



Universidad de Valladolid



PROGRAMA DE DOCTORADO EN
QUÍMICA: QUÍMICA DE SÍNTESIS,
CATÁLISIS Y MATERIALES
AVANZADOS

TESIS DOCTORAL:

**Understanding Palladium-Mediated
Transformations: Aerobic C-H Alkenylation of
Arenes via Metal-Ligand Cooperation and
Reactions with Carbene Precursors**

Presentada por Francisco Villalba de
Pando para optar al grado de
Doctor por la Universidad de Valladolid

Dirigida por:
Ana Carmen Albéniz Jiménez

AUTORIZACIÓN DE LA DIRECTORA DE TESIS

Ana Carmen Albéniz Jiménez, Catedrática de Química Inorgánica de la Universidad de Valladolid e investigadora del I. U. CINQUIMA

CERTIFICA:

Que la memoria titulada *Understanding Palladium-Mediated Transformations: Aerobic C-H Alkenylation of Arenes via Metal-Ligand Cooperation and Reactions with Carbene Precursors* ha sido realizada en el I. U. CINQUIMA y el Área de Química Inorgánica de la Facultad de Ciencias de la Universidad de Valladolid por D. Francisco Villalba de Pando, alumno del programa de doctorado “*Doctorado en Química: Química de Síntesis, Catálisis y Materiales Avanzados*” y autoriza su presentación para que sea calificada como Tesis Doctoral.

Valladolid, 12 de diciembre de 2022

La Directora de la Tesis

Fdo: Ana Carmen Albéniz Jiménez



La Tesis Doctoral titulada “*Understanding Palladium-Mediated Transformations: Aerobic C-H Alkenylation of Arenes via Metal-Ligand Cooperation and Reactions with Carbene Precursors*” ha sido realizada gracias al apoyo económico del MICINN/AEI (proyectos CTQ-2016-80913-P y PID2019-111406GB-I00), de la Junta de Castilla y León-Feder (proyectos VA051P17 y VA224P20; ayuda para contratos predoctorales Orden EDU/1100/2017, de 12 de diciembre) y del MECD (beca predoctoral FPU-17/04559). La asistencia a algunos congresos ha sido objeto de ayudas por parte de la UVa (asistencia a congresos relevantes para el desarrollo de tesis doctorales, convocatoria 2022) y de la S.T. de Castilla de la RSEQ.

Hasta el momento el trabajo presentado en esta Tesis ha dado lugar a las siguientes publicaciones:

“Non-Chelate-Assisted Palladium-Catalyzed Aerobic Oxidative Heck Reaction of Fluorobenzenes and Other Arenes: When Does the C–H Activation Need Help?”.

Villalba, F.; Albéniz, A. C. *Adv. Synth. Catal.* **2021**, *363*, 4795–4804.
<https://doi.org/https://doi.org/10.1002/adsc.202100677>

“Diazo Compounds and Palladium-Aryl Complexes: Trapping the Elusive Carbene Migratory Insertion Organometallic Products”.

Villalba, F.; Albéniz, A. C. *Dalton Trans.* **2022**, *51*, 14847–14851.
<https://doi.org/10.1039/D2DT02775E>

“Palladium Hydrazonato Complexes and Their Role in the Pd-Catalyzed Cross-Coupling Reactions of Hydrazones as Carbene Precursors”.

Villalba, F.; Albéniz, A. C. *Dalton Trans.* **2022**, *51*, 17733–17742.
DOI <https://doi.org/10.1039/D2DT03251A>

Quiero empezar estas líneas agradeciendo a todas aquellas personas que han hecho posible que esta tesis doctoral se materialice en la forma final que aquí se presenta, acompañándome durante todo el camino.

A la Profesora Ana Carmen Albéniz, primero por darme la posibilidad de formar parte de su grupo durante estos años y segundo por transmitirme su visión crítica y meticulosa a la hora de abordar cualquier tipo de problema ya fuese químico o de la vida cotidiana.

A todos los técnicos y profesores del área de Química Inorgánica y Química Física, por compartir su conocimiento y ayudarme cuando lo he necesitado con los múltiples problemas que me ha ido planteando la Química. A J.M. por ser capaz de tener cualquier cosa que necesitará, ya fuese un adaptador para bomba o una charla motivadora. Quiero agradecer al profesor Agustí Lledós su tiempo y sus consejos los cuales me han acercado un poco más al vasto mundo de la Química Computacional.

A todos los compañeros de laboratorio con lo que he tenido la suerte de coincidir durante esta etapa, todos ellos han aportado algo bueno que me ha permitido seguir adelante en los malos momentos. A Rodri por ser mi maestro de ceremonias y enseñarme toda su experiencia cuando llegué por primera vez, allá por aquellas prácticas de laboratorio de tercero. A Beto, por ser compañero de laboratorio, comidas, viajes en la Regional y siempre estar ahí. A Vanesa por su inestimable ayuda y paciencia durante mi TFG y mi TFM.

Me gustaría dedicar unas líneas para dar un especial agradecimiento a aquellas personas con las que he compartido la mayor parte de mi tiempo durante la tesis. A Jaime, Rebeca, Sandra, Sarah, Noelia, Leo, Dani, Adriana, Clara y especialmente a Álvaro por su ayuda en la resolución de estructuras de rayos X.

A la familia que se ha formado y con la que he tenido la suerte de compartir comidas, cenas, casas rurales, cañas y en definitiva cualquier tipo de plan descabellado liderado por Miguelu y secundado por Nacho, Cintya, Charly, Wonka, Iker y Jorge siendo Safer y Marta las maquiavélicas mentes pensantes.

Por supuesto al grupo de la Mery-House. A María por ser el mayor ejemplo de resiliencia y de amor incondicional que conozco. A María-B por nuestras interminables discusiones en las más interminables horas invertidas en la Regional. A Estefa por compartir sus puntos de vista y consejos conmigo, gracias a ellos he podido encarar los problemas que me venían desde otro punto de vista. A Sergio, por transmitir tu gran pasión, aunque no te dieras cuenta, cada vez que me hablabas del mundo del RMN y sin el cual habría sido

imposible sostener gran parte de las discusiones de esta tesis. A Olmo y Estela, de los cuales he podido aprender la importancia de la paciencia y la humildad.

A mi variopinto grupo de amigos palentinos que me han permitido evadirme de mis problemas cuando más lo necesitaba y me han enseñado que siempre estarán ahí cuando lo necesite. A Alberto por ser la mecha que lo inició todo. A David, Andoni, Elena, Bea, Natalia y Leti.

Por último y no menos importante: a Laura por su paciencia y por haber sido la puerta a un mundo que no había conocido. A Sandra por ser de las personas que más han tenido que sufrir mis frustraciones durante los últimos años.

A todos vosotros, gracias por estar ahí.

A mi madre y a mis hermanas.

TABLE OF CONTENTS

<i>Preface</i>	1
<i>Part I: Pd-Catalyzed C-C Cross-Coupling Reactions with C-H Activation Steps</i>	5
<i>Chapter 1</i>	7
1. Introduction	9
1.1 Conventional Pd-catalysed C-C cross-coupling reactions	9
1.2 Pd-catalysed C-C cross-coupling reactions with C-H activation steps	11
1.3 Oxidative C-C cross-coupling reactions	13
1.4 Mechanistic features for aerobic oxidations	16
1.5 Mechanisms of C-H activation	19
1.6 Cooperating ligands in the C-H cleavage	25
<i>Chapter 2</i>	31
2. Oxidative Heck Reaction of Fluorobenzenes and Other Arenes: When Does the C-H Activation Need Help?	33
2.1 Introduction	33
2.2 Results and discussion	38
2.2.1 Oxidative Heck reactions of fluorinated and non-fluorinated arenes	38
2.2.2 Mechanistic aspects and the role of bipy-6-OH	49
2.3 Conclusions	54
2.4 Experimental part	55
2.4.1 General considerations	55
2.4.2 Synthesis of palladium complexes	55
2.4.3 Catalytic reactions	56
2.4.4 Additional catalytic experiments and test reactions	72
2.4.5 Mechanistic experiments	75
2.4.6 Kinetic experiments for the oxidative Heck reaction of toluene	78
2.4.7 Computational details	84
2.4.8 Data for X-Ray structure determinations	85

Chapter 3 _____ **89**

3. Shedding Light on the Precatalytic Mixture of [Pd(OAc)₂] and Cooperating Pyridone-Type Ligands for the C-H Activation of Arenes _____ **91**

3.1 Introduction	91
3.2 Results and discussion	96
3.2.1 Reactivity of bipy-6-OH	96
3.2.2 Reactivity of phen-2-OH	103
3.2.3 Reactivity of phen-2-OH and bipy-6-OH with pyridine and [Pd(OAc) ₂]	105
3.2.4 Catalytic reactions	110
3.3 Conclusions	114
3.4 Experimental part	115
3.4.1 General considerations	115
3.4.2 Synthesis of palladium complexes	115
3.4.3 Catalytic reactions	120
3.4.4 Decomposition of 23a in toluene at high temperature	122
3.4.5 Reactivity of bipy-6-OH and phen-2-OH with [Pd(OAc) ₂] in different solvents (CDCl ₃ , DMA and DMSO). Reorganization studies	123
3.4.6 DOSY experiments	124
3.4.7 Mass spectrometry	125
3.4.8 Data for X-Ray structure determinations	127

Part II: Reactions of Pd(II) Complexes with Carbene Precursors _____ **131**

Chapter 4 _____ **133**

4. Introduction _____ **135**

4.1 The carbene fragment and metal carbenes	135
4.2 Approaches to the generation of reactive metal-carbenes	144
4.3. Pd-catalyzed C-C coupling reactions with carbene precursors <i>via</i> migratory insertion	150

Chapter 5 _____ **157**

5. Diazo Compounds, Hydrazones and Their Reactions with Palladium-Aryl Complexes _____ **159**

5.1 Introduction	159
------------------	-----

5.2 Results and discussion	163
5.2.1 Reactions with diazo compounds	163
5.2.2 Reactions with hydrazone derivatives	174
5.2.3 Ligand substitution reactions	184
5.3 Conclusions	187
5.4 Experimental part	189
5.4.1 General considerations	189
5.4.2 Synthesis of palladium complexes	190
5.4.3 Decomposition of the diazoalkane 30 and <i>N</i> -tosylhydrazone 34	201
5.4.4 Decomposition of individual complexes	203
5.4.5 Crossover experiments	204
5.4.6 General procedure for the ligand substitution reactions	205
5.4.7 Attempts at detection of intermediate complexes before the migratory insertion	206
5.4.8 Data for X-Ray molecular structure determinations	207
5.4.9 Computational details	214
Chapter 6	217
6. Understanding the Ligand Influence in the Multistep Reaction of Diazo Derivatives with Palladium Complexes Leading to Carbene-Aryl Coupling	219
6.1 Introduction	219
6.2 Results and discussion	224
6.2.1 Synthesis of palladium(II) precursors	224
6.2.2 Reactions with diazo compounds: chelating diphosphine ligands	227
6.2.3 Reactions with diazo compounds: triphenylphosphine	234
6.2.4 Reactions with diazo compounds: bipyridine	236
6.2.5 DFT studies	240
6.3 Conclusions	254
6.4 Experimental part	255
6.4.1 General considerations	255
6.4.2 Synthesis of palladium complexes	255
6.4.3 Experiments to evaluate the reactivity of palladium complexes with diazo compounds	262

6.4.4 Data for X-Ray molecular structure determinations	263
6.4.5 Computational details	266
Chapter 7	271
7. Reactions of the Simplest Amino Carbene CH(NEt₂): Transmetallation from Cu(I) to Pd(II) and Migratory Insertion	273
7.1 Introduction	273
7.2 Results and discussion	278
7.2.1 Carbene transmetallation from Cu(I) to Pd(II): Preparation of Pd(II)-aminocarbene complexes	278
7.2.2 Study of the transmetallation and migratory insertion reaction in Pd-aryl complexes	286
7.3 Conclusions	297
7.4 Experimental part	298
7.4.1 General considerations	298
7.4.2 Synthesis of palladium complexes	298
7.4.3 Evidence for the chloride bridge cleavage by acetonitrile in complex [Pd ₂ (μ-Cl) ₂ (Cl) ₂ (PPh ₃) ₂]	301
7.4.4 Follow up of the carbene transmetallation from Cu(I) to Pd(II)	302
7.4.5 Attempts at detection of a [Tp ^{Ms} Cu(PPh ₃)] adduct	303
7.4.6 Mass spectra	304
7.4.7 Computational details	306
Transformaciones Mediadas por Paladio: C-H Alquenilación Aeróbica de Arenos Asistida por Cooperación Metal-Ligando y Reacciones con Precursores de Carbeno	307
Resumen	307
Prefacio	309
Capítulo 1: Introducción Parte I	311
Capítulo 2: Reacción de Heck oxidativa de fluorobencenos y otros arenos: ¿En qué casos necesita ayuda la activación C-H?	314
Capítulo 3: Arrojando luz sobre las especies presentes en la mezcla precatalítica de [Pd(OAc) ₂] y ligandos cooperativos de tipo bipyridona para activaciones C-H de arenos	319
Capítulo 4: Introducción Parte II	324

Capítulo 5: Diazo-compuestos, hidrazonas y sus reacciones con complejos arílicos de paladio _____	328
Capítulo 6: Entendiendo la influencia de los ligandos en la reacción multietapa de diazo compuestos con complejos de paladio con acoplamiento carbeno-arilo __	333
Capítulo 7: Reacciones del aminocarbeno más simple CH(NEt ₂): Transmetalación desde Cu(I) a Pd(II) e inserción migratoria _____	337
Conclusiones Generales _____	340
Appendix _____	343
List of abbreviations and acronyms _____	345
References _____	347
Compound index _____	363

Preface

Preface

One of the main goals of research in Chemistry nowadays is to achieve more efficient chemical syntheses. The work in this thesis is intended to contribute to this goal by improving the efficiency of palladium catalyzed processes. With this aim, the research is focused on the use of novel catalysts in combination with mechanistic studies of the steps that constitute the catalytic cycles. Two different types of catalytic processes were chosen: cross-coupling reactions of arenes that involve C-H activation, and cross-coupling processes that use carbene precursors. Both are attractive reactions to achieve molecular complexity in a reduced number of synthetic steps: The first one because no prefunctionalization of the arenes, the available raw materials, is needed; the second one because the formation of more than one C-C or C-X bonds occurs in just one synthetic step. The analysis of catalytic and stoichiometric reactions along with kinetic and computational studies, led us to gain insight into the mechanistic aspects of these reactions that could help to a rational design of better catalytic systems.

This dissertation is organized into two main blocks, each block focusing in one of the reaction types mentioned above and comprising a general introductory chapter, to establish the main context and to define the basic concepts that will be used throughout the block, and several chapters describing the work done.

The first block describes the research on Pd-catalysed C-C cross-coupling reactions with C-H activation steps. After a general introduction (*Chapter 1*), *Chapter 2* describes the aerobic oxidative Heck-type reaction of fluorinated and non-fluorinated arenes catalyzed by well-defined Pd-complexes bearing cooperating bipyridone-type ligands which assist in the C-H cleavage transition state. The optimal set of conditions using oxygen as a sole oxidant and catalytic amounts of additives were investigated, increasing, by doing so, the

Preface

sustainability of the global process. *Chapter 3* explores the solution speciation of the bipyridone cooperating ligands, employed in the abovementioned reaction and useful in other arene functionalization reactions, with commercial Pd(II) salts. These studies led us to determine the complexes that are most efficient precatalysts in cross-coupling reactions with simple arenes.

The second part is a contribution to palladium-mediated carbene chemistry, focusing on the less studied non-stabilized monosubstituted palladium carbenes with alkyl or phenyl as a substituent ($:\text{CHR}^1$) or palladium-carbenes bearing only one heteroatom substituent ($:\text{CH}(\text{X})$, $\text{X} = \text{NEt}_2$). *Chapters 5* and *6* describe a thorough study, by experimental and computationally methods, of the migratory insertion processes of elusive palladium carbene intermediates formed by reaction of diazoalkanes and hydrazones. This is the key C-C bond-forming step in Pd-catalyzed cross-coupling reactions involving carbene precursors. Finally, *Chapter 7* aims to explore the behaviour of palladium complexes with the unusual $:\text{CHNR}_2$ carbene-fragment *via* transmetalation from a well-defined Cu(I) complex to Pd(II) complexes. This work was carried out in collaboration with the group of Prof. Pedro. J. Pérez (CIQSO, Universidad de Huelva) and with Prof. Agustí Lledós (Universidad Autònoma de Barcelona) who has been responsible for the DFT calculations in this chapter.

The present dissertation is written in English as a part of my doctoral training. Those chapters describing the results of this work (*Chapters 2, 3, 5-7*) are self-contained and are subdivided into four sections: Introduction, Results and Discussion, Conclusions and Experimental Part. This dissertation contains an Appendix with a list of abbreviations used and an index of the compounds described in each chapter, numbered in order of appearance. The references are presented as footnotes in every chapter and are also collected in the appendix as a list. Since this thesis is written in English, to comply with the current regulations of the UVA a brief summary of the results is presented in Spanish with its own bibliography and the general conclusions.

Part I

*Pd-Catalyzed C-C Cross-Coupling Reactions
with C-H Activation Steps*

Chapter 1

1. Introduction

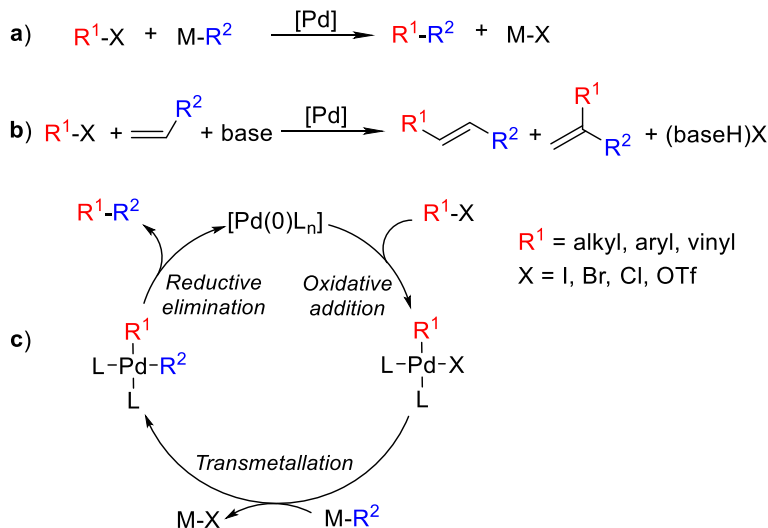
1.1 Conventional Pd-catalysed C-C cross-coupling reactions

Among the versatile synthetic approaches known to date, transition metal-catalyzed cross-coupling reactions have been considered as one of the great discoveries of the last century. The 2010 Nobel Prize in chemistry was awarded to Professors Richard F. Heck, Ei-ichi Negishi and Akira Suzuki because of their research contributions to cross-coupling reactions as the most important keystone on palladium catalysis. These C-C bond formation reactions represent a powerful strategy in both academic and industrial fields to access complex molecular scaffolds in synthetic chemistry.¹

In a simplified way, these reactions involve two main reagents: an organic electrophile R^1-X and an organometallic nucleophile $M-R^2$ that couple in the presence of a metal catalyst (Scheme 1.1). In most cases, cross-coupling reactions use late-transition metals as catalysts, mainly palladium, and in this chapter, the discussion will focus on this metal. In addition to organometallic nucleophiles, with a direct “M-C” bond, there are other nucleophiles as coupling partners capable of carrying out those transformations. Cross-coupling reactions can involve alkenes, commonly referred to as Heck-type

¹ A presentation of the topic can be found in: a) de Meijere, A.; Negishi, E-i. *Handbook of Organopalladium Chemistry for Organic Synthesis, Vol 1 and 2*, Wiley-Interscience, New York, **2002**. b) Miyaura, N.; *Cross-Coupling Reactions: A practical Guide; Topics in Current Chemistry*, Series 219; **2002**, Springer, Berlin. c) De Meijere, A; Dietrich, F.; *Metal-Catalyzed Cross-Coupling Reactions*, 2nd ed. **2004**, Wiley-VCH: Weinheim. d) de Meijere, A.; Bräse, S.; Oestreich, M. *Metal-Catalyzed Cross-Coupling Reactions and More, Vol 1, 2 and 3.*; Wiley-VCH: Weinheim, **2013**.

reactions,² amines (Buchwald-Hartwig amination),^{3,4} organosulfur compounds (sulfenylation reactions)^{4,5} or alcohols (and other *O*-containing surrogates such as vinyl ethers, phenols or epoxides).⁴



Scheme 1.1 General equations of Pd-catalyzed cross-coupling reactions. **a)** $M-R^2$: Li-R^2 , MgXR^2 (Kumada),⁶ ZnR^2X (Negishi),⁷ R_2AlR^2 , Bu_3SnR^2 , (Stille),⁸ R_2BR^2 (Miyaura-Suzuki),⁹ R_3SiR^2 (Hiyama),¹⁰ CuR^2 (Sonogashira).¹¹ **b)** Olefin (Heck).² R^1-X : $R^1 = \text{alkyl, aryl, vinyl, heteroaryl}$; $X = \text{I, Br, Cl, OTf}$. **c)** General catalytic cycle for reactions in Equation. **a)**.

A general accepted mechanistic interpretation of a cross-coupling catalytic cycle involves three fundamental steps: **a)** oxidative addition of the organic electrophile

² a) Heck, R. F. *J. Am. Chem. Soc.* **1968**, *90*, 5518–5526. b) Mizoroki, T.; Mori, K.; Ozaki, A. *Bull. Chem. Soc. Jpn.* **1971**, *44*, 581–581. c) Heck, R. F. *Org. React.* **1982**, *27*, 345–390.

³ a) Louie, J.; Hartwig, J. F. *Tetrahedron Lett.* **1995**, *36*, 3609–3612. b) Guram, A. S.; Rennels, R. A.; Buchwald, S. L. *Angew. Chem., Int. Ed.* **1995**, *34*, 1348–1350. For recent reviews see: a) Ruiz-Castillo, P.; Buchwald, S. L. *Chem. Rev.* **2016**, *116*, 12564–12649. b) Heravi, M. M.; Kheilkordi, Z.; Zadsirjan, V.; Heydari, M.; Malmir, M. *J. Organomet. Chem.* **2018**, *861*, 17–104. c) Dorel, R.; Grugel, C. P.; Haydl, A. M. *Angew. Chem. Int. Ed.* **2019**, *58*, 17118–17129.

⁴ Zhao, B.; Rogge, T.; Ackermann, L.; Shi, Z. *Chem. Soc. Rev.* **2021**, *50*, 8903–8953.

⁵ a) Li, J.; Yang, S.; Wu, W.; Jiang, H. *Org. Chem. Front.* **2020**, *7*, 1395–1417. b) Beletskaya, I. P.; Ananikov, V. P. *Chem. Rev.* **2022**, *122*, 16110–16293.

⁶ Kumada, M. *Pure Appl. Chem.* **1980**, *52*, 669–679.

⁷ Negishi, E.-I. *Acc. Chem. Res.* **1982**, *15*, 340–348.

⁸ a) Stille, J. K. *Angew. Chem. Int. Ed.* **1986**, *25*, 508–524. b) Stille, J. K. *Angew. Chem.* **1986**, *98*, 504–519. c) Espinet, P.; Echavaren, A. M. *Angew. Chem. Int. Ed.* **2004**, *43*, 4704–4734.

⁹ a) Miyaura, N.; Yanagi, T.; Suzuki, A. *Synth. Commun.* **1981**, *11*, 513–519. b) Miyaura, N.; Suzuki, A. *Chem. Rev.* **1995**, *95*, 2457–2483.

¹⁰ a) Hiyama, T.; Shirakawa, E. *Top. Curr. Chem.* **2002**, *219*, 61–85. b) Hiyama, T.; *J. Organomet. Chem.* **2002**, *653*, 58–61.

¹¹ a) Sonogashira, K.; Tohda, Y.; Hagihara, N. *Tetrahedron Lett.* **1975**, 4467–4470.

b) Sonogashira, K. in *Comprehensive Organic Synthesis* (Eds.: B. M. Trost, I. Fleming), Pergamon Press, Oxford, **1991**, Vol. 3, pp. 521–549.

R¹-X to palladium(0) to form a Pd(II) complex intermediate, [PdL₂R¹X];
b) transmetallation of the nucleophile M-R² to form intermediate [PdL₂R¹R²];
c) reductive elimination to release the desired coupling product R¹-R² and regenerate the Pd(0) species, thus completing a catalytic cycle (Scheme 1.1, **c**). Several additional steps including off-cycle precatalyst activation, isomerization processes and ligand substitutions could take place.

1.2 Pd-catalysed C-C cross-coupling reactions with C-H activation steps

In the previous conventional cross-coupling reactions, electrophiles and nucleophiles as reactants are obtained by prefunctionalization of their corresponding hydrocarbons as raw materials. In this aspect the poor atom- and step-economy of these prefunctionalizations is not ideal, and it does not fit well with the Green Chemistry concept.¹² During the last decades, tremendous efforts have been devoted to develop novel synthetic methodologies to achieve C-C or C-X cross-coupling reactions by direct activation and functionalization of C-H bonds.¹³

To clarify some of the terminology used throughout this introduction and the following chapters, *Chapter 2* and *Chapter 3*, with regard to the “C-H activation or C-H functionalization” concepts it is worth mention that we talk about C-H bond activation to refer to the formation of a metal complex in which the C-H bond has been broken affording a new M-C bond. Conversely, the term C-H bond functionalization refers to the process of transforming a C-H bond to a new C-X bond where X could be carbon or heteroatom. In most cases the C-H functionalization is preceded by a C-H activation event.¹⁴

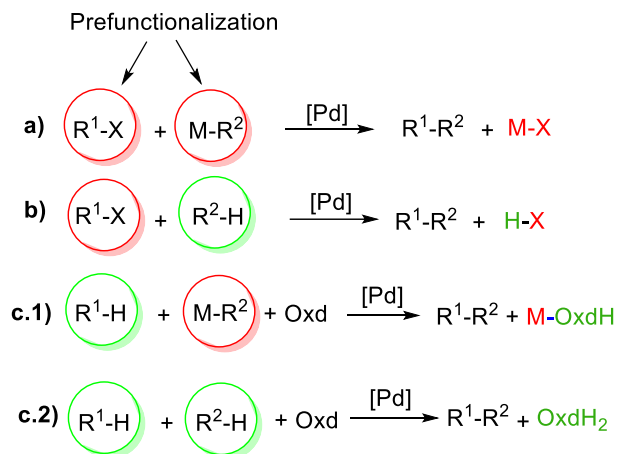
There is, at least, one C-H activation step involved in the catalytic cycle for those strategies that replace one or two coupling partners of a conventional cross-coupling reaction by a hydrocarbon (*cf.* **a** and **b-c** in Scheme 1.2). In the direct arylation scenario (Scheme 1.2, **b**), no prefunctionalization to give an organometallic compound is required since the hydrocarbon is directly used, avoiding this way multiple

¹² a) Anastas, P. T.; Mary, M. *Acc. Chem. Res.* **2002**, *35*, 686–694. b) Dalton, T.; Faber, T.; Glorius, F. *ACS Cent. Sci.* **2021**, *7*, 245–261.

¹³ a) He, J.; Wasa, M.; Chan, K. S. L.; Shao, Q.; Yu, J-Q. *Chem. Rev.* **2017**, *117*, 8754–8786. b) Newton, C. G.; Wang, S.-G.; Oliveira, C. C.; Cramer, N. *Chem. Rev.* **2017**, *117*, 8908–8976. c) Crabtree, R. H.; Lei, A. *Chem. Rev.* **2017**, *117* (13), 8481–8482. d) Zhang, L.; Ritter, T. *J. Am. Chem. Soc.* **2022**, *144*, 2399–2414.

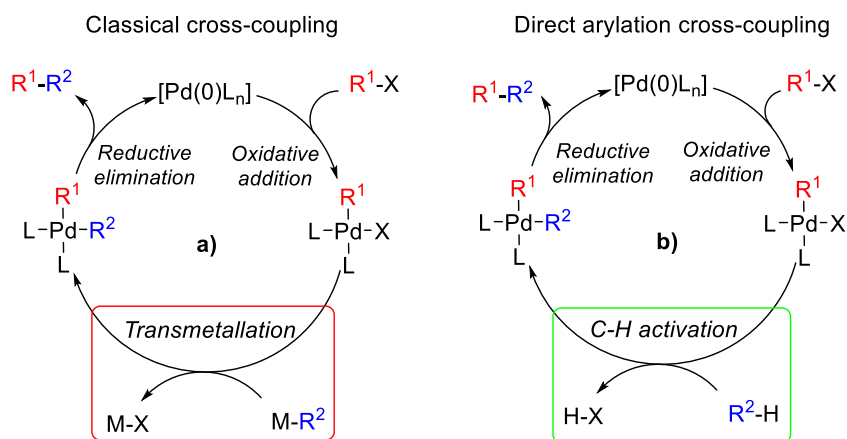
¹⁴ Altus, K. M.; Love, J. A. *Commun. Chem.* **2021**, *4*, 173.

synthetic steps. The substitution of either the organic electrophile or both coupling partners by hydrocarbons is also possible (Scheme 1.2, c), but usually requires the presence of an oxidant and they are called oxidative C-C couplings (see the following section).



Scheme 1.2 C-C bond formation strategies. **a)** Traditional/conventional C-C coupling, **b)** Direct arylation reaction, **c)** Oxidative C-C couplings.

Mechanistically, the transmetalation step is replaced by a C-H activation step for a direct arylation reaction (*cf.* **a**) and **b**) in Scheme 1.3). Overall, this methodology implies a considerable reduction of useless byproducts at the end of the reaction which makes these chemical processes more sustainable.

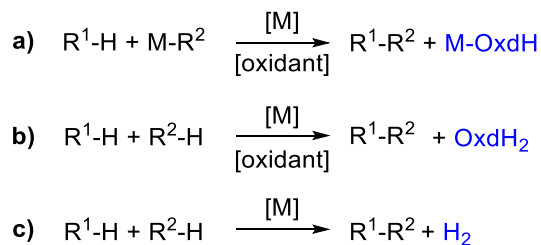


Scheme 1.3 General catalytic cycles of palladium-catalysed **a)** traditional cross-coupling reactions. **b)** cross coupling reactions by direct arylation.

1.3 Oxidative C-C cross-coupling reactions

An oxidative coupling is a process that creates a new bond between two nucleophiles,¹⁵ which could be non-functionalized hydrocarbons as mentioned before, heteroatom centered nucleophiles such as amines, alcohols and also organometallic reagents (Scheme 1.4). These reactions usually need an oxidant that makes the reaction thermodynamically more favoured.

The most environmentally attractive method, in terms of improving step economy and reducing the waste, is the direct cross-coupling of two hydrocarbons by double C-H activation (Scheme 1.4, **b**) and **c**).¹⁶ These reactions in which the C-C bond formation has been carried out by the consecutive cleavage of two C-H bonds, are called “cross-dehydrogenative couplings” (CDC).¹⁷



Scheme 1.4 Different oxidative C-C bond formation.

Among these cross-dehydrogenative couplings, one of the first works was reported by Fujiwara and Moritani describing the coupling between simple arenes and styrene using stoichiometric amounts of a styrene-palladium chloride complex.¹⁸ When palladium is used in sub-stoichiometric amounts (catalytic conditions), an external oxidant is required. This Pd-catalyzed coupling of arenes with alkenes are called

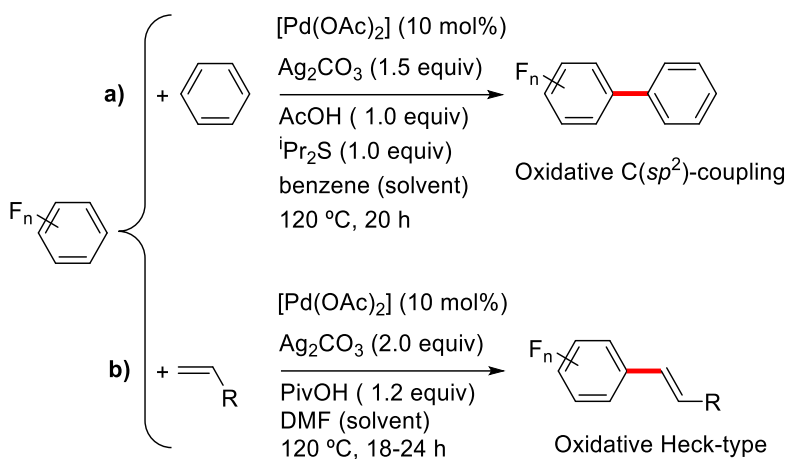
¹⁵ In the context of fundamental organometallic chemistry oxidative coupling has a different meaning: it is a reaction where two coordinated ligands form a new bond to each other while changing from 2 L ligands to an X₂ ligand and therefore producing the oxidation of the metal center.

¹⁶ Li, H.; Liu, J.; Sun, C.-L.; Li, B.-J.; Shi, Z.-J. *Org. Lett.* **2011**, *13*, 276–279.

¹⁷ a) Li, C.-J. *Acc. Chem. Res.* **2009**, *42*, 335–344. b) Scheuermann, C. *J. Chem. Asian J.* **2010**, *5*, 436–451. c) Krylov, I. B.; Vil', V. A.; Terent'ev, A. O. *Beilstein J. Org. Chem.* **2015**, *11*, 92–146. d) Yang, Y.; Lan, J.; You, J.-Q. *Chem. Rev.* **2017**, *117*, 8787–8863. e) Huang, C.-Y.; Kang, H.; Li, J.; Li, C.-J. *J. Org. Chem.* **2019**, *84*, 12705–12721.

¹⁸ Moritani, I.; Fujiwara, Y. *Tetrahedron Lett.* **1967**, *8*, 1119–1122.

oxidative Heck, dehydrogenative Heck (DHR) or Fujiwara-Moritani reaction (Scheme 1.5, **b**).¹⁹



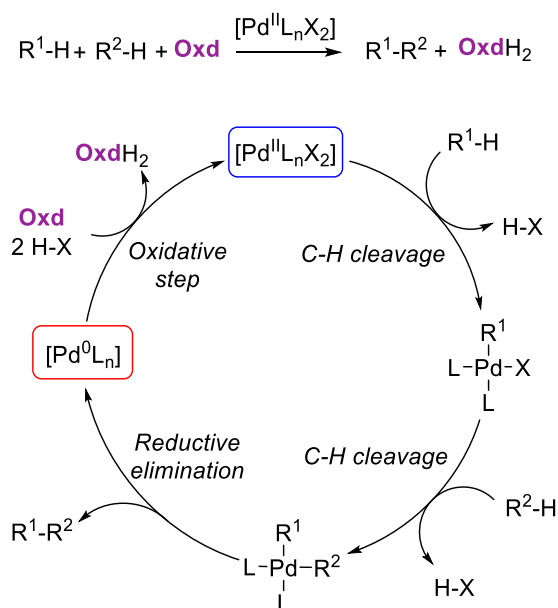
Scheme 1.5 Examples of cross-dehydrogenative coupling between **a**) a polyfluorinated arene and a simple arene (ref: 16) and **b**) a polyfluorinated arene an alkene (ref: 19).

A simplified catalytic cycle for the oxidative cross-coupling of two hydrocarbons is depicted in Scheme 1.6. Usually, the catalyst initiates the catalytic cycle as a palladium(II) species which has two monoanionic groups (X^-) acting as ligands. In these reactions, one of the hydrocarbons, R^1H , reacts with the palladium catalyst to form an organometallic complex by C-H activation. The second organic fragment, R^2 , is introduced in the metal coordination sphere *via* C-H cleavage in a second C-H activation process. For reactions where the second coupling partner is an organometallic derivative MR^2 (Scheme 1.4, **a**), the latter step is a transmetalation. Finally, reductive elimination affords the desired coupling product R^1-R^2 and releases a palladium(0) species. In order to restart the catalytic cycle, an external oxidant is needed to re-oxidize Pd(0) to Pd(II). It is important to note that the oxidant only acts as an electron acceptor without going into the coupling products. The mechanism of the oxidative Heck reaction differs with respect to the cross-coupling of two simple arenes since one of the coupling partners is an alkene. After the C-H cleavage step for the R^1-H reactant, a coordination of the olefin followed by a migratory insertion into the metal-carbon bond is proposed ($M-R^1$).

Very recent achievements have been carried out in oxidative cross-coupling reactions, trying to circumvent the use of oxidants. In this way, the ideal coupling process

¹⁹ Zhang, X.; Fan, S.; He, C.-Y.; Wan, X.; Min, Q.-Q.; Yang, J.; Jiang, Z.-X. *J. Am. Chem. Soc.* **2010**, *132*, 4506–4507.

is depicted in Scheme 1.4, c) in which no oxidant is required and H₂ as the only byproduct is generated, leading to a reaction with great atom economy. In this context, thermal transition metal catalysis, photochemistry and electrochemistry have emerged as powerful tools for R¹-H/R²-H cross-coupling reactions with hydrogen evolution.²⁰ However, most oxidative coupling processes still require the presence of an oxidant.



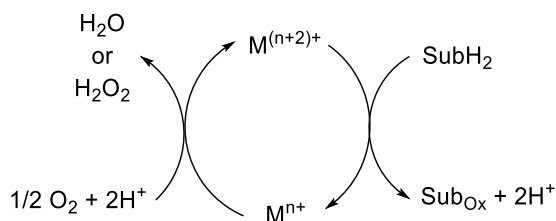
Scheme 1.6 General catalytic cycle for palladium-catalyzed oxidative cross-coupling reactions involving two C-H activation steps with oxygen as an oxidant.

Among all effective oxidants known in oxidative reactions, metal salts such as silver(I), copper(II), Mn(VII) have been widely reported (see examples in Scheme 1.5). Likewise, organic oxidants such as benzoquinone derivatives (*p*-BQ, DDQ), hypervalent iodine derivatives or various peroxides derivatives have been also used. Many of them are associated with a negative environmental impact due to their toxic properties or byproduct generation, so the choice of oxidant in these reactions is very important to keep them sustainable. Molecular oxygen is readily available, inexpensive and non-toxic, being the ideal green oxidant since hydrogen peroxide or water are the only byproducts.

²⁰ a) Tang, S.; Zeng, L.; Lei, A. *J. Am. Chem. Soc.* **2018**, *140*, 13128–13135. b) Zhang, D.; Hui, X.; Wu, C.; Zhu, Y. *ChemCatChem* **2021**, *13*, 3370–3380. c) Liu, Q.; Wu, L.-Z. Cross-Coupling Hydrogen Evolution to Avoid the Use of External Oxidants BT - Springer Handbook of Inorganic Photochemistry; Bahnemann, D., Patrocínio, A. O. T., Eds.; Springer International Publishing: Cham, **2022**; pp 1457–1480.

1.4 Mechanistic features for aerobic oxidations

When the oxidative step in palladium-catalyzed reactions is performed using molecular oxygen as a terminal oxidant, it generally acts as a two electron/ two proton acceptor in the metal oxidation and it is not involved in oxygen-atom transfer to the substrates. These reactions are called oxidase-type (Scheme 1.7),^{21c} in contrast to the oxygenase-type reactions where there is oxygen-atom transfer to the substrate.



Scheme 1.7 Representation of a general Pd-catalyzed oxidase-type process.

Recent developments in the selective transformation of organic molecules by transition-metal catalyzed aerobic oxidation reactions provide a broad scope of value-added products.²¹ However, it is well-known that the use of oxygen is a challenge for several reasons: it is very stable, both thermodynamically and kinetically, and the ground state is a triplet, hindering the activation on a singlet potential energy surface. Thus, this gives rise to higher energetic barriers for electron transfer leading to unfavourable kinetics associated with this process. To circumvent these issues, some electron-transfer mediators (ETMs) have been used in combination with oxygen to successfully achieve the oxidation of Pd(0), such as a sub-stoichiometric amount of copper salts, hydroquinone (HQ), cobalt Schiff base complex [Co(salophen)], iron phthalocyanines, NaNO₃ or NaNO₂, among others.²²

The solubility of oxygen in organic solvents or in binary mixtures is an important property to take into account. For oxidative metal-catalyzed reactions, it has been observed that at elevated catalyst loading, the rate of catalytic turnover is limited

²¹ For reviews on transition-metal catalyzed oxidative reactions with oxygen see: a) Stahl, S. S. *Angew. Chem. Int. Ed.* **2004**, *43*, 3400–3420. b) Piera, J.; Bäckvall, J.-E. *Angew. Chem. Int. Ed.* **2008**, *47*, 3506–3523. c) Campbell, A. N.; Stahl, S. S. *Acc. Chem. Res.* **2012**, *45*, 851–863. d) Shi, Z.; Zhang, C.; Tanga, C.; Jiao, N. *Chem. Soc. Rev.*, **2012**, *41*, 3381–3430.

²² a) Liu, J.; Guðmundsson, A.; Bäckvall, J.-E. *Angew. Chem. Int. Ed.* **2021**, *60*, 15686–15704.

by the oxygen solubility when a polar solvent is used (DMSO, amides).²³ Therefore, the mass-transfer of oxygen gas into solution can be rate-limiting and it can govern the kinetics of the overall process albeit the actual oxidation reaction is not the turnover-limiting step of the catalysis. This is important in the oxidation of Pd(0) to Pd(II) by molecular oxygen. The intrinsic instability of homogenous Pd(0) species can lead to decomposition to Pd black if the oxidation by O₂, in a rate-limiting mass-transfer scenario, is not fast enough. To overcome this gas-liquid mass-transfer limitation, several strategies can be used, like the increase of the concentration of dissolved oxygen by conducting the reaction at elevated oxygen pressures or the use of solvents with higher oxygen solubility (*i.e.* solvents with low polarity).

Scheme 1.8 represents the accepted mechanisms for the direct oxidation of reduced palladium species [Pd(0)L_n] with molecular oxygen. The oxidation route is strongly dependent on the palladium complex and its specific set of ligands.²⁴ Isolated complexes that illustrate both types of reactivity have been reported.

Mechanism A): A η²-peroxo palladium(II) complex is formed as a result of molecular oxygen activation by reduced palladium(0) species. A large array of evidence for this pathway has been reported by different authors such as Stahl and Goldberg, among others.²⁵ Computational studies and one experimental observation employing a bulky carbene (IPr),^{25b} indicate that O₂ reacts with the Pd(0) species by initial formation of an *end-on* superoxo-Pd(I) complex that rearranges to form a η²-peroxo palladium(II) complex (Scheme 1.8, **A**). A double sequential protonation of this complex regenerates the active catalytic species [PdL_nX₂] with the concomitant production of H₂O₂.

²³ a) Steinhoff, B. A.; Stahl, S. S. *J. Am. Chem. Soc.* **2006**, *128*, 4348–4355 b) Quaranta, M.; Murkovic, M.; Klimant, I. *Analyst* **2013**, *138*, 6243–6245. c) Sato, T.; Hamada, Y.; Sumikawa, M.; Araki, S.; Yamamoto, H. *Ind. Eng. Chem. Res.* **2014**, *53*, 19331–19337.

²⁴ a) Muzart, J. *Chem. Asian J.* **2006**, *1*, 508–515. b) Wang, D.; Weinstein, A. B.; White, P. B.; Stahl, S. S. *Chem. Rev.* **2018**, *118*, 5, 2636–2679.

²⁵ a) Stahl, S. S.; Thorman, J. L.; Nelson, R. C.; Kozee, M. A. *J. Am. Chem. Soc.* **2001**, *123*, 7188–7189. b) Steinhoff, B. A.; Fix, S. R.; Stahl, S. S. *J. Am. Chem. Soc.* **2002**, *124*, 766–767. c) Steinhoff, B. A.; Guzei, I. A.; Stahl, S. S. *J. Am. Chem. Soc.* **2004**, *126*, 11268–11278. d) Rogers, M. M.; Wendlandt, J. E.; Guzei, I. A.; Stahl, S. S. *Org. Lett.* **2006**, *8*, 2257–2260. e) Cai, X.; Majumdar, S.; Fortman, G. C.; Cazin, C. S. J.; Slawin, A. M. Z.; Lhermitte, C.; Prabhakar, R.; Germain, M. E.; Palluccio, T.; Nolan, S. P.; Rybak-Akimova, E. V.; Temprado, M.; Captain, B.; Hoff, C. D. *J. Am. Chem. Soc.* **2011**, *133*, 1290–1293. f) Scheuermann, M. L.; Boyce, D. W.; Grice, K. A.; Kaminsky, W.; Stoll, S.; Tolman, W. B.; Swang, O.; Goldberg, K. I. *Angew. Chem. Int. Ed.* **2014**, *53*, 6492–6495.

[Pd(0)L_n] which can react with oxygen to give a peroxo derivative (mechanism A).²⁶ The elucidation of the mechanism that operates in the oxidation of Pd(0) species is difficult and, in some systems, both pathways are plausible.²⁷

Waymouth *et al.* have reported how peroxopalladium(II) species bearing *N,N'*-chelating ligands can react with reduced palladium species to give dinuclear complexes “Pd₂(μ-OH)₂²⁺”, or with Pd(II) species to afford trinuclear complexes with a [(Pd₃L_nO₂)]²⁺ core.²⁸ Therefore the involvement of polynuclear species in the oxidation process is also possible.

1.5 Mechanisms of C-H Activation

C-H bond activation is a necessary step in direct arylation and oxidative cross-coupling reactions of hydrocarbons. However, the C-H activation processes entail significant challenges such as:

Reactivity: C-H bonds possess large bond dissociation energies, in the range of 100-120 Kcal mol⁻¹.²⁹ This along with the low polarity of C-H bonds make them fairly unreactive in comparison to C-X or M-C bonds.

Site-selectivity: performing a good control in site selectivity in molecules that contain multiple C-H bonds with similar electronic environments is troublesome since C-H bonds are ubiquitous in organic compounds. Reactions that afford multiple regioisomers can benefit molecular diversity (compound bank in Medicinal Chemistry, for instance) as long as all the isomers can be separated and obtained as pure compounds. This strategy has been widely employed in late-stage functionalization of C-H bonds (C-H LSF).^{13d} However, the separation of regioisomers is not always easy and to develop regioselective C-H functionalization is an important challenge. In these cases, the use of directing groups (DGs) have become the strategy of choice to allow site-selective

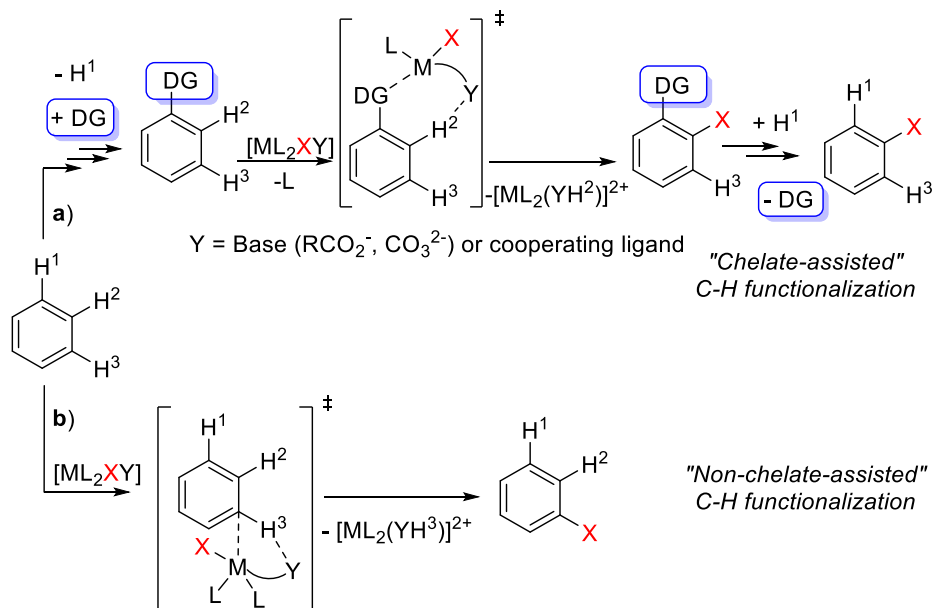
²⁶ a) Popp, B. V.; Stahl, S. S. *J. Am. Chem. Soc.* **2007**, *129*, 4410–4422. b) Konnick, M. M.; Stahl, S. S. *J. Am. Chem. Soc.* **2008**, *130*, 5753–5762. c) Popp, B. V.; Stahl, S. S. *Chem. Eur. J.* **2009**, *15*, 2915–2922.

²⁷ a) Keith, J. M.; Goddard III, W. A. *J. Am. Chem. Soc.* **2009**, *131*, 1416–1425. b) Konnick, M. M.; Decharin, N.; Popp, B. V.; Stahl, S. S. *Chem. Sci.* **2011**, *2*, 326–330.

²⁸ a) Ingram, A. J.; Solis-Ibarra, D.; Zare, R. N.; Waymouth, R. M. *Angew. Chem. Int. Ed.* **2014**, *53*, 5648–5652. b) Ingram, A. J.; Walker, K. L.; Zare, R. N.; Waymouth, R. M. *J. Am. Chem. Soc.* **2015**, *137*, 13632–13646.

²⁹ Luo, Y. R. *Comprehensive Handbook of Chemical Bond Energies*, CRC Press, **2007**.

functionalization (Scheme 1.9, **a**).³⁰ Since most of these reactions proceed through cyclometallated chelate complexes as intermediates, the term “chelate-assisted” has been introduced to describe these transformations. The general accepted mechanism initiates by DG coordination to the catalyst and this directs the activation to the aromatic C-H bond in the proximity of the metal. This results in high levels of regioselectivity and also in the increase in the reactivity because the coordination of the arene is easier in a chelate ligand. Beyond these advantages, the use of DGs present certain limitations. For example, the C-H functionalization commonly occurs at the C-H bond *ortho* to the DG (*ortho*-functionalized products) since the formation of 5- or 6-membered chelate complexes are energetically favoured. Furthermore, additional synthetic steps are often required to install and remove the DG from the starting material, thus reducing the step economy of the overall process. A more appealing strategy for C-H functionalization would be to avoid the DGs and at the same time to maintain the selectivity control (“non-chelate-assisted” C-H activation) (Scheme 1.9, **b**).³¹



Scheme 1.9 Comparison between direct C-H functionalization by non-chelate assisted strategy vs. preinstallation of directing group.

³⁰ For a comprehensive revision see: a) Chen, Z.; Wang, B.; Zhang, J.; Yu, W.; Liu, Z.; Zhang, Y. *Org. Chem. Front.* **2015**, 2, 1107–1295. b) Ghosh, K.; Rit, R. K.; Shankar, M.; Mukherjee, K.; Sahoo, A. K. *Chem. Rec.* **2020**, 20, 1017–1042.

³¹ Kuhl, N.; Hopkinson, M. N.; Wencel-Delord, J.; Glorius, F. *Angew. Chem. Int. Ed.* **2012**, 51, 10236–10254.

With the collected data previously published, several accepted general mechanistic pathways for the C-H activation step can be proposed. Although the C(sp^3)-H activation is possible, most of the studies focus on the C-H bond cleavage in arenes (C(sp^2)-H) (Scheme 1.10).³² The most important mechanisms are:

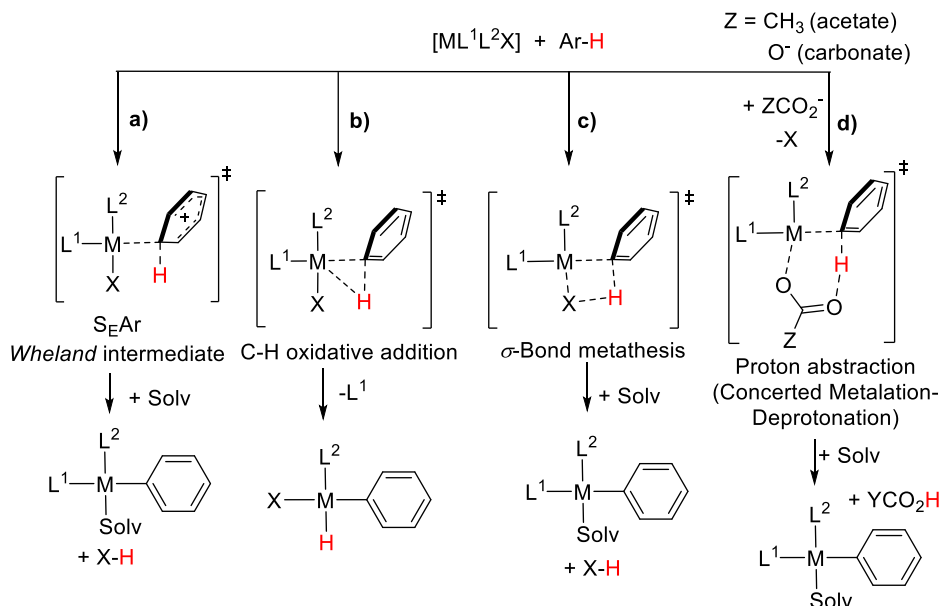
- a) Electrophilic aromatic substitution (S_EAr).³³
- b) C-H oxidative addition. This has been observed for low valent electron-rich metal complexes bearing strong donating ligands. In this mechanism the metal's oxidation state and coordination number increase in two units.³⁴
- c) σ -Bond metathesis. It is most common for "early" transition metals with d^0 electronic configurations where the -H atom from the C-H bond is transferred to an existing M-C bond (X = hydrocarbyl). No change in the oxidation state of the metal occurs in this mechanism.³⁵
- d) Proton abstraction: Inter/intramolecular concerted metalation-deprotonation (CMD).

³² Balcells, D.; Clot, E.; Eisenstein, O. *Chem. Rev.* **2010**, *110*, 749–823.

³³ a) Fujiwara, Y.; Moritani, I.; Danno, S.; Asano, R.; Teranishi, S. *J. Am. Chem. Soc.* **1969**, *91*, 7166–7169. b) Ryabov, A. D.; Sakodinskaya, I. K.; Yatsimirsky, A. K. *J. Chem. Soc., Dalton Trans.* **1985**, 2629–1638. c) Yokoyama, Y.; Matsumoto, T.; Murakami, Y. *J. Org. Chem.* **1995**, *60*, 1486–1487. d) Jia, C.; Piao, D.; Oyamada, J.; Lu, W.; Kitamura, T.; Fujiwara, Y. *Science* **2000**, *287*, 1992–1995. e) Lane, B. S.; Brown, M. A.; Sames, D. *J. Am. Chem. Soc.* **2005**, *127*, 8050–8057. f) Lebrasseur, N.; Larrosa, I. *J. Am. Chem. Soc.* **2008**, *130*, 2926–2927.

³⁴ Canty, A. J.; van Koten, G. *Acc. Chem. Res.* **1995**, *28*, 406–413.

³⁵ a) Watson, P. L. *J. Am. Chem. Soc.* **1983**, *105*, 6491–6493. b) Thompson, M. E.; Baxter, S. M.; Bulls, A. R.; Burger, B. J.; Nolan, M. C.; Santarsiero, B. D.; Schaefer, W. P.; Bercaw, J. E. *J. Am. Chem. Soc.* **1987**, *109*, 203–219. c) Lin, Z. *Coord. Chem. Rev.* **2007**, *251*, 2280–2291.



Scheme 1.10 Mechanistic proposal for the C(*sp*²)-H cleavage in transition metal complexes.

It is worth mentioning that in many cases, the assignment of the reaction mechanism is not trivial. Although none of these four types of mechanism can be discarded for Pd-mediated C-H bond activation, the most commonly operating are the electrophilic aromatic substitution and, specially, the concerted metalation-deprotonation (CMD). The latter has been widely proposed and found to be the most favourable for C-H bonds of low C-H bond pK_a and less steric hindrance in most cases.

The CMD mechanism relies on the basic carboxylate/carbonate ligand coordinated to the metal which serves as an internal base to deprotonate the C-H bond during the interaction of the metal with the π -system of the arene (Scheme 1.10, **d**)).

The earliest proposal of a CMD mechanism is probably that reported by Winstein and Traylor in 1955 for the protodemallation of diphenylmercury by acetic acid.³⁶ But, it was in 1985 when, in the course of a detailed mechanistic study on the *ortho*-palladation of *N,N*-dimethylbenzylamine, Ryabov and co-workers^{33b,37} postulated the formation of a “highly ordered and compact transition state”, supported by a large negative activation entropy in which the proton is abstracted by an acetate ligand (Figure 1.1).

³⁶ Winstein, S.; Traylor, T. G. *J. Am. Chem. Soc.* **1955**, *77*, 3747–3752.

³⁷ a) Kurzev, S. A.; Kazankov, G. M.; Ryabov, A. D. *Inorganica Chim. Acta* **2002**, *340*, 192–196.

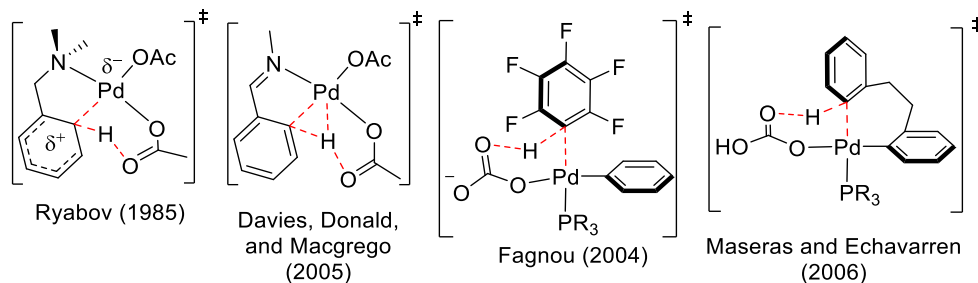


Figure 1.1 Conceptually concerted metalation-deprotonation (CMD) proposals for Pd(II) systems.

In 2005, Davies, Donald and Macgregor performed a computational study based on Ryabov's system and mechanistic work.³⁸ They found that the most favourable reaction pathway proceeds through an agostic C-H complex rather than a *Wheland* intermediate. In the transition state, the C-H bond is polarized, making the hydrogen more acidic and an acetate or carboxylate ligand assists the cleavage *via* a six-membered cyclic transition state.³⁹ Some experimental and computational work in the formation of biaryls by C-H activation through a CMD mechanism were performed by the groups of Maseras, Echavarren⁴⁰ and Fagnou.⁴¹ In these works, they observe that the C-H bond functionalization was not influenced by the electronic nature of the arene whereas in the case of a $S_{E}Ar$ mechanism it should be highly favoured for electron-rich arenes, which rules out this mechanism. Also, large values for the KIEs (3.5-6.7) were obtained. These results are in line with a CMD mechanism.

When investigating the CMD mechanism two pathways can be considered:

The inner-sphere mechanism (intramolecular) is characterized by the presence of a base coordinated to palladium which is responsible for the proton abstraction. This base could be a halide or carbonate/carboxylate anion.^{41b}

In the outer-sphere mechanism (intermolecular) the proton abstraction is performed by an external base which does not coordinate to the palladium.⁴²

³⁸ Davies, D. L.; Donald, S. M. A.; Macgregor, S. A. *J. Am. Chem. Soc.* **2005**, *127*, 13754–13755.

³⁹ a) Ackermann, L. *Chem. Rev.* **2011**, *111*, 1315–1345. b) Davies, D. L.; Macgregor, S. A.; McMullin, C. L. *Chem. Rev.* **2017**, *117*, 8649–8709.

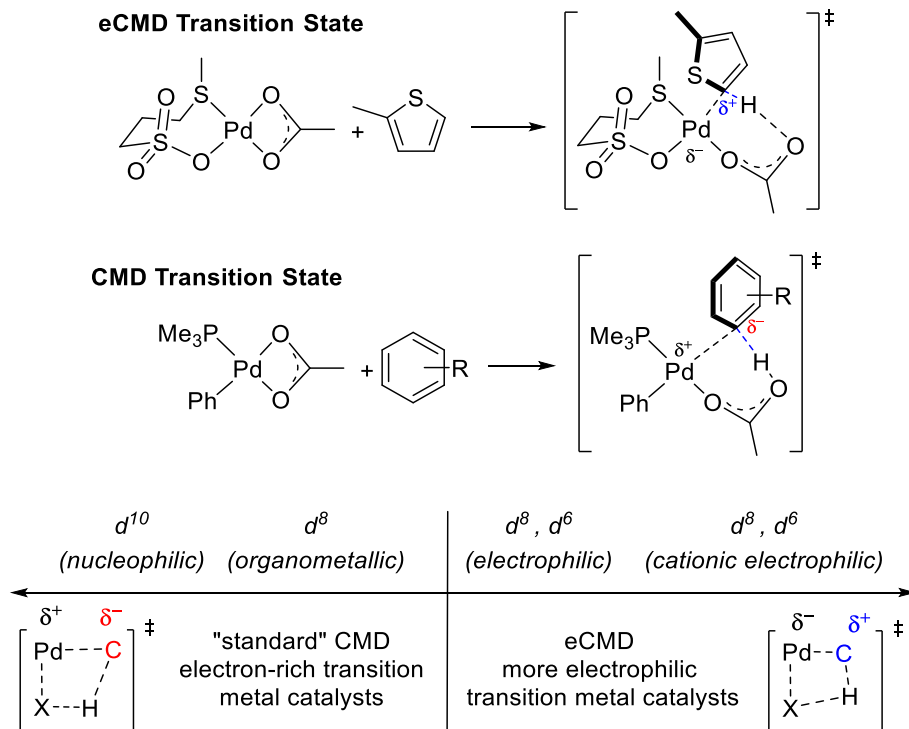
⁴⁰ a) García-Cuadrado, D.; Braga, A. A. C.; Maseras, F.; Echavarren, A. M. *J. Am. Chem. Soc.* **2006**, *128*, 1066–1067. b) García-Cuadrado, D.; de Mendoza, P.; Braga, A. A. C.; Maseras, F.; Echavarren, A. M. *J. Am. Chem. Soc.* **2007**, *129*, 6880–6886.

⁴¹ a) Campeau, L.-C.; Parisien, M.; Leblanc, M.; Fagnou, K. *J. Am. Chem. Soc.* **2004**, *126*, 9186–9187. b) Lafrance, M.; Rowley, C. N.; Woo, T. K.; Fagnou, K. *J. Am. Chem. Soc.* **2006**, *128*, 8754–8756. c) Stuart, D. R.; Fagnou, K. *Science*. **2007**, *316*, 1172–1175. d) Gorelsky, S. I.; Lapointe, D.; Fagnou, K. *J. Am. Chem. Soc.* **2008**, *130*, 10848–10849.

⁴² a) Pascual, S.; de Mendoza, P.; Braga, A. A. C.; Maseras, F.; Echavarren, A. M. *Tetrahedron* **2008**, *64*, 6021–6029. b) Sun, H.-Y.; Gorelsky, S. I.; Stuart, D. R.; Campeau, L.-C.; Fagnou, K. *J. Org. Chem.* **2010**, *75*, 8180–8189.

Recently, different authors have considered that there is not only a “standard” concerted metalation-deprotonation (CMD) model for the metal-catalyzed C-H activation reactions and the situation can be more complex. In some cases, the C-H cleavage transition state is not fully synchronized, *i.e.* the Pd-C bond formation exceeds the C-H bond breaking, which results in a positive charge build-up on the arene. Since this feature (partial or complete Pd-C bond formation prior to the C-H bond cleavage) is characteristic of the S_EAr -type mechanism, the term electrophilic CMD (*e*CMD) has been introduced by Carrow to reflect this situation.⁴³ In this C-H activation mechanism the kinetic barrier for activation of electron-rich heteroarenes (such as thiophene or pyrrole derivatives) with electrophilic complexes is lower and also changes the site selectivity of the C-H bond functionalization, favouring more π -basic sites. These features differ from the standard CMD model which typically operates on C-H bonds with lower pK_a and less steric hindrance and electron-rich organometallic species (typically bearing a Pd-aryl bond). In this regard, the existence of a mechanistic continuum for C-H cleavage has been postulated, providing a more accurate description in the C-H bond activation concerted pathways (Scheme 1.11).

⁴³ a) Wang, L.; Carrow, B. P. *ACS Catal.* **2019**, *9*, 6821–6836. b) Carrow, B. P.; Sampson, J.; Wang, L. *Isr. J. Chem.* **2020**, *60*, 230–258. c) Evans, R.; Sampson, J.; Wang, L.; Lückemeier, L.; Carrow, B. P. *Chem. Commun.* **2021**, *57*, 9076–9079.



Scheme 1.11 Mechanistic continuum proposals for C-H cleavage mediated by transition metals.

1.6 Cooperating ligands in the C-H cleavage

One of the major challenges in the C-H activation field is the lack of reactivity of the robust C-H bonds. This generally entails the use of high temperatures (kinetic factors) and large amounts of the reactant arene (usually employed as a solvent or co-solvent). To efficiently promote these reactions, great efforts have been made in the design of cooperating ligands which present a suitable structure to actively assist in the C-H activation, accelerating the reactions by lowering the energetic barriers. The concept of metal-ligand cooperation (MLC) has become important in homogeneous catalysis by transition metal complexes in the last 15 years. In this context, the ligands do not play a traditional spectator role in the chemical transformations during catalysis. Milstein and Khusnutdinova discussed this topic in a review on MLC in which they propose that a cooperating ligand has to satisfy the following criteria:⁴⁴

⁴⁴ Khusnutdinova, J. R.; Milstein, D. *Angew. Chem. Int. Ed.* **2015**, *54*, 12236–12273.

- 1) Both the metal and the ligand participate in the bond cleavage or bond formation steps.
- 2) Both the metal and the ligand are chemically modified during bond activation.
- 3) The coordination mode of the cooperative ligand undergoes significant changes in the 1st coordination sphere as a result of bond activation.

Some of the most prominent cooperating ligands in the context of C-H activation by palladium complexes and the first to be studied were mono-*N*-protected amino acids (MPAAs) introduced by Yu *et al.* (Figure 1.2, **a**).⁴⁵ These cooperating ligands have demonstrated to be efficient in several catalytic transformations that activate C(*sp*²)-H and C(*sp*³)-H bonds. Recently, the group of Yu and Maiti reported the synergistic behavior of dual ligands systems (electron-deficient 2-pyridone in combination with pyridine-based ligands or mono-*N*-protected amino acids).⁴⁶

The MPAA effect in the catalytic reactions and the mechanism in which the amino acid assists the C-H bond cleavage have been interrogated by computational methods.⁴⁷ Just a few experimental examples have been reported to reveal how MPAAs coordinate to [Pd(OAc)₂] and only by mass spectrometry. In these publications Yu's group demonstrated the formation of monomeric [Pd(MPAA)(solv)₂] (solv = NCMe or MeOH) species, which are considered responsible of the reactivity and the selectivity observed in the C-H activation reactions.⁴⁸ With these experimental data along with all computational results collected, it has been proposed that MPAAs coordinate to the palladium center as dianionic ligands (X₂-type) by the deprotonated carboxylate and the deprotonated amidate groups. The oxygen in the amidate group (commonly *N*-acyl group, Figure 1.2, **a**) is the one that participates in the C-H bond cleavage during the transition state. Also, chelate S,O-ligands, typically thioethercarboxylic acid, have been employed in C-H activation reactions.⁴⁹

⁴⁵ Shi, B.-F.; Mangel, N.; Zhang, Y.-H.; Yu, J.-Q. *Angew. Chem. Int. Ed.* **2008**, *47*, 4882–4886.

⁴⁶ a) Liu, L.-Y.; Qiao, J. X.; Yeung, K.-S.; Ewing, W. R.; Yu, J.-Q. *Angew. Chem. Int. Ed.* **2020**, *59*, 13831–13835. b) Park, H. S.; Fan, Z.; Zhu, R.-Y.; Yu, J.-Q. *Angew. Chem. Int. Ed.* **2020**, *59*, 12853–12859. c) Sinha, S. K.; Panja, S.; Grover, J.; Hazra, P. S.; Pandit, S.; Bairagi, Y.; Zhang, X.; Maiti, D. *J. Am. Chem. Soc.* **2022**, *144*, 12032–12042.

⁴⁷ a) Yang, Y.-F.; Hong, X.; Yu, J.-Q.; Houk, K. N. *Acc. Chem. Res.* **2017**, *50*, 2853–2860. b) Shao, Q.; Wu, K.; Zhuang, Z.; Qian, S.; Yu, J.-Q. *Acc. Chem. Res.* **2020**, *53*, 833–851.

⁴⁸ Cheng, G.-J.; Yang, Y.-F.; Liu, P.; Chen, P.; Sun, T.-Y.; Li, G.; Zhang, X.; Houk, K. N.; Yu, J.-Q.; Wu, Y.-D. *J. Am. Chem. Soc.* **2014**, *136*, 894–897.

⁴⁹ a) Naksomboon, K.; Valderas, C.; Gómez-Martínez, M.; Álvarez-Casao, Y.; Fernández-Ibáñez, M. Á. *ACS Catal.* **2017**, *7*, 6342–6346. b) Álvarez-Casao, Y.; Fernández-Ibáñez, M. Á. *European J. Org. Chem.* **2019**, 2019, 1842–1845. c) Sukowski, V.; Jia, W.-L.; van Diest, R.; van Borselen, M.; Fernández-Ibáñez, M. Á. *European J. Org. Chem.* **2021**, 2021, 4132–4135.

Other important cooperating ligand types are represented by the monodentate pyridone-based ligands derived from 2-hydroxypyridine (or 2-pyridone) (Figure 1.2, b).⁵⁰ Within this family of cooperating ligands, chelate-bipyridone ligands whose two coordination sites on the metal afford a more robust coordination mode in the C-H activation step have been described. In this context, our group has used the cooperating bipyridone ligands [2,2'-bipyridin]-6(1*H*)-one (bipy-6-OH) and 1,10-phenanthrolin-2(1*H*)-one (phen-2-OH) and also well-defined Pd(II)-complexes bearing these ligands as catalysts in C-H activation reactions. The key feature of the abovementioned ligands is a basic functional group able to act as a base in the proton abstraction by an intramolecular CMD mechanism (Figure 1.2, c). Also, the chelate sulfoxide-2-hydroxypyridine ligand has demonstrated to afford successful outcomes.⁵¹

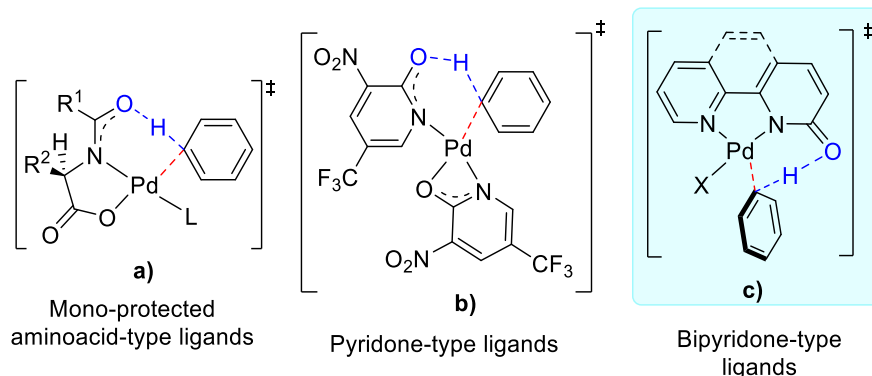


Figure 1.2 Representative examples of transition states with MPAA (a), pyridone (b) and bipyridone (c) ligands.

The precoordination of an external base (acetate or carbonate) to the metal center is not required because this role is played by the bipyridone ligand coordinated to the palladium. This is an important advantage because no predissociation of a ligand is needed to incorporate the external base and, at the same time, by this strategy we can minimize the ligands that compete with the incoming arene for coordination. The bipy-6-OH ligand has demonstrated an accelerating effect in the direct arylation of simple arenes with arylhalides due to its cooperating behaviour in the catalysis. The

⁵⁰ Wang, P.; Verma, P.; Xia, G.; Shi, J.; Qiao, J. X.; Tao, S.; Cheng, P. T. W.; Poss, M. A.; Farmer, M. E.; Yeung, K. S.; Yu, J.-Q. *Nature*, **2017**, *551*, 489–493.

⁵¹ Wang, Y.-J.; Yuan, C.-H.; Chu, D.-Z.; Jiao, L. *Chem. Sci.* **2020**, *11*, 11042–11054.

cooperating role of the bipy-6-OH ligand in C-H activation reactions was demonstrated experimentally for the first time by our group (Figure 1.3).⁵²

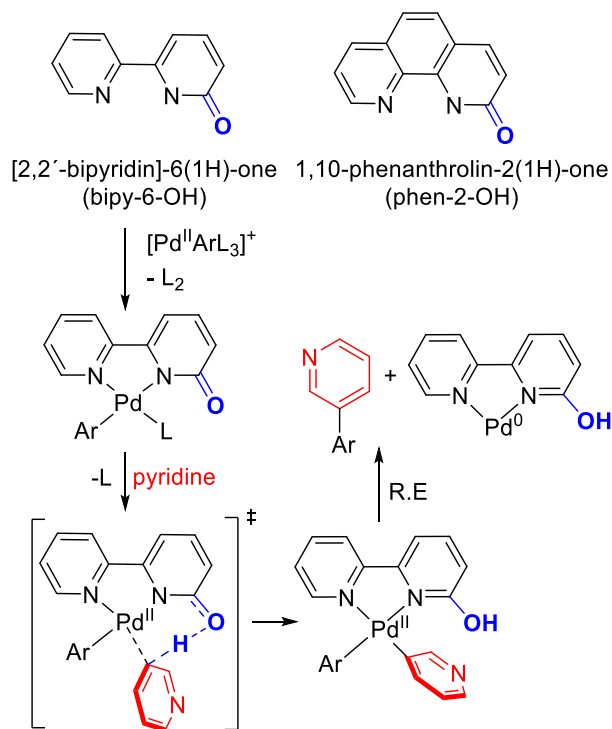


Figure 1.3 Bipy-6-O-assisted cleavage of the *meta* C–H bond of pyridine.

Bipy-6-OH and phen-2-OH ligands had been previously used in proton-transfer reactions and also in coordination chemistry for the study of photophysical properties. Different transition metals were studied in combination with these ligands, such as Ir,⁵³

⁵² a) Salamanca, V.; Toledo, A.; Albéniz, A. C. *J. Am. Chem. Soc.* **2018**, *140*, 17851–17856.

b) Salamanca, V.; Albéniz, A. C. *Org. Chem. Front.* **2021**, *8*, 1941–1951.

⁵³ a) Kawahara, R.; Fujita, K.; Yamaguchi, R. *J. Am. Chem. Soc.* **2012**, *134*, 3643–3646. b) Wang, W.-H.; Muckerman, J. T.; Fujita, E.; Himeda, Y. *ACS Catal.* **2013**, *3*, 856–860. c) Zheng, G.; Sakaki, S.; Fujita, K.; Sano, H.; Yamaguchi, R. *ACS Catal.* **2014**, *4*, 1010–1020. d) Fujita, K.; Tanaka, Y.; Kobayashi, M.; Yamaguchi, R. *J. Am. Chem. Soc.* **2014**, *136*, 4829–4832. e) Wang, R.; Ma, J.; Li, F. *J. Org. Chem.* **2015**, *80*, 10769–10776. f) Xu, Z.; Yan, P.; Li, H.; Liu, K.; Liu, X.; Jia, S.; Zhang, Z. C. *ACS Catal.* **2016**, *6*, 3784–3788. g) Suna, Y.; Himeda, Y.; Fujita, E.; Muckerman, J. T.; Ertem, M. Z. *ChemSusChem*. **2017**, *10*, 4535–4543. h) Siek, S.; Burks, D. B.; Gerlach, D. L.; Liang, G.; Tesh, J. M.; Thompson, C. R.; Qu, F.; Shankwitz, J. E.; Vasquez, R. M.; Chambers, N.; Szulczewski, G. J.; Grotjahn, D. B.; Webster, C. E.; Papish, E. T. *Organometallics* **2017**, *36*, 1091–1106.

Ru,⁵⁴ or Mn⁵⁵ among others.⁵⁶ However, the use of bipy-6-OH as a cooperating ligand in Pd-catalyzed cross-coupling reaction with C-H activation steps was unprecedented when we started our work. Only one example of the use of phen-2-OH in the oxidative Heck reaction was reported. The authors hypothesised that the accelerating effect observed in the reaction was a result of the easy dissociation of an acetate in the Pd-complex bearing the monoanionic phen-2-O ligand when compared to that with the neutral 1,10-phen ligand. In this way, the coordination of the incoming arene is easier. No cooperating role in the C-H cleavage step was attributed to phen-2-OH.⁵⁷

In the last two years, the use of chelating bipyridone ligands (bipy-6-OH and derivatives) in palladium catalyzed C-H functionalization has been expanded.⁵⁸

The following chapters included in *Part I* of this dissertation collect the study and application of bipyridone cooperating ligands that assist in the C-H cleavage by a CMD mechanism. The work described in *Chapter 2* deals with the oxidative Heck reaction of simple arenes (fluorinated and non-fluorinated) to obtain alkenylated arenes via C-C bond formation employing oxygen as the sole oxidant. A detailed study on the coordination chemistry of ligands bipy-6-OH and phen-2-OH with Pd(II) precursors is presented in *Chapter 3*, with the aim of learning about the nature of the precatalytic palladium species formed and their impact in the direct arylation catalytic reaction.

⁵⁴ a) Nieto, L.; Livings, M. S.; Sacci, J. B., III; Reuther, L. E.; Zeller, M.; Papish, E. T. *Organometallics* **2011**, *30*, 6339–6342. b) Moore, C. M.; Szymczak, N. K. *Chem. Commun.* **2013**, *49*, 400–402. c) Roy, B. C.; Chakrabarti, K.; Shee, S.; Paul, S.; Kundu, S. *Chem. Eur. J.* **2016**, *22*, 18147–18155. d) Yu, F.; Shen, C.; Zheng, T.; Chu, W.-K.; Xiang, J.; Luo, Y.; Ko, C.-C.; Guo, Z.-Q.; Lau, T.-C. *Eur. J. Inorg. Chem.* **2016**, *2016*, 3641–3648. e) Shen, C.; Yu, F.; Chu, W.-K.; Xiang, J.; Tan, P.; Luo, Y.; Feng, H.; Guo, Z.-Q.; Leung, C.-F.; Lau, T.-C. *RSC Adv.* **2016**, *6*, 87389–87399.

⁵⁵ Zhang, C.; Hu, B.; Chen, D.; Xia, H. *Organometallics* **2019**, *38*, 3218–3226.

⁵⁶ a) Tomás-Mendivil, E.; Díez, J.; Cadierno, V. *Catal. Sci. Technol.* **2011**, *1*, 1605–1615. b) Hu, L.-L.; Shen, C.; Chu, W.-K.; Xiang, J.; Yu, F.; Xiang, G.; Nie, Y.; Kwok, C.-L.; Leung, C.-F.; Ko, C.-C. *Polyhedron* **2017**, *127*, 203–211.

⁵⁷ a) Ying, C.-H.; Yan, S.-B.; Duan, W.-L. *Org. Lett.* **2014**, *16*, 500–503. b) Ying, C.-H.; Duan, W.-L. *Org. Chem. Front.* **2014**, *1*, 546–550. c) Zhen Li, Z.; Duan, W.-L. *Angew. Chem. Int. Ed.* **2018**, *57*, 16041–16045.

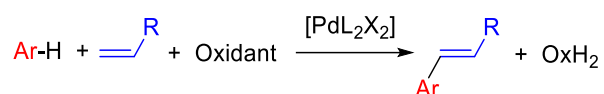
⁵⁸ a) Wang, Z.; Hu, L.; Chekshin, N.; Zhuang, Z.; Qian, S.; Qiao, J. X.; Yu, J.-Q. *Science*. **2021**, *374*, 1281–1285. b) Zhen, L.; Zhen, W.; Nikita, C.; Qian, S.; Qiao, J. X.; Cheng, P. T.; Yeung, K.-S.; Ewing, W. R.; Yu, J.-Q. *Science*. **2021**, *372*, 1452–1457. c) Chan, H. S. S.; Yang, J.-M.; Yu, J.-Q. *Science*. **2022**, *376*, 1481–1487. d) Hu, L.; Meng, G.; Yu, J.-Q. *J. Am. Chem. Soc.* **2022**, *144*, 20550–20553.

Chapter 2

2. Oxidative Heck Reaction of Fluorobenzenes and Other Arenes: When Does the C-H Activation Need Help?

2.1 INTRODUCTION

The Fujiwara-Moritani or oxidative Heck reaction of arenes has gained great importance in the cross-coupling toolbox of the synthetic chemist (Equation 2.1).¹⁸



Equation 2.1

Mostly catalyzed by palladium complexes, it has been applied in an intra- and intermolecular fashion for the alkenylation of arenes, often bearing directing groups (chelate-assisted functionalization), and these advances have been collected in several

reviews.⁵⁹ The use of arenes as reactants instead of the aryl halides in the conventional Heck reaction is a clear advantage as far as sustainability is concerned. However, as mentioned in *Chapter 1*, the reaction needs a stoichiometric amount of an oxidant and, depending on its identity, this may erode the atom economy of the reaction and introduce toxicity issues. This is the case of the common copper derivatives, silver salts,⁶⁰ benzoquinone or peroxides.⁵¹ Aerobic oxidative Heck reactions lack these problems and oxygen as the sole oxidant is the cleanest and most attractive choice. A compromise approach that uses oxygen and a catalytic amount of the above-mentioned oxidants or other redox mediators such as ferrocenium salts or iron phthalocyanine derivatives has also been applied.⁶¹

Oxygen as oxidant has been used in chelate-assisted oxidative Heck reactions and also in the alkenylation of arenes with no directing groups (simple arenes). Some examples are shown in Scheme 2.1, **a**) and **b**).^{62,63} The latter are more difficult to activate since they lack a coordinating group that provides the approach of the arene to the metal in a chelating fashion which facilitates the subsequent C-H activation. However, a variety of conditions have been developed for fluoroarenes,⁶⁴ heterocycles,⁶⁵ and other simple arenes,^{57a,61,66} which are often very specific for the particular reactant combination (Scheme 2.1, **b**), **c**) and **d**)).

⁵⁹ a) Le Bras, J.; Muzart, J. *Chem. Rev.* **2011**, *111*, 1170–1214. b) Yeung, C. D.; Dong, V. M. *Chem. Rev.* **2011**, *111*, 1215–1292. c) Odell, L. R.; Sävmarker, J.; Lindh, J.; Nilsson, P.; Larhed, M. *Addition Reactions with Formation of Carbon-Carbon Bonds: (V) The Oxidative Heck Reaction*, Elsevier Ltd., **2014**. d) Kancherla, S.; Jørgensen, K. M.; Fernández-Ibáñez, M. A. *Synthesis*, **2019**, *51*, 643–663. e) Gunnoe, T. B.; Schinski, W. L.; Jia, X.; Zhu, W. *ACS Catal.* **2020**, *10*, 14080–14092. f) Ali, W.; Prakash, G.; Maiti, D. *Chem. Sci.* **2021**, *12*, 2735–2759. g) Zhu, W.; Gunnoe, T. B. *J. Am. Chem. Soc.* **2021**, *143*, 6746–6766.

⁶⁰ Mondal, A.; van Gemmeren, M. *Angew. Chem. Int. Ed.* **2022**, e202210825.

⁶¹ Babu, B. P.; Meng, X.; Bäckvall, J. E. *Chem. Eur. J.* **2013**, *19*, 4140–4145.

⁶² Zhang, Y.-H.; Shi, B.-F.; Yu, J.-Q. *J. Am. Chem. Soc.* **2009**, *131*, 5072–5074.

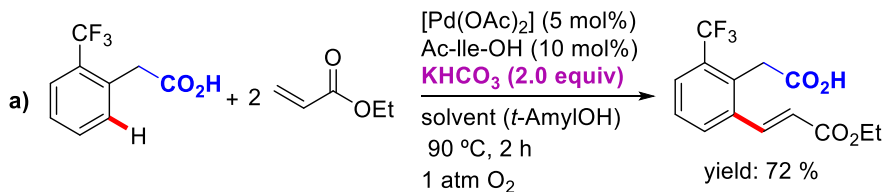
⁶³ a) Engle, K. M.; Wang, D. H.; Yu, J.-Q. *J. Am. Chem. Soc.* **2010**, *132*, 14137–14151. b) Baxter, R. D.; Sale, D.; Engle, K. M.; Yu, J.-Q.; Blackmond, D. G. *J. Am. Chem. Soc.* **2012**, *134*, 4600–4606.

⁶⁴ a) He, C. Y.; Qing, F. L.; Zhang, X. *Tetrahedron Lett.* **2014**, *55*, 2962–2964. b) Huang, Q.; Zhang, X.; Qiu, L.; Wu, J.; Xiao, H.; Zhang, X.; Lin, S. *Adv. Synth. Catal.* **2015**, *357*, 3753–3757

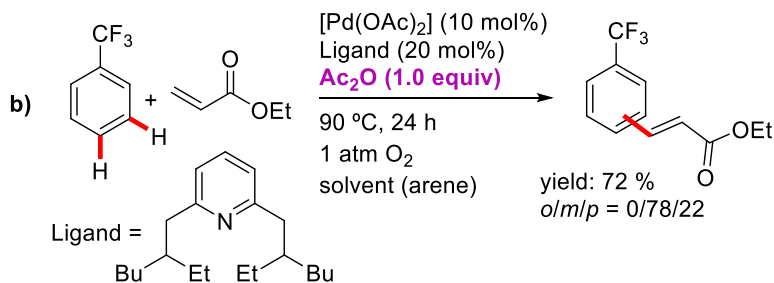
⁶⁵ a) Beck, E. M.; Grimster, N. P.; Hatley, R.; Gaunt, M. J. *J. Am. Chem. Soc.* **2006**, *128*, 2528–2529. b) Ye, M.; Gao, G. L.; Yu, J.-Q. *J. Am. Chem. Soc.* **2011**, *133*, 6964–6967. c) Chen, W. L.; Gao, Y. R.; Mao, S.; Zhang, Y. L.; Wang, Y. F.; Wang, Y. Q. *Org. Lett.* **2012**, *14*, 5920–5923. d) Vasseur, A.; Harakat, D.; Muzart, J.; Le Bras, J. *Adv. Synth. Catal.* **2013**, *355*, 59–67. e) Zhang, X.; Su, L.; Qiu, L.; Fan, Z.; Zhang, X.; Lin, S.; Huang, Q. *Org. Biomol. Chem.* **2017**, *15*, 3499–3506. f) Gorsline, B. J.; Wang, L.; Ren, P.; Carrow, B. P. *J. Am. Chem. Soc.* **2017**, *139*, 9605–9614.

⁶⁶ a) Yokota, T.; Tani, M.; Sakaguchi, S.; Ishii, Y. *J. Am. Chem. Soc.* **2003**, *125*, 1476–1477. b) Dams, M.; De Vos, D. E.; Celen, S.; Jacobs, P. A. *Angew. Chem. Int. Ed.* **2003**, *42*, 3512–3515. c) Cong, X.; Hang, H.; Wu, C.; Zeng, X. *Organometallics* **2013**, *32*, 6565–6575. d) Harada, S.; Yano, H.; Obora, Y. *ChemCatChem* **2013**, *5*, 121–125. e) Gigant, N.; Bäckvall, J. E. *Org. Lett.* **2014**, *16*, 1664–1667. f) Kim, H. T.; Kang, E.; Kim, M.; Joo, J. M. *Org. Lett.* **2021**, *23*, 3657–3662.

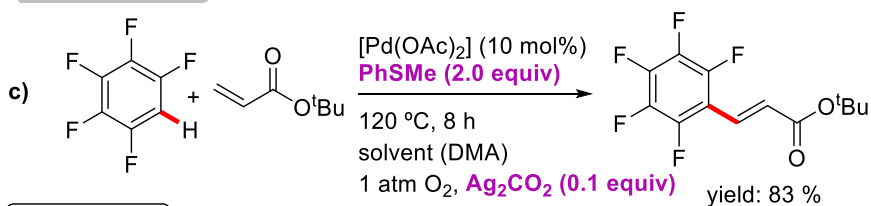
Arenes with DGs



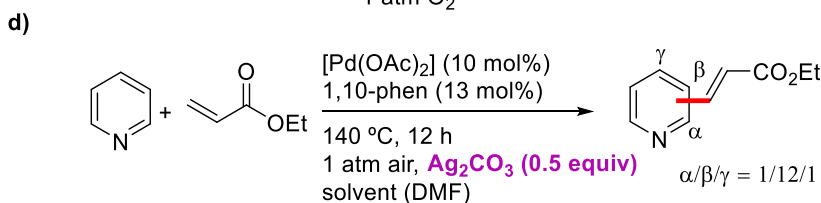
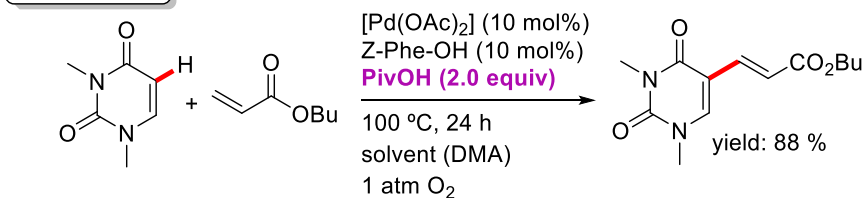
Simple arenes



Polyfluoroarenes

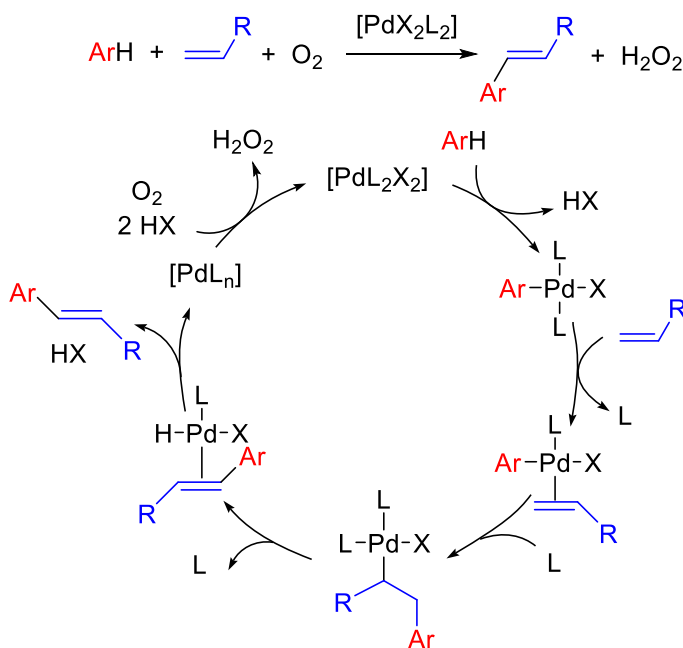


Heterocycles



Scheme 2.1 Examples of aerobic oxidative Heck reactions with different arenes behaviour and reactions condition. **a)** Non-chelate-assisted arenes (ref: 60). **b)** Arenes with directing groups (ref: 61). **c)** Polyfluoroarene with silver salt as co-oxidant (ref: 64a). **d)** Heterocycles with silver salt as co-oxidant or acidic media (ref: 65b and 65e).

In order to further improve these processes and within the framework of the accepted mechanism for this reaction (Scheme 2.2), the attention is generally focused in the two steps which are considered crucial to reach an efficient catalytic aerobic arene alkenylation reaction: The usual energy demanding C-H activation step, and the palladium(0) oxidation step which can compete with metal aggregation and catalyst deactivation. The Pd(0) oxidation by oxygen has been studied, and this step is not usually rate limiting although other factors such as the intrinsic solubility of the gas and mass-transfer problems can play a role in the efficiency of the oxidation and the catalyst performance, as mentioned in *Chapter 1*.²³



Scheme 2.2 Palladium catalysed oxidative Heck reaction of arenes and general mechanism.

As can be gathered from the catalytic cycle in Scheme 2.2 the C-H activation step can benefit from the presence of a base (also the palladium hydride decomposition to Pd(0)), but the oxidation step needs the protonation of the putative η^2 -peroxo palladium complex formed by reaction with oxygen. Therefore, the choice of additives in these reactions is not always straightforward and a delicate balance is required. A wide range of reaction conditions can be found in the literature for the aerobic oxidative Heck reactions, and this can be seen in the selected examples shown in Scheme 2.1 which required completely different reaction conditions to work efficiently (highlighted in purple, Scheme 2.1).

The C-H activation step can be favored by the use of cooperating ligands that act as an intramolecular base in the C-H activation transition state by a concerted metalation-deprotonation (CMD) mechanism. In the context of the oxidative Heck reaction of arenes, acyl *N*-monoprotected amino acids (MPAA), a potential cooperating type of ligands, have been used,^{47b} sometimes in combination with a second ligand,⁶⁷ and they have shown a positive effect in the aerobic olefination of arenes bearing directing groups.^{50,68} Pyridone-type ligands can also assist the C-H cleavage step, and there are a few examples of their use in olefination processes with silver oxidants,⁶⁹ and with stoichiometric Cu(II) salts or a O₂/Cu(II) salt mixture.^{51,57} Upon lowering the activation energy of the C-H cleavage step in the presence of a cooperating ligand, other steps in the catalytic cycle can become turnover limiting and this has been shown recently in the change in regioselectivity observed in the Cu(II)/O₂ mediated alkenylation of indole derivatives.⁵¹

This chapter describes the efficient oxidative Heck reaction with oxygen at atmospheric pressure as the sole oxidant of a number of fluoroarenes and other arenes with different substituents using the cooperating ligand [2,2'-bipyridin]-6(1*H*)-one (bipy-6-OH). We have previously employed this ligand for the direct arylation of arenes and shown its role in assisting the C-H activation step.⁵² Now, a set of reaction conditions have been developed for the oxidative Heck reaction that use minimum amount of additives (acids or bases) and can be applied to a variety of simple arenes. The nature of the arene influences the step that controls the alkenylation reaction and we have studied when the cooperation of the ligand is crucial and those cases where the C-H cleavage is fast enough, so the assistance of the ligand in the C-H activation is not required.

⁶⁷ a) Chen, H.; Wedi, P.; Meyer, T.; Tavakoli, G.; van Gemmeren, M. *Angew. Chem. Int. Ed.* **2018**, *57*, 2497–2501. b) Yin, B.; Fu, M.; Wang, L.; Liu, J.; Zhu, Q. *Chem. Commun.* **2020**, *56*, 3293–3296. c) Wedi, P.; Farizyan, M.; Bergander, K.; Mück-Lichtenfeld, C.; van Gemmeren, M. *Angew. Chem. Int. Ed.* **2021**, *60*, 15641–15649.

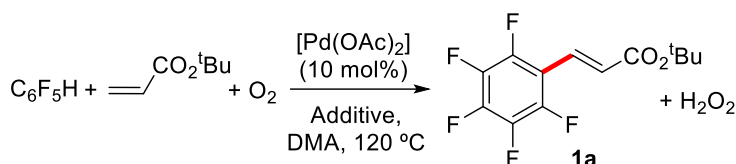
⁶⁸ a) Wang, D-H.; Engle, K. M.; Shi, B-F.; Yu, J-Q. *Science*, **2010**, *327*, 315–319. b) Xiao, K. J.; Chu, L.; Yu, J-Q. *Angew. Chem. Int. Ed.* **2016**, *55*, 2856–2860.

⁶⁹ a) Chen, X. Y.; Wu, Y.; Zhou, J.; Wang, P.; Yu, J-Q. *Org. Lett.* **2019**, *21*, 1426–1429. b) Fan, Z.; Bay, K. L.; Chen, X.; Zhuang, Z.; Park, H. S.; Yeung, K.; Houk, K. N.; Yu, J-Q. *Angew. Chem. Int. Ed.* **2020**, *59*, 4770–4777.

2.2 RESULTS AND DISCUSSION

2.2.1 Oxidative Heck reactions of fluorinated and non-fluorinated arenes

The reaction of pentafluorobenzene with *t*-butyl acrylate was first tested and used to set up suitable reaction conditions (Equation 2.2).



Equation 2.2

The reaction was carried out using a moderate excess of the arene (C₆F₅H:olefin = 2.5:1) in DMA as solvent. Acids and/or bases, sometimes in excess, are commonly used as additives in these reactions, and which one to choose is often difficult to anticipate. They are not reactants in the aerobic Heck reaction, as shown in Scheme 2.2 and Equation 2.2, although several proton transfer processes occur in the reaction that can be favored by these additives. We found that just a catalytic amount of base (10 mol%) is needed to ensure good yields, whereas an excess of base or an acid is detrimental (entries 1-6, Table 2.1). This has also been observed in other aerobic Pd-catalyzed oxidative couplings.⁷⁰ Sodium molybdate (pK_a(HMoO₄⁻) = 3.5–4.5)⁷¹ gives excellent results and works better than other bases (entries 4-6, Table 2.1). We have no evidence that Na₂MoO₄ is playing a role as redox mediator in the reaction and it may just be acting as a weak base. We run several tests that support that the presence of such a high-valent metal species is not influencing the oxidation process. Mo(VI) is not acting as a terminal oxidant (entry 10, Table 2.1) and oxygen is necessary (*cf.* entries 6, 8 (air) and 9 (under N₂), Table 2.1).

⁷⁰ A. Toledo, I. Funes-Ardoiz, F. Maseras, A. C. Albéniz, *ACS Catal.* **2018**, *8*, 7495–7506.

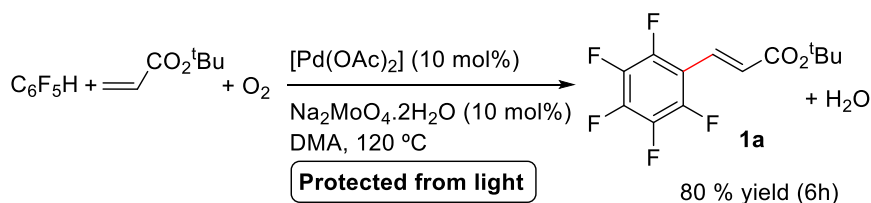
⁷¹ a) Cruywagen, J. J.; Rohwer, E. F. C. H. *Inorg. Chem.* **1975**, *14*, 3136–3137. b) Liu, X.; Cheng, J.; Sprik, M.; Lu, X. *J. Phys. Chem. Lett.* **2013**, *4*, 2926–2930.

Table 2.1 Oxidative Heck reaction of C₆F₅H according to Equation 2.2.^a

Entry	[Pd]	Additive (equiv)	1a , crude yield, % ^b , 6 h ^b
1	[Pd(OAc) ₂]	-	0
2	[Pd(OAc) ₂]	AcOH (1.5)	15
3	[Pd(OAc) ₂]	Cs ₂ CO ₃ (1.5)	0
4	[Pd(OAc) ₂]	Cs ₂ CO ₃ (0.1)	76
5	[Pd(OAc) ₂]	NaOAc (0.1)	61
6	[Pd(OAc) ₂]	Na ₂ MoO ₄ ·2H ₂ O (0.1)	99 (88 ^{isol})
7	-	Na ₂ MoO ₄ ·2H ₂ O (0.1)	0
8 ^c	[Pd(OAc) ₂]	Na ₂ MoO ₄ ·2H ₂ O (0.1)	67
9 ^d	[Pd(OAc) ₂]	Na ₂ MoO ₄ ·2H ₂ O (0.1)	5
10 ^d	[Pd(OAc) ₂]	Na ₂ MoO ₄ ·2H ₂ O (1)	0
11 ^d	[Pd(OAc) ₂]	Na ₂ MoO ₄ ·2H ₂ O (0.1) + H ₂ O ₂ (1)	7
12 ^e	[Pd(OAc) ₂]	Na ₂ MoO ₄ ·2H ₂ O (0.1)	81
13 ^f	[Pd(OAc) ₂]	Na ₂ MoO ₄ ·2H ₂ O (0.1)	27 ^g
14	[Pd(OAc) ₂] ^h	Na ₂ MoO ₄ ·2H ₂ O (0.1)	86
15	[PdCl ₂ (NCMe) ₂]	Na ₂ MoO ₄ ·2H ₂ O (0.1)	30
16	[PdCl ₂ (NCMe) ₂]	Na ₂ MoO ₄ ·2H ₂ O (0.3)	51
17	[PdCl ₂ (NCMe) ₂]	Na ₂ MoO ₄ ·2H ₂ O (0.1) + NaOAc 3H ₂ O (0.2)	68
18 ⁱ	[Pd(OAc) ₂] ^g	Na ₂ MoO ₄ ·2H ₂ O (0.1)	68 (62 ^{isol})

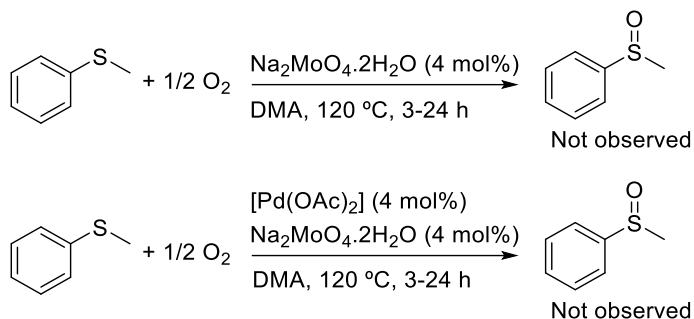
^a Reaction conditions: [Pd(OAc)₂] (0.034 mmol, 10 mol %), C₆F₅H (0.853 mmol), *t*-butyl acrylate (0.341 mmol), DMA (3 mL), 120 °C, O₂ (1 atm), unless otherwise noted. ^b Crude yields were determined by ¹H NMR using dodecane as internal standard. ^c Air instead of O₂. ^d Under N₂. ^e 90 °C. ^f 60 °C. ^g 88 % yield in 48 h. ^h 5 mol%. ⁱ Styrene as olefin and C₆F₅CH=CHPh (**1b**) as product.

It is known that singlet oxygen can be generated by photochemical processes.⁷² Equation 2.3 shows that the catalytic reaction is efficient when carried out protected from light, indicating that the photochemical generation of a more reactive singlet oxygen in the presence of molybdate can be ruled out.

**Equation 2.3**

⁷² a) Adam, W. A.; Kazakov, D. V.; Kazakov, V. P. *Chem. Rev.* **2005**, *105*, 3371–3387.
 b) Montagnon, T.; Tofi, M.; Vassilikogiannakis, G. *Acc. Chem. Res.* **2008**, *41*, 1001–1011.
 c) Ghogare, A. A.; Greer, A. *Chem. Rev.* **2016**, *116*, 9994–10034.

In addition, thioether oxidation to a sulfoxide does not work in the reaction conditions used here. The oxidation of a sulfide to sulfoxide, was carried out to check the possible mediation of sodium molybdate in the generation of singlet oxygen or other oxygen reactive species (Scheme 2.3).⁷³



Scheme 2.3 Attempted thioanisole oxidation.

The generation of singlet oxygen by decomposition of hydrogen peroxide in the presence of molybdate has been reported,⁷⁴ and this could occur in the reaction course upon generation of H₂O₂ (Equation 2.2). Hydrogen peroxide is the common reduction product of oxygen in Pd-catalyzed reactions, although metal catalyzed decomposition of H₂O₂ can occur leading to water as the final byproduct. The formation of H₂O₂ was detected in the reaction shown in entry 5, Table 2.1. The reaction in the presence of Na₂MoO₄, *i.e.* entry 6, Table 2.1, does not lead to the accumulation of H₂O₂, most probably because of the fast disproportionation catalyzed by molybdate (see *Experimental part*, Figure 2.4). However, H₂O₂ in the presence of molybdate is not a suitable oxidant in this reaction (entry 11, Table 2.1). We found that sodium tungstate is as efficient as sodium molybdate (entry 2, Table 2.2) but other dioxomolybdenum complexes that are active in oxygen-transfer reaction or singlet oxygen generator do not work (entries 3-5, Table 2.2).

⁷³ a) Aubry, J. M.; Bouttemy, S. *J. Am. Chem. Soc.* **1997**, *119*, 5286–5294. b) Li, W.; Li, L.; Xiao, H.; Qi, R.; Huang, Y.; Xie, Z.; Jing, X.; Zhang, H. *RSC Adv.* **2013**, *3*, 13417–13421.

⁷⁴ Boehme, K.; Brauer, H. D. *Inorg. Chem.* **1992**, *31*, 3468–3471.

Table 2.2 Use of other additives of high-valent elements for the reaction in Equation 2.2.^a

Entry	[Pd]	Additive (equiv)	1a , Crude yield (%), 6 h ^b
1	[Pd(OAc) ₂]	Na ₂ MoO ₄ ·2H ₂ O (0.1)	99
2	[Pd(OAc) ₂]	Na ₂ WO ₄ ·2H ₂ O (0.1)	82
3	[Pd(OAc) ₂]	MoO ₂ Cl ₂ (DMSO) ₂ (0.1) ^c	0
4	[Pd(OAc) ₂]	MoO ₂ Cl ₂ (DMSO) ₂ (1) ^c	0
5	[Pd(OAc) ₂]	KIO ₄ (0.1) ^d	38

^a Reaction conditions: [Pd(OAc)₂] (0.034 mmol, 10 mol %), *t*-butyl acrylate (0.341 mmol), C₆F₅H (0.853 mmol), DMA (3 mL total volume), 120 °C, O₂ (1 atm). ^b Crude yields were determined by ¹H NMR using dodecane as internal standard. ^c These dioxomolybdenum(VI) complexes have been used as mediators in oxygen transfer reactions (see ref: 75). ^d Besides being a potential oxidant, periodate can generate singlet oxygen under basic conditions (see ref: 76).

Sodium molybdate dihydrate has not been used in this type of reactions and it may seem an unconventional choice, since it is a non-hygroscopic, inexpensive and available salt, which can be used in a very convenient way. It has to be noted that heteropolymolybdates containing redox active vanadium(V) centers have been used as redox mediators in Pd-catalyzed oxidative C-H activation reactions,⁷⁷ and greatly developed by Ishii, Obora and coworkers.^{66a,78} They found that the presence of V(V) is necessary for the redox mediation (in the absence of vanadium other phosphomolybdates were inactive) as tested in the oxidation of hydroquinone to benzoquinone with oxygen.⁷⁹ We performed the same reaction that Ishii and coworkers reported using Na₂MoO₄ instead of H₄PMo₁₁VO₄₀ and found that the oxidation is inefficient (Scheme 2.4).

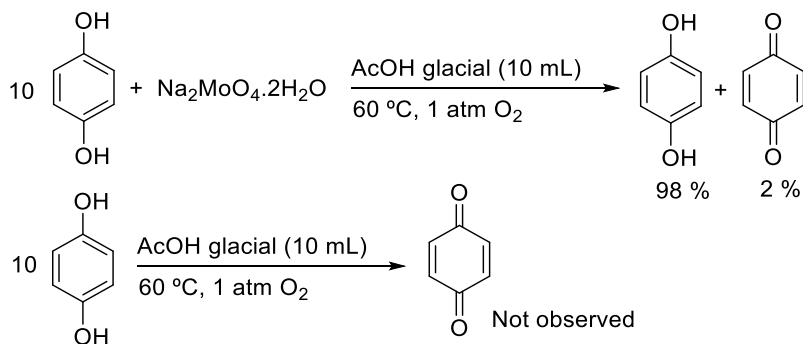
⁷⁵ a) Rubio-Presa, R.; Fernández-Rodríguez, M. A.; Pedrosa, M. R.; Arnáiz, F. J.; Sanz, R. *Adv. Synth. Catal.* **2017**, *359*, 1752–1757. b) García, N.; García-García, P.; Fernández-Rodríguez, M. A.; García, D.; Pedrosa, M. R.; Arnáiz, F. J.; Sanz, R. *Green Chem.* **2013**, *15*, 999–1005.

⁷⁶ Bokare, A. D.; Choi, W. *Environ. Sci. Technol.* **2015**, *49*, 14392–14400.

⁷⁷ a) Tarabanko, V. E.; Kozhevnikov, I. V.; Matveev, K. I. *React. Kinet. Catal. Lett.* **1978**, *8*, 77–79. b) Weinstock, A.; Schreiber, R. E.; Neumann, R. *Chem. Rev.* **2018**, *118*, 2680–2717.

⁷⁸ a) Yokota, T.; akakura, A.; Tani, M.; Sakaguchi, S.; Ishii, Y. *Tetrahedron Lett.* **2002**, *43*, 8887–8891. b) Yamada, T.; Sakaguchi, S.; Ishii, Y. *J. Org. Chem.* **2005**, *70*, 5471–5474. c) Mizuta, Y.; Obora, Y.; Shimizu, Y.; Ishii, Y. *ChemCatChem* **2012**, *4*, 187–191.

⁷⁹ Yokota, T.; Fujibayashi, S.; Nishiyama, Y.; Sakaguchi, S.; Ishii, Y. *J. Mol. Catal. A Chem.* **1996**, *169*, 113–122.



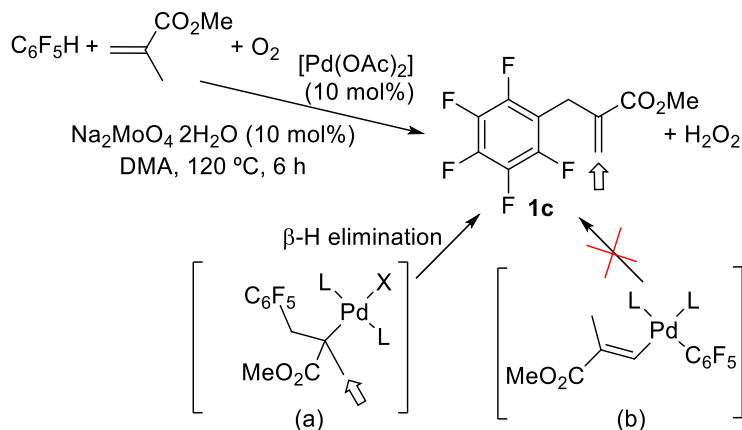
Scheme 2.4 Attempted benzoquinone oxidation.

All these experiments show that, as mentioned above, Na_2MoO_4 is not a redox mediator in the reaction and its role as an additive is just that of a weak base.

The reaction can be carried out under milder conditions and the temperature can be lowered to $90\text{ }^\circ\text{C}$ or even $60\text{ }^\circ\text{C}$, provided the reaction times are extended to 48 h for the latter (entries 12 and 13, Table 2.1). The amount of catalyst can be reduced to 5 mol% (entry 14, Table 2.1). $[\text{Pd}(\text{OAc})_2]$ is the best catalyst precursor (*cf.* entries 6 and 15, Table 2.1) and for less basic ligands in the precatalyst coordination sphere (Cl *vs.* OAc) the reaction benefits from the presence of additional base and acetate (entries 15-17, Table 2.1). Other precursor complexes such as $[\text{Pd}(\text{acac})_2]$ or $[\text{Pd}(\text{TFA})_2]$ in the same conditions as entry 15 were even less efficient (see *Experimental part*, Table 2.5).

Pentafluorostilbene (**1b**) can be prepared by arylation of styrene using this reaction (entry 18, Table 2.1), but the fluoroarylation of olefins with no electron-withdrawing groups such as 1-hexene or 2,3-dihydrofuran could not be achieved.

The formation of **1a** (Equation 2.2) could be either the result of an oxidative Heck reaction (Scheme 2.2) or the product of a double $\text{C}(sp^2)\text{-H}$ activation (arene and alkene) and reductive elimination. The reaction of pentafluorobenzene with methyl methacrylate rules out the second route, since the product of this reaction, the terminal olefin **1c**, can only be formed by insertion of the olefin into the Pd- C_6F_5 bond and subsequent β -hydride elimination, much more favorable for the methyl hydrogens (Scheme 2.5).

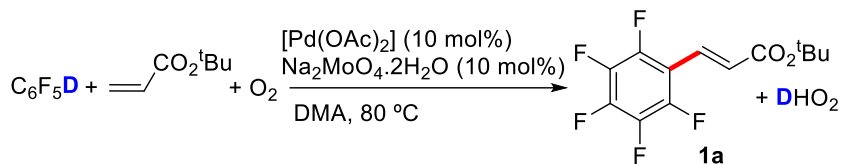


Scheme 2.5 Perfluoroarylation of methyl methacrylate: it rules out the double C-H activation pathway (intermediate b) vs. a Heck route (intermediate a).

The reaction course was monitored at $80\text{ }^\circ\text{C}$ by NMR and the rate of the reaction showed no dependence on the concentration of olefin, arene and catalyst (see *Experimental part*, Figure 2.6). This points to O_2 , whose solubility is quite low in DMA (5.2 mM),^{23c} as the factor controlling the reaction rate by keeping the amount of available oxidant as the limiting reagent. This has been observed before for other aerobic reactions in solvents of low oxygen solubility such as DMSO.²³ An increase of the O_2 pressure leads to a higher yield (68 % yield at 2 atm vs. 52 % at 1 atm after 20 min).

These results show that the aerobic alkenylation of pentafluorophenyl is efficient without the addition of a cooperating ligand. Indeed, the C-H cleavage of C_6F_5H is facile as can be seen in the monitoring of the reaction in Equation 2.4 using C_6F_5D as reagent at $80\text{ }^\circ\text{C}$. In the first hour almost all the deuterated arene is converted into C_6F_5H . Figure 2.1 shows a faster disappearance of the *t*-butyl acrylate than the formation of the Heck product in the first two hours. This indicates a competitive reaction route for the alkene that also occurs in the absence of arene as tested independently (see *Experimental part*, Figure 2.5). No new alkene was formed suggesting a possible polymerization pathway.⁸⁰

⁸⁰ See for example: Albéniz, A. C.; Espinet, P.; López-Fernández, R.; *Organometallics*, **2003**, *22*, 4206–4212.



Equation 2.4

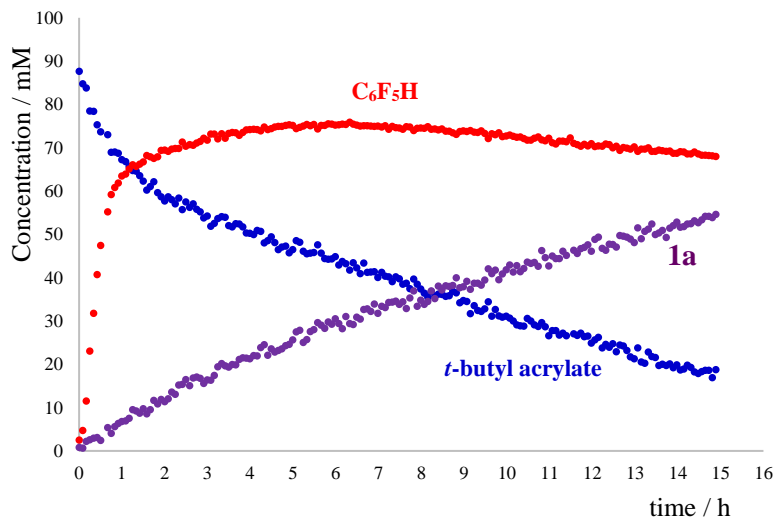
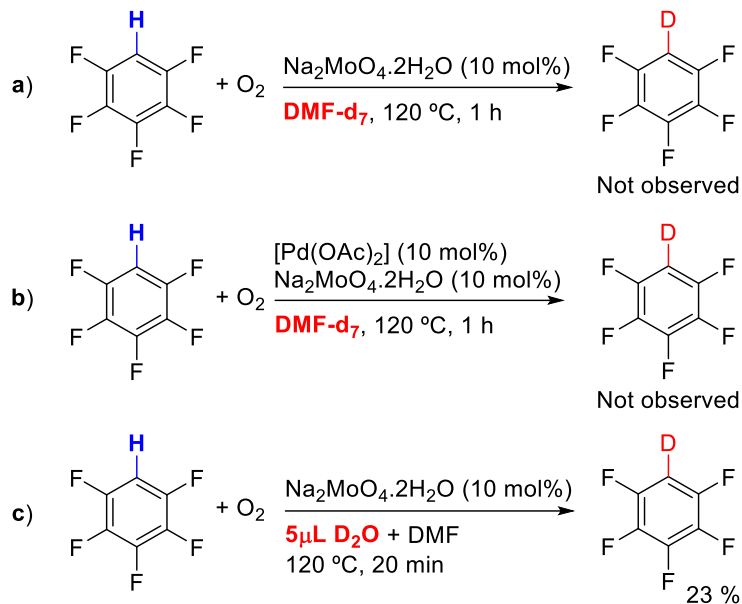


Figure 2.1 Evolution of the reaction of C₆F₅D and *t*-butyl acrylate at 80 °C showing the fast H/D exchange of the arene.

The H/D exchange in pentafluorobenzene is easy in the presence of base and does not require metal catalysis as has been reported before.⁸¹ In this case just the presence of a catalytic amount of sodium molybdate in the presence of traces of H₂O is enough for the conversion, as we tested independently (Scheme 2.6, Figure 2.2). Nonetheless, the presence of acetate in the reaction plays a beneficial role which points to the occurrence of an acetate-mediated CMD route to generate the Pd-C₆F₅ bond (entry 17, Table 2.1).

⁸¹ Salamanca, V.; Albéniz, A. C. *Eur. J. Org. Chem.* **2020**, 3206–3212.



Scheme 2.6 Conversion of C_6F_5H to C_6F_5D promoted by sodium molybdate dihydrate in presence of deuterated water. The reactions were followed by ^{19}F NMR with C_6F_6 as an internal standard (5 μ L) (Figure 2.2).

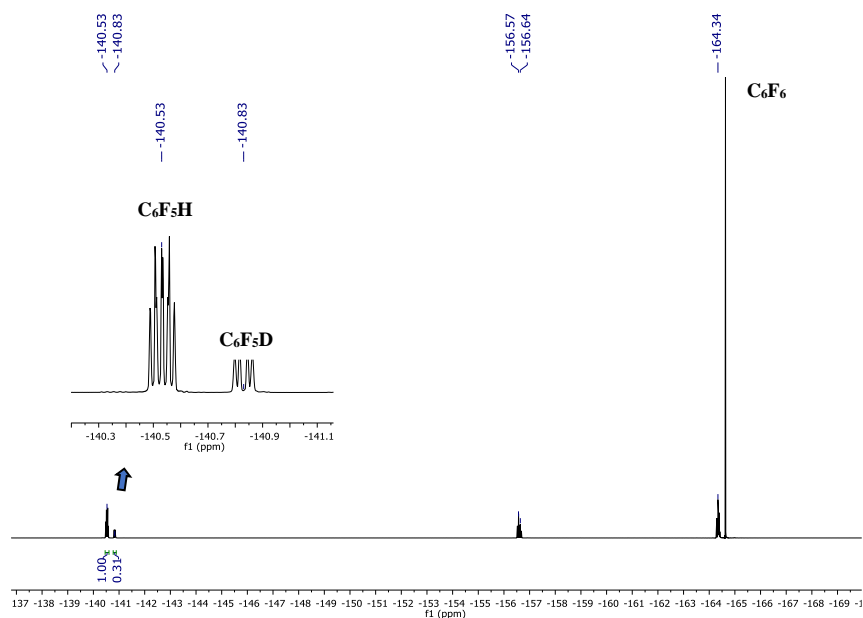
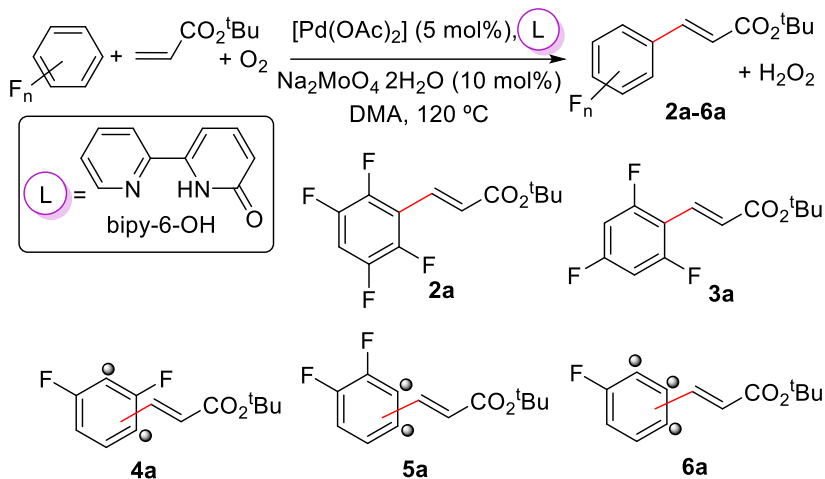


Figure 2.2 Formation of C_6F_5D from C_6F_5H in presence sodium molybdate and traces of deuterated water (Scheme 2.6, c).

The alkenylation of other fluorinated arenes can also be carried out and the best reaction conditions found show the increasing importance of the C-H cleavage in the reaction upon decreasing the number of fluorine substituents (Scheme 2.7 and Table 2.3).



Scheme 2.7 Aerobic oxidative Heck reaction of fluorinated arenes (° alkenylated positions).

Table 2.3 Oxidative Heck reaction of C₆F_nH_{6-n} according to Scheme 2.7.^a

Entry	Arene (equiv)	Arene:alkene (mol ratio)	L mol %	Crude yield (%) 6 h ^b	Crude yield (isol.) (%) 24 h ^b
1	1,2,4,5-C ₆ F ₄ H ₂	2.5:1	-	2a , 48	
2	1,2,4,5-C ₆ F ₄ H ₂	5:1	-	2a , 50	2a , 56 (42)
3	1,3,5-C ₆ F ₃ H ₃	2.5:1	-	3a , 52	
4	1,3,5-C ₆ F ₃ H ₃	5:1	-	3a , 71	3a , 71 (60)
5	1,3-C ₆ F ₂ H ₄	2.5:1	-	3a , 46	
6	1,3-C ₆ F ₂ H ₄	5:1	-	4a , 68	4a , 99 ^c (85)
7 ^d	1,3-C ₆ F ₂ H ₄	2.5:2	-	4a , 44	
8	1,2-C ₆ F ₂ H ₄	2.5:1	-	5a , 13	
9 ^e	1,2-C ₆ F ₂ H ₄	44:1	-	5a , 20	
10 ^e	1,2-C ₆ F ₂ H ₄	44:1	5	5a , 60	5a , 86 ^f (75)
11 ^e	C ₆ FH ₅	47:1	-	6a , 18	
12 ^e	C ₆ FH ₅	47:1	5	6a , 75	6a , 87 ^g (78)

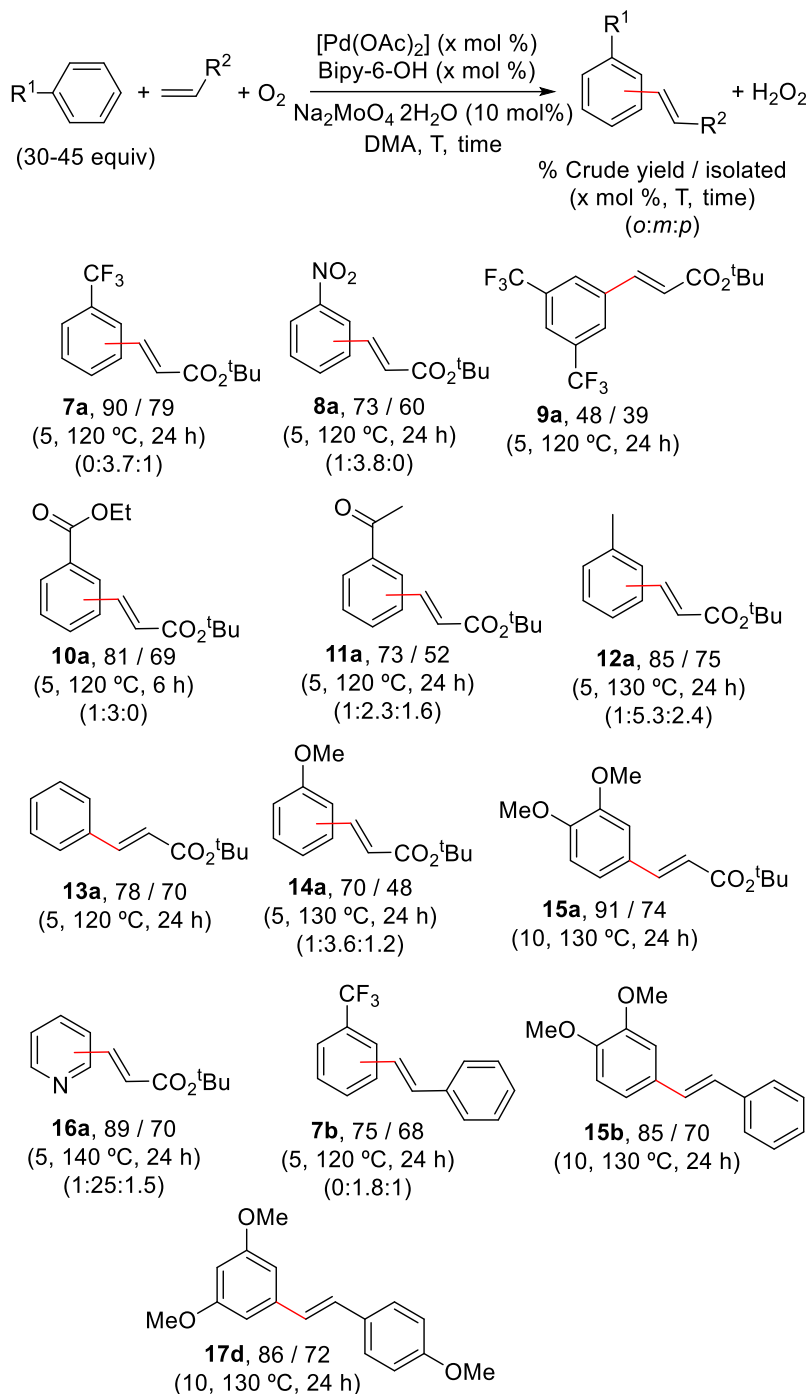
^a Reaction conditions: [Pd(OAc)₂] (0.017 mmol, 5 mol %), *t*-butyl acrylate (0.341 mmol), Na₂MoO₄·2H₂O (0.034 mmol, 10 mol %), DMA as solvent (3 mL), 120 °C, O₂ (1 atm), unless otherwise noted. ^b Crude yields were determined by ¹H NMR using dodecane as internal standard. ^c Isomer ratio 2,6-F₂:2,4-F₂ = 2:1. ^d *t*-Butyl acrylate (arene:olefin = 2.5:2 mol ratio). ^e Arene:DMA = 1:1 v/v. ^f Isomer ratio 2,3-F₂:3,4-F₂ = 1.8/1. ^g Isomer ratio *o*:*m*:*p* = 2.8:3.8:1.

Tetrafluorobenzene can be alkenylated in moderate yield using a 2.5-fold excess of the arene in the same way used for pentafluorobenzene. In both cases the use of a higher amount of the arene has no influence in the reaction outcome (entries 1 and 2,

Table 2.3). In contrast, the reactions with trifluorobenzene and 1,3-difluorobenzene clearly benefit from the use of a larger excess of arene (5-fold, *cf.* entries 3, 4 and 5, 6, Table 2.3). This indicates that the arene activation is kinetically relevant for these arenes but the excess of olefin has no effect (entries 5-7, Table 2.3). The alkenylation of 1,2-difluorobenzene or fluorobenzene is inefficient even when using a large excess of arene, and it reaches good yields only in the presence of the ligand bipy-6-OH. The observed reactivity for the fluoroarenes fits the acidity trend of the C-H bond that is cleaved,⁸¹ which in turn parallels the ease of C-H activation also favored by the stronger Pd-C bond for fluoroaryls with *ortho* fluorines.⁸² As the F-substitution decreases, the C-H activation becomes turnover limiting and eventually needs the assistance of bipy-6-OH. It has to be noted that, in fact, the presence of bipy-6-OH is detrimental for the most reactive penta- tetra- tri- and 1,3-difluorobenzenes, as will be discussed below.

Other non-fluorinated simple arenes were alkenylated using the bipy-6-OH ligand and a catalytic amount of sodium molybdate, in the same way as the less substituted fluoroarenes. Scheme 2.8 shows the products obtained and the best reaction conditions ([Pd] mol %, T and time) in each case. The reaction is useful for arenes bearing electron-withdrawing and electron-donating groups. The alkene stereochemistry in all these products is *trans*, but the C-H activation is not regioselective for the mono-substituted arenes and mixtures of two or three of the *ortho*, *meta* and *para* isomers were found. The *meta* isomer is always the major one, specially in the case of pyridine. This regiochemistry in the C-H activation is the same observed in the non-oxidative direct arylation reactions with the same ligand.⁵² The presence of an ester (**10a**) or keto (**11a**) substituent in the arene does not provide a directing effect in this reaction that could shift the regioselectivity towards the *ortho* isomer. On the other hand, the disubstituted arenes lead to just one isomer regioselectively. In the case of the di-methoxy substituted arenes, this has been used for the synthesis of the resveratrol precursor **17d** with success.

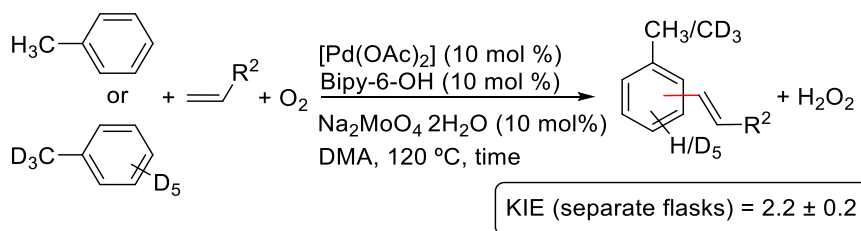
⁸² Eisenstein, O.; Milani, J.; Perutz, R. N. *Chem. Rev.* **2017**, *117*, 8710–8753.



Scheme 2.8 Aerobic oxidative Heck reaction of non-fluorinated arenes (isomer ratio in the crude mixture).

2.2.2 Mechanistic aspects and the role of bipy-6-OH

The role of a ligand in a complex catalytic cycle such as that operating in the aerobic oxidative Heck reaction of arenes can be manifold. However, the experimental data point to a cooperating role of bipy-6-OH in the C-H cleavage step in these reactions. Using toluene as a model arene, the kinetic isotope effect was determined using the conditions shown in Scheme 2.8 (L = bipy-6-OH) for separate reactions using toluene in one experiment and toluene-d₈ in the other (Equation 2.5).



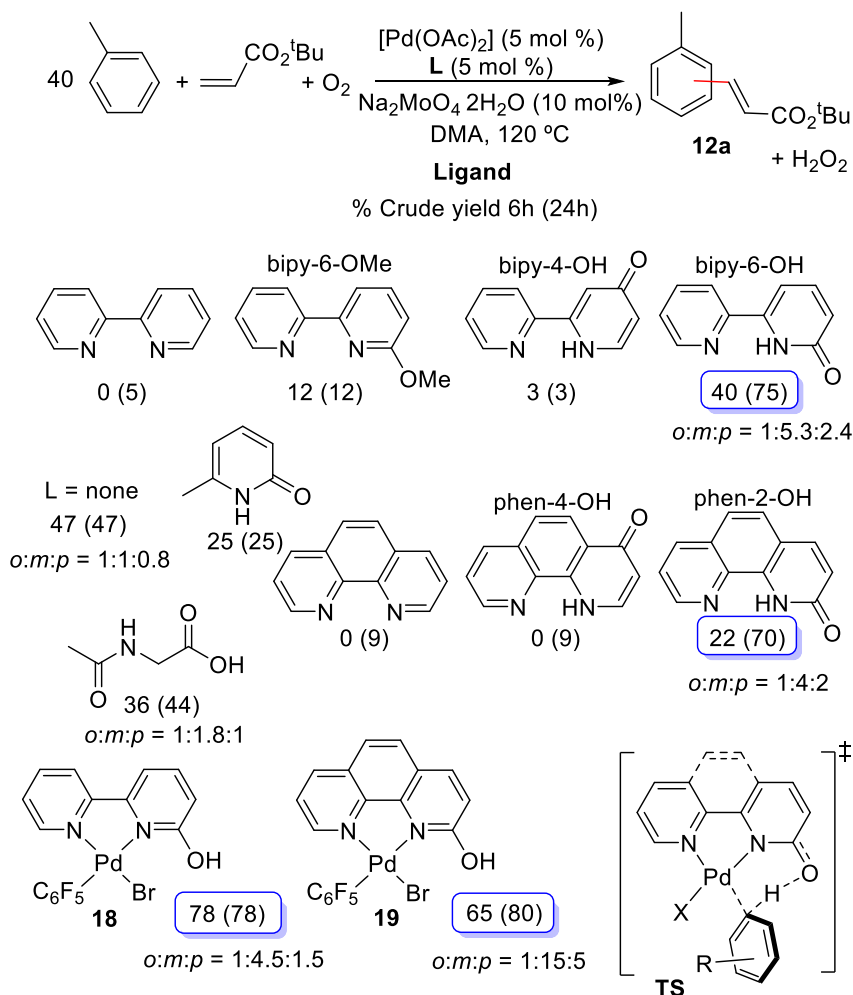
Equation 2.5

A value of $\text{KIE} = 2.2 \pm 0.2$ was obtained, showing that the C-H cleavage is turnover limiting. This value is lower than the one expected for a situation where the C-H activation is the only rate limiting step ($\text{KIE} \approx 3.6$), indicating that a preceding step, either the coordination of the arene or the actual reoxidation rate with O_2 , may also be influencing the overall reaction rate, with the C-H cleavage TS being nonetheless the highest in energy and therefore the most influential. This has been studied before.^{52b}

Several catalytic reactions were carried out with different ligands. As can be seen in Scheme 2.9, only bipy-6-OH and the analogous phen-2-OH have a beneficial effect in the reaction which, along with the KIE found, support the involvement of these ligands in the C-H cleavage *via* the transition state shown in Scheme 2.9. Neither the unsubstituted ligands in both *N*-chelating series (2,2'-bipy or 1,10-phen) nor bipy-6-OMe are effective. The position of the pyridone moiety is also crucial, and neither bipy-4-OH nor phen-4-OH enable the reaction. Even if the latter ligands can lead to an anionic ligand by deprotonation, the pyridone moiety cannot engage in the C-H cleavage.

Phen-2-OH has been used before by Duan *et al.* in the oxidative Heck reaction of arenes using Cu(II) salts as oxidants or redox mediators.^{57a} The authors attributed the observed effect to the anionic (X,L) nature the ligand upon deprotonation which, when compared to a neutral L-L chelating ligand, could facilitate the decoordination of an acetate and the opening of a coordination site on the metal. Although this is certainly

plausible, the differences observed between the regioisomers phen-2-OH and phen-4-OH strongly support the direct involvement of the former in the C-H cleavage.



Scheme 2.9 Aerobic oxidative Heck reaction of toluene with different ligands.

The use of a preformed palladium complex $[\text{PdBr}(\text{C}_6\text{F}_5)(\text{L-L})]$ (L-L = bipy-6-OH, **18**; phen-2-OH, **19**) as precatalyst instead of the mixture $[\text{Pd}(\text{OAc})_2]$ + ligand is also effective (Scheme 2.9). This shows that the presence of acetate is not needed in these reactions, although the moderate yield obtained in the absence of ligand ($\text{L} = \text{none}$, Scheme 2.9) indicates that the C-H cleavage could also occur *via* a CMD process with an acetato ligand. In fact, when the mixture $[\text{Pd}(\text{OAc})_2]$ + bipy-6-OH is used as precatalyst a putative intermediate complex with both coordinated acetato and bipy-6-O ligands could be involved in the C-H activation step. Which one reacts

preferentially is impossible to ascertain experimentally but DFT calculations on the isolated C-H cleavage step show that the assistance of the bipy-6-OH ligand leads to a lower energy transition state, so the cooperation of this ligand is expected (Figure 2.3).

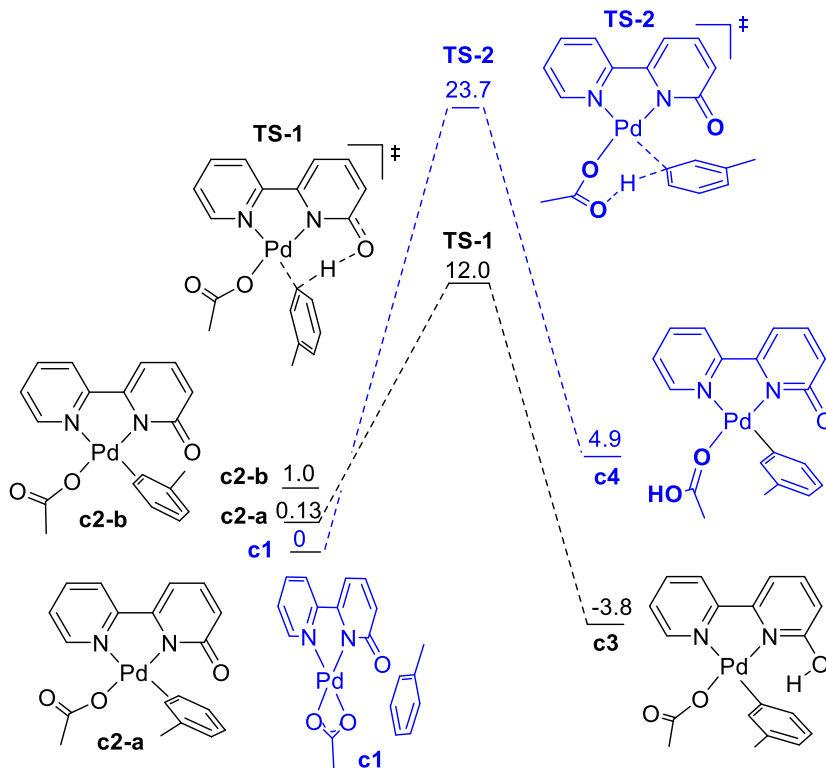


Figure 2.3 Gibbs energy barriers for the C-H activation step assisted by bipy-6-O or by the acetato ligand. Energies in kcal mol⁻¹.

Interestingly, a higher selectivity in the alkenylation of toluene towards the *meta* substitution is observed when bipy-6-OH or phen-2-OH are used (*o:m:p* = 1:5.3:2.4) than when no ligand is added (*o:m:p* = 1:1:0.8). This may reflect the different steric requirements in the C-H activation TS for different coordination environments. Recently, the work of Jiao *et al.* showed that in the alkenylation of indoles using a pyridone derivative as ligand, the regioselectivity is determined by the olefin insertion step.⁵¹ In our case, the lack of deuteration of **12a** when the reaction was carried out in the presence of D₂O supports an irreversible C-H activation. Also, in contrast to Jiao's work, the reaction is not accelerated when an excess of *t*-butyl acrylate is used. Although deeper studies are needed, these results support that regioselectivity might be determined upon C-H cleavage.

Table 2.4 shows the effect of bipy-6-OH in the aerobic oxidative Heck reaction of different arenes. An increase of the final yield of the product is observed upon addition of bipy-6-OH in all cases except for the most acidic polyfluoroarenes, where the effect of the ligand is clearly detrimental (entries 1-4, Table 2.4).

Table 2.4 Effect of the use of the ligand bipy-6-OH for the aerobic alkenylation of different arenes with *t*-butyl acrylate.^a

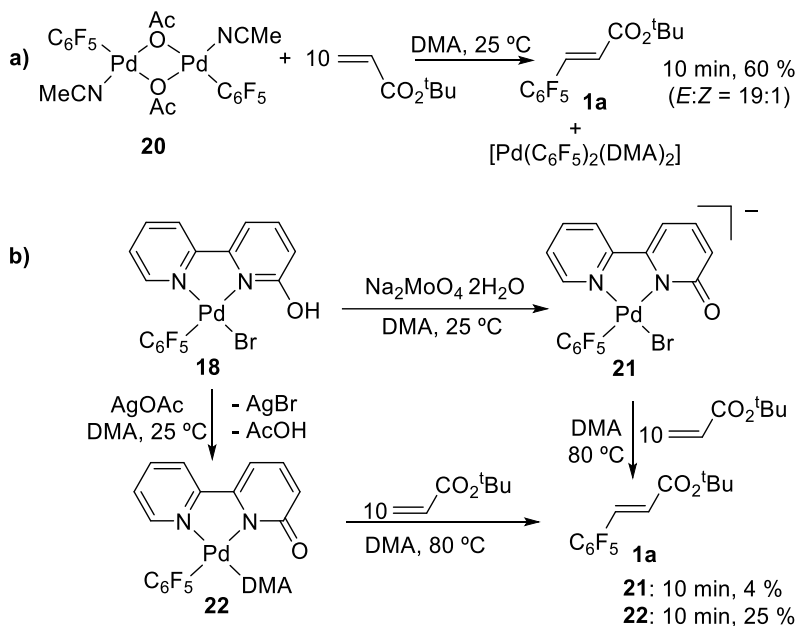
Entry	L	Arene	Cpd.	Crude yield, %	
				6 h ^b	24 h ^b
1 ^c	bipy-6-OH	C ₆ F ₅ H	1a	0	0
2 ^c	–	C ₆ F ₅ H	1a	86	90
3 ^c	bipy-6-OH	1,3-C ₆ F ₂ H ₄	3a	13	18
4 ^c	–	1,3-C ₆ F ₂ H ₄	3a	46	46
5	bipy-6-OH	1,2-C ₆ F ₂ H ₄	5a	60	86
6	–	1,2-C ₆ F ₂ H ₄	5a	20	28
7	bipy-6-OH	PhF	6a	75	87
8	–	PhF	6a	18	18
9	bipy-6-OH	PhCF ₃	7a	72	90
10	–	Ph-CF ₃	7a	40	40
11	bipy-6-OH	PhMe	12a	40	75
12	–	PhMe	12a	47	47
13 ^d	bipy-6-OH	1,2-(OMe) ₂ -C ₆ H ₄	15a	73	91
14 ^d	–	1,2-(OMe) ₂ -C ₆ H ₄	15a	26	32
15 ^{d,e}	bipy-6-OH	1,3-(OMe) ₂ -C ₆ H ₄	17d	56	86
16 ^{d,e}	–	1,3-(OMe) ₂ -C ₆ H ₄	17d	0	0

^a Reaction conditions: [Pd(OAc)₂] (0.017 mmol, 5 mol %), Na₂MoO₄·2H₂O (0.034 mmol, 10 mol %), alkene (0.341 mmol), Arene:DMA = 1:1 v/v (total volume, 3 mL), O₂ (1 atm), 120 °C, unless otherwise noted.^b Crude yields were determined by ¹H NMR using dodecane as internal standard. Yields refer to the mixture of isomers, whose distribution can be found in the *Experimental part* (Table 2.6). ^c Arene:olefine = 2.5:1 mol ratio.^d [Pd(OAc)₂] (10 mol %), L (10 mol %), 130 °C. ^e 4-methoxy styrene instead of *t*-butyl acrylate.

Since the C-H activation in these arenes is more facile, the ligand must be hampering other steps in the catalytic cycle, *i.e.* the coordination-insertion of the olefin.⁸³ To test this, we monitored the reaction of *t*-butyl acrylate with two palladium complexes that mimic plausible reaction intermediates in both scenarios (Scheme 2.10, **a**) and **b**). The *trans*-dimeric complex **20** (see molecular structure in Figure 2.12, *Experimental part*) represents the species that could be formed after C-H activation of C₆F₅H when only [Pd(OAc)₂] is used as precatalyst. The reaction of **20** in DMA with the olefin is fast and about 60 % of the perfluorophenyl acrylate is observed after 10 min at room

⁸³ These two elementary steps are inseparable when analyzing the reaction experimentally in Heck processes and therefore are referred to as one.

temperature (Scheme 2.10, **a**). A small amount of the *cis* olefination product was also observed as well as the aryl reorganization of the complex to give $[\text{Pd}(\text{C}_6\text{F}_5)_2(\text{DMA})_2]$.



Scheme 2.10 Stoichiometric reactions of model palladium complexes with *t*-butyl acrylate.

In contrast, complexes **21** and **22** bearing the bipy-6-O ligand only react with *t*-butyl acrylate slowly at 80 °C (Scheme 2.10, **b**). Thus, when the C-H activation is not problematic, the presence of a good chelating ligand, which renders a less accessible metal center, disfavors the coordination of the olefin and the reaction is less efficient. The strong Pd-aryl bond for polyfluoroarenes with *ortho* substituents also disfavors the insertion of the olefin. The conventional Heck reaction of polyfluoroarenes shows a related situation with the coordination-insertion of the olefin as turnover limiting vs. the most commonly slow oxidative addition.⁸⁴ For some of the arenes in Table 2.4, the acceleration upon addition of the ligand after 6 h is not very important but, whereas the catalysis does not proceed further without the ligand, it reaches almost completion when bipy-6-OH is added. These results are consistent with the ligand being involved in the stabilization of intermediate species in the cycle. Therefore, the ligand is instrumental to lower the C-H activation energy but its role in the reaction can be more complex affecting other reaction steps, which overall gives a useful olefination reaction.

⁸⁴ a) Albéniz, A. C.; Espinet, P.; Martín-Ruiz, B.; Milstein, D. *J. Am. Chem. Soc.* **2001**, *123*, 11504–11505. b) Albéniz, A. C.; Espinet, P.; Martín-Ruiz, B.; Milstein, D. *Organometallics* **2005**, *24*, 3679–3684.

2.3 CONCLUSIONS

The oxidative Heck reaction of arenes with oxygen as terminal oxidant and no redox mediators can be carried out using a set of reaction conditions that employ a minimum amount of additives, just sodium molybdate in catalytic amounts, and avoids strongly acidic or basic conditions. The presence of the cooperating [2,2'-bipyridin]-6(1*H*)-one (bipy-6-OH) ligand enables the reaction for mono and disubstituted arenes of different electronic properties by assisting the C-H activation step. The ligand is detrimental in the olefination of polyfluorinated arenes $C_6F_nH_{6-n}$ ($n \geq 3$) and 1,3- $C_6F_2H_4$ where the easier C-H activation does not need an additional cooperating ligand, but the latter can disfavor the coordination-insertion of the olefin. Therefore a “ligandless” catalytic system is more suitable for the alkenylation of *ortho* disubstituted fluoroarenes. The C-H activation of any other arene needs the help of an enabling ligand and the cooperating bipy-6-OH and phen-2-OH are suitable for this transformation.

2.4 EXPERIMENTAL PART

2.4.1 General considerations

^1H , ^{13}C and ^{19}F NMR spectra were recorded on Bruker AV-400 or Agilent MR-500 spectrometers at the LTI-UVa. Chemical shifts (in δ units, ppm) were referenced to SiMe_4 (^1H and ^{13}C) and CFCl_3 (^{19}F). Homonuclear (^1H -COSY) and heteronuclear (^1H - ^{13}C HSQC and HMBC) experiments were used to help with the signal assignments. Solvents were dried using a solvent purification system SPS PS-MD-5 or distilled from appropriate drying agents under nitrogen prior to use and stored over 3 Å or 4 Å molecular sieves. $[\text{Pd}(\text{OAc})_2]$, *N*-acetylglycine, 2,2'-bipyridine, 1,10-phenanthroline, 6-methyl-2(1*H*)-pyridinone, the arenes and the alkenes used are commercially available and were used as received unless otherwise indicated. $[\text{Pd}(\text{bipy-6-OH})\text{Br}(\text{C}_6\text{F}_5)]$ (**18**),^{52a} $(\text{NBu}_4)[\text{Pd}(\text{bipy-6-O})\text{Br}(\text{C}_6\text{F}_5)]$ (**21**),^{52a} $[\text{PdBr}(\text{CH}_3\text{CN})_2(\text{C}_6\text{F}_5)]$,⁸⁵ $(\text{NBu}_4)_2[\text{Pd}_2(\mu\text{-Br})_2\text{Br}_2(\text{C}_6\text{F}_5)_2]$,⁸⁶ [2,2'-bipyridin]-6(1*H*)-one (bipy-6-OH),⁸⁷ 1,10-phenanthrolin-2(1*H*)-one (phen-2-OH),⁸⁸ 1,10-phenanthrolin-4(1*H*)-one (phen-4-OH),⁸⁹ [2,2'-bipyridin]-4(1*H*)-one (bipy-4-OH),⁹⁰ 6-methoxy-2,2'-bipyridine (bipy-6-OMe),⁸⁷ and $\text{C}_6\text{F}_5\text{D}$,⁸¹ were prepared according to the procedures in the literature.

2.4.2 Synthesis of palladium complexes

[Pd(phen-2-OH)Br(C₆F₅)] (19). 1,10-phen-2(1*H*)-one (71 mg, 0.364 mmol) was added to a solution of $(\text{NBu}_4)_2[\text{Pd}_2(\mu\text{-Br})_2\text{Br}_2(\text{C}_6\text{F}_5)_2]$ (0.245 g, 0.181 mmol) in 20 mL of acetone. The mixture was stirred at room temperature for 2 h. During this time the orange solution became lighter and also an abundant precipitate was observed. The solvent was evaporated to ca. 5 mL and cold EtOH (10 mL) was added to the suspension. The yellow solid obtained was filtered, washed with cold EtOH (3 x 5 mL) and air-dried. Yield: 0.16 g (80 %).

^1H NMR (499.73 MHz, δ , $(\text{CD}_3)_2\text{CO}$): 11.61 (br, 1H, OH), 8.90 (d, $J = 8.3$ Hz, 1H, H¹⁰), 8.77 (d, $J = 8.8$ Hz, 1H, H³), 8.23 (m, 2H, H⁶, H⁸), 8.13 (d, $J = 8.7$ Hz, 1H, H⁵), 7.86 (dd, $J = 8.3, 5.3$ Hz, 1H, H⁹), 7.46 (d, $J = 8.8$ Hz, 1H, H²). $^{13}\text{C}\{^1\text{H}\}$ NMR (125.67 MHz, δ , $(\text{CD}_3)_2\text{CO}$): 166.8 (C¹), 151.7 (C⁸), 146.5 (C¹²), 143.2 (C¹¹), 142.6 (C³), 140.1 (C⁷), 139.9 (C¹⁰), 130.8 (C⁴), 127.9 (C⁶), 125.3 (C⁹), 124.6 (C⁵), 117.0 (C²). * ^{19}F NMR (470.17 MHz, δ , $(\text{CD}_3)_2\text{CO}$): -119.72 (m, 2F, F_{ortho}), -162.01 (t, $J = 19.7$ Hz, 1F, F_{para}), -164.77 (m, 2F, F_{meta}). IR (neat, cm^{-1}): $\nu(\text{C}_6\text{F}_5)$ (1507, 1462, 1063, 950, 793); $\nu(\text{OH}, \text{st})$ 3031. Anal. Calcd

⁸⁵ Albéniz, A. C.; Espinet, P. *Organometallics* **1990**, *9*, 1079–1085.

⁸⁶ Usón, R.; Forniés, J.; Nalda, J. A.; Lozano, M. J.; Espinet, P.; Albéniz, A. C. *Inorg. Chim. Acta* **1989**, *156*, 251–256.

⁸⁷ Tomon, T.; Koizumi, T. A.; Tanaka, K. *Eur. J. Inorg. Chem.* **2005**, *2005*, 285–293.

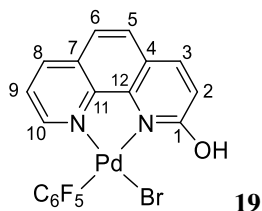
⁸⁸ Krapcho, A. P.; Sparapani, S. *J. Heterocycl. Chem.* **2008**, *45*, 1167–1170.

⁸⁹ Ferretti, F.; Ragaini, F.; Lariccia, R.; Gallo, E.; Cenini, S. *Organometallics* **2010**, *29*, 1465–1471.

⁹⁰ a) Wenkert, D.; Woodward, R. B. *J. Org. Chem.* **1983**, *48*, 283–289. b) Hong, Y. R.; Gorman, C. B. *J. Org. Chem.* **2003**, *68*, 9019–9025.

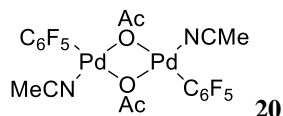
for $C_{18}H_8N_2F_5BrOPd$: C, 39.34 %; H, 1.47 %; N, 5.10 %. Found: C, 39.15 %; H, 1.21 %; N, 5.53 %.

*The ^{13}C signals for the C_6F_5 group, heavily coupled to ^{19}F , could not be observed due to the low solubility of this complex. The stereochemistry of **19** could not be determined as the 1H - ^{19}F HOESY NMR experiments were inconclusive due to the low solubility of the complex; it is tentatively assigned by analogy to complex **18** bearing the similar bipy-6-OH ligand.



[Pd₂(μ-OAc)₂(C₆F₅)₂(CH₃CN)₂] (20). A solution of complex $[PdBr(C_6F_5)(CH_3CN)_2]$ (145 mg, 0.33 mmol) in dry- CH_3CN (3 mL) was added to a solution of $AgOAc$ (55 mg, 0.33 mmol) in 5 mL of dry- CH_3CN under nitrogen atmosphere. The mixture was stirred at room temperature for 2 h protected from light. During this time an abundant precipitate was observed which was filtered. The filtrate was evaporated to dryness and diethyl ether (3 mL) was added. The yellow solid obtained was filtered, washed with ether (2 x 3 mL) and air-dried. Yield: 0.11 g (88 %).

1H NMR (499.73 MHz, δ , $CDCl_3$): 2.30 (s, 6H, $COOCH_3$), 1.89 (s, 6H, $NCCH_3$). ^{13}C $\{^1H\}$ NMR (125.67 MHz, δ , $CDCl_3$): 183.5 ($COOCH_3$), 148.7 (dm, $^1J_{C-F} = 233.8$ Hz, C_{ortho}), 138.3 (dm, $^1J_{C-F} = 245.9$ Hz, C_{para}), 135.2 (dm, $^1J_{C-F} = 252.5$ Hz, C_{meta}), 120.3 ($NCCH_3$), 97.4 (d, $^2J_{C-F} = 42.2$ Hz, C_{ipso}), 23.3 ($COOCH_3$), 3.2 ($NCCH_3$). ^{19}F NMR (470.17 MHz, δ , $CDCl_3$): -121.74 (m, 2F, F_{ortho}), -159.33 (t, $J = 20$ Hz, 1F, F_{para}), -164.09 (m, 2F, F_{meta}). Anal. Calcd for $C_{20}H_{12}F_{10}N_2O_4Pd_2$: C, 32.15 %; H, 1.62 %; N, 3.75 %. Found: C, 32.10 %; H, 1.41 %; N, 3.75 %. IR (neat, cm^{-1}): $\nu(C_6F_5)$ (1463, 1063, 959, 796, 689); $\nu(CN, st)$ 2340.



2.4.3 Catalytic reactions

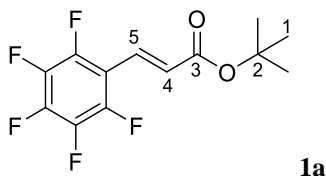
General procedure A: Oxidative Heck reaction of pentafluorobenzene. $[Pd(OAc)_2]$ (7.65 mg, 0.034 mmol), and sodium molybdate dihydrate (8.25 mg, 0.034 mmol) were introduced in a Schlenk tube with a screw cap in an oxygen atmosphere. Then, C_6F_5H (94 μL , 0.853 mmol), *t*-butyl acrylate (50 μL , 0.341 mmol), dodecane (40 μL , 0.176 mmol) as internal standard and *N,N*-dimethylacetamide (3 mL) were added. Oxygen was bubbled through the mixture (5 min) and the vessel was closed. The mixture was heated in a bath at 120 °C for 6 h. The yield of the reaction was checked by ^{19}F and 1H NMR of

the crude mixture. *N,N*-dimethylacetamide was then removed under vacuum and *n*-hexane was added to the residue to extract the product. The suspension was filtered and the filtrate was evaporated to dryness obtaining an oily residue. Finally, the product was purified by column chromatography using silica gel and EtOAc: hexane = 1:50 as eluent. The product was obtained as a colorless oil. Yield 90 mg (88 %). The reaction can also be carried out using 5 mol % of [Pd(OAc)₂] (0.017 mmol).

Compound **1b** was obtained following the same procedure. The other tetra-, tri- and 1,3-di-fluorobenzenes can be olefinated in the same way using a fluoroarene:alkene = 2.5:1 or 5:1 mol ratio and sometimes longer reaction times (Table 2.3). The products were purified by column chromatography using silica gel and a solvent mixture for each product that are specified below.

***tert*-Butyl (2*E*)-3-(2,3,4,5,6-pentafluorophenyl)-2-propenoate (**1a**).⁹¹**

¹H NMR (399.86 MHz, δ , CDCl₃): 7.53 (d, *J* = 16.4 Hz, 1H, H⁵), 6.65 (d, *J* = 16.4 Hz, 1H, H⁴), 1.52 (s, 9H, H¹). ¹³C{¹H} NMR (100.56 MHz, δ , CDCl₃): 165.1 (C³), 145.4 (m, ¹J_{C-F} = 255.6 Hz, C_{ortho}), 141.4 (m, ¹J_{C-F} = 251.8 Hz, C_{para}), 137.6 (m, ¹J_{C-F} = 253.47 Hz, C_{meta}), 128.2 (C⁵), 126.9 (C⁴), 110.0 (td, ²J_{C-F} = 13.6, 4.3 Hz, C_{ipso}), 81.4 (C²), 27.9 (C¹). ¹⁹F NMR (376.38 MHz, δ , CDCl₃): -139.85 (m, 2F, F_{ortho}), -151.94 (tt, *J* = 19.5, 2.8 Hz, 1F, F_{para}), -161.93 (m, 2F, F_{meta}). MS (EI⁺, 70 eV): *m/z* (%) 294.1 (4) [M⁺], 220.93 (8), 142.99 (9), 57.07 (100).

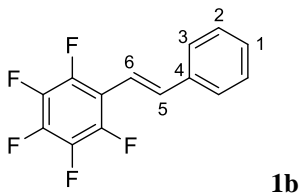


***trans*-2,3,4,5,6-pentafluorostilbene (**1b**).¹⁹**

This compound was obtained as a white solid. Eluent, *n*-hexane:CH₂Cl₂ = 1:1. Yield 57 mg (62 %).

¹H NMR (399.86 MHz, δ , CDCl₃): 7.53 (m, *J* = 7.3 Hz, 2H, H³), 7.41 (d, *J* = 16.7 Hz, 1H, H⁶), 7.37-7.34 (m, 3H, H¹, H²), 6.97 (d, *J* = 16.7 Hz, 1H, H⁵). ¹³C{¹H} NMR (100.62 MHz, δ , CDCl₃): 144.8 (m, ¹J_{C-F} = 250 Hz, C_{ortho}), 139.4 (m, ¹J_{C-F} = 254.3 Hz, C_{para}), 137.2 (m, ¹J_{C-F} = 247.1 Hz, C_{meta}), 137.2 (t, *J*_{C-F} = 8.2 Hz, C⁶), 136.4 (C⁴), 128.9 (C¹), 128.8 (C²), 126.8 (C³), 112.5 (C⁵), 112.3 (td, ²J_{C-F} = 13.4, 4.0 Hz, C_{ipso}). ¹⁹F NMR (376.38 MHz, δ , CDCl₃): -142.79 (m, 2F, F_{ortho}), -156.60 (t, *J* = 19.5 Hz, 1F, F_{para}), -163.01 (m, 2F, F_{meta}). MS (EI⁺, 70 eV): *m/z* (%) 270.01 (24) [M⁺], 250.02 (31), 219.00 (21), 78.06 (30), 51.05 (100).

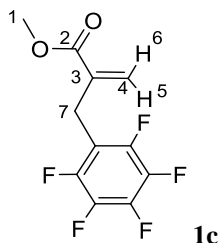
⁹¹ Wu, C-Z.; He, C-Y.; Huang, Y.; Zhang, X. *Org. Lett.* **2013**, *15*, 5266–5269.



Methyl 2,3,4,5,6-pentafluoro- α -methylenebenzenepropenoate (1c).¹⁹

This compound was obtained as a colorless oil. Eluent, *n*-hexane:CH₂Cl₂ = 1:1. Yield 27 mg (30 %) for a reaction conversion of 40 %.

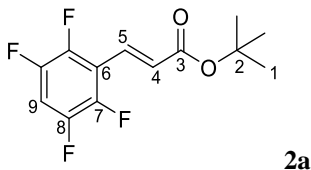
¹H NMR (399.86 MHz, δ , CDCl₃): 6.24 (s, 1H, H⁶), 5.40 (s, 1H, H⁵), 3.73 (s, 3H, H¹), 3.66 (s, 2H, H⁷). ¹³C{¹H} NMR (100.56 MHz, δ , CDCl₃): 166.3 (C²), 145.2 (m, ¹J_{C-F} = 250 Hz, C_{ortho}), 140.5 (d, ¹J_{C-F} = 252 Hz, C_{para}), 137.5 (m, ¹J_{C-F} = 244 Hz, C_{meta}), 135.9 (C³), 126.6 (C⁴), 111.8 (m, C_{ipso}), 52.1 (C¹), 24.8 (t, ³J_{C-F} = 22.1 Hz, C⁷). ¹⁹F NMR (399.19 MHz, δ , CDCl₃): -142.62 (m, 2F, F_{ortho}), -156.48 (t, J = 19.5 Hz, 1F, F_{para}), -162.60 (m, 2F, F_{meta}). MS (EI+, 70 eV): m/z (%) 266.03 (45) [M⁺], 235.05 (23), 207.12 (32), 203.04 (24), 187.05 (100), 59.13 (37).



***tert*-Butyl (2*E*)-3-(2,3,5,6-tetrafluorophenyl)-2-propenoate (2a).**⁹¹

This compound was obtained as a white solid. Eluent, *n*-hexane: CH₂Cl₂ = 1:1. Yield 40 mg (42 %).

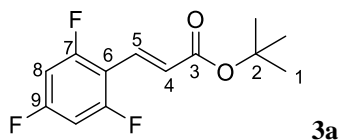
¹H NMR (499.73 MHz, δ , CDCl₃): 7.61 (d, J = 16.4 Hz, 1H, H⁵), 7.07 (m, 1H, H⁹), 6.70 (d, J = 16.4 Hz, 1H, H⁴), 1.54 (s, 9H, H¹). ¹³C{¹H} NMR (125.67 MHz, δ , CDCl₃): 165.3 (C³), 145.7 (m, ¹J_{C-F} = 248.2 Hz, C⁸), 144.9 (m, ¹J_{C-F} = 253.0 Hz, C⁷), 128.6 (t, ⁴J_{C-F} = 8.5 Hz, C⁴), 128.0 (br, C⁵), 115.2 (t, ²J_{C-F} = 13.3 Hz, C⁶), 106.4 (t, ²J_{C-F} = 22.9 Hz, C⁹), 81.4 (C²), 28.0 (C¹). ¹⁹F NMR (470.17 MHz, δ , CDCl₃): -138.98 (m, 2F), -140.52 (m, 2F). MS (EI+, 70 eV): m/z (%) 276.01 (3) [M⁺], 220.97 (44), 202.94 (91), 199.94 (13), 174.99 (33), 154.99 (20), 57.07 (100).



***tert*-Butyl (2*E*)-3-(2,4,6-trifluorophenyl)-2-propenoate (3a).**⁹¹

This compound was obtained as a white solid. Eluent, *n*-hexane:CH₂Cl₂ = 1:3. Yield 52.8 mg (60 %).

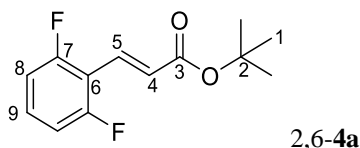
¹H NMR (499.73 MHz, δ, CDCl₃): 7.60 (d, J = 16.5 Hz, 1H, H⁵), 6.72 (t, J = 8.5 Hz, 2H, H⁸), 6.60 (d, J = 16.5 Hz, 1H, H⁴), 1.52 (s, 9H, H¹). ¹³C{¹H} NMR (125.67 MHz, δ, CDCl₃): 166.0 (C³), 162.85 (dt, ¹J_{C-F} = 253.7, 15.6 Hz, C⁹), 161.9 (ddd, ¹J_{C-F} = 256.4, 14.6, 9.8 Hz, C⁷), 128.6 (q, ³J_{C-F} = 1.9 Hz, C⁵), 125.7 (td, J = 8.4, 2.5 Hz, C⁴), 109.3 (td, J = 15.3, 4.9 Hz, C⁶), 100.8 (m, C⁸), 80.8 (C²), 28.1 (C¹). ¹⁹F NMR (470.17 MHz, δ, CDCl₃): -104.60 (quintet, J = 8.3 Hz, 1F, F_{para}), -106.8 (t, J = 8.4 Hz, 2F, F_{ortho}). MS (EI+, 70eV): m/z (%) 258.04 (5) [M⁺], 203.02 (49), 184.99 (100), 157.02 (40), 57.08 (90).

***tert*-Butyl (2*E*)-3-(difluorophenyl)-2-propenoate (4a) from 1,3 difluorobenzene.**¹⁹

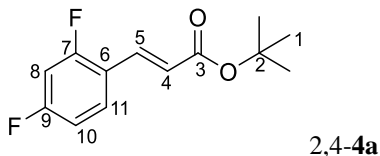
White solid, mixture of two isomers in a ratio 2,6-F₂:2,4-F₂ = 1.5:1. Eluent, *n*-hexane:CH₂Cl₂ = 1:1. Yield 70 mg (85%).

***tert*-Butyl (2*E*)-3-(2,6-difluorophenyl)-2-propenoate (2,6-4a).**¹⁹

¹H NMR (499.73 MHz, δ, CDCl₃): 7.67 (d, J = 16.5 Hz, 1H, H⁵), 7.26 (m, 1H, H⁹), 6.92 (t, J = 8.5 Hz, 2H, H⁸), 6.66 (d, J = 16.5 Hz, 1H, H⁴), 1.53 (s, 9H, H¹). ¹³C{¹H} NMR (125.78 MHz, δ, CDCl₃): 166.1 (C³), 161.6 (m, ¹J_{C-F} = 255 Hz, C⁷), 130.7 (t, ³J_{C-F} = 11.0 Hz, C⁹), 129.5 (t, ³J_{C-F} = 2.1 Hz, C⁵), 126.2 (t, ⁴J_{C-F} = 8.5 Hz, C⁴), 112.6 (t, ²J_{C-F} = 14.8 Hz, C⁶), 111.8 (dd, ²J_{C-F} = 21.2, ⁴J_{C-F} = 5.0 Hz, C⁸), 80.7 (C²), 28.1 (C¹). ¹⁹F NMR (470.17 MHz, δ, CDCl₃): -110.46 (t, J = 7.32 Hz, 2F). MS (EI+, 70 eV): m/z (%) 276.01 (3) [M⁺], 220.97 (44), 202.94 (91), 199.94 (13), 174.99 (33), 154.99 (20), 57.07 (100).

***tert*-Butyl (2*E*)-3-(2,4-difluorophenyl)-2-propenoate (2,4-4a).**¹⁹

¹H NMR (499.73 MHz, δ, CDCl₃): 7.64 (d, J = 16.1 Hz, 1H, H⁵), 7.50 (m, 1H, H¹¹), 6.91 (m, 1H, H¹⁰), 6.85 (m, 1H, H⁸), 6.39 (d, J = 16.1 Hz, 1H, H⁴), 1.53 (s, 9H, H¹). ¹³C{¹H} NMR (125.78 MHz, δ, CDCl₃): 165.9 (C³), 163.6 (dd, ¹J_{C-F} = 275.3, 12.1 Hz, C⁹), 161.5 (dd, ¹J_{C-F} = 278.5, ³J_{C-F} = 11.9 Hz, C⁷), 135.0 (t, ³J_{C-F} = 1.6 Hz, C⁵), 129.9 (dd, ³J_{C-F} = 9.8, 4.5 Hz, C¹¹), 122.5 (dd, ⁴J_{C-F} = 6.5, ⁶J_{C-F} = 2.4 Hz, C⁴), 111.9 (dd, ²J_{C-F} = 21.8, ⁴J_{C-F} = 3.6 Hz, C¹⁰), 104.5 (t, ²J_{C-F} = 25.5 Hz, C⁸), 80.7 (C²), 28.1 (C¹). ¹⁹F NMR (470.17 MHz, δ, CDCl₃): -106.71 (m, J = 7.7 Hz, 1F), -110.22 (m, J = 9.9 Hz, 1F).



General procedure B: Oxidative Heck reaction of arenes using [2,2'-bipyridin]-6(1*H*)-one.

[Pd(OAc)₂] (3.82 mg, 0.017 mmol), [2,2'-bipyridin]-6(1*H*)-one (bipy-6-OH, 2.93 mg, 0.017 mmol) and sodium molybdate dihydrate (8.25 mg, 0.034 mmol) were introduced in a Schlenk tube with a screw cap in an oxygen atmosphere. Then, the arene (1.5 mL), *t*-butyl acrylate (50 μL, 0.341 mmol), dodecane (40 μL, 0.176 mmol) as internal standard, and *N,N*-dimethylacetamide (1.5 mL) were added. Oxygen was bubbled through the mixture (5 min) and the vessel was closed. The mixture was heated in a bath at 120 °C for 6-24 h. The yield of the reaction was checked by ¹⁹F and ¹H NMR of the crude mixture. *N,N*-dimethylacetamide was then removed under vacuum and *n*-hexane was added to the residue to extract the product. The suspension was filtered and the filtrate was evaporated to dryness obtaining an oily residue. Finally, the product was purified by column chromatography using silica gel and a solvent mixture for each product that are specified below.

Isomeric mixtures could not be separated and the ratio of isomers in the isolated product is given below (ratios of isomers in the crude mixture are given in the main text). For some of the complexes, mixtures enriched in one isomer were obtained by column chromatography and their spectra are shown in the selected spectra section.

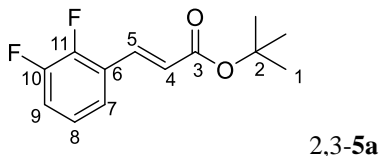
***tert*-Butyl (2*E*)-3-(difluorophenyl)-2-propenoate (5a) from 1,2-difluorobenzene.**⁹²

White solid, mixture of two isomers in a ratio of 2,3-F₂:3,4-F₂ = 1.2:1. Eluent, *n*-hexane: CH₂Cl₂ = 1:1. Yield 61 mg (75 %).

***tert*-Butyl (2*E*)-3-(2,3-difluorophenyl)-2-propenoate (2,3-5a).**⁹²

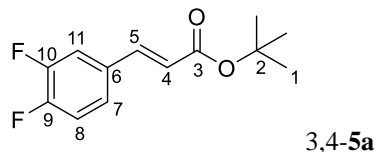
¹H NMR (499.73 MHz, δ, CDCl₃): 7.67 (d, *J* = 16.2 Hz, 1H, H⁵), 7.27 (m, 1H, H⁷), 7.15 (m, 1H, H⁹), 7.07 (m, 1H, H⁸), 6.46 (d, *J* = 16.2 Hz, 1H, H⁴), 1.53 (s, 9H, H¹). ¹³C{¹H} NMR (125.67 MHz, δ, CDCl₃): 165.7 (C³), 150.9 (dd, ¹J_{C-F} = 248.6, ²J_{C-F} = 12.8 Hz C¹⁰), 149.1 (dd, ¹J_{C-F} = 254.8, ²J_{C-F} = 13.3 Hz, C¹¹), 134.9 (t, *J*_{C-F} = 2.9 Hz, C⁶), 134.8 (t, ³J_{C-F} = 2.8 Hz, C⁵), 124.1 (dd, ³J_{C-F} = 6.8, ⁴J_{C-F} = 4.7 Hz, C⁸), 124.0 (d, ⁴J_{C-F} = 6.4 Hz, C⁴), 123.5 (dd, ³J_{C-F} = 3.5, ⁴J_{C-F} = 1.8 Hz, C⁷), 118.1 (d, ²J_{C-F} = 17.5 Hz, C⁹), 80.9 (C²), 28.1 (C¹). ¹⁹F NMR (470.17 MHz, δ, CDCl₃): -137.74 (m, 1F), -140.31 (dt, *J* = 20.0, 6.6 Hz, 1F). MS (EI+, 70 eV): *m/z* (%) 240 (4) [M⁺], 184.98 (58), 166.94 (100), 118.93 (43), 57.07 (89).

⁹² Davies, S. G.; Fletcher, A. M.; Lv, L.; Roberts, P. M.; Thomson, J. E. *Tetrahedron: Asymmetry*, **2012**, *23*, 910–925.



tert-Butyl (2E)-3-(3,4-difluorophenyl)-2-propenoate (3,4-5a).⁹²

¹H NMR (499.73 MHz, δ , CDCl₃): 7.47 (d, J = 16 Hz, 1H, H⁵), 7.32 (m, 1H, H⁷), 7.21 (m, 1H, H⁸), 7.15 (m, 1H, H¹¹), 6.27 (d, J = 16 Hz, 1H, H⁴), 1.53 (s, 9H, H¹). ¹³C{¹H} NMR (125.67 MHz, δ , CDCl₃): 165.7 (C³), 151.2 (dd, ¹J_{C-F} = 252.5, ²J_{C-F} = 13.0 Hz C¹⁰), 150.5 (dd, ¹J_{C-F} = 249.4, ²J_{C-F} = 12.8 Hz, C⁹), 141.0 (t, ⁴J_{C-F} = 1.8 Hz, C⁵), 131.9 (dd, J_{C-F} = 5.7, 3.8 Hz, C⁶), 124.5 (dd, ²J_{C-F} = 6.5, ³J_{C-F} = 3.3 Hz, C⁸), 121.1 (d, ⁵J_{C-F} = 2.4 Hz, C⁴), 117.7 (dd, ²J_{C-F} = 17.7, ³J_{C-F} = 0.7 Hz, C¹¹), 116.1 (dd, J_{C-F} = 17.5, 0.9 Hz, C⁷), 80.9 (C²), 28.1 (C¹). ¹⁹F NMR (470.17 MHz, δ , CDCl₃): -134.85 (m, 1F), -136.88 (m, 1F). MS (EI+, 70 eV): m/z (%) 240 (4) [M⁺], 184.98 (58), 166.94 (100), 118.93 (43), 57.07 (89).

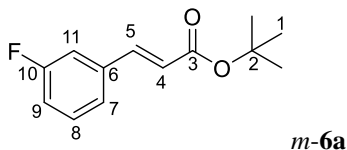


tert-Butyl (2E)-3-(fluorophenyl)-2-propenoate (6a).

Colorless oil, mixture of three isomers in a ratio of o:m:p = 2.8:3.8:1. Eluent, *n*-hexane:CH₂Cl₂ = 1:1. Yield 59 mg (78%).

tert-Butyl (2E)-3-(3-fluorophenyl)-2-propenoate (m-6a).⁹³

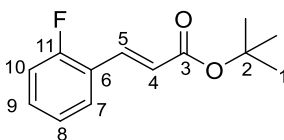
¹H NMR (499.73 MHz, δ , CDCl₃): 7.53 (d, J = 15.9 Hz, 1H, H⁵), 7.26 (d, J = 7.6 Hz, 1H, H⁷), 7.03 (m, 1H, H⁹), 7.14 (td, J = 7.6, 0.9 Hz, 1H, H⁸), 7.17 (m, J = 7.6, 2.0 Hz, 1H, H¹¹), 6.36 (d, J = 15.9 Hz, 1H, H⁴), 1.53 (s, 9H, H¹). ¹³C{¹H} NMR (125.67 MHz, δ , CDCl₃): 165.8 (C³), 162.9 (d, ¹J_{C-F} = 246.7 Hz C¹⁰), 142.0 (d, ⁴J_{C-F} = 2.0 Hz C⁵), 136.9 (d, ³J_{C-F} = 7.6 Hz C⁶), 124.3 (d, ³J_{C-F} = 3.4 Hz C⁸), 123.8 (d, ⁴J_{C-F} = 2.8 Hz C⁷), 121.5 (C⁴), 115.9 (d, ²J_{C-F} = 21.9 Hz C⁹), 114.1 (d, ²J_{C-F} = 21.9 Hz C¹¹), 80.6 (C²), 28.1 (C¹). ¹⁹F NMR (470.17 MHz, δ , CDCl₃): -112.78 (td, J = 9.06, 5.50 Hz, 1F). MS (EI+, 70 eV): m/z (%) 222.04 (6) [M⁺], 166.01 (77), 149.00 (100), 101.02 (37), 57.07 (74).



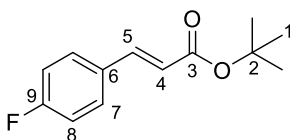
⁹³ Liu, J.; Zhao, Y.; Zhou, Y.; Li, L.; Zhang, T. Y.; Zhang, H. *Org. Biomol. Chem.* **2003**, *1*, 3227–3231.

***tert*-Butyl (2*E*)-3-(2-fluorophenyl)-2-propenoate (*o*-6a).⁹²**

¹H NMR (499.73 MHz, δ , CDCl₃): 7.72 (d, *J* = 16.2 Hz, 1H, H⁵), 7.51 (td, *J* = 7.7, 1.5 Hz, 1H, H⁹), 7.32 (m, 1H, H⁸), 7.13 (td, *J* = 7.7, 1.1 Hz, 1H, H⁷), 7.07 (ddd, *J* = 10.6, 8.2, 1.0 Hz, 1H, H¹⁰), 6.46 (d, *J* = 16.2 Hz, 1H, H⁴), 1.53 (s, 9H, H¹). ¹³C{¹H} NMR (125.67 MHz, δ , CDCl₃): 166.0 (C³), 161.2 (d, ¹J_{C-F} = 253.6 Hz C¹¹), 136.0 (d, ⁴J_{C-F} = 3.0 Hz C⁵), 131.29 (d, ⁴J_{C-F} = 8.5 Hz C⁸), 130.3 (d, ³J_{C-F} = 8.4 Hz C⁹), 128.9 (d, ³J_{C-F} = 3.2 Hz C⁷), 122.7 (d, ⁴J_{C-F} = 6.2 Hz, C⁴), 122.6 (d, ²J_{C-F} = 11.6 Hz C⁶), 116.0 (d, ²J_{C-F} = 22.2 Hz C¹⁰), 80.5 (C²), 28.1 (C¹). ¹⁹F NMR (470.17 MHz, δ , CDCl₃): -114.71 (m, *J* = 11.1, 7.8, 5.5 Hz, 1F). MS (EI+, 70 eV): *m/z* (%) 222.04 (6) [M⁺], 166.01 (77), 149.00 (100), 101.02 (37), 57.07 (74).

*o*-6a***tert*-Butyl (2*E*)-3-(4-fluorophenyl)-2-propenoate (*p*-6a).⁹⁴**

¹H NMR (499.73 MHz, δ , CDCl₃): 7.52 (d, *J* = 15.9 Hz, 1H, H⁵), 7.46 (d, *J* = 7.7 Hz, 2H, H⁸), 7.01 (d, *J* = 7.7 Hz, 2H, H⁷), 6.26 (d, *J* = 15.9 Hz, 1H, H⁴), 1.53 (s, 9H, H¹). ¹³C{¹H} NMR (125.67 MHz, δ , CDCl₃): 166.0 (C³), 163.6 (d, ¹J_{C-F} = 250.5 Hz, C⁹), 142.1 (C⁵), 130.8 (d, ⁴J_{C-F} = 3.3 Hz, C⁶), 129.7 (d, ³J_{C-F} = 8.5 Hz, C⁷), 119.9 (C⁴), 116.7 (d, ²J_{C-F} = 21.4 Hz, C⁸), 80.4 (C²), 28.1 (C¹). ¹⁹F NMR (470.17 MHz, δ , CDCl₃): -110.30 (m, 1F). MS (EI+, 70 eV): *m/z* (%) 222.04 (6) [M⁺], 166.01 (77), 149.00 (100), 101.02 (37), 57.07 (74).

*p*-6a***tert*-Butyl (2*E*)-3-[(trifluoromethyl)phenyl]-2-propenoate (7a).⁶²**

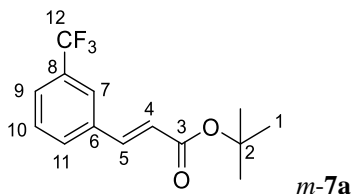
This compound was obtained as a yellow oil, mixture of two isomers in a ratio of *m*:*p* = 3.7:1. Eluent, *n*-hexane:EtOAc = 8:1. Yield 73 mg (79 %).

***tert*-Butyl (2*E*)-3-[3-(trifluoromethyl)phenyl]-2-propenoate (*m*-7a).⁶²**

¹H NMR (399.86 MHz, δ , CDCl₃): 7.73 (s, 1H, H⁷), 7.65 (d, *J* = 7.8 Hz 1H, H¹¹), 7.62 (d, *J* = 7.6 Hz 1H, H⁹), 7.59 (d, *J* = 16 Hz, 1H, H⁵), 7.49 (t, *J* = 7.7 Hz, 1H, H¹⁰), 6.42 (d, *J* = 16 Hz, 1H, H⁴), 1.48 (s, 9H, H¹). ¹³C{¹H} NMR (100.56 MHz, δ , CDCl₃): 165.6 (C³), 141.6 (C⁵), 138.0 (q, *J* = 1.3 Hz, C⁶), 131.4 (q, ²J_{C-F} = 32.3 Hz, C⁸), 130.9 (C¹¹), 129.3 (C¹⁰), 128.0 (C⁵), 125.7 (q, ³J_{C-F} = 3.8 Hz, C⁹), 124.4 (q, ³J_{C-F} = 3.8 Hz, C⁷), 123.8 (q, ¹J_{C-F} = 272.3 Hz, C¹²), 122.1 (C⁴), 80.8 (C²), 28.1 (C¹). ¹⁹F NMR (399.19 MHz, δ ,

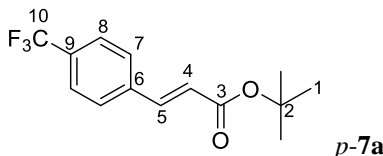
⁹⁴ Zhu, M-K.; Zhao, J-F.; Loh, T-P. *Org. Lett.* **2011**, *13*, 6308–6311.

CDCl₃): -62,75 (s, 3F, CF₃). MS (EI+, 70 eV): m/z (%) 272.06 (6) [M⁺], 217.03 (49), 216.04 (39), 215.00 (38), 199.01 (91), 151.00 (50), 57.07 (100).



tert-Butyl (2E)-3-[4-(trifluoromethyl)phenyl]-2-propenoate (p-7a).⁹⁵

¹H NMR (399.86 MHz, δ, CDCl₃): 7.62-7.57 (m, 5H, H⁸, H⁷, H⁵), 6.43 (d, J = 16 Hz 1H, H⁴), 1.52 (s, 9H, H¹). ¹³C{¹H} NMR (100.56 MHz, δ, CDCl₃): 165.6 (C³), 141.6 (C⁵), 138.0 (C⁶), 131.4 (q, ²J_{C-F} = 32.3 Hz, C⁹), 128.3 (C⁷), 126.3 (q, ³J_{C-F} = 3.7 Hz, C⁸), 123.9 (q, ¹J_{C-F} = 270.6 Hz, C¹⁰), 122.1 (C⁴), 80.9 (C²), 28.1 (C¹). ¹⁹F NMR (399.19 MHz, δ, CDCl₃): -62.67 (s, 3F, CF₃). MS (EI+, 70 eV): m/z (%) 272.06 (6) [M⁺], 217.03 (49), 216.04 (39), 215.00 (38), 199.01 (91), 151.00 (50), 57.07 (100).

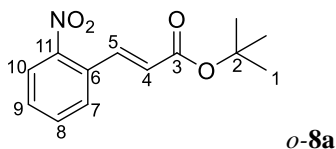


tert-Butyl (2E)-3-(nitrophenyl)-2-propenoate (8a).

This compound was obtained as a yellow oil, mixture of two isomers in a ratio of o:m = 1:3.8. Eluent, hexane: CH₂Cl₂ = 1:1. Yield 51 mg (60 %).

tert-Butyl (2E)-3-(2-nitrophenyl)-2-propenoate (o-8a).⁹⁴

¹H NMR (499.73 MHz, δ, CDCl₃): 8.03 (m, 1H, H¹⁰), 8.00 (d, J = 15.7 Hz, 1H, H⁵), 7.62-7.66 (m, 2H, H⁹, H⁷), 7.49-7.56 (m, 1H, H⁸), 6.29 (d, J = 15.7 Hz, 1H, H⁴), 1.54 (s, 9H, H¹). ¹³C{¹H} NMR (125.67 MHz, δ, CDCl₃): 165.3 (C³), 148.3 (C¹¹), 138.6 (C⁵), 130.7 (C⁶), 130.0 (C⁸), 128.8 (C⁹), 127.3 (C⁷), 125.3 (C⁴), 124.8 (C¹⁰), 81.1 (C²), 28.1 (C¹). MS (EI+, 70 eV): m/z (%) 249.06 (3) [M⁺], 194.01 (32), 176.01 (57), 57.07 (100).



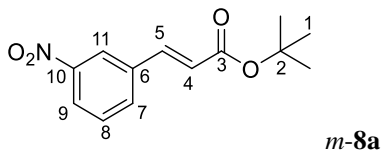
tert-Butyl (2E)-3-(3-nitrophenyl)-2-propenoate (m-8a).⁹⁶

¹H NMR (499.73 MHz, δ, CDCl₃): 8.36 (s, 1H, H¹¹), 8.21 (m, 1H, H⁹), 7.79 (d, J = 7.7 Hz, 1H, H⁷), 7.63 (m, 1H, H⁸), 7.57 (d, J = 16 Hz, 1H, H⁵), 6.48 (d, J = 16 Hz, 1H, H⁴),

⁹⁵ Youn, S. W.; Kim, B. S.; Jagdale, B. A. R. *J. Am. Chem. Soc.* **2012**, *134*, 11308–11311.

⁹⁶ Lakshminarayana, B.; Mahendar, L.; Ghosal, P.; Sreedhar, B.; Satyanarayana, G.; Subrahmanyam, C. *New J. Chem.* **2018**, *42*, 1646–1654.

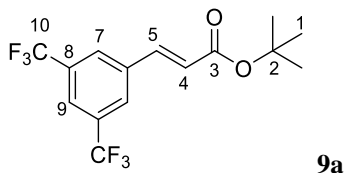
1.54 (s, 9H, H¹). ¹³C{¹H} NMR (125.67 MHz, δ, CDCl₃): 165.3 (C³), 148.6 (C¹⁰), 140.6 (C⁵), 136.4 (C⁶), 133.6 (C⁷), 128.5 (C⁸), 124.1 (C⁹), 123.4 (C⁴), 122.2 (C¹¹), 81.1 (C²), 28.1 (C¹). MS (EI+, 70 eV): m/z (%) 249.06 (3) [M⁺], 194.01 (32), 176.01 (57), 57.07 (100).



***tert*-Butyl (2*E*)-3-(3,5-bis(trifluoromethylphenyl)-2-propenoate (9a).**

This compound was obtained as a colorless oil. Eluent, CH₂Cl₂. Yield 45 mg (40 %).

¹H NMR (499.73 MHz, δ, CDCl₃): 7.91 (s, 2H, H⁷), 7.85 (s, 1H, H⁹), 7.60 (d, J = 16.0 Hz, 1H, H⁵), 6.50 (d, J = 16.0 Hz, 1H, H⁴), 1.54 (s, 9H, H¹). ¹³C{¹H} NMR (125.78 MHz, δ, CDCl₃): 165.0 (C³), 139.7 (C⁵), 132.3 (q, ²J_{C-F} = 33.8 Hz, C⁸), 127.5 (m, C⁷), 124.4 (C⁴), 123.1 (sept, ³J_{C-F} = 3.7 Hz, C⁹), 81.3 (C²), 28.0 (C¹). ¹⁹F NMR (470.17 MHz, δ, CDCl₃): -63.16 (s, 6F). MS (EI+, 70 eV): m/z (%) 339.96 (2) [M⁺], 284.98 (17), 266.93 (50), 57.06 (100).

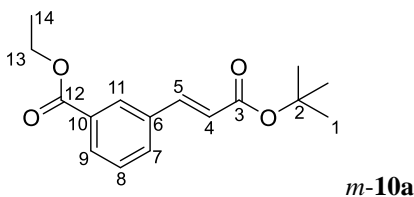


Ethyl (E)-3-(*tert*-butoxy)-3-oxoprop-1-en-1-yl)benzoate (10a).

This compound was obtained as a colorless oil, mixture of two isomers in a ratio of o:m = 1:7. Eluent, hexane:CH₂Cl₂ (3:1). Yield 65 mg (69 %).

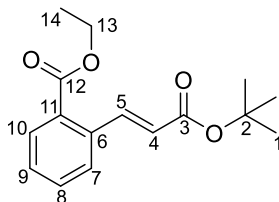
Ethyl (E)-3-(3-(*tert*-butoxy)-3-oxoprop-1-en-1-yl)benzoate (*m*-10a).

¹H NMR (499.73 MHz, δ, CDCl₃): 8.18 (t, J = 1.6 Hz, 1H, H¹¹), 8.02 (dt, J = 7.8, 1.4 Hz, 1H, H⁹), 7.66 (dt, J = 7.7, 1.4 Hz, 1H, H⁷), 7.60 (d, J = 16 Hz, 1H, H⁵), 7.44 (t, J = 7.7 Hz, 1H, H⁸), 6.44 (d, J = 16 Hz, 1H, H⁴), 4.39 (quartet, J = 7.1 Hz, 2H, H¹³), 1.54 (s, 9H, H¹), 1.40 (t, J = 7.1 Hz, 3H, H¹⁴). ¹³C{¹H} NMR (125.67 MHz, δ, CDCl₃): 166.0 (C³), 165.9 (C¹²), 142.3 (C⁵), 136.3 (C⁶), 132.0 (C⁷), 130.7 (C⁹), 130.3 (C¹⁰), 128.9 (C⁸), 128.7 (C¹¹), 121.4 (C⁴), 80.7 (C²), 61.2 (C¹³), 28.1 (C¹), 14.3 (C¹⁴). MS (EI+, 70 eV): m/z (%) 276.03 (3) [M⁺], 220.01 (76), 202.99 (25), 192.00 (32), 175.00 (100), 147.02 (25), 57.07 (94).



Ethyl (*E*)-2-(3-(*tert*-butoxy)-3-oxoprop-1-en-1-yl)benzoate (*o*-10a).

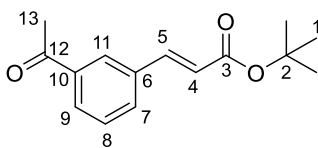
^1H NMR (499.73 MHz, δ , CDCl_3): 8.3 (d, $J = 15.8$ Hz, 1H, H^5), 7.93 (dd, $J = 7.8, 1.3$ Hz, 1H, H^{10}), 7.57 (m, 1H, H^7), 7.50 (td, $J = 7.8, 1.3$ Hz, 1H, H^8), 7.41 (td, $J = 7.5, 1.3$ Hz, 1H, H^9), 6.22 (d, $J = 15.8$ Hz, 1H, H^4), 4.39 (quartet, $J = 7.1$ Hz, 2H, H^{13}), 1.53 (s, 9H, H^1), 1.41 (t, $J = 7.1$ Hz, 3H, H^{14}). $^{13}\text{C}\{^1\text{H}\}$ NMR (125.67 MHz, δ , CDCl_3): 166.9 (C^3), 165.8 (C^{12}), 142.6 (C^5), 138.8 (C^6), 132.0 (C^8), 130.6 (C^{10}), 129.0 (C^{11}), 127.8 (C^7), 127.7 (C^9), 122.8 (C^4), 80.5 (C^2), 61.4 (C^{13}), 28.0 (C^1), 14.2 (C^{14}). MS (EI+, 70 eV): m/z (%) 276.03 (3) [M^+], 220.01 (76), 202.99 (25), 192.00 (32), 175.00 (100), 147.02 (25), 57.07 (94).

***o*-10a*****tert*-Butyl (*2E*)-3-(acetylphenyl)-2-propenoate (**11a**).**

This compound was obtained as a colorless oil, mixture of two isomers in a ratio of *o*:*m*:*p* = 1:2.8:2. Eluent, hexane:EtOAc (2:1). Yield 43 mg (52 %).

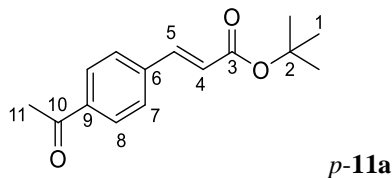
***tert*-Butyl (*2E*)-3-(3-acetylphenyl)-2-propenoate (*m*-11a).⁹⁷**

^1H NMR (499.73 MHz, δ , CDCl_3): 8.08 (t, $J = 1.8$ Hz, 1H, H^{11}), 7.94 (m, 1H, H^7), 7.69 (m, 1H, H^9), 7.60 (d, $J = 16$ Hz, 1H, H^5), 7.48 (t, $J = 7.7$ Hz, 1H, H^8), 6.44 (d, $J = 16$ Hz, 1H, H^4), 2.63 (s, 3H, H^{13}), 1.54 (s, 9H, H^1). $^{13}\text{C}\{^1\text{H}\}$ NMR (125.67 MHz, δ , CDCl_3): 197.5 (C^{12}), 165.8 (C^3), 141.9 (C^5), 137.6 (C^{10}), 135.2 (C^6), 132.1 (C^9), 129.5 (C^7), 129.1 (C^8), 127.5 (C^{11}), 121.6 (C^4), 80.8 (C^2), 28.1 (C^1), 26.6 (C^{13}). MS (EI+, 70 eV): m/z (%) 246.05 (4) [M^+], 190.01 (36), 174.99 (100), 155.00 (23), 57.07 (43).

***m*-11a*****tert*-Butyl (*2E*)-3-(4-acetylphenyl)-2-propenoate (*p*-11a).⁹⁷**

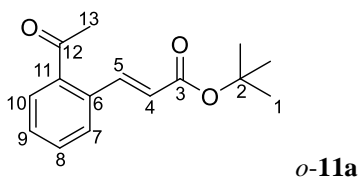
^1H NMR (499.73 MHz, δ , CDCl_3): 7.95 (m, 2H, H^8), 7.60 (m, 2H, H^7), 7.62 (d, $J = 16$ Hz, 1H, H^5), 6.45 (d, $J = 16$ Hz, 1H, H^4), 2.61 (s, 3H, H^{13}), 1.54 (s, 9H, H^1). $^{13}\text{C}\{^1\text{H}\}$ NMR (125.67 MHz, δ , CDCl_3): 197.3 (C^{10}), 165.7 (C^3), 142.2 (C^5), 139.0 (C^6), 135.2 (C^9), 128.8 (C^8), 128.0 (C^7), 122.7 (C^4), 80.9 (C^2), 28.1 (C^1), 26.6 (C^{13}).

⁹⁷ Enquist, P. A.; Lindh, J.; Nilsson, P.; Larhed, M. *Green Chem.* **2006**, *8*, 338–343.



***tert*-Butyl (2*E*)-3-(2-acetylphenyl)-2-propenoate (*o*-11a).⁹⁸**

¹H NMR (499.73 MHz, δ , CDCl₃): 8.04 (d, *J* = 15.8 Hz, 1H, H⁵), 7.71 (dd, *J* = 7.7, 1.4 Hz, 1H, H¹⁰), 7.58 (m, 1H, H⁷), 7.50 (ddd, *J* = 7.6, 1.4, 0.5 Hz, 1H, H⁹), 7.43 (td, *J* = 7.5, 1.4 Hz, 1H, H⁸), 6.21 (d, *J* = 15.8 Hz, 1H, H⁴), 2.61 (s, 3H, H¹³), 1.53 (s, 9H, H¹). ¹³C{¹H} NMR (125.67 MHz, δ , CDCl₃): 200.9 (C¹²), 165.8 (C³), 142.6 (C⁵), 138.3 (C¹¹), 134.9 (C⁶), 129.1 (C⁸), 129.0 (C¹⁰), 128.3 (C⁷), 122.9 (C⁴), 80.5 (C²), 28.1 (C¹), 26.6 (C¹³). MS (EI+, 70 eV): *m/z* (%) 246.05 (4) [M⁺], 190.01 (36), 174.99 (100), 155.00 (23), 57.07 (43).

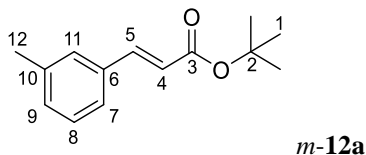


***tert*-Butyl (2*E*)-3-(methylphenyl)-2-propenoate (12a).**

This compound was obtained as a colorless oil, mixture of isomers in a ratio of o:m:p = 1:5.3:2.4. Eluent, hexane: CH₂Cl₂ = 1:1. Yield 51 mg (68 %).

***tert*-Butyl (2*E*)-3-(3-methylphenyl)-2-propenoate (*m*-12a).⁹⁴**

¹H NMR (499.73 MHz, δ , CDCl₃): 7.56 (d, *J* = 15.9 Hz, 1H, H⁵), 7.40 (d, *J* = 7.7 Hz, 1H, H⁷), 7.32 (s, 1H, H¹¹), 7.26 (t, *J* = 7.5 Hz, 1H, H⁸), 7.17 (d, *J* = 7.6 Hz, 1H, H⁹), 6.36 (d, *J* = 15.9 Hz, 1H, H⁴), 2.36 (s, 3H, H¹²), 1.53 (s, 9H, H¹). ¹³C{¹H} NMR (125.67 MHz, δ , CDCl₃): 166.3 (C³), 143.7 (C⁵), 138.4 (C¹⁰), 134.6 (C⁶), 130.7 (C⁹), 128.7 (C⁸), 127.9 (C⁷), 125.1 (C¹¹), 119.9 (C⁴), 80.3 (C²), 28.2 (C¹), 21.3 (C¹²). MS (EI+, 70 eV): *m/z* (%) 218.1 (20) [M⁺], 162.05 (97), 147.03 (100), 115.02 (50), 57.07 (47).

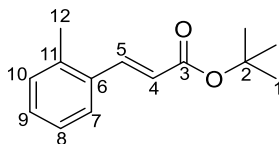


***tert*-Butyl (2*E*)-3-(2-methylphenyl)-2-propenoate (*o*-12a).⁹⁴**

¹H NMR (499.73 MHz, δ , CDCl₃): 7.89 (d, *J* = 15.9 Hz, 1H, H⁵), 7.54 (d, *J* = 8.1 Hz, 1H, H⁷), 7.24-7.28 (m, 1H, H⁸), 7.17 (m, 2H, H⁹, H¹⁰), 6.29 (d, *J* = 15.9 Hz, 1H, H⁴), 2.43 (s, 3H, H¹²), 1.54 (s, 9H, H¹). ¹³C{¹H} NMR (125.67 MHz, δ , CDCl₃): 166.5 (C³), 141.2

⁹⁸ Patureau, F. W.; Besset, T.; Glorius, F. *Angew. Chem. Int. Ed.* **2011**, *50*, 1064–1067.

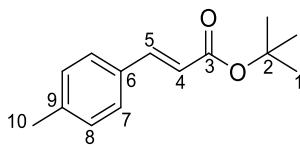
(C⁵), 137.4 (C¹¹), 133.6 (C⁶), 130.7 (C¹⁰), 129.7 (C⁷), 126.3 (C⁹), 126.2 (C⁸), 121.1 (C⁴), 80.2 (C²), 28.2 (C¹), 19.7 (C¹²). MS (EI+, 70 eV): m/z (%) 218.10 (20) [M⁺], 162.05 (97), 147.03 (100), 115.02 (50), 57.07 (47).

***o*-12a**

***tert*-Butyl (2E)-3-(4-methylphenyl)-2-propenoate (*p*-12a).**^{99,94}

¹H NMR (499.73 MHz, δ , CDCl₃): 7.56 (d, J = 15.9 Hz, 1H, H⁵), 7.40 (m, 2H, H⁷), 7.17 (m, 2H, H⁸), 6.33 (d, J = 15.9 Hz, 1H, H⁴), 2.36 (s, 3H, H¹⁰), 1.53 (s, 9H, H¹). ¹³C{¹H} NMR (125.67 MHz, δ , CDCl₃): 166.5 (C³), 143.5 (C⁵), 140.2 (C⁹), 131.9 (C⁶), 129.5 (C⁷), 127.9 (C⁸), 119.1 (C⁴), 80.3 (C²), 28.2 (C¹), 21.3 (C¹⁰). MS (EI+, 70 eV): m/z (%) 218.1 (20) [M⁺], 162.05 (97), 147.03 (100), 115.02 (50), 57.07 (47).

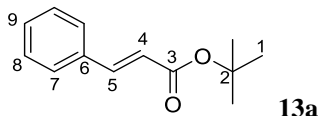
* Most signals are overlapped with the *meta*-isomer. The spectra of the isomeric mixture were compared to a sample of *p*-12a prepared independently *via* a conventional Heck reaction of *p*-bromotoluene and *t*-butyl acrylate.

***p*-12a**

***tert*-Butyl (2E)-3-phenyl-2-propenoate (13a).**⁹⁴

This compound was obtained as a yellow oil. Eluent, hexane: EtOAc = 4:1. Yield 49 mg (70 %).

¹H NMR (499.73 MHz, δ , CDCl₃): 7.59 (d, J = 15.9 Hz, 1H, H⁵), 7.51 (m, 2H, H⁷), 7.36 (m, 3H, H⁸, H⁹), 6.37 (d, J = 15.9 Hz, 1H, H⁴), 1.55 (s, 9H, H¹). ¹³C{¹H} NMR (125.67 MHz, δ , CDCl₃): 166.3 (C³), 143.5 (C⁵), 134.6 (C⁶), 129.9 (C⁹), 128.8 (C⁸), 128.0 (C⁷), 120.2 (C⁴), 80.4 (C²), 28.2 (C¹). MS (EI+, 70 eV): m/z (%) 204.07 (6) [M⁺], 147.01 (100), 131.01 (59), 103.03 (28), 57.07 (70).

**13a**

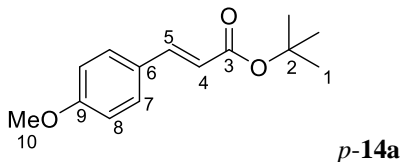
***tert*-Butyl (2E)-3-(methoxyphenyl)-2-propenoate (14a).**

This compound was obtained as a colorless oil, mixture of three isomers in a ratio *o*:*m*:*p* = 1:12:4. Eluent, hexane: CH₂Cl₂ = 1:1. Yield 55 mg (69 %).

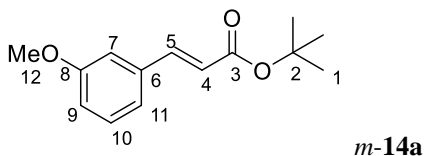
⁹⁹ Jadhav, S. N.; Rode, C. V. *Green Chem.* **2017**, *19*, 5958–5970.

***tert*-Butyl (2E)-3-(4-methoxyphenyl)-2-propenoate (*p*-14a).**⁹⁴

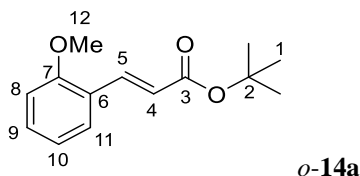
¹H NMR (499.73 MHz, δ , CDCl₃): 7.54 (d, *J* = 15.9 Hz, 1H, H⁵), 7.45 (d, *J* = 8.5 Hz, 2H, H⁷), 6.89 (d, *J* = 8.5 Hz, 2H, H⁸), 6.24 (d, *J* = 15.9 Hz, 1H, H⁴), 3.88 (s, 3H, H¹⁰), 1.51 (s, 9H, H¹). ¹³C{¹H} NMR (125.67 MHz, δ , CDCl₃): 166.6 (C³), 161.1 (C⁹), 143.1 (C⁵), 129.5 (C⁷), 127.4 (C⁶), 117.7 (C⁴), 114.2 (C⁸), 80.2 (C²), 55.3 (C¹⁰), 28.2 (C¹). MS (EI+, 70 eV): *m/z* (%) 234.11 (26) [M⁺], 178.04 (77), 161.05 (44), 147.05 (100), 118.04 (39), 57.07 (46).

***tert*-Butyl (2E)-3-(3-methoxyphenyl)-2-propenoate (*m*-14a).**¹⁰⁰

¹H NMR (499.73 MHz, δ , CDCl₃): 7.55 (d, *J* = 15.9 Hz, 1H, H⁵), 7.28 (m, 1H, H¹⁰), 7.10 (m, 1H, H¹¹), 7.01 (s, 1H, H⁷), 6.91 (m, 1H, H⁹), 6.35 (d, *J* = 15.9 Hz, 1H, H⁴), 3.82 (s, 3H, H¹²), 1.54 (s, 9H, H¹). ¹³C{¹H} NMR (125.67 MHz, δ , CDCl₃): 166.2 (C³), 159.8 (C⁸), 143.4 (C⁵), 129.8 (C¹⁰), 123.7 (C⁶), 120.6 (C¹¹), 120.5 (C⁴), 115.8 (C⁹), 112.7 (C⁷), 80.5 (C²), 55.2 (C¹²), 28.1 (C¹). MS (EI+, 70 eV): *m/z* (%) 234.11 (26) [M⁺], 178.04 (77), 161.05 (44), 147.05 (100), 118.04 (39), 57.07 (46).

***tert*-Butyl (2E)-3-(2-methoxyphenyl)-2-propenoate (*o*-14a).**¹⁰⁰

¹H NMR (499.73 MHz, δ , CDCl₃): 7.91 (d, *J* = 16.1 Hz, 1H, H⁵), 7.49 (dd, *J* = 7.8, 1.3 Hz, 1H, H¹¹), 7.33-7.29 (m, 1H, H⁹), 6.98-6.83 (m, 2H, H¹⁰, H⁸), 6.44 (d, *J* = 16.1 Hz, 1H, H⁴), 3.88 (s, 3H, H¹²), 1.52 (s, 9H, H¹). ¹³C{¹H} NMR (125.67 MHz, δ , CDCl₃): 166.8 (C³), 158.1 (C⁷), 138.9 (C⁵), 136.0 (C⁶), 129.6 (C⁹), 128.7 (C¹¹), 120.7 (C¹⁰), 120.6 (C⁴), 111.0 (C⁸), 80.1 (C²), 55.4 (C¹²), 28.2 (C¹). GC-MS: MS (EI+, 70eV): *m/z* (%) 234.11 (100) [M⁺].

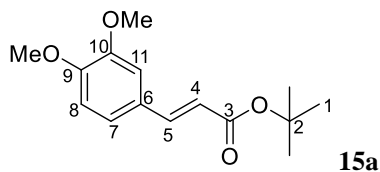


¹⁰⁰ Davies, S. G.; Mulvaney, A. W.; Russell, A. J.; Smith, A. D. *Tetrahedron: Asymmetry*, **2007**, *18*, 1554–1566.

tert-Butyl (2E)-3-(3,4-dimethoxyphenyl)-2-propenoate (15a).⁹³

This compound was obtained as a yellow oil. Eluent, hexane: EtOAc = 4:1. Yield 67 mg (74 %).

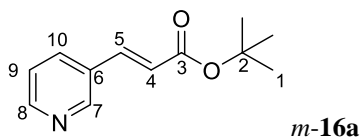
¹H NMR (499.73 MHz, δ , CDCl₃): 7.52 (d, J = 15.9 Hz, 1H, H⁵), 7.07 (d, J = 8.3 Hz 1H, H⁸), 7.03 (d, J = 1.9 Hz, 1H, H¹¹), 6.85 (d, J = 8.3 Hz, 1H, H⁷), 6.24 (d, J = 15.8 Hz, 1H, H⁴), 3.89 (s, OMe, 6H), 1.52 (s, 9H, H¹). ¹³C{¹H} NMR (125.67 MHz, δ , CDCl₃): 166.5 (C³), 150.8 (C¹⁰), 149.1 (C⁹), 143.4 (C⁵), 127.6 (C⁶), 122.4 (C⁷), 117.8 (C⁴), 110.9 (C¹¹), 109.5 (C⁸), 80.2 (C²), 55.8 (OMe), 28.1 (C¹). MS (EI+, 70 eV): m/z (%) 264.12 (21) [M⁺], 208.07 (100), 193.02 (24), 191.06 (24), 57.07 (30).

**tert-Butyl (2E)-3-(pyridinyl)-2-propenoate (16a).**

Colorless oil, mixture of two isomers in a ratio of o:m:p = 1.4:15.5:1. Eluent, AcOEt:hexane = 10:1. Yield 50 mg (70 %).

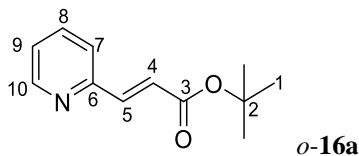
tert-Butyl (2E)-3-(3-pyridinyl)-2-propenoate (m-16a).^{65b}

¹H NMR (499.73 MHz, δ , CDCl₃): 8.69 (d, J = 1.9 Hz, 1H, H⁷), 8.55 (dd, J = 4.8, 1.9 Hz, 1H, H⁸), 7.78 (dt, J = 8.2, 1.9 Hz, 1H, H¹⁰), 7.53 (d, J = 16 Hz, 1H, H⁵), 7.27 (dd, J = 8.2, 4.8 Hz, 1H, H⁹), 6.4 (d, J = 16 Hz, 1H, H⁴), 1.5 (s, 9H, H¹). ¹³C{¹H} NMR (125.67 MHz, δ , CDCl₃): 165.5 (C³), 150.7 (C⁸), 149.5 (C⁷), 139.7 (C⁵), 134.0 (C¹⁰), 130.3 (C⁶), 123.6 (C⁹), 122.3 (C⁴), 80.9 (C²), 28.1 (C¹). MS (EI+, 70 eV): m/z (%) 205.00 (5) [M⁺], 160.07 (35), 150.03 (73), 132.03 (93), 105.05 (47), 57.07 (100).

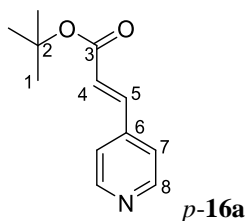
**tert-Butyl (2E)-3-(2-pyridinyl)-2-propenoate (o-16a).**¹⁰¹

¹H NMR (499.73 MHz, δ , CDCl₃): 8.63 (d, J = 4.7 Hz, 1H, H¹⁰), 7.69 (td, J = 7.6, 1.8 Hz, 1H, H⁸), 7.58 (d, J = 15.7 Hz, 1H, H⁵), 7.42 (dt, J = 7.8, 1.0 Hz, 1H, H⁷), 7.24 (ddd, J = 7.6, 4.7, 1.0 Hz, 1H, H⁹), 6.82 (d, J = 15.7 Hz, 1H, H⁴), 1.5 (s, 9H, H¹). ¹³C{¹H} NMR (125.67 MHz, δ , CDCl₃): 165.9 (C³), 153.3 (C⁶), 150.0 (C¹⁰), 142.3 (C⁵), 136.6 (C⁸), 124.4 (C⁴), 123.9 (C⁷), 123.7 (C⁹), 80.7 (C²), 28.1 (C¹). MS (EI+, 70 eV): m/z (%) 205.00 (5) [M⁺], 160.07 (35), 150.03 (73), 132.03 (93), 105.05 (47), 57.07 (100).

¹⁰¹ Li, J.-H.; Wang, D.-P.; Xie, Y.-X.; *Synthesis*, **2005**, *13*, 2193–2197.

***tert*-Butyl (2*E*)-3-(4-pyridinyl)-2-propenoate (*p*-16a).**

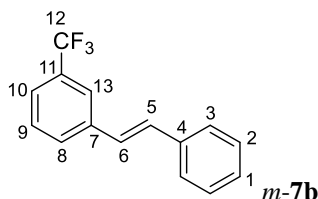
^1H NMR (499.73 MHz, δ , CDCl_3): 8.63 (d, $J = 4.4$ Hz, 2H, H^8), 7.49 (d, $J = 16$ Hz, 1H, H^5), 7.34 (d, $J = 4.4$ Hz, 2H, H^7), 6.52 (d, $J = 16$ Hz, 1H, H^4), 1.5 (s, 9H, H^1). $^{13}\text{C}\{^1\text{H}\}$ NMR (125.67 MHz, δ , CDCl_3): 165.2 (C^3), 150.5 (C^8), 141.9 (C^6), 140.5 (C^5), 124.8 (C^7), 121.7 (C^4), 81.2 (C^2), 28.1 (C^1). MS (EI+, 70 eV): m/z (%) 205.00 (5) [M^+], 160.07 (35), 150.03 (73), 132.03 (93), 105.05 (47), 57.07 (100).

**(*E*)-(Trifluoromethyl)stilbene (7b).**

White solid, mixture of two isomers in a ratio $m:p = 1.8:1$. Eluent, *n*-hexane. Yield 58 mg (68 %).

(*E*)-3-(Trifluoromethyl)stilbene (*m*-7b).¹⁰²

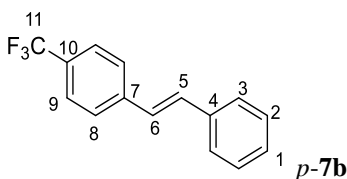
^1H NMR (499.73 MHz, δ , CDCl_3): 7.76 (s, 1H, H^{13}), 7.68 (d, $J = 7.50$ Hz, 1H, H^8), 7.56-7.45 (m, 4H, H^{10} , H^9 , H^3), 7.39 (t, $J = 7.5$ Hz, 2H, H^2), 7.3 (m, 1H, H^1), 7.19 (m, AB system, $J = 16.3$ Hz, 1H, H^6), 7.13 (m, AB system, $J = 16.3$ Hz, 1H, H^5). $^{13}\text{C}\{^1\text{H}\}$ NMR (125.67 MHz, δ , CDCl_3): 138.1 (C^7), 136.6 (C^4), 131.2 (q, $^2J_{\text{C-F}} = 32.0$ Hz, C^{11}), 130.5 (C^6), 129.5 (C^8), 128.7 (C^2), 128.1 (C^1), 127.0 (C^5), 126.7 (C^3), 125.6 (q, $^4J_{\text{C-F}} = 4.0$ Hz, C^9), 124.1 (d, $^1J_{\text{C-F}} = 272.4$ Hz, C^{12}), 124.0 (q, $^3J_{\text{C-F}} = 3.8$ Hz, C^{10}), 123.0 (q, $^3J_{\text{C-F}} = 3.8$ Hz, C^{13}). ^{19}F NMR (470.17 MHz, δ , CDCl_3): -62.79 (s, 3F). MS (EI+, 70 eV): m/z (%) 248.02 (93) [M^+], 179.04 (100), 178.03 (86).



¹⁰² Sore, H. F.; Boehner, C. M.; MacDonald, S. J. F.; Norton, D.; Fox, D. J.; Spring, D. R. *Org. Biomol. Chem.* **2009**, *7*, 1068–1072.

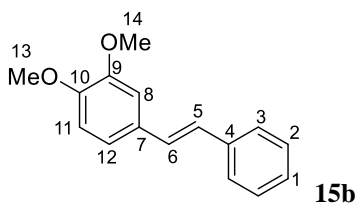
(E)-4-(Trifluoromethyl)stilbene (p-7b).¹⁰³

¹H NMR (499.73 MHz, δ , CDCl₃): 7.6 (m, 4H, H⁸, H⁹), 7.53 (m, 2H, H³), 7.39 (m, 2H, H²), 7.3 (m, 1H, H¹), 7.2 (m, AB system, $J = 16.4$ Hz, 1H, H⁶), 7.12 (m, AB system, $J = 16.4$ Hz, 1H, H⁵). ¹³C{¹H} NMR (125.67 MHz, δ , CDCl₃): 140.8 (C⁴), 140.6 (C⁷), 136.2 (C⁶), 132.1 (q, ²J_{C-F} = 32.0 Hz, C¹⁰), 128.8 (C²), 128.6 (C³), 128.2 (C¹), 127.2 (C⁵), 126.5 (C⁸), 125.6 (q, ⁴J_{C-F} = 4.0 Hz C⁹), 124.1 (d, ¹J_{C-F} = 272.4 Hz C¹¹). ¹⁹F NMR (470.17 MHz, δ , CDCl₃): -62.48 (s, 3F). MS (EI+, 70 eV): m/z (%) 248.02 (93) [M⁺], 179.04 (100), 178.03 (86).

**trans-3,4-Dimethoxystilbene (15b).**⁹³

This compound was obtained as a white solid. Eluent, AcOEt:hexane = 1:5. Yield 53 mg (70 %).

¹H NMR (499.73 MHz, δ , CDCl₃): 7.51 (d, $J = 7.7$ Hz, 2H, H³), 7.34 (t, $J = 7.6$ Hz, 2H, H²), 7.24 (t, $J = 7.4$ Hz, 1H, H¹), 7.06 (m, 2H, H⁸, H¹²), 7.04 (m, AB system, $J = 16.3$ Hz, 1H, H⁶), 6.99 (m, AB system, $J = 16.3$ Hz, 1H, H⁵), 6.86 (d, $J = 8.1$ Hz, 1H, H¹¹), 3.96 (s, 3H, H¹⁴), 3.91 (s, 3H, H¹³). ¹³C{¹H} NMR (125.67 MHz, δ , CDCl₃): 149.1 (C⁹), 148.9 (C¹⁰), 137.5 (C⁴), 130.4 (C⁷), 128.6 (C²), 128.4 (C¹²), 127.3 (C¹), 126.8 (C⁵), 126.2 (C³), 119.8 (C⁶), 111.2 (C¹¹), 108.7 (C⁸), 55.9 (C¹⁴), 55.8 (C¹³). MS (EI+, 70 eV): m/z (%) 240.03 (100) [M⁺], 224.95 (36), 165.04 (44).

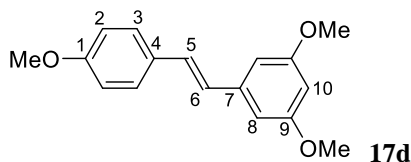
**trans-Trimethoxyresveratrol (17d).**¹⁰⁴

This compound was obtained as a white solid. Eluent, CH₂Cl₂:hexane = 1:1. Yield 66 mg (72 %).

¹H NMR (499.73 MHz, δ , CDCl₃): 7.45 (d, $J = 8.6$ Hz, 2H, H³), 7.04 (d, $J = 16.2$ Hz, 1H, H⁶), 6.91 (d, $J = 16.2$ Hz, 1H, H⁵), 6.90 (d, $J = 8.6$ Hz, 2H, H²), 6.66 (d, $J = 2.3$ Hz, 2H, H⁸), 6.38 (t, $J = 2.3$ Hz, 1H, H¹⁰), 3.83 (s, 9H, OMe). ¹³C{¹H} NMR (125.67 MHz, δ , CDCl₃): 160.9 (C⁹), 159.4 (C¹), 139.7 (C⁷), 129.9 (C⁴), 128.7 (C⁶), 127.8 (C³), 126.5 (C⁵), 114.1 (C²), 104.3 (C⁸), 99.6 (C¹⁰), 55.3 (C, OMe). MS (EI+, 70 eV): m/z (%) 270.08 (100) [M⁺], 239.08 (21).

¹⁰³ Liu, J.; Liu, H.; Wang, L. *Appl. Organomet. Chem.* **2010**, *24*, 386–391.

¹⁰⁴ Borate, H. B.; Dumbre, D. K.; Wakharkar, R. D.; Choudhary, V. R. *J. Chem. Res.* **2008**, 495–499.



2.4.4 Additional catalytic experiments and test reactions

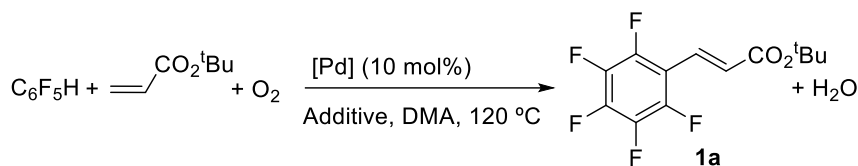


Table 2.5 Additional screening experiments for the reaction shown in Equation 2.6.^a

Entry	[Pd]	Additive (equiv)	T (°C)	C ₆ F ₅ H:acrylate (mol ratio)	1a , Crude yield (%), 6 h ^b
1	[Pd(OAc) ₂]	Na ₂ MoO ₄ ·2H ₂ O (0.1)	120	2.5:1	99
2	[Pd(OAc) ₂]	Na ₂ MoO ₄ anhydrous (0.1)	120	2.5:1	80
3	[Pd(OAc) ₂]	Na ₂ MoO ₄ ·2H ₂ O (0.1) + H ₂ O (1)	120	2.5:1	88
4	[Pd(OAc) ₂]	NaOAc anhydrous (0.1)	120	2.5:1	61
5	[Pd(OAc) ₂]	NaOAc·3H ₂ O (0.1)	120	2.5:1	51
6	[Pd(OAc) ₂]	KOAc anhydrous (0.1)	120	2.5:1	54
7	[PdCl ₂ (NCMe) ₂]	Na ₂ MoO ₄ ·2H ₂ O (0.1)	120	2.5:1	30
8	[PdCl ₂ (NCMe) ₂]	Na ₂ MoO ₄ ·2H ₂ O (0.3)	120	2.5:1	51
9	[PdCl ₂ (NCMe) ₂]	Na ₂ MoO ₄ ·2H ₂ O (0.1) + NaOAc 3H ₂ O (0.2)	120	2.5:1	68
10	[Pd(acac) ₂]	Na ₂ MoO ₄ ·2H ₂ O (0.1)	120	2.5:1	23
11	[Pd(TFA) ₂]	Na ₂ MoO ₄ ·2H ₂ O (0.1)	120	2.5:1	11
12	[Pd(OAc) ₂]	Na ₂ MoO ₄ ·2H ₂ O (0.1)	90	2.5:1	81
13	[Pd(OAc) ₂]	Na ₂ MoO ₄ ·2H ₂ O (0.1)	60	2.5:1	27
14	[Pd(OAc) ₂]	Na ₂ MoO ₄ ·2H ₂ O (0.1)	60	5:1	26
15	[Pd(OAc) ₂]	Na ₂ MoO ₄ ·2H ₂ O (0.1)	60	2.5:2	16

^a Reaction conditions: [Pd] (0.034 mmol, 10 mol %), *t*-butyl acrylate (0.341 mmol), DMA (3 mL total volume), 120 °C, O₂ (1 atm). ^b Crude yields were determined by ¹H NMR using dodecane as internal standard.

Table 2.6 Effect of the use of the ligand bipy-6-OH for the aerobic alkenylation of different arenes with *t*-butyl acrylate.^a

Entry	Ligand	Arene	Cpd.	Crude yield, %		Isomer distribution ^c
				6 h ^b	24 h ^b	
1 ^d	bipy-6-OH	C ₆ F ₅ H	1a	0	0	
2 ^d	–	C ₆ F ₅ H	1a	86	90	
3 ^d	bipy-6-OH	1,3-C ₆ F ₂ H ₄	3a	13	18	2,6-F ₂ :2,4-F ₂ =1:1.4
4 ^d	–	1,3-C ₆ F ₂ H ₄	3a	46	46	2,6-F ₂ :2,4-F ₂ =1.6:1
5	bipy-6-OH	1,2-C ₆ F ₂ H ₄	5a	60	86	2,3-F ₂ :3,4-F ₂ =1.8:1
6	–	1,2-C ₆ F ₂ H ₄	5a	20	28	2,3-F ₂ :3,4-F ₂ =3.3:1
7	bipy-6-OH	PhF	6a	75	87	<i>o</i> : <i>m</i> : <i>p</i> = 2.8:3.8:1
8	–	PhF	6a	18	18	<i>o</i> : <i>m</i> : <i>p</i> = 5.5:1:1
9	bipy-6-OH	PhCF ₃	7a	72	90	<i>o</i> : <i>m</i> : <i>p</i> = 0:3.7:1
10	–	Ph-CF ₃	7a	40	40	<i>o</i> : <i>m</i> : <i>p</i> = 0:1.8:1
11	bipy-6-OH	PhMe	12a	40	75	<i>o</i> : <i>m</i> : <i>p</i> = 1:5.3:2.4
12	–	PhMe	12a	47	47	<i>o</i> : <i>m</i> : <i>p</i> = 1:1:0.8
13 ^e	bipy-6-OH	1,2-(OMe) ₂ -C ₆ H ₄	15a	73	91	
14 ^e	–	1,2-(OMe) ₂ -C ₆ H ₄	15a	26	32	
15 ^{e,f}	bipy-6-OH	1,3-(OMe) ₂ -C ₆ H ₄	17d	56	86	
16 ^{e,f}	–	1,3-(OMe) ₂ -C ₆ H ₄	17d	0	0	

^a Reaction conditions: [Pd(OAc)₂] (0.017 mmol, 5 mol %), Na₂MoO₄·2H₂O (0.034 mmol, 10 mol%), alkene (0.341 mmol), Arene:DMA = 1:1 v/v (total volume, 3 mL), O₂ (1 atm), 120 °C, unless otherwise noted.^b Crude yields were determined by ¹H NMR using dodecane as internal standard. Yields refer to the mixture of isomers.^c Molar ratio of isomers; only one isomer was found for blank cells. ^d Arene:alkene = 2.5:1 mol ratio.^e [Pd(OAc)₂] (10 mol%), L (10 mol%), 130 °C. ^f 4-methoxy styrene instead of *t*-butyl acrylate.

Test on the ability of molybdate to behave as oxidation mediator

Conditions for thioanisole oxidation: Na₂MoO₄·2H₂O (0.034 mmol), [Pd(OAc)₂] (0.034 mmol), thioanisole (100 μL, 0.85 mmol), DMA (0.5 mL), 1 atm O₂, 120 °C, dodecane (5 μL, 0.022 mmol) as internal standard. The crude reaction mixture was checked by ¹H NMR.

Conditions for hydroquinone oxidation: Na₂MoO₄·2H₂O (48.4 mg, 0.2 mmol), hydroquinone (220.2 mg, 2.0 mmol), acetic acid (10 mL), 1 atm O₂, 60 °C, 4 h. The crude reaction mixture was checked by ¹H NMR.

Qualitative experiments for the detection of H₂O₂ in the formation of **1a**

[Pd(OAc)₂] (7.65 mg, 0.034 mmol), and a base (0.034 mmol) were introduced in a Schlenk tube with a screw cap in an oxygen atmosphere. Then, C₆F₅H (94 μL, 0.853 mmol), *t*-butyl acrylate (50 μL, 0.341 mmol), dodecane (40 μL, 0.176 mmol) as internal standard and *N,N*-dimethylacetamide (3 mL) were added. Oxygen was bubbled through the mixture for 5 min and the vessel was closed. The mixture was heated in a bath at 120 °C.

The formation of hydrogen peroxide was tested by taking aliquots at 30- and 60-min reaction times and adding them to 10 mL of a saturated aqueous NaHCO_3 solution containing 0.25 mL of a 0.07 M $\text{CoSO}_4 \cdot 7\text{H}_2\text{O}$ (aq) solution. The presence of hydrogen peroxide in the crude mixture was detected by the color change of the initial solution (pinkish) to an intense green.¹⁰⁵

As shown in Figure 2.4, the experiments show the clear formation of H_2O_2 when the base used is NaOAc . Hydrogen peroxide was not detected when Na_2MoO_4 was used but it is known that this salt catalyzes the disproportionation reaction of H_2O_2 and therefore a fast decomposition in the reaction conditions could account for the absence of this oxygen reduction byproduct.^{74, 106}

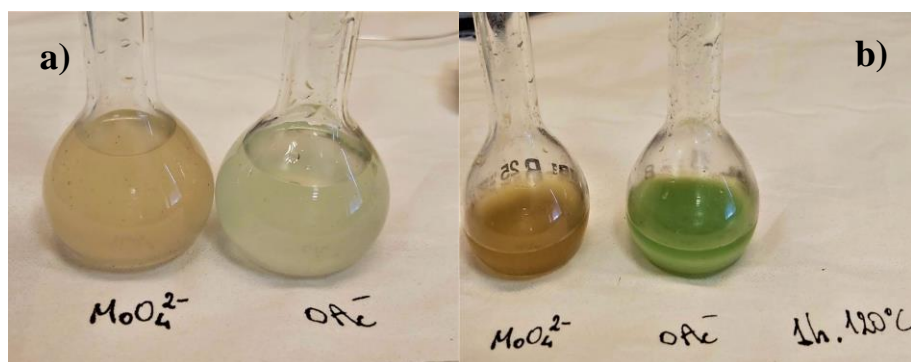
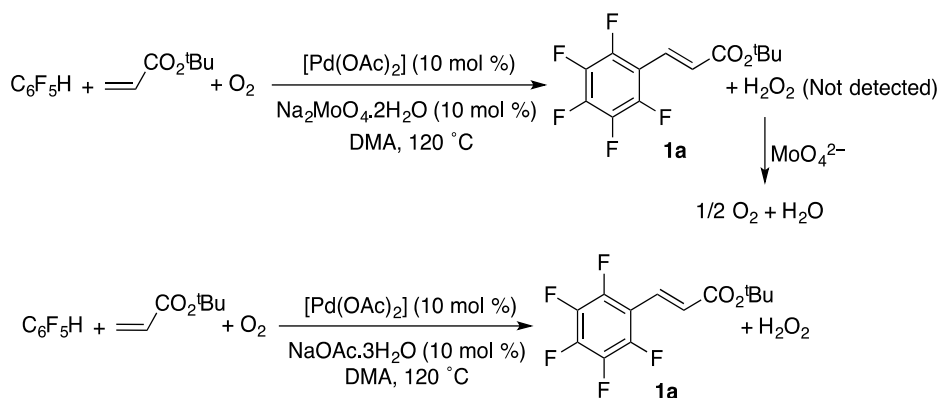


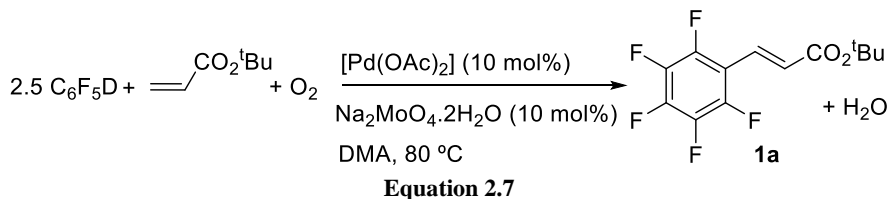
Figure 2.4 Qualitative detection of H_2O_2 in the oxidative Heck reaction of $\text{C}_6\text{F}_5\text{H}$ in the presence of different additive bases. **a)** reaction time 30 min; **b)** reaction time 60 min.

¹⁰⁵ Belhatche, D.; Symons, J. M. *Journal AWWA*, **1991**, *83*, 70–73.

¹⁰⁶ Aubry, J. M. *J. Am. Chem. Soc.* **1985**, *107*, 5844–5849.

2.4.5 Mechanistic experiments

Follow up of the oxidative Heck reaction of C₆F₅D



In an NMR tube equipped with a J. Young-stopcock and filled with oxygen, [Pd(OAc)₂] (1.02 mg, 0.0045 mmol) and Na₂MoO₄·2H₂O (1.1 mg, 0.0045 mmol) were added. C₆F₅D (12.5 μL, 0.112 mmol), *t*-butyl acrylate (6.7 μL, 0.045 mmol), DMA (0.5 mL), dodecane as an internal standard (5 μL, 0.022 mmol) and a sealed glass capillary filled with (CD₃)₂SO as an NMR reference were added. Finally, oxygen was bubbled through the resulting solution for 30 seconds at room temperature. The NMR tube was closed and shaken just before its introduction in the NMR probe, previously thermostated at 80 °C. The change in the concentration of *t*-butyl acrylate, C₆F₅H and product (**1a**) (by the integration of the corresponding signals) was used to obtain the kinetic time courses (Figure 2.1). The reaction was followed for 15 h with data collected every 5 minutes. The disappearance of the acrylate is faster than the formation of the Heck product in the first two hours (see Figure 2.1). This indicates a competitive reaction route for the alkene. This was also observed by monitoring the reaction shown in Equation 2.7 without C₆F₅D in the same conditions described above (Figure 2.5). No new alkene was formed suggesting a possible polymerization pathway (see for example: Albéniz, A. C.; Espinet, P.; López-Fernández, R. *Organometallics* **2003**, *22*, 4206-4212).

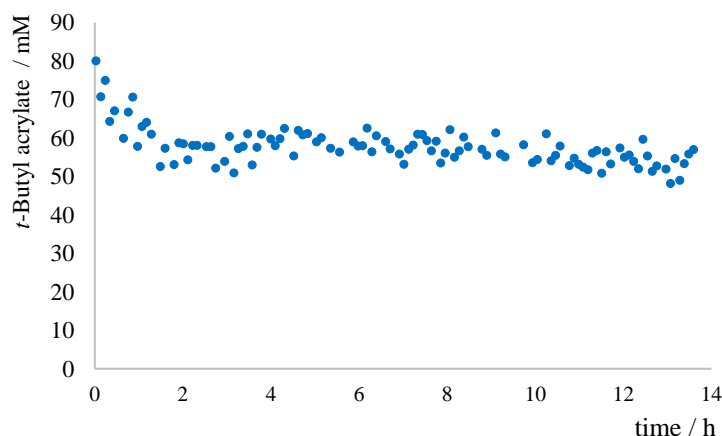


Figure 2.5 Kinetic time course of the evolution of *t*-butyl acrylate in the absence of C₆F₅D.

Kinetic experiments

Kinetic experiments for the oxidative Heck reaction of pentafluorobenzene

In an NMR tube equipped with a J. Young-stopcock and filled with oxygen, [Pd(OAc)₂] and sodium molybdate dihydrate were added. C₆F₅H, *t*-butyl acrylate, dodecane as an internal standard, *N,N*-dimethylacetamide (0.5 mL) and a capillary filled with deuterated DMSO as an NMR reference were added (see concentration in Table 2.7). Finally, oxygen was bubbled through the resulting solution for 30 seconds at room temperature. The NMR tube was closed and shaken just before its introduction in the NMR probe, previously thermostated at 80 °C (353 K). The changes in the concentration of *t*-butyl acrylate, C₆F₅H and product (**1a**) were determined by the integration of the corresponding signals.

The *variable time normalization analysis* (VTNA) reported by Burés,¹⁰⁷ was used to determine the order on the reactants of the catalytic reaction. Four experiments were performed each time varying one of the reagent's initial concentrations (Table 2.7). The resulting plots are represented in Figure 2.6. The oxygen concentration is limited by the solubility of the gas in *N,N*-dimethylacetamide and was calculated from the values in the literature.²³ Enough oxygen in the closed Young-NMR tube is available for a complete reaction provided the diffusion into the solution is effective.

Table 2.7 Initial concentration values for the kinetic experiments on the oxidative Heck reaction of C₆F₅H.

Experiment	[Olefin] / M	[Arene] / M	[cat] / M	[O ₂] / M
1	0.090	0.224	0.009	0.0054
2	0.090	0.448	0.009	0.0054
3	0.180	0.224	0.009	0.0054
4	0.090	0.224	0.027	0.0054

¹⁰⁷ a) Burés, J. *Angew. Chem. Int. Ed.* **2016**, *55*, 16084–16087. b) Burés, J. *Angew. Chem. Int. Ed.* **2016**, *55*, 2028–2031.

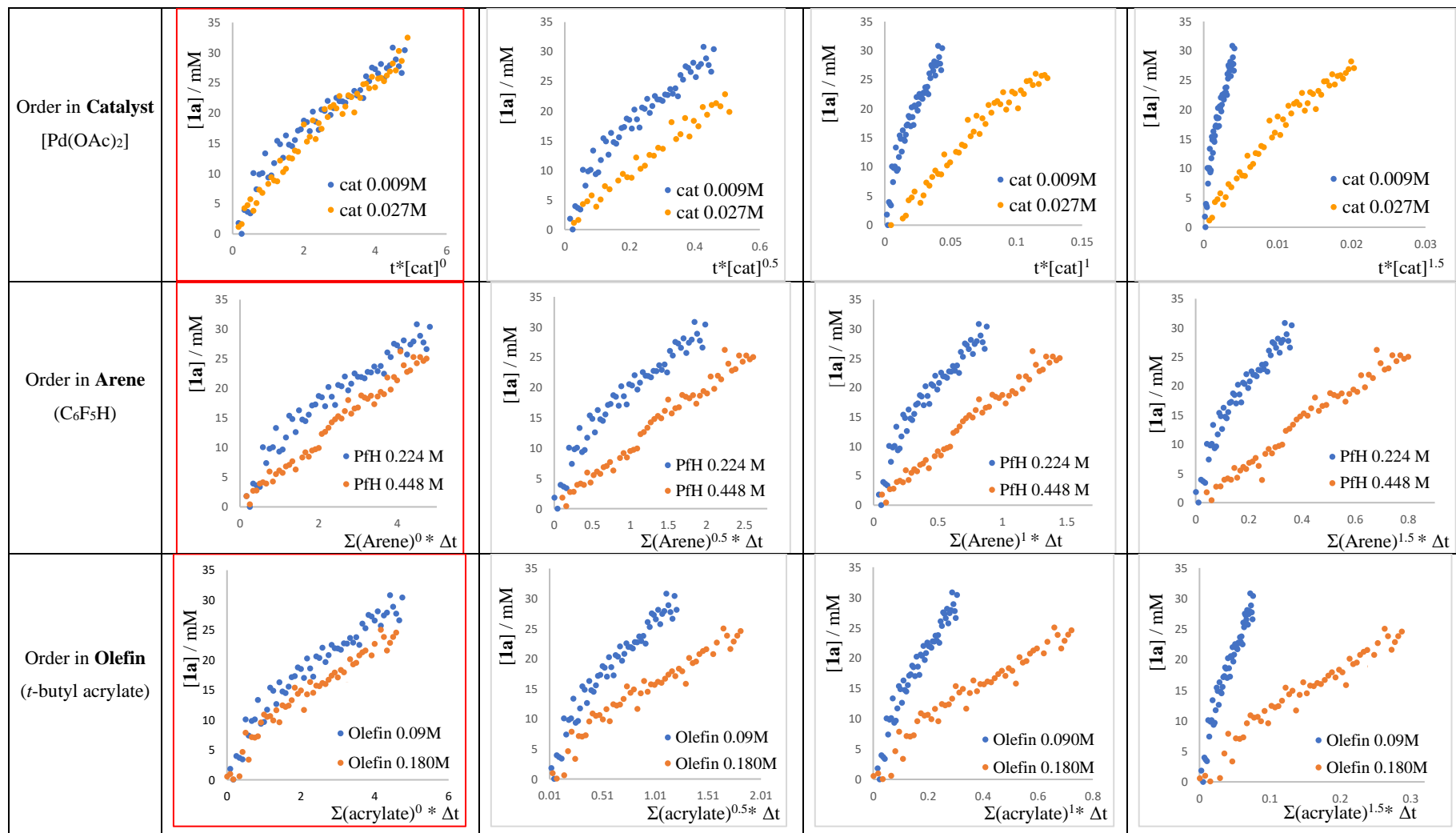


Figure 2.6 Plots derived from the variable time normalization analysis (VTNA). Overlay of plots from two different experiments gives the order in the reagent whose initial concentration is changed (power value in abscissa axis).

2.4.6 Kinetic experiments for the oxidative Heck reaction of toluene

General procedure for the determination of the KIE

Two Schlenk flasks equipped with a screw cap and a Teflon stirring bar were charged with $[\text{Pd}(\text{OAc})_2]$ (3.82 mg, 0.017 mmol) sodium molybdate dihydrate (8.25 mg, 0.034 mmol) and [2,2'-bipyridin]-6(1*H*)-one (2.93 mg, 0.017 mmol) in an oxygen atmosphere. *t*-Butyl acrylate (50 μL , 0.341 mmol), DMA (1.5 mL) and dodecane (40 μL , 0.176 mmol) as an internal standard were added to each flask. Then, toluene- d_8 (1.5 mL) was added to one flask and toluene (1.5 mL) to the other. The Schlenk flasks were placed in a pre-heated oil bath at 120 $^\circ\text{C}$ with constant stirring. The reactions were monitored by taking aliquots at different reaction times and analyzing them by ^1H NMR using a sealed glass capillary filled with $\text{DMSO-}d_8$ as NMR reference. The concentration of the product was determined by integration of the distinct olefin proton signals of the product and those of the internal standard.

The KIE ($k_{\text{obs}(\text{toluene})}/k_{\text{obs}(\text{toluene-}d_8)}$) was determined by comparing the initial rates for the reactions of toluene and toluene- d_8 in independent experiments (Figure 2.7).

The mean value of KIE for two determinations at different initial concentrations (KIE = 2.36 and KIE = 1.97, Figure 2.7) is KIE = 2.2 ± 0.2 .

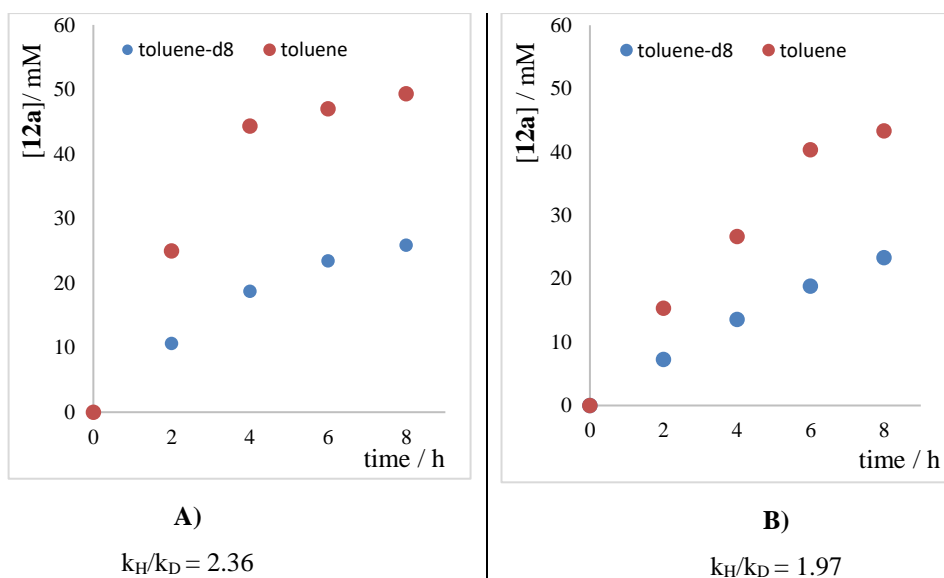


Figure 2.7 Concentration time-plots for the oxidative Heck reaction of toluene and toluene- d_8 carried out in separate flasks. A) Initial concentrations $[\text{Pd}(\text{OAc})_2] = 4.7$ mM, $[\text{acrylate}] = 94.7$ mM, $[\text{arene}] = 3.92$ M; $k_{\text{obs}(\text{toluene})} = 11.1$ mM h^{-1} , $k_{\text{obs}(\text{toluene-}d_8)} = 4.7$ mM h^{-1} . B) Initial concentrations $[\text{Pd}(\text{OAc})_2] = 2.3$ mM, $[\text{acrylate}] = 47$ mM, $[\text{arene}] = 3.92$ M; $k_{\text{obs}(\text{toluene})} = 5.6$ mM h^{-1} , $k_{\text{obs}(\text{toluene-}d_8)} = 2.8$ mM h^{-1} .

The KIE determination in the absence of cooperating ligand was carried out in the same way as described above but without the addition of bipy-6-OH. The value found was KIE = 3.6.

Additional kinetic experiments

Following the same procedure described above for the determination of the KIE, the initial k_{obs} were determined for two reactions at different initial concentrations of *t*-butyl acrylate or palladium acetate showing that the reaction is independent on the concentration of the olefin and first order in the catalyst (Table 2.8).

Table 2.8 Initial rate constants for several kinetic experiments on the oxidative Heck reaction of toluene.

Entry	[Olefin] ₀ (mM)	[Arene] ₀ (M)	[Pd(OAc) ₂] ₀ (mM)	[O ₂] (mM)	k_{obs} (mM/h)
1	94.7	3.92	4.72	6.0	11.1
2	47.3	3.92	4.72	6.0	11.3
3	47.3	3.92	2.36	6.0	5.6

H/D exchange experiments

[Pd(OAc)₂] (3.82 mg, 0.017 mmol), [2,2'-bipyridin]-6(*H*)-one (bipy-6-OH, 2.93 mg, 0.017 mmol) and sodium molybdate dihydrate (8.25 mg, 0.034 mmol) were introduced in a Schlenk tube with a screw cap in an oxygen atmosphere. Then, the arene (fluorobenzene) (1.5 mL), *t*-butyl acrylate (50 μ L, 0.341 mmol), dodecane (40 μ L, 0.176 mmol) as internal standard, and *N,N*-dimethylacetamide (1.5 mL) and D₂O (6.2 μ L, 0.341 mmol) were added. Oxygen was bubbled through the mixture (5 min) and the vessel was closed. The mixture was heated in a bath at 120 °C for 5 h. The crude reaction mixture was checked by ¹⁹F and ¹H NMR. *N,N*-dimethylacetamide was then removed under vacuum and *n*-hexane was added to the residue to extract the product. The suspension was filtered and the filtrate was evaporated to dryness obtaining an oily residue. This residue was analyzed by NMR and GC-MS showing the same product mixture described above for **12a** and **6a**. The ²H NMR spectra showed no deuterated products.

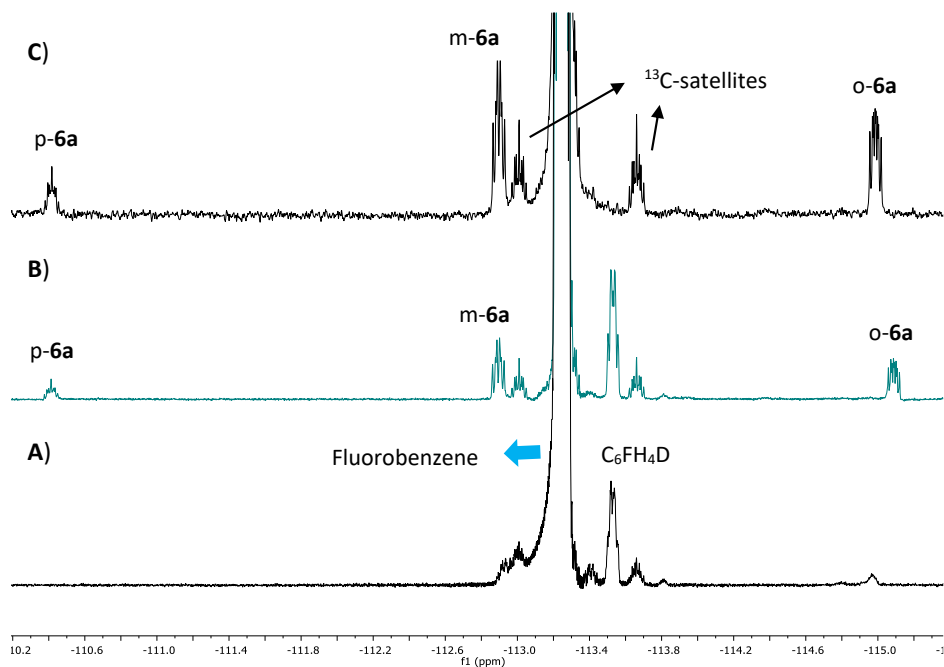
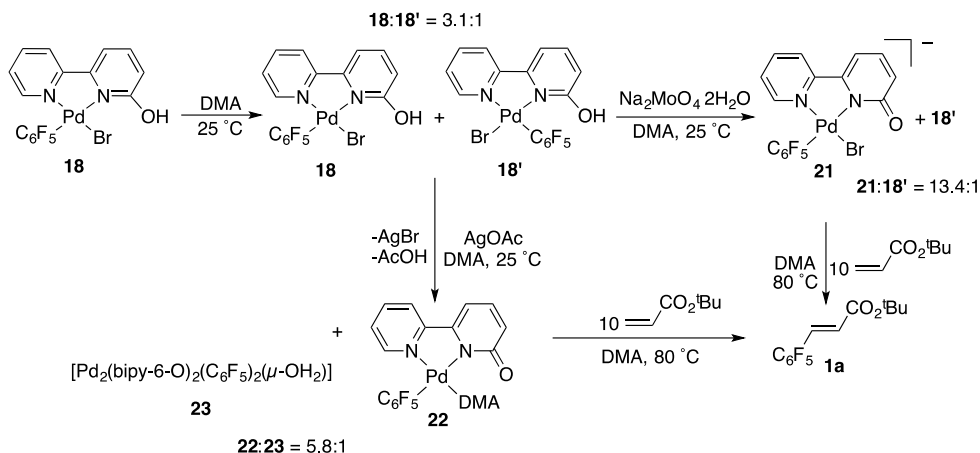


Figure 2.8 ^{19}F NMR (399.19 MHz, CDCl_3) of the crude mixture of several reactions of $\text{C}_6\text{H}_5\text{F}$: **A)** reaction carried out in the same way described above in the absence of *t*-butyl acrylate. The presence of $\text{C}_6\text{H}_4\text{DF}$ is observed and this deuteration can occur in the absence of Pd (see ref.81). **B)** Alkenylation reaction with D_2O as additive. **C)** Alkenylation reaction without D_2O as additive. (o; *ortho*), (p; *para*), (m; *meta*).

Stoichiometric reactions of pentafluorophenyl palladium complexes and *t*-butyl acrylate

Reactions of bipy-6-OH complexes

[Pd(bipy-6-OH)Br(C_6F_5)] (**18**, 0.0068 mmol) and 0.6 mL of *N,N*-dimethylacetamide were added into an NMR tube along with a sealed glass capillary filled with $(\text{CD}_3)_2\text{SO}$ as an NMR reference. The corresponding additive in equimolar amount (0.0068 mmol) was added and the mixture was monitored by ^1H and ^{19}F NMR at 25 °C. The identified complexes are depicted in Scheme 2.11. Then, *t*-butyl acrylate (10 μL , 0.068 mmol) and C_6F_6 (5 μL as internal standard) were added to the NMR tube and the mixture was monitored at 80 °C (Scheme 2.11).



Scheme 2.11 Species formed *in situ* from complex [Pd(bipy-6-OH)(Br)(C₆F₅)] (**18**) and their reactions with *t*-butyl acrylate to give **1a** (see Figure 2.9).

The spectroscopic data of the identified palladium species in DMA with (CD₃)₂SO capillary as an NMR reference are given below:

18: ¹H NMR (499.73 MHz, δ, DMA/(CD₃)₂SO capillary): 13.40 (s, broad, OH), 9.30 (d, J = 5.24 Hz, 1H), 8.55 (d, J = 8.21 Hz, 1H), 8.21 (t, J = 7.03 Hz, 1H), 8.08 (d, J = 7.55 Hz, 1H), 8.01 (t, J = 7.88 Hz, 1H), 7.71 (t, J = 6.42 Hz, 1H), 6.97 (d, J = 8.21 Hz, 1H). ¹⁹F NMR (470.17 MHz, 25 °C, δ, DMA/(CD₃)₂SO capillary): -119.30 (m, 2F, F_{ortho}), -166.50 (t, J = 20.2 Hz, 1F, F_{para}), -168.30 (m, 2F, F_{meta}).

18': ¹H NMR (499.73 MHz, δ, DMA/(CD₃)₂SO capillary): 10.90 (s, broad, 1H, OH), 8.66 (d, J = 7.83 Hz, 1H), 8.27 (t, J = 7.87 Hz, 1H), 8.2 (1H), 8.14 (t, J = 7.87 Hz, 1H), 7.81 (d, J = 5.21 Hz, 1H), 7.53 (t, J = 6.68 Hz, 1H), 7.09 (d, J = 8.25 Hz, 1H). ¹⁹F NMR (470.17 MHz, 25 °C, δ, DMA/(CD₃)₂SO capillary): -119.51 (m, 2F, F_{ortho}), -161.70 (t, J = 19.8 Hz, 1F, F_{para}), -164.41 (m, 2F, F_{meta}). The structure of **18'** in Scheme 2.11 is tentatively assigned.

21: ¹H NMR (499.73 MHz, δ, DMA/(CD₃)₂SO capillary): 9.26 (dd, J = 5.57, 1.18 Hz, 1H), 8.32 (dd, J = 7.92, 3.12 Hz, 1H), 8.08 (t, J = 7.70 Hz, 1H), 7.56 (m, 1H), 7.50-7.38 (m, 2H), 6.09 (m, 1H). ¹⁹F NMR (470.17 MHz, 25 °C, δ, DMA/(CD₃)₂SO capillary): -118.81 (m, 2F, F_{ortho}), -167.90 (t, J = 20.2 Hz, 1F, F_{para}), -169.04 (m, 2F, F_{meta}).

The identity of complex **21** was checked independently by dissolving the isolated complex (NBu₄)[PdBr(bipy-6-O)(C₆F₅)] in DMA.

E-1a: ¹H NMR (499.73 MHz, δ, DMA/(CD₃)₂SO capillary): 7.37 (d, J = 16.35 Hz, 1H), 6.52 (d, J = 16.35 Hz, 1H). ¹⁹F NMR (470.17 MHz, 25 °C, δ, DMA/(CD₃)₂SO capillary): -141.81 (m, 2F, F_{ortho}), -154.05 (t, J = 19.9 Hz, 1F, F_{para}), -164.06 (m, 2F, F_{meta}).

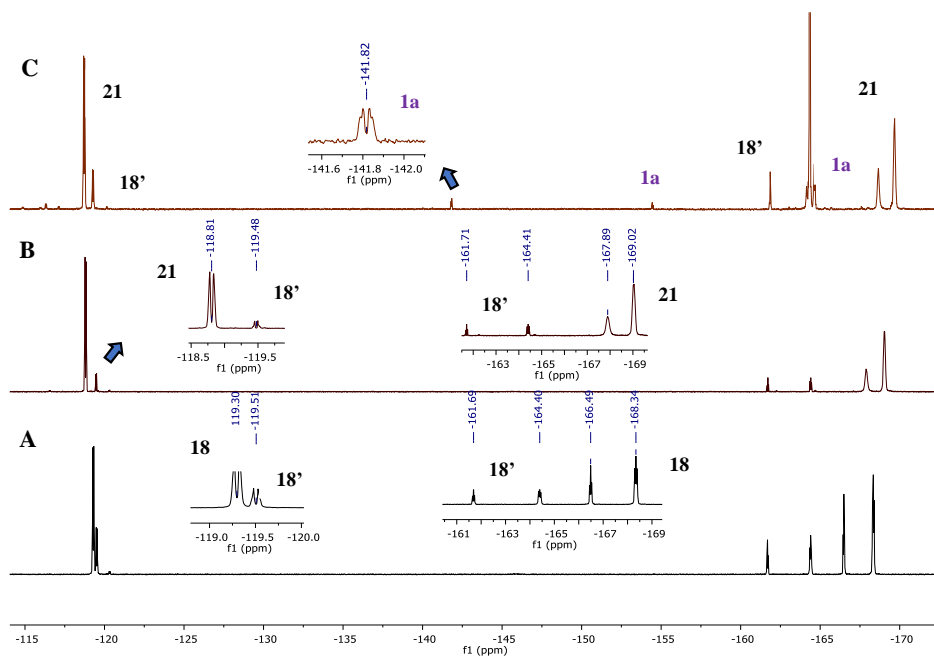


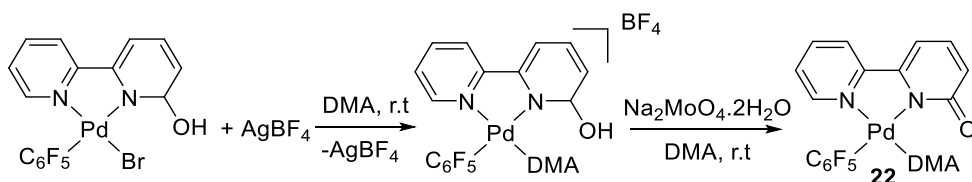
Figure 2.9 ^{19}F NMR spectra (470.17 MHz) of: **A**) the mixture of **18** and **18'** in DMA at room temperature. **B**) The mixture in **A**) upon addition of the sodium molybdate at room temperature. **C**) The mixture in **B**) upon addition of *t*-butyl acrylate. Formation of **1a** at 80 °C, 10 min.

22: ^1H NMR (499.73 MHz, δ , DMA/ $(\text{CD}_3)_2\text{SO}$ capillary): 8.37 (d, $J = 8.09$ Hz, 1H), 8.11 (t, $J = 7.90$ Hz, 1H), 7.88 (d, $J = 5.68$ Hz, 1H), 7.51 (dd, $J = 8.7, 5.7$ Hz, 1H), 7.36 (m, 2H), 6.33 (d, $J = 8.63$ Hz, 1H). ^{19}F NMR (470.17 MHz, 25 °C, δ , DMA/ $(\text{CD}_3)_2\text{SO}$ capillary): -118.80 (m, 2F, F_{ortho}), -162.25 (t, $J = 19.7$ Hz, 1F, F_{para}), -164.69 (m, 2F, F_{meta}).

23: ^{19}F NMR (470.17 MHz, 25 °C, δ , DMA/ $(\text{CD}_3)_2\text{SO}$ capillary): -114.73 (m, 2F, F_{ortho}), -114.12 (m, 2F, $F_{\text{ortho}'}$), -162.15 (t, $J = 19.8$ Hz, 1F, F_{para}), -165.56 (m, 2F, F_{meta}).

The identity of complex **23** was checked independently by comparing the spectrum with that of a solution in DMA of an authentic sample prepared as described before.^{52b}

Complex **22** was also prepared *in situ* by dissolving $[\text{PdBr}(\text{bipy-6-OH})(\text{C}_6\text{F}_5)]$ in DMA in presence of an equimolecular amount of AgBF_4 and sodium molybdate dihydrate (Scheme 2.12).



Scheme 2.12 Alternative formation in solution of complex **22**.

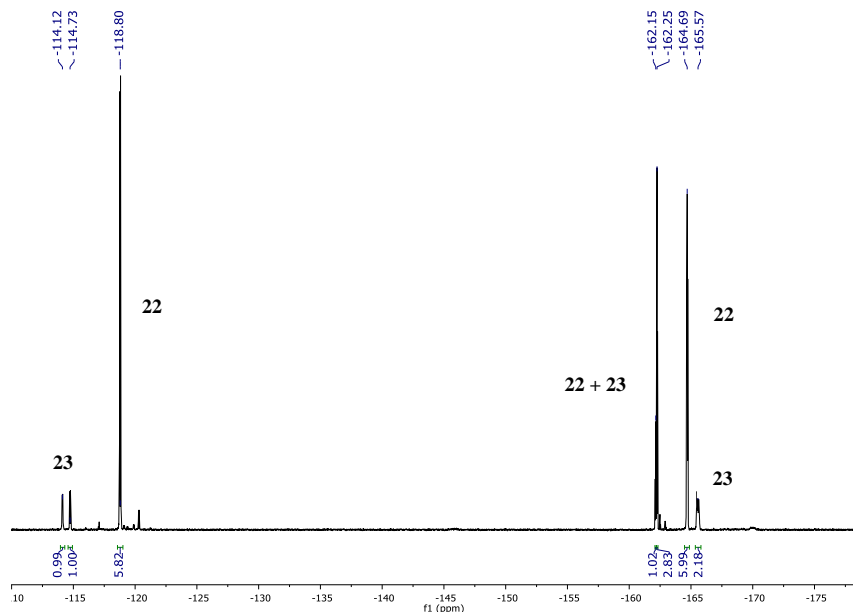
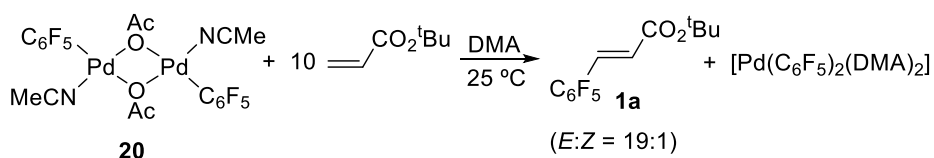


Figure 2.10 ^{19}F NMR (470.17 MHz) spectrum of complexes **22** and **23** formed by treatment of the mixture **18** and **18'** with AgOAc in DMA at room temperature (Scheme 2.12).

Reaction of the acetato complex **20**

$[\text{Pd}_2(\mu\text{-OAc})_2(\text{C}_6\text{F}_5)_2(\text{NCMe})_2]$ (**20**, 0.0034 mmol), *t*-butyl acrylate (10 μL , 0.068 mmol), C_6F_6 (5 μL as internal standard) and 0.6 mL of *N,N*-dimethylacetamide were added into an NMR tube along with a sealed glass capillary filled with $(\text{CD}_3)_2\text{SO}$ as an NMR reference. The mixture was monitored at 25 $^\circ\text{C}$ (Equation 2.8 and Figure 2.11).



Equation 2.8

The spectroscopic data of the identified palladium-species in DMA with $(\text{CD}_3)_2\text{SO}$ capillary as an NMR internal standard are given below:

$[\text{Pd}(\text{C}_6\text{F}_5)_2(\text{DMA})_2]$: ^{19}F NMR (470.17 MHz, 25 $^\circ\text{C}$, δ , DMA/ $(\text{CD}_3)_2\text{SO}$ capillary): -116.38 (m, 2F, F_{ortho}), -163.55 (t, $J = 20$ Hz, 1F, F_{para}), -166.19 (m, 2F, F_{meta}).

Z-**1a**: ^{19}F NMR (470.17 MHz, 25 $^\circ\text{C}$, δ , DMA/ $(\text{CD}_3)_2\text{SO}$ capillary): -140.74 (m, 2F, F_{ortho}), -157.09 (t, $J = 21$ Hz, 1F, F_{para}), -165.28 (m, 2F, F_{meta}).

The identity of $[\text{Pd}(\text{C}_6\text{F}_5)_2(\text{DMA})_2]$ was confirmed independently by dissolving $(\text{NBu}_4)_2[\text{Pd}_2(\mu\text{-Br})_2(\text{C}_6\text{F}_5)_4]$ in DMA in presence of AgBF_4 (Pd:Ag = 1:1 mol ratio).

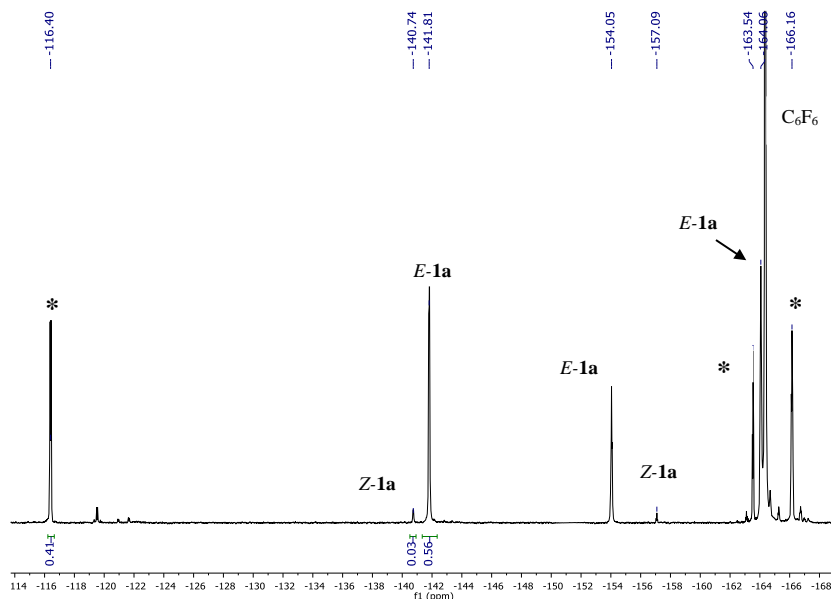


Figure 2.11 ^{19}F NMR (470.17 MHz) of the reaction shown in Equation 2.8 after 10 min at room temperature. The formation of the oxidative Heck product (*E*-**1a** and *Z*-**1a**) and $[\text{Pd}(\text{C}_6\text{F}_5)_2(\text{DMA})_2]$ (*) can be observed.

2.4.7 Computational details

All calculations were initially performed using the DFT approach with the M06 functional,^{108,109} using Gaussian09 as program package.¹¹⁰ The selected basis set was 6-31+G(d) for C, O, N and H^{111,112}, and LANL2TZ(f) for Pd^{113,114} (Basis set I). Solvation

¹⁰⁸ Zhao, Y.; Truhlar, D. G. *J. Chem. Phys.* **2006**, *125*, 194101–194118.

¹⁰⁹ Zhao, Y.; Truhlar, D. G. *Theor. Chem. Acc.* **2006**, *120*, 215–241.

¹¹⁰ Gaussian 09, Revision D.01, Frisch, M. J.; Trucks, G. W.; Schlegel, H. B.; Scuseria, G. E.; Robb, M. A.; Cheeseman, J. R.; Scalmani, G.; Barone, V.; Mennucci, B.; Petersson, G. A.; Nakatsuji, H.; Caricato, M.; Li, X.; Hratchian, H. P.; Izmaylov, A. F.; Bloino, J.; Zheng, G.; Sonnenberg, J. L.; Hada, M.; Ehara, M.; Toyota, K.; Fukuda, R.; Hasegawa, J.; Ishida, M.; Nakajima, T.; Honda, Y.; Kitao, O.; Nakai, H.; Vreven, T.; Montgomery, J. A., Jr.; Peralta, J. E.; Ogliaro, F.; Bearpark, M.; Heyd, J. J.; Brothers, E.; Kudin, K. N.; Staroverov, V. N.; Kobayashi, R.; Normand, J.; Raghavachari, K.; Rendell, A.; Burant, J. C.; Iyengar, S. S.; Tomasi, J.; Cossi, M.; Rega, N.; Millam, J. M.; Klene, M.; Knox, J. E.; Cross, J. B.; Bakken, V.; Adamo, C.; Jaramillo, J.; Gomperts, R.; Stratmann, R. E.; Yazyev, O.; Austin, A. J.; Cammi, R.; Pomelli, C.; Ochterski, J. W.; Martin, R. L.; Morokuma, K.; Zakrzewski, V. G.; Voth, G. A.; Salvador, P.; Dannenberg, J. J.; Dapprich, S.; Daniels, A. D.; Farkas, Ö.; Foresman, J. B.; Ortiz, J. V.; Cioslowski, J.; Fox, D. J. Gaussian, Inc., Wallingford CT, 2009.

¹¹¹ Francl, M. M.; Petro, W. J.; Hehre, W. J.; Binkley, J. S.; Gordon, M. S.; DeFrees, D. J.; Pople, J. A. *J. Chem. Phys.* **1982**, *77*, 3654–3665.

¹¹² Clark, T.; Chandrasekhar, J.; Schleyer, P. V. R. *J. Comput. Chem.* **1983**, *4*, 294–301.

¹¹³ Ehlers, A. W.; Böhme, M.; Dapprich, S.; Gobbi, A.; Höllwarth, A.; Jonas, V.; Köhler, K. F.; Stegmann, R.; Veldkamp, A.; Frenking, G. *Chem. Phys. Lett.* **1993**, *208*, 111–114.

¹¹⁴ Roy, L. E.; Hay, P. J.; Martin, R. L. *J. Chem. Theory Comput.* **2008**, *4*, 1029–1031.

was introduced in all the optimizations, frequency calculations and potential energy refinement through the SMD model, where we applied the solvent *N,N*-dimethylformamide ($\epsilon = 37.219$). All geometry optimizations were carried out in solution with no symmetry restrictions. Free energy corrections were calculated at 393.15 K and 10^5 Pa pressure, including zero-point energy corrections (ZPE), and the energies were converted to 1M standard state in solution (adding/subtracting 1.89 kcal/mol for non-unimolecular processes). Vibrational frequency calculations were performed to establish the stationary points were minima (without imaginary frequencies) or transition states (with one imaginary frequency). Connectivity of the transition state structures were confirmed by relaxing the transition state geometry towards both the reactant and the product. Final potential energies were refined by performing additional single-point energy calculations (also in solution), Pd was still described with LANL2TZ(f) basis set, and the remaining atoms were treated with 6-311++G(d,p) basis set (Basis set II). All reported energies in the manuscript correspond to Gibbs energies in solution, obtained from potential energies (including solvation) with basis set II plus Gibbs energy corrections with basis set I and are given in kcal mol⁻¹ (see SCF energy and free energy correction values in *Supporting information*).

2.4.8 Data for X-Ray structure determinations

The crystal suitable for X-ray analyses was obtained by slow diffusion of *n*-hexane layered onto a solution of the complex in CH₂Cl₂ at -28 °C. The crystal was attached to the tip of a glass fiber and transferred to an Agilent Supernova diffractometer with an Atlas CCD area detector. Data collection was performed with Mo K α radiation (0.71073 Å) at 298 K. Data integration and empirical absorption correction was carried out using the CrysAlisPro program package.¹¹⁵ The structure was solved by direct methods and refined by full-matrix least squares against F² with SHELX,¹¹⁶ in OLEX2.¹¹⁷ The non-hydrogen atoms were refined anisotropically and hydrogen atoms were constrained to ideal geometries and refined with fixed isotropic displacement parameters. Refinement proceeded smoothly to give the residuals shown in Table 2.9.

Three independent molecules were found in the asymmetric unit for **20**.

¹¹⁵ CrysAlisPro Software system, version 1.171.33.51, 2009, Oxford Diffraction Ltd, Oxford, UK.

¹¹⁶ Sheldrick, G. M. *Acta Crystallogr. Sect. C* **2015**, *71*, 3–8.

¹¹⁷ Dolomanov, O. V; Bourhis, L. J.; Gildea, R. J.; Howard, J. A. K.; Puschmann, H. *J. Appl. Crystallogr.* **2009**, *42*, 339–341.

Table 2.9 Crystal data and structure refinement parameters for complex **20**.

Compound number	20
Empirical formula	C ₆₀ H ₃₆ F ₃₀ N ₆ O ₁₂ Pd ₆
Formula weight	2241.35
Temperature/K	298
Crystal system	monoclinic
Space group	I2/a
a/Å	19.9447(7)
b/Å	16.0542(5)
c/Å	47.4558(18)
α /°	90
β /°	100.807(4)
γ /°	90
Volume/Å ³	14925.7(9)
Z	8
$\rho_{\text{calc}}/\text{cm}^3$	1.995
μ/mm^{-1}	1.550
F(000)	8640.0
Crystal size/mm ³	0.518 × 0.301 × 0.177
Radiation	MoK α (λ = 0.71073)
2 θ range for data collection/°	6.736 to 59.558
Index ranges	-27 ≤ h ≤ 20, -20 ≤ k ≤ 22, -40 ≤ l ≤ 64
Reflections collected	32341
Independent reflections	17522 [R _{int} = 0.0368, R _{sigma} = 0.0623]
Data/restraints/parameters	17522/0/1039
Goodness-of-fit on F ²	1.040
Final R indexes [I >= 2 σ (I)]	R ₁ = 0.0494, wR ₂ = 0.1148
Final R indexes [all data]	R ₁ = 0.0838, wR ₂ = 0.1356
Largest diff. peak/hole / e Å ⁻³	0.73/-0.85

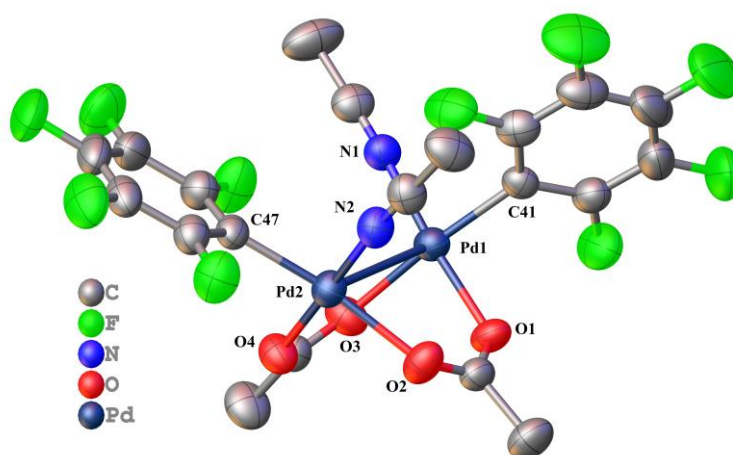
**Figure 2.12** X-ray molecular structure of **20** (ORTEP 40% probability ellipsoids). Hydrogen atoms are omitted for clarity.

Table 2.10 Selected bond lengths (Å) and angles (°) for complex **20** (for numbering scheme see Figure 2.12).

Pd(1)-Pd(2)	3.0941(5)	O(1)-Pd(1)-O(3)	89.82(15)
Pd(1)-O(1)	2.006(4)	C(41)-Pd(1)-N(1)	90.39(19)
Pd(1)-O(3)	2.097(4)	O(12)-Pd(2)-O(2)	90.67(15)
Pd(1)-N(1)	2.097(4)	N(2)-Pd(2)-C(47)	90.64(19)
Pd(1)-C(41)	1.984(5)		
Pd(2)-O(4)	1.998(3)		
Pd(2)-O(2)	2.100(4)		
Pd(2)-N(2)	1.977(5)		
Pd(2)-C(47)	1.980(5)		

Chapter 3

3. Shedding Light on the Precatalytic Mixture of [Pd(OAc)₂] and Cooperating Pyridone-Type Ligands for the C-H Activation of Arenes

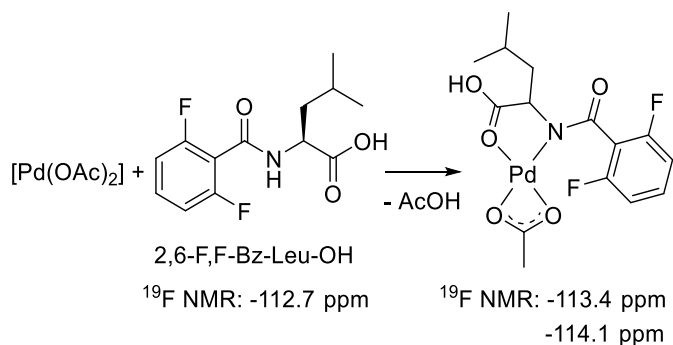
3.1 INTRODUCTION

As stated in *Chapter 1*, addressing C-H functionalization reactions of unactivated carbon-hydrogen bonds is extremely important and great advances have been done over the last decades. This enables the direct use of the raw materials with no necessity of prefunctionalization, saving time-consuming synthetic steps and increasing the atom-economy of the whole process.

In this regard, the use of cooperating ligands is often necessary and among them, [2,2'-bipyridin]-6(1*H*)-one (bipy-6-OH) and 1,10-phenanthrolin-2(1*H*)-one (phen-2-OH), have been developed by our group. These bipyridone ligands have demonstrated the accelerating effect in the directing-group-free (non-chelate assisted) C-H activation of arenes and heteroarenes (pyridine) with arylhalides.⁵² Furthermore, these cooperating ligands give rise to excellent functional group tolerance in aerobic oxidative conditions as it has been shown in the alkenylation of simple arenes using oxygen as the sole oxidant described in *Chapter 2*.¹¹⁸

¹¹⁸ Villalba, F.; Albéniz, A. C. *Adv. Synth. Catal.* **2021**, *363*, 4795–4804.

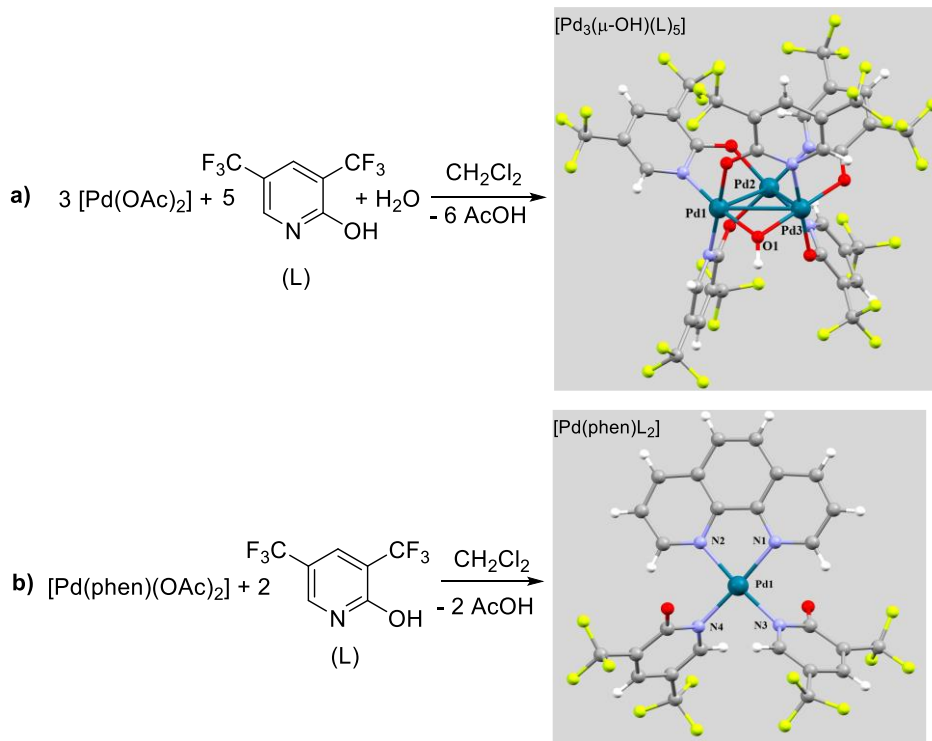
For most Pd-catalyzed reactions which involve cooperating ligands, the use of a mixture of $[\text{Pd}(\text{OAc})_2]$ or other Pd-accessible salts and the ligand or ligands is widely used. While some of the fundamental steps involved in the catalytic cycles are well established, detailed information about the intermediate species formed from these starting mixtures, almost always in an off-cycle step, is still scarce. This is important because the formation of the actual catalytically active species might be slow and it can result in inconvenient induction periods or even produce inactive metal species. Only a few examples of how several cooperating ligands interact with $[\text{Pd}(\text{OAc})_2]$ have been reported by experimental studies. A collaboration among the groups of Yu, Musaev and Blackmond revealed, by ^{19}F NMR, the interaction between the $[\text{Pd}(\text{OAc})_2]$ and the ligand 2,6-F₂-Bz-Leu-OH and they proposed the rapid and quantitative deprotonation of the -NH coordinated to palladium to form the monomeric Pd(II) complex depicted in Equation 3.1.¹¹⁹



Equation 3.1

Additionally, Yu *et al.* have characterized by X-ray crystallography two Pd(II) complexes bearing a highly electron-deficient pyridone ligand (Scheme 3.1, L = 3,5-bis(trifluoromethyl)-pyridin-2(1H)-one). A trimeric $[\text{Pd}_3(\mu\text{-OH})(\text{L})_5]$ and a monomeric $[\text{Pd}(\text{phen})\text{L}_2]$ complexes were obtained at room temperature when $[\text{Pd}(\text{OAc})_2]$ or $[\text{Pd}(\text{phen})(\text{OAc})_2]$ reacts with the pyridone ligand (L). The coordination mode of L in these complexes is shown to be analogous to that found with carboxylate ligands, acting as a X-type in a monodentate and bidentate bridging fashion to palladium and also as an internal base to cleavage the C-H bond *via* concerted metalation-deprotonation mechanism.⁵⁰

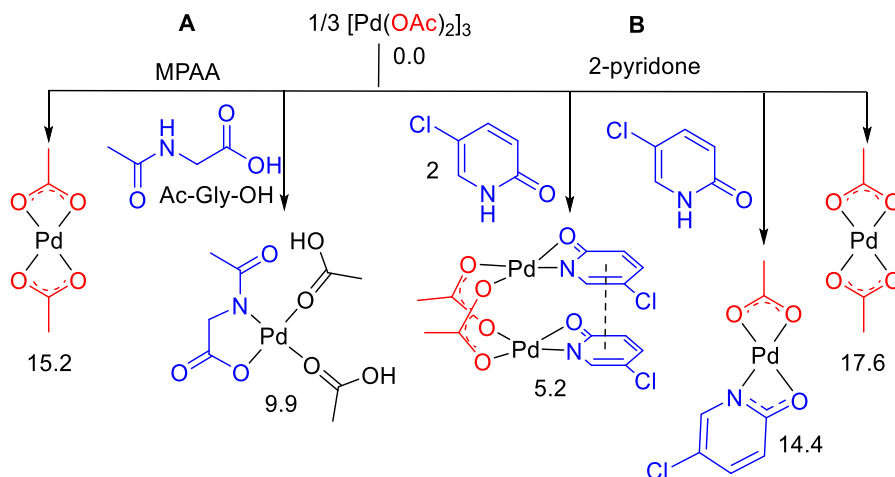
¹¹⁹ Plata, R. E.; Hill, D. E.; Haines, B. E.; Musaev, D. G.; Chu, L.; Hickey, D. P.; Sigman, M. S.; Yu, J. Q.; Blackmond, D. G. *J. Am. Chem. Soc.* **2017**, *139*, 9238–9245.



Scheme 3.1 Synthesis of Pd(II) complexes with the 2-pyridone ligand (3,5-bis(trifluoromethyl)-pyridin-2(1*H*)-one) and molecular X-ray structures (ref: 50). **a)** selected bond lengths (Å): Pd1-O1, 2.011; Pd1-Pd2, 3.093; Pd1-Pd3, 2.899, Pd2-Pd3, 2.955; Pd3-O1, 2.006; N1-N2. **b)** selected bond lengths (Å): Pd1-N1, 2.042; Pd1-N2, 2.037; Pd1-N3, 2.014; Pd1-N4, 2.020.

The acetate bridge cleavage in the trimeric palladium acetate complex $[\text{Pd}_3(\text{OAc})_6]$ by both monoprotected amino acids MPAA and 2-pyridone ligands has been studied by computational methods, showing that the formation of Pd(II) species bearing the cooperating ligand is thermodynamically more favoured than the monomeric $[\text{Pd}(\text{OAc})_2]$ species.^{48,120} The double deprotonation of the MPPA by both acetates is highly favoured, leading to a stable bidentate Pd-MPAA complex with a bidentate ligand and two coordinated acetic acid molecules (Scheme 3.2, **A**). In this case, the normally unfavorable deprotonation of the N-H bond in the amino acid is promoted by the strong binding of the deprotonated -N to the palladium center. In the 2-pyridone case, the formation of a dimeric Pd(II) complex, with acetate acting as a bridge, is preferred and the higher stability of the final complex is due to the π - π stacking of the two 2-pyridone ligands (Scheme 3.2, **B**).

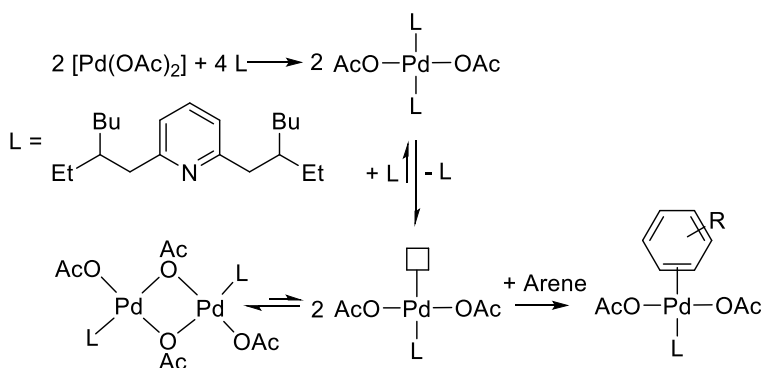
¹²⁰ Mandal, N.; Datta, A. *J. Org. Chem.* **2020**, *85*, 13228–13238.



Scheme 3.2 Calculated free energies for Pd(II)-complexes with MPA and 2-pyridone ligands using $[\text{Pd}_3(\text{OAc})_6]$ as a precursor. **A)** B3LYP and LANL2DZ (Pd), SMD solvation model at 298.15 K. **B)** Minnesota M06 functional, ECP (Pd), SMD solvation model at 298.15 K. Optimized structures obtained from refs: 48 and 120.

As it can be seen in these examples, the cooperating ligands usually have several donor atoms in their structures that can give different coordination modes and even different complex nuclearity. The acetato ligand can also behave as a mono, a bidentate and a bridging ligand. This makes the study of these species more complicated.

Despite not being cooperating ligands in the C-H cleavage, the behavior of other useful ligands in C-H activation reactions with palladium acetate has been reported. Yu and co-workers described the olefination of electron-deficient arenes using 2,6-dialkylpyridine ligands with minimal steric hindrance immediately surrounding the nitrogen atom and with steric hindrance placed on the side chain carbon atoms (Scheme 3.3).⁶² In this scenario, the coordination of two pyridyl ligands to $[\text{Pd}(\text{OAc})_2]$ generates significant mutual steric repulsion and, as a consequence, the decoordination of one pyridyl ligand is favored, allowing for arene coordination to take place.



Scheme 3.3 Solution behaviour of $[\text{Pd}(\text{OAc})_2(\text{L})_2]$ complex (L = bulky pyridyl ligand).

Carrow *et al.* reported the C-H olefination of heteroarenes enabled by $[\text{Pd}(\text{OAc})_2]$ and electron-rich alkyl aryl thioethers as ligands. The authors examined the catalyst speciation since thioether ligands have high tendency to form polynuclear species $[\text{Pd}(\text{OAc})_2(\text{thioether})]_n$ ($n > 1$). A titration experiment was carried out varying the thioether concentration at constant $[\text{Pd}(\text{OAc})_2]$ concentration at room temperature. By ^1H NMR, ESI-MS and Diffusion-Ordered Spectroscopy (DOSY NMR) the authors postulate the formation of different palladium complexes bearing thioether ligand in different ratios ($[\text{L}_2\text{Pd}(\text{OAc})_2]$, $[\text{L}_2\text{Pd}_2(\text{OAc})_4]$ and $[\text{L}_2\text{Pd}_3(\text{OAc})_6]$, $\text{L} = 4\text{-(ethylthio)-}N,N\text{-dimethylaniline}$).^{65f}

Herein, we have analyzed an array of possible scenarios when $[\text{Pd}(\text{OAc})_2]$ and the ligands bipy-6-OH and phen-2-OH are mixed, to determine the complexes formed. Depending on how they evolve into the active species, it could strongly influence the efficiency of the catalysis. The reactivity of the analogous bipyridine derivatives (bipy and phen, L,L-type ligands) was also analyzed. Bipy-6-OH and phen-2-OH could act as a L,L-type ligands (pyridine-pyridine) or L,X-type ligand (pyridine-pyridone) depending on the remaining ligands in the coordination sphere of the metal (Figure 3.1).⁵⁸ The identification of the complexes and the analysis of the factors that favor the neutral and anionic coordination modes could also be important.

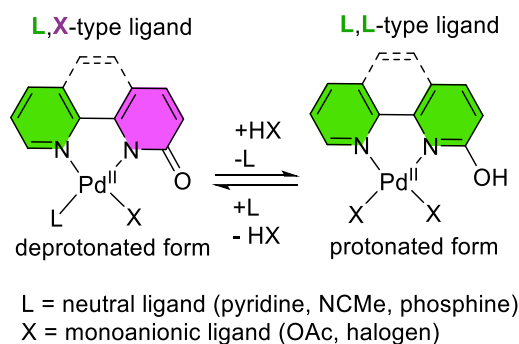
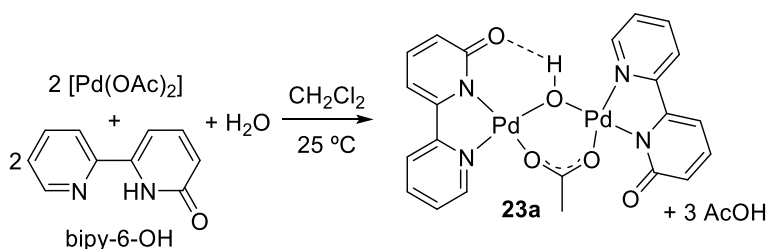


Figure 3.1 Ligand coordination-modes for bipy-6-OH and phen-2-OH with Pd(II).

3.2 RESULTS AND DISCUSSION

3.2.1 Reactivity of bipy-6-OH

Equation 3.2 shows the reactivity of the bipy-6-OH ligand with $[\text{Pd}(\text{OAc})_2]$ in a polar aprotic solvent (CH_2Cl_2). An equimolecular amount of the bipy-6-OH ligand reacts completely with $[\text{Pd}(\text{OAc})_2]$ in 2 h at room temperature affording a dimeric palladium complex with mixed bridges (**23a**) as the only species (Equation 3.2). The structure of **23a** has been determined by conductivity measurements, ^1H , 2D- ^1H DOSY, gHSQC and gHMBC NMR experiments and mass spectrometry.



Equation 3.2

The conductivity value obtained for **23a** is very low ($\Lambda_{\text{M}} = 3.4 \text{ S cm}^2 \text{ mol}^{-1}$) showing a neutral complex in solution. The ^1H NMR unveils two sets of signals for the inequivalent bipy-6-O ligands, along with only one signal for the methyl group of the acetate ligand and a broad singlet at 9.0 ppm (Figure 3.2). This signal has been assigned to a hydroxo bridge ($\mu\text{-OH}$), probably H-bonded to the keto group of one of the bipy-O ligands as indicated by the high chemical shift of the signal in ^1H NMR, and as it has been observed in the related dimer $[\text{Pd}_2(\text{bipy-6-O})_2(\text{C}_5\text{F}_5)_2(\mu\text{-OH}_2)]$.^{52b} The trimeric Pd(II) complex bearing a pyridone-type cooperating ligand also exhibits a hydroxo bridge ($\mu\text{-OH}$) (see Scheme 3.1, **a**) in the *Introduction section*).^{69a}

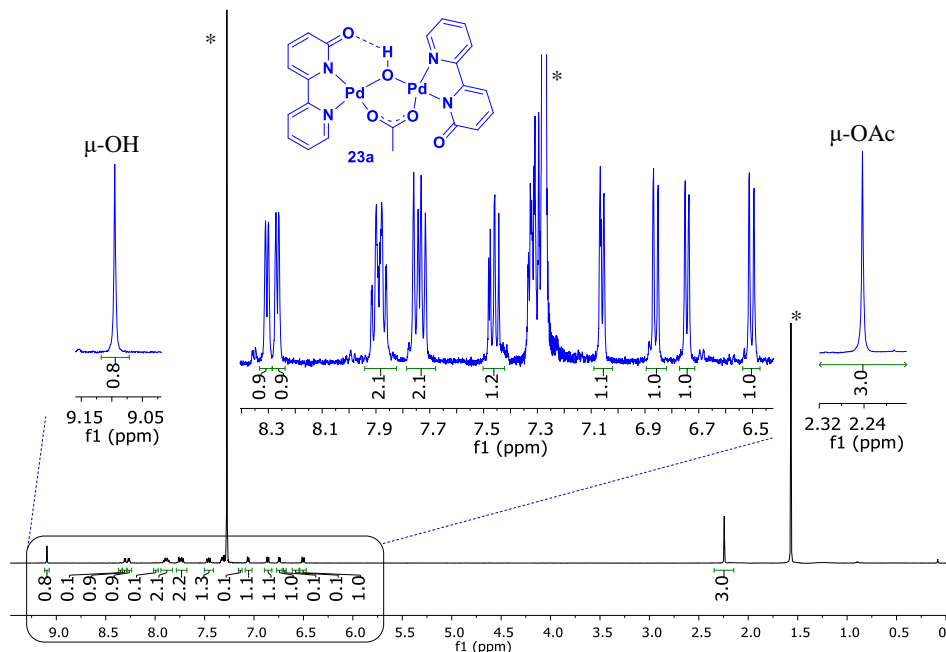
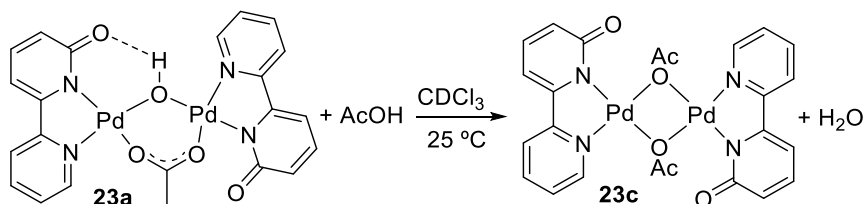


Figure 3.2 ^1H NMR spectrum in CDCl_3 of complex **23a** at 298 K. * Signal corresponding to H_2O and CHCl_3 .

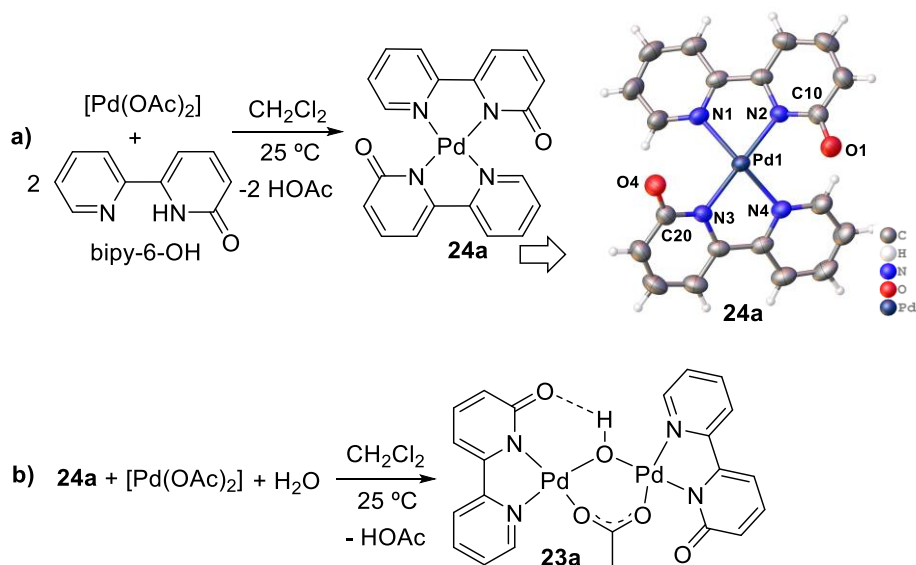
The molecular weight of **23a** was estimated by 2D-DOSY experiments using internal standards for calibration. The results obtained by 2D DOSY (DMSO- d_6 as a solvent) along with the mass spectrum (ESI-TOF) corroborate that a dimeric structure is present in solution. The molecular structure of complex **23a** could not be determined by X-ray diffraction, but the stereochemistry corresponds to a *trans*-**23a** complex because of the ^1H NMR pattern: Two inequivalent bipy-6-O ligands are clearly observed and that fact does not fit with the *cis*-**23a** isomer, which shows a symmetry plane assuming a rapid interconversion in solution between the hydrogen bond of the $\mu\text{-OH}$ bridge and the oxygens of the bipyridones.

The addition of acetic acid to **23a** generates a new symmetric complex which has been tentatively assigned to $[\text{Pd}_2(\mu\text{-OAc})_2(\text{bipy-6-O})_2]$ (**23c**) (Equation 3.3). This experiment illustrates the basic behaviour of the $\mu\text{-OH}$ group.



Equation 3.3

An excess of bidentate or monodentate ligands are sometimes used (ratio ligand:Pd > 1 or 2) and it has been found to be crucial in several catalytic reactions.^{63a,68a,121} We decided to test the reaction of [Pd(OAc)₂] and the cooperating ligand bipy-6-OH in a Pd:ligand = 1:2 mol ratio to study the speciation in solution (Scheme 3.4, a)). In this case, the complex obtained was the monomeric **24a** with two deprotonated coordinated bipy-6-O ligands. The stereochemistry of **24a** was unequivocally determined by X-ray diffraction of a monocrystal.



Scheme 3.4 L,X-type coordination mode of bipy-6-OH with [Pd(OAc)₂]. Molecular structure of **24a** (ORTEP 40% probability ellipsoids). Selected distances (Å): O1–C10, 1.263(3); O4–C20, 1.259(4); N2–Pd1–N1, 79.27(8); N3–Pd1–N4, 79.49(9).

The coordination of the second bipy-6-O to the metal generates a very distorted square planar geometry with a tilted bipy-6-O so the *trans* keto-moieties can alleviate the steric clash with the pyridine ring of the other ligand (Figure 3.3). Three molecules of water are trapped in the crystal lattice which establish hydrogen bonds with the keto-groups. The crystallization of water molecules in complexes with the bipy-6-O

¹²¹ Selected examples of Pd-catalyzed C-H activation reaction with a ratio of ligand:Pd > 1 or 2: a) Engle, K. M.; Wang, D.-H.; Yu, J.-Q. *Angew. Chem. Int. Ed.* **2010**, *49*, 6169–6173. b) Ye, M.; Gao, G. L.; Edmunds, A. J. F.; Worthington, P. A.; Morris, J. A.; Yu, J. Q. *J. Am. Chem. Soc.* **2011**, *133*, 19090–19093. c) Provencher, P. A.; Hoskin, J. F.; Wong, J. J.; Chen, X.; Yu, J.-Q.; Houk, K. N.; Sorensen, E. J. *J. Am. Chem. Soc.* **2021**, *143*, 20035–20041.

ligand (deprotonated form) is favored as observed in another similar palladium complex with the same bipy-6-O ligand.¹²²

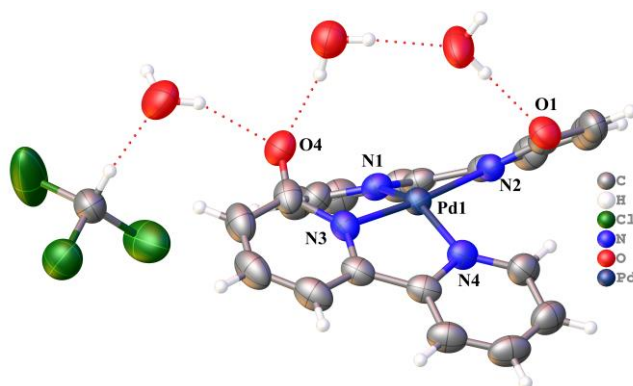
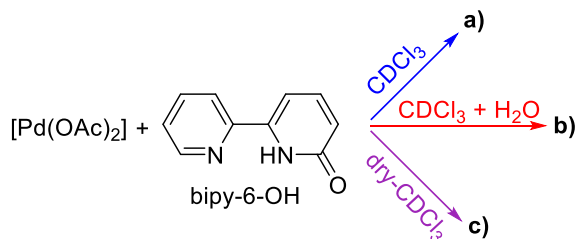


Figure 3.3 Molecular structure of complex **24a** (ORTEP plot; 40 % probability ellipsoids). The co-crystallized water molecules and chloroform are shown. Selected angles (°): N1-Pd1-N4, 153.14(9); N2-Pd1-N3, 173.39(8).

When an equimolecular amount of $[\text{Pd}(\text{OAc})_2]$ was added to isolated complex **24a**, a rapid reorganization in solution was observed to afford complex **23a** at room temperature (Scheme 3.4, **b**). This indicates a strong tendency to form the thermodynamically stable dimeric structure when the ratio Pd:Ligand is 1:1.

The reaction of $[\text{Pd}(\text{OAc})_2]$ with bipy-6-OH in a ratio Pd:ligand = 1:1 in chloroform was monitored by ^1H NMR looking at the aromatic region of the ligand. Three experiments were carried out using different solvent conditions to test the influence of the water present (Scheme 3.5). A mixture of complexes is formed: The dimeric complexes **23a** and **23c** in different ratios depending on the water in the chloroform along with complex **24a** at the beginning of the reaction (Figure 3.4).



Scheme 3.5 Monitored reaction with Pd:bipy-6-OH = 1:1 mol ratio in: **a**) CDCl_3 , **b**) CDCl_3 + one drop of water and **c**) dry- CDCl_3 at room temperature.

¹²² Pinilla, C.; Salamanca, V.; Lledós, A.; Albéniz, A. C. *ACS Catal.* **2022**, *12*, 14527–14532.

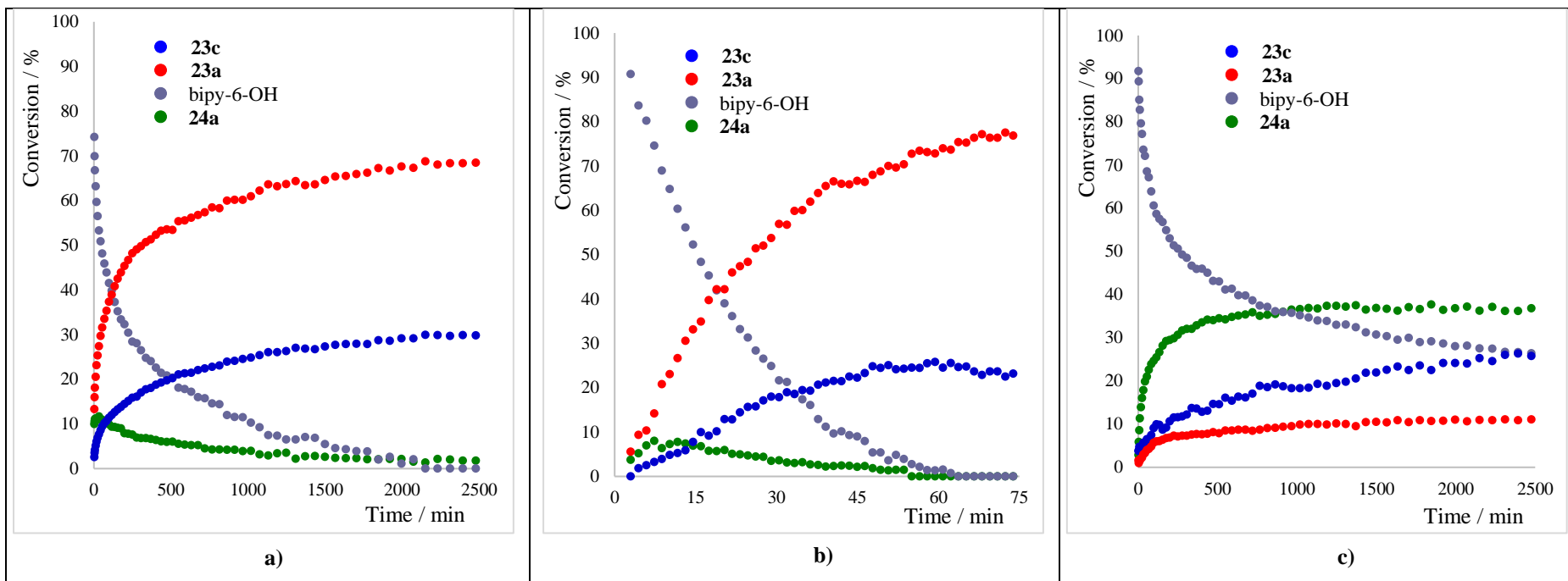


Figure 3.4 Plot of conversion vs. time for reactions shown in Scheme 3.5. **a)** CDCl₃; **b)** CDCl₃ + drop of water; **c)** dry-CDCl₃ under nitrogen atmosphere.

The monitored reactions shown in Scheme 3.5 reveals the formation of complexes **23a** and **23c**, being the latter favoured by the presence of the acetic acid formed in the reaction media. There is a strong dependence on the formation of complex **23a** depending on the amount of water contained in the solvent (*cf.* **b**) and **c**) in Figure 3.4). The H₂O present in the chloroform stored under air conditions is enough to produce **23a** as the major complex at the end of the reaction *cf.* **a**) and **b**) in Figure 3.4). One of the first products observed in the reaction is the bis-ligand derivative **24a** with the concomitant disappearance of the free ligand. Complex **24a** reacts promptly with the [Pd(OAc)₂] that remains unreacted to afford complex **23a**, proving that there is enough H₂O present in the reaction medium (**a**) and **b**), Figure 3.4). When the reaction was carried out under dry conditions complex **24a** is barely transformed and remains as the major component. The formation of complex **23c** is less affected by the water present. Table 3.1 collects the amount of complexes formed for the three reactions after 60 min. These data clearly show that water strongly increases the reaction rate to give complex **23a**.

Table 3.1 Crude yield of the complexes formed after 60 min in the reaction shown in Scheme 3.5.^a

Crude yield (%), 60 min, 25 °C	a) (CDCl ₃)	b) (CDCl ₃ + H ₂ O)	c) (dry-CDCl ₃)
Bipy-6-OH	46	1.5	67.1
24a	10.5	0	22.5
23c	10	24.5	6.1
23a	33.5	74	4.3

^a The percentages of the palladium complexes shown are determined by integration of the signals in ¹H NMR spectra using an internal standard (1,4-dioxane) and given in % H corresponding to the aromatic region of the bipyridines.

Considering that C-H functionalization reactions commonly require high temperatures, most of the solvents used have high boiling points and moderate coordinating ability. We decided to study the reaction of bipy-6-OH with [Pd(OAc)₂] in DMSO-d₆ and DMA, and the results are collected in Table 3.2. The almost complete formation of complex **23a** takes place in DMSO in the first 10 min at room temperature and it is stable in solution since no decomposition was observed after 24 h. In harsh conditions, 120 °C, complex **23a** decomposes in 30 min into **24a** and other non-identified species as well as Pd black. The reaction in DMA is slower than in DMSO and only complex **24a** (26 %) can be observed in the first 10 min at room temperature. After 3 h at room temperature the amount of **24a** increases (56 %) and the reaction of **24a** with the remaining [Pd(OAc)₂] also occurs leading to **23a** (44 %). Complex **23a** is the only

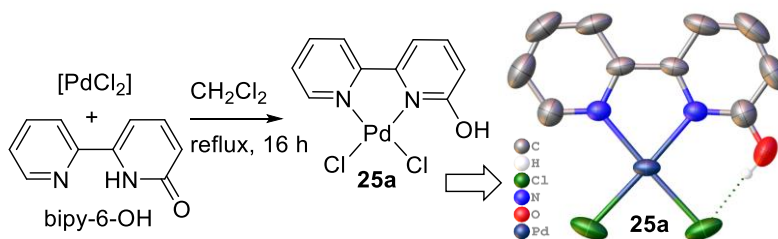
species observed in DMA when the reaction time is extended to 24 h, but this complex is not stable when it was heated to 120 °C for 30 min resulting in the decomposition to other non-identified species and Pd black. These experiments tell us that the bipy-6-OH complexation and the subsequent reorganization reaction that leads to a complex with a ratio Pd:bipy-6-O = 1:1 is analogous in different solvents but occurs faster in DMSO. However the amount of water present, which could be different depending on the solvent, can also influence this rate, as observed in Figure 3.4.

Table 3.2 Complexes formed by reaction of bipy-6-OH and [Pd(OAc)₂] (1:1 mol ratio) in different solvents.^a

Time, T	DMSO ^b	DMA ^b
10 min, 25 °C	23a (91 %), 24a (9 %).	24a (26 %), bipy-6-OH (74 %)
24 h, 25 °C	23a (100 %)	23a (100 %)
30 min, 120 °C	23a (11 %), 24a (23 %), other unidentified species (66 %)	23a (23 %), other unidentified species (77 %)

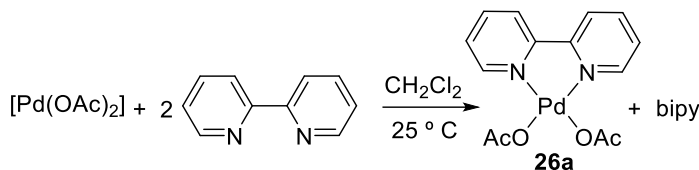
^a Reaction conditions: bipy-6-OH (2.5 mg, 0.014 mmol), [Pd(OAc)₂] (3.26 mg, 0.014 mmol), solvent (0.6 mL). ^b Crude yields determined by ¹H NMR in the reaction mixture. See spectra in the Supporting information.

In the reactions with palladium acetate, the deprotonation of the ligand occurs to generate a monoanionic bipy-6-O ligand (L,X-type coordination) and acetic acid. In contrast, when PdCl₂ is used as precursor, the absence of a base affords the monomeric Pd(II) complex **25a** with bipy-6-OH (L,L-type coordination) (Scheme 3.6). The molecular structure of this complex shows a hydrogen bond between the OH of the ligand and the closest chloro atom.



Scheme 3.6 L,L-type coordination mode of bipy-6-OH. Molecular structure of **25a** (ORTEP 40% probability ellipsoids). Hydrogen atoms are omitted for clarity except for the bridging fragment.

The reaction of $[\text{Pd}(\text{OAc})_2]$ with an equimolar amount of 2,2'-bipyridine has been reported before,¹²³ and the monomeric $[\text{Pd}(\text{bipy})(\text{OAc})_2]$ complex is the only species isolated. With a 2-fold excess of bipyridine, the formation of a bisbipyridine cationic complex with acetates as counterions $[\text{Pd}(\text{N}_2\text{N})_2](\text{OAc})_2$ could be possible.¹²⁴ However, the reaction shows the formation of the complex $[\text{Pd}(\text{bipy})(\text{OAc})_2]$ and one equivalent of free bipyridine (Equation 3.4).

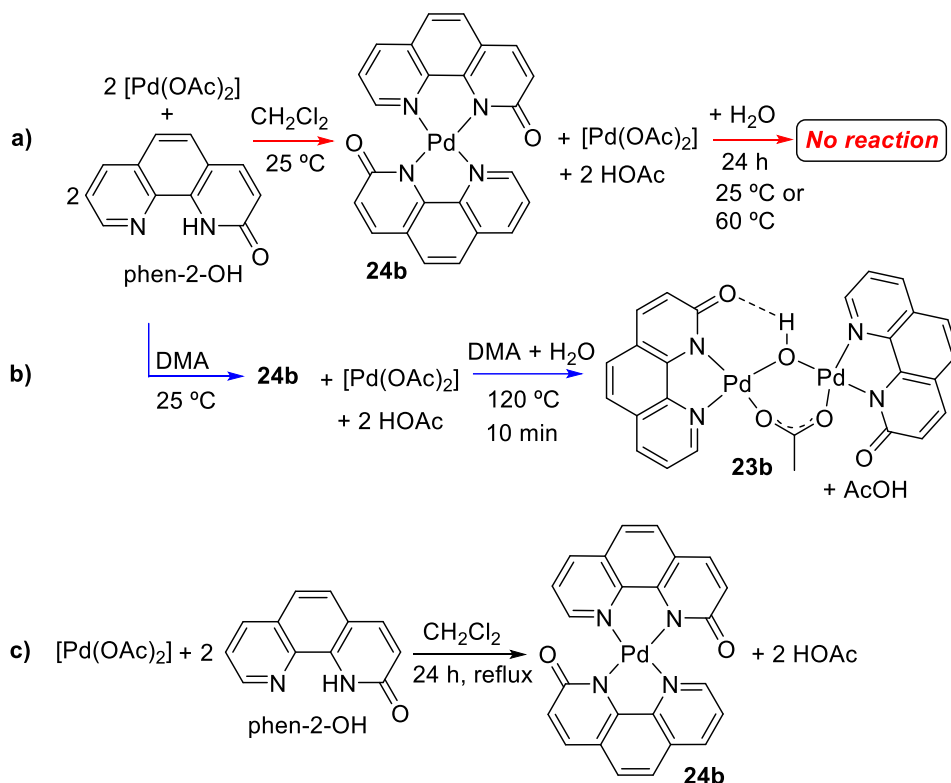


3.2.2 Reactivity of phen-2-OH

The same analysis as above was applied to phen-2-OH and a different behavior was observed in comparison to bipy-6-OH. When $[\text{Pd}(\text{OAc})_2]$ and phen-2-OH were mixed in CH_2Cl_2 at room temperature only complex **24b** was observed starting from a Pd:Ligand ratio both 1:1 and 1:2 (*cf.* **a**) and **c**) in Scheme 3.7). When the ratio is 1:1, half of the palladium source, palladium acetate, is available in the reaction media but no reorganization was observed when the reaction mixture was allowed to stand for 24 h at room temperature or it was heated at 60 °C. Only when the reaction was carried out in DMA as a solvent, we observed the initial formation of complex **24a** and the reorganization to a new dimeric complex **23b** upon heating at 120 °C for 10 min (Scheme 3.7, **b**). Thus, the formation of complex **24b** is controlled by kinetic factors whereas complex **23b** is the thermodynamic product. Nonetheless, the low solubility of complex **24b** could be responsible for the lack of reactivity in CH_2Cl_2 .

¹²³ Milani, B.; Alessio, E.; Mestroni, G.; Sommazzi, A.; Garbassi, F.; Zangrando, E.; Bresciani-Pahor, N.; Randaccio, L. *J. Chem. Soc. Dalton Trans.* **1994**, 1903–1911.

¹²⁴ Milani, B.; Anzilutti, A.; Vicentini, L.; Sessanta o Santi, A.; Zangrando, E.; Geremia, S.; Mestroni, G. *Organometallics* **1997**, *16*, 5064–5075.



Scheme 3.7 L,X-type coordination mode of phen-2-OH with $[\text{Pd}(\text{OAc})_2]$.

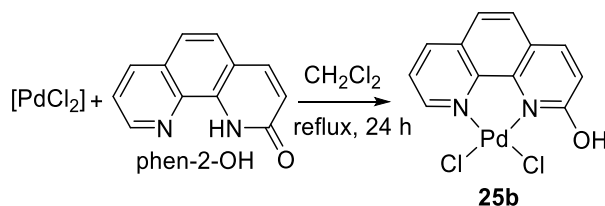
The reluctant reactivity that phen-2-OH presents in comparison with bipy-6-OH becomes apparent when we analyze the speciation in DMSO- d_6 and DMA (Table 3.3). When DMSO is used, the major complex obtained is **23b** (80 %) taking only 10 min at room temperature (similar results were obtained for the bipy-6-OH). After 24 h at room temperature, **23b** is the only product observed. When heating at 120 °C for 30 min, the decomposition of **23b** to generate **24b** and Pd black was clearly observed. In DMA the reactions are slower than in DMSO. After 10 min at room temperature no complex formation was observed and it takes 5 h for the complete formation of complex **24b** which remains unaltered for 24 h. Heating to 120 °C for 30 min produces the full conversion to **23b**.

Table 3.3 Complexes formation from phen-2-OH + [Pd(OAc)₂] (1:1 ratio) in different solvents.^a

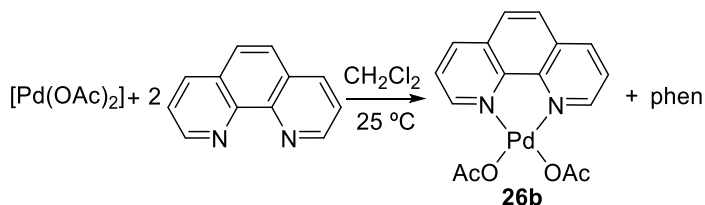
Time, T	DMSO ^b	DMA ^b
10 min, 25 °C	23b (80 %), 24b (20 %)	phen-2-OH (100%)
24 h, 25 °C	23b (100%)	24b (100%)
30 min, 120 °C	24b + Pd(0)	23b (100%)

^a Reaction conditions: phen-2-OH (2.84 mg, 0.014 mmol), [Pd(OAc)₂] (3.26 mg, 0.014 mmol), solvent (0.6 mL). ^b Crude yields determined by ¹H NMR in the reaction mixture. See spectra in the Supporting information.

Phen-2-OH acts as a neutral L,L-type ligand when it reacts with PdCl₂, affording complex **25b**, the same behavior than the one observed for bipy-6-OH (Equation 3.5).



Phenanthroline reacts with [Pd(OAc)₂] to give complex **26b**, even if an excess of ligand is used (2-fold molar amount) (Equation 3.6). This complex **26b** is analogous to complex **26a**.



3.2.3 Reactivity of phen-2-OH and bipy-6-OH with pyridine and [Pd(OAc)₂]

The use of pyridine ligands in combination with other cooperating ligands (dual ligand systems) has emerged in the last years as a powerful strategy in the development of directing-group-free arenes functionalization reactions.^{67a,67c,125} It has been suggested

¹²⁵ a) Farizyan, M.; Mondal, A.; Mal, S.; Deufel, F.; van Gemmeren, M. *J. Am. Chem. Soc.* **2021**, *143*, 16370–16376. b) Santiago, C.; Chen, H.; Mondal, A.; van Gemmeren, M. *Synlett*, **2022**, *33*, 357–360.

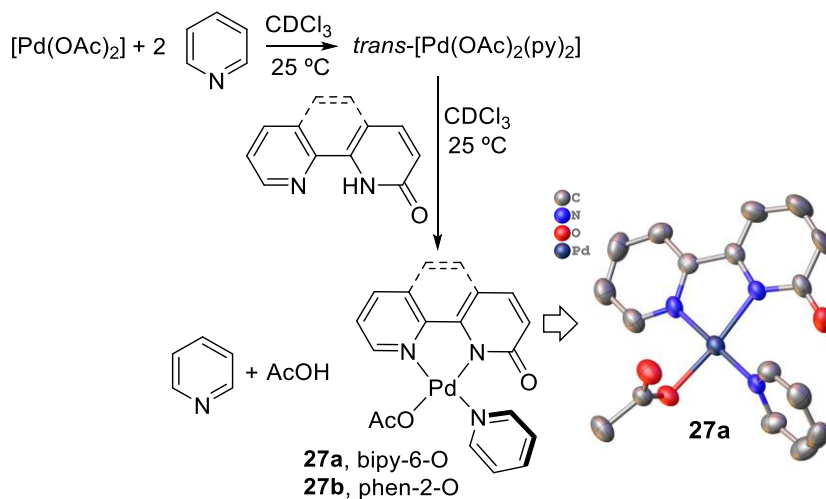
that pyridine could be acting as a trigger ligand in the formation of discrete and well-defined intermediates, both inside and outside of catalytic cycles. These mechanistic proposals pointed to monomeric complexes containing a chelating cooperating ligand and pyridine “[Pd(Ligand)(py)(X)]⁺” as key-intermediates in the catalytic cycle or resting states.^{65b,121d,126} Thus, the study of how pyridine interacts with the initial precatalyst mixture could be important to improve the efficiency of the active catalytic species. Therefore, the solution speciation of [Pd(OAc)₂] in the presence of pyridine and bipy-6-OH or phen-2-OH bipyridone ligands has been analyzed.

Starting from an *in situ* preformed *trans*-[Pd(OAc)₂(py)₂] and adding an equimolecular amount of bipyridone ligand, the formation of complexes **27a** and **27b** was observed in solution (Scheme 3.8). In both cases, the internal acetate deprotonates the bipyridone ligand which displaces one pyridine to afford a neutral [Pd(Ligand)(OAc)(py)] complex (Ligand = bipy-6-O or phen-2-O).¹²⁷ The identity of complex **27a** was further established by the determination of its molecular structure by X-ray diffraction. The acetate ligand coordinates in a monodentate fashion (κ^1 -OAc) in a *trans* position to the keto group of the bipy-6-O. This discrete well-defined palladium species with a 1:1:1 ratio (Ligand:py:OAc) provide a significant advantage in comparison with other non-well-known species in solution when starting from the trimeric [Pd(OAc)₂]₃.¹²⁸

¹²⁶ a) Zhang, S.; Shi, L.; Ding, Y. *J. Am. Chem. Soc.* **2011**, *133*, 20218–20229. b) Chen, H.; Mondal, A.; Wedi, P.; van Gemmeren, M. *ACS Catal.* **2019**, *9*, 1979–1984.

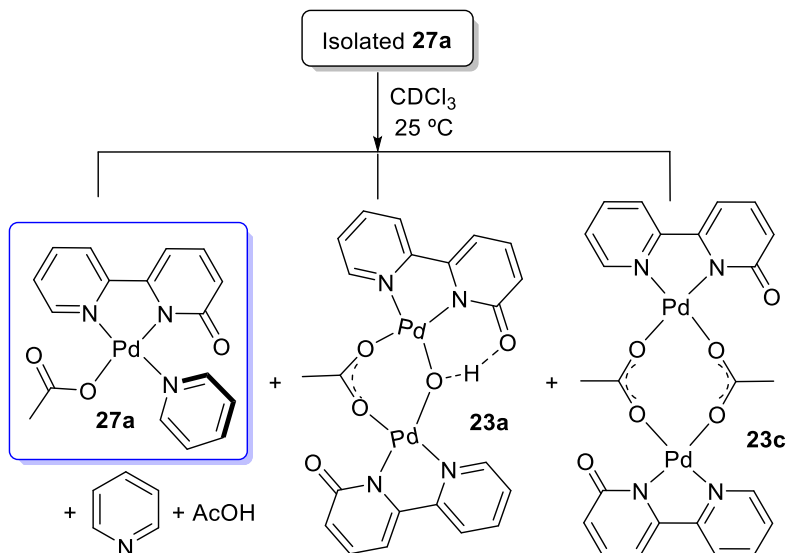
¹²⁷ It is not possible to determine if the deprotonation of the bipyridone ligand occurs inside or outside the palladium coordination sphere.

¹²⁸ Ritter, S.K. A User’s Guide for Palladium Acetate. *C&EN Glob. Enterp.* **2016**, *94*, 20–21.



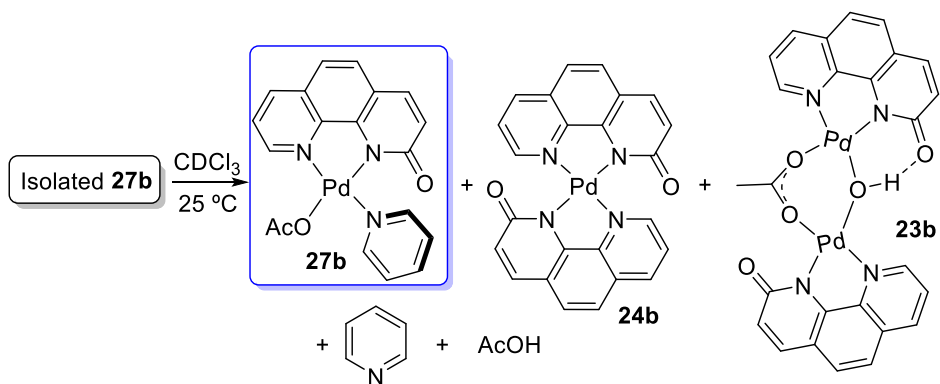
Scheme 3.8 *In situ* formation of complexes **27(a-b)**. Molecular structure of **27a** (ORTEP 40% probability ellipsoids). Hydrogen atoms are omitted for clarity.

The dissociation of pyridine in complexes **27** is a very facile process. Isolated samples of **27a-b** lead to a mixture of species in solution, such as **27a-b**, **23a-b** or **24b** and free pyridine. Figure 3.5, **a**) shows that complex **27a** is the major species in solution only in the presence of an excess of free pyridine, which shifts the dissociation equilibrium. Isolated **27a** leads in solution to a mixture of complexes **27a**, **23a** and **23c** as well as free pyridine (see Scheme 3.9) and the ratio of complexes is very dependent on the amount of water in the solvent, the latter favoring the formation of the hydroxo dimer **23a** (*cf.* **d**) and **e**) Figure 3.5). Therefore, the formation of dimeric species is very much favored, and in the presence of pyridine a mixture of monomeric and dimeric species can be found.



Scheme 3.9 Palladium species observed when **27a** was dissolved in CDCl₃.

An analogous situation was found for complex **27b** with the formation in solution of a mixture of **27b**, **23b**, **24b** and free pyridine (Scheme 3.10 and Figure 3.6).



Scheme 3.10 Palladium species observed when **27a** was dissolved in CDCl₃.

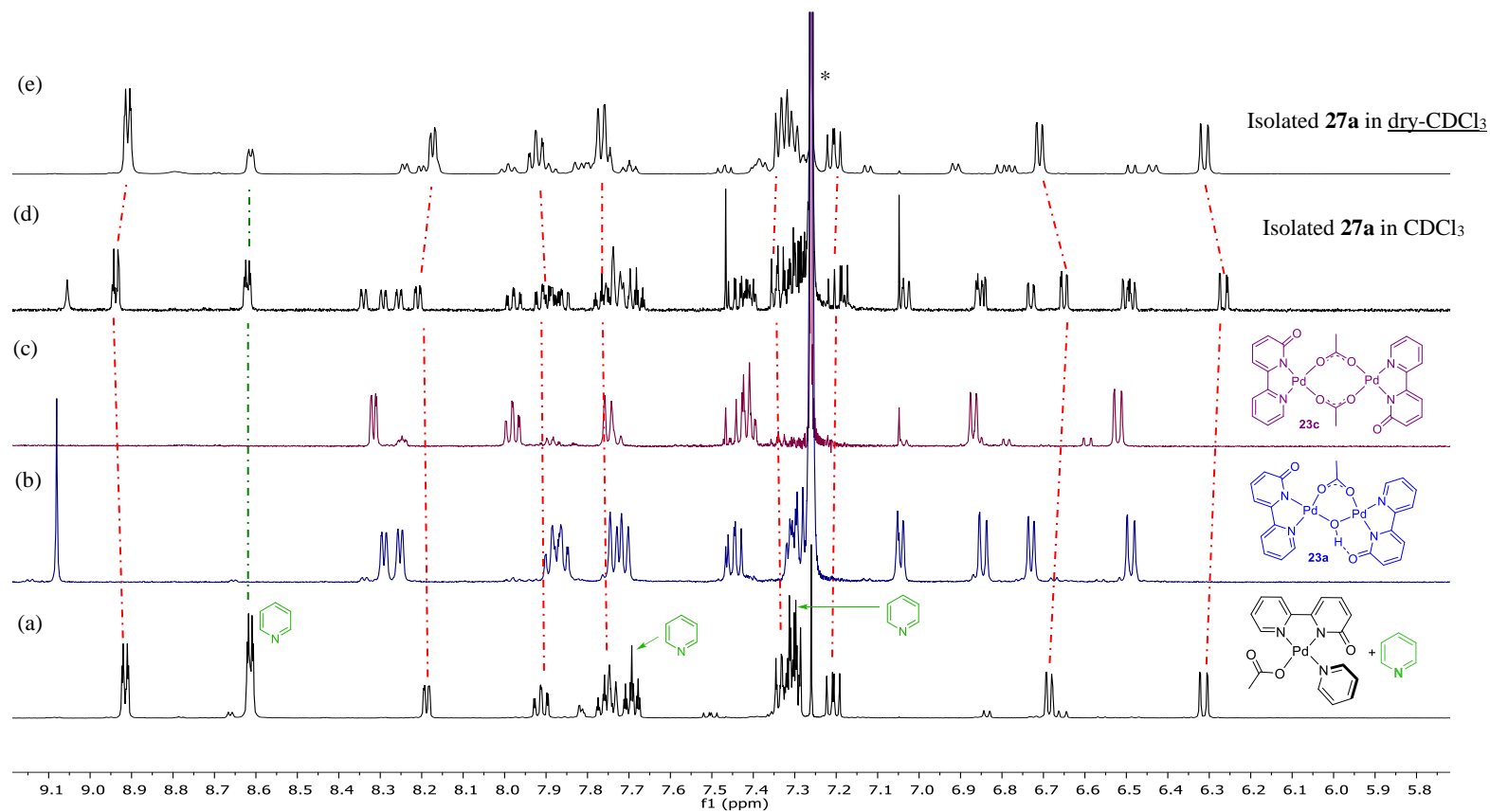


Figure 3.5 ^1H NMR (499.73 MHz, CDCl_3) spectra of: (a) *in situ* formation of complex **27a**. (b) Complex **23a**. (c) Complex **23c**. (d) and (e) Spectra of isolated **27a** in solution giving the mixture of compounds shown in Scheme 3.9. Only the aromatic region is shown for clarity. * Signal corresponding to the chloroform.

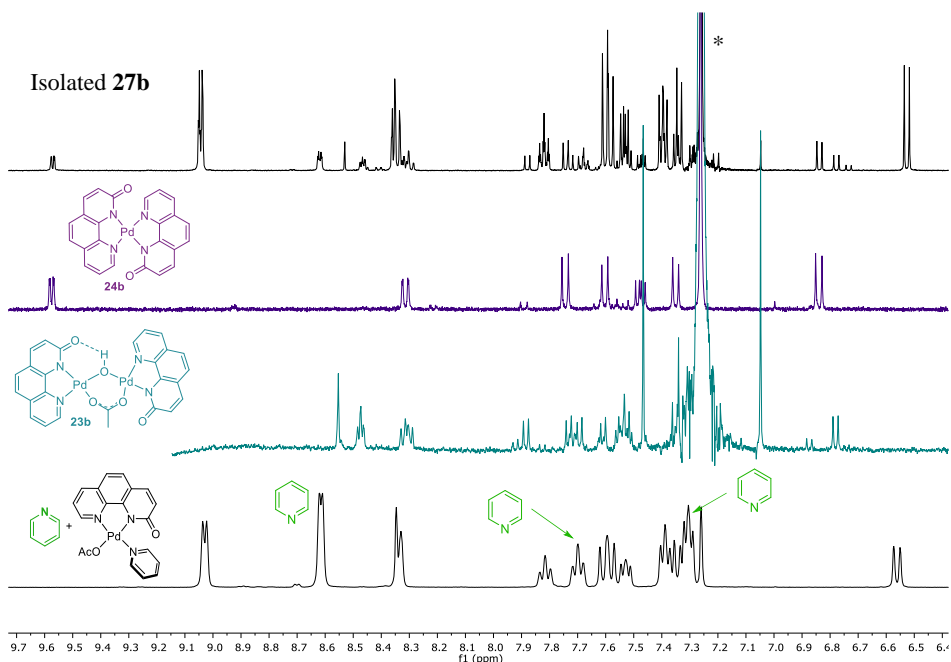
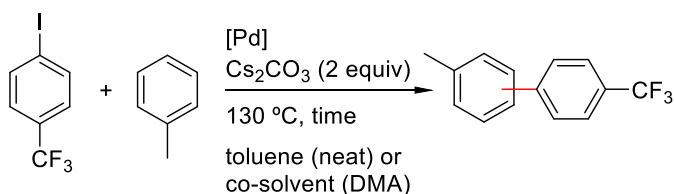


Figure 3.6 ^1H NMR (499.73 MHz, dry- CDCl_3) spectrum of isolated **27b** to give the mixture of complexes shown in Scheme 3.10 and comparison with the isolated complexes **23b** and **24b** synthesized by independent routes. Only the aromatic region is shown for clarity. * Signal corresponding to the chloroform.

3.2.4 Catalytic reactions

To evaluate the catalytic activity of the synthesized palladium complexes, a direct arylation reaction of toluene with arylhalides, previously reported, was chosen as a model reaction (Equation 3.7).^{52b} Three regioisomers were obtained (*o:m:p*) in different distributions, being the *meta*-isomer the major one (see Tables 3.5 and 3.6 in *Experimental part* for details). The reaction was carried out using the arene as reagent and solvent (toluene for this particular case) but, in order to decrease the amount of arene used, DMA can be chosen as co-solvent with toluene in a ratio 1:1 (v/v). The co-solvent has a significant accelerating effect in this arylation reaction as has been studied before.^{52b}



Equation 3.7

Table 3.4 collects the combined crude-yield of the three cross-coupling isomeric products and the reaction time for different precatalyst.

The reaction does not work in the absence of palladium or using $[\text{Pd}(\text{OAc})_2]$ as precatalyst in neat toluene (less than 1 % of conversion). The same results were found when non-cooperating ligands such as 2,2'-bipy or 1,10-phen were used along with $[\text{Pd}(\text{OAc})_2]$ (entries 1-4, Table 3.4). The precatalytic mixture of $[\text{Pd}(\text{OAc})_2]$ + bipy-6-OH increases the yield up to 91 % in the same solvent (toluene), in 24 h (entry 5, Table 3.4). Significant differences were observed when the preformed bipy-6-OH complexes described above (**23a-25a**) were used. Dimeric complex **23a** affords an 82 % of the cross-coupling product in just 6 h with toluene as a solvent (entry 6, Table 3.4). The highest catalytic activity observed when complex **23a** is used can be attributed to the no necessity to *in situ* preform it from $[\text{Pd}(\text{OAc})_2]$ + bipy-6-OH mixture in toluene. The μ -OAc and μ -OH bridges may easily break when heating leading to two monomeric complexes with one bipyridone L,X-type ligand per palladium and an available coordination site in the palladium sphere for interaction with the incoming arene. We next explored the activity of complex **24a**, which presents two bipy-6-O ligands chelating the palladium center and thus could confer high stability and robustness to this precatalyst. An 18 % of the final product was observed in toluene in 6 h and it is necessary to extend the reaction time to 24 h to obtain good yield (entry 7, Table 3.4). Finally, complex **25a** which present L,L-type coordination mode was analysed. The reaction proceeds very efficiently in toluene affording a 65 % in 6 h (entry 8, Table 3.4). These results show that a preformed Pd-precatalyst with one coordinated bipy-6-O ligand per palladium is optimal to accelerate the overall reaction and get shorter reaction times.

A reluctant behavior in the catalysis was observed for phen-2-OH in comparison with the bipy-6-OH, probably due to the lower solubility of the palladium species bearing phen-2-OH ligand. The mixture of $[\text{Pd}(\text{OAc})_2]$ + phen-2-OH only affords an 18 % yield in 24 h using toluene (entry 9, Table 3.4). Complex **23b** as precatalyst affords a slight enhancement of the conversion when compared to the mixture of $[\text{Pd}(\text{OAc})_2]$ + phen-2-OH (*cf.* entries 9 and 10). In contrast, complex **24b** produces an improvement in the catalytic reaction, but it takes longer times (24 h) (entry 11). Similar conversion to the mixture $[\text{Pd}(\text{OAc})_2]$ + phen-2-OH was obtained when complex **25b** was used (entry 12).

All reactions give excellent yields when DMA as co-solvent was used and the reaction time is significantly reduced to 6 h (entries 13-20, Table 3.4). The formation of the active catalytic species is expected to be fast under the reaction conditions in this solvent as can be seen in Tables 3.2. and 3.3.

Table 3.4 Direct arylation of toluene with *p*-CF₃C₆H₄I using different catalysts according to Equation 3.7.^a

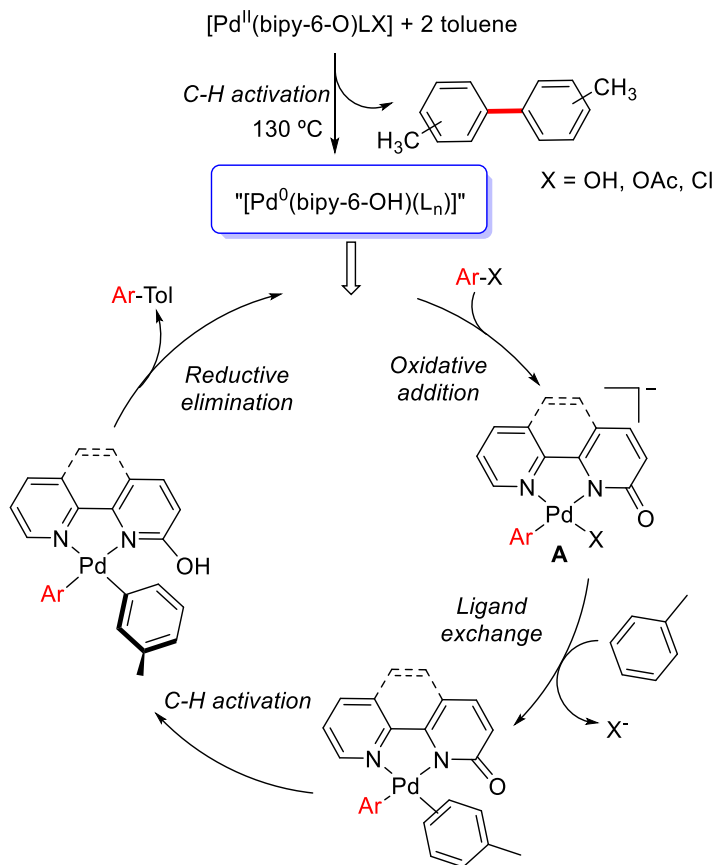
Entry	Toluene/ DMA (v/v %)	[Pd] (mol %)	Crude yield, %, (react. time) ^b
1	1/0	-	- (24h)
2	1/0	[Pd(OAc) ₂] (5)	- (24h)
3	1/0	[Pd(OAc) ₂] (5) + bipy (5)	0 (6h), 1 (24h)
4	1/0	[Pd(OAc) ₂] (5) + 1,10-phen (5)	0 (6h), 1 (24h)
5	1/0	[Pd(OAc) ₂] (5) + bipy-6-OH (5)	20 (6h), 91 (24h)
6	1/0	23a (2.5)	82 (6h)
7	1/0	24a (5)	18 (6h), 94 (24 h)
8	1/0	25a (5)	65 (6h), 89 (24h)
9	1/0	[Pd(OAc) ₂] (5) + phen-2-OH (5)	6 (6h), 18 (24h)
10	1/0	23b (2.5)	15 (6h), 29 (24h)
11	1/0	24b (5)	3 (6h), 50 (24h)
12	1/0	25b (5)	4 (6h), 19 (24h)
13	1/1	[Pd(OAc) ₂] (5) + bipy-6-OH (5)	96 (6h)
14	1/1	23a (2.5)	93 (6h)
15	1/1	24a (5)	95 (6h)
16	1/1	25a (5)	88 (6h)
17	1/1	[Pd(OAc) ₂] (5) + phen-2-OH (5)	79 (6h)
18	1/1	23b (2.5)	93 (6h)
19	1/1	24b (5)	97 (6h)
20	1/1	25b (5)	88 (6h)

^a Reaction conditions: *p*-CF₃C₆H₄I (51 μL, 0.34 mmol), toluene (3 mL) or toluene/DMA (1.5/1.5 mL), [Pd] (5 mol %), Cs₂CO₃ (222 mg, 0.68 mmol); 130 °C. ^b Crude yields determined by ¹⁹F NMR of the reaction mixture. The reduction product of the aryl iodide (ArH) and the homocoupling derivative (Ar–Ar) are the observed byproducts. Regioisomer distribution for the cross-coupling products and byproduct amount (%) are specified in Tables 3.5 and 3.6 in the *Experimental part*.

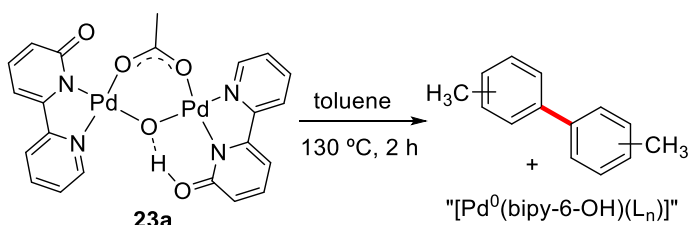
The proposed general catalytic cycle for the direct arylation of toluene with cooperating bipyridone ligands is shown in Scheme 3.11. This is a Pd(0)/Pd(II) cycle analogous to the one that operates in the direct arylation of pyridine with the same cooperating ligand. Intermediate **A** represents the result of an oxidative addition of the arylhalide (*p*-CF₃C₆H₄I) on Pd(0) species. Since all the precatalyst employed in Table 3.4 are Pd(II) species, an off-cycle decomposition of the starting precatalyst to generate Pd(0) species, capable to start the catalytic cycle, needs to occur.¹²⁹ Thus, the decomposition of the precatalysts has been analyzed. When the dimeric complex **23a** was heated in toluene at 130 °C for 2 h, Pd black was formed in the reaction medium. A white solid was obtained from the reaction mixture and its analysis by mass spectrometry (GC-MS) and ¹H NMR indicated the presence of six different homocoupling

¹²⁹ A recent review on the most common palladium precatalyst in conventional cross-coupling reactions and their activation pathways can be found in: Shaughnessy, K. H. *Isr. J. Chem.* **2020**, *60*, 180–194.

regioisomeric biphenyl products from the dimerization of toluene (Equation 3.8). This experiment proves that the double C-H activation of toluene followed by a reductive elimination to give the homocoupling product is a feasible pathway to decompose complex **23a** to Pd(0)-species and start the catalytic cycle. In the case that other solvent is used such as DMA (co-solvent mixture), Tables 3.2 and 3.3. shown that under the same temperature conditions the formation of Pd black by other decomposition reactions is also feasible.



Scheme 3.11 Proposed catalytic cycle for the arylation of toluene with Pd(II) precursors bearing bipyridone cooperating ligands.



Equation 3.8

3.3 CONCLUSIONS

The complexes obtained by reaction of the bipyridone ligands bipy-6-OH and phen-2-OH with $[\text{Pd}(\text{OAc})_2]$ exhibit an anionic L,X-type coordination mode to Pd(II). Despite the Pd:Ligand ratio used the formation of the neutral monomeric $[\text{Pd}(\text{L},\text{X})_2]$ (L,X = bipy-6-O, phen-2-O, **24**) occurs first. This is the only product observed for a ratio Pd:Ligand = 1:2. If the ratio Pd:Ligand is 1:1, a subsequent ligand reorganization of complexes **24a-b** with the remaining $[\text{Pd}(\text{OAc})_2]$ is possible, leading to the formation of dimeric complexes $[\text{Pd}_2(\text{L},\text{X})_2(\mu\text{-OAc})(\mu\text{-OH})]$ (L,X = bipy-6-O, phen-2-O, **23**) which have been isolated and characterized. The formation of complexes **23** is faster in the more coordinating DMSO and, in the case of the ligand bipy-6-OH, water accelerates the reaction and influences the distribution of palladium complexes. Phen-2-OH, usually forming less soluble complexes, shows a more reluctant behaviour, requiring high temperatures for the reorganization to take place.

In contrast to palladium acetate, the reaction with PdCl_2 as metal precursor affords a neutral L,L-coordination mode for the bipyridone ligands leading to complexes $[\text{Pd}(\text{bipy-6-OH})\text{Cl}_2]$ (**25a**) $[\text{PdCl}_2(\text{phen-2-OH})]$ (**25b**).

The activity as precatalysts of the isolated complexes has been tested in the direct arylation of toluene and compared to the mixture $\text{Pd}(\text{OAc})_2/\text{bipy-6-OH}$. When the catalytic reaction is carried out in a solvent such as a toluene/DMA mixture, there is hardly any difference on the final yield regardless the precatalyst used, most probably because of the rapid Pd/Ligand coordination-reorganization in the medium to form the active species. However, when the reaction is run in a non-polar non-coordinating solvent (neat toluene) complexes **23a** and **25a** show faster reactions by increasing the final yield in the first 6 h by comparison with the precatalyst mixture of $[\text{Pd}(\text{OAc})_2]/\text{bipy-6-OH}$. This shows that the precoordination of the ligand to the metal in a Pd:ligand = 1:1 ratio facilitates the formation of the active species. Therefore, we expect that complexes **23a** and **25a**, easy to synthesize, can be convenient and effective precatalyst in C-H activation reactions in non-polar solvents. The Pd(II) precatalyst can be transformed into Pd(0) species, active in the direct arylation reaction, *via* double C-H activation and reductive elimination.

3.4 EXPERIMENTAL PART

3.4.1 General considerations

^1H and $^{13}\text{C}\{^1\text{H}\}$ spectra were recorded on Agilent MR-500 spectrometer at the *Laboratorio de Técnicas Instrumentales* (LTI) of the UVa. Chemical shifts (in δ units, ppm) were referenced to SiMe_4 (^1H and ^{13}C). The spectral data were recorded at 298 K unless otherwise noted. Homonuclear (^1H -COSY, ^1H -2D-DOSY) and heteronuclear (^1H - ^{13}C HSQC and HMBC) experiments were used to help with the signal assignments. Elemental analyses were carried out in a Carlo Erba 1108 microanalyser (at Vigo University). Infrared spectra were recorded (in the range 4000-200 cm^{-1}) on a Perkin-Elmer FT-IR Spectrum Frontier with an ATR diamond accessory. Conductivity measurements were carried out by a Mettler Toledo MC226 conductivity meter. Acetone was chosen as a solvent for the measurements. The values of the molar conductivities were compared to the reported values for different electrolytes.¹³⁰ Solvents were dried using a solvent purification system SPS PS-MD-5 (ether, hexane, THF and CH_2Cl_2) or distilled from appropriate drying agents under nitrogen prior to use and stored over 3 Å or 4 Å molecular sieves (pyridine, *N,N*-dimethylacetamide and CDCl_3). $[\text{Pd}(\text{OAc})_2]$, 2,2'-bipyridine, 1,10-phenanthroline are commercially available and were purchased from Johnson Matthey, Sigma-Aldrich or Alfa Aesar. All commercial reagents and solvents were used as received unless otherwise indicated.

[2,2'-bipyridin]-6(1*H*)-one (bipy-6-OH),⁸⁷ 1,10-phenanthrolin-2(1*H*)-one (phen-2-OH),⁸⁸ $[\text{Pd}(\text{bipy-6-OH})\text{Br}(\text{C}_6\text{F}_5)]^{52\text{a}}$ and $[\text{PdBr}(\text{C}_6\text{F}_5)(\text{phen-2-OH})]^{118}$ were prepared according to the procedures in the literature.

3.4.2 Synthesis of Palladium complexes

$[\text{Pd}_2(\mu\text{-OAc})(\mu\text{-OH})(\text{bipy-6-O})_2]$ (23a)

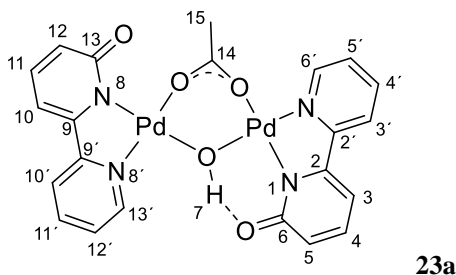
[2,2'-Bipyridin]-6(1*H*)-one (bipy-6-OH) (43.5 mg, 0.253 mmol) was added to a solution of $[\text{Pd}(\text{OAc})_2]$ (56.7 g, 0.253 mmol) in CH_2Cl_2 (12 mL). The mixture was stirred at room temperature for 2 h. During this time the orange solution became yellow and a precipitate was observed. The solvent was evaporated to *ca.* 3 mL and Et_2O (10 mL) was added to the suspension. The yellow solid was filtered, washed with Et_2O (3 x 5 mL), acetone (3 x 5 mL) and air-dried. Yield: 52 mg (52 %).

^1H NMR (499.73 MHz, CDCl_3): δ 9.08 (s, 1H, H^7), 8.29 (dd, $J = 5.7$, 1 Hz, 1H, $\text{H}^{6'}$ or $\text{H}^{13'}$), 8.25 (d, $J = 5.7$, 1 Hz, 1H, $\text{H}^{13'}$ or $\text{H}^{6'}$), 7.87 (m, 2H, H^4 , H^{11}), 7.72 (m, 2H, $\text{H}^{3'}$, $\text{H}^{10'}$), 7.45 (m, 1H, H^4), 7.36-7.29 (m, 3H, H^5 , $\text{H}^{12'}$, H^{11}), 7.04 (d, $J = 8.8$ Hz, 1H, H^3), 6.85 (d, $J = 8.8$ Hz, 1H, H^5), 6.73 (d, $J = 6.8$ Hz, 1H, H^{10}), 6.49 (d, $J = 8.8$ Hz, 1H, H^{12}), 2.23 (s, 3H, H^{15}). $^{13}\text{C}\{^1\text{H}\}$ NMR (125.58 MHz, δ , CDCl_3): 178.6 (C^{14}), 172.9 (C^{13}) 170.3

¹³⁰ Geary, W. J. *Coord. Chem. Rev.* **1971**, 7, 81–122.

(C⁶), 159.4 (C⁹), 158.1 (C²), 153 (C²), 149.8 (C^{6'} or C^{13'}), 149.5 (C⁹), 147.1 (C^{13'} or C^{6'}), 138.7 (C^{4'}, C^{11'}), 137.6 (C⁴), 136.5 (C¹¹), 124.6 (C^{5'} or C^{12'}), 123.8 (C^{12'} or C^{5'}), 123.4 (C¹²), 120.8 (C^{3'}, C^{10'}) 120.7 (C⁵), 109.5 (C³) 106.1 (C¹⁰), 23.3 (C¹⁵).

IR (neat, cm⁻¹): ν (μ-OH, st) 3466; (μ-OAc) 1601, 1470. HRMS (ESI-TOF) m/z calcd for C₂₀H₁₅N₄O₃Pd₂ [[Pd₂(μ-OH)(bipy-6-O)₂]⁺ 570.9222. Found 570.9233. Λ_M = 3.4 Scm²/mol.

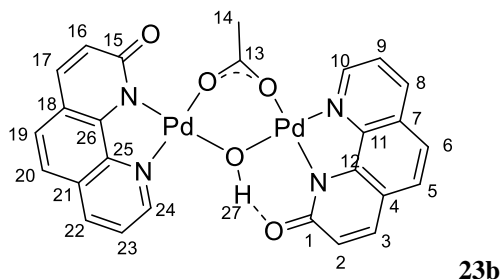


[Pd₂(μ-OAc)(μ-OH)(phen-2-O)₂] (23b)

1,10-phenanthroline-2(*H*)-one (phen-2-OH) (53.2 mg, 0.27 mmol) was added to a solution of [Pd(OAc)₂] (60.9 g, 0.27 mmol) in DMA (10 mL). The mixture was stirred at room temperature for 15 min. During this time an abundant precipitate was observed ([Pd(phen-2-O)₂]). The mixture was heated at 120 °C for 10 min. After that time the black solution formed was treated with activated charcoal and filtered. The filtrate was evaporated to dryness giving a light brown solid. After being triturated with Et₂O (5 mL) the solid was filtered off and washed with Et₂O (3 x 5 mL) and acetone (3 x 5 mL) and air-dried. Yield: 55 mg (60 %).

¹H NMR (499.73 MHz, CDCl₃): 8.52 (s, 1H, H²⁷), 8.47 (dd, J = 5.2, 1.4 Hz, 1H, H⁸ or H²²), 8.46 (dd, J = 5.2, 1.4 Hz, 1H, H⁸ or H²²), 8.32 (dd, J = 8.2, 1.3 Hz, 1H, H¹⁰ or H²⁴), 8.30 (dd, J = 8.3, 1.3 Hz, 1H, H¹⁰ or H²⁴), 7.88 (d, J = 8.9 Hz, 1H, H³), 7.74 (d, J = 9.1 Hz, 1H, H¹⁷), 7.69 (d, J = 8.5 Hz, 1H, H⁶ or H²⁰), 7.61 (d, J = 8.4 Hz, 1H, H⁶ or H²⁰), 7.54 (m, 2H, H⁹, H²³), 7.53 (d, J = 8.5 Hz, 1H, H⁵ or H¹⁹), 7.36 (d, J = 8.4 Hz, 1H, H⁵ or H¹⁹), 7.21 (d, J = 8.9 Hz, 1H, H²), 6.78 (d, J = 9.1 Hz, 1H, H¹⁶), 2.32 (s, 3H, H¹⁴). ¹³C{¹H} NMR (125.67 MHz, CDCl₃): 179.1 (C¹³), 172.05 (C¹⁵), 169.5 (C¹), 145.8 (C⁸ or C²²), 149.0 (C⁸ or C²²), 137.7 (C¹⁰ or C²⁴), 137.9 (C¹⁰ or C²⁴), 137.4 (C³), 135.9 (C¹⁷), 127.7 (C⁶ or C²⁰), 127.0 (C⁶ or C²⁰), 125.7 (C¹⁶), 123.0 (C⁹, C²³), 122.5 (C²), 121.8 (C⁹, C²³), 120.8 (C⁵ or C¹⁹), 118.1 (C⁵ or C¹⁹), 23.6 (C¹⁴). HRMS (ESI-TOF) m/z calcd for C₂₀H₁₅N₄O₃Pd₂ [[Pd₂(μ-OH)(phen-2-O)₂]⁺ 618.9223. Found 618.9226. Λ_M = 1.7 Scm²/mol.

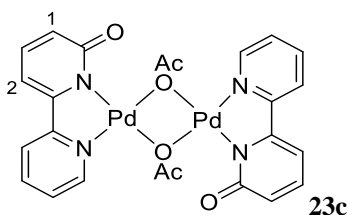
* The ¹³C NMR signals for the quaternary carbons could not be assigned due to the low solubility of the complex.



[Pd₂(μ-OAc)₂(bipy-6-O)₂] (23c)

[Pd₂(bipy-6-O)₂(μ-OAc)(μ-OH)] (0.2 mg, 0.0003 mmol) and acetic acid (0.5 μL, 0.008 mmol) were dissolved in CDCl₃ (0.6 mL) and the solution placed in an NMR tube. The ¹H NMR of the mixture showed the formation of **23c**, which was analysed *in situ*.

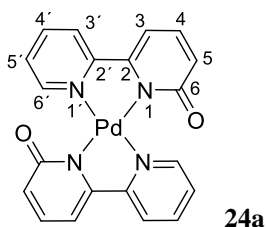
¹H NMR (499.73 MHz, CDCl₃): 8.31 (dd, J = 5.7, 1.0 Hz, 2H), 7.98 (td, J = 7.9, 1.4 Hz, 2H), 7.75 (d, J = 8.1 Hz, 2H), 7.4 (m, J = 7.1 Hz, 2H), 6.87 (d, J = 7.0 Hz, 2H, H²), 6.52 (d, J = 8.8 Hz, 2H, H¹), 2.10 (s, 6H, CH₃).



[Pd(bipy-6-O)₂] (24a)

[2,2'-Bipyridin]-6(1*H*)-one (bipy-6-OH) (192.3 mg, 1.11 mmol) was added to a solution of [Pd(OAc)₂] (125.1 g, 0.557 mmol) in CH₂Cl₂ (15 mL). The mixture was stirred at room temperature for 1 h. During this time the orange solution became yellow and a precipitate was observed. The solvent was evaporated to *c.a.* 5 mL and Et₂O (10 mL) was added to the suspension. The yellow solid was filtered, washed with Et₂O (3 x 5 mL), acetone (3 x 5 mL) and air-dried. Yield: 181 mg (72 %).

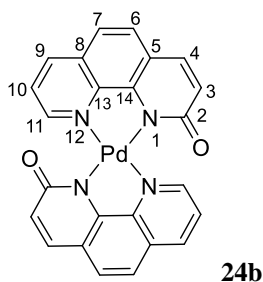
¹H NMR (499.73 MHz, δ, CDCl₃): 9.15 (dd, J = 5.7, 1.1 Hz, 1H, H^{6'}), 7.86 (td, J = 7.6, 1.5 Hz, 1H, H⁴), 7.70 (d, J = 8.2 Hz, 1H, H^{3'}), 7.31 (dd, J = 8.5, 6.9 Hz, 1H, H^{4'}), 7.21 (td, J = 6.8, 1.5 Hz, 1H, H^{5'}), 6.66 (dd, J = 6.8, 1.0 Hz, 1H, H⁵), 6.51 (dd, J = 8.5, 1.0 Hz, 1H, H³). ¹³C {¹H} NMR (125.58 MHz, δ, CDCl₃): 169.4 (C⁶), 160.4 (C^{2'}), 153.7 (C^{6'}), 153.3 (C²), 138.9 (C^{4'}), 137.2 (C⁴), 123.7 (C^{5'}), 122.1 (C⁵), 120.2 (C^{3'}), 105.9 (C³). IR (neat, cm⁻¹): ν (CO, st) 1616 cm⁻¹.



[Pd(phen-2-O)₂] (24b)

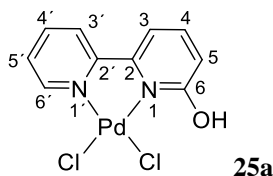
1,10-phen-2(*H*)-one (phen-2-OH) (237.3 mg, 1.2 mmol) was added to a solution of [Pd(OAc)₂] (135.6 g, 0.60 mmol) in CH₂Cl₂ (20 mL). The mixture was stirred at room temperature for 1 h. During this time the orange solution became yellow and a precipitate was observed. The solvent was evaporated to *c.a.* 5 mL and Et₂O (10 mL) was added to the suspension. The yellow solid was filtered, washed with Et₂O (3 x 5 mL), acetone (3 x 5 mL) and air-dried. Yield: 240.8 mg (80 %).

¹H NMR (499.73 MHz, δ, CDCl₃): 9.57 (dd, *J* = 5.5, 1.4 Hz, 1H, H¹¹), 8.31 (dd, *J* = 8.2, 1.4 Hz, 1H, H⁹), 7.74 (d, *J* = 9.1 Hz, 1H, H⁴), 7.60 (d, *J* = 8.4 Hz, 1H, H⁶), 7.47 (dd, *J* = 8.2, 5.5 Hz, 1H, H¹⁰), 7.35 (d, *J* = 8.4 Hz, 1H, H⁷), 6.83 (d, *J* = 9.1 Hz, 1H, H³). ¹³C {¹H} NMR (125.58 MHz, δ, CDCl₃): 168.9 (C²), 153.6 (C¹¹), 148.7 (C¹⁴), 146.5 (C¹³), 138.5 (C⁹), 136.4 (C⁴), 129.1 (C⁵), 127.0 (C⁶), 125.6 (C³), 122.1 (C¹⁰), 121.1 (C⁸), 118.1 (C⁷). IR (neat, cm⁻¹): ν (CO, st) 1626 cm⁻¹. Anal. Calcd. For: C₂₄H₁₄N₄O₂Pd: C, 58.02 %; H, 2.84 %; N, 11.28 %. found: C, 58.30 %; H, 3.14 %; N, 11.12 %.

**[Pd(bipy-6-OH)Cl₂] (25a)**

[2,2'-Bipyridin]-6(*H*)-one (bipy-6-OH) (72.0 mg, 0.41 mmol) was added to a solution of PdCl₂ (74.1 mg, 0.41 mmol) in CH₂Cl₂ (30 mL). The mixture was stirred at reflux for 16 h. During this time the brown suspension became yellow and a precipitate was observed. The yellow solid was filtered, washed with cold CH₂Cl₂ (3 x 5 mL), Et₂O (3 x 5 mL) and air-dried. Yield: 105 mg (72 %).

¹H NMR (499.73 MHz, δ, DMSO-*d*₆): 11.97 (br, 1H, OH), 9.10 (d, *J* = 5.4 Hz, 1H, H^{6'}), 8.47 (d, *J* = 8.1 Hz, 1H, H³), 8.29 (td, *J* = 7.7, 1.2 Hz, 1H, H^{4'}), 8.14 (t, *J* = 7.2 Hz, 1H, H⁴), 8.08 (br, 1H, H³), 7.72 (t, *J* = 7.7 Hz, 1H, H^{5'}), 7.07 (d, *J* = 8.0 Hz, 1H, H⁵). ¹³C {¹H} NMR (125.58 MHz, δ, DMSO-*d*₆): 167.3 (C⁶), 158.3 (C²), 153.8 (C²), 143.6 (C⁴), 141.8 (C⁴), 127.1 (C⁵), 124.4 (C³), 117.1 (C⁵), 116.5 (C³), 105.1 (C⁶). IR (neat, cm⁻¹): ν (OH, st) 3078; ν (Pd-Cl), 337, 329.



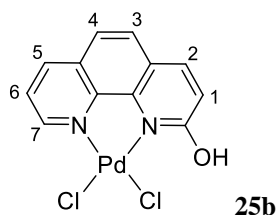
[Pd(phen-2-OH)Cl₂] (25b)

1,10-phen-2(*H*)-one (phen-2-OH) (131.1 mg, 0.67 mmol) was added to a solution of PdCl₂ (118.5 mg, 0.68 mmol) in CH₂Cl₂ (90 mL). The mixture was stirred at reflux for 24 h. During this time the brown suspension became yellow and a precipitate was observed. The yellow solid was filtered, washed with cold CH₂Cl₂ (3 x 5 mL), Et₂O (3 x 5 mL) and air-dried. Yield: 200 mg (80 %).

¹H NMR (499.73 MHz, δ, CDCl₃, 323 K): 12.96 (s, 1H, OH), 9.67 (d, J = 5.0 Hz, 1H, H⁷), 8.51 (d, J = 8.1 Hz, 1H, H⁵), 8.30 (d, J = 8.7 Hz, 1H, H²), 7.88 (d, J = 8.6 Hz, 1H, H⁴), 7.82 (d, J = 8.6 Hz, 1H, H³), 7.78 (dd, J = 7.8, 5.5 Hz, 1H, H⁶), 7.25 (1H, H¹).*

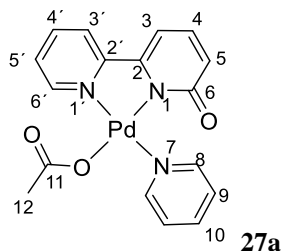
¹H NMR (499.73 MHz, δ, CD₃CN, 323 K): 12.64 (s, 1H, OH), 9.50 (d, J = 5.0 Hz, 1H), 8.73 (d, J = 8.1 Hz, 1H), 8.55 (d, J = 8.7 Hz, 1H), 8.05 (d, J = 8.6 Hz, 1H), 7.99 (d, J = 8.6 Hz, 1H), 7.90 (dd, J = 7.8, 5.5 Hz, 1H), 8.27 (d, J = 8.7 Hz, 1H). IR (neat, cm⁻¹): ν (OH, st) 3054; ν (Pd-Cl) 333 (br).

* Signal overlapped with chloroform. The ¹³C signals could not be observed due to the low solubility of this complex.

**[Pd(bipy-6-O)(κ¹-OAc)(py)] (27a)**

Pyridine (194 μL, 2.4 mmol) was added to a solution of [Pd(OAc)₂] (54.0 mg, 0.24 mmol) in 12 mL of CH₂Cl₂. After 15 min at room temperature, ligand phen-2-OH (41.5 mg, 0.24 mmol) was added. The mixture was stirred at room temperature for 2 h. During this time the orange solution became intense yellow. The solvent was evaporated to *c.a.* 3 mL and hexane (10 mL) was added to the suspension. The yellow solid obtained was filtered, washed with cold Et₂O (3 x 5 mL) and air-dried. Yield: 60 mg (60 %).

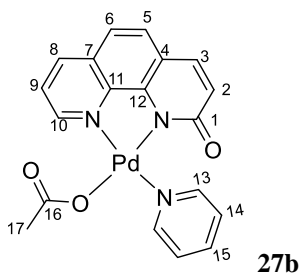
¹H NMR (499.73 MHz, CDCl₃): δ 8.91 (d, J = 6.5 Hz, 2H, H⁸), 8.19 (d, J = 5.7 Hz, 1H, H^{6'}), 7.91 (td, J = 8.0, 1.5 Hz, 1H, H⁴), 7.77 (tt, J = 7.7, 1.6 Hz, 1H, H¹⁰), 7.75 (m, 1H, H³), 7.33 (t, 2H, H⁹), 7.30 (m, 1H, H^{4'}), 7.21 (dd, J = 8.8, 6.9 Hz, 1H, H⁵), 6.69 (dd, J = 7.0, 1.0 Hz, 1H, H³), 6.32 (dd, J = 8.8, 1.1 Hz, 1H, H⁵), 2.0 (s, 3H, H¹²).



[Pd(phen-2-O)(κ^1 -OAc)(py)] (27b)

Pyridine (200 μ L, 2.5 mmol) was added to a solution of [Pd(OAc)₂] (51.0 mg, 0.227 mmol) in 20 mL of CH₂Cl₂. After 10 min at room temperature, ligand phen-2-OH (44.5 mg, 0.227 mmol) was added. The mixture was stirred at room temperature for 2 h. During this time the orange solution became intense yellow. The solvent was evaporated to *c.a.* 5 mL and cold Et₂O/acetone (1:0.5 v/v) (10 mL) was added to the suspension. The yellow solid obtained was filtered, washed with cold Et₂O (3 x 5 mL) and air-dried. Yield: 73 mg (75 %).

¹H NMR (499.73 MHz, CDCl₃): 9.04 (m, 2H, H¹³), 8.36-8.34 (m, 2H, H⁸, H¹⁰), 7.82 (tt, J = 7.7, 1.5 Hz, 1H, H¹⁵), 7.60 (d, J = 9.0 Hz, 1H, H³), 7.58 (d, J = 8.3 Hz, 1H, H⁶), 7.53 (dd, J = 8.2, 5.2 Hz, 1H, H⁹), 7.40 (m, 2H, H¹⁴), 7.34 (d, J = 8.3, 1H, H⁵), 6.53 (d, J = 9.0 Hz, 1H, H²), 2.02 (s, 3H, H¹⁷). ¹³C{¹H} NMR (125.67 MHz, CDCl₃): 178.3 (C¹⁶), 168.9 (C¹), 153.2 (C¹³), 147.1 (C¹², C¹⁰), 145.5 (C¹¹), 138.7 (C⁸), 138.1 (C¹⁵), 136.0 (C³), 129.0 (C⁷), 127.7 (C⁶), 125.8 (C²), 124.4 (C¹⁴), 121.7 (C⁹), 121.1 (C⁴), 117.6 (C⁵), 23.0 (C¹⁷).

**3.4.3 Catalytic reactions****General Procedure for direct arylation of toluene****Method A (toluene as solvent):**

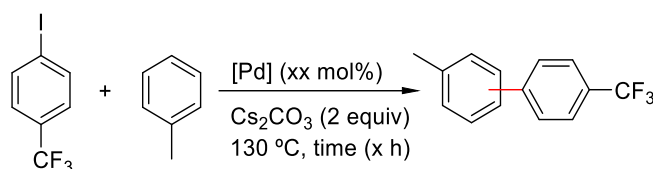
[Pd(OAc)₂] (3.8 mg, 0.017 mmol), bipy-6-OH (2.93 mg, 0.017 mmol) and cesium carbonate (222 mg, 0.68 mmol) were introduced in a Schlenk flask with a screw cap in a nitrogen atmosphere. Then, toluene (3 mL) and the aryl iodide (*p*-CF₃C₆H₄I) (51 μ L, 0.34 mmol) were added. The mixture was kept in a preheated-bath at 130 °C for 6-24 h. After this time, the conversion was checked by ¹⁹F NMR of the crude mixture. The crude yields and isomer distribution are collected in Tables 3.5 and 3.6. The number and ratio of isomers was determined by ¹⁹F NMR. The arene was then removed under vacuum and *n*-hexane (3 mL) and EtOAc (0.3 mL) were added to the residue to extract the organic product. The suspension was filtered off. The filtrate was evaporated to dryness obtaining a yellowish residue. Finally, the product was purified by column chromatography using silica gel (see ref: 52). The characterization of the three isomers: 3-methyl-4'-(trifluoromethyl)-1,1'-biphenyl,^{52a,131} 4-methyl-4'-(trifluoromethyl)-1,1'-biphenyl,^{52a,132} and 2-methyl-4'-(trifluoromethyl)-1,1'-biphenyl,^{52a,132} has been reported before.

¹³¹ Lian, Z.-Y.; Yuan, J.; Yan, M.-Q.; Liu, Y.; Luo, X.; Wu, Q.-G.; Liu, S.-H.; Chen, J.; Zhu, X.-L.; Yu, G.-A. *Org. Biomol. Chem.* **2016**, *14*, 10090–10094.

¹³² Shi, S.; Meng, G.; Szostak, M. *Angew. Chem. Int. Ed.* **2016**, *55*, 6959–6963.

Method B (DMA as co-solvent):

[Pd(OAc)₂] (3.8 mg, 0.017 mmol), bipy-6-OH (2.93 mg, 0.017 mmol) and cesium carbonate (222 mg, 0.68 mmol) were introduced in a Scklenk flask with a screw cap in a nitrogen atmosphere. Then, toluene (1.5 mL), *N,N*-dimethylacetamide (1.5 mL) and the aryl iodide (*p*-CF₃C₆H₄I) (51 μL, 0.34 mmol) were added. The mixture was kept in a preheated-bath at 130 °C for 6-24 h. After this time, the conversion was checked by ¹⁹F NMR of the crude mixture.

**Equation 3.9****Table 3.5** Direct arylation of toluene with *p*-CF₃C₆H₄I and precatalyst Pd-complexes bearing bipy-6-OH according to Equation 3.9.^a

Entry	Toluene/ DMA (v/v %)	[Pd] (5 mol %)	Crude yield, %, (reaction time) ^b	Crude yield ratio (<i>o</i> / <i>m</i> / <i>p</i>)	Byproducts Crude yield, %, (reaction time) ^b
1	1/0	-	- (24h)	-	
2	1/0	[Pd(OAc) ₂]	- (24h)	-	
3	1/0	[Pd(OAc) ₂]+ bipy	0 (6h), 1 (24h)	-	-
4	1/0	[Pd(OAc) ₂]+bipy-6-OH	20 (6h), 91 (24h)	0.1:1:0.45	9 (24h)
5	1/0	23a	82 (6h)	0:1:0.5	18 (6h)
6	1/0	24a	18 (6h), 94 (24 h)	0.17:1:0.6	4 (6h), 6 (24 h)
7	1/0	25a	65 (6h), 89 (24h)	0.48/1/0.0 6	3 (6h), 11 (24h)
8	1/0	[Pd(bipy-6OH)Br(C ₆ F ₅)]	61 (6h), 90 (24h)	0.1:1:0.45	10 (24h)
9	1/1	[Pd(OAc) ₂]+bipy-6-OH	96 (6h)	0.6:1:0.77	4 (6h)
10	1/1	23a	93 (6h)	0.84:1:0.7 7	7 (6h)
11	1/1	24a	95 (6h)	0.8:1:0.77	5 (6h)
12	1/1	25a	88 (6h)	0.6/1/0.7	12 (6h)
13	1/1	[Pd(bipy-6-OH)Br(C ₆ F ₅)]	94 (6h)	0.25:1:0.7 5	6 (24h)

^a Reaction conditions: *p*-CF₃C₆H₄I (51 μL, 0.34 mmol), toluene (3 mL) or toluene/DMA (1.5/1.5 mL), [Pd] (5 mol%), Cs₂CO₃ (222 mg, 0.68 mmol); 130 °C. ^b Crude yields determined by ¹⁹F NMR of the reaction mixture. The reduction product of the aryl iodide (ArH) and the homocoupling derivative (Ar-Ar) are the observed byproducts.

Table 3.6 Direct arylation of toluene with *p*-CF₃C₆H₄I and precatalyst Pd-complexes bearing phen-2-OH according to Equation 3.9.^a

Entry	Toluene/ DMA (v/v %)	[Pd]/Ligand (5 mol%)	Crude yield, %, (reaction time) ^b	Crude yield ratio (<i>o</i> / <i>m</i> / <i>p</i>)	Byproducts Crude yield, %, (reaction time) ^b
1	1/0	[Pd(OAc) ₂] + 1,10-phen	0 (6h), 1 (24h)	-	3 (24h)
2	1/0	[Pd(OAc) ₂] + phen-2-OH	6 (6h), 18 (24h)	0.35:1:0.5	8 (24h)
3	1/0	23b	15 (6h), 29 (24h)	0.37:1:0.5	7 (6h), 12 (24h)
4	1/0	24b	3 (6h), 50 (24h)	0.48:1:0.56	1 (6h), 7 (24h)
5	1/0	25b	4 (6h), 19 (24h)	0.46/1/0.12	1 (6h), 12 (24h)
6	1/0	[Pd(phen-2-OH)Br(C ₆ F ₅)]	17 (6h), 31 (24h)	0.26:1:0.56	4 (24h)
7	1/1	[Pd(OAc) ₂] + phen-2-OH	79 (6h)	0.2:1:0.6	21 (6h)
8	1/1	23b	93 (6h)	1.3:1:0.8	2 (6h)
9	1/1	24b	97 (6h)	1.7:1:0.85 (1.5:1:0.84) ^c	3 (6h)
10	1/1	25b	88 (6h)	0.64/1/0.8	12 (6h)
11	1/1	[Pd(phen-2-OH)Br(C ₆ F ₅)]	18 (6h), 30 (24h)	0.2:1:0.5	39 (24h)

^a Reaction conditions: *p*-CF₃C₆H₄I (51 μL, 0.34 mmol), toluene (3 mL) or toluene/DMA (1.5/1.5 mL), [Pd] (5 mol%), Cs₂CO₃ (222 mg, 0.68 mmol); 130 °C. ^b Crude yields determined by ¹⁹F NMR of the reaction mixture. The reduction product of the aryl iodide (ArH) and the homocoupling derivative (Ar–Ar) are the observed byproducts. ^c Isolated isomer distribution.

3.4.4 Decomposition of 23a in toluene at high temperature

Complex **23a** (8.0 mg, 0.013 mmol) was added to an NMR tube with 0.6 mL of toluene. The mixture was heated to 130 °C for 2 h and then the suspension was filtered through Kieselghur and activated charcoal to remove the Pd black formed. The solution was evaporated to dryness and analysed by mass spectrometry (GC_MS).

Isomer 1 (retention time 15.89 min); Isomer 2 (retention time 15.92 min); Isomer 3 (retention time 16.04 min); Isomer 4 (retention time 16.08 min); Isomer 5 (retention time 16.19 min); Isomer 6 (retention time 16.22 min). MS (EI+, 70 eV): *m/z* (100 %) 182.12 [M⁺],

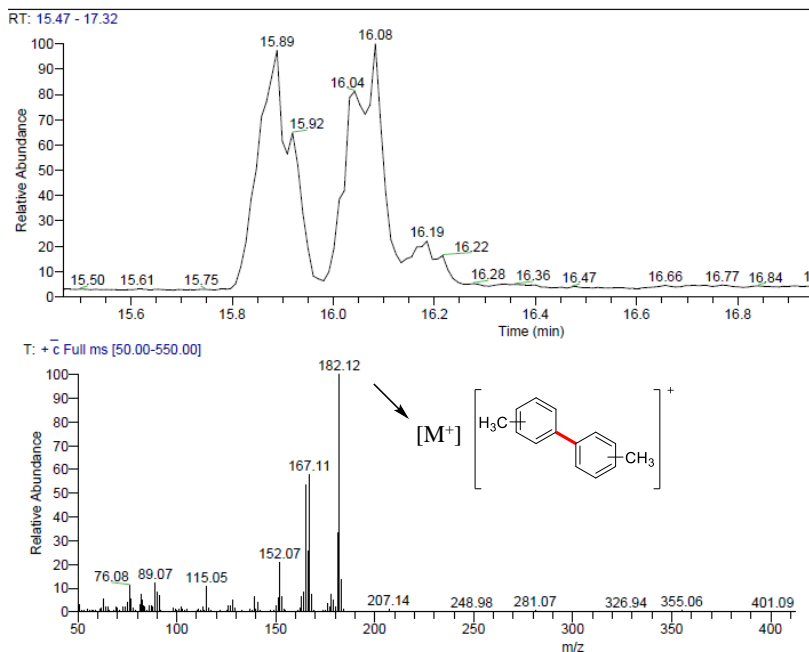


Figure 3.7 Chromatogram and mass spectrum for the extracted residue of reaction depicted in Equation 3.8.

3.4.5 Reactivity of *bipy-6-OH* and *phen-2-OH* with $[Pd(OAc)_2]$ in different solvents ($CDCl_3$, DMA and DMSO). Reorganization studies

Ligand *bipy-6-OH* (2.5 mg, 0.014 mmol) or *phen-2-OH* (2.84 mg, 0.014 mmol) was added to a solution of $[Pd(OAc)_2]$ (3.14 mg, 0.014 mmol) in 0.6 mL of the corresponding solvent ($CDCl_3$, DMA and DMSO) in an NMR tube. The reaction was monitored by 1H NMR, using a sealed glass capillary filled with DMSO- d_6 as NMR lock reference in the case of DMA as a solvent. In the specified cases, the mixture was heated to 120 °C (see Figure 3.4 and Tables 3.1, 3.2 and 3.3).

Complex $[Pd(bipy-6-O)_2]$ (**24a**) (5.38 mg, 0.012 mmol) or $[Pd(phen-2-O)_2]$ (**24b**) (5.96 mg, 0.012 mmol) was added to a solution of $[Pd(OAc)_2]$ (2.70 mg, 0.012 mmol) in 0.6 mL of ($CDCl_3$ or DMA) in an NMR tube at room temperature. The reaction was monitored by 1H NMR using a sealed glass capillary filled with DMSO- d_6 as NMR lock reference in the case of DMA as a solvent. In the course of the reaction a yellow precipitate appears, which was filtered and washed with diethyl-ether (2 x 5 mL). The identity of the obtained yellow solid was checked by redissolving a small amount in $CDCl_3$ at room temperature.

3.4.6 DOSY experiments

The experiments were recorded with an Agilent MR-500 spectrometer. All spectra were acquired at 298.15 K in 5 mm tubes. All 2D ^1H DOSY experiments were performed using 2D DOSY with convection compensation using a Gradient Compensated Stimulated Echo with Spin Lock pulse sequence (dgcsteSL_cc). In each NMR experiment a series of 16 dgcsteSL_cc spectra on 16 K data points were collected, the value of d (diffusion gradient length) was of 2.0 ms duration (unless otherwise indicated) duration with a diffusion delay (Δ) of 50 ms and the relaxation time (t_1) between acquisition was set to 1 s.

Experiments in DMSO- d_6 as a solvent

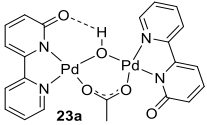
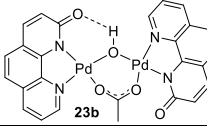
For the calibration line, different tubes were charged with standard substances with a molecular weight in the range of 88–1030 / g mol^{-1} that are soluble in DMSO- d_6 . The quantities of the standard used were chosen to obtain a similar signal intensity on the final spectrum. High-viscosity solvents such as DMSO- d_6 are the most suitable choice for DOSY experiments since it creates less temperature convection.

Table 3.7 Results of diffusion experiments of different compounds in DMSO- d_6 for the calibration line.^a

Entry	Standards	MW / g mol^{-1}	$D / \times 10^{-10} \text{ m}^2 \text{ s}^{-1}$ (DMSO- d_6)	+/-std.err. $\text{m}^2 \text{ s}^{-1}$ (DMSO- d_6)
1	$\text{Si}(\text{CH}_3)_4$	A 88.22	6.096	1.097E-03
2	Hexamethylbenzene	B 162.27	4.221	2.597E-03
3	1,3,5-triphenylbenzene	C 306.41	2.800	3.234E-03
4	$\text{Pd}(\text{bipy})\text{Cl}_2$	D 333.51	2.856	7.546E-03
5	$\text{Pd}(\text{bipy}-6\text{-OH})(\text{Pf})(\text{Br})$	E 524.56	2.282	5.954E-03
6	Dppb	F 554.38	2.005	7.868E-03
7	$[\text{PdCl}_2(\text{PPh}_3)_2]$	G 701.89	1.807	2.984E-03
8	$[\text{Pd}(\text{Pf})_2(\text{dppe})]$	H 838.96	1.750	7.298E-03
9	$[\text{Pd}(\text{Rf})_2(\text{PPh}_3)_2]$	I 1030.93	1.612	5.242E-03

^a Diffusion gradient length optimized (2.0 ms); diffusion delay was set to 50 ms.

Table 3.8 Results of diffusion experiments for **23a** and **23b** in DMSO- d_6

Complex	MW _(theoretical) / g mol^{-1}	MW _{det} (^1H DOSY) / g mol^{-1}	$D / \times 10^{-10} \text{ m}^2 \text{ s}^{-1}$ (DMSO- d_6)	+/-std.err. $\text{m}^2 \text{ s}^{-1}$ (DMSO- d_6)
 23a	631.25	642.23	1.974	6.890E-03
 23b	679.29	680.84	1.911	2.023E-02

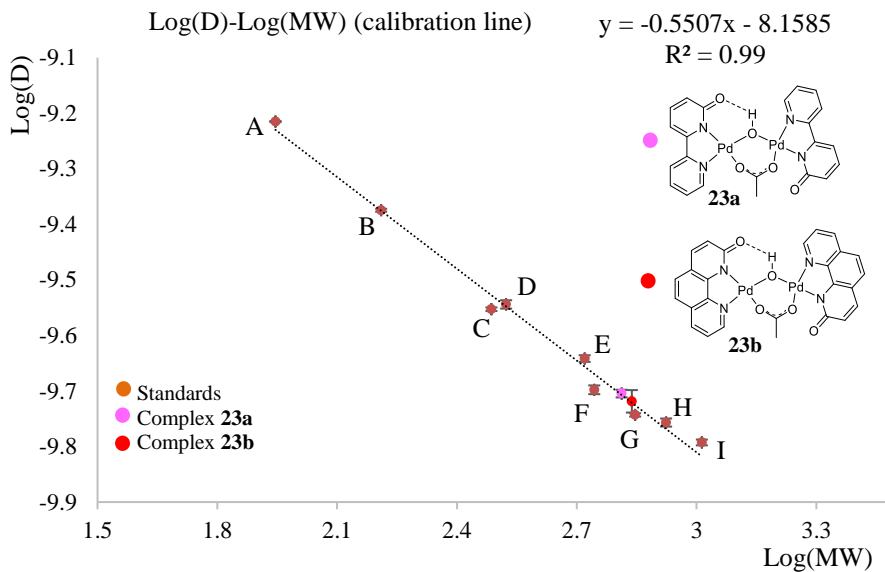


Figure 3.8 LogD–LogMW plot from the ^1H DOSY NMR data obtained for the standards at 298 K in DMSO-d_6 . The MW determined for **23a** (5.0 mM) and **23b** (2.3 mM) were 642 and 680, respectively.

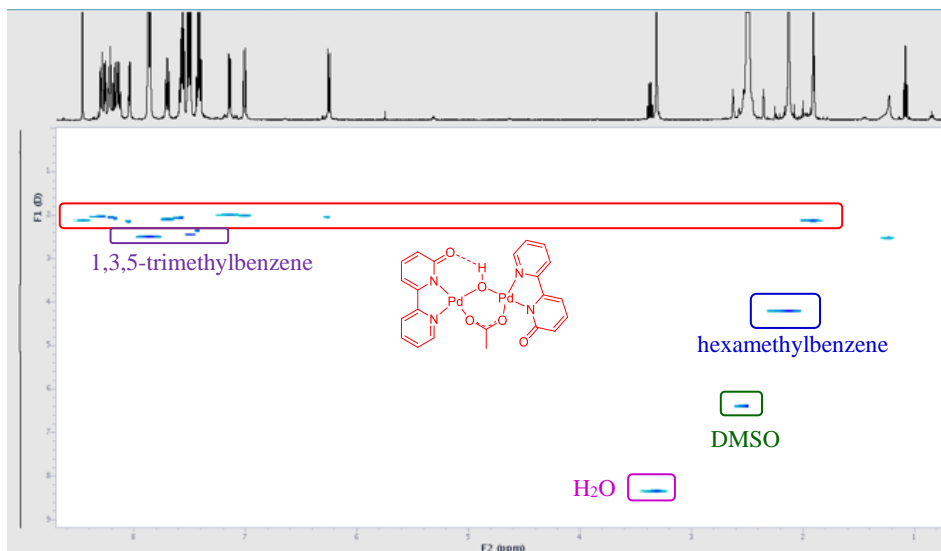


Figure 3.9 ^1H -DOSY NMR spectrum of complex **23a** in DMSO-d_6 (5.0 mM) at 298 K in presence of the standards (hexamethylbenzene and 1,3,5-trimethylbenzene).

3.4.7 Mass spectrometry

Mass spectrometry experiments on the isolated dimeric complexes **23a** and **23b** showed the presence of a species of composition “[$\text{Pd}_2(\mu\text{-OH})(\text{ligand})_2$]” (ligand = bipy-6-O or phen-2-O) without the acetato bridging fragment.

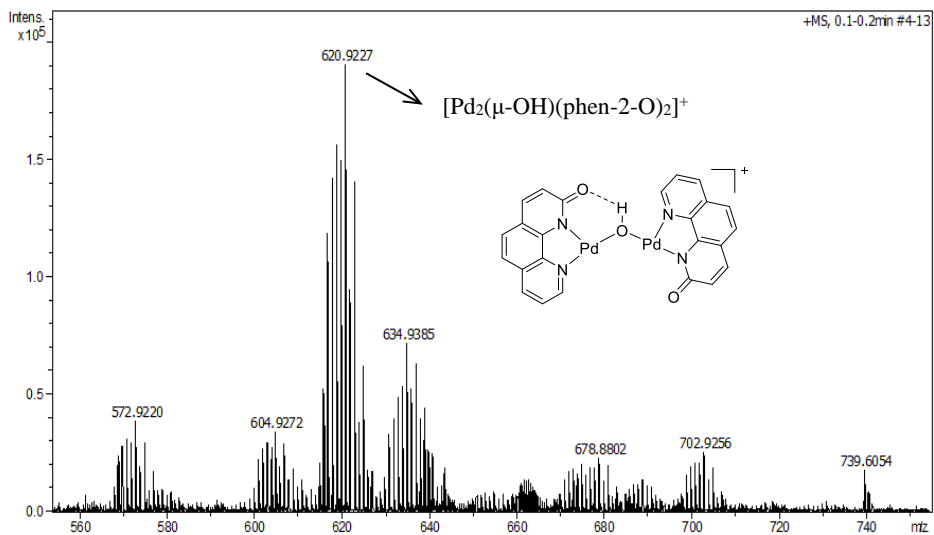


Figure 3.10 HR-MS (ESI-TOF) (positive mode) of complex **23b**.

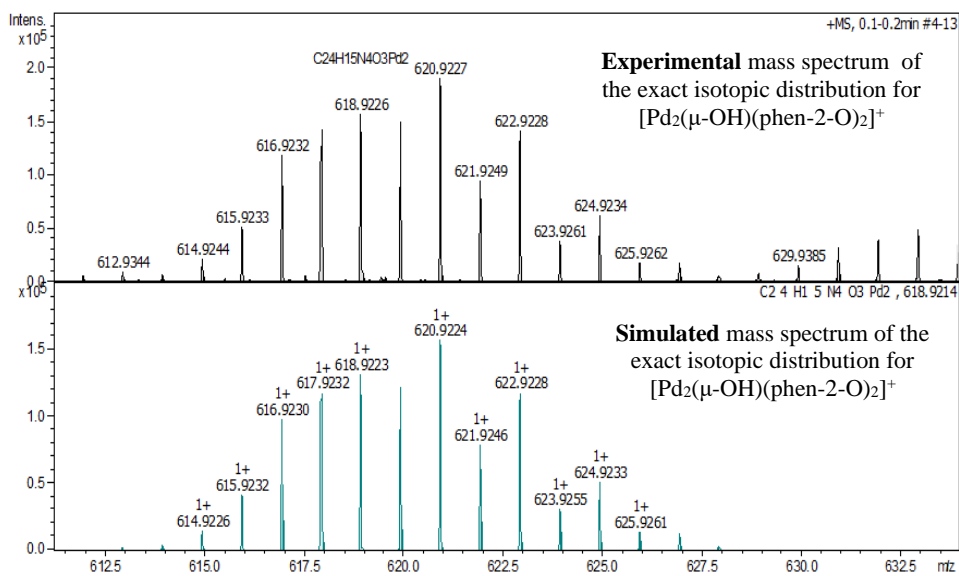


Figure 3.11 HR-MS (ESI-TOF) (positive mode) comparison between simulated and experimental isotopic distribution of $[\text{Pd}_2(\text{phen-2-O})_2(\mu\text{-OH})]^+$ fragment.

Meas. m/z	m/z	err [ppm]	mSigma	Ion Formula
618.9226	618.9223	-0.4	13.9	$\text{C}_{24}\text{H}_{15}\text{N}_4\text{O}_3\text{Pd}_2$

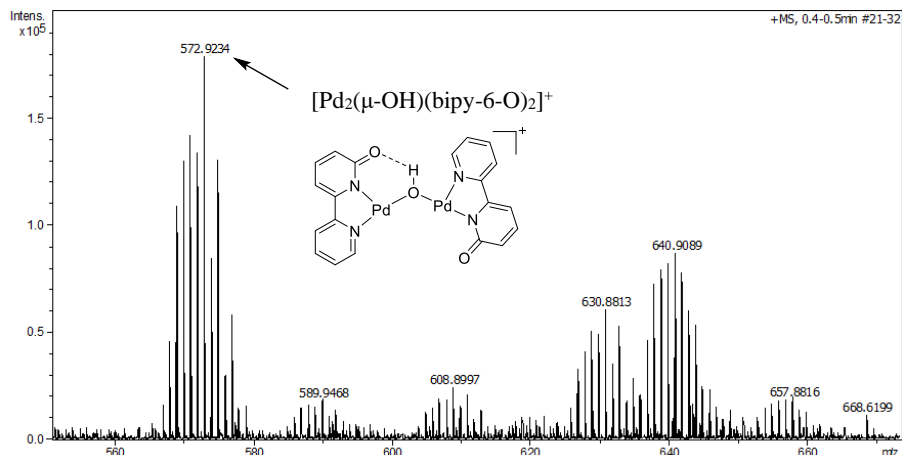


Figure 3.12 HR-MS (ESI-TOF) (positive mode) of complex **23a**.

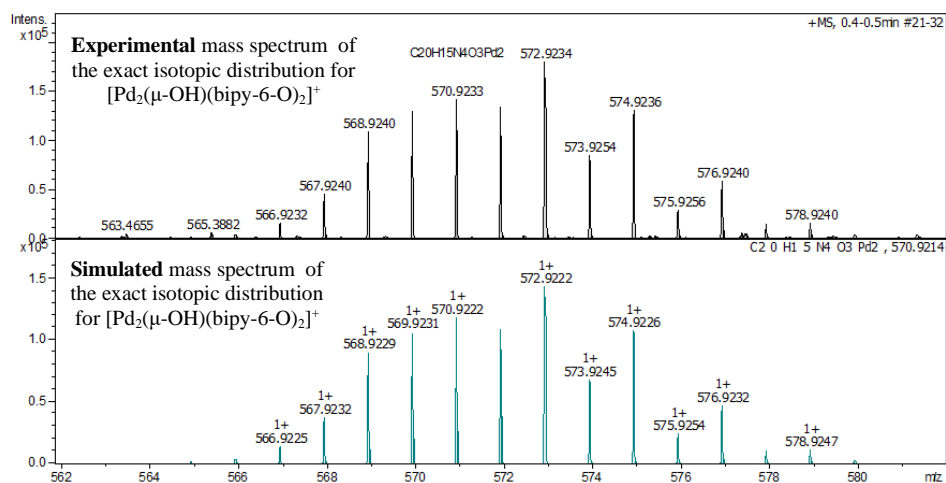


Figure 3.13 HR-MS (ESI-TOF) (positive mode) comparison between simulated and experimental isotopic distribution of $[\text{Pd}_2(\text{bipy-6-O})_2(\mu\text{-OH})]^+$ fragment.

Meas. m/z	m/z	err [ppm]	mSigma	Ion Formula
570.9233	570.9222	-1.9	13.1	$\text{C}_{20}\text{H}_{15}\text{N}_4\text{O}_3\text{Pd}_2$

3.4.8 Data for X-Ray structure determinations

Crystals suitable for X-ray analyses were obtained by slow evaporation of the solvent (CHCl_3 or CH_2Cl_2) at room temperature. In each case, the crystal was attached to the tip of a glass fiber and transferred to an Agilent Supernova diffractometer with an Atlas CCD area detector. Data collection was performed with Mo $K\alpha$ radiation (0.71073 Å) at 298 K. Data integration and empirical absorption correction was carried out using the CrysAlisPro program package.¹¹⁵ The structures were solved by direct methods and

refined by full-matrix least squares against F^2 with SHELX,¹¹⁶ in OLEX2.¹¹⁷ The non-hydrogen atoms were refined anisotropically and hydrogen atoms were constrained to ideal geometries and refined with fixed isotropic displacement parameters. Refinement proceeded smoothly to give the residuals shown in Table 3.9.

Complex **24a** crystallizes with a chloroform molecule and three H₂O molecules. The molecular structure of complex **25a** is affected by positional disorder (see below). Two independent molecules were found in the asymmetric unit for complex **27a** that crystallizes with an acetic acid molecule.

Table 3.9 Crystal data and structure refinement parameters for complexes **24a**, **25a** and **27a**.

Compound number	24a	25a	27a
Empirical formula	C ₂₁ H ₂₁ Cl ₃ N ₄ O ₅ Pd	C ₁₀ H ₈ Cl ₂ N ₂ OPd	C ₃₆ H ₃₄ N ₆ O ₈ Pd ₂
Formula weight	622.17	349.48	891.49
Temperature/K	298	298	298
Crystal system	triclinic	orthorhombic	triclinic
Space group	P-1	Cmcm	P-1
a/Å	10.5926(4)	18.0668(11)	12.1782(6)
b/Å	10.6027(4)	9.1840(3)	12.4021(9)
c/Å	12.3597(3)	6.7915(3)	12.7344(8)
α /°	101.831(3)	90	70.416(6)
β /°	102.824(3)	90	81.812(5)
γ /°	108.565(4)	90	79.554(5)
Volume/Å ³	1224.66(8)	1126.88(9)	1775.1(2)
Z	2	4	2
$\rho_{\text{calc}}/\text{cm}^3$	1.687	2.060	1.668
μ/mm^{-1}	1.125	2.097	1.074
F(000)	624.0	680.0	896.0
Crystal size/mm ³	0.359 × 0.348 × 0.139	0.238 × 0.068 × 0.043	0.835 × 0.113 × 0.079
Radiation	Mo K α (λ = 0.71073)	Mo K α (λ = 0.71073)	Mo K α (λ = 0.71073)
2 θ range for data collection/°	6.654 to 59.382	7.796 to 59.082	6.818 to 59.066
Index ranges	-13 ≤ h ≤ 14, -13 ≤ k ≤ 14, -15 ≤ l ≤ 15	-22 ≤ h ≤ 24, -12 ≤ k ≤ 12, -9 ≤ l ≤ 8	-16 ≤ h ≤ 12, -16 ≤ k ≤ 13, -16 ≤ l ≤ 11
Reflections collected	20110	9036	12207
Independent reflections	6092 [R _{int} = 0.0269, R _{sigma} = 0.0291]	853 [R _{int} = 0.0373, R _{sigma} = 0.0190]	8090 [R _{int} = 0.0270, R _{sigma} = 0.0689]
Data/restraints/parameters	6092/0/316	853/0/54	8090/0/472
Goodness-of-fit on F ²	1.042	1.153	1.068
Final R indexes [I ≥ 2 σ (I)]	R ₁ = 0.0341, wR ₂ = 0.0779	R ₁ = 0.0262, wR ₂ = 0.0521	R ₁ = 0.0512, wR ₂ = 0.0974
Final R indexes [all data]	R ₁ = 0.0426, wR ₂ = 0.0850	R ₁ = 0.0357, wR ₂ = 0.0561	R ₁ = 0.0948, wR ₂ = 0.1230
Largest diff. peak/hole / e Å ⁻³	0.85/-0.87	0.38/-0.40	1.03/-0.98

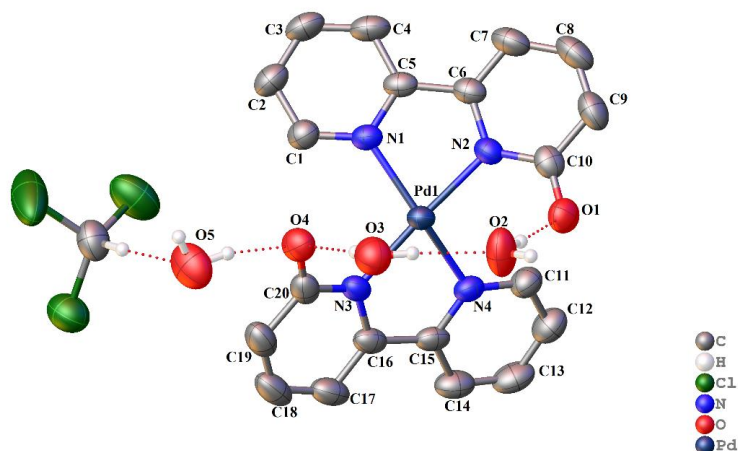


Figure 3.14 X-ray molecular structure of **24a** (ORTEP 40 % probability ellipsoids). The co-crystallized water molecules and chloroform are shown. Hydrogen atoms are omitted for clarity except those involved in hydrogen bonds between the keto-moieties and the water molecules.

Table 3.10 Selected bond lengths [Å] and angles [°] for complex **24a** (for numbering scheme see Figure 3.14).

Pd(1)-N(2)	2.014(2)	Pd(1)-N(3)	2.024(2)
Pd(1)-N(1)	2.0500(19)	Pd(1)-N(4)	2.040(2)
C(10)-C(9)	1.429(4)	C(20)-C(19)	1.425(4)
C(9)-C(8)	1.352(5)	C(19)-C(18)	1.347(5)
C(8)-C(7)	1.402(5)	C(18)-C(17)	1.398(5)
C(7)-C(6)	1.359(4)	C(17)-C(16)	1.370(4)
O(1)-C(10)	1.263(3)	O(4)-C(20)	1.259(4)
<hr/>		<hr/>	
N(2)-Pd(1)-N(1)	79.27(8)	N(3)-Pd(1)-N(4)	79.49(9)

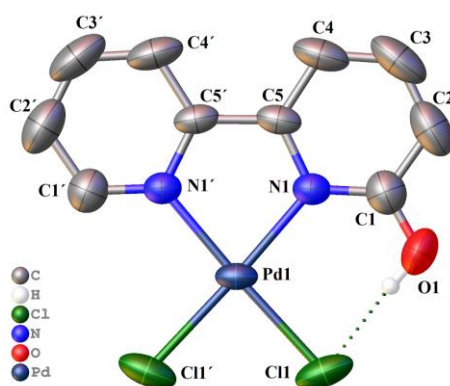
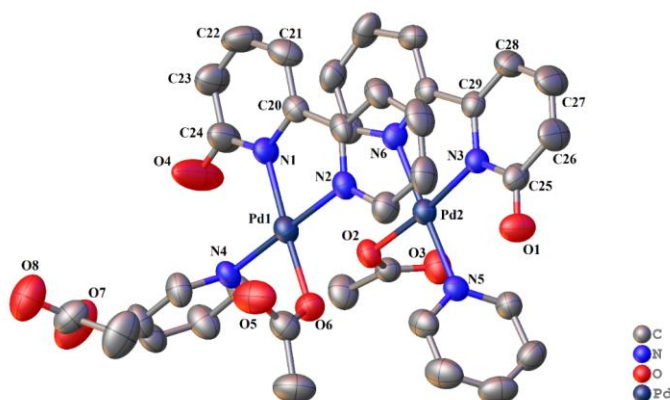


Figure 3.15 X-ray molecular structure of **25a** (ORTEP 40 % probability ellipsoids). Hydrogen atoms are omitted for clarity except for the hydrogen bond between the phenol-moiety and the chloride ligand.

Table 3.11 Selected bond lengths [Å] and angles [°] for complex **25a** (for numbering scheme see Figure 3.15).

Pd(1)-Cl(1')	2.2959(10)	C(5)-C(5')	1.460(8)
Pd(1)-Cl(1)	2.2959(10)	C(5)-C(4)	1.375(5)
Pd(1)-N(1)	2.038(3)	C(3)-C(2)	1.350(8)
Pd(1)-N(1')	2.038(3)	C(2)-C(1)	1.386(6)
N(1)-C(5)	1.358(4)	C(1)-O(1)	1.202(8)
N(1)-C(1)	1.320(5)	Cl(1)-O(1)	1.716(0)
Cl(1)-Pd(1)-Cl(1')	85.99(7)	N(1')-Pd(1)-N(1)	80.86(16)

This X-ray molecular structure of **25a** is affected by a positional disorder in the lattice of the crystal. The crystallographic solution is a superposition of molecular forms where the OH and H substituents in C1 and C1' exchange their positions. As a consequence, the resulting C-O bond distance will be an average of these situations (C-H and C-O). This site occupancy disorder could not be solved since the crystal belongs to a high symmetry space group and the structure grows by symmetry. Therefore, the C1-O1 bond length found, being 1.202(8) Å, differs from the expected single bond distance (C-O = 1.43 Å) and it is closer to the value for a typical C=O distance (1.21 Å).

**Figure 3.16** X-ray molecular structure of **27a** (ORTEP 40 % probability ellipsoids). Hydrogen atoms are omitted for clarity. The two independent molecules are shown as well as the co-crystallized acetic acid molecule.**Table 3.12** Selected bond lengths [Å] and angles [°] for complex **27a** (for numbering scheme see Figure 3.16).

Pd(1)-N(4)	2.025(4)	Pd(2)-O(2)	2.019(3)
Pd(1)-N(2)	2.000(4)	Pd(2)-N(5)	2.025(4)
Pd(1)-N(1)	2.019(4)	Pd(2)-N(6)	1.996(4)
Pd(1)-O(6)	2.034(4)	Pd(2)-N(3)	2.025(4)
C(20)-C(21)	1.368(8)	C(29)-C(28)	1.364(7)
C(21)-C(22)	1.403(9)	C(27)-C(28)	1.402(8)
C(22)-C(23)	1.325(9)	C(26)-C(27)	1.335(9)
C(24)-C(23)	1.416(9)	C(25)-C(26)	1.430(8)
C(24)-O(4)	1.233(8)	C(25)-O(1)	1.254(6)
N(2)-Pd(1)-N(1)	80.72(17)	O(2)-Pd(2)-N(5)	87.59(15)
N(4)-Pd(1)-O(6)	84.23(16)	N(6)-Pd(2)-N(3)	80.70(16)

Part II

*Reactions of Pd(II) Complexes with Carbene
Precursors*

Chapter 4

4. Introduction

4.1 The carbene fragment and metal carbenes

A carbene is a well-established chemical entity defined as an electrically neutral compound “:CR₂” that features a divalent carbon atom with only six valence electrons: Two bonding electron pairs for the R-C_{carbenic} bonds and two non-bonding electrons remaining at the carbene center (C_{carbenic}). These two electrons can adopt two different spin states: singlet (↑↓) or triplet (↑↑).¹³³

Singlet carbene compounds exhibit a bent geometry since the carbenic carbon bears a lone pair of electrons in a *sp*² hybridized orbital while a *p* orbital remains vacant. The two non-bonding electrons are spin-paired in the energetically more favourable σ orbital, leading to a singlet ground state (Figure 4.1).

A *triplet carbene* can adopt either linear or bent geometry. The carbenic carbon can be *sp*-hybridized with two non-bonding energetically degenerate *p* orbitals (*p*_x and *p*_y) or *sp*²-hybridized. In both cases, the triplet carbene exhibits two “spin up” unpaired electrons, giving rise to S=1 (Figure 4.1).

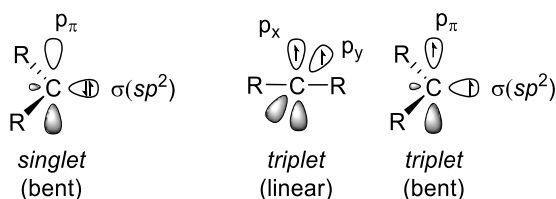


Figure 4.1 Electronic configurations of carbenes.

¹³³ a) Bourissou, D.; Guerret, O.; Gabbai, F. P.; Bertrand, G. *Chem. Rev.* **2000**, *100*, 39-91. b) Crabtree, R. H. *The Organometallic Chemistry of the Transition Metals*. 6th ed.; Wiley-VCH: Weinheim, **2014**.

The most important contribution to the electronic stabilization of the carbene fragment is the donation of electron density from the substituents that are directly bound to the carbenic carbon. In the case of atoms with electron lone pairs ($-X = -N, -O$ or $-P$), they can stabilize the carbene by decreasing the HOMO orbital energy by virtue of their higher electronegativity. More significantly, the overlap of the occupied p -orbital of the $-X$ substituent with the empty p -orbital of the carbenic carbon leads to a π -donation and thereby to reduce its electron deficiency (Figure 4.2). The electronic effect of two and to a lesser extent one $-X$ substituent and the steric hindrance exerted by the substituents in $-X$ contribute to the extraordinary stability in some of these carbene structures (Figure 4.2).

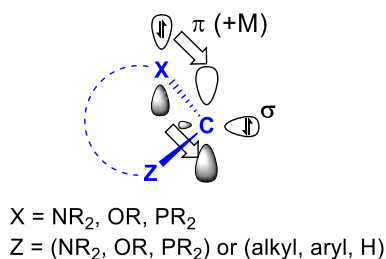


Figure 4.2 Stabilization of the carbene by adjacent electron-donating substituents.

The preparation of stable carbenes that could be isolated in a pure form was achieved by Bertrand,¹³⁴ Arduengo,¹³⁵ and co-workers who described the synthesis of the first stable phosphinocarbene and *N*-heterocyclic carbene (NHC) respectively. These pioneering works opened the door to numerous breakthroughs in transition metal catalysis among other research areas. The simplest way to describe NHC carbenes can be as compounds featuring a carbene center as part of an aromatic imidazole heterocyclic ring containing two nitrogen atoms adjacent to the carbene center. Related to these imidazolylidenes, but displaying different reactivity, are their saturated imidazolinylidene analogs (Figure 4.3). There is also no requirement for two nitrogen atoms to be adjacent to the carbene center and this leads to various NHC classes featuring other heteroatoms such as oxygen, sulfur or even carbon in place of one nitrogen.

¹³⁴ Igau, A.; Grutzmacher, H.; Baceiredo, A.; Bertrand, G. *J. Am. Chem. Soc.* **1988**, *110*, 6463–6466.

¹³⁵ a) Arduengo, A. J.; Harlow, R. L.; Kline, M. *J. Am. Chem. Soc.* **1991**, *113*, 361–363.
 b) Arduengo, A. J.; Bertrand, G. *Chem. Rev.* **2009**, *109*, 3209–3210.

Those carbenes which feature one nitrogen as the only heteroatom in a pyrrolidinylidene ring can also be stable and they are commonly referred to as cyclic (amino)(alkyl)carbenes (CAACs) or cyclic (amino)(aryl)carbenes (CAArCs)¹³⁶ (Figure 4.3).

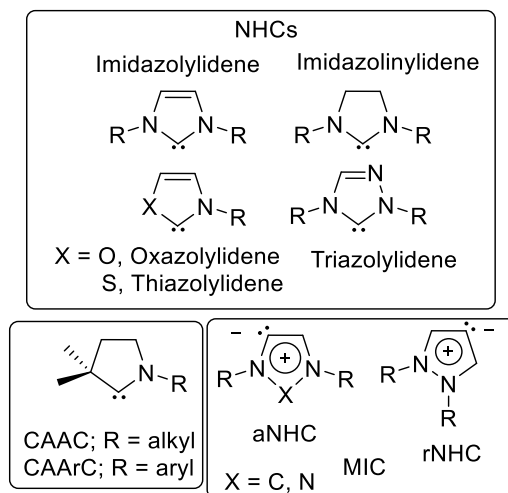


Figure 4.3 The vast family of NHCs and related carbenes.

A subclass of special NHC carbenes can be synthesized at the 4-position of imidazolylidenes. In this case, a less heteroatom stabilization allowed modulation in the donor and reactivity properties of the generated carbene. For these carbenes no reasonable canonical resonance forms containing the carbenic carbon can be drawn without additional charges and these carbenes have been named as abnormal (aNHC)

¹³⁶ a) Nolan, S. P. *N-Heterocyclic Carbenes: Effective Tools for Organometallic Synthesis*; Wiley-VCH: Weinheim, **2014**. b) Huynh, H. V. *The Organometallic Chemistry of N-Heterocyclic Carbenes*. Wiley-VCH: Weinheim, **2017**. c) Biju, A. T. *N-Heterocyclic Carbenes in Organocatalysis*. Wiley-VCH: Weinheim, **2019**. d) Jazsar, R.; Soleilhavoup, M.; Bertrand, G. *Chem. Rev.* **2020**, *120*, 4141–4168. e) Kim, H.; Lee, E. *Bull. Korean Chem. Soc.* **2022**. <https://doi.org/10.1002/bkcs.12620>.

and remote (rNHC). The term mesoionic compound (MICs)^{137,138,139} encompasses both subclasses of carbene compounds (Figure 4.3).

Attending to the two main types of bonding of the “:CR₂” to the metal and their reactivity, metal carbenes are named and classified as Fischer,¹⁴⁰ and Schrock carbenes.¹⁴¹

Schrock carbenes: Early transition metal complexes with strong donor ligands are usually involved in the formation of this type of carbenes. Due to the high energy of the *d* orbitals of the metal, a strong π -backdonation $M \rightarrow C_{\text{carbenic}}$ prevails and the carbene carbon acts as a nucleophilic center (Figure 4.4). The carbene is better described as a dianionic 4e⁻ donor ligand.

Fischer carbenes: Are usually found for late transition metals in low oxidation states and, often, the carbene fragment bears π -donor substituents (-OR or -NR₂) on the carbenic carbon. Therefore, the carbene ligand receives reduced π -backdonation from the metal since the metal *d* orbitals are strongly stabilized and the metal π -backdonation decreases. A σ -donor bond *via* the lone pair in the carbene center is the predominant feature and the carbene carbon is considered as a neutral 2e⁻ donor ligand acting as an electrophile (Figure 4.4).

¹³⁷ Mesoionic compound can be defined as: *dipolar five- (possibly six-) membered heterocyclic compounds in which both the negative and the positive charge are delocalized, for which a totally covalent structure cannot be written, and which cannot be represented satisfactorily by any one polar structure. The formal positive charge is associated with the ring atoms, and the formal negative charge is associated with ring atoms or an exocyclic nitrogen or chalcogen atom.* PAC, **1995**, 67, 1307. (Glossary of class names of organic compounds and reactivity intermediates based on structure (IUPAC Recommendations 1995)) on page 1349. <https://doi.org/10.1351/goldbook.M03842>.

¹³⁸ For reviews of MICs see: a) Vivancos, A.; Segarra, C.; Albrecht, M. *Chem. Rev.* **2018**, *118*, 9493–9586. b) Sierra, M. A.; de la Torre, M. C. *ACS Omega*, **2019**, *4*, 12983–12994.

¹³⁹ For isolation of crystalline “abnormal” *N*-heterocyclic carbene see: a) Aldeco-Perez, E.; Rosenthal, A. J.; Donnadiu, B.; Parameswaran, P.; Frenking, G.; Bertrand, G. *Science*. **2009**, *326*, 556–559. b) Guisado-Barrios, G.; Bouffard, J.; Donnadiu, B.; Bertrand, G. *Angew. Chem. Int. Ed.* **2010**, *49*, 4759–4762.

¹⁴⁰ Fischer, E. O.; Maasböl, A. *Angew. Chem. Int. Ed.* **1964**, *3*, 580–581.

¹⁴¹ Schrock, R. R. *J. Am. Chem. Soc.* **1974**, *96*, 6796–6797.

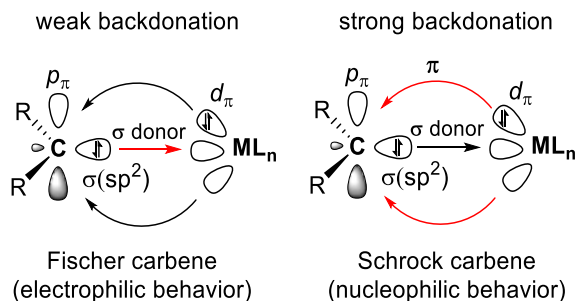


Figure 4.4

Palladium carbene complexes, which are the object of study of this thesis, fall into the Fisher-type carbene category and the discussion that follows is centered on the late transition metals, mainly palladium.

NHC-metal complexes have been deeply studied and are the best-known among all carbenes types. They are Fisher-type carbenes, with a strong σ -donor behaviour of the carbene ligand, which is easily modulated by varying the substituents on the carbenic carbon. These metal complexes are highly stable due to the reduced electrophilicity of the carbene, with generally two *N*-substituents. For all the reasons abovementioned, *N*-heterocyclic carbenes are currently used as spectator/ancillary ligands in transition metal-catalyzed transformation providing effective catalysts.¹⁴²

Compared with the rather robust metal-carbene complexes (NHC and related), those carbene ligands stabilized by only one heteroatom or none, are less common. Many of them are difficult to detect or even isolate due to their inherent high reactivity. The main role of these carbene species is proposed to be intermediates in many metal-catalyzed reactions where the carbenes are acting as building blocks rather than ancillary ligands. The electronegativity of the donor atom ($X = -N$ or $-O$) and the number of donor-substituents strongly impact on the carbene electrophilicity and the following reactivity trend is observed: $[:C(NR^1R^1)_2] < :CR^2(NR^1R^1) < :CR^1(OR^2) < :CR^1(R^2) \leq :CH(R^1)$. The electrophilicity of these carbenes can be roughly correlated with the experimental ¹³C NMR resonance of the C_{carbenic} atom for those metal-carbene complexes that can be isolated and fully characterized. For instance, a strong increase in the chemical shift of the C_{carbenic} ¹³C NMR signal is observed on going from Pd-carbene complex **A** (313.4 ppm) to Pd-carbene(NHC) complex **B** (191.4 ppm) (Figure 4.5).¹⁴³

¹⁴² Selected reviews: a) Nelson, D. J.; Nolan, S. P. *Chem. Soc. Rev.* **2013**, *42*, 6723–6753. b) Hopkinson, M. N.; Richter, C.; Schedler, M.; Glorius, F. *Nature* **2014**, *510*, 485–496. c) Zhao, Q.; Meng, G.; Nolan, S. P.; Szostak, M. *Chem. Rev.* **2020**, *120*, 1981–2048.

¹⁴³ Albéniz, A. C. *Eur. J. Inorg. Chem.* **2018**, *33*, 3693–3705.

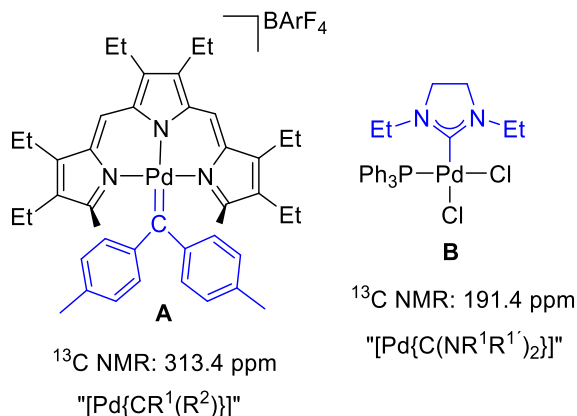


Figure 4.5 Differences in the ^{13}C NMR signal for the carbenic carbon atom depending on the number and nature of the carbene-substituents.

Several strategies to synthesize palladium carbenes bearing only one donor heteroatom as push-stabilizing substituent are collected in Scheme 4.1. All carbene complexes depicted in Scheme 4.1 have been drawn with a single Pd-C_{carbenic} bond and a multiple C-X bond as supported by the spectroscopic and X-Ray diffraction data. Short distances between the heteroatom and the carbenic carbon show an effective electron donation of the -X lone pair, leading to the formation of a C=X double bond (Figure 4.2, X = -N, -O or -S) rather than a C-X bond.

Carbene transfer reactions from group 6 metals to late transition metals have become common since Fischer *et al.* reported the transmetalation from a [Mo(C₆H₅)(CO)(NO){C(OCH₃)(C₆H₅)}] Fischer carbene to Fe(0) and Ni(0) complexes.¹⁴⁴ Hitherto, numerous reports have described the synthesis of palladium carbene complexes by this methodology. Scheme 4.1 outlines the four most representative pathways to synthesize monoamino or monoalkoxo palladium carbenes.

Various examples employing the transmetalation strategy have been reported in our group by direct transmetalation from Fischer group 6 carbenes to palladium(II) complexes which contain labile ligands, allowing a convenient carbene substitution step (Scheme 4.1, **a.1-a.3**). **Route a.1**) shows the transmetalation from the corresponding tungsten complex to [PdBr(C₆F₅)(NCMe)₂] leading to the dimeric palladium carbene **A**,

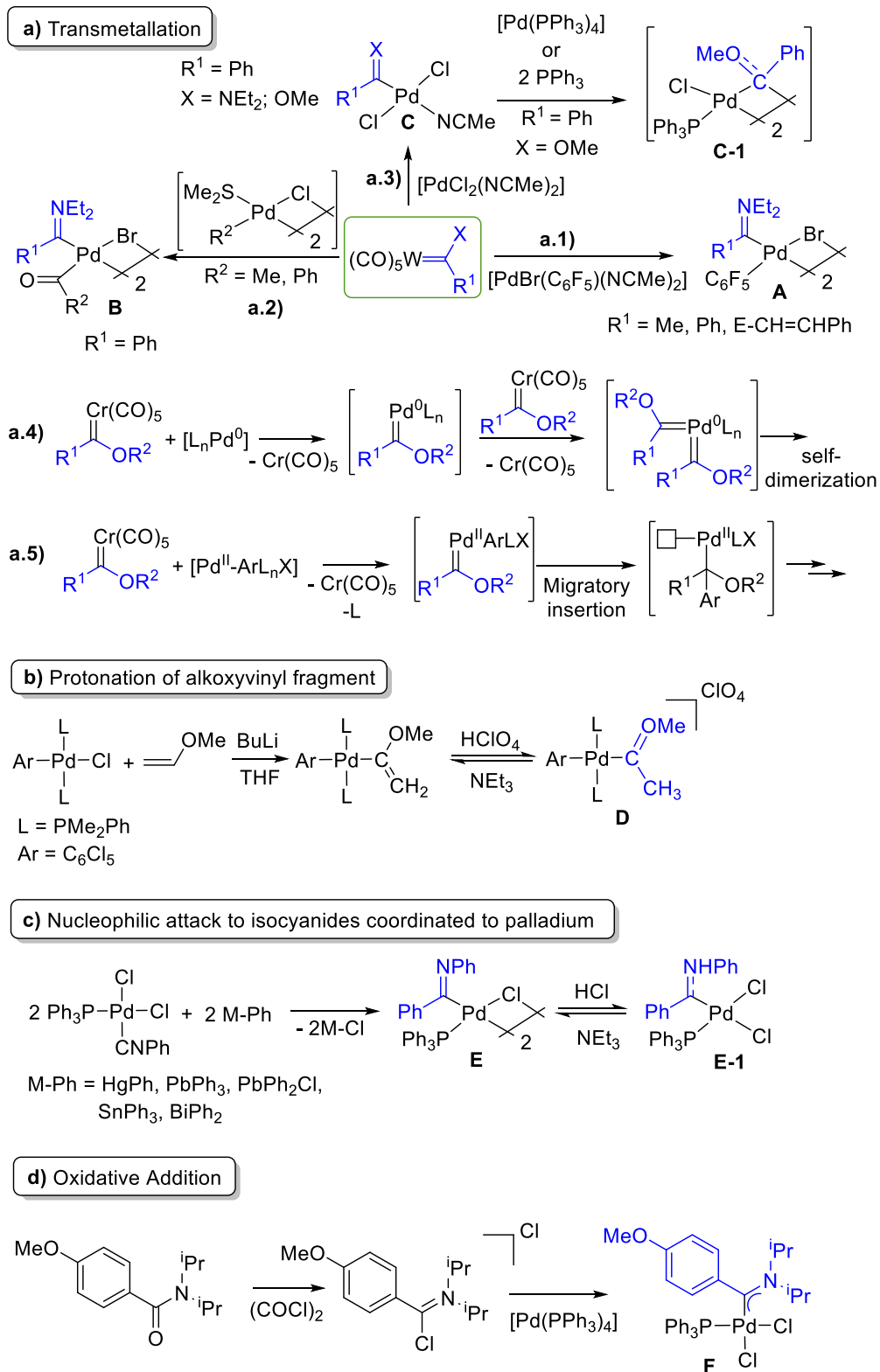
¹⁴⁴ Fischer, E. O.; Beck, H.-J. *Angew. Chem. Int. Ed.* **1970**, *9*, 72–73.

which can be isolated only in the case of the aminocarbene (Scheme 4.1, **a.1**).¹⁴⁵ **Route a.2**) depicts the transmetallation to dimeric $[\text{Pd}(\mu\text{-Cl})\text{R}(\text{SMe})_2]$ ($\text{R} = \text{Me}, \text{Ph}$) where the transfer of the carbene fragment occurs as well as the transfer of a CO ligand. The CO ligand undergoes a rapid migratory insertion into the Pd-R² bond when R is a methyl or phenyl group affording the corresponding acyl-carbene palladium complex **B** (Scheme 4.1, **a.2**).¹⁴⁶ Finally **Route a.3**) shows that the monocarbene palladium complex **C** can be synthesized by transmetallation from the tungsten carbene to $[\text{PdCl}_2(\text{NCMe})_2]$ which no -R groups preinstalled in the Pd. When the donor substituent is -OMe, complex **C** reacts in presence of palladium(0) source to afford a genuine palladium(I) alkoxocarbene complex **C-1**, where the CR(OR') carbene fragment is acting as a bridge between two palladium(I) centers (Scheme 4.1, **a.3**).¹⁴⁷

¹⁴⁵ a) Albéniz, A. C.; Espinet, P.; Manrique, R.; Pérez-Mateo, A. *Angew. Chem. Int. Ed.* **2002**, *41*, 2363–2366. b) Albéniz, A. C.; Espinet, P.; Manrique, R.; Pérez-Mateo, A. *Chem. Eur. J.* **2005**, *11*, 1565–1573. c) Albéniz, A. C.; Espinet, P.; Pérez-Mateo, A.; Nova, A.; Ujaque, G. *Organometallics*, **2006**, *25*, 1293–1297. d) Perez-Mateo, A.; Espinet, P.; Albeniz, A. C. *J. Organomet. Chem.* **2010**, *695*, 441–445.

¹⁴⁶ Meana, I.; Albéniz, A. C.; Espinet, P. *Organometallics*, **2008**, *27*, 4193–4198.

¹⁴⁷ Meana, I.; Toledo, A.; Albéniz, A. C.; Espinet, P. *Chem. Eur. J.* **2012**, *18*, 7658–7661.



Scheme 4.1 Representative methodologies for preparation of monoamino or monoalkoxo palladium complexes.

The group of Sierra has also thoroughly explored the transmetallation from group 6 monoamino or monoalkoxo carbene complexes to palladium(0).¹⁴⁸ The resulting undetected Pd(0)-carbene complexes can catalyse the self-dimerization of the parent carbene through reductive elimination in a Pd(0)-biscarbene species (Scheme 4.1, **a.4**) but other transformations such as β -elimination to afford vinyl ethers or alkyl/vinyl C-H insertions can be possible as the authors proved by experimental¹⁴⁹ and computational studies.¹⁵⁰

Along similar lines, Wang *et al.* reported the catalytic cross-coupling application of a putative aryl-Pd-alkoxocarbene that is generated from transmetallation of chromium(0)-alkoxocarbene with Pd(II)-aryl complexes (Scheme 4.1, **a.5**). The mechanism of the catalytic cycle is consistent with a transmetallation and migratory insertion step as it was supported by DFT calculations and mechanistic experiments.¹⁵¹

Heterocyclic monoamino or diamino-substituted Pd-carbenes can be synthesized by reaction with group 6 metal carbene complexes in the same vein.¹⁵²

In the case of palladium alkoxocarbenes another synthetic route has been reported by Wada *et al.*¹⁵³ (Scheme 4.1, **b**). The protonation of alkoxyvinyl palladium complex affords a cationic Pd(II)-monoalkoxo complex (**D**). This synthesis is an alternative to the transmetallation of alkoxocarbenes from group 6.

Crociani and coworkers reported in 1971 the nucleophilic attack of a phenyl group, transferred from heavy metal organometallic derivatives, to a coordinated isonitrile according to Scheme 4.1, **c**) to afford the dimeric intermediate **E**. This complex **E** undergoes bridge-splitting and reversible protonation to give the aminocarbene palladium complex **E-1**.¹⁵⁴

¹⁴⁸ Gómez-Gallego, M.; Mancheño, M. J.; Sierra, M. A. *Acc. Chem. Res.* **2005**, *38*, 44–53.

¹⁴⁹ a) Sierra, M. A.; Mancheño, M. J.; Sáez, E.; del Amo, J. C. *J. Am. Chem. Soc.* **1998**, *120*, 6812–6813. b) Sierra, M. A.; del Amo, J. C.; Mancheño, M. J.; Gómez-Gallego, M. *J. Am. Chem. Soc.* **2001**, *123*, 851–861. c) Lage, M. L.; Curiel, D.; Fernández, I.; Mancheño, M. J.; Gómez-Gallego, M.; Molina, P.; Sierra, M. A. *Organometallics* **2011**, *30*, 1794–1803.

¹⁵⁰ Fernández, I.; Mancheño, M. J.; Vicente, R.; López, L. A.; Sierra, M. A. *Chem. – A Eur. J.* **2008**, *14*, 11222–11230. López-Alberca, M. P.; Fernández, I.; Mancheño, M. J.; Gómez-Gallego, M.; Casarrubios, L.; Sierra, M. A. *European J. Org. Chem.* **2011**, 3293–3300.

¹⁵¹ Wang, K.; Lu, Y.; Hu, F.; Yang, J.; Zhang, Y.; Wang, Z.-X.; Wang, J. *Organometallics* **2018**, *37*, 1–10.

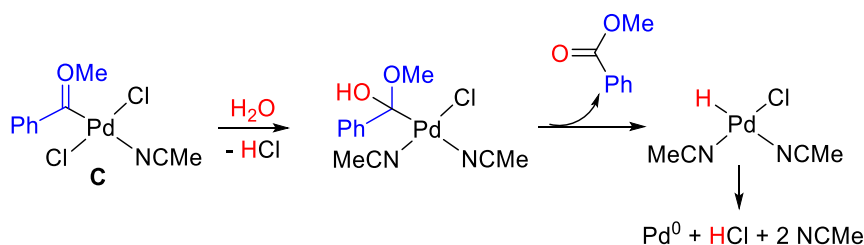
¹⁵² a) Liu, S.-T.; Hsieh, T.-Y.; Lee, G.-H.; Peng, S.-M. *Organometallics* **1998**, *17*, 993–995. b) Ku, R.-Z.; Huang, J.-C.; Cho, J.-Y.; Kiang, F.-M.; Reddy, K. R.; Chen, Y.-C.; Lee, K.-J.; Lee, J.-H.; Lee, G.-H.; Peng, S.-M.; Liu, S.-T. *Organometallics* **1999**, *18*, 2145–2154. c) Kessler, F.; Szesni, N.; Maaß, C.; Hohberger, C.; Weibert, B.; Fischer, H. *J. Organomet. Chem.* **2007**, *692*, 3005–3018.

¹⁵³ a) Wada, M.; Koyama, Y. *J. Organomet. Chem.* **1980**, *201*, 477–491. b) Wada, M.; Koyama, Y.; Sameshima, K. *J. Organomet. Chem.* **1981**, *209*, 115–121.

¹⁵⁴ Crociani, B.; Nicolini, M.; Boschi, T. *J. Organomet. Chem.* **1971**, *33*, C81–C83.

The last route, the oxidative addition, was explored by Fürstner's group (Scheme 4.1, **d**). $[\text{Pd}^0(\text{PPh}_3)_4]$ undergoes the oxidative addition of a C-Cl bond in 2-chloroimidazolium salts, affording both diamino- and monoaminocarbene Pd-complexes. Scheme 4.1, **d**) shows only the synthesis of palladium monoaminocarbene **F**.¹⁵⁵

One of the stability issues that present these palladium carbenes bearing just one heteroatom-containing substituent is the high reactivity towards nucleophiles, revealing their characteristic Fisher-type behaviour. This feature is exacerbated for the carbenic carbon with the highly electronegative -OR substituent. Complex **C** in Scheme 4.2 bearing an alkoxycarbene is highly sensitive to water due to the electrophilic character of the carbenic carbon. The decomposition by hydrolysis to the corresponding methylbenzoate and Pd(0) could be explained by nucleophilic attack of water on the carbenic carbon followed by a β -H elimination process (Scheme 4.2).¹⁴⁷



Scheme 4.2 Hydrolysis reaction of an alkoxycarbene Pd-complex by nucleophilic attack of water

However, despite the high reactivity shown by the isolated monocarbene palladium complexes in Scheme 4.1, there are a more reactive Pd-carbenes that are discussed in the next section.

4.2 Approaches to the generation of reactive metal-carbenes

The most extreme situation in terms of reactivity can be found for those late transition metal carbenes which no heteroatom adjacent to the carbenic carbon ($:\text{CR}^2(\text{R}^1)$; $\text{R}^2, \text{R}^1 = \text{hydrocarbyl}, \text{H}$). The latter are by far the most reactive and they have used as reactants in emergent and innovative synthetic methodologies. The common strategy to access these metal carbenes is the *in situ* generation from the corresponding precursors. Then, they react further leading to products that contain the carbene fragment in their

¹⁵⁵ Kremzow, D.; Seidel G.; Lehmann, C. W; Fürstner, A. *Chem. Eur. J.* **2005**, *11*, 1833–1853.

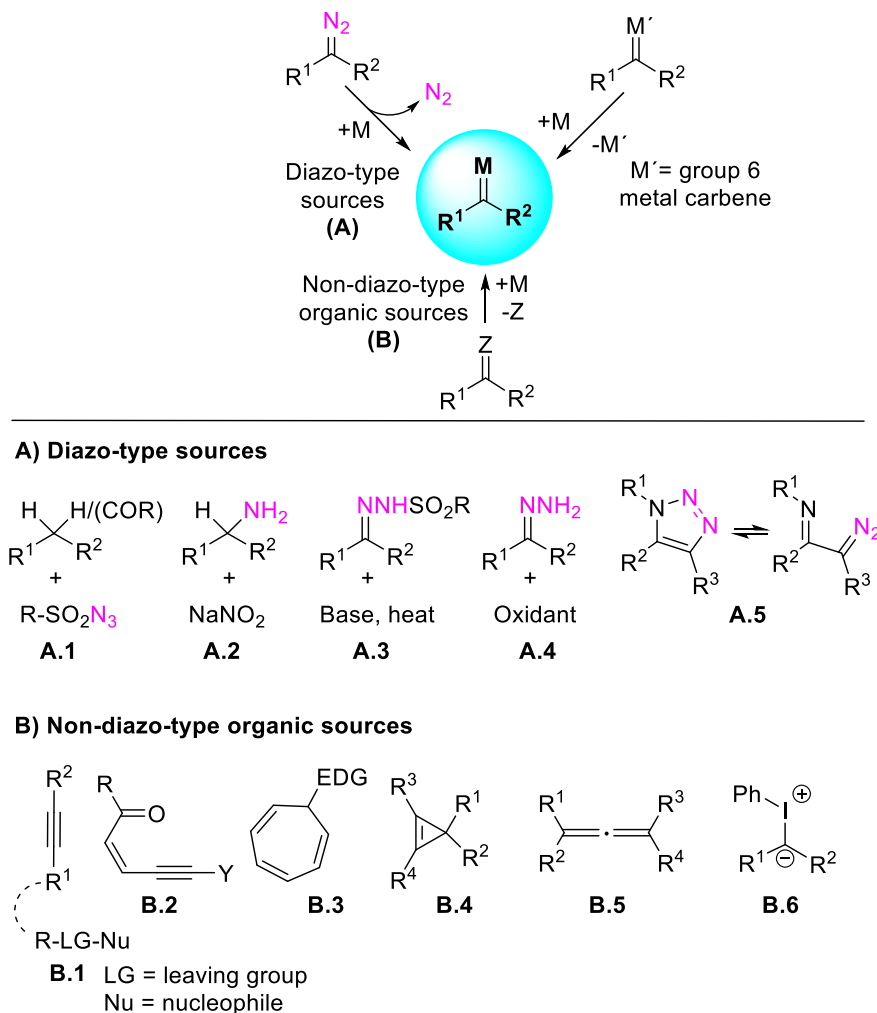
structure. The carbene precursors can be classified into three main types: diazo-type sources, non-diazo-type organic sources and group 6 metal carbenes. An array of synthetic routes for metal carbene complexes is shown in Scheme 4.3. The transmetallation from group 6 metal carbenes has been one of the strategies for the synthesis of reactive metal carbenes as it was discussed in the previous section.

Diazo-type sources include several compound types that give access to the diazo compound *via* different pathways.¹⁵⁶ In all cases the generated diazoalkane reacts with the metal precursor and, *via* N₂ extrusion, gives the corresponding metal carbene. Diazoalkanes can be generated by: i) Diazo-group transfer, from sulfonyl azide-derivatives or other electron-deficient organoazide derivatives, onto an activated methylene or methine fragment (**A.1**). ii) Diazotization of α -acceptor substituted primary aliphatic amines by treatment with sodium nitrite in aqueous media (**A.2**). iii) Decomposition by heating in the presence of base of tosylhydrazones *via* a Bamford-Stevens reaction (**A.3**). iv) Dehydrogenation/oxidation of hydrazones with oxidants. Mercuric oxide, silver oxide, manganese dioxide or organic oxidants such as TsNIK, TEMPO and oxalyl chloride have been commonly used (**A.4**). v) *N*-heterocycles such as triazole derivatives have emerged as suitable diazo compounds precursors since they exist in equilibrium with their diazoimine tautomer (**A.5**).

Non-diazo-type organic sources are precursor that lead to metal carbenes by reaction in the coordination sphere of the metal.¹⁵⁷ As shown in Scheme 4.3, they include: i) Alkynes, *via* attack of a nucleophile containing a leaving group and the intermediacy of vinyl metal species (**B.1**). ii) Ene-yne-substituted ketones or imines can generate metal carbenes under metal catalysis through 5-*exo* cyclization (**B.2**). iii) Retro-Buchner reaction of cycloheptatrienes (**B.3**). iv) Ring-opening of small, strained ring systems such as cyclopropenes (**B.4**). v) Allenes derivatives (**B.5**). vi) Hypervalent iodonium(III)-ylides (**B.6**).

¹⁵⁶ a) Regitz, M.; Maas, G. *Diazo Compounds-Properties and Synthesis*, Academic Press, Orlando, **1986**. b) Gerhard Maas, G. *Angew. Chem. Int. Ed.* **2009**, *48*, 8186–8195. c) Akter, M.; Rupa, K.; Anbarasan, P. *Chem. Rev.* **2022**, *122*, 13108–13205.

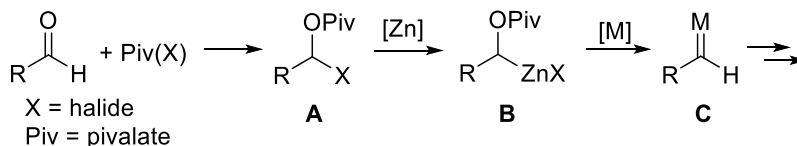
¹⁵⁷ a) Jia, M.; Ma, S. *Angew. Chem. Int. Ed.* **2016**, *55*, 9134–9166. b) Wang, K.; Wang, J. *Synlett*, **2019**, *30*, 542–551. c) Mayakrishnan, S.; Tamizmani, M.; Maheswari, N. U. *Chem. Commun.* **2020**, *56*, 15462–15465. d) Zhu, D.; Chen, L.; Fan, H.; Yao, Q.; Zhu, S. *Chem. Soc. Rev.* **2020**, *49*, 908–950.



Scheme 4.3 Major routes for the synthesis of reactive metal carbene complexes.

A very recent ground-breaking report by Nagib's group has demonstrated an alternative methodology to access this metal-carbene reactivity employing just accessible and commercial carbonyl compounds (Scheme 4.4). This approach has been tested in an array of common carbene-based catalytic reactions such as dimerization, X-H and C-C insertion, cyclopropanation, epoxidation and aziridination reactions, providing excellent results. The aldehyde compounds are readily converted in stable pivaloyl halides (**A**) which permits the formation of stable α -acyloxy Zn carbenoid intermediate (*via* Zn insertion into α -acyloxy halide intermediate) (**B**). The α -acyloxy elimination by a metal catalyst (earth-abundant metal salts of Fe, Co or Cu) forms reactive metal carbene **C**.¹⁵⁸

¹⁵⁸ a) Zhang, L.; DeMuyck, B. M.; Paneque, A. N.; Rutherford, J. E.; Nagib, D. A. *Science*. **2022**, 377, 649–654. b) West, M. S.; Rousseaux, S. A. L. *Science*. **2022**, 377, 580–581.



Scheme 4.4 Strategy to generate nonstabilized metal-carbene reactivity from aldehydes.

Among all carbene precursors known in the literature, diazo compounds are the most commonly used because of their easy decomposition through the release of nitrogen to generate the corresponding metal-carbenes. Due to their inherent handling problems, since they are potentially explosive,¹⁵⁹ some considerations must be taken into account to minimize the risk associated with working with these carbene precursors. The *in situ* generation of diazo-compounds along with “on-demand” preparation using a continuous-flow,¹⁶⁰ or photochemical transformation,¹⁶¹ methodologies are attracting special interest to incorporate these diazo compounds into synthetic applications. Only in a few cases, the isolation and purification can be achieved as long as the diazo compound are stabilized by electron-withdrawing groups (EWG-stabilized) (Figure 4.6).

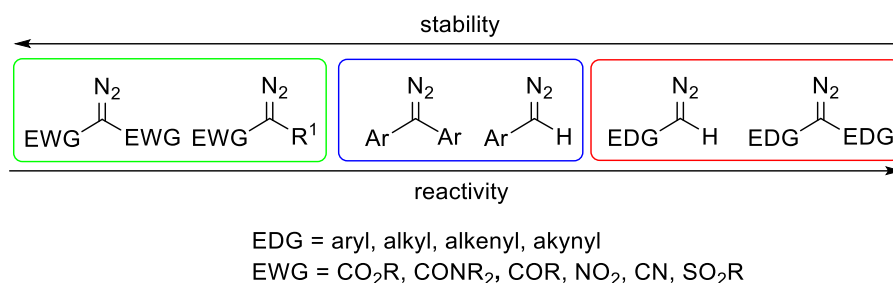


Figure 4.6 Types and reactivity of diazo compounds.

Diazo compounds have the capability to coordinate to a metal center¹⁶² and several cases have been reported in the literature with different transition metal such as

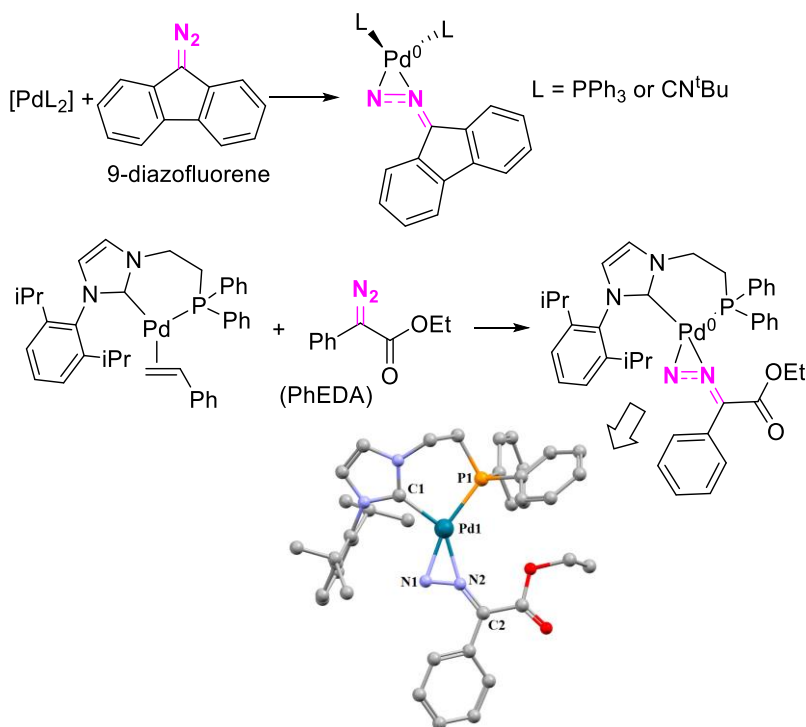
¹⁵⁹ Proctor, L. D.; Warr, A. J. *Org. Process. Res. Dev.* **2002**, *6*, 884–892.

¹⁶⁰ a) Poh, J.-S.; Tran, D. N.; Battilocchio, C.; Hawkins, J. M.; Ley, S. V. *Angew. Chem. Int. Ed.* **2015**, *54*, 7920–7923. b) Hock, K. J.; Koenigs, R. M. *Chem. Eur. J.* **2018**, *24*, 10571–10583. c) Sullivan, R. J.; Freure, G. P. R.; Newman, S. G. *ACS Catal.* **2019**, *9*, 5623–5630. d) Empel, C.; Koenigs, R. M. *J. Flow Chem.* **2020**, *10*, 157–160.

¹⁶¹ a) Dingwall, P.; Greb, A.; Crespin, L. N. S.; Labes, R.; Musio, B.; Poh, J.-S.; Pasau, P.; Blakemore, D. C.; Ley, S. V. *Chem. Commun.*, **2018**, *54*, 11685–11688. b) Ciszewski, Ł. W.; Rybicka-Jasińska, K.; Gryko, D. *Org. Biomol. Chem.*, **2019**, *17*, 432–448. c) Jana, S.; Li, F.; Empel, C.; Verspeek, D.; Aseeva, P.; Koenigs, R. M. *Chem. Eur. J.* **2020**, *26*, 2586–2591.

¹⁶² Sutton, D. *Chem. Rev.* **1993**, *93*, 995–1022.

Cu,¹⁶³ Rh,¹⁶⁴ Ru¹⁶⁵ or Ni.¹⁶⁵ Specifically, in the case of palladium, only a few cases are known where the authors were able to isolate and fully characterize the resulting palladium(0) complex where the diazo compound is coordinated (Scheme 4.5).¹⁶⁶ These palladium-diazo adducts have been formed by ligand displacement and coordination of the diazo functional group to a zerovalent palladium complex. In these complexes the bent diazoalkane is bound unsymmetrically by its two -N atoms as a bidentate ligand (*side-on* coordination mode) (Scheme 4.6, A)).



Scheme 4.5 Synthesis of palladium-diazo adduct and molecular X-ray structure (ref: 166b)). selected bond lengths (Å): Pd1-N1, 2.026; Pd1-N2, 2.084; N2-C2, 1.345; Pd1-P1, 2.281; Pd1-C1, 2.036; N1-N2, 1.266(7).

Diazoalkanes can interact with the metal center and adopt other coordination modes such as a monodentate ligand *via* the terminal -N atom or *via* the central -C atom

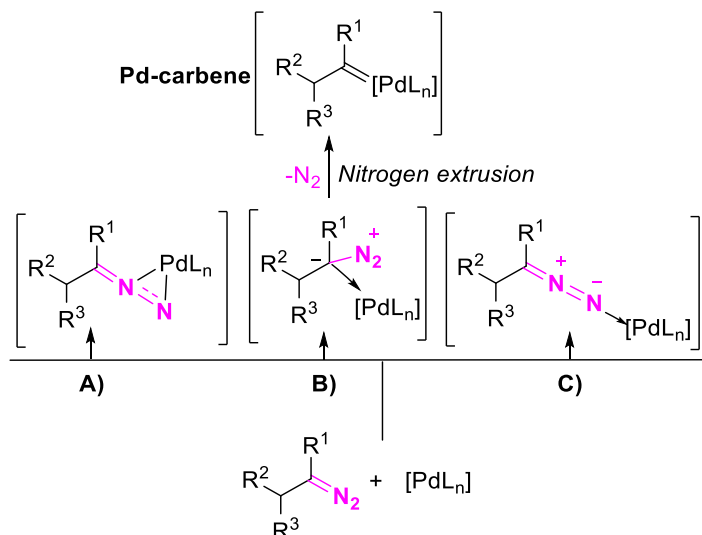
¹⁶³ Pereira, A.; Champouret, Y.; Martín, C.; Álvarez, E.; Etienne, M.; Belderrain, T. R.; Pérez, P. *J. Chem. Eur. J.* **2015**, *21*, 9769–9775.

¹⁶⁴ Deydier, E.; Menu, M.-J.; Dartiguenave, M.; Dartiguenave, Y.; Simard, M.; Beauchamp, A. L.; Brewer, J. C.; Gray, H. B. *Organometallics*. **1996**, *15*, 1166–1175.

¹⁶⁵ Schramm, K. D.; Ibers, J. A. *Inorg. Chem.* **1980**, *19*, 2441–2448.

¹⁶⁶ a) Otsuka, S.; Nakamura, A.; Koyama, T.; Tatsuno, Y. *Justus Liebigs Ann. Chem.* **1975**, 626–635. b) Rull, S. G.; Álvarez, E.; Fructos, M. R.; Belderrain, T. R.; Pérez, P. *J. Chem. Eur. J.* **2017**, *23*, 7667–7671.

(Scheme 4.6, **B**) and **C**). These coordination modes have been proposed but no experimental evidence has been reported beyond DFT calculations for palladium complexes. The palladium species where the coordination occurs by the -C atom (Scheme 4.6, **B**) is considered responsible for the nitrogen extrusion, a crucial step to generate the metal carbene.¹⁶⁷

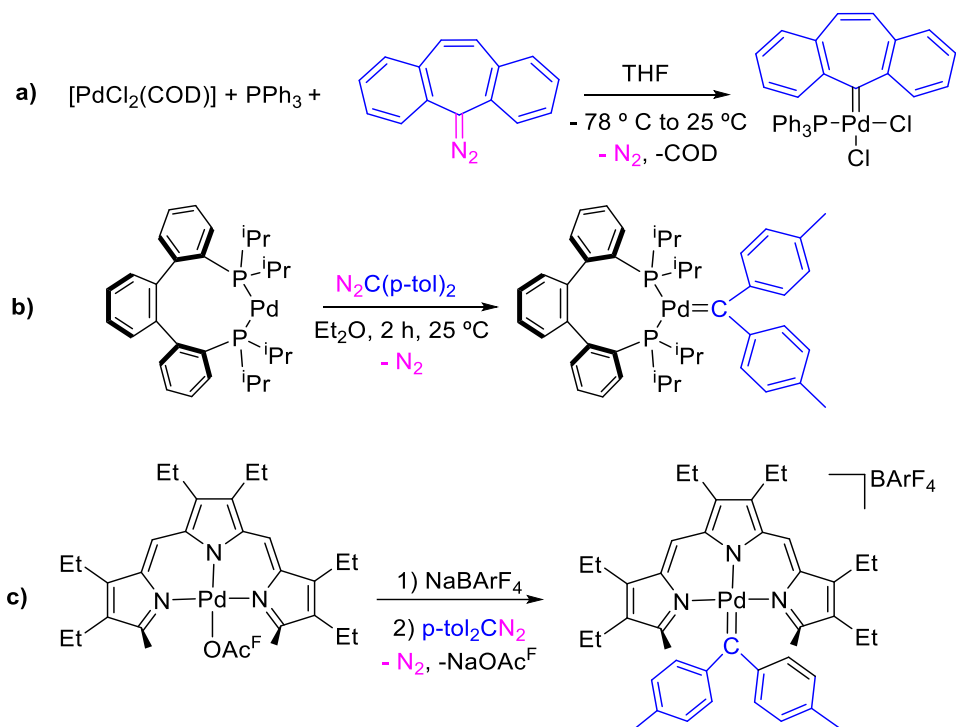


Scheme 4.6 Different proposed coordination modes of diazo compound in monometallic Pd-complexes.

Because of the high reactivity of the resulting palladium carbene species, only a few examples have been reported where the complex is stable enough to be characterized thanks to the high steric demand of the auxiliary ligands (Scheme 4.7).¹⁶⁸

¹⁶⁷ a) Murahashi, S-I.; Kitani, Y.; Hosokawa, T.; Miki, K.; Kasai, N. *J. Chem. Soc., Chem. Commun.*, **1979**, 450–451. b) Murahashi, S-I.; Kitani, Y.; Uno, T.; Hosokawa, T.; Miki, K.; Yonezawa, T.; Kasai, N. *Organometallics*, **1986**, *5*, 356–365.

¹⁶⁸ a) M. Bröring, C. D. Brandt, S. Stellwag. *Chem. Commun.* **2003**, 2344–2345. b) Taubmann, C.; Ofele, K.; Herdtweck, E.; Herrmann, W. A. *Organometallics*, **2009**, *28*, 4254–4257. c) Barrett, B. J.; Iluc, V. M. *Organometallics*, **2017**, *36*, 730–741



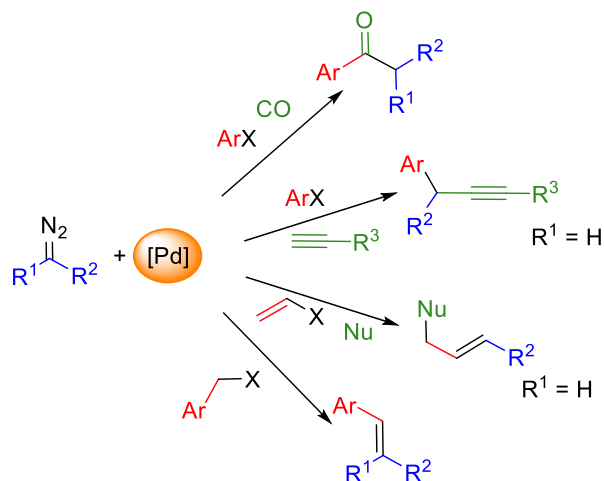
Scheme 4.7 Previously reported work of non-heteroatom stabilised carbene ligand coordinated to palladium from diazo compounds precursors.

4.3. Pd-catalyzed C-C coupling reactions with carbene precursors via migratory insertion

A large number of palladium catalyzed C-C and C-X coupling reactions involve a reactive carbene species in some steps of the catalytic cycle. A strategy to generate C-C and C-X bonds is by migratory insertion reactions and in this regard, the abovementioned metal carbenes represent an ideal option. In the case of unstable palladium-carbene species, this particular step is favored by the interaction of an electrophilic carbene carbon atom with the electron density of the “R” group (Pd-R, σ -bond). This leads to a new palladium alkyl complex that can react further, so the carbene fragment is amenable to afford a double functionalization that leads to cascade reactions and therefore to a more efficient building up of molecular complexity. Following the pioneering work of Van Vranken *et al.*¹⁶⁹ a lot of progress has been done in type of reaction and as a

¹⁶⁹ a) Greenman, K. L.; Carter, D. S.; Van Vranken, D. L. *Tetrahedron* **2001**, *57*, 5219–5225. b) Greenman, K. L.; Van Vranken, D. L. *Tetrahedron* **2005**, *61*, 6438–6441.

consequence it has now a prominent position among the Pd-catalyzed cross-coupling processes (Scheme 4.8).^{170,171}



Scheme 4.8 Some examples of Pd-catalyzed coupling reactions with diazo-compounds as carbene precursors.

These reactions use non-stabilized carbene fragments (*i.e.* $:\text{CHR}^1$ or $:\text{CR}^2\text{R}^1$) as coupling partners and the most common carbene precursors are diazo compounds as shown in the preceding section.^{172,173} The proposed general mechanism involves the formation of a palladium carbene from the diazoalkane (Scheme 4.9, intermediate **B**), followed by a migratory insertion of the carbene fragment into the Pd-R bond (intermediate **C**), the R group being previously installed on palladium (intermediate **A**).

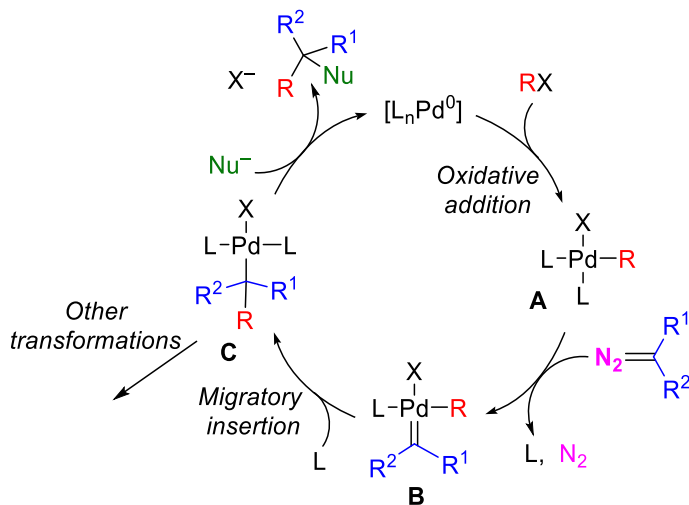
¹⁷⁰ Selected reviews: a) Liu, Z.; Wang, J. *J. Org. Chem.* **2013**, *78*, 10024–10030. b) Barroso, R.; Cabal, M. P.; Valdés, C. *Synth.* **2017**, *49*, 4434–4447 c) Xia, Y.; Qiu, D.; Wang, J. *Chem. Rev.* **2017**, *117*, 13810–13889. d) Chen, G.; Yu, Y.; Huang, X. *Synlett* **2018**, *29*, 2087–2092. e) Wang, X.; Wang, X.; Wang, J. *Tetrahedron* **2019**, *75*, 949–964. f) Xiang, Y.; Wang, C.; Ding, Q.; Peng, Y. *Adv. Synth. Catal.* **2019**, *361*, 919–944. g) Jha, N.; Khot, N. P.; Kapur, M. *Chem. Rec.* **2021**, *21*, 4088–4122.

¹⁷¹ a) Liu, Y.; Zhang, Z.; Zhang, S.; Zhang, Y.; Wang, J.; Zhang, Z. *Chem. – An Asian J.* **2018**, *13*, 3658–3663. b) Zhou, Q.; Gao, Y.; Xiao, Y.; Yu, L.; Fu, Z.; Li, Z.; Wang, J. *Polym. Chem.* **2019**, *10*, 569–573. c) Pérez-Gómez, M.; Azizollahi, H.; Franzoni, I.; Larin, E. M.; Lautens, M.; García-López, J.-A. *Organometallics* **2019**, *38*, 973–980. d) Yu, Y.; Ma, L.; Xia, J.; Xin, L.; Zhu, L.; Huang, X. *Angew. Chem. Int. Ed.* **2020**, *59*, 18261–18266. e) Yu, Y.; Chakraborty, P.; Song, J.; Zhu, L.; Li, C.; Huang, X. *Nat. Commun.* **2020**, *11*, 461. f) Huo, J.; Zhong, K.; Xue, Y.; Lyu, M.; Ping, Y.; Liu, Z.; Lan, Y.; Wang, J. *J. Am. Chem. Soc.* **2021**, *143*, 12968–12973. g) Cheng, M.; Huang, X.-Y.; Yang, F.; Zhao, D.-M.; Ji, K.; Chen, Z.-S. *Org. Lett.* **2022**, *24*, 1237–1242. h) X.-Q.; Wang, Y.-S.; Wang, J. *Chem. Commun.* **2022**, *58*, 4032–4035.

¹⁷² Xiao, Q.; Zhang, Y.; Wang, J. *Acc. Chem. Res.* **2013**, *46*, 236–247.

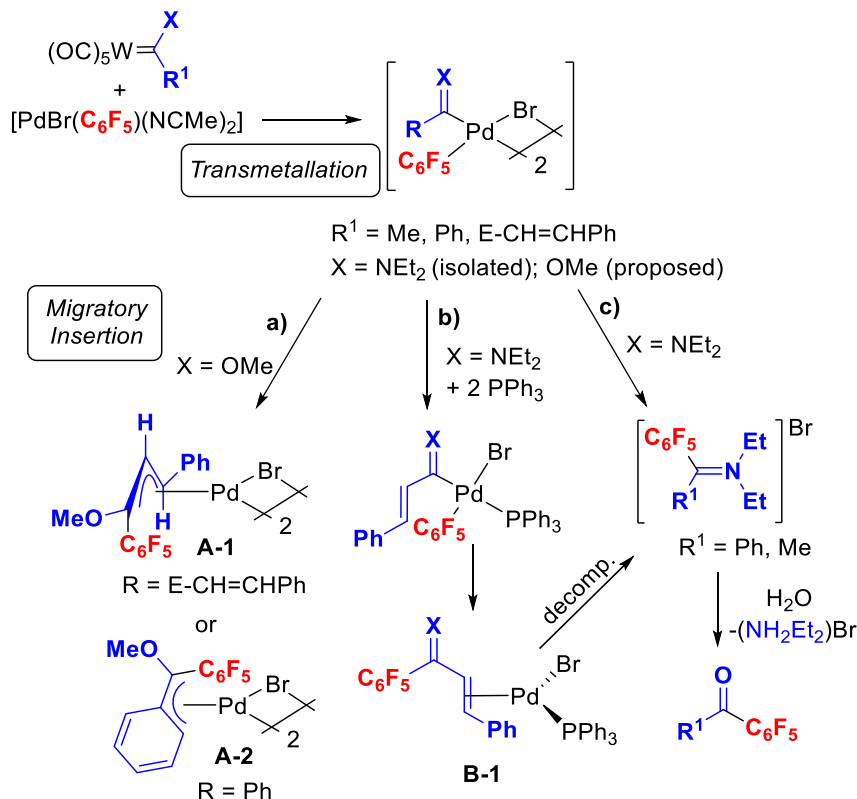
¹⁷³ a) Wang, H.; Deng, Y. H.; Shao, Z. *Synth.* **2018**, *50*, 2281–2306 b) Xia, Y.; Wang, J. *J. Am. Chem. Soc.* **2020**, *142*, 10592–10605. c) Radolko, J.; Ehlers, P.; Langer, P. *Adv. Synth. Catal.* **2021**, *363*, 3616–3654.

Intermediates **A-C** are common to all cross-coupling reactions that involve a carbene fragment as a reactant, although the formation of **A** and the evolution of **C** can occur by different routes depending on the specific reaction.



Scheme 4.9 General catalytic cycle proposed for Pd-catalyzed coupling reactions with diazo compounds as carbene precursors (the formation of Pd-R is shown here as the results of oxidative addition on Pd(0)).

The catalytic cycle depicted in Scheme 4.9 represents a plausible proposal, supported by DFT calculations, but very few experimental studies have been done to probe and support the steps of the reaction, in particular, the key bond-forming migratory insertion step. The feasibility of the carbene migratory insertion on palladium organometallic complexes has been shown for stabilized monoamino or monoalkoxo Fisher-type carbenes as shown in Scheme 4.10.¹⁴⁵

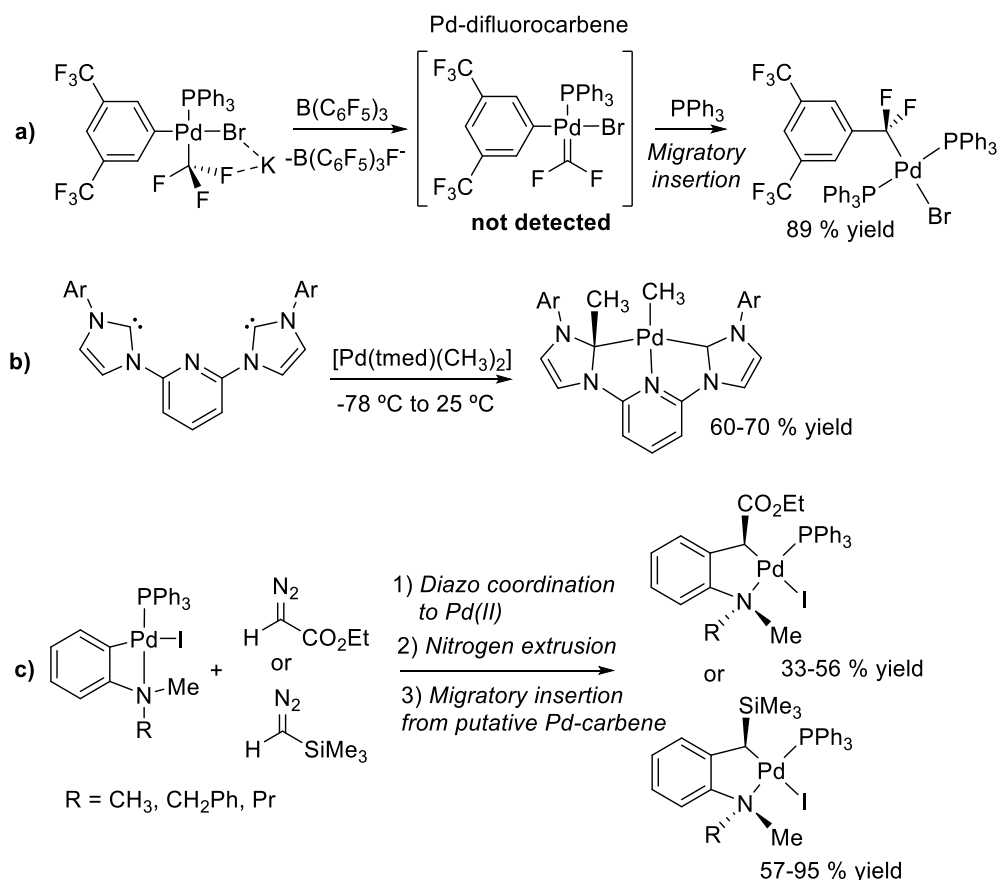


Scheme 4.10 Study of the key bond-forming migratory insertion process from well-defined amino or alkoxo Pd-carbenes.

The migratory insertion step has been demonstrated by isolation and characterization of the alkyl palladium derivatives **A-1** (η^3 -allyl-complex) and **A-2** (η^3 -benzylic-complex) (Scheme 4.10, **a**). The stabilization of these alkyl complexes is favored by coordination of the double bond or the phenyl ring present in the substituents of the initial alkoxo carbenes. The migratory insertion of a vinylamino carbene into the Pd-C₆F₅ bond, gives a three-coordinated Pd(0) complex where the vinyliminium ligand is bound to the Pd through the C=C bond (**B-1**) (Scheme 4.10, **b**).¹⁴⁵ Once the migratory insertion step occurs, a common decomposition pathway for those still reactive intermediates is *via* iminium salt formation and their subsequent hydrolysis (Scheme 4.10, **c**).

Other few examples where the resulting organometallic complexes after the migratory insertion were isolated have been reported. The haloalkyl-palladium derivatives in Scheme 4.11, **a**) leads to an organometallic complex whose formation could be explained *via* dehalogenation, formation of a putative Pd-difluorocarbene and a migratory insertion reaction. All these steps are promoted by addition of Lewis acid

($B(C_6F_5)_3$).¹⁷⁴ Only one example of migratory insertion of a *N*-heterocyclic carbene complex with the isolation of the resulting palladium organometallic products has been reported (Scheme 4.11, b).¹⁷⁵ To our knowledge, there is only one example of the insertion of a non-stabilized ($:CR^2R^1$) carbene fragment derived from a diazoalkane in a palladium metallacyclic complex (Scheme 4.11, c).¹⁷⁶



Scheme 4.11 Isolation of organometallic product from migratory insertion reaction of unstable Pd-carbenes.

¹⁷⁴ Wade Wolfe, M. M.; Shanahan, J. P.; Kampf, J. W.; Szymczak, N. K. *J. Am. Chem. Soc.* **2020**, *142*, 18698–18705.

¹⁷⁵ Danopoulos, A. A.; Tsoureas, N.; Green, J. C.; Hursthouse, M. B. *Chem. Commun.* **2003**, *6*, 756–757.

¹⁷⁶ Solé, D.; Vallverdú, L.; Solans, X.; Font-Bardia, M.; Bonjoch, J. *Organometallics* **2004**, *23*, 1438–1447.

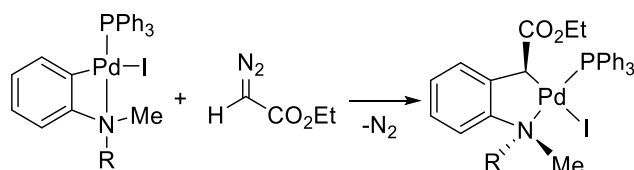
The development of synthetic applications involving carbene migratory insertion reactions has been achieved much faster than the detailed knowledge of the steps proposed in the mechanism of these reactions. In the following chapters, we explore the reactivity of palladium-aryl complexes with precursors of “CHR¹” fragments, *i.e.* diazoalkanes and hydrazones. Relevant palladium coordination complexes and organometallic migratory insertion products were isolated in *Chapter 5*. The influence of the auxiliary ligands in the reactions of aryl palladium complexes with diazoalkanes is described in *Chapter 6*. Finally, a study of the transmetallation of the unusual aminocarbene :CH(NEt₂) from a Cu(I) complex to Pd(II) and its migratory insertion reactions are discussed in *Chapter 7*, the latter work is a collaboration with Prof. Pedro Pérez’s group and Prof. Agustí Lledós.

Chapter 5

5. Diazo Compounds, Hydrazones and Their Reactions with Palladium-Aryl Complexes

5.1 INTRODUCTION

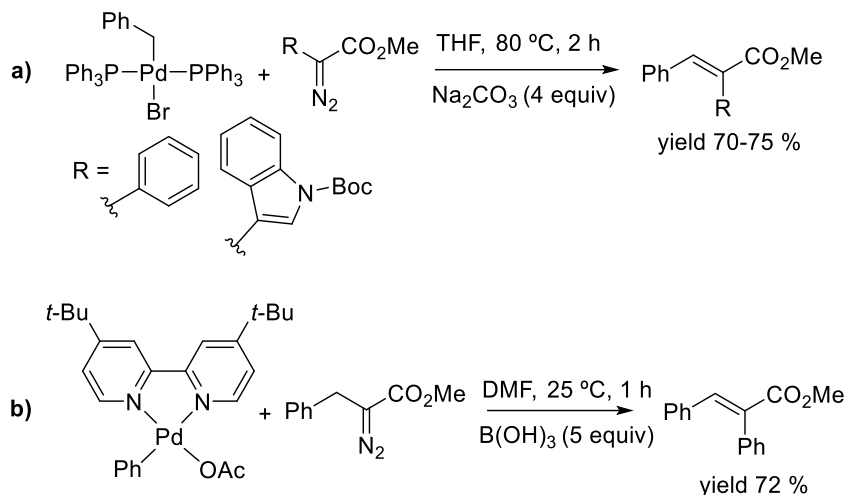
As discussed in the previous Chapter, only one example has been reported in the literature in which the organometallic species, resulting from the migratory insertion in a putative palladium carbene generated from a diazo precursor, was isolated (Equation 5.1).¹⁷⁶



Equation 5.1

Apart from that, only a couple of examples of the formation of the migratory insertion organic products from well-defined palladium aryl complexes have been reported but no organometallic intermediates were detected (Scheme 5.1).¹⁷⁷

¹⁷⁷ a) Yu, W.-Y.; Tsoi, Y.-T.; Zhou, Z.; Chan, A. S. C. *Org. Lett.* **2009**, *11*, 469–472. b) Tsoi, Y.-T.; Zhou, Z.; Chan, A. S. C.; Yu, W.-Y. *Org. Lett.* **2010**, *12*, 4506–4509.



Scheme 5.1 Isolation of the organic migratory insertion products from well-defined palladium complex bearing bipyridine with diazo compounds.

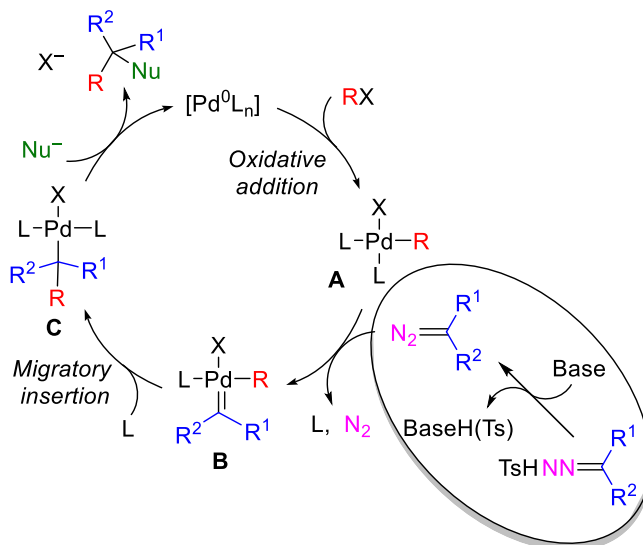
As mentioned in *Chapter 4*, diazo compounds as well as hydrazones are excellent carbene precursors. *N*-sulfonylhydrazones instead of diazo compounds have been extensively used in the transition-metal-catalyzed cross-coupling reactions over the past years.^{173f,178} *N*-tosylhydrazones are easily synthesized by condensation of the corresponding carbonyl compounds (aldehydes or ketones) and tosylhydrazides.¹⁷⁹ Also, the manipulation and storage of these compounds are chemically safe. Because of these properties, *N*-tosylhydrazones have become the focus of interest, trying to avoid the inherent stability issues and non-safety problems related to diazo compounds, often hazardous.¹⁸⁰ *N*-tosylhydrazones are suitable diazo precursors through an *in situ* decomposition by the Bamford-Stevens reaction in basic medium (Scheme 5.2).¹⁸¹

¹⁷⁸ a) Shao, Z.; Zhang, H. *Chem. Soc. Rev.* **2012**, *41*, 560–572.

¹⁷⁹ *N*-tosylhydrazones are the most commonly *N*-sulfonylhydrazones used, but other hydrazone derivatives such as *N*-2-(trifluoromethyl)benzenesulfonylhydrazone (*i.e.* *N*-triflylhydrazone) have been reported since 2014 by Xihe Bi's group as an efficient diazo surrogate that decomposes at very low temperatures (-40 °C). These mild reaction conditions allow them to carry out a range of challenging transformations that require functional group tolerance and/or chemo- and stereoselectivity. Liu, Z.; Sivaguru, P.; Zandoni, G.; Bi, X. *Acc. Chem. Res.* **2022**, *55*, 1763–1781.

¹⁸⁰ a) Fulton, J. R.; Aggarwal, V. K.; de Vicente, J. *Eur. J. Org. Chem.* **2005**, 1479–1492. b) Green, S. P.; Wheelhouse, K. M.; Payne, A. D.; Hallett, J. P.; Miller, P. W.; Bull, J. A. *Org. Process. Res. Dev.* **2020**, *24*, 67–84.

¹⁸¹ Bamford, W. R.; Stevens, T. S. *J. Chem. Soc.* **1952**, 4735–4740.



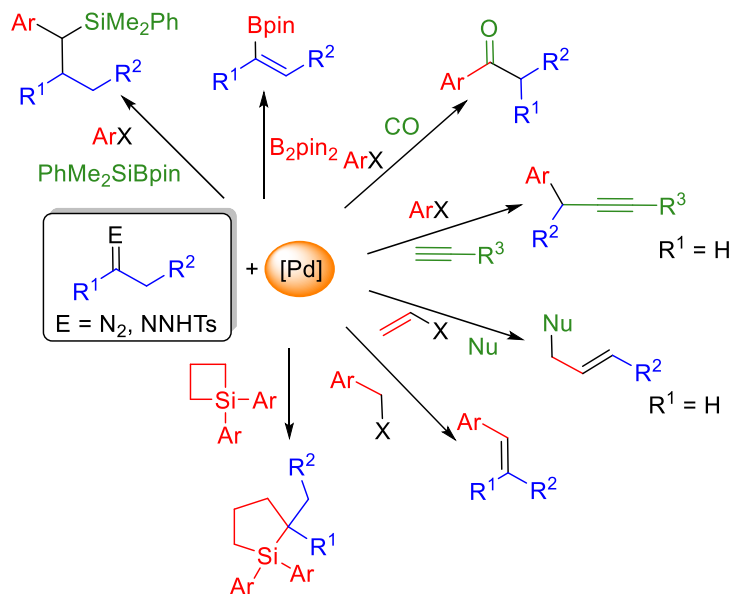
Scheme 5.2 Simplified catalytic cycle with the fundamental steps for the palladium cross-coupling reaction using *N*-tosylhydrazone as a diazoalkane precursor.

The employment of *N*-tosylhydrazones was the pioneering strategy reported by Barluenga, Valdés and co-workers who used these nitrogenated reagents as diazoalkane surrogates in Pd-catalyzed cross-coupling reactions.¹⁸² This finding triggered extraordinary progress to extend the scope of transition metal-catalyzed C-C or C-E (E = B, Si)^{171f,183} bond-forming reactions with *N*-tosylhydrazones as a coupling partner.^{170c} Some examples of palladium-catalyzed cascade transformations are depicted in Scheme 5.3, which lead to multiple bond formation from diazo compounds or tosylhydrazones assuming a carbene-hydrocarbyl migratory insertion step. However, this key migratory insertion step has been only supported by DFT calculations.

¹⁸² a) Barluenga, J.; Moriel, P.; Valdés, C.; Aznar, F. *Angew. Chem. Int. Ed.* **2007**, *46*, 5587–5590.

b) Barluenga, J.; Valdés, C. *Angew. Chem. Int. Ed.* **2011**, *50*, 7486–7500.

¹⁸³ a) Ping, Y.; Wang, R.; Wang, Q.; Chang, T.; Huo, J.; Lei, M.; Wang, J. *J. Am. Chem. Soc.* **2021**, *143*, 9769–9780. b) Yang, B.; Cao, K.; Zhao, G.; Yang, J.; Zhang, J. *J. Am. Chem. Soc.* **2022**, *144*, 15468–15474.



Scheme 5.3 Some examples of Pd-catalyzed coupling reactions with carbene precursors.

In the mechanistic proposals collected in the literature, the role of the reactant hydrazone is exclusively the generation of a diazoalkane by its decomposition outside the catalytic cycle, and no interaction with the metal has been considered (Scheme 5.2). However, hydrazones and the corresponding hydrazoneates formed upon deprotonation in basic medium are potential ligands used in large excess during the catalysis and likely to coordinate to the metal.

In this Chapter, the reactions of palladium aryl complexes with diazoalkanes and also the interaction with *N*-tosylhydrazones in basic media are described. The results reported here give a more accurate picture of the catalytic scenario in the Pd-catalyzed cross-coupling reactions of carbenes.

5.2 RESULTS AND DISCUSSION

Complexes [PdArBr(dppe)] (**28**) and [PdAr(dppe)(NCMe)]BF₄ (**29**) (Ar = C₆F₅, Ph; dppe = diphenylphosphinoethane) were used as models of intermediate **A** in Scheme 5.2 and tested in the reactions with diazo compounds and hydrazones. Pentafluorophenyl was used because of its advantageous spectroscopic features in ¹⁹F NMR. However, since the strong Pd-C bond for this aryl makes the reactions that require the Pd-C cleavage generally slower, reactions of the analogous phenyl complexes were also carried out. Intermediate **A** can be formed in a catalytic process by an oxidative addition process, as it is very common and it is shown in Scheme 5.2, but it could also arise from a transmetallation reaction from a main group organometallic or even by a C-H activation process.^{170a-d}

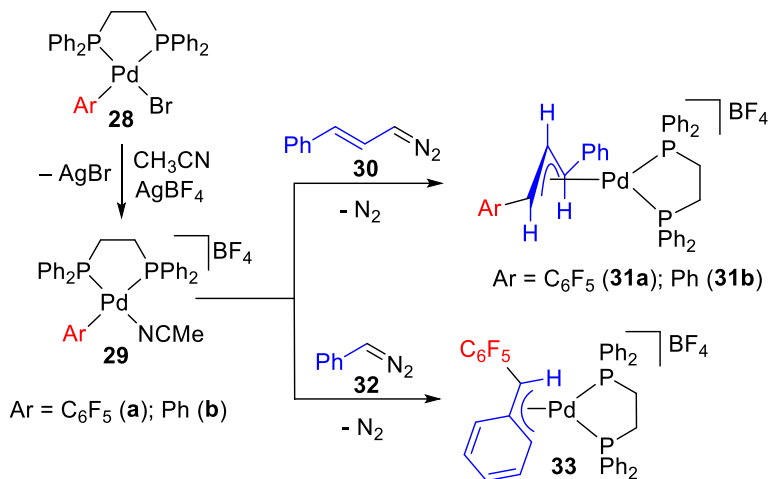
By selecting diazoalkanes N₂CHR with R = CH=CHPh, Ph we provide a way to stabilize the expected alkyl intermediate **C**, Scheme 5.2 by coordination of the unsaturated (double bond or aryl) to the metal (see Scheme 4.10 in *Chapter 4*). Both diazo compounds are common reagents in palladium catalyzed processes, as well as the corresponding tosylhydrazone derivatives TsNHNCHR (R = CH=CHPh, Ph).^{184,185}

5.2.1 Reactions with diazo compounds

The reaction of the solvento acetonitrile complexes **29** with the diazoalkane **30** at room temperature in acetonitrile leads immediately to the formation of the η³-allylic derivatives **31** (Scheme 5.4).

¹⁸⁴ a) Gutman, E. S.; Arredondo, V.; Van Vranken, D. L. *Org. Lett.* **2014**, *16*, 5498–5501. b) Wu, Q.; Muto, K.; Yamaguchi, J. *Org. Lett.* **2022**, *24*, 4129–4134.

¹⁸⁵ a) Zhou, P.-X.; Luo, J.-Y.; Zhao, L.-B.; Ye, Y.-Y.; Liang, Y.-M. *Chem. Commun.* **2013**, *49*, 3254–3256. b) Zhou, P.-X.; Ye, Y.-Y.; Zhao, L.-B.; Hou, J.-Y.; Kang, X.; Chen, D.-Q.; Tang, Q.; Zhang, J.-Y.; Huang, Q.-X.; Zheng, L.; Ma, J.-W.; Xu, P.-F.; Liang, Y.-M. *Chem. – A Eur. J.* **2014**, *20*, 16093–16096. c) Li, J.; Qin, G.; Liu, Y.; Huang, H. *Org. Chem. Front.* **2016**, *3*, 259–267.



Scheme 5.4 Reactions of Pd-aryl complexes with diazoalkanes.

The formation of a new Ar-C bond is very clear for Ar = C₆F₅ since the signals for the *ortho* fluorine atoms in ¹⁹F NMR shift about 20 ppm when a Pd-C₆F₅ moiety (about -120 ppm) is transformed into a C-C₆F₅ bond (about -142 ppm) (Figure 5.1).

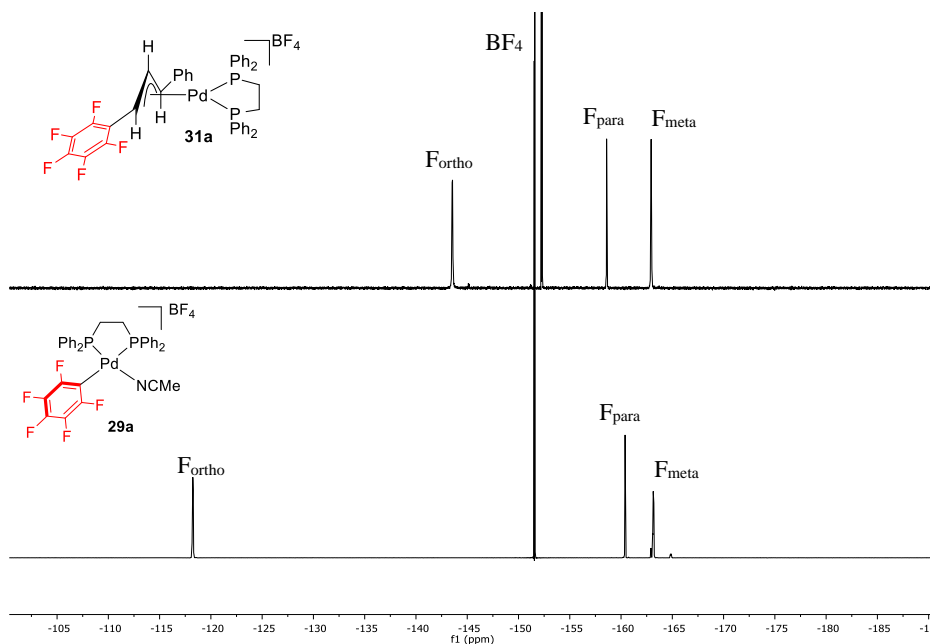


Figure 5.1 ¹⁹F NMR (470.17 MHz, CH₃CN/(CD₃)₂SO capillary) at 298 K of complexes **29a** and **31a** showing the dramatic shift of the F_{ortho} signals.

Characteristic signals for the asymmetric η^3 -allyl complex **31a** are observed in the ^1H , and ^{31}P NMR spectra whereas a symmetric η^3 -allyl was found for **31b** (Figure 5.2 and Figure 5.3).

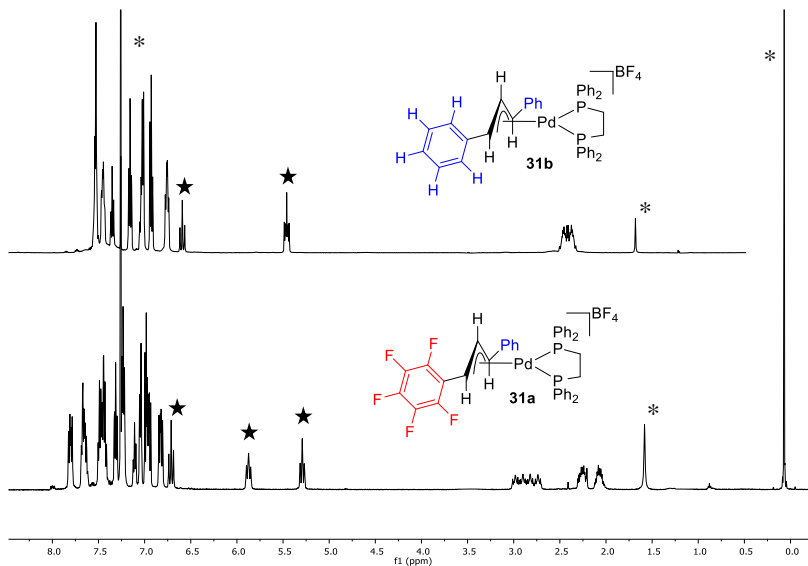


Figure 5.2 ^1H NMR (399.86 MHz, CDCl_3) of $[\text{Pd}(\text{dpe})(\eta^3\text{-Ph-CH-CH-CH-C}_6\text{F}_5)](\text{BF}_4)$ (**31a**) and $[\text{Pd}(\text{dpe})(\eta^3\text{-Ph-CH-CH-CH-Ph})](\text{BF}_4)$ (**31b**) at 298 K. Signals corresponding to the C-H in the η^3 -allylic fragments are labeled (black star). * Signals corresponding to the solvent (H_2O , chloroform and silicone grease).

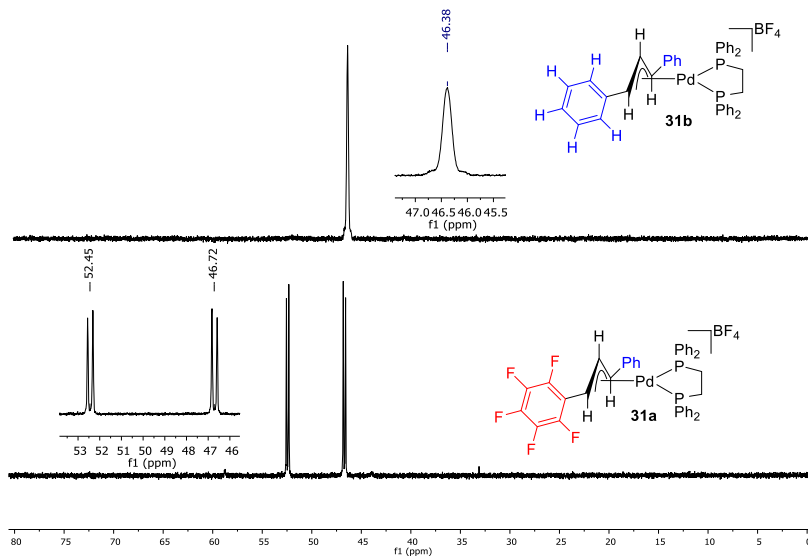
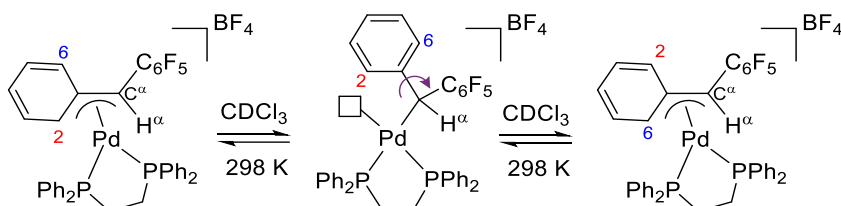


Figure 5.3 ^{31}P NMR (161.87 MHz, CDCl_3) of $[\text{Pd}(\text{dpe})(\eta^3\text{-Ph-CH-CH-CH-C}_6\text{F}_5)](\text{BF}_4)$ (**31a**) and $[\text{Pd}(\text{dpe})(\eta^3\text{-Ph-CH-CH-CH-Ph})](\text{BF}_4)$ (**31b**) at 298 K.

The analogous reaction of the diazo compound **32** with **29a** leads to the benzylic palladium complex **33**. Again, the migration of the pentafluorophenyl group to the organic fragment is clearly seen by ^{19}F NMR. The spectroscopic features of **33** show the typical behavior of a fluxional benzylic derivative with broad *ortho* phenyl signals in the ^1H NMR at room temperature by exchange *via* a $\eta^3\text{-}\sigma\text{-}\eta^3$ fluxional process (Scheme 5.5 and Figure 5.4).¹⁸⁶



Scheme 5.5 H^2 and H^6 exchange by rotation of the phenyl ring in a fast $\eta^3\text{-}\sigma\text{-}\eta^3$ equilibrium at 298 K.

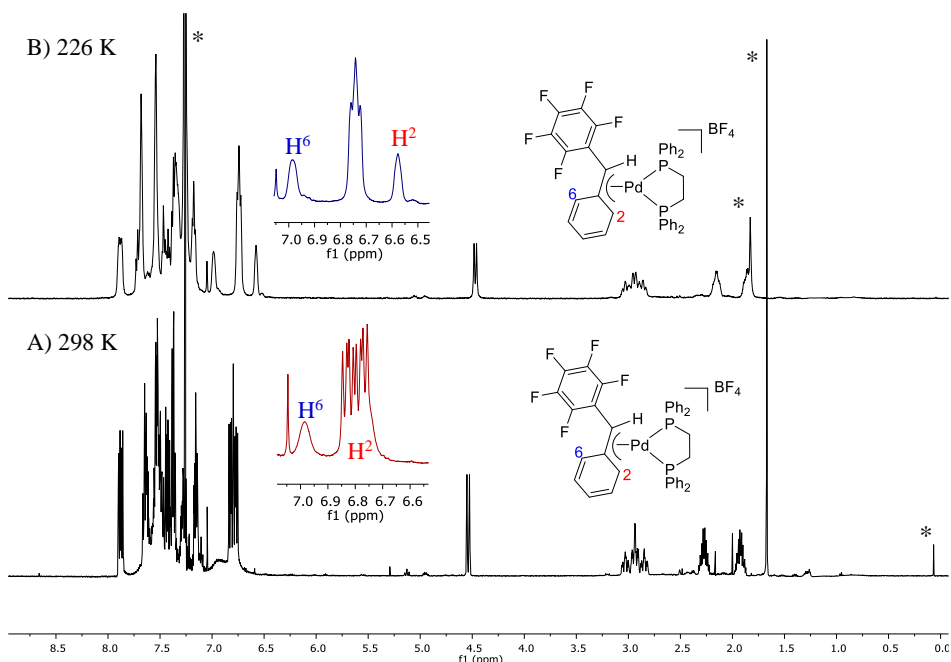


Figure 5.4 ^1H NMR (399.86 MHz, CDCl_3) of: A) $[\text{Pd}(\text{dppe})(\eta^3\text{-Ph-CH-CH-CH-Ph})](\text{BF}_4)$ (**33**) at 298 K (H^2 is overlapped with other signals at 6.8 ppm) and B) complex **33** at 226 K. * Signals corresponding to the solvent (H_2O , chloroform and silicone grease).

¹⁸⁶ a) Becker, Y.; Stille, J. K. *J. Am. Chem. Soc.* **1978**, *100*, 845–850. b) Crascall, L. E.; Spencer, J. L. *J. Chem. Soc. Dalton Trans.* **1992**, 3445–3452. c) Gatti, G.; López, J. A.; Mealli, C.; Musco, A. *J. Organomet. Chem.* **1994**, *483*, 77–89. d) Rix, F. C.; Brookhart, M.; White, P. S. *J. Am. Chem. Soc.* **1996**, *118*, 2436–2448. e) Martín-Ruiz, B.; Pérez-Ortega, I.; Albéniz, A. C. *Organometallics* **2018**, *37*, 1074–1085.

In this η^3 -benzylic complex **33** the $-\text{C}_6\text{F}_5$ substituent is in a *syn* position, far from the metal center. The presence of this isomer was confirmed by ^1H 2D-ROESY NMR experiment at low temperature (226 K), which showed an intense cross-peak between H^α and H^2 (Figure 5.5).

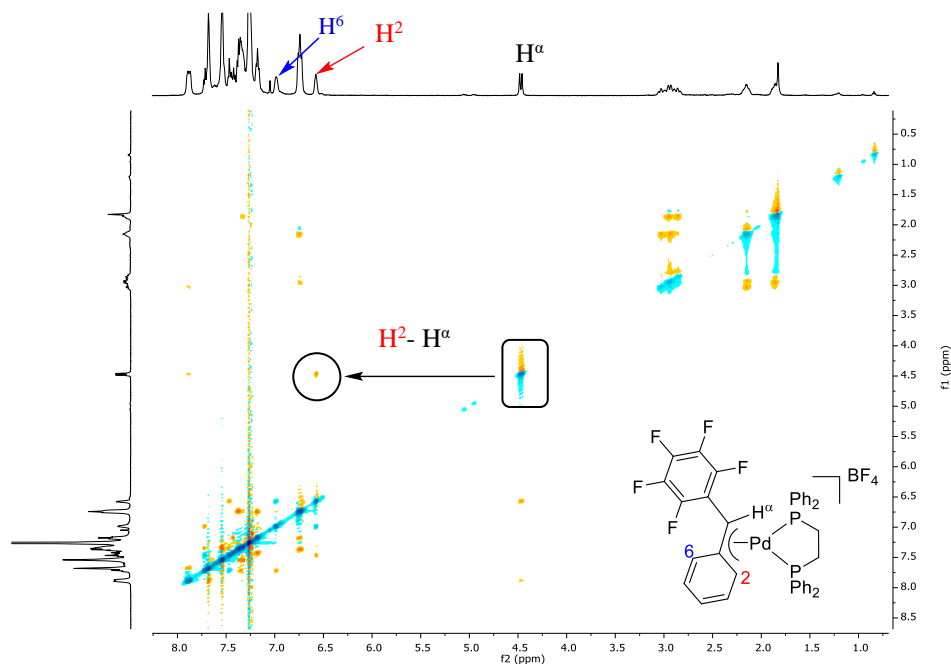


Figure 5.5 Phase sensitive ^1H 2D-ROESY NMR of $[\text{Pd}(\text{dppe})(\eta^3\text{-Ph-CH-C}_6\text{F}_5)](\text{BF}_4)$ (**33**) in CDCl_3 at 226 K.

The formation of complex **33** supports the intermediacy of benzylic palladium derivatives in catalytic coupling reactions of phenyldiazomethane derivatives, as has been suggested before.¹⁸⁴ The molecular structures of complexes **31a** and **33** were obtained by X-ray crystal diffraction and they are shown in Figure 5.6.

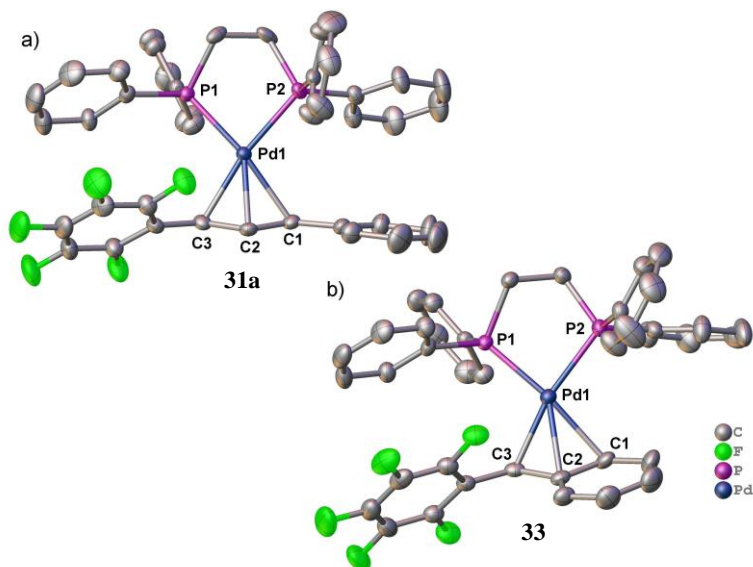
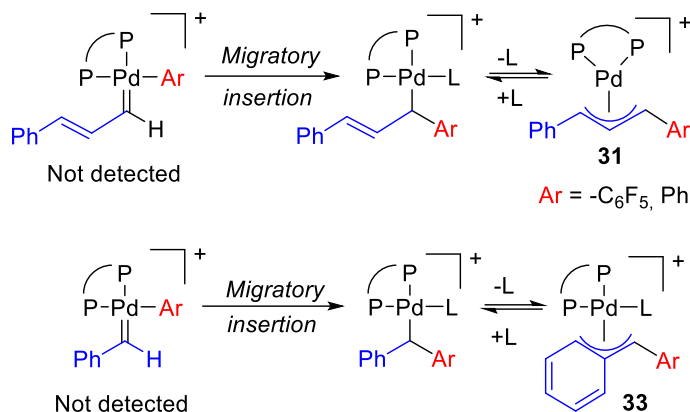


Figure 5.6 X-ray molecular structures of **31a** (a) and **33** (b) (ORTEP 40% probability ellipsoids). Hydrogen atoms and the counterion BF_4^- are omitted for clarity.

Complex **31a** is an η^3 -allyl with both substituents in a *syn* arrangement. The η^3 -benzylic derivative **33** also shows a *syn*-pentafluorophenyl arrangement, as it is the case in solution. In this derivative, the Pd-C3 bond length (2.155(4) Å) is clearly shorter than the Pd-C distances for the coordinated phenyl ring (Pd-C2, 2.275(4) Å and Pd-C1, 2.284(4) Å) reflecting a weaker interaction that involves the loss of aromaticity. This is characteristic of other η^3 -benzylic complexes.¹⁸⁷

Complexes **31** and **33** are the result of the migratory insertion reaction of the aryl into a putative palladium carbene complex, as shown in Scheme 5.6, and they model intermediate **C** in Scheme 5.2. The palladium alkyl complex formed right after the migratory insertion can be trapped and stabilized by coordination of the double bond (**31**) or the phenyl ring (**33**) present in the substituents of the diazoalkanes used.

¹⁸⁷ a) Hosokawa, T.; Maitlis, P. M. *J. Am. Chem. Soc.* **1972**, *94*, 3238–3240. b) Johns, A. M.; Utsunomiya, M.; Incarvito, C. D.; Hartwig, J. F. *J. Am. Chem. Soc.* **2006**, *128*, 1828–1839.

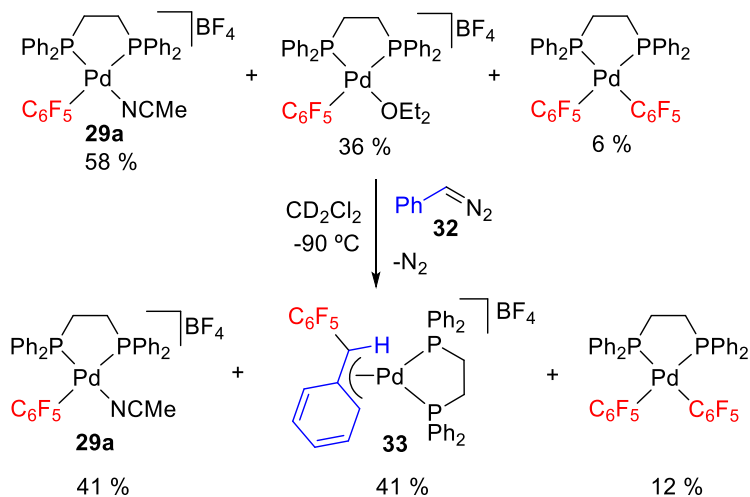


Scheme 5.6 Generation of complexes **31** and **33** by migratory insertion in a putative palladium carbene and stabilization of the generated palladium alkyl.

With the aim of detecting some of the intermediates involved before the migratory insertion, we carried out the reaction of **29a** with diazoalkanes **30** and **32** in CD₂Cl₂ at -90 °C and monitored it by ¹⁹F NMR. Upon addition of the diazo compound, complexes **31a** and **33** were the only new species formed and they coexist with the starting solvento complex (Scheme 5.7 and Scheme 5.8). Neither the coordination of the diazo compounds nor the formation of the palladium carbene was detected.

Figure 5.7 shows the variable temperature ¹⁹F NMR follow up of the reaction of **29a** with N₂CHPh (**32**). The first spectrum in Figure 5.7 shows the mixture of the starting solvento Pd-complexes [Pd(C₆F₅)(dppe)S]BF₄ (S = NCMe, OEt₂) and a small amount of the reorganization [Pd(C₆F₅)₂(dppe)] complex. The latter is inevitably formed during the isolation of **29a** (see *Experimental part*). A small amount of Et₂O in the sample along with a slow ligand exchange at that temperature leads to the coexistence of **29a** and [Pd(C₆F₅)(dppe)(OEt₂)]BF₄. Analogous species have been reported before.¹⁸⁸ Et₂O is readily substituted upon addition of NCMe as tested independently (see *Experimental part*, Figure 5.23). Upon addition of N₂CHPh (**32**, Pd:**32** = 1:1.5 mol ratio) only the formation of η³-benzylic complex **33** and the small amount of the aryl reorganization complex [Pd(dppe)(C₆F₅)₂] was observed. The slow rotation of the C₆F₅ group is observed at this temperature (broad inequivalent F_{ortho} and F_{meta} signals at -90 °C). As the temperature increases, in the range of -80 to -70 °C, the disappearance of the F_{ortho} resonances due to coalescence was observed and they become equivalent due to fast rotation at room temperature.

¹⁸⁸ a) Shultz, C. S.; Ledford, J.; DeSimone, J. M.; Brookhart, M. *J. Am. Chem. Soc.* **2000**, *122*, 6351–6356. b) Ledford, J.; Shultz, C. S.; Gates, D. P.; White, P. S.; DeSimone, J. M.; Brookhart, M. *Organometallics* **2001**, *20*, 5266–5276.



Scheme 5.7 Reaction of the solvent complexes $[\text{Pd}(\text{C}_6\text{F}_5)(\text{dppe})\text{S}]\text{BF}_4$ ($\text{S} = \text{MeCN}, \text{OEt}_2$) with N_2CHPh (**32**, $\text{Pd}:\mathbf{32} = 1:1.5$ mol ratio) at -90°C in CD_2Cl_2 (see Figure 5.7, a) and b)).

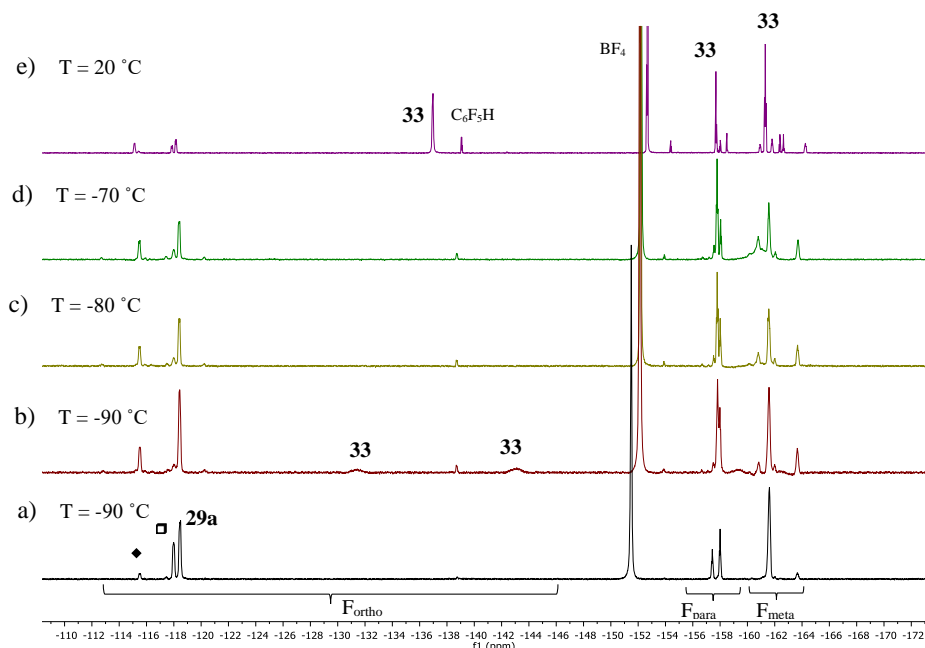
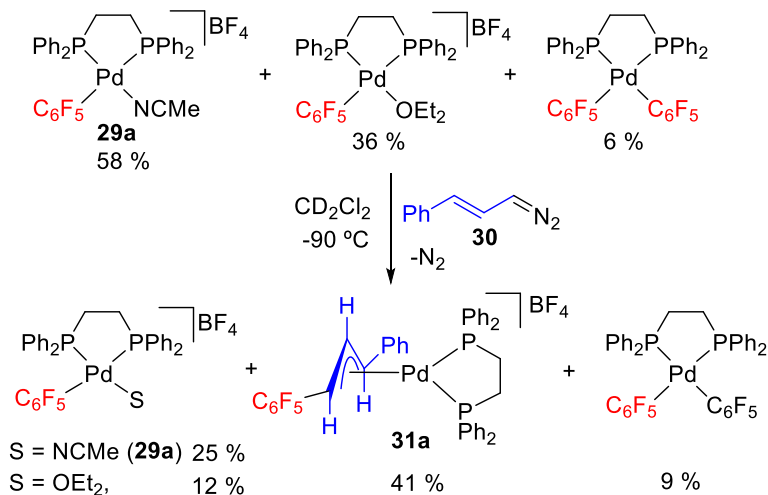


Figure 5.7 ^{19}F NMR (376.46 MHz, δ , CD_2Cl_2) of: a) a mixture of complexes **29a**, $[\text{Pd}(\text{C}_6\text{F}_5)(\text{dppe})(\text{OEt}_2)]\text{BF}_4$ (\square) and $[\text{Pd}(\text{C}_6\text{F}_5)_2(\text{dppe})]$ (\blacklozenge) formed when a sample of **29a** was dissolved in dichloromethane at low temperature. b) Sample a) upon addition of diazoalkane **32** ($\text{Pd}:\mathbf{32} = 1:1.5$ mol ratio). c-e) Sample b) upon increasing the temperature.

The analogous reaction with $\text{N}_2\text{CH-CH=CHPh}$ (**30**) is shown in Scheme 5.8 and the variable temperature monitoring in Figure 5.8. Identical results were observed for diazo compound $\text{N}_2\text{CH-CH=CHPh}$ (**30**, $\text{Pd}:\mathbf{30} = 1:1.5$ mol ratio) when it was added to the starting solvent Pd-complexes at -90°C . At low temperature the slow rotation of the

Pd-C₆F₅ bond is observed and inequivalent signals for the F_{ortho} and F_{meta} appear, which become equivalent at room temperature due to fast rotation.



Scheme 5.8 Reaction of the solvento complexes [Pd(C₆F₅)(dppe)S]BF₄ (S = MeCN, OEt₂) with N₂CH-CH=CHPh (**30**, Pd:**32** = 1:1.5 mol ratio) at -90 °C in CD₂Cl₂ (see Figure 5.8, a) and b)).

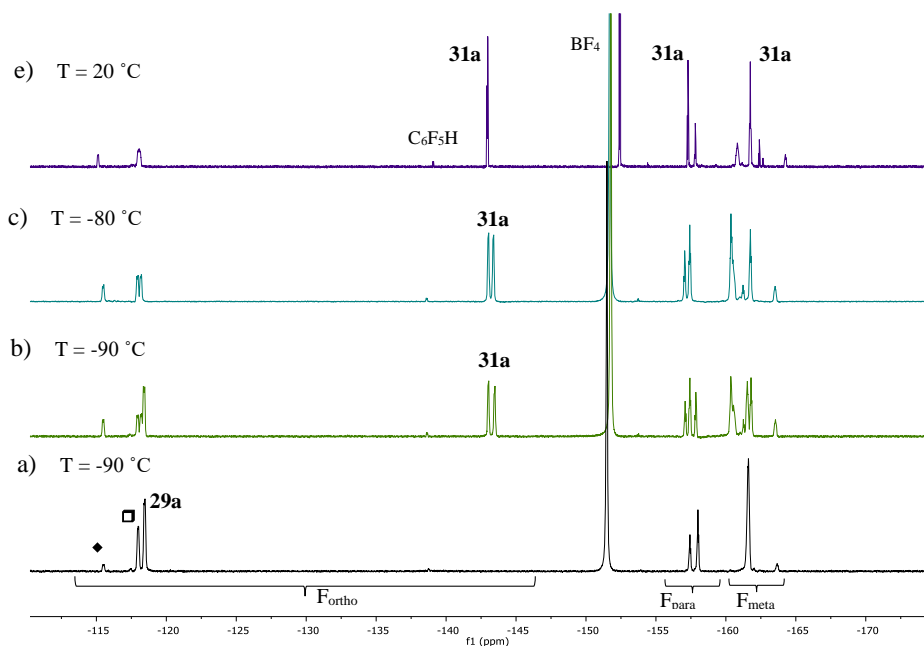


Figure 5.8 ¹⁹F NMR (376.46 MHz, δ, CD₂Cl₂) of: a) a mixture of complexes **29a**, [Pd(C₆F₅)(dppe)(OEt₂)]BF₄ (□) and [Pd(C₆F₅)₂(dppe)] (◆) formed when a sample of **29a** was dissolved in dichloromethane at low temperature. b) Sample a) upon addition of equimolar amount of diazoalkane **30**. c-e) Sample b) upon increasing the temperature.

This failure at observing any intermediate preceding the formation of the aryl-carbene insertion product indicates that the steps involved in the overall reaction are fast and they cannot be experimentally studied separately. Therefore, to obtain more information, we modeled the reaction using Density Functional Theory (DFT) calculations using the M06 functional and including solvation (MeCN) through the SMD implicit solvent method (see computational details in the *Experimental part*). The calculated reaction profile for the reaction with the diazoalkane **30** is shown in Figure 5.9.

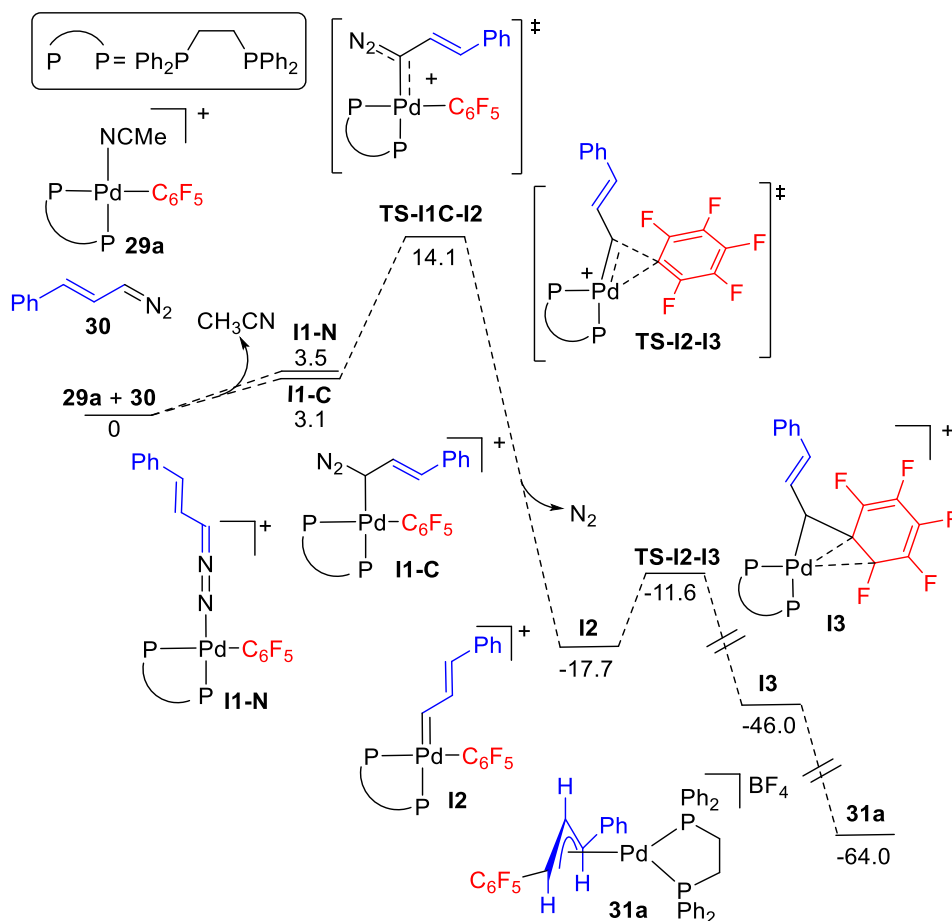


Figure 5.9 Gibbs energy profile for the reaction of complex **29a** and the diazo compound **30** to give the migratory insertion complex **31a**. Energies in kcal mol⁻¹.

The coordination of the diazoalkane either in a $\kappa^1\text{-N}$ (**I1-N**) or in a $\kappa^1\text{-C}$ (**I1-C**) coordination mode leads to intermediates that are less stable than the starting solvento complex (**29a**) by about 3 kcal mol⁻¹. **I1-C** can undergo extrusion of nitrogen to give a

palladium carbene (**12**) via a transition state with an accessible energy barrier (14.1 kcal mol⁻¹, **TS-11C-12**).

Although formation of palladium carbene **12** is quite exergonic, it evolves through a very low-barrier migratory insertion (6.1 kcal mol⁻¹) to give the very stable η^3 -allyl complex **31a**. This reaction profile is consistent with our experimental results. The energetic span for this reaction has a low value (14.1 kcal mol⁻¹), so the reaction occurs at low temperatures, and the rate determining state is the nitrogen extrusion to give the palladium carbene (**12**). Only the complex before this step, the starting solvento derivative **29a**, can be observed considering that the coordinated κ^1 -C diazo derivative is 3.1 kcal mol⁻¹ less stable and therefore the plausible equilibrium between **29a** and **11-C** is shifted toward **29a** ($K \approx 5 \times 10^{-3}$). Once the palladium carbene is formed the migratory insertion is very fast and just the final product is observed. This is in agreement with previous calculations carried out by other authors on related systems, where they find that the migratory insertion reaction usually has a very low energy barrier.^{171d,189} This is expected for these very electrophilic, non-stabilized carbenes in contrast with the heteroatom-stabilized fragments CR(XR'_n), which in some cases can be isolated before a more reluctant migratory insertion follows (see Scheme 4.10, *Chapter 4*).¹⁴⁵ The very few examples of the formation of Pd(II) carbene complexes from diazoalkanes occur on palladium precursors with no Pd-R bonds, *i.e.* no migratory insertion can take place.^{168a} The energy profile for the reaction of diazoalkane **32** with complex **29a** was also calculated (Figure 5.10) and it is analogous to that in Figure 5.9.

¹⁸⁹ a) Ye, F.; Qu, S.; Zhou, L.; Peng, C.; Wang, C.; Cheng, J.; Hossain, M. L.; Liu, Y.; Zhang, Y.; Wang, Z.-X.; Wang, J. *J. Am. Chem. Soc.* **2015**, *137*, 4435–4444. b) Yu, Y.; Lu, Q.; Chen, G.; Li, C.; Huang, X. *Angew. Chem. Int. Ed.* **2018**, *57*, 319–323. c) Yue, X.; Shan, C.; Qi, X.; Luo, X.; Zhu, L.; Zhang, T.; Li, Y.; Li, Y.; Bai, R.; Lan, Y. *Dalton Trans.* **2018**, *47*, 1819–1826. d) Qi, X.; Lan, Y. *Acc. Chem. Res.* **2021**, *54*, 2905–2915.

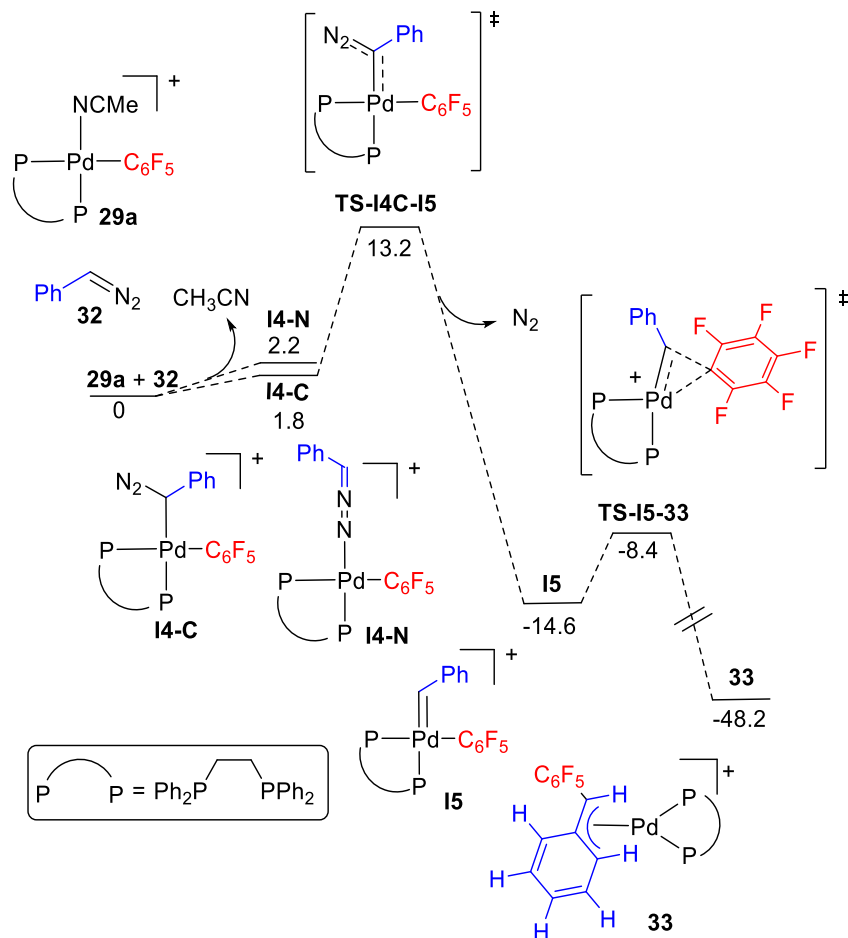
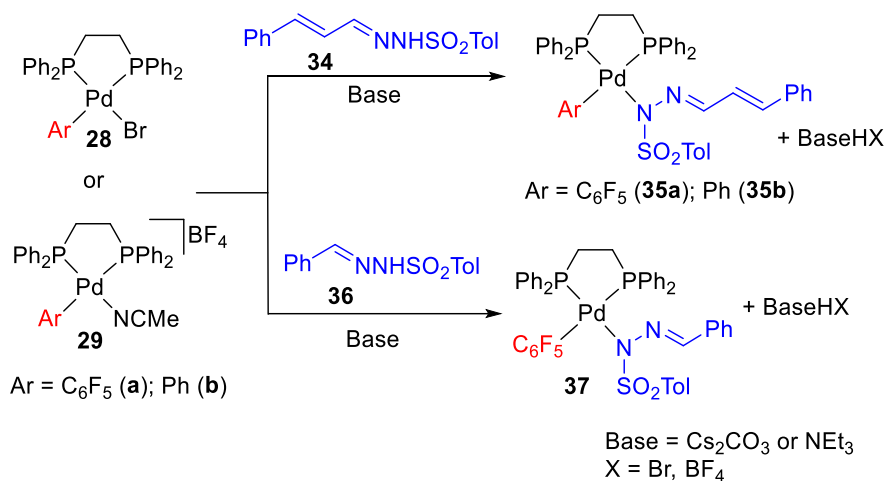


Figure 5.10 Gibbs energy profile for the reaction of complex **29a** and the diazo compound **32** to give the migratory insertion complex **33**. Energies in kcal mol⁻¹.

5.2.2 Reactions with hydrazone derivatives

As it was mentioned above, the use of hydrazones as diazoalkane surrogates in the catalytic coupling reactions that involve carbenes is widespread. The easy synthesis and handling of these derivatives when compared to the diazo compounds is a great advantage. Thus, many catalytic reactions use a combination of a tosylhydrazone and a base to generate a hydrazone that decomposes *in situ* to the diazoalkane. Hydrazones are good ligands and, indeed, in the presence of a mixture of a tosylhydrazone and a base, complexes **28** or the solvento complexes **29** form the hydrazone derivatives **35** and **37** (Scheme 5.9). This means that, under catalytic conditions (excess of hydrazone), intermediate [PdXRL₂] (**A**) in Scheme 5.2 is likely to be the analogous derivative to **35** or **37** (X = TsNNCHR).

Palladium derivatives with monodentate hydrazone ligands are rare and, to our knowledge, only one structurally characterized complex of this type has been reported before.¹⁹⁰ Complexes **35** and **37** were isolated in good yields and characterized. Figure 5.11 shows the molecular structure of complex **37** and the analogous diphenylphosphinoferrocene (dppf) derivative $[\text{Pd}(\text{C}_6\text{F}_5)(\text{dppf})\{(\text{PhSO}_2)\text{N}=\text{N}=\text{CH}-\text{CH}=\text{CH}-\text{Ph}\}]$ (**35c**). The hydrazone ligand is quite bulky and, in solution, restricted rotation about the Pd-N bond leads to broad signals at room temperature in the ^1H and ^{19}F NMR for most derivatives (**35a-c** and **37**). The slow rotation limit is observed at 233 K for **35a** (Figure 5.12) but this process is already slow at 298 K for the more constrained derivative **35c**.



Scheme 5.9 Reactions of Pd-aryl complexes with hydrazones.

¹⁹⁰ Hartwig, J. F. *Angew. Chem. Int. Ed.* **1998**, *37*, 2090–2093.

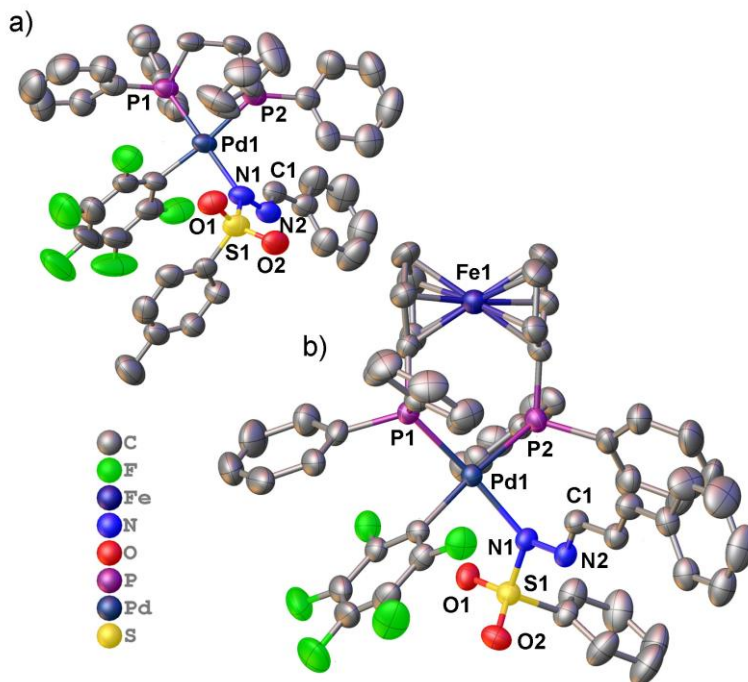


Figure 5.11 Molecular structures of complexes **37** (a) and **35c** (b) (ORTEP plots 40 % probability ellipsoids). Hydrogens have been omitted for clarity. Selected distances (Å) **37**: Pd1–N1, 2.105(5); N1–N2, 1.382(6); N2–C1 1.270(7); **35c**: Pd1–N1, 2.109(4); N1–N2, 1.380(5); N2–C1 1.282(5).

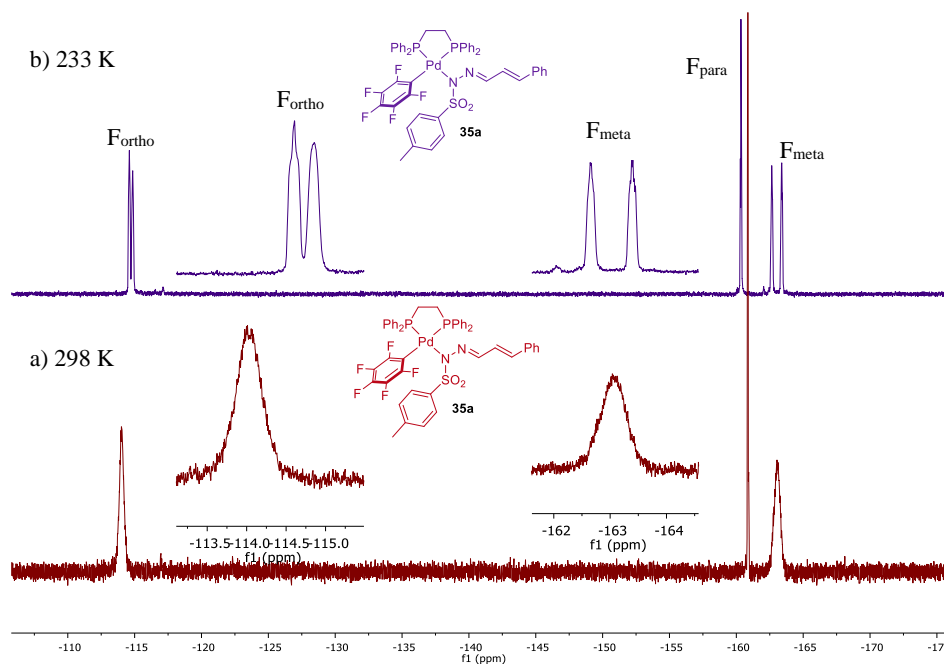


Figure 5.12 ^{19}F NMR (376.19 MHz, CDCl_3) of $[\text{Pd}(\text{C}_6\text{F}_5)(\text{dppe})\{(p\text{-TolSO}_2)\text{N-N}=\text{CH-CH}=\text{CHPh}\}]$ (**35a**) at 298 K (a) and 233 K (b).

Since the coordination of the hydrazone derivatives to palladium is so facile, we wondered if the metal played any role in the decomposition of this moiety to the diazoalkane, a necessary step in the catalysis. The decomposition of the free hydrazone **34** in the presence of triethylamine as a base in acetonitrile at 50 °C leads to 5-phenyl-1*H*-pyrazole (5-Ph-pzH), via the *in situ* generation and subsequent cyclization of the diazo compound **30** (Equation 5.2 and Figure 5.13).¹⁹¹ NEt₃ was used as a base to ensure the formation of the soluble ammonium hydrazone. The use of an alkali carbonate leads to very insoluble hydrazone salts and therefore the decomposition is controlled by the small concentration of the reactant hydrazone. This is the reason why the use of ammonium halides as PTC (Phase Transfer Catalyst) agents is common in many catalytic processes that use hydrazones.

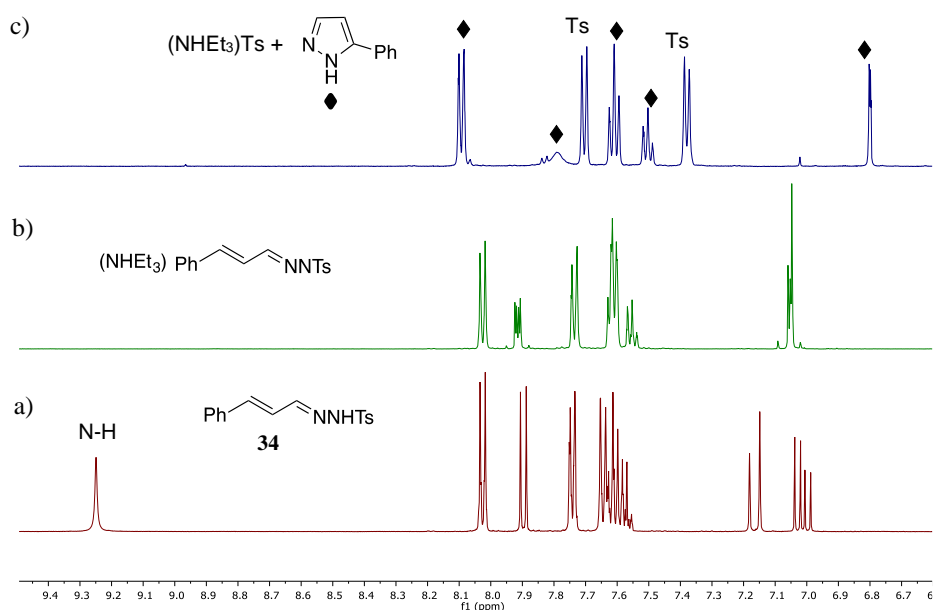
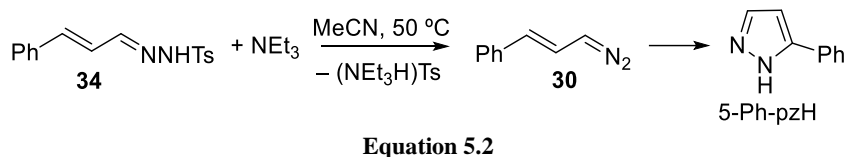


Figure 5.13 ¹H NMR (499.73, MHz, CD₃CN, 298 K) of: a) Hydrazone **34**; b) the ammonium hydrazone formed upon addition of NEt₃ to sample a); c) sample b) after heating at 50 °C for 16 h, showing the complete transformation into 5-Ph-pzH (Ts = SO₂-*p*-Tol).

¹⁹¹ Brewbaker, J. L.; Hart, H. *J. Am. Chem. Soc.* **1969**, *91*, 711–715.

The decomposition of *N*-tosylhydrazone **34** was monitored for 4 h at 50 °C by ¹H NMR using 1,4-dioxane as an internal standard. The only product observed in this reaction is 5-Ph-pzH which comes from the *in situ* generation of diazo compound N₂CH-CH=CHPh. The progress of the reaction is shown in Figure 5.14.

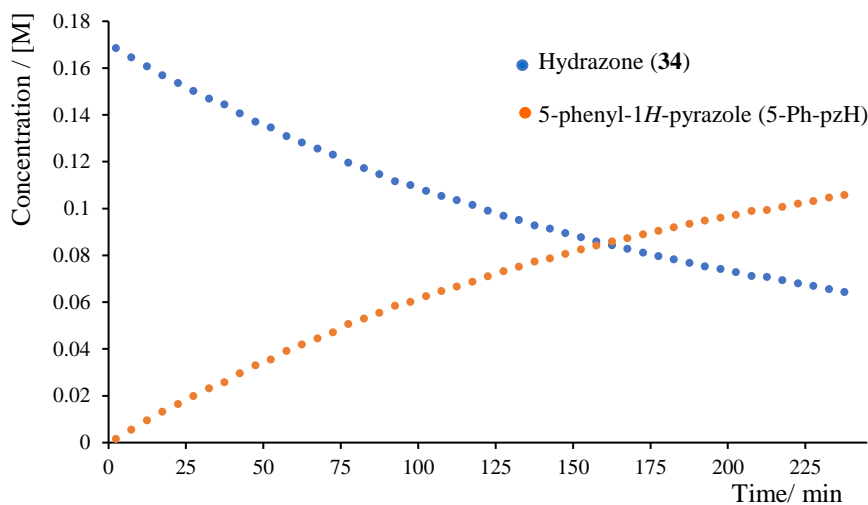
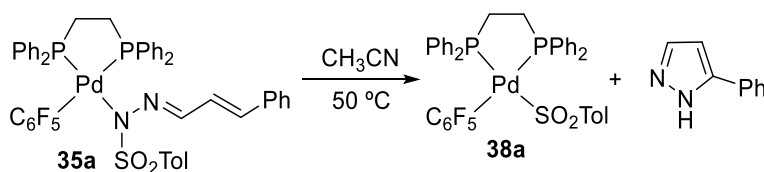


Figure 5.14 Plot of concentration vs. time for the decomposition of *p*-TolSO₂NHNCH-CH=CHPh (**34**) in CD₃CN at 50 °C.

Complex **35a** decomposes under the same conditions to give the tosylate complex **38a** as well as 5-Ph-pzH (Equation 5.3).¹⁹² For this complex, tosylate coordinates better than the diazoalkane to palladium and no migratory insertion product, *i.e.* **31a**, was formed. The tosyl fragment is coordinated to palladium *via* the -S atom, as expected and supported by the analysis of the molecular structures of complexes **38a** and **38c** (Figure 5.15).



Equation 5.3

¹⁹² a) Pelzer, G.; Herwig, J.; Keim, W.; Goddard, R. *Russ. Chem. Bull.* **1998**, *47*, 904–912.
 b) Shavnya, A.; Hesp, K. D.; Mascitti, V.; Smith, A. C. *Angew. Chem. Int. Ed.* **2015**, *54*, 13571–13575.

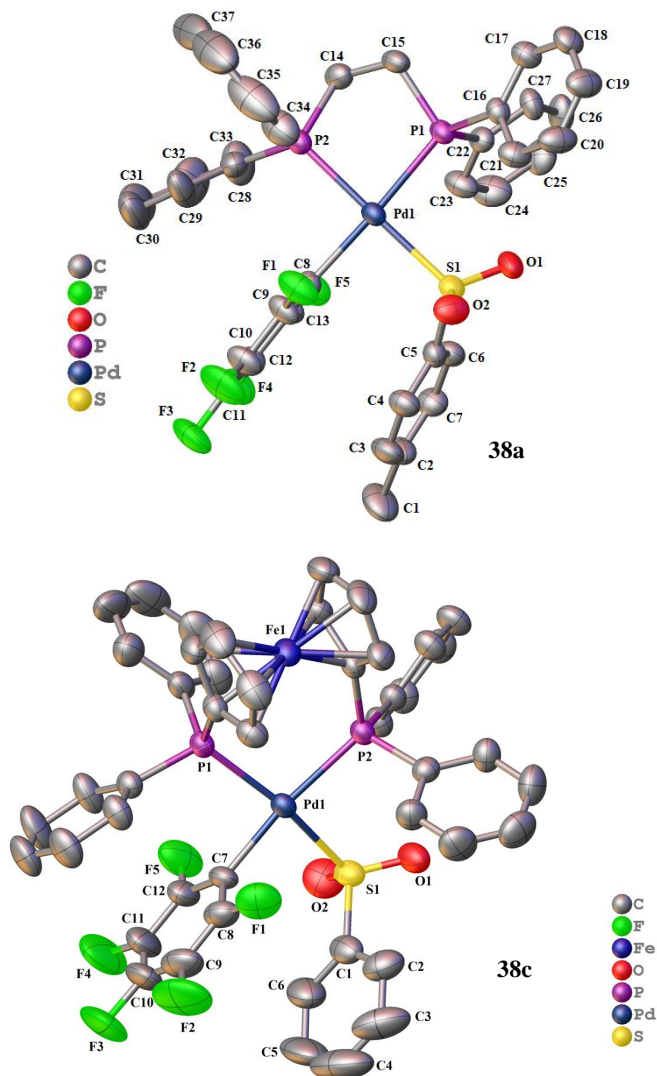


Figure 5.15 Molecular structures of complexes **38a** (ORTEP plots 40 % probability ellipsoids). Hydrogens have been omitted for clarity. Selected distances (Å) **38a**: Pd1–S1, 2.337(2); Pd1–C8, 2.058(7); Pd1–P1, 2.3203(19); Pd1–P2, 2.278(2). **38c**: Pd1–S1, 2.3656(8); Pd1–C7, 2.038(3); Pd1–P1, 2.3427(8); Pd1–P2, 2.3611(8).

Interestingly, the monitoring of the decomposition of **35a** at 50 °C shows a very slow decomposition at the beginning of the reaction that undergoes a strong acceleration when about 10 % conversion is reached (Figure 5.16, **a**). The observed profile conforms to a situation where, in the course of the decomposition, a species is formed that catalyzes the reaction.

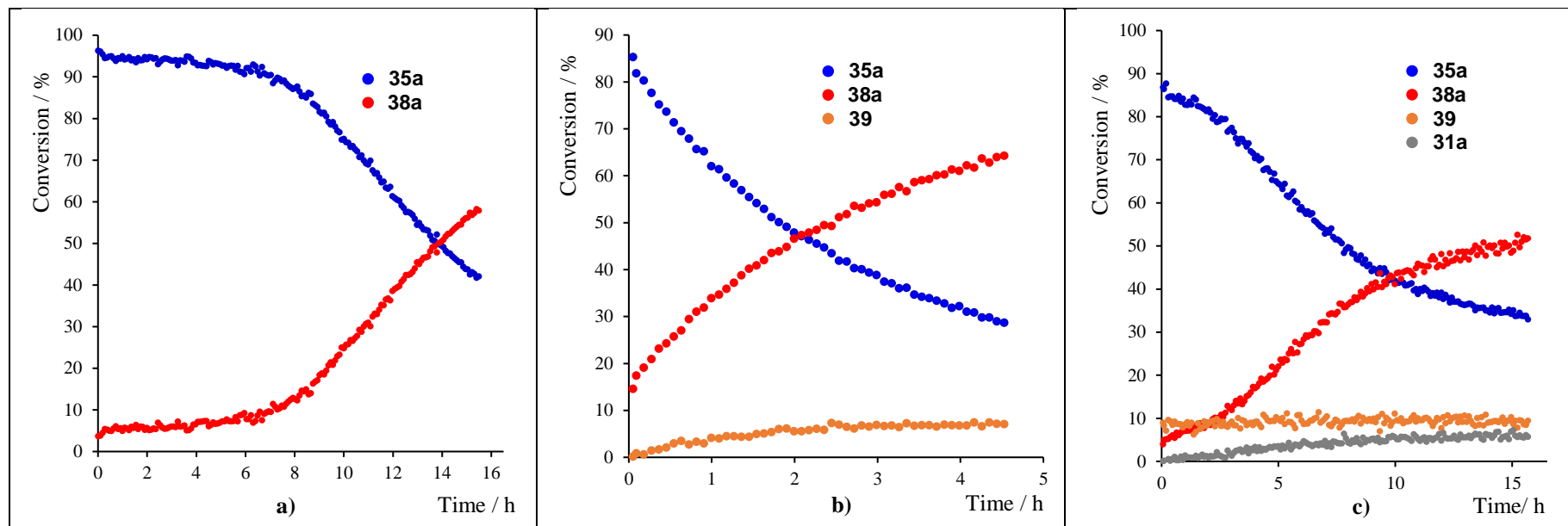
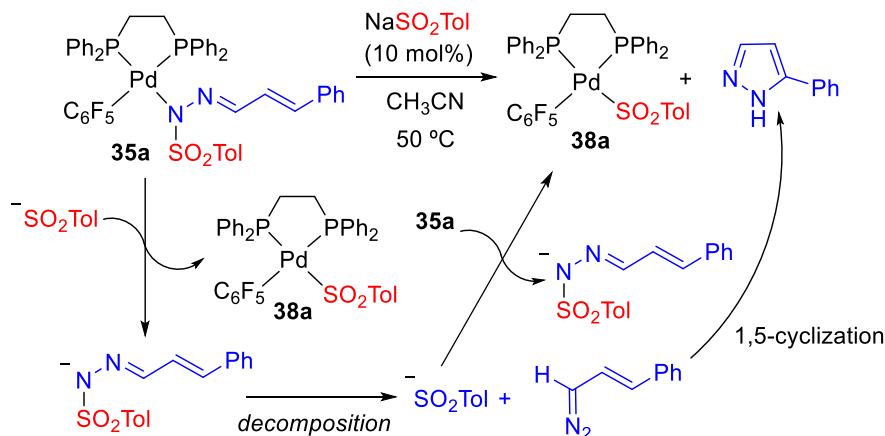


Figure 5.16 Plot of conversion vs. time for the decomposition of **a)** **35a** in MeCN at 50 °C; **b)** **35a** and NaSO₂Tol (10 mol %) in MeCN at 50 °C (the formation of a small amount of [Pd(C₆F₅)(dppe)(κ¹-5-Ph-pz)] (**39**) was also observed); **c)** (**35a**) and 5-Ph-pzH (10 mol %) in MeCN at 50 °C (the formation of a small amount of η³-allylic complex **31a** was also observed).

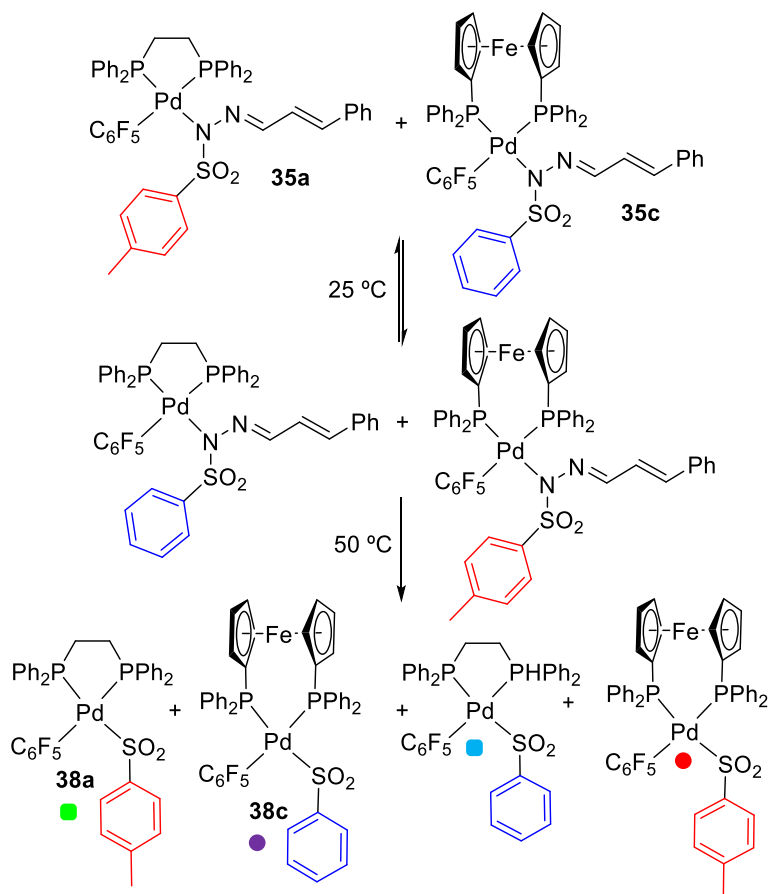
When the same monitoring was carried out in the presence of 10 mol% of NaSO₂Tol the reaction is faster and reproduces the concentration-time evolution in the later stage of the decomposition of **35a** (Figure 5.16, **b**). This is consistent with tosylate increasing the rate of substitution of the coordinated hydrazonate (Scheme 5.10). The same experiment was carried out adding 10 mol% of 5-Ph-pzH, also a product formed in the decomposition of **35a**, instead of sodium tosylate. A small increase of the rate was observed (half-life of **35a**, $t_{1/2} = 7.8$ h) consistent with the lower coordination ability of 5-Ph-pzH (Figure 5.16, **c**).

The half-life of the free hydrazone **34** in the decomposition reaction shown in Equation 5.2 ($t_{1/2} = 2.6$ h, Figure 5.14) is similar to that of **35a** in the presence of sodium tosylate ($t_{1/2} = 2$ h, Figure 5.16, **b**) indicating that the most plausible scenario is the decomposition of the hydrazonate outside the coordination sphere of palladium.



Scheme 5.10 Decomposition of complex **35a** favoured by the addition of NaSO₂Tol according to the kinetic shown in Figure 5.16, **b**).

The crossover experiment depicted in Scheme 5.11 shows that the scrambling of the hydrazonato ligands in the mixture **35a/35c** occurs at room temperature (see Figure 5.17). When the mixture **35a/35c** was heated at 50 °C in acetonitrile both complexes decompose to a mixture of tosylate derivatives (Figures 5.18 and Figure 5.19). The half-life of the mixture **35a/35c** is $t_{1/2} = 2.9$ h (Figure 5.21 in the *Experimental part*) similar to that observed for the decomposition of the free hydrazone. This indicates that the decoordination of the hydrazonato ligand is easier in the more constrained dppf palladium complex **35c**. Altogether, these experiments show that the metal does not promote the hydrazonato decomposition and the latter process occurs outside the catalytic cycle.



Scheme 5.11 Crossover experiment showing the facile exchange of hydrazonato ligands (25 °C) and of the sulfinate ligands upon decomposition at 50 °C.

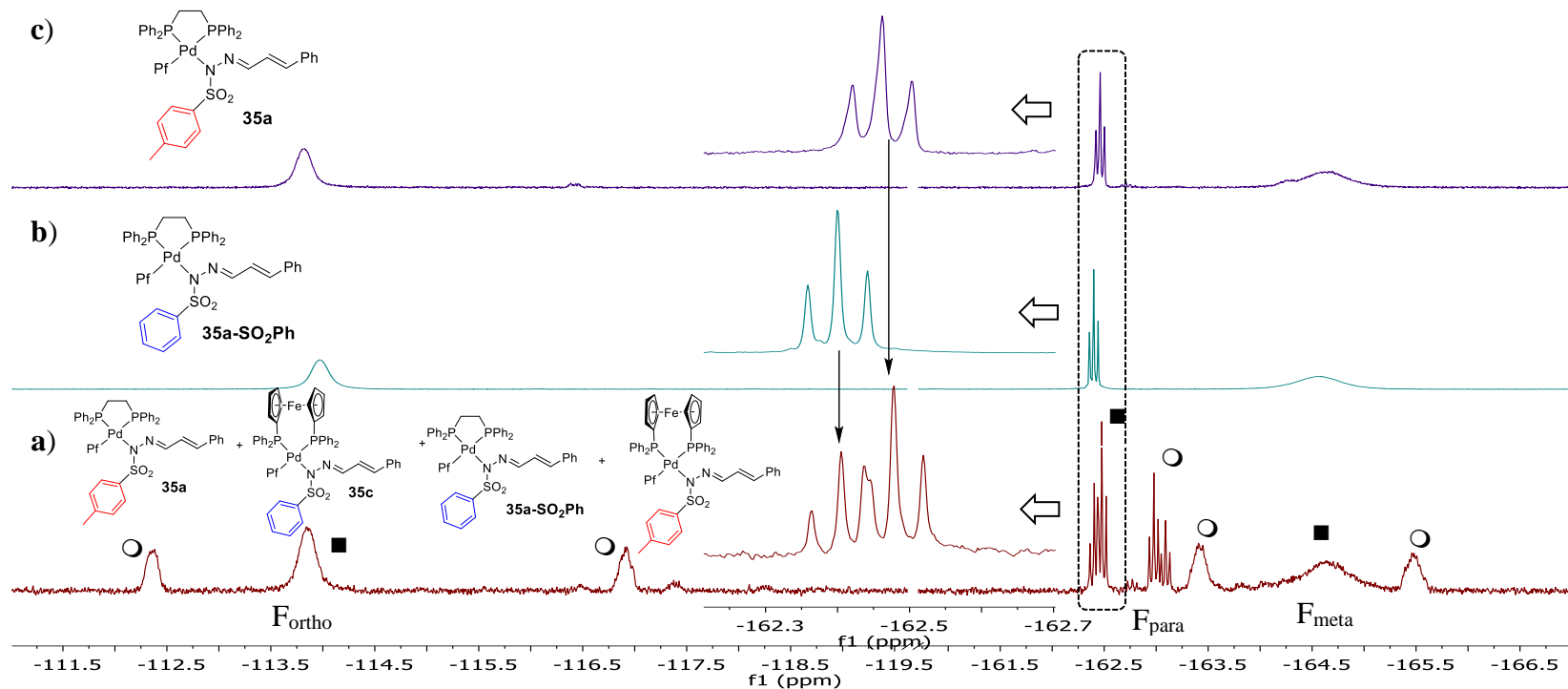


Figure 5.17 ^{19}F NMR (470.17 MHz, $\text{CH}_3\text{CN}/\text{DMSO-d}_6$ capillary) spectra of: (a) The reaction of complexes **35a** and **35c** at room temperature for 30 min, showing the formation of two new species by scrambling of the hydrazonato ligands. These species can be clearly seen in the F_{para} region (the F_{ortho} and F_{meta} signals overlap with the starting complexes). The F_{para} region for the dppe complexes is enlarged and can be compared with the spectra of the *N*-phenylsulfinyl-hydrazonato complex **35a-SO₂Ph** (b) and the *N*-tosylhydrazonato derivative **35a** (c). ■ dppe complexes; ○ dpfp complexes (restricted rotation of the $-\text{C}_6\text{F}_5$ group leads to inequivalent F_{ortho} and F_{meta} signals). Pf = $-\text{C}_6\text{F}_5$.

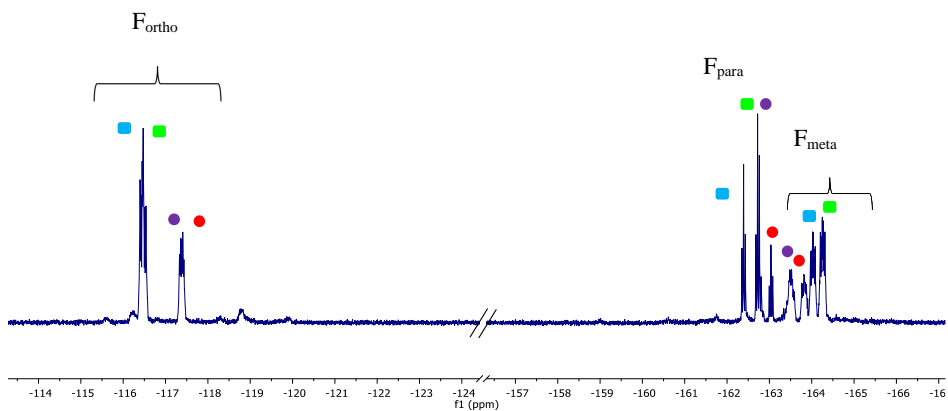


Figure 5.18 ^{19}F NMR (470.17 MHz, $\text{CH}_3\text{CN}/\text{DMSO-d}_6$ capillary) of the reaction of complexes **35a** and **35c** for 2 h at 80 °C leading to a mixture of the four possible sulfinato palladium complexes (for label key, see Scheme 5.11).

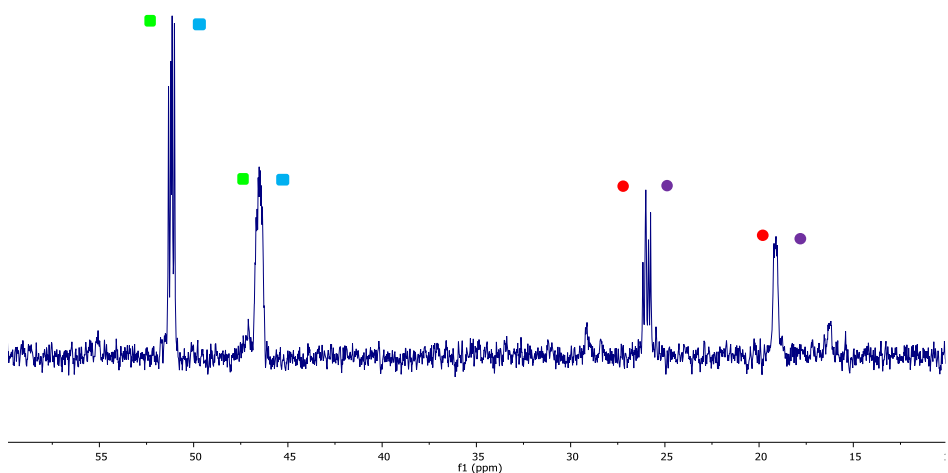


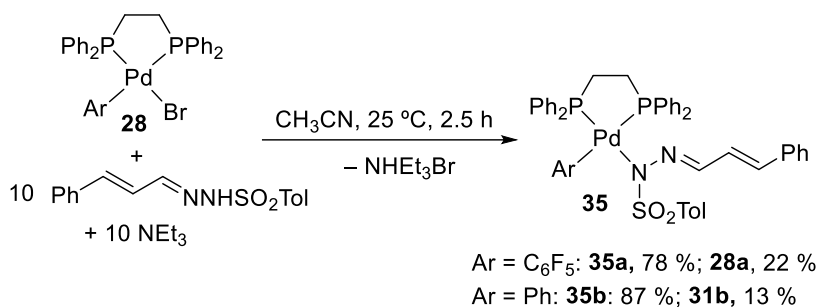
Figure 5.19 $^{31}\text{P}\{^1\text{H}\}$ NMR (202.31, MHz, $\text{CH}_3\text{CN}/\text{DMSO-d}_6$ capillary) of the reaction of complexes **35a** and **35c** for 2 h at 80 °C leading to a mixture of the four possible sulfinato-Pd complexes (for label key, see Scheme 5.11).

5.2.3 Ligand substitution reactions

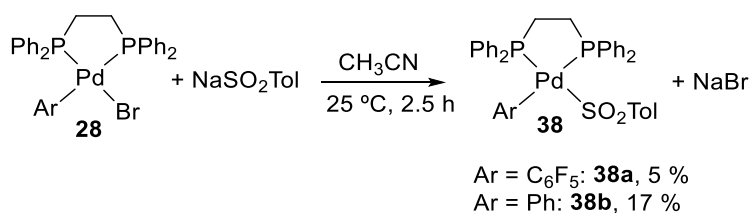
The experiments shown before indicate that, in the course of a reaction with tosylhydrazones as carbene precursors, there are several competing ligands that influence the speciation of palladium, *i.e.* $[\text{PdArL}_2\text{Y}]$ $\text{Y} = \text{halide, hydrazonate or Ts}$. Equations 5.4 and 5.5 show substitution reactions using the ligands in mol ratios close to those under catalytic conditions. In the presence of an excess of hydrazonate, the substitution of

hydrazone for bromide is favored and complexes **35** are the predominant species (Equation. 5.4). The substitution of tosylate for bromide can also occur (Equation. 5.5) but it is less facile at least at the beginning of the reaction when the amount of free tosylate is low. Nonetheless the actual ratio of species will be dependent on the concentration of free X ligands, which will be in turn controlled by the relative solubility of the formed byproduct salts MX ($M^+ = \text{alkali cation}, \text{NR}_4^+$), according to the base chosen to deprotonate the hydrazone. Since the reactions are usually conducted using a large excess of hydrazone and base, the complex $[\text{PdArL}_2(\text{hydrazone})]$ is likely the most abundant and a plausible resting state.

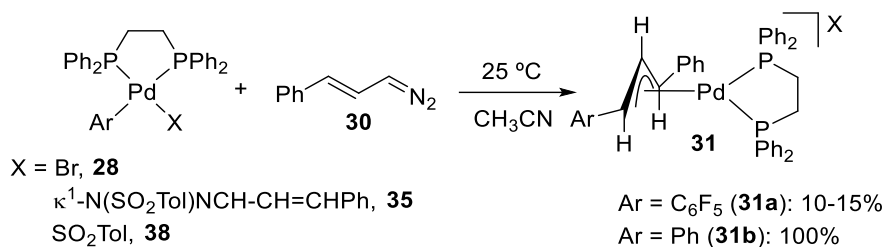
For the reaction to proceed, the *in situ* generated diazoalkane by decomposition of the free hydrazone has to enter into the metal coordination sphere. Therefore, the feasibility of the substitution of diazoalkane for X was evaluated. Equation. 5.6 shows the reactions tested at room temperature (see also Table 5.2 in the *Experimental part*).



Equation 5.4



Equation 5.5



Equation 5.6

The diazoalkane can substitute all X ligands with similar ability, but the most significant difference is introduced by the aryl group, the phenyl group leading to a more efficient formation of the migratory insertion product **31b** (Equation 5.6). The phenyl group is a better donor and can reduce the electrophilicity of the metal making the substitution of the anionic X ligand by the entering neutral diazo compound more facile. The subsequent formation of the carbene (by N₂ extrusion) and migratory insertion will also be affected by the nature of the aryl but given the low barriers for these steps (Figure 5.9), it is unlikely that they control the reactivity observed.

5.3 CONCLUSIONS

Using well-defined model aryl palladium complexes, it is possible to gather information about the interaction of diazoalkanes and tosylhydrazones with these complexes, relevant to the catalytic C-C coupling processes that involve the abovementioned carbene precursors. A more detailed catalytic cycle could be derived from this information that completes the general one shown above (Scheme 5.2, *Introduction section*) and it is depicted in Scheme 5.12.

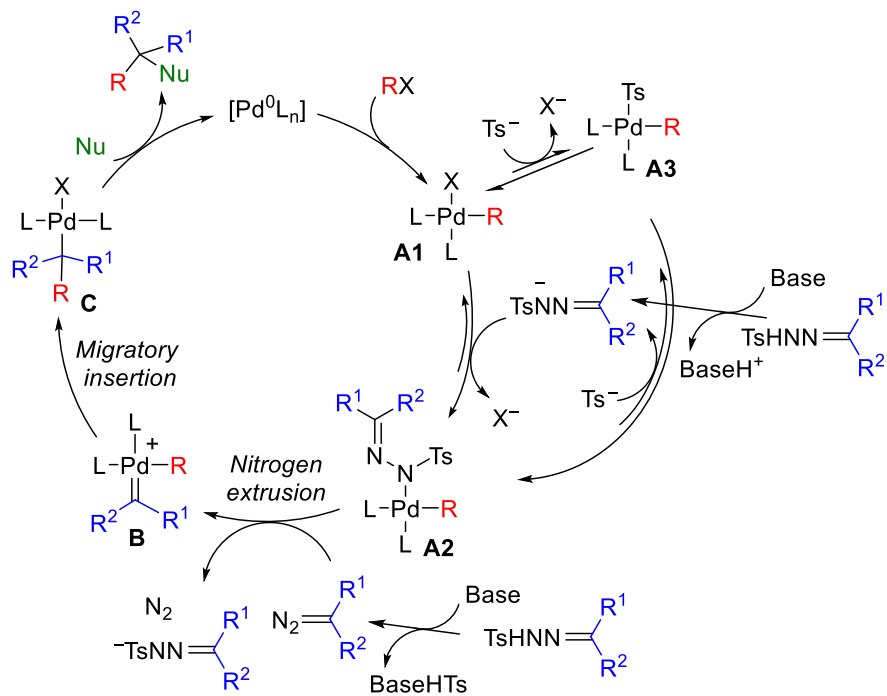
Hydrazonates are excellent ligands that coordinate to palladium and, in the presence of an excess of hydrazone and a base, a common mixture in catalytic reactions, these species are easily formed by halide substitution. When the hydrazonato decomposes *via* the Bamford-Stevens reaction to the diazoalkane, free tosylate is generated than can also coordinate to palladium. Therefore, a mixture of aryl species [PdArL₂Y], Y = halide, hydrazonate, Ts coexist in equilibrium (**A1-A3** in Scheme 5.12, analogous to the isolated complexes **28**, **35** and **38**), the hydrazonato complexes being the more abundant.

The decomposition of the hydrazonato moiety to a diazoalkane is not promoted by coordination to the metal and it does not occur in the coordination sphere of palladium. A previous decoordination is needed, so the conventional evolution of the free hydrazonato to the corresponding diazo compound takes place.

The coordination of the diazoalkane to palladium occurs by substitution of the hydrazonato ligand, as has been tested independently. The substitution of halide or tosylate by the diazoalkane is also possible. The formation of a palladium carbene (**B**, Scheme 5.12) from the diazoalkane occurs by a low barrier N₂ extrusion. It was not possible to detect this intermediate since the very electrophilic palladium carbene undergoes a fast migratory insertion that leads to a new palladium alkyl. The palladium derivatives right after migratory insertion of these non-stabilized carbenes (**C**, Scheme 5.12) could be isolated by selecting appropriate substituents in the carbene moiety CHR that could stabilize the new organometallic complex *via* formation of an η^3 -allyl complex (R = CH=CHPh, **31**) or a η^3 -benzylic one (R = Ph, **33**). In this way intermediate **C** could be trapped and its decomposition hampered.

The hydrazonato species **A2** is a likely resting state of these reactions. Once the diazoalkane is formed from the non-coordinated hydrazonato in solution, the substitution of the metal-bound hydrazonato is possible and the steps that follow are fast. The use of hydrazones instead of diazoalkanes has many practical advantages and a myriad of reactions have been successfully implemented with these precursors. In order to use the

optimal catalytic conditions with these substrates it is necessary to take into account that a hydrazone species are likely formed and that the reaction conditions (excess of hydrazone and base, solubility of the hydrazone) should not impede the substitution equilibria with the diazoalkane, formed in lower concentration, that is key for turnover.



Scheme 5.12 A more detailed catalytic cycle for Pd-catalyzed coupling reactions with hydrazones.

5.4 EXPERIMENTAL PART

5.4.1 General considerations

^1H , $^{13}\text{C}\{^1\text{H}\}$ ^{31}P and ^{19}F NMR spectra were recorded on Bruker AV-400 or an Agilent MR-500 and MR-400 spectrometers equipped with variable-temperature probes at the *Laboratorio de Técnicas Instrumentales* (LTI) of the UVa. Chemical shifts (in δ units, ppm) were referenced to SiMe_4 (^1H and ^{13}C) and CFCl_3 (^{19}F) and H_3PO_4 (85%, ^{31}P). For the NMR spectra registered in non-deuterated solvents, a coaxial tube containing DMSO-d_6 was used to maintain the lock to the ^2H signal. The temperature for the NMR probe was calibrated with a methanol standard (low temperature).¹⁹³ Homonuclear (^1H -COSY and ^1H -ROESY) and heteronuclear (^1H - ^{13}C HSQC and HMBC) experiments were used to help with the signal assignments. NMR data are given at 298 K unless otherwise noted. The GC-MS analyses were performed in a Thermo-Scientific Focus DSQ II GC/MS apparatus. The intensities are reported as percentages relative to the base peak after the corresponding m/z value. Elemental analyses were carried out in a Carlo Erba 1108 microanalyser (at the Vigo University, Spain). Infrared spectra were recorded (in the range 4000–200 cm^{-1}) on a Perkin-Elmer FT-IR Spectrum Frontier with an ATR diamond accessory. All reactions were conducted under a N_2 atmosphere. Solvents were dried using a solvent purification system SPS PS-MD-5 (ether, hexane, THF and CH_2Cl_2) or distilled from appropriate drying agents under nitrogen prior to use and stored over 3 Å or 4 Å molecular sieves (acetonitrile). Sodium *p*-toluenesulfinate (NaTs), sodium benzenesulfinate (NaSO_2Ph), 1,1'-bis(diphenylphosphino)ferrocene (dppf), 1,2-bis(diphenylphosphino)ethane (dppe) and PPh_3 are commercially available and were purchased from Aldrich, Alfa Aesar or Fluorochem. All commercial reagents and solvents were used as received unless otherwise indicated. The syntheses of the hydrazone derivatives (**34**, **36** and $(\text{PhSO}_2)\text{NH-N}=\text{CH-CH}=\text{CHPh}$),¹⁹⁴ the diazo compounds (**30**, **32**),¹⁹⁵ 5-Ph-pzH,¹⁹⁶ and (*E*)-3-phenylprop-2-enal azine,¹⁹⁷ were carried out according to the literature methods. All diazoalkanes were prepared and kept as dichloromethane solutions for no longer than 10 days under a nitrogen atmosphere at $-28\text{ }^\circ\text{C}$ in the dark. The concentrations of these solutions were determined by ^1H NMR using $\text{CF}_3\text{CH}_2\text{I}$ as internal standard. The palladium complexes $[\text{PdBr}(\text{C}_6\text{F}_5)(\text{dppe})]$,⁸⁶ $[\text{PdBr}(\text{C}_6\text{F}_5)(\text{dppf})]$,⁸⁶ and $[\text{PdBr}(\text{dppe})\text{Ph}]$,⁸⁶ were prepared as reported before.

¹⁹³ Ammann, C.; Meier, P.; Merbach, A. E. *J. Magn. Reson.* **1982**, *321*, 319–321.

¹⁹⁴ a) Aggarwal, V. K.; Alonso, E.; Bae, I.; Hynd, G.; Lydon, K. M.; Palmer, M. J.; Patel, M.; Porcelloni, M.; Richardson, J.; Stenson, R. A.; Studley, J. R.; Vasse, J.-L.; Winn, C. L. *J. Am. Chem. Soc.* **2003**, *125*, 10926–10940. b) Li, P.; Zhao, J.; Wu, C.; Larock, R. C.; Shi, F. *Org. Lett.* **2011**, *13*, 3340–3343.

¹⁹⁵ a) Morrison, H.; Danishefsky, S.; Yates, P. *J. Org. Chem.* **1961**, *26*, 2617–2618. b) Doyle, M. P.; Yan, M. *J. Org. Chem.* **2002**, *67*, 602–604. c) Friscourt, F.; Fahrni, C. J.; Boons, G.-J. *Chem. – A Eur. J.* **2015**, *21*, 13996–14001.

¹⁹⁶ Wen, J.; Fu, Y.; Zhang, R.-Y.; Zhang, J.; Chen, S.-Y.; Yu, X.-Q. *Tetrahedron* **2011**, *67*, 9618–9621.

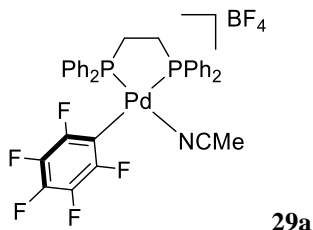
¹⁹⁷ Russavskaya, N. V.; Grabel'nykh, V. A.; Levanova, E. P.; Sukhomazova, E. N.; Deryagina, E. N. *Russ. J. Org. Chem.* **2002**, *38*, 1498–1500.

5.4.2 Synthesis of Palladium complexes

[Pd(C₆F₅)(dppe)(NCCH₃)](BF₄) (29a). Equimolar amounts of [PdBr(C₆F₅)(dppe)] (152.80 mg, 0.20 mmol) and AgBF₄ (39.5 mg, 0.20 mmol) were mixed in dry MeCN (10 mL) and stirred for 15 min at room temperature under nitrogen. The suspension was filtered through Kieselghur and the filtrate was evaporated to dryness. The resulting yellow oil (**29a**) was characterized by NMR. The yellow oil was triturated with diethyl ether and *n*-hexane until the formation of a white solid that was filtered, washed with *n*-hexane and air-dried. Yield: 108.3 mg, (67 %). This solid is contaminated by small amounts of the reorganization product [Pd(C₆F₅)₂(dppe)].

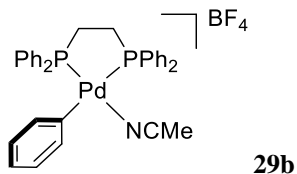
¹H NMR (499.73 MHz, δ, CD₃CN): 7.85 (m, 4H, H^{arom}), 7.75-7.70 (m, 2H, H^{arom}), 7.69-7.52 (m, 10H, H^{arom}), 7.50-7.43 (m, 4H, H^{arom}), 2.92 (m, 2H, CH₂), 2.50 (2H, C'H₂). ¹³C{¹H} NMR (125.67 MHz, δ, CD₃CN): 146.5 (m, ¹J_{C-F} = 227.7 Hz, CF_{ortho}), 138.3 (m, ¹J_{C-F} = 253 Hz, CF_{para}), 136.3 (m, ¹J_{C-F} = 254.0 Hz, CF_{para}), 133.2 (d, J_{C-P} = 11.5 Hz, C^{arom}), 133.0 (d, J_{C-P} = 11.8 Hz, C^{arom}), 132.9 (d, J_{C-P} = 3.4 Hz, C^{arom}), 132.6 (d, J_{C-P} = 2.5 Hz, C^{arom}), 129.8 (d, J_{C-P} = 10.5 Hz, C^{arom}), 129.1 (d, J_{C-P} = 11.9 Hz, C^{arom}), 128.0 (d, ¹J_{C-P} = 45.3 Hz, C^{ipso,arom}), 126.8 (d, ¹J_{C-P} = 59.9 Hz, C^{ipso,arom}), 29.8 (dd, J_{C-P} = 36.1, 16.6 Hz, CH₂), 22.3 (dd, J_{C-P} = 32.4, 8.1 Hz, CH₂). * ¹⁹F NMR (470.17 MHz, δ, CD₃CN): -118.24 (m, 2F, F_{ortho}), -151.58 (BF₄), -160.39 (t, J = 19.4 Hz, 1F, F_{para}), -163.15 (m, 2F, F_{meta}). ³¹P{¹H} NMR (202.31, MHz, δ, CD₃CN): 62.64 (m, 1P), 52.59 (m, 1P). IR (neat, cm⁻¹): C₆F₅, 1495, 1040, 951, 742, 689; CH₃CN, 2308; BF₄⁻, 1046.

*The ¹³C signal for the C_{ipso} of the C₆F₅ group could not be observed.



[Pd(dppe)(NCCH₃)Ph](BF₄) (29b). [PdBr(dppe)Ph] (12.0 mg, 0.018 mmol) and AgBF₄ (3.5 mg, 0.018 mmol) were mixed in dry MeCN (0.6 mL) and stirred for 15 min at room temperature under nitrogen. The suspension was filtered through Kieselghur and the resulting colorless solution was characterized by NMR.

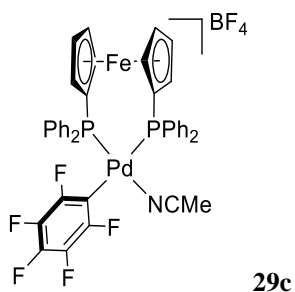
¹H NMR (499.73 MHz, δ, CH₃CN, (CD₃)₂SO capillary): 8.04 (m, 4H, H^{arom}), 7.92-7.84 (m, 6H, H^{arom}), 7.81 (m, 2H, H^{arom}), 7.74-7.66 (m, 8H, H^{arom}), 7.27 (m, 2H, H^{ortho, Pd-Ph}), 7.08 (m, 2H, H^{meta + para, Pd-Ph}), 2.94 (m, 2H, CH₂), 2.62 (m, 2H, CH₂). ³¹P{¹H} NMR (202.31, MHz, δ, CH₃CN, (CD₃)₂SO capillary): 54.51 (d, J = 26.8 Hz, 1P), 41.07 (d, J = 26.8 Hz, 1P).



[Pd(C₆F₅)(dppf)(NCCH₃)](BF₄) (29c). Equimolar amounts of [PdBr(C₆F₅)(dppf)] (128.2 mg, 0.14 mmol) and AgBF₄ (27.5 mg, 0.14 mmol) were mixed in dry CH₃CN (10 mL) and stirred for 15 min at room temperature under nitrogen. The suspension was filtered through Kieselghur and the filtrate was evaporated to dryness. The resulting orange oil (**29c**) was characterized by NMR. The orange oil was triturated with diethyl ether and *n*-hexane until the formation of an orange solid that was filtered, washed with *n*-hexane and air-dried. Yield: 98 mg, (73 %). This solid is contaminated by small amounts of reorganization products.

¹H NMR (499.73 MHz, δ, CDCl₃): 7.79-7.67 (m, 10H, H^{arom}), 7.46-7.32 (m, 6H, H^{arom}), 7.17 (m, 4H, H^{arom}), 5.03 (s, 2H, H^{Cp}), 4.80 (s, 2H, H^{Cp}), 4.39 (s, 2H, H^{Cp}), 3.61 (s, 2H, H^{Cp}), 2.00 (s, 3H, NCMe). ¹³C{¹H} NMR (125.67 MHz, δ, CDCl₃): 145.1 (m, ¹J_{C-F} = 225.6 Hz, CF_{ortho}), 138.5 (m, ¹J_{C-F} = 248.0 Hz, CF_{para}), 136.1 (m, ¹J_{C-F} = 249.1 Hz, CF_{meta}), 133.6 (d, J_{C-P} = 12.0 Hz, C^{arom}), 133.1 (d, J_{C-P} = 12.0 Hz, C^{arom}), 132.3 (C^{arom}), 132.1 (C^{arom}), 130.6 (d, ¹J_{C-P} = 63.0 Hz, C^{arom}), 129.7 (d, ¹J_{C-P} = 49 Hz, C^{arom}), 129.8 (d, J_{C-P} = 10.3 Hz, C^{arom}), 128.5 (d, J_{C-P} = 11.9 Hz, C^{arom}), 116.8 (NCMe), 78.2 (d, J_{C-P} = 12.8 Hz, C^{Cp}), 75.4 (d, J_{C-P} = 8.9 Hz, C^{Cp}), 74.9 (d, J_{C-P} = 9.6 Hz, C^{Cp}), 74.0 (d, J_{C-P} = 6.6 Hz, C^{Cp}), 73.5 (dd, ¹J_{C-P} = 64.7 Hz, J_{C-P} = 7.2 Hz, C^{Cp}), 68.0 (dd, ¹J_{C-P} = 55.8 Hz, J_{C-P} = 2.7 Hz, C^{Cp}), 1.9 (NCMe). * ¹⁹F NMR (470.17 MHz, δ, CDCl₃): -119.65 (m, 2F, F_{ortho}), -153.55 (BF₄), -157.59 (t, J = 20.5 Hz, 1F, F_{para}), -160.21 (m, 2F, F_{meta}). ³¹P{¹H} NMR (202.31, MHz, δ, CDCl₃): 36.86 (m, 1P), 18.28 (m, 1P). IR (neat, cm⁻¹): C₆F₅: 1499, 1040, 950, 742, 692; CH₃CN, 2292; BF₄⁻ 1045.

*The ¹³C signal for the C_{ipso} of the C₆F₅ group could not be observed.



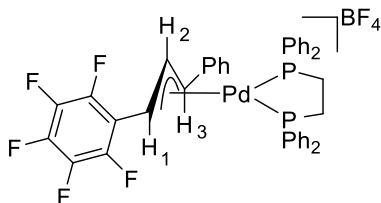
[Pd(dppe)(η³-Ph-CH-CH-CH-C₆F₅)](BF₄) (31a). [PdBr(C₆F₅)(dppe)] (199.2 mg, 0.265 mmol) and AgBF₄ (51.68 mg, 0.265 mmol) were mixed in dry MeCN (5 mL) and stirred for 15 min at room temperature under nitrogen. The resulting suspension was filtered through Kieselghur to remove the AgBr. The addition of a dichloromethane solution of the diazo alkene N₂CH-CH=CHPh (**30**, 12 mL, 0.0248 M) afforded an intense yellow solution, which was stirred at room temperature for 30 min. The solution was

evaporated to dryness and the addition of Et₂O (3 mL) led to a yellow solid, which was collected by filtration, washed with cold Et₂O (2 x 5 mL), and air dried. Yield: 0.2 g (86 %).

¹H NMR (399.86 MHz, δ, CDCl₃): 7.80 (m, 2H, H^{arom}), 7.67 (m, 3H, H^{arom}), 7.47 (m, 5H, H^{arom}), 7.32 (m, 2H, H^{arom}), 7.24 (m, 4H, H^{arom}), 7.11 (t, J = 7.2 Hz, 1H, H_{para}, Ph-allyl), 7.05 (d, J = 7.7 Hz, 2H, H_{ortho} Ph-allyl), 7.00 (m, J = 7.5 Hz, 2H, H_{meta}, Ph-allyl), 6.96 (m, 2H, H^{arom}), 6.83 (m, 2H, H^{arom}), 6.67 (t, J = 13 Hz, 1H, H²), 5.81 (t, J_{H-H} = J_{H-P} = 13 Hz, 1H, H¹), 5.24 (t, J_{H-H} = J_{H-P} = 13 Hz, 1H, H³), 2.91 (m, 1H, CH₂), 2.78 (m, 1H, C'^H₂), 2.26 (m, 1H, CH₂), 2.0 (m, 1H, C'^H₂).[†] ¹³C{¹H} NMR (100.56 MHz, δ, CDCl₃): 143.3 (m, ¹J_{C-F} = 250.5 Hz, CF_{ortho}), 137.2 (m, ¹J_{C-F} = 252.0 Hz, CF_{para}), 134.5 (d, J_{C-P} = 14.0 Hz, C^{arom}), 133.1 (d, J_{C-P} = 2.4 Hz, C^{arom}), 132.8 (d, J_{C-P} = 13.0 Hz, C^{arom}), 132.1 (d, J_{C-P} = 11.9 Hz, C^{arom}), 131.9 (d, J_{C-P} = 2.5 Hz, C^{arom}), 131.8 (d, J_{C-P} = 2.7 Hz, C^{arom}), 131.1 (d, J_{C-P} = 2.7 Hz, C^{arom}), 130.5 (d, J_{C-P} = 11.3 Hz, C^{arom}), 130.2 (d, J_{C-P} = 11.2 Hz, C^{arom}), 129.6 (d, J_{C-P} = 10.5 Hz, C^{arom}), 129.1 (d, J_{C-P} = 10.6 Hz, C^{arom}), 128.8 (C_{meta}-Ph-allyl), 128.5 (d, J_{C-P} = 11.3 Hz, C^{arom}), 128.2 (C_{para}-Ph-allyl), 127.6 (d, ¹J_{C-P} = 44.8 Hz, C^{arom}), 126.8 (C_{ortho}-Ph-allyl), 126.3 (d, ¹J_{C-P} = 42.6 Hz, C^{arom}), 125.8 (d, ¹J_{C-P} = 45.5 Hz, C^{arom}), 125.2 (d, ¹J_{C-P} = 45.3 Hz, C^{arom}), 113.2 (t, J = 6.2 Hz, C²), 112.3 (m, CF_{ipso}), 96.8 (dd, J_{C-P} = 23.1, 5.5 Hz, C¹), 67.2 (d, J_{C-P} = 30.0 Hz, C³), 29.0 (dd, J_{C-P} = 33.1, 13.1 Hz, CH₂), 27.1 (dd, J_{C-P} = 32.1, 13.6 Hz, C'^H₂).^{*†} ¹⁹F NMR (376.19 MHz, δ, CDCl₃): -142.11 (m, 2F, F_{ortho}), -151.84 (BF₄), -157.15 (t, J = 21 Hz, 1F, F_{para}), -161.38 (m, 2F, F_{meta}). ³¹P{¹H} NMR (161.87 MHz, δ, CDCl₃): 52.44 (d, J = 48.3 Hz, 1P), 46.70 (d, J = 48.3 Hz, 1P). IR (neat, cm⁻¹): C₆F₅, 1503, 1046, 998, 952, 689; BF₄⁻ 1040. Anal. Calcd. for C₄₁H₃₂BF₉P₂Pd: C, 56.29 %; H, 3.69 %. Found: C, 56.51 %; H, 3.73 %.

[†] The signal assignment of H¹/C¹ and H³/C³ is tentative and could be reversed.

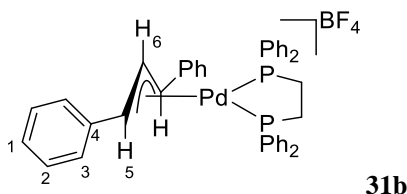
^{*}The ¹³C signal for the C_{meta} of the C₆F₅ group was not observed.



31a

[Pd(dppe)(η³-Ph-CH-CH-CH-Ph)](BF₄) (31b). [PdBr(C₆H₅)(dppe)] (137.3 mg, 0.207 mmol) and AgBF₄ (40.4 mg, 0.207 mmol) were mixed in dry MeCN (3 mL) and stirred for 15 min at room temperature under nitrogen. The suspension was filtered through Kieselghur to remove the AgBr. The addition of a dichloromethane solution of the diazo compound N₂CH-CH=CHPh (**30**, 2.3 mL, 0.09 M) afforded an intense yellow solution, which was stirred at room temperature for 30 min. The solution was evaporated to dryness and the addition of Et₂O (5 mL) afforded complex **31b** as a yellow solid, which was collected by filtration, washed with cold Et₂O (2 x 5 mL), and air dried. Yield: 0.130 g (80 %).

^1H NMR (399.86 MHz, δ , CDCl_3): 7.53 (m, 6H, H^{arom}), 7.45 (m, 4H, H^{arom}), 7.35 (t, $J = 7.2$ Hz, 2H, H^1), 7.16 (t, $J = 7.3$ Hz, 4H, H^2), 7.02 (m, 6H, H^{arom}), 6.93 (m, 4H, H^{arom}), 6.76 (m, 4H, H^3), 6.59 (t, $J = 12.9$ Hz, 1H, H^6), 5.46 (m, 2H, H^5), 2.51-2.33 (m, 4H, CH_2). $^{13}\text{C}\{^1\text{H}\}$ NMR (100.56 MHz, δ , CDCl_3): 136.3 (t, $J_{\text{C-P}} = 4.6$ Hz, C^4), 133.3 (t, $J_{\text{C-P}} = 6.4$ Hz, C^{arom}), 131.9 (C^{arom}), 131.6 (t, $J_{\text{C-P}} = 5.7$, C^3), 131.1 (C^1), 129.7 (t, $J_{\text{C-P}} = 5.5$ Hz, C^{arom}), 129.3 (t, $J_{\text{C-P}} = 5.2$ Hz, C^2), 128.7 (t, $J_{\text{C-P}} = 1.9$ Hz, C^{arom}), 128.0 (m, $\text{C}^{\text{ipso-arom}}$), 127.4 (t, $J_{\text{C-P}} = 2.6$ Hz, C^{arom}), 126.8 (t, $J_{\text{C-P}} = 3.1$ Hz, C^{arom}), 126.6 (m, $\text{C}^{\text{ipso-arom}}$), 111.6 (t, $J_{\text{C-P}} = 7.3$ Hz, C^6), 90.1 (t, $J_{\text{C-P}} = 15.8$ Hz, C^5), 28.0 (t, $J_{\text{C-P}} = 23.0$ Hz, CH_2). $^{31}\text{P}\{^1\text{H}\}$ NMR (161.87 MHz, δ , CDCl_3): 46.38 (s, 2P). IR (neat, cm^{-1}): BF_4 , 1044 br. Anal. Calcd. for $\text{C}_{41}\text{H}_{37}\text{BF}_4\text{P}_2\text{Pd}$: C, 62.74 %; H, 4.75 %. Found: C, 62.79 %; H, 4.79 %.



[Pd(dppe)(η^3 -Ph-CH-C $_6$ F $_5$)](BF $_4$) (33). Equimolar amounts of [PdBr(C $_6$ F $_5$)(dppe)] (113.23 mg, 0.150 mmol) and AgBF $_4$ (29.32 mg, 0.150 mmol) were mixed in dry MeCN (5 mL) and stirred for 15 min at room temperature under nitrogen. The suspension was filtered through Kieselghur to remove the AgBr. Addition of a dichloromethane solution of the diazo compound N $_2$ CHPh (**32**, 1 mL, 0.146 M) afforded an intense yellow solution, which was stirred at room temperature for 30 min. Then, the solution was evaporated to dryness to give a yellow residue, which was triturated with *n*-hexane (3 mL) affording a yellow solid. The yellow solid was collected by filtration, washed with *n*-hexane (2 x 5 mL), and air dried. Yield: 63.31 mg (50 %).

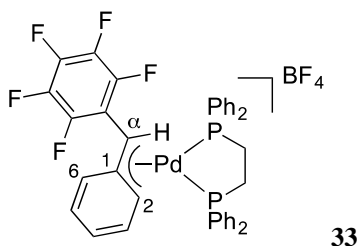
^1H NMR (399.86 MHz, δ , CDCl_3 , 298 K): 7.82 (m, 2H, H^{arom}), 7.6-7.68 (m, 3H, H^{arom}), 7.48-7.57 (m, 6H, H^{arom}), 7.35-7.45 (m, 6H, H^{arom}), 7.16 (td, $J = 7.9, 2.5$ Hz, 2H, H^{arom}), 6.98 (m, br, 1H, H^6), 6.80 (m, 4H, H^{arom}), 6.75 (m, br, 1H, H^2), 4.54 (d, $^3J_{\text{H-P}} = 12.3$ Hz, 1H, H^a), 2.94 (m, 2H, CH_2 , $\text{C}'\text{H}_2$), 2.28 (m, 1H, CH_2), 1.92 (m, 1H, $\text{C}'\text{H}_2$). $^{13}\text{C}\{^1\text{H}\}$ NMR (100.56 MHz, δ , CDCl_3 , 298 K): 143.6 (m, $^1J_{\text{C-F}} = 248.8$ Hz, CF_{ortho}), 137.2 (m, $^1J_{\text{C-F}} = 251.3$ Hz, CF_{para}), 134.7 (d, $J_{\text{C-P}} = 13.7$ Hz, C^{arom}), 133.3 (C^{arom}), 132.8 (d, $J_{\text{C-P}} = 13.5$ Hz, C^{arom}), 132.4 (C^{arom}), 131.8 (d, $J_{\text{C-P}} = 12.4$ Hz, C^{arom}), 130.9 (d, $J_{\text{C-P}} = 2.2$ Hz, C^{arom}), 130.3 (d, $J_{\text{C-P}} = 10.9$ Hz, C^{arom}), 130.2 (d, $J_{\text{C-P}} = 9.7$ Hz, C^{arom}), 129.7 (d, $J_{\text{C-P}} = 10.3$ Hz, C^{arom}), 129.6 (d, $J_{\text{C-P}} = 9.9$ Hz, C^{arom}), 129.2 (t, $J_{\text{C-P}} = 4.1$ Hz, C^{arom}), 128.8 (d, $J_{\text{C-P}} = 10.9$ Hz, C^{arom}), 128.4 (d, $^1J_{\text{C-P}} = 49.9$ Hz, C^{arom}), 127.0 (d, $^1J_{\text{C-P}} = 48.9$ Hz, C^{arom}), 126.1 (d, $^1J_{\text{C-P}} = 46.1$ Hz, C^{arom}), 125.2 (d, $^1J_{\text{C-P}} = 42.0$ Hz, C^{arom}), 125.4 (br, C^6), 120.7 (dd, $J_{\text{C-P}} = 8.5, 3.8$ Hz, C^1), 112.3 (t, $^2J_{\text{C-F}} = 15.5$ Hz, CF_{ipso}), 100.6 (br, C^2), 49.6 (dd, $J = 48.8, 11.0$ Hz, C^a), 28.3 (dd, $J_{\text{C-P}} = 34.5, 15.2$ Hz, CH_2), 24.2 (dd, $J_{\text{C-P}} = 31.2, 10.6$ Hz, $\text{C}'\text{H}_2$). * ^{19}F NMR (376.19 MHz, δ , CDCl_3 , 298 K): -136.41 (m, 2F, F_{ortho}), -152.79 (BF_4), -157.44 (t, $J = 21.1$ Hz, 1F, F_{para}), -160.87 (m, 2F, F_{meta}). $^{31}\text{P}\{^1\text{H}\}$ NMR (161.87 MHz, δ , CDCl_3 , 298 K): 57.76 (dm, $J = 49.8$ Hz, 1P), 46.91 (dd, $J = 49.8, 3.0$ Hz, 1P). IR (neat, cm^{-1}): C $_6$ F $_5$, 1435, 1050, 996, 964, 690; BF_4^- , 1054. Anal. Calcd. for $\text{C}_{39}\text{H}_{30}\text{BF}_9\text{P}_2\text{Pd}$: C, 55.19 %; H, 3.56 %. Found: C, 55.51 %; H, 3.46 %

* ^{13}C signals for the C_{para} and C_{meta} of the benzylic fragment could not be located.

^1H NMR (499.73 MHz, δ , CDCl_3 , 226 K): 7.88 (m, 2H, H^{arom}), 7.73-7.30 (m, 15H, H^{arom} , H^3 , H^5), 7.17 (t, $J = 7.6$ Hz, 2H, H^{arom}), 6.98 (s, 1H, H^6), 6.74 (m, 4H, H^{arom}), 6.58 (s, 1H, H^2), 4.47 (d, $^3J_{\text{H-P}} = 12.3$ Hz, 1H, H^{α}), 2.94 (m, 2H, CH_2 , $\text{C}'\text{H}_2$), 2.16 (m, 1H, CH_2), 1.86 (m, 1H, $\text{C}'\text{H}_2$). * ^{19}F NMR (470.17 MHz, δ , CDCl_3 , 226 K): -156.96 (t, $J = 21.9$ Hz, 1F, F_{para}), -160.11 (m, 2F, F_{meta}). † $^{31}\text{P}\{^1\text{H}\}$ NMR (202.31 MHz, δ , CDCl_3 , 226 K): 59.15 (d, $J = 48.1$ Hz, 1P), 47.28 (d, $J = 48.1$ Hz, 1P).

† Restricted rotation about the C-C $_6\text{F}_5$ bond leads to coalescence of the F_{ortho} signals at 226 K and they could not be observed.

The stereochemistry of the complex was unequivocally determined by the observation of a positive NOE effect observed between H^{α} and H^2 in a ^1H 2D-ROESY experiment at 226 K.



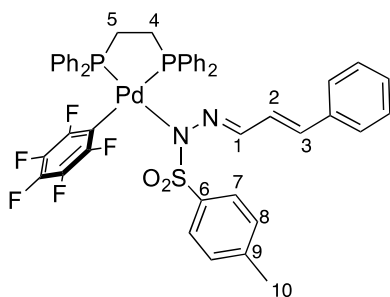
[Pd(C $_6\text{F}_5$)(dppe){(*p*-TolSO $_2$)N=N-CH=CH-CHPh}] (**35a**). [PdBr(C $_6\text{F}_5$)(dppe)] (102.18 mg, 0.135 mmol) and AgBF $_4$ (26.46 mg, 0.135 mmol) were mixed in dry MeCN (3 mL) and stirred for 15 min at room temperature under nitrogen. The suspension was filtered through Kieselghur to remove the AgBr. The resulting solution was added to a mixture of the *N*-tosylhydrazone **34** (40.82 mg, 0.135 mmol) and Cs $_2$ CO $_3$ (265.71 mg, 0.815 mmol) in MeCN (5 mL) and then stirred for 2 h at room temperature. The reaction mixture was filtered and the filtrate was evaporated to dryness. Addition of Et $_2$ O (5 mL) afforded complex **35a** as a yellow solid, which was collected by filtration, washed with cold Et $_2$ O (2 x 5 mL), and air dried. Yield: 0.11 mg, (83 %).

^1H NMR (399.86 MHz, δ , CDCl_3 , 298 K): 7.95 (d, $J = 9.1$ Hz, 1H, H^1), 7.86-7.27 (m, 24H, H^{arom}), 7.33 (d, $J = 8.2$ Hz, 2H, H^7), 7.20 (m, 1H, H^{arom}), 6.87 (d, $J = 8.2$ Hz, 2H, H^8), 6.61 (dd, $J = 15.9, 9.1$, Hz, 1H, H^2), 6.10 (d, $J = 15.9$ Hz, 1H, H^3), 2.51 (br, 2H, H^5), 2.27 (m, 2H, H^4), 2.20 (s, 3H, H^{10}). $^{13}\text{C}\{^1\text{H}\}$ NMR (100.56 MHz, δ , CDCl_3 , 298 K): 146.1 (m, $^1J_{\text{C-F}} = 229.6$ Hz, CF_{ortho}), 137.8 (m, $^1J_{\text{C-F}} = 247.1$ Hz, CF_{para}), 141.6 (C^1), 140.6 (C^9), 140.2 (C^6), 137.5 ($\text{C}^{\text{ipso-Ph}}$), 134.0 (d, $J_{\text{C-P}} = 11.6$ Hz, C^{arom}), 132.9 (br, C^{arom}), 132.1 (C^3), 131.9 (s br, C^{arom}), 129.5 (d, $^1J_{\text{C-P}} = 42.0$ Hz, C^{arom}), 129.2 (d, $J_{\text{C-P}} = 10.5$ Hz, C^{arom}), 128.9 (d, $J_{\text{C-P}} = 10.5$ Hz, C^{arom}), 128.5 (C^{arom}), 128.3 (C^{arom}), 127.8 (C^8), 127.4 (C^2), 127.1 ($\text{C}^{\text{para-Ph}}$), 126.1 (C^7), 126.1 (d, $J_{\text{C-P}} = 10.0$ Hz, C^{arom}), 27.7 (dd, $J = 31.8, 17.4$ Hz, C^5), 24.1 (dd, $J = 29.5, 11.5$ Hz, C^4), 21.0 (C^{10}). * ^{19}F NMR (376.19 MHz, δ , CDCl_3 , 298 K): -114.05 (br, 2F, F_{ortho}), -160.89 (t, $J = 21$ Hz, 1F, F_{para}), -163.10 (br, 2F, F_{meta}). † $^{31}\text{P}\{^1\text{H}\}$ NMR (161.87, MHz, δ , CDCl_3 , 298 K): 52.78 (dt, $J = 17.5, 4.4$ Hz, 1P), 42.74 (m, 1P). IR (neat, cm^{-1}): C $_6\text{F}_5$, 1453, 1048, 952, 747, 685; SO $_2$, 1137. Anal. Calcd. for C $_{48}\text{H}_{39}\text{F}_5\text{N}_2\text{O}_2\text{P}_2\text{PdS}$: C, 59.36 %; H, 4.05 %; N, 2.88 %. Found: C, 59.36 %; H, 4.12 %; N, 2.88 %.

*The ^{13}C signals for the C_{meta} and C_{ipso} of the C_6F_5 group, heavily coupled to ^{19}F , could not be observed.

† Restricted rotation about the Pd- C_6F_5 or Pd-N bonds leads to broad F_{ortho} and F_{meta} signals at 298 K.

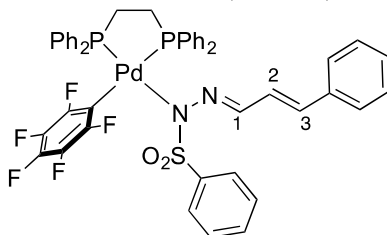
^1H NMR (499.73 MHz, δ , CDCl_3 , 233 K): 8.15 (m, 2H, H^{arom}), 8.03 (m, 1H, H^1), 7.84 (m, 2H, H^{arom}), 7.62 (m, 4H, H^{arom}), 7.52 (m, 5H, H^{arom}), 7.33 (m, 11H, H^{arom}), 7.22 (m, 3H, H^{arom}), 6.88 (d, $J = 8.2$ Hz, 2H, H^8), 6.67 (dd, $J = 15.9, 9.4$, Hz, 1H, H^2), 6.13 (d, $J = 15.9$ Hz, 1H, H^3), 2.62 (m, 1H, H^5), 2.37 (m, 2H, $\text{H}^{5'}$, H^4), 2.36 (m, 1H, H^4), 2.25 (m, 1H, H^4), 2.20 (s, 3H, H^8). ^{19}F NMR (470.17 MHz, δ , CDCl_3 , 233 K): -114.61 (m, 1F, F_{ortho}), -114.86 (m, 1F, F_{ortho}), -160.34 (t, $J = 21$ Hz, 1F, F_{para}), -162.66 (m, 1F, F_{meta}), -163.40 (m, 1F, F_{meta}). $^{31}\text{P}\{^1\text{H}\}$ NMR (202.31, MHz, δ , CDCl_3 , 233 K): 53.06 (m, 1P), 44.06 (m, 1P).



35a

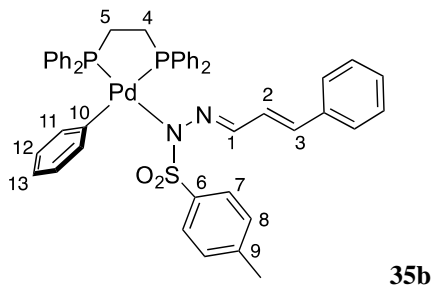
[Pd(C_6F_5)(dppf)]{(PhSO₂)N=N=CH-CH=CHPh} (35a-PhSO₂). [PdBr(C_6F_5)(dppf)] (34.0 mg, 0.045 mmol) and AgBF₄ (9.0 mg, 0.045 mmol) were mixed in dry MeCN (0.6 mL) and stirred for 15 min at room temperature under nitrogen. The suspension was filtered through Kieselghur to remove the AgBr. The resulting colorless solution was added to a mixture of the *N*-phenylsulfonyl hydrazone (PhSO₂)NH-N=CH-CH=CH-Ph (13.2 mg, 0.045 mmol) and Cs₂CO₃ (29.3 mg, 0.09 mmol) and then stirred for 2 h at room temperature. The reaction mixture was filtered and the resulting yellow solution was characterized by NMR.

^1H NMR (499.73 MHz, δ , $\text{CH}_3\text{CN}/(\text{CD}_3)_2\text{SO}$ capillary): 8.20 (d, $J = 9.0$ Hz, 1H, H^1), 8.14-7.42 (m, 28H, H^{arom}), 7.39 (t, $J = 7.5$ Hz, 2H, H^{arom}), 6.64 (m, $J = 15.9, 9.0$ Hz, 1H, H^2), 6.53 (d, $J = 15.9$ Hz, 1H, H^3), 2.60 (m, 2H, CH_2), 2.47 (m, 2H, $\text{C}'\text{H}_2$). ^{19}F NMR (470.17 MHz, δ , $\text{CH}_3\text{CN}/(\text{CD}_3)_2\text{SO}$ capillary): -113.96 (br, 2F, F_{ortho}), -162.40 (t, $J = 19.4$ Hz, 1F, F_{para}), -164.57 (br, 2F, F_{meta}). $^{31}\text{P}\{^1\text{H}\}$ NMR (202.31, MHz, δ , $\text{CH}_3\text{CN}/(\text{CD}_3)_2\text{SO}$ capillary): 54.49 (dt, $J = 16.2, 4.1$ Hz, 1P), 44.50 (m, 1P).

35a-PhSO₂

[PdPh(dppe)]{(p-TolSO₂)N-N=CH-CH=CHPh} (35b). [PdBr(dppe)(Ph)] (290.0 mg, 0.438 mmol) and AgBF₄ (85.3 mg, 0.438 mmol) were mixed in dry MeCN (5 mL) and stirred for 15 min at room temperature under nitrogen. The suspension was filtered through Kieselghur to remove the AgBr. The resulting solution was added to a mixture of the *N*-tosylhydrazone **34** (200.0 mg, 0.665 mmol) and Cs₂CO₃ (420.0 mg, 1.3 mmol) in MeCN (5 mL) and then stirred for 2 h at room temperature. The reaction mixture was filtered and the filtrate was evaporated to dryness. Addition of Et₂O (5 mL) afforded complex **35b** as a yellow solid, which was collected by filtration, washed with Et₂O (2 x 5 mL), MeOH (3 x 5 mL) and air dried. Yield: 0.243 g (63 %).

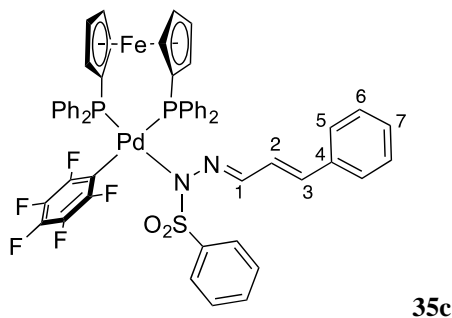
¹H NMR (399.86 MHz, δ, CDCl₃): 8.14 (d, J = 9.1 Hz, 1H, H¹), 8.27-7.21 (m, 24H, H^{arom}), 7.16 (tt, J = 6.7, 1.9 Hz, 1H, H^{arom}), 7.05 (t, J = 7.5 Hz, 2H, H¹¹), 6.97 (d, J = 8.5 Hz, 2H, H⁷), 6.78 (d, J = 8.5 Hz, 2H, H⁸), 6.72 (m, 1H, H¹³), 6.67 (m, 2H, H¹²), 6.64 (dd, J = 15.9, 9.1 Hz, 1H, H²), 6.05 (d, J = 15.9 Hz, 1H, H³), 2.48 (m, 2H, H⁵), 2.24 (m, 2H, H⁴), 2.18 (s, 3H, Me). ¹³C{¹H} NMR (100.56 MHz, δ, CDCl₃): 156.9 (d, J_{C-P} = 123.9 Hz, C¹⁰), 140.3 (C¹, C⁹), 139.9 (C⁶), 137.7 (C^{arom}), 137.2 (C¹¹), 133.3 (d, ¹J_{C-P} = 10.0 Hz, C^{arom}), 131.2 (C^{arom}), 130.9 (C³), 129.7 (C^{arom}), 129.0 (d, J_{C-P} = 8.8 Hz, C^{arom}), 128.8 (d, J_{C-P} = 10.1 Hz, C^{arom}), 128.5 (C^{arom}), 128.1 (C⁸), 127.7 (C²), 127.5 (C⁷), 127.2 (C¹²), 127.2 (C^{arom}), 126.9 (C^{arom}), 126.8 (C^{arom}), 125.9 (C^{arom}), 122.9 (C¹³), 29.1 (dd, J_{C-P} = 30.8, 20.9 Hz, C⁵), 24.2 (dd, J_{C-P} = 25.6, 11.5 Hz, C⁴), 21.22 (Me). ³¹P{¹H} NMR (161.87, MHz, δ, CDCl₃): 47.72 (d, J = 24.5 Hz, 1P), 32.65 (d, J = 24.5 Hz, 1P). IR (neat, cm⁻¹): SO₂, 1136. Anal. Calcd. for C₄₈H₄₄N₂O₂P₂PdS: C, 65.42 %; H, 5.03 %; N, 3.18 %. Found: C, 65.39 %; H, 5.22 % N, 3.21 %.



[Pd(C₆F₅)(dppf)]{(PhSO₂)N-N=CH-CH=CHPh} (35c). Equimolar amounts of [PdBr(C₆F₅)(dppf)] (110.0 mg, 0.12 mmol) and AgBF₄ (23.6 mg, 0.12 mmol) were mixed in dried MeCN (3 mL) and stirred for 15 min at room temperature under nitrogen. The suspension was filtered through Kieselghur to remove the AgBr. The resulting solution was added to a mixture of the *N*-phenylsulfonyl hydrazone (PhSO₂)NH-N=CH-CH=CH-Ph (34.7 mg, 0.12 mmol) and Cs₂CO₃ (78.9 mg, 0.24 mmol) and then stirred for 2 h at room temperature. The reaction mixture was filtered and the filtrate was evaporated to dryness. Addition of *n*-hexane (5 mL) afforded the complex as an orange solid, which was collected by filtration, washed with *n*-hexane (2 x 5 mL), and air dried. Yield: 94 mg (70 %). It can be crystallized from slow diffusion of hexane into a dichloromethane solution (orange crystals).

^1H NMR (399.86 MHz, δ , CDCl_3): 8.35 (m, 3H, H^{arom} , H^1), 8.12 (m, 2H, H^{arom}), 7.64 (m, 4H, H^{arom}), 7.56 (m, 2H, H^{arom}), 7.48 (m, 2H, H^{arom}), 7.41-7.25 (m, 7H, H^{arom}), 7.22 (m, 2H, H^{arom}), 7.14 (m, 3H, H^{arom}), 7.10-7.00 (m, 6H, H^{arom}), 6.55 (dd, $J = 16.0, 8.8$ Hz, 1H, H^2), 6.41 (d, $J = 15.7$ Hz, 1H, H^3), 4.82 (s, 1H, $\text{H}^{\text{Cp}1}$), 4.56 (s, 1H, $\text{H}^{\text{Cp}2}$), 4.43 (s, 1H, $\text{H}^{\text{Cp}1}$), 4.38 (s, 1H, $\text{H}^{\text{Cp}2}$), 4.35 (s, 1H, $\text{H}^{\text{Cp}1}$), 4.26 (s, 1H, $\text{H}^{\text{Cp}2}$), 4.20 (s, 1H, $\text{H}^{\text{Cp}1}$), 3.91 (s, 1H, $\text{H}^{\text{Cp}2}$). $^{13}\text{C}\{^1\text{H}\}$ NMR (100.56 MHz, δ , CDCl_3): 143.7 ($\text{C}^{\text{ipso}}(\text{SO}_2\text{-Ph})$), 141.2 (C^1), 137.5 (C^4), 137.3 (d, $J_{\text{C-P}} = 13.1$ Hz, C^{arom}), 135.5 (d, $J_{\text{C-P}} = 12.4$ Hz, C^{arom}), 133.0 (d, $J_{\text{C-P}} = 10.6$ Hz, C^{arom}), 132.3 (d, $J_{\text{C-P}} = 11.6$ Hz, C^{arom}), 132.2 (C^3), 132.1 (d, $J_{\text{C-P}} = 12.1$ Hz, C^{arom}), 132.0 (C^{arom}), 131.0 (d, $J_{\text{C-P}} = 54.3$ Hz, C^{arom}), 130.1 (C^{arom}), 130.0 (d, $J_{\text{C-P}} = 46.1$ Hz, C^{arom}), 129.6 (C^{arom}), 128.6 (C^{arom}), 128.3 (d, $J_{\text{C-P}} = 10.9$ Hz, C^{arom}), 128.0 (d, $J_{\text{C-P}} = 9.8$ Hz, C^{arom}), 127.3 (d, $J_{\text{C-P}} = 12$ Hz, C^{arom}), 127.2 (C^{arom}), 127.6 (C^2), 127.0 (C^7), 126.1 (C^5), 126.0 (C^6), 76.6 ($\text{C}^{\text{Cp}1}$), 75.6 (d, $J = 5.6$ Hz, $\text{C}^{\text{Cp}2}$), 74.8 (br, $2\text{C}^{\text{Cp}1}$, $1\text{C}^{\text{Cp}1}$), 74.3 (d, $J = 4.2$ Hz, $\text{C}^{\text{Cp}1}$), 72.7 (d, $J = 5.5$ Hz, $\text{C}^{\text{Cp}1}$), 72.5 (d, $J = 5.2$ Hz, $\text{C}^{\text{Cp}2}$). * ^{19}F NMR (376.19 MHz, δ , CDCl_3): -113.23 (m, 1F, F^{ortho}), -116.72 (m, 1F, F^{ortho}), -160.88 (t, $J = 20.5$ Hz, 1F, F^{para}), -161.44 (m, 1F, F^{meta}), -163.30 (m, 1F, F^{meta}). $^{31}\text{P}\{^1\text{H}\}$ NMR (161.87, MHz, δ , CDCl_3): 20.57 (t, $J = 11.8$ Hz, 1P), 12.84 (m, 1P). IR (neat, cm^{-1}): C_6F_5 , 1499, 1029, 953, 692, 616; SO_2 , 1150. Anal. Calcd. for $\text{C}_{55}\text{H}_{41}\text{F}_5\text{FeN}_2\text{O}_2\text{P}_2\text{PdS} \cdot \text{CH}_2\text{Cl}_2$: C, 56.14 %; H, 3.62 %; N, 2.34 %. Found: C, 56.15 %; H, 3.88 % N, 2.48 %.

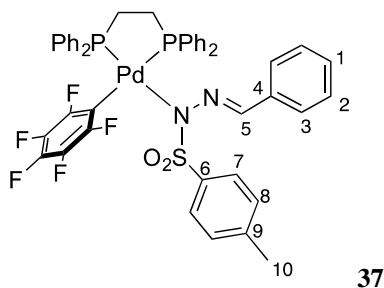
* The signals for the Cp carbons bound to P could not be observed.



[Pd(C₆F₅)(dppe){(*p*-TolSO₂)N-N=CHPh}] (37). [PdBr(C₆F₅)(dppe)] (111.0 mg, 0.14 mmol) and AgBF₄ (28.75 mg, 0.14 mmol) were mixed in dry MeCN (3 mL) and stirred for 15 min at room temperature under nitrogen. The suspension was filtered through Kieselghur to remove the AgBr. The resulting solution was added to a mixture of the *N*-tosylhydrazone **36** (60.77 mg, 0.22 mmol) and Na₂CO₃ (46.74 mg, 0.44 mmol) in MeCN (5 mL) and then stirred for 2 h at room temperature. The reaction mixture was filtered and the filtrate was evaporated to dryness. Addition of Et₂O (5 mL) to the residue afforded complex **37** as a yellow solid, which was collected by filtration, washed with cold Et₂O (2 x 5 mL), and air dried. Yield: 0.12 g, (87%). It can be crystallized from slow diffusion of hexane into a dichloromethane solution.

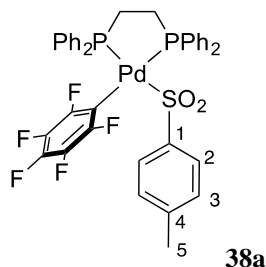
^1H NMR (499.73 MHz, δ , CDCl_3): 8.02 (s, 1H, H^5), 7.99-7.49 (m, 9H, H^{arom}), 7.54 (t, $J = 7.4$ Hz, H^{arom}), 7.42 (m, 5H, H^{arom}), 7.37 (d, $J = 8.3$ Hz, 2H, H^7), 7.21-7.0 (m, 6H, H^{arom}), 6.89 (d, $J = 8.3$ Hz, 2H, H^8), 2.52 (m, 2H, CH_2), 2.24 (m, 2H, $\text{C}'\text{H}_2$), 2.21 (s, 3H, H^{10}). $^{13}\text{C}\{^1\text{H}\}$ NMR (125.67 MHz, δ , CDCl_3): 140.6 (C^6), 140.0 (C^9), 138.5 (C^5), 136.4 (C^4), 132.9 (br, 2C^{arom}), 132.0 (C^{arom}), 131.5 (C^{arom}), 129.6 (d, $J_{\text{C-P}} = 41.8$ Hz, C^{arom}), 129.0 (d,

$J_{C-P} = 10.6$ Hz, C^{arom}), 128.9 (d, $J_{C-P} = 10.9$ Hz, C^{arom}), 128.7 (d, $^1J_{C-P} = 42.3$ Hz, C^{arom}), 127.8 (C^8), 127.6 (C^2), 126.8 (C^1), 126.4 (C^7), 126.0 (C^3), 27.7 (dd, $J_{C-P} = 31.5, 17.4$ Hz, CH_2), 24.1 (dd, $J_{C-P} = 28.8, 12.2$ Hz, C^{H_2}), 21.1 (C^{10}). ^{19}F NMR (470.17 MHz, δ , $CDCl_3$): -113.83 (br, 2F, F_{ortho}), -161.04 (t, $J = 19.9$ Hz, 1F, F_{para}), -163.18 (br, 2F, F_{meta}). $^{31}P\{^1H\}$ NMR (202.31, MHz, δ , $CDCl_3$): 52.74 (dt, $J = 17.4, 4.5$, Hz, 1P), 42.45 (m, 1P). IR (neat, cm^{-1}): C_6F_5 , 1454, 1046, 952, 689, 746; (SO_2 , st), 1145. Anal. Calcd. for $C_{46}H_{37}F_5N_2O_2P_2PdS \cdot CH_2Cl_2$: C, 54.80 %; H, 3.82 %; N, 2.72 %. Found: C, 54.59 %; H, 3.80 % N, 2.60 %.



[Pd(C_6F_5)(dppe)(SO_2 -*p*-Tol)] (38a). Equimolar amounts of $[PdBr(C_6F_5)(dppe)]$ (76.42 mg, 0.101 mmol) and $AgBF_4$ (19.79 mg, 0.101 mmol) were mixed in dry MeCN (10 mL) and stirred for 15 min at room temperature under nitrogen. The solution was filtered through Kieselghur and the filtrate was added to a solution of sodium *p*-toluenesulfonate (18.10 mg, 0.101 mmol) in CH_3CN (5 mL). The mixture was stirred for 3 h at room temperature and an almost colorless solution was formed. The reaction mixture was filtered and the filtrate was evaporated to dryness. A mixture of MeOH/ H_2O (1:5 mL) was added to the residue and the resulting white solid was filtered, washed with water (3 x 5 mL) and air-dried. Yield: 49.63 mg (60 %).

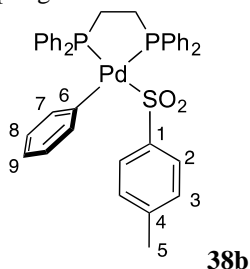
1H NMR (499.73 MHz, δ , $CDCl_3$): 8.00 (m, 4H, H^{arom}), 7.61-7.52 (m, 6H, H^{arom}), 7.49 (m, 2H, H^{arom}), 7.43-7.32 (m, 9H, H^{arom}), 7.20 (d, $J = 8.0$ Hz, 2H, H^2), 6.84 (d, $J = 8.0$ Hz, 2H, H^3), 2.37-2.22 (m, 4H, CH_2), 2.20 (s, 3H, H^5). $^{13}C\{^1H\}$ NMR (125.67 MHz, δ , $CDCl_3$): 150.8 (d, $J_{C-P} = 19.4$ Hz, C^1), 145.4 (d, $^1J_{C-F} = 226.2$ Hz, CF_{ortho}), 139.7 (C^4), 137.7 (d, $^1J_{C-F} = 230.3$ Hz, CF_{para}), 135.7 (d, $^1J_{C-F} = 246.1$ Hz, CF_{meta}), 134.0 (d, $J_{C-P} = 11.7$ Hz, C^{arom}), 132.9 (d, $J_{C-P} = 11.4$ Hz, C^{arom}), 132.0 (d, $J_{C-P} = 2.6$ Hz, C^{arom}), 131.7 (d, $J_{C-P} = 2.5$ Hz, C^{arom}), 129.1 (d, $J_{C-P} = 11.0$ Hz, C^{arom}), 128.9 (d, $J_{C-P} = 11.0$ Hz, C^{arom}), 128.6 (d, $^1J_{C-P} = 45.2$ Hz, C^{arom}), 128.1 (d, $^1J_{C-P} = 47.8$ Hz, C^{arom}), 127.7 (C^3), 125.27 (C^2), 26.8 (dd, $J_{C-P} = 28.4, 15.1$ Hz, CH_2), 26.3 (dd, $J_{C-P} = 30.0, 14.6$ Hz, C^{H_2}), 21.0 (C^5). ^{19}F NMR (470.17 MHz, δ , $CDCl_3$): -116.08 (m, 2F, F_{ortho}), -161.18 (t, $J = 21$ Hz, 1F, F_{para}), -162.79 (m, 2F, F_{meta}). $^{31}P\{^1H\}$ NMR (202.31, MHz, δ , $CDCl_3$): 49.31 (d, $J = 25.7$ Hz, 1P), 44.61 (m, 1P). IR (neat, cm^{-1}): C_6F_5 , 1460, 1089, 959, 829, 699; SO_2 , 1186. Anal. Calcd. for $C_{39}H_{31}F_5O_2P_2PdS$: C, 56.64 %; H, 3.78 %. Found: C, 56.48 %; H, 3.47 %.



[PdPh(dppe)(SO₂-*p*-Tol)] (38b). [PdBr(Ph)(dppe)] (130.8 mg, 0.197 mmol) and AgBF₄ (38.5 mg, 0.197 mmol) were mixed in dry MeCN (10 mL) and stirred for 15 min at room temperature under nitrogen. The suspension was filtered through Kieselghur and the filtrate was added to a solution of sodium *p*-toluenesulfinate (42.3 mg, 0.237 mmol) in dry CH₃CN (5 mL). The mixture was stirred for 3 h at room temperature to give an almost colorless solution, which was filtered. The filtrate was evaporated to *c.a.* 2 mL and Et₂O (5 mL) was added to the suspension. The white solid was filtered, washed with diethyl ether (3 x 5 mL), MeOH (3 x 5 mL) and air-dried. Yield: 78 mg (54 %).

¹H NMR (399.86 MHz, δ, CDCl₃): 8.02 (m, 4H, H^{arom}), 7.53 (m, 6H, H^{arom}), 7.40 (td, J = 7.3, 1.8 Hz, 2H, H^{arom}), 7.30-7.22 (m, 10H, H^{arom}), 7.01 (d, J = 8.1 Hz, 2H, H²), 6.75 (d, J = 8.1 Hz, 2H, H³), 6.73 (m, 2H, H⁷), 6.57 (t, J = 7.0 Hz, 1H, H⁹), 6.46 (td, J = 7.5, 2.1 Hz, 2H, H⁸), 2.35 (m, 2H, CH₂), 2.22 (m, 2H, CH₂), 2.18 (s, 3H, H⁵). ¹³C{¹H} NMR (100.56 MHz, δ, CDCl₃): 158.5 (C⁶), 150.6 (C¹), 138.3 (C⁴), 136.4 (C³), 133.6 (C^{arom}), 133.8 (C^{arom}), 133.2 (C^{arom}), 131.1 (C^{arom}), 130.9 (C^{arom}), 128.9 (C^{arom}), 128.8 (C^{arom}), 128.2 (C^{arom}), 127.6 (C⁷), 126.8 (C⁸), 126.0 (C²), 122.5 (C⁹), 28.4 (dd, J_{C-P} = 27.5, 18.5 Hz, CH₂), 25.6 (dd, J_{C-P} = 26.6, 12.9 Hz, C[']CH₂), 21.1 (C⁵). * ³¹P{¹H} NMR (161.87, MHz, δ, CDCl₃): 43.50 (d, J = 22.1 Hz, 1P), 35.83 (d, J = 22.1 Hz, 1P). IR (neat, cm⁻¹): SO₂, 1102. Anal. Calcd. for C₃₉H₃₆O₂P₂PdS: C, 63.55 %; H, 4.92 %. Found: C, 63.59 %; H, 5.20 %.

* The complex is not very stable in solution and most chemical shifts were determined using ¹H-¹³C HSQC and HMBC NMR experiments. The direct ¹³C NMR spectrum only allows to determine the J_{P-C} coupling constants for the -CH₂ carbons of the dppe ligand.

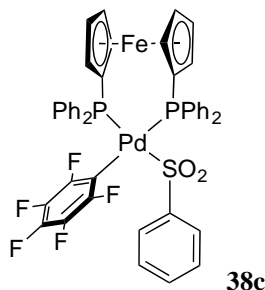


[Pd(C₆F₅)(dppf)(SO₂Ph)] (38c). Equimolar amounts of [PdBr(C₆F₅)(dppf)] (111.9 mg, 0.123 mmol) and AgBF₄ (24.0 mg, 0.123 mmol) were mixed in dry MeCN (10 mL) and stirred for 15 min at room temperature under nitrogen. The solution was filtered through Kieselghur to remove the AgBr. The filtrate was added to a solution of sodium benzenesulfinate (30.4 mg, 0.18 mmol) in CH₃CN (5 mL). The mixture was stirred for 3

h at room temperature and then, it was filtered. The resulting solution was evaporated to dryness and a 1:5 v/v ratio of MeOH/H₂O (6 mL) was added to the residue. A white solid appeared which was filtered, washed with water (3 x 5 mL) and air-dried. Yield: 93 mg (78 %).

¹H NMR (499.73 MHz, δ, CDCl₃): 8.13 (m, 4H, H^{arom}), 7.60 (m, 6H, H^{arom}), 7.38 (m, 4H, H^{arom}), 7.30 (t, J = 7.4 Hz, 2H, H^{arom}), 7.15 (m, 3H, H^{arom}), 7.10 (m, 4H, H^{arom}), 7.04 (t, J = 7.4 Hz, 2H, H^{arom}), 4.88 (s, 2H, H^{Cp}), 4.60 (s, 2H, H^{Cp}), 4.16 (s, 2H, H^{Cp}), 3.49 (s, 2H, H^{Cp}). ¹³C{¹H} NMR (125.67 MHz, δ, CDCl₃): 153.3 (d, J_{C-P} = 18.5 Hz, C^{ipso}-(SO₂-Ph)), 134.9 (d, J_{C-P} = 12.7 Hz, C^{arom}), 133.4 (d, J_{C-P} = 11.8 Hz, C^{arom}), 132.5 (d, ¹J_{C-P} = 50.7 Hz, C^{arom}), 131.3 (d, ¹J_{C-P} = 44.4 Hz, C^{arom}), 131.0 (2C^{arom}), 129.4 (C^{arom}), 128.5 (d, J_{C-P} = 10.8 Hz, C^{arom}), 128.0 (d, J_{C-P} = 10.8 Hz, C^{arom}), 127.1 (C^{arom}), 125.3 (C^{arom}), 77.2 (C^{Cp}), 76.4 (m, C^{Cp}), 74.9 (d, J_{C-P} = 8.4 Hz, C^{Cp}), 74.1 (d, J_{C-P} = 7.6 Hz, C^{Cp}), 72.7 (m, C^{Cp}), 72.4 (d, J_{C-P} = 5.8 Hz, C^{Cp}). * ¹⁹F NMR (470.17 MHz, δ, CDCl₃): -117.26 (m, 2F, F_{ortho}), -160.99 (t, J = 21 Hz, 1F, F_{para}), -162.02 (m, 2F, F_{meta}). ³¹P{¹H} NMR (202.31, MHz, δ, CDCl₃): 25.64 (d, J = 27.6 Hz, 1P), 17.73 (m, 1P). IR (neat, cm⁻¹): C₆F₅, 1461, 1046, 953, 743, 687; ν(S=O): 1199. Anal. Calcd. for C₄₆H₃₃F₅O₂P₂SPd: C, 57.02 %; H, 3.43 %. Found: C, 57.38 %; H, 3.49 %.

*The ¹³C signals for the C₆F₅ group, heavily coupled to ¹⁹F, could not be observed.



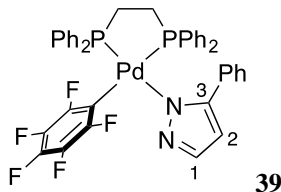
38c

[Pd(C₆F₅)(dppf)(N₂C₃H₂Ph)] (39). Equimolar amounts of [PdBr(C₆F₅)(dppf)] (39.8 mg, 0.053 mmol) and AgBF₄ (10.3 mg, 0.053 mmol) were mixed in dry MeCN (5 mL) and stirred for 15 min at room temperature under nitrogen. The solution was filtered through Kieselgur to remove the AgBr. The filtrate was added to a mixture of 5-Ph-pzH (7.6 mg, 0.053 mmol) and Cs₂CO₃ (34.5 mg, 0.10 mmol) in dry CH₃CN (5 mL) and then stirred for 3 h at room temperature to give a colorless suspension. The reaction mixture was filtered and the filtrate was evaporated to *c.a.* 2 mL. Diethyl ether (5 mL) was added to the residue to give a white solid, which was filtered, washed with diethyl ether (3 x 5 mL), MeOH (3 x 5 mL) and air-dried. Yield: 21 mg (48 %).

¹H NMR (499.73 MHz, δ, CDCl₃): 7.81 (m, 4H, H^{arom}), 7.58 (m, 4H, H^{arom}), 7.51 (m, 3H, H^{arom}), 7.47 (m, 2H, H^{arom}), 7.39 (m, 8H, H^{arom}), 7.14 (d, J = 7.9 Hz, 2H, H^{ortho}-Ph-pz), 7.05 (t, J = 7.1 Hz, 2H, H^{meta}-Ph-pz), 6.99 (t, J = 7.1 Hz, 1H, H^{para}-Ph-pz), 6.95 (d, J = 1.7 Hz, 1H, H¹), 6.25 (t, J = 1.7 Hz, 1H, H²), 2.50 (m, 2H, CH₂), 2.19 (m, 2H, C²H₂). ¹³C{¹H} NMR (125.67 MHz, δ, CDCl₃): 151.0 (m, C³), 140.2 (C¹), 136.2 (C^{ipso}-Ph-pz), 133.7 (d, J_{C-P} = 11.6 Hz, C^{arom}), 133.0 (d, J_{C-P} = 11.4 Hz, C^{arom}), 131.8 (d, J_{C-P} = 2.7 Hz, C^{arom}), 130.9 (d,

$J_{C-P} = 2.4$ Hz, C^{arom}), 130.0 (d, $^1J_{C-P} = 44.6$ Hz, C^{arom}), 128.9 (d, $^1J_{C-P} = 35.6$ Hz, C^{arom}), 128.8 (d, $J_{C-P} = 11.0$ Hz, C^{arom}), 128.7 (d, $J_{C-P} = 10.6$ Hz, C^{arom}), 127.6 ($C^{\text{meta-Ph-pz}}$), 125.1 ($C^{\text{ortho-Ph-pz}}$), 124.9 ($C^{\text{para-Ph-pz}}$), 99.7 (C^2), 28.8 (dd, $J_{C-P} = 31.7, 17.5$ Hz, CH_2), 25.5 (dd, $J_{C-P} = 29.8, 12.9$ Hz, $C'H_2$). * ^{19}F NMR (MHz, δ , $CDCl_3$): -115.39 (br, 2F, F_{ortho}), -160.24 (t, $J = 20.8$ Hz, 1F, F_{para}), -162.31 (br, 2F, F_{meta}). $^{31}P\{^1H\}$ NMR (202.31 MHz, δ , $CDCl_3$): 53.63 (m, 1P), 44.71 (m, 1P). IR (neat, cm^{-1}): C_6F_5 , 1451, 1057, 949, 740, 688. Anal. Calcd. for $C_{41}H_{31}F_5N_2P_2Pd$: C, 60.42 %; H, 3.83 %; N, 3.44 %. Found: C, 60.67 %; H, 3.87; N, 3.41 %.

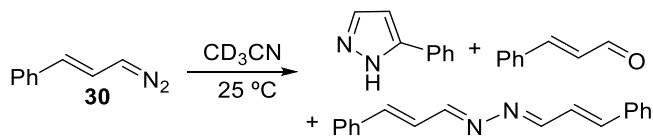
*The ^{13}C signals for the C_6F_5 group, heavily coupled to ^{19}F , could not be observed.



5.4.3 Decomposition of the diazoalkane **30** and *N*-tosylhydrazone **34**

Decomposition of $N_2CH-CH=CHPh$ (**30**)

A dichloromethane solution of the diazo compound **30** (0.12 mmol) in dry CD_3CN (total volume 0.7 mL) was monitored by 1H NMR at 298 K using 1,4-dioxane as an internal standard under a nitrogen atmosphere. The collection of data started 13 min after the preparation of the solution at 298 K. The decomposition products observed are 5-Ph-pzH and minor compounds such as the corresponding azine-derivate and *trans*-cinnamaldehyde. The progress of the reaction (Equation 5.7) is shown in Figure 5.20.



Equation 5.7

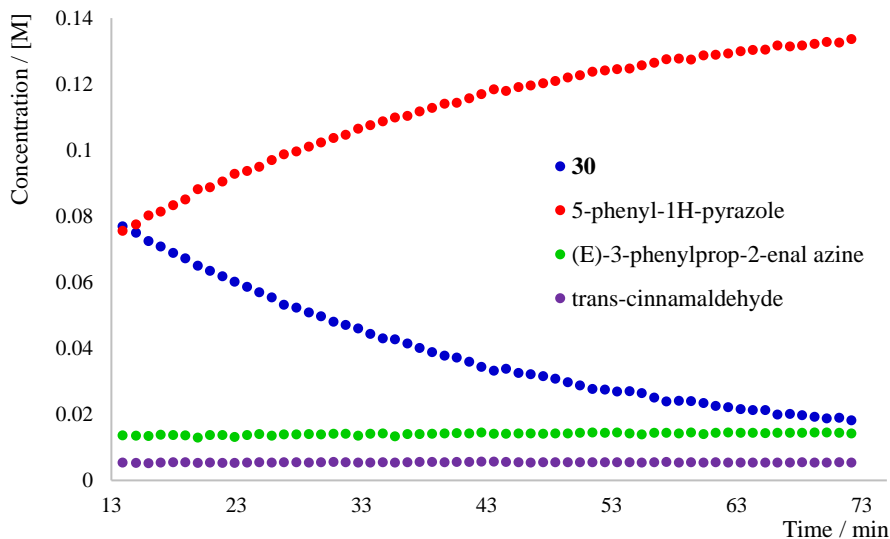
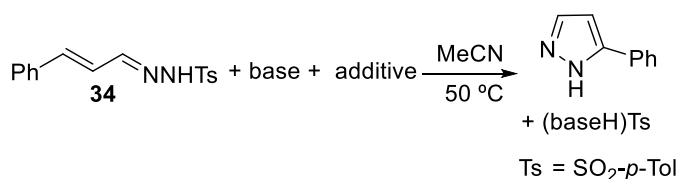


Figure 5.20 Plot of concentration vs. time for the decomposition of the diazoalkane **30** in CD₃CN at 298 K.

Decomposition of the *N*-tosylhydrazone. *N*-tosylhydrazone **34** (0.033 mmol), base (0.05 mmol), additive (0.033 mmol) and solvent (0.6 mL) were added into an NMR tube along with a sealed glass capillary filled with (CD₃)₂SO as NMR lock signal. The species formed after 16 h at 50 °C were examined by ¹H NMR and quantified using 1,4-dioxane as an internal standard. The product observed in these reactions, 5-Ph-pzH, comes from the *in situ* generation and subsequent decomposition of the diazo compound (Equation 5.8 and Table 5.1).



Equation 5.8

Table 5.1 Decomposition of *N*-tosylhydrazone.^a

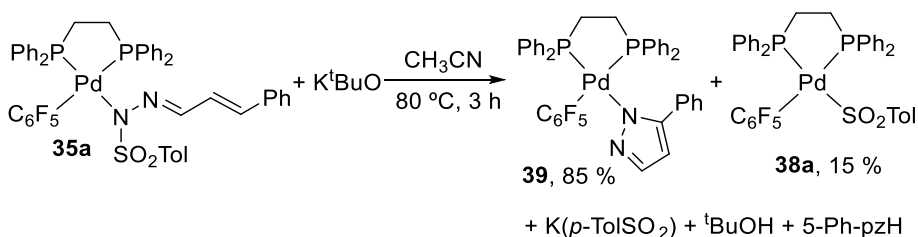
Entry	Hydrazone	Base	Additive	(% Conversion, 16 h) ^b
1	34	-	-	0
2	34	Na ₂ CO ₃	-	28
3	34	Na ₂ CO ₃	BnEt ₃ NCl	100
4	34	(NBu ₄) ₂ CO ₃	-	100
5	34	Et ₃ N	-	100

^a Reaction conditions: **34** (0.033 mmol), base (0.05 mmol), additive (0.033 mmol), solvent (0.6 mL), 50 °C, 16 h. ^b Conversion was quantified by ¹H NMR using 1,4-dioxane as internal standard.

The solubility of the sodium hydrazonates is very low in acetonitrile whereas the ammonium salts are completely soluble. The higher conversion observed in the presence of a trialkylammonium chloride (entry 3) and when a base provides an ammonium counterion (entries 4 and 5) reflects this solubility difference. The decomposition of *N*-tosylhydrazone **34** in the presence of triethylamine (leading to a soluble ammonium hydrazonate) was monitored by ^1H NMR. **34** (0.12 mmol), Et_3N (0.18 mmol) and CD_3CN (0.7 mL) were added into an NMR tube and the evolution of the mixture was followed by ^1H NMR at regular intervals (see Figure 5.14).

5.4.4 Decomposition of individual complexes

$[\text{Pd}(\text{C}_6\text{F}_5)(\text{dppe})\{(p\text{-TolSO}_2)\text{N}=\text{N}=\text{CH}-\text{CH}=\text{CHPh}\}]$ (**35a**, 0.006 mmol) was dissolved in CH_3CN (0.6 mL) and the solution was placed in an NMR tube along with a sealed glass capillary filled with $(\text{CD}_3)_2\text{SO}$ as NMR lock signal. The species formed in solution at the specified temperature and time were examined by ^{19}F and ^{31}P NMR (Equation 5.9). The same result shown in Equation 5.9 was obtained when Li_2CO_3 (0.012 mmol) was added to the solution. However, in the presence of the strong base K^tBuO (0.012 mmol) the pyrazolate complex **39** was formed (Equation 5.9). The identity of the complexes was determined by comparison with independently prepared samples.



Equation 5.9

Complex **35a** (13.6 mg, 0.014 mmol) and dry CH_3CN (0.6 mL) were added to a 5 mm NMR tube along with a sealed glass capillary filled with $(\text{CD}_3)_2\text{SO}$ as NMR lock signal. The formation of the palladium tosyl complex **38a** was monitored by ^{19}F NMR at $50\text{ }^\circ\text{C}$ for 15 h (Figure 5.16, **a**). Analogous experiments were carried out adding 10 mol % of NaSO_2Tol (Figure 5.16, **b**) and 10 mol % of 5-Ph-pzH (Figure 5.16, **c**).

5.4.5 Crossover experiments

Reaction of $[\text{Pd}(\text{C}_6\text{F}_5)(\text{dppe})\{(\text{p-TolSO}_2)\text{N-N=CH-CH=CHPh}\}]$ (**35a**) and $[\text{Pd}(\text{C}_6\text{F}_5)(\text{dppf})\{(\text{PhSO}_2)\text{N-N=CH-CH=CHPh}\}]$ (**35c**)

Complex **35c** (3.0 mg, 0.0027 mmol), complex **35a** (2.6 mg, 0.0027 mmol) and dry CH_3CN (0.6 mL) were added to a 5 mm NMR tube along with a sealed glass capillary filled with $(\text{CD}_3)_2\text{SO}$ as NMR lock signal. The species formed in solution at room temperature were examined by ^{31}P and ^{19}F NMR. The resulting mixture was heated at 80°C and checked after 2 h. The same experiment was carried out and monitored by ^{19}F NMR at 50°C for 4 h (Figure 5.21). The species formed were identified by comparison with samples of the complexes prepared independently.

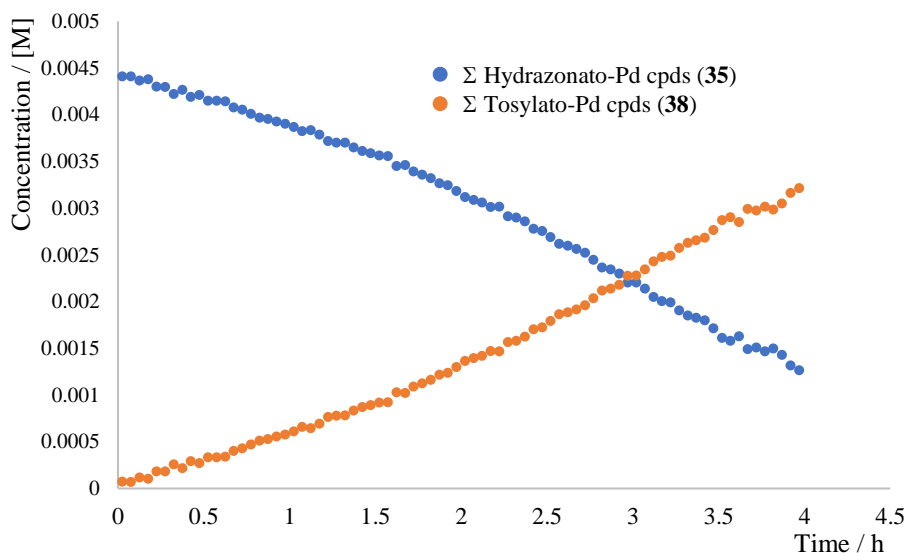


Figure 5.21 Plot of concentration vs. time for the decomposition of the mixture of hydrazonato complexes to give a mixture of arylsulfonato derivatives as shown in Scheme 5.11. Reaction conditions: MeCN, 50°C .

Reaction of $[\text{Pd}(\text{C}_6\text{F}_5)(\text{dppe})(\text{p-TolSO}_2)]$ (**38a**) and $[\text{Pd}(\text{C}_6\text{F}_5)(\text{dppf})(\text{PhSO}_2)]$ (**38c**)

Complex **38a** (2.2 mg, 0.0027 mmol), complex **38c** (2.6 mg, 0.0027 mmol) and dry CH_3CN (0.6 mL) were added to a 5 mm NMR tube along with a sealed glass capillary filled with $(\text{CD}_3)_2\text{SO}$ as NMR lock signal. The species formed in solution at room temperature were examined by ^{31}P and ^{19}F NMR (Figure 5.22).

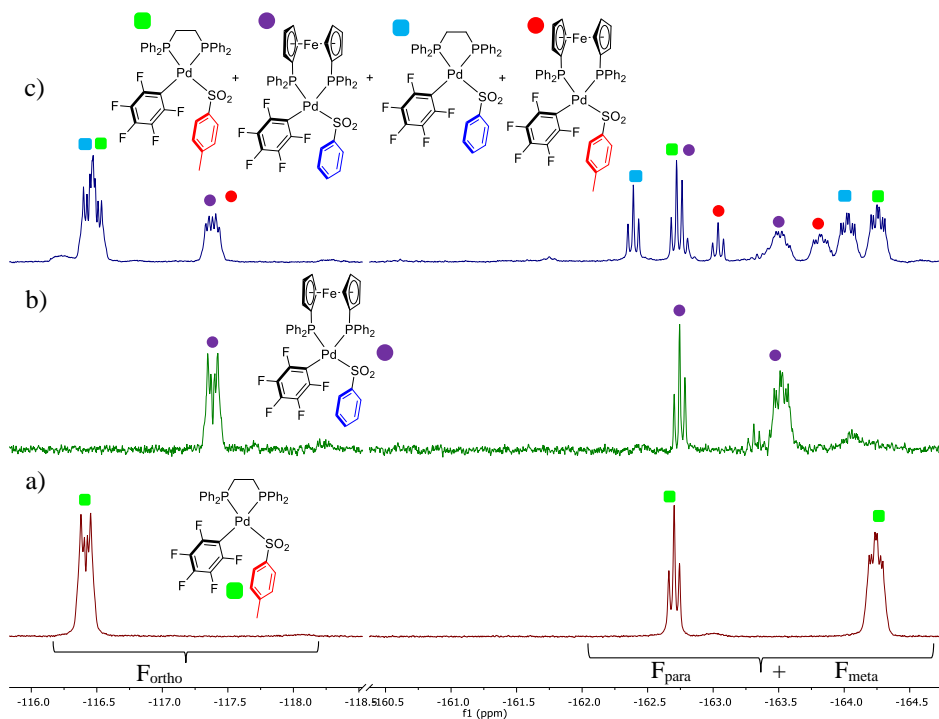


Figure 5.22 ^{19}F NMR (470.17 MHz, δ , $\text{CH}_3\text{CN}/(\text{CD}_3)_2\text{SO}$ capillary) at 298 K of: a) complex **38a**; b) complex **38c**; c) a mixture of **38a** and **38c** showing the scrambling of the sulfinato groups after heating.

5.4.6 General procedure for the ligand substitution reactions

Ligand substitution reactions by diazoalkanes

The corresponding palladium complex (0.01 mmol) was placed into an NMR tube along with CH_3CN (0.6 mL) and a sealed glass capillary filled with $(\text{CD}_3)_2\text{SO}$ as NMR lock signal. After that, a solution of the diazoalkane (0.01 mmol) in dichloromethane was added to the NMR tube under a nitrogen atmosphere. The tube was introduced into the NMR probe and the species formed in solution at room temperature were examined by ^1H ^{19}F and ^{31}P NMR nuclei depending on the complexes (Table 5.2).

Table 5.2 Products of the reaction of diazoalkanes with palladium complexes **28**, **29**, **35** and **38** (Ts = SO₂-*p*-Tol).^a

Entry	[Pd]	Diazoalkane	Products (%) ^b
1	[Pd(C ₆ F ₅)(Br)(dppe)] (28a)	30	31a (10) ^c
2	[Pd(Ph)(Br)(dppe)] (28b)	30	31b (100)
3	[Pd(C ₆ F ₅)(Br)(dppe)] (28a)	32	No reaction
4	[Pd(C ₆ F ₅)(NCMe)(dppe)]BF ₄ (29a)	30	31a (100)
5	[Pd(Ph)(NCMe)(dppe)]BF ₄ (29b)	30	31b (100)
6	[Pd(C ₆ F ₅)(NCMe)(dppe)]BF ₄ (29a)	32	33 (100)
7	[Pd(C ₆ F ₅)(Ts)N-N=CH-CH=CHPh)(dppe)] (35a)	30	31a (10), 38a (5), 39 (6) ^c
8	[Pd(Ph)Ts N-N=CH-CH=CHPh)(dppe)] (35b)	30	31b (100)
9	[Pd(C ₆ F ₅)(SO ₂ - <i>p</i> -Tol)(dppe)] (38a)	30	31a (15) ^c
10	[Pd(Ph)(SO ₂ - <i>p</i> -Tol)(dppe)] (38b)	30	31b (100)

^a Reaction conditions: MeCN as solvent at 298 K for 10 min. ^b The new species formed were determined by ¹⁹F NMR and ³¹P NMR. ^c Unreacted starting material accounts for the remaining percentage.

Bromide substitution reactions in [PdArBr(dppe)]

The corresponding palladium complex (0.01 mmol) was placed into an NMR tube along with CH₃CN (0.6 mL) and a sealed glass capillary filled with (CD₃)₂SO as NMR lock signal. *N*-tosylhydrazone **34** (0.1 mmol) and NEt₃ (0.1 mmol) in one experiment set or NaSO₂(*p*-Tol) (0.01 mmol) in the second experiment set were added. The mixture was allowed to stand for 1-2.5 h and then checked by ¹⁹F and ³¹P NMR.

5.4.7 Attempts at detection of intermediate complexes before the migratory insertion

[Pd(C₆F₅)(NCMe)(dppe)]BF₄ (**29a**) (0.0175 mmol) and 0.6 mL of dry CD₂Cl₂ were added into an NMR tube under a nitrogen atmosphere, and placed in cooled bath at -105 °C. Then, a precooled diazo compound (-50 °C, Pd:**32** = 1:1.5 mol ratio) was added and the tube was closed. The resulting mixture was frozen during the setup of the NMR experiment. Finally, the NMR tube was introduced into another cool bath at -90 °C for 5 minutes to allow the equilibration of the temperature. After this time, the sample was shaken vigorously inside the cool bath, wiped externally and introduced in the NMR probe already set at the measurement temperature (-90 °C). The reaction was monitored by ¹⁹F NMR, at -90 °C first and then at higher temperature (10-degree intervals). Figure 5.23 shows the mixture of palladium complexes formed when **29a** was dissolved in

CD_2Cl_2 at $-90\text{ }^\circ\text{C}$. The latter is transformed in **29a** upon addition of MeCN. The reorganization product $[\text{Pd}(\text{C}_6\text{F}_5)_2(\text{dppe})]$ (6 %) was also present.

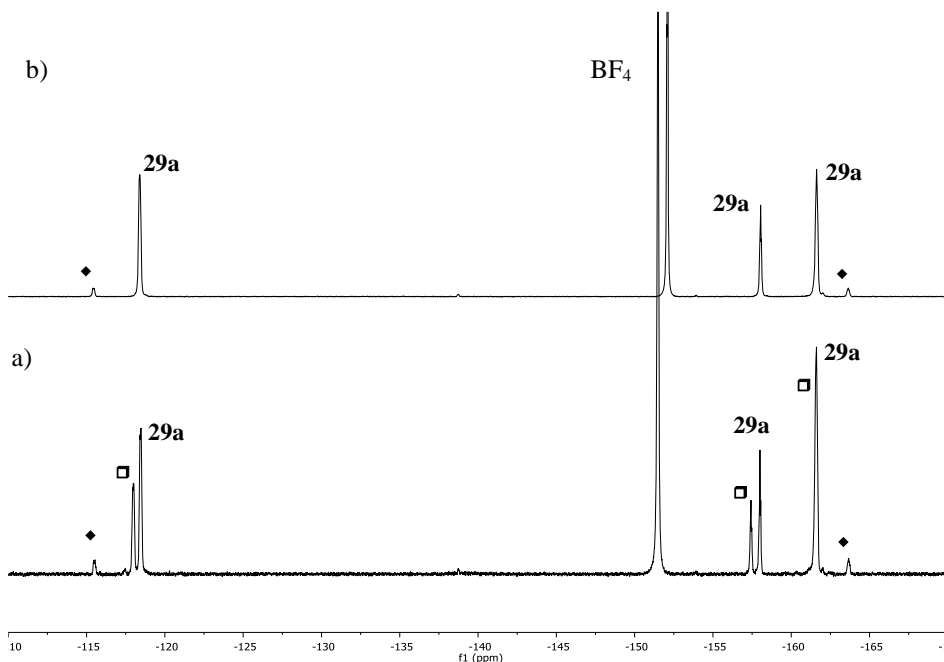


Figure 5.23 ^{19}F NMR (376.46 MHz, δ , CD_2Cl_2) at $-90\text{ }^\circ\text{C}$ of: **a**) a mixture of complexes **29a**, $[\text{Pd}(\text{C}_6\text{F}_5)(\text{dppe})(\text{OEt}_2)]\text{BF}_4$ (\square) and $[\text{Pd}(\text{C}_6\text{F}_5)_2(\text{dppe})]$ (\blacklozenge) formed when a sample of **29a** was dissolved in dichloromethane at low temperature ; **b**) the mixture shown in (**a**) upon addition of MeCN (Pd:NMe = 1:10 mol ratio).

5.4.8 Data for X-Ray molecular structure determinations

Crystals suitable for X-ray analyses were obtained by: a) slow diffusion of *n*-hexane layered onto a solution of the complex in CH_2Cl_2 at $-28\text{ }^\circ\text{C}$ (**31a** and **33**); b) slow diffusion of Et_2O layered onto a solution of the complex in CH_2Cl_2 at $-28\text{ }^\circ\text{C}$ (**35c** and **37**); c) slow evaporation of the complex in CH_2Cl_2 (**38a** and **38c**). In each case, the crystal was attached to the tip of a glass fiber and transferred to an Agilent Supernova diffractometer with an Atlas CCD area detector. Data collection was performed with Mo $K\alpha$ radiation (0.71073 \AA) at 298 K. Data integration and empirical absorption correction was carried out using the CrysAlisPro program package. The structures were solved by direct methods and refined by full-matrix least squares against F^2 with SHELX, in OLEX2. The non-hydrogen atoms were refined anisotropically and hydrogen atoms were constrained to ideal geometries and refined with fixed isotropic displacement parameters. Refinement proceeded smoothly to give the residuals shown in Tables 5.3 and 5.4. The crystal structures have deposited in the CCDC database: CCDC-2184725 (complex **31a**), CCDC-2184716 (complex **33**), CCDC-2184726 (complex **35c**), CCDC-2184731 (complex **37**) and CCDC-2184733 (complex **38a**).

Complex **38a** crystallized with a CH₂Cl₂ solvent molecule that was modeled. Two independent molecules were found in the asymmetric unit for **35c** and a solvent mask was used for the CH₂Cl₂ co-crystallized solvent.

Table 5.3 Crystal data and structure refinement parameters for complexes **31a**, **33**, **38a**.

Compound number	31a	33	38a
Empirical formula	C ₄₁ H ₃₂ BF ₉ P ₂ Pd	C ₃₉ H ₃₀ BF ₉ P ₂ Pd	C ₄₀ H ₃₃ Cl ₂ F ₅ O ₂ P ₂ PdS
Formula weight	874.81	848.78	911.96
Temperature/K	298	298.15	298
Crystal system	monoclinic	triclinic	monoclinic
Space group	P2 ₁ /n	P-1	C2/c
a/Å	10.1431(4)	8.5211(4)	22.5623(15)
b/Å	22.7544(7)	10.1127(4)	11.1264(8)
c/Å	16.9793(5)	21.1960(7)	31.1487(13)
α/°	90	91.301(3)	90
β/°	104.335(4)	95.754(3)	94.857(4)
γ/°	90	93.117(4)	90
Volume/Å ³	3796.8(2)	1813.87(13)	7791.4(8)
Z	4	2	8
ρ _{calc} /g/cm ³	1.530	1.554	1.555
μ/mm ⁻¹	0.647	0.675	0.808
F(000)	1760.0	852.0	3680.0
Crystal size/mm ³	0.269 × 0.17 × 0.057	0.253 × 0.161 × 0.049	0.28 × 0.11 × 0.064
Radiation	MoKα (λ = 0.71073)	MoKα (λ = 0.71073)	MoKα (λ = 0.71073)
2θ range for data collection/°	6.662 to 59.076	6.91 to 59.392	6.628 to 59.22
Index ranges	-13 ≤ h ≤ 13, -31 ≤ k ≤ 23, -23 ≤ l ≤ 17	-10 ≤ h ≤ 10, -12 ≤ k ≤ 13, -29 ≤ l ≤ 29	-30 ≤ h ≤ 31, -14 ≤ k ≤ 15, -43 ≤ l ≤ 24
Reflections collected	20113	13812	20606
Independent reflections	8931 [R _{int} = 0.0370, R _{sigma} = 0.0641]	8440 [R _{int} = 0.0336, R _{sigma} = 0.0759]	9211 [R _{int} = 0.0635, R _{sigma} = 0.1199]
Data/restraints/parameters	8931/0/487	8440/0/469	9211/0/479
Goodness-of-fit on F ²	1.033	1.069	1.045
Final R indexes [I ≥ 2σ (I)]	R ₁ = 0.0544, wR ₂ = 0.1122	R ₁ = 0.0552, wR ₂ = 0.0922	R ₁ = 0.0904, wR ₂ = 0.1749
Final R indexes [all data]	R ₁ = 0.0961, wR ₂ = 0.1320	R ₁ = 0.0891, wR ₂ = 0.1114	R ₁ = 0.1820, wR ₂ = 0.2111
Largest diff. peak/hole / e Å ⁻³	1.23/-0.52	0.43/-0.46	0.61/-0.69

Table 5.4 Crystal data and structure refinement parameters for complexes **35c**, **37** and **38c**.

Compound number	35c	37	38c
Empirical formula	C ₅₅ H ₄₁ F ₅ FeN ₂ O ₂ P ₂ PdS	C ₉₂ H ₇₄ F ₁₀ N ₄ O ₄ P ₄ Pd ₂ S ₂	C ₄₆ H ₃₃ F ₅ FeO ₂ P ₂ PdS
Formula weight	1113.15	1890.35	968.97
Temperature/K	298	298(2)	298
Crystal system	orthorhombic	triclinic	monoclinic
Space group	Pca2 ₁	P-1	P2 ₁ /n
a/Å	23.4624(8)	12.9823(5)	12.9070(6)
b/Å	10.2943(3)	14.2919(5)	10.8331(5)
c/Å	20.1369(6)	26.8298(11)	31.6024(13)
α/°	90	88.413(3)	90
β/°	90	89.913(3)	100.506(5)
γ/°	90	73.042(3)	90
Volume/Å ³	4863.7(3)	4759.6(3)	4344.7(3)
Z	4	2	4
ρ _{calc} /g/cm ³	1.520	1.319	1.481
μ/mm ⁻¹	0.841	0.557	0.927
F(000)	2256.0	1920.0	1952.0
Crystal size/mm ³	0.295 × 0.197 × 0.104	0.176 × 0.134 × 0.079	0.398 × 0.21 × 0.128
Radiation	Mo Kα (λ = 0.71073)	MoKα (λ = 0.71073)	MoKα (λ = 0.71073)
2θ range for data collection/°	5.264 to 59.516	3.384 to 50.054	6.754 to 59.568
Index ranges	-25 ≤ h ≤ 29, -12 ≤ k ≤ 14, -23 ≤ l ≤ 27	-15 ≤ h ≤ 14, -15 ≤ k ≤ 17, -30 ≤ l ≤ 31	-17 ≤ h ≤ 17, -14 ≤ k ≤ 11, -32 ≤ l ≤ 43
Reflections collected	36962	32504	19107
Independent reflections	10888 [R _{int} = 0.0428, R _{sigma} = 0.0487]	16805 [R _{int} = 0.0675, R _{sigma} = 0.1451]	10169 [R _{int} = 0.0309, R _{sigma} = 0.0545]
Data/restraints/parameters	10888/1/622	16805/0/1065	10169/0/523
Goodness-of-fit on F ²	1.054	0.946	1.024
Final R indexes [I >= 2σ (I)]	R ₁ = 0.0356, wR ₂ = 0.0589	R ₁ = 0.0646, wR ₂ = 0.0967	R ₁ = 0.0417, wR ₂ = 0.0778
Final R indexes [all data]	R ₁ = 0.0575, wR ₂ = 0.0686	R ₁ = 0.1515, wR ₂ = 0.1261	R ₁ = 0.0688, wR ₂ = 0.0907
Largest diff. peak/hole / e Å ⁻³	0.42/-0.62	0.47/-0.33	0.43/-0.52

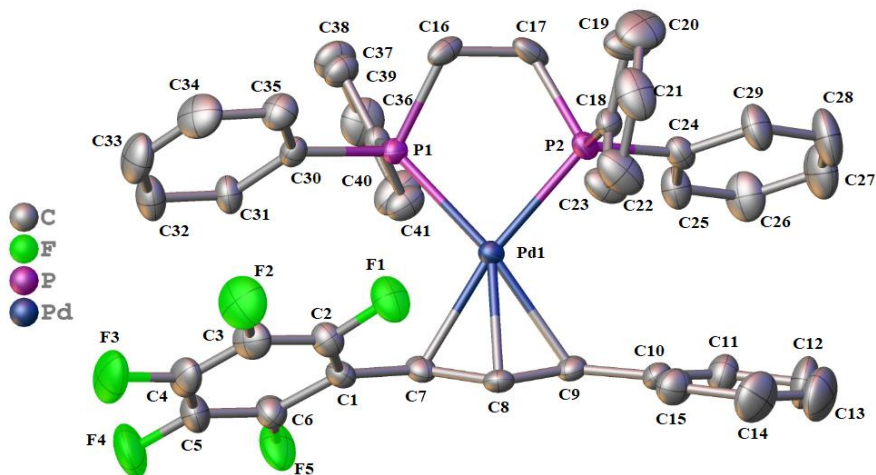


Figure 5.24 X-ray molecular structure of **31a** (ORTEP 40% probability ellipsoids). Hydrogen atoms and the BF_4^- anion are omitted for clarity.

Table 5.5 Selected bond lengths (Å) and angles ($^\circ$) for complex **31a** (for numbering scheme see Figure 5.24).

Pd(1)-P(1)	2.2881(10)	P(1)-Pd(1)-P(2)	85.17(4)
Pd(1)-P(2)	2.2914(10)	C(7)-Pd(1)-C(9)	66.27(15)
Pd(1)-C(7)	2.179(4)	C(9)-C(8)-C(7)	119.4(4)
Pd(1)-C(8)	2.177(4)		
Pd(1)-C(9)	2.253(4)		
C(7)-C(8)	1.416(5)		
C(8)-C(9)	1.392(6)		

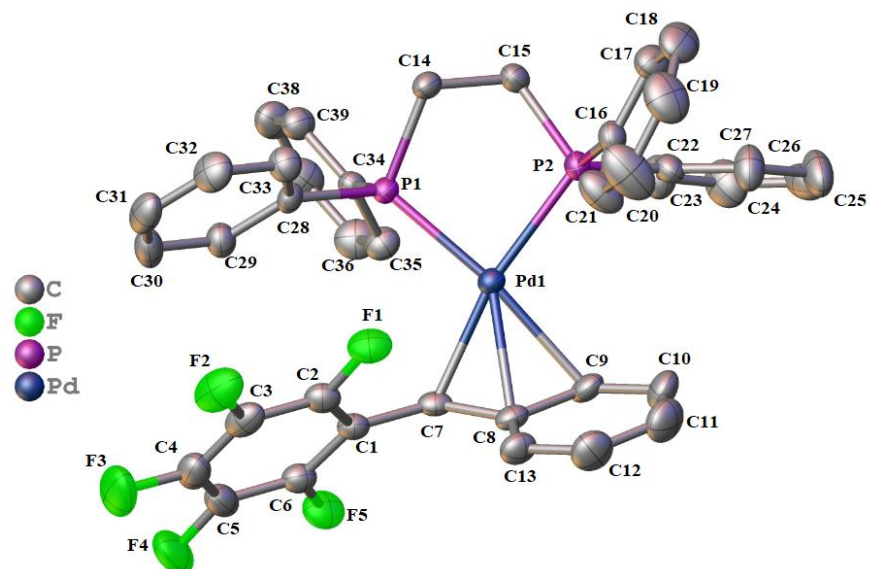
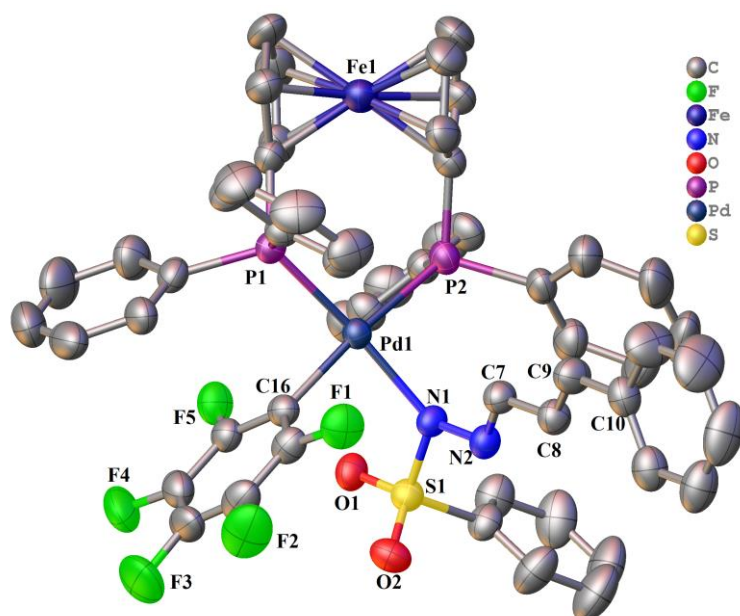


Figure 5.25 X-ray molecular structure of **33** (ORTEP 40% probability ellipsoids). Hydrogen atoms and the BF_4^- anion are omitted for clarity.

Table 5.6 Selected bond lengths [\AA] and angles [$^\circ$] for complex **33** (for numbering scheme see Figure 5.25).

Pd(1)-P(1)	2.2609(11)	C(8)-C(9)	1.417(5)
Pd(1)-P(2)	2.3018(10)	C(8)-C(13)	1.418(5)
Pd(1)-C(7)	2.155(4)	C(13)-C(12)	1.347(6)
Pd(1)-C(8)	2.275(4)	C(12)-C(11)	1.393(7)
Pd(1)-C(9)	2.284(4)	C(11)-C(10)	1.350(7)
C(7)-C(8)	1.447(6)	C(10)-C(9)	1.405(6)
<hr/>			
P(1)-Pd(1)-P(2)	86.25(4)	C(7)-Pd(1)-C(9)	66.80(15)
C(7)-C(8)-C(9)	117.3(3)		

**Figure 5.26** X-ray molecular structure of **35c** (ORTEP 40% probability ellipsoids). Hydrogen atoms are omitted for clarity.**Table 5.7** Selected bond lengths [\AA] and angles [$^\circ$] for complex **35c** (for numbering scheme see Figure 5.26).

Pd(1)-P(1)	2.3011(12)	N(2)-C(7)	1.282(5)
Pd(1)-P(2)	2.3698(12)	C(7)-C(8)	1.430(6)
Pd(1)-N(1)	2.109(4)	C(8)-C(9)	1.338(6)
Pd(1)-C(16)	2.047(4)	C(9)-C(10)	1.463(6)
N(1)-N(2)	1.380(5)		
<hr/>			
P(1)-Pd(1)-P(2)	101.17(4)	C(16)-Pd(1)-N(1)	87.66(16)

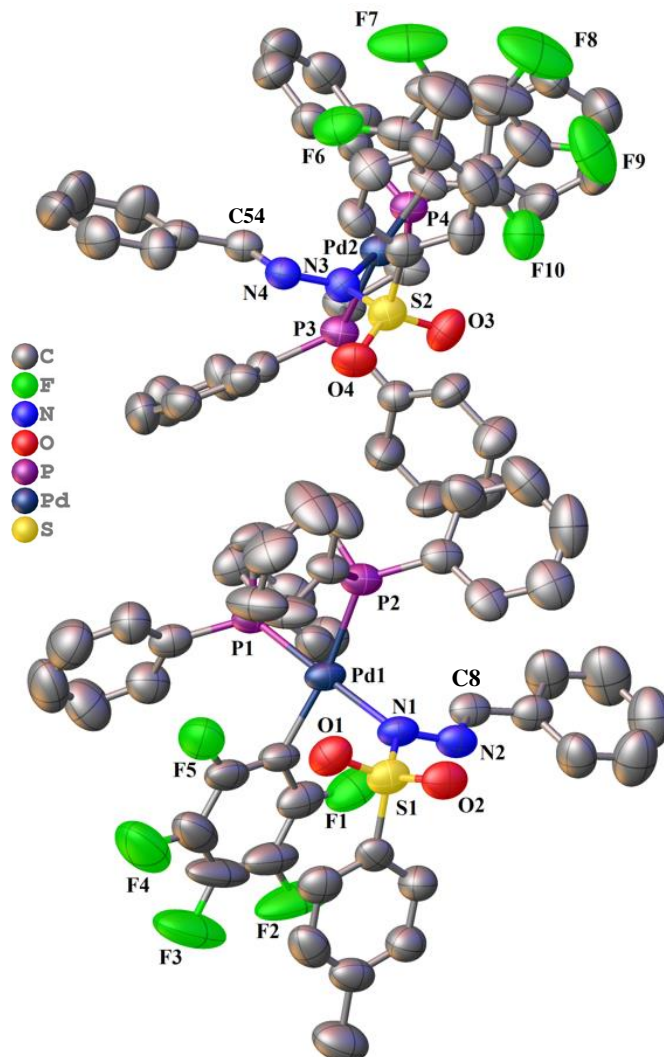


Figure 5.27 X-ray molecular structure of **37** (ORTEP 40% probability ellipsoids). Hydrogen atoms are omitted for clarity.

Table 5.8 Selected bond lengths [Å] and angles [°] for complex **37** (for numbering scheme see Figure 5.27).

Pd(1)-P(1)	2.2461(16)	Pd(2)-P(3)	2.3281(18)
Pd(1)-P(2)	2.3317(18)	Pd(2)-P(4)	2.2502(16)
Pd(1)-N(1)	2.105(5)	Pd(2)-N(3)	2.120(4)
Pd(1)-C(15)	2.045(7)	Pd(2)-C(73)	2.051(6)
N(2)-N(1)	1.382(6)	N(3)-N(4)	1.366(6)
N(2)-C(8)	1.270(7)	N(4)-C(54)	1.290(6)
<hr/>			
P(1)-Pd(1)-P(2)	84.56(6)	P(4)-Pd(2)-P(3)	84.49(6)
C(15)-Pd(1)-N(1)	88.8(2)	C(73)-Pd(2)-N(3)	89.4(2)

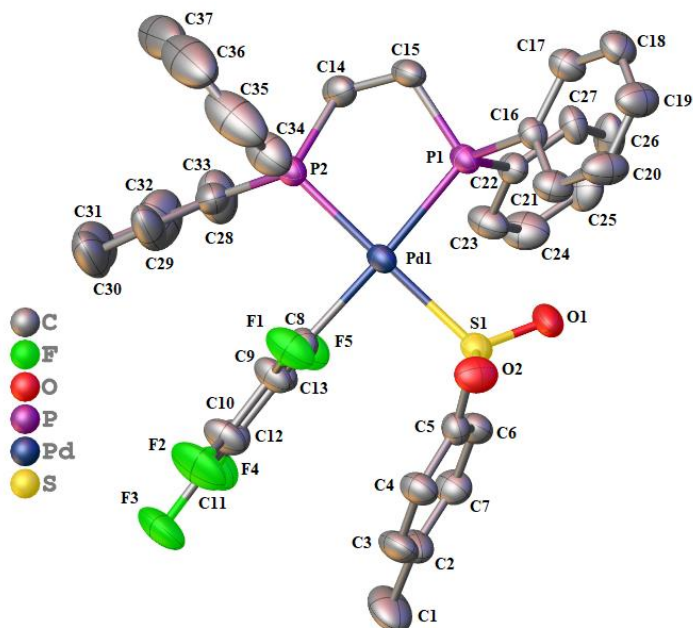


Figure 5.28 X-ray molecular structure of **38a** (ORTEP 40% probability ellipsoids). Hydrogen atoms and the solvent molecule of CH₂Cl₂ are omitted for clarity.

Table 5.9 Selected bond lengths [Å] and angles [°] for complex **38a** (for numbering scheme see Figure 5.28).

Pd(1)-P(1)	2.3203(19)
Pd(1)-S(1)	2.337(2)
Pd(1)-P(2)	2.278(2)
Pd(1)-C(8)	2.058(7)
P(2)-Pd(1)-P(1)	84.68(8)
C(8)-Pd(1)-S(1)	89.3(2)

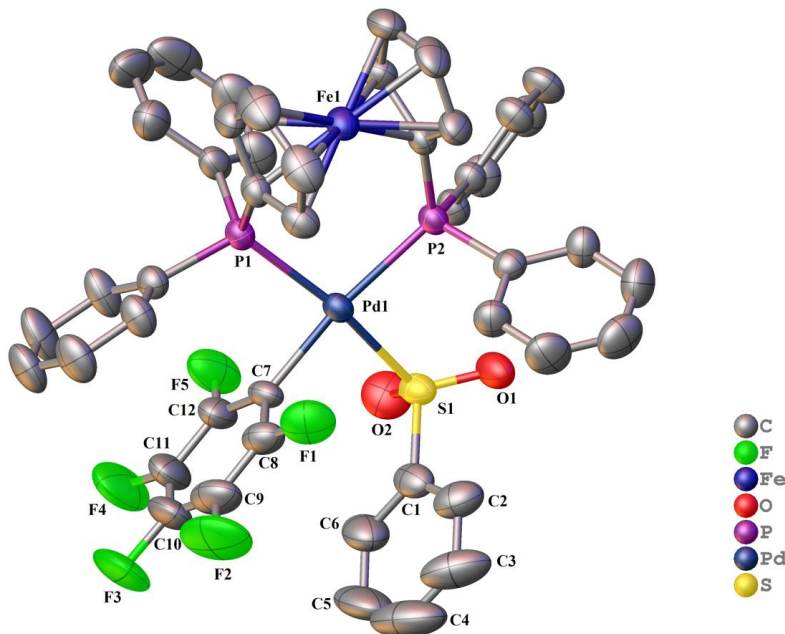


Figure 5.29 X-ray molecular structure of **38c** (ORTEP 40% probability ellipsoids). Hydrogen atoms are omitted for clarity.

Table 5.10 Selected bond lengths [Å] and angles [°] for complex **38c** (for numbering scheme see Figure 5.29).

Pd(1)-P(2)	2.3611(8)
Pd(1)-P(1)	2.3427(8)
Pd(1)-S(1)	2.3656(8)
Pd(1)-C(7)	2.038(3)
<hr/>	
P(1)-Pd(1)-P(2)	97.65(3)
C(7)-Pd(1)-S(1)	85.68(8)

5.4.9 Computational details

Computational methods

All calculations were performed using the DFT approach with the M06 functional, using Gaussian09 as program package. The selected basis set was 6-31+G(d) for C, N, F and H, and LANL2TZ(f) for Pd (Basis set I). Solvation was introduced in all the optimizations, frequency calculations and potential energy refinement through the SMD model, where we applied the experimental solvent, acetonitrile ($\epsilon = 37.5$, at 25 °C). All geometry optimizations were carried out in solution with no symmetry restrictions. Free energy corrections were calculated at 298.15 K and 10^5 Pa pressure, including zero-point energy corrections (ZPE), and the energies were converted to 1M standard state in solution (adding/subtracting $1.89 \text{ kcal mol}^{-1}$ for non-unimolecular processes). Vibrational frequency calculations were performed to establish the stationary points were

minima (without imaginary frequencies) or transition states (with one imaginary frequency). Connectivity of the transition state structures were confirmed by relaxing the transition state geometry towards both the reactant and the product. Final potential energies were refined by performing additional single-point energy calculations (also in solution), Pd was still described with LANL2TZ(f) basis set, and the remaining atoms were treated with 6-311++G(d,p) basis set (Basis set II). All reported energies in the manuscript correspond to Gibbs energies in solution, obtained from potential energies (including solvation) with basis set II plus Gibbs energy corrections with basis set I and are given in kcal mol⁻¹ (see SCF energy and free energy correction values in *Supporting information*).

Chapter 6

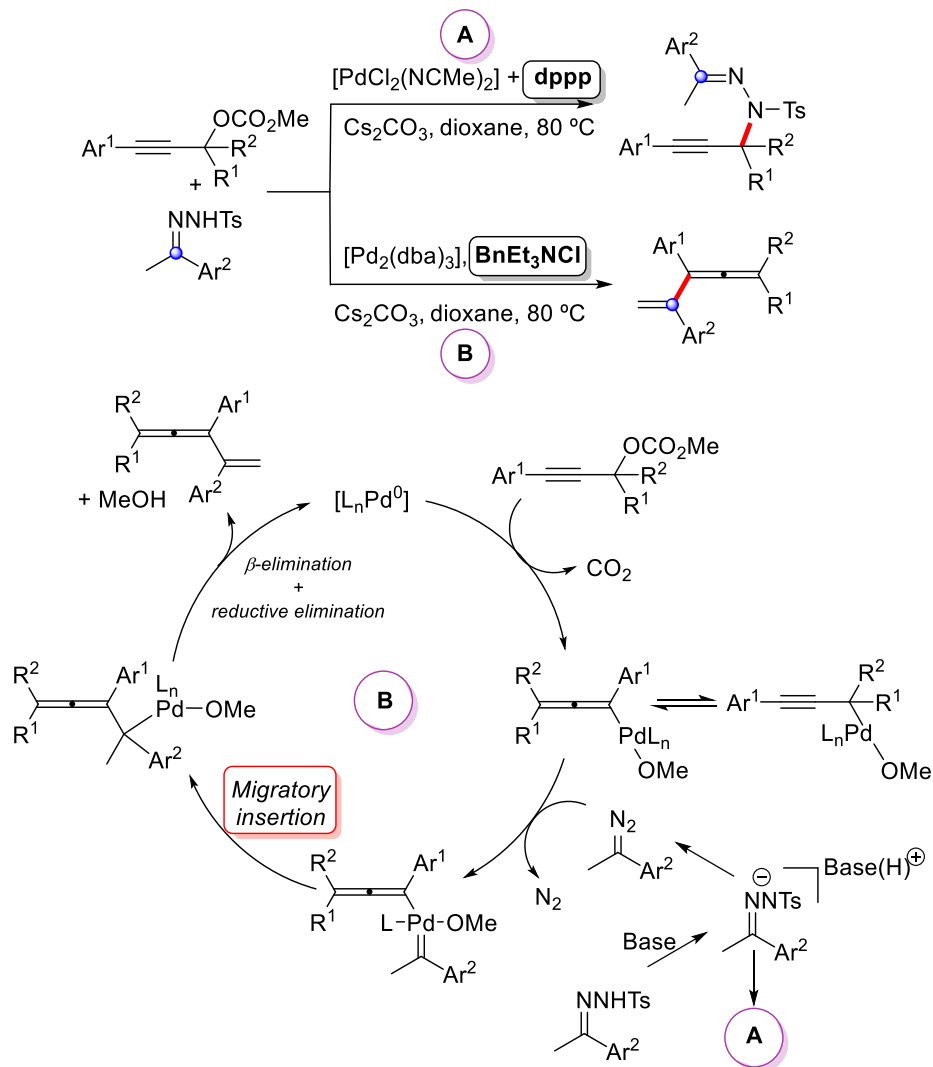
6. Understanding the Ligand Influence in the Multistep Reaction of Diazo Derivatives with Palladium Complexes Leading to Carbene-Aryl Coupling

6.1 INTRODUCTION

Understanding the fundamental steps that take place in palladium carbene coupling reactions can help the rational election of better ancillary ligands. In some cases, it has been observed that the ligands chosen in combination with the proper precatalyst can control the whole chemoselectivity of the reaction. For example, the group of Lian *et al.* reported the functionalization of propargylic carbonates with *N*-tosylhydrazones, where the suitable election of the precatalyst leads to different products. When [PdCl₂(NCMe)₂] combined with dppp as ancillary ligand is used, the substituted propargylic *N*-sulfonylhydrazones can be prepared, whereas vinylallenes derivatives are obtained in absence of P-donor ligand (Scheme 6.1).¹⁹⁸ In fact, the first reaction is a nucleophilic substitution by the hydrazone and no carbene fragment is involved, but in the second reaction (vinylallene derivatives), a carbene transfer and C-C bond formation by migratory insertion was proposed and supported by computational methods.¹⁹⁹

¹⁹⁸ Chen, Z.-S.; Duan, X.-H.; Wu, L.-Y.; Ali, S.; Ji, K.-G.; Zhou, P.-X.; Liu, X.-Y.; Liang, Y.-M. *Chem. – A Eur. J.* **2011**, *17*, 6918–6921.

¹⁹⁹ Ping, W.-W.; Jin, L.; Wu, Y.; Xue, X.-Y.; Zhao, X. *Tetrahedron* **2014**, *70*, 9373–9380.



Scheme 6.1 Synthesis of propargylic *N*-sulfonylhydrazones (**A**) and Pd-catalyzed synthesis of vinylallenes derivatives (**B**) depending on the ligand combination used.

Taking the model complexes $[\text{Pd}(\text{C}_6\text{F}_5)(\text{L-L})(\text{NCMe})](\text{BF}_4)$ where L-L = dppe, dppp, dppb, bipy, the influence of the ancillary ligand in the reaction with diazoalkanes was analyzed and it is described in this chapter. As it was mentioned in *Chapter 5*, from an experimental point of view, some steps such as migratory insertion or nitrogen extrusion from diazo derivatives are not easy to separate from the steps preceding and following them. To gain mechanistic insight into these steps, Density Functional Theory (DFT) calculations have been done, which represent a powerful tool for accessing the information that otherwise will be impossible.

Diphosphine ligands are characterized as being good ligands and also introduce a better control of the coordination environment since they occupy two, usually *cis*, coordination sites on a transition metal center. Among the numerous steric and electronic parameters reported for *P*-donor ligands,²⁰⁰ the parameter called “natural bite angle” (β_n)²⁰¹ represents a ligand descriptor in which the preferred chelation angle is determined by the ligand backbone constraints and not by the metal valence angle, so it is based solely on steric considerations. The interaction between the ligand and the groups-to-be-coupled can be associated with the “pocket angle” (θ) descriptor, which was introduced by Barron *et al.*²⁰² and defined as the interior cone angle created by the ligand at the metal center (Figure 6.1).

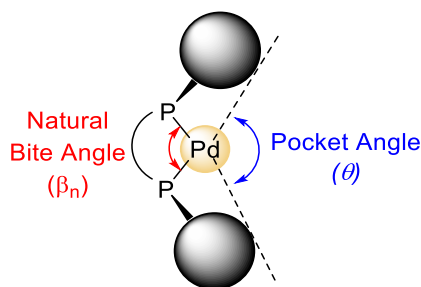


Figure 6.1 Natural Bite Angle (β_n) and Pocket Angle (θ) of chelating phosphines ligands.

The efficacy of bulky chelate ligands to promote C-C coupling is long known. For example, in a reductive elimination process, palladium complexes with chelating ligands containing large bite angles undergo faster C-C coupling than complexes with small bite angles. The bidentate Xantphos ligand, among others, with a bite angle of 102.07° produces a clear enhancement in the rate of the reductive elimination of the challenging Ar-CF₃ couplings.²⁰³

Migratory insertion reactions are also favoured by a large natural bite angle. The greater the bite angle, the closer the -R groups that have to couple.

²⁰⁰ a) Gillespie, J. A.; Dodds, D. L.; Kamer, P. C. J. *Dalton Trans.* **2010**, 39, 2751–2764. b) Durand, D. J.; Fey, N. *Chem. Rev.* **2019**, 119, 6561–6594.

²⁰¹ Casey, C. P.; Whiteker, G. T. *Isr. J. Chem.* **1990**, 30, 299–304.

²⁰² Koide, Y.; Bott, S. G.; Barron, A. R. *Organometallics* **1996**, 15, 2213–2226.

²⁰³ a) Kamer, P. C.J.; van Leeuwen, P. W. N. M.; Reek, J. N. H. *Acc. Chem. Res.* **2001**, 34, 895–904. b) Grushin, V. V.; Marshall, W. J. *J. Am. Chem. Soc.* **2006**, 128, 12644–12645. c) Ferguson, D. M.; Bour, J. R.; Canty, A. J.; Kampf, J. W.; Sanford, M. S. *Organometallics*, **2019**, 38, 2, 519–526.

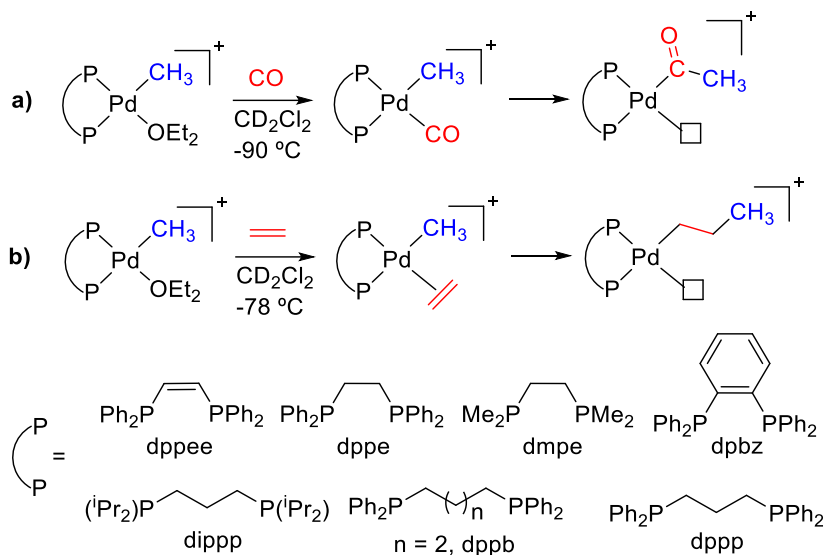
This intuitive idea means that the complex is closer to the transition state in which the C-Pd-C angles are forced to “compress” for a lateral orbital overlap.²⁰⁴ Very few studies have been devoted to investigate how the bite angle in diphosphine ligands affect the migratory insertion steps, mostly in the insertion of CO into a Pd-alkyl bond.

A series of well-defined bidentate phosphine Pd(II)-complexes used as models to study the migratory insertion step, were examined by Brookhart *et al.* They observed that the kinetic barriers for the migratory insertion of CO into the Pd-methyl bond decrease with increasing the P-Pd-P bond angle of the complex for the family of dppe, dppp and dppb diphosphine ligands (Scheme 6.2, **a**).^{188b} The authors observed that the rigidity of the ligand backbone does not have any effect but the steric bulk of the diphosphine has a significant effect on the methyl carbonyl insertion barriers, being the bulkiest ligand (dipp) the one with the smallest activation barrier. The observed order for the migratory insertion barriers was the following: dipp ~ dppb < dppp << dppe ~ dpbz ~ dppe < dmpe.

For the case of the 1,2 migratory insertion of ethylene into the Pd-methyl bond, the activation barriers are not directly related to either the steric crowding of the diphosphine or the P-Pd-P bond angle, even though the highest kinetic barrier is presented by the dmpe ligand which possesses the smallest P-Pd-P angle (Scheme 6.2, **b**). The migratory insertion of CO into Pd-alkyl bonds has been analyzed using other Pd(II) complexes bearing chelate *P,N*-donor ligands, but the influence of the bite angle and bulkiness of the ligands was not studied.²⁰⁵

²⁰⁴ a) Brown, J. M.; Guiry, P. J. *Inorg. Chim. Acta.* **1994**, *220*, 249–259. b) Hamann, B. C.; Hartwig, J. F. *J. Am. Chem. Soc.* **1998**, *120*, 3694–3703. c) Freixa, Z.; van Leeuwen, P. W. N. M. *Dalton Trans.* **2003**, 1890–1901.

²⁰⁵ a) Luinstra, G. A.; Brinkmann, P. H. P. *Organometallics* **1998**, *17*, 5160–5165. b) Reddy, K. R.; Surekha, K.; Lee, G.-H.; Peng, S.-M.; Chen, J.-T.; Liu, S.-T. *Organometallics* **2001**, *20*, 1292–1299.



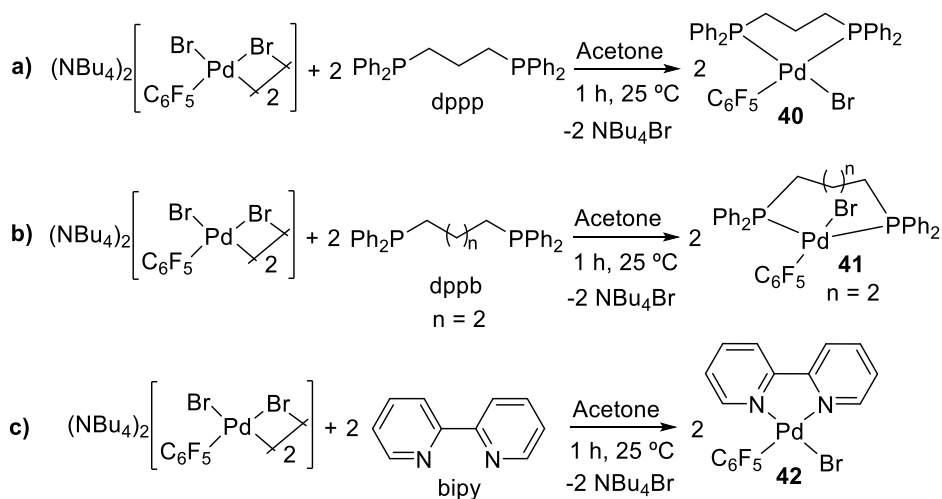
Scheme 6.2 Migratory insertion reactions of CO or ethylene into well-defined Pd(II)-complexes.

Although the migratory insertion of CO and carbenes have many analogies, no study of the influence of the ligands on the coupling of a carbene fragment and a Pd-R moiety has been reported. This Chapter contains both experimental and computational work done on the reactivity of palladium aryl complexes with different monodentate and bidentate ligands (phosphines and bipyridine) and diazoalkanes, leading to C-C coupling through Pd-carbene based systems.

6.2 RESULTS AND DISCUSSION

6.2.1 Synthesis of palladium(II) precursors

Complexes $[\text{PdBr}(\text{C}_6\text{F}_5)(\text{L-L})]$ (Scheme 6.3), $[\text{Pd}(\text{C}_6\text{F}_5)(\text{L-L})(\text{NCMe})](\text{BF}_4)$ ($\text{L-L} = \text{dppe}, \text{dppp}, \text{dppb}$ and bipy) (Scheme 6.4) and $[\text{Pd}(\text{C}_6\text{F}_5)(\text{NCMe})(\text{PPh}_3)_2](\text{BF}_4)$ were used as models to evaluate the ligand-dependent reactivity with diazoalkanes **30** and **32**. These diazoalkanes have already proved to be suitable for stabilizing the expected alkyl intermediate after the migratory insertion step, by coordination of the unsaturated double bond or aryl group to the metal, at least, with dppe as a ligand (Chapter 5). The synthesis of all precursors was carried out using the same dimeric complex $(\text{NBu}_4)_2[\text{Pd}(\mu\text{-Br}_2)\text{Br}_2(\text{C}_6\text{F}_5)_2]$ in the presence of the stoichiometric amount of the chelate ligand. The chosen phosphine ligands belong to the same family of diphosphines, seeking to maintain the electronic properties unchanged, and only modifying the separation between the phosphorous atoms and therewith the “bite angle” (P-M-P). Additionally, the N,N -chelate ligand 2,2'-bipyridine was also tested.



Scheme 6.3 Synthesis of the model diphosphine Pd(II)-complexes.

The molecular structure of complex **40** was determined by X-ray diffraction and it shows a *cis* arrangement of the $\text{-C}_6\text{F}_5$ and -Br ligands in a palladium square-planar geometry (Figure 6.2). The P-Pd-P and $\text{C}_6\text{F}_5\text{-Pd-Br}$ angles are 93.44° and 88.28° respectively, being in the expected range for other similar X-ray structures of $[\text{PdAr}(\text{dppp})(\text{X})]$ complexes reported in the literature, e.g., $[\text{Pd}(\text{dppp})(\text{Ph})(\text{X})]$:

$X = -CF_3$,²⁰⁶ P-Pd-P and C_{Ph} -Pd-X angles are 93.36° and 84.85° ; $X = Cl$,²⁰⁷ P-Pd-P and C_{Ph} -Pd-X angles are 96.70° and 89.04° ; $X = OH$,²⁰⁸ P-Pd-P and C_{Ph} -Pd-X angles are 95.21° and 86.52° respectively. The *cis* arrangement is also present in solution as clearly shown by the appearance of two inequivalent ^{31}P NMR resonances (see *Experimental part*).

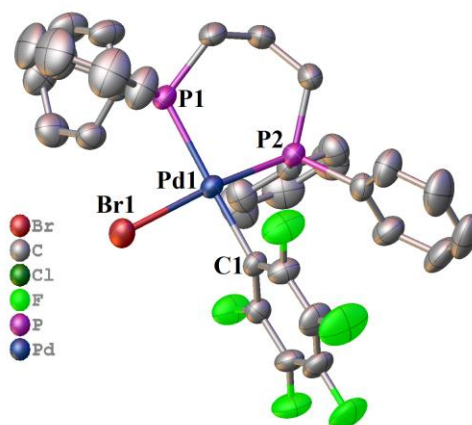


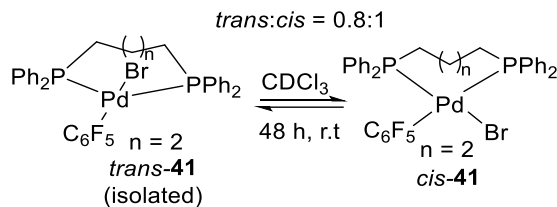
Figure 6.2 X-ray molecular structure of **40** (ORTEP 40% probability ellipsoids). Hydrogen atoms are omitted for clarity. Selected bond lengths (Å) and angles ($^\circ$): Pd1-Br1, 2.4756(4); Pd1-P1, 2.3286(9); Pd1-P2, 2.2483(8); Pd1-Cl1, 2.062(3); P2-Pd1-P1, $93.44(3)$; Cl1-Pd1-Br1, $88.28(8)$.

However, a different behavior was observed for the dppb complex $[PdBr(C_6F_5)(L-L)]$ and for the analogous solvento complex $[Pd(C_6F_5)(L-L)(NCMe)](BF_4)$ ($L-L = dppb$) as is shown in Equation 6.1 and 6.2. Initially, the isolated complex **41** is a *trans*-species as shown by the appearance of only one ^{31}P NMR resonance at 18.92 ppm (see *Experimental part*). In a chloroform solution at room temperature, **41** isomerizes to give a *trans:cis* mixture in a 0.8:1 mol ratio after 48 h (Equation 6.1).

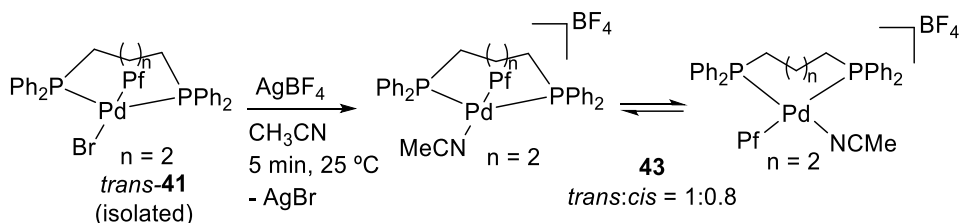
²⁰⁶ Grushin, V. V.; Marshall, W. J. *J. Am. Chem. Soc.* **2006**, *128*, 4632–4641.

²⁰⁷ Herrmann, W. A.; Broßmer, C.; Priermeier, T.; Öfele, K. *J. Organomet. Chem.* **1994**, *481*, 97–108.

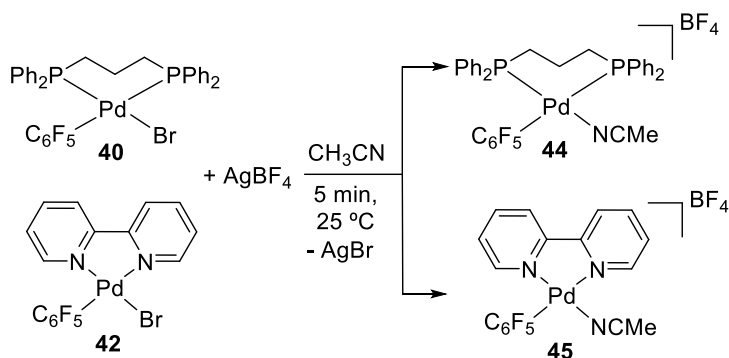
²⁰⁸ Takemoto, S.; Grushin, V. V. *J. Am. Chem. Soc.* **2013**, *135*, 16837–16840.



When the isolated complex *trans*-**41** is treated with AgBF_4 to remove the -Br ligand in acetonitrile at room temperature, complex **43** was obtained as a mixture of isomers *trans:cis* = 1:0.8 mol ratio. This was observed by ^{19}F and ^{31}P NMR indicating a dynamic equilibrium in solution for this complex.

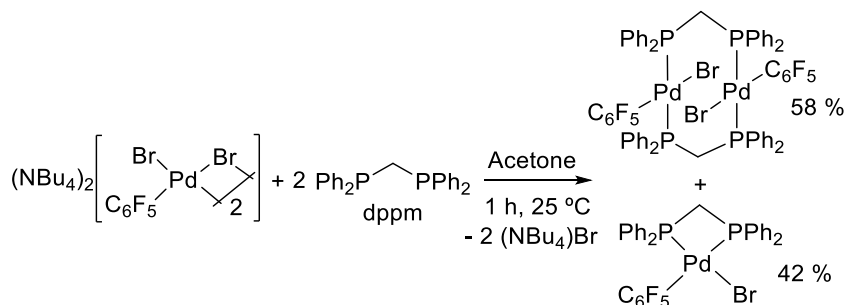


This behavior is only observed for the dppb ligand because of its inherent wide P-Pd-P angle in comparison to dppe or dppp ligands. For the remaining complexes **40** and **42** their treatment with AgBF_4 affords the corresponding *cis*-solvento acetonitrile complexes **44** and **45** (Scheme 6.4). Complex *trans*-[Pd(C_6F_5)(NCMe)(PPh₃)₂](BF₄) was prepared in the same way from the known *trans*-[PdBr(C_6F_5)(PPh₃)₂] complex.



Scheme 6.4 Synthesis of the solvento acetonitrile palladium complexes.

The diphosphine, 1,1-bis(diphenylphosphino)methane (dppm), with the smallest bite angle, was excluded from the study since the parent palladium complex of composition “PdBr(C₆F₅)dppm” was obtained as a mixture of the binuclear [Pd(μ-dppm)Br(C₆F₅)]₂ (58 %) with a bridging dppm and the monomeric [PdBr(C₆F₅)dppm] (42 %) (Equation 6.3).²⁰⁹ This behavior of dppm has been observed before,²¹⁰ and the presence of the bridging phosphine does not allow to evaluate the influence of the bite angle properly.



Equation 6.3

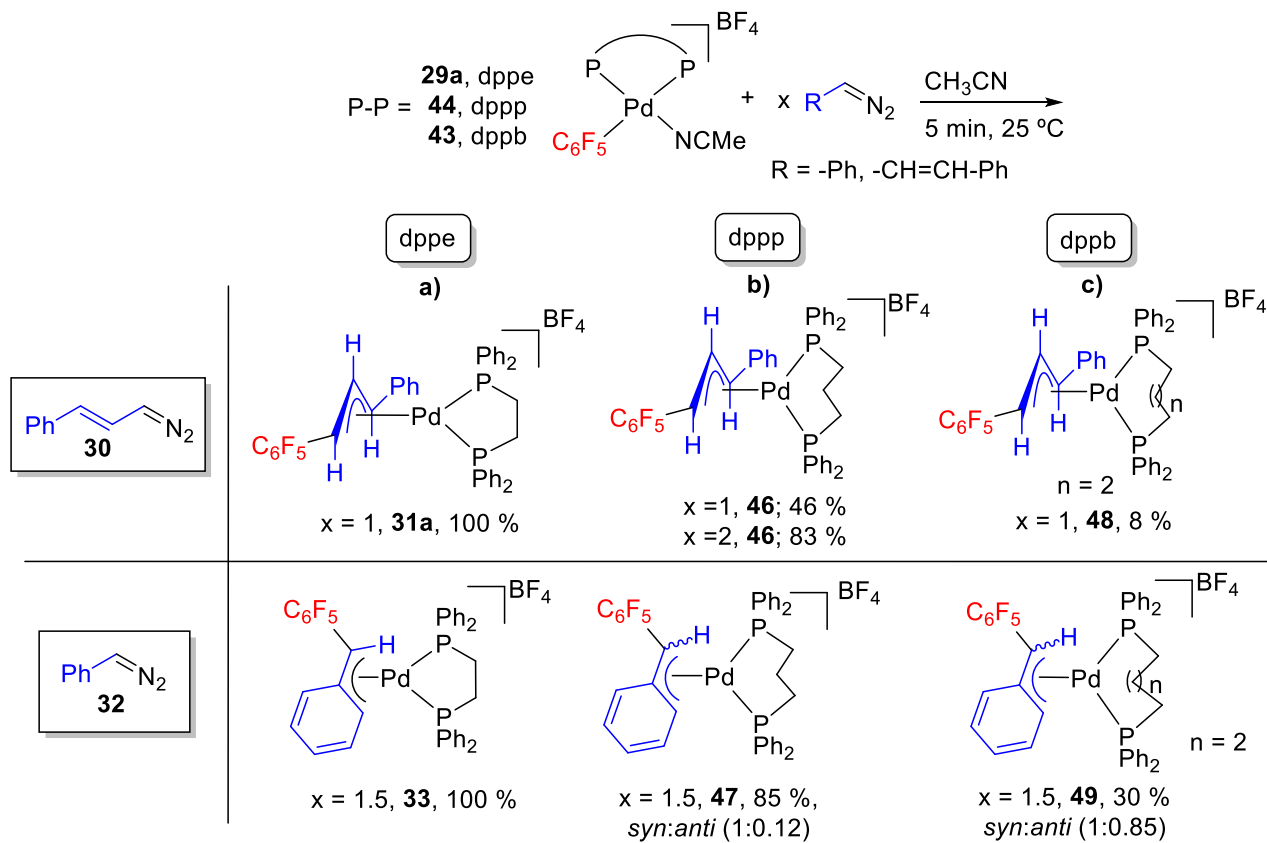
6.2.2 Reactions with diazo compounds: chelating diphosphine ligands

As described in *Chapter 5*, the solvento acetonitrile complex **29a** readily reacts with diazoalkanes **30** and **32** giving the organometallic η^3 -allylic-complex **31a** or the η^3 -benzylic complex **33** in full conversion regardless the solvent employed (Scheme 6.5, a)).²¹¹ Figure 6.3 shown the characteristic ¹⁹F NMR signals of the starting solvento complex **29a** (Pd-C₆F₅, about -120 ppm) and the organometallic complexes obtaining after the migratory insertion (C-C₆F₅, about -140 ppm).

²⁰⁹ The percentage given for the mixture of the monomeric and dimeric “PdBr(C₆F₅)dppm” was obtained from the crude reaction mixture by ¹⁹F and ³¹P NMR integration.

²¹⁰ a) Puddephatt, R. *J. Chem. Soc. Rev.* **1983**, *12*, 99–127. b) Usón, R.; Forniés, J.; Espinet, P.; Navarro, R.; Fortuño, C. *J. Chem. Soc. Dalton Trans.* **1987**, *8*, 2077–2081.

²¹¹ Chlorinated solvents (CDCl₃ or CD₂Cl₂) and coordinating solvent such as acetonitrile have been tested in these reactions. All the following reactions with different ligands have been carried out in acetonitrile as a solvent to prevent side-reactions like reorganizations of the -C₆F₅ groups, observed for complex **29a** in CD₂Cl₂.



Scheme 6.5 Reactions of $[\text{Pd}(\text{C}_6\text{F}_5)(\text{NCMe})(\text{P-P})](\text{BF}_4)$ complexes with diazoalkanes. x = mol ratio of diazoalkane / Pd.

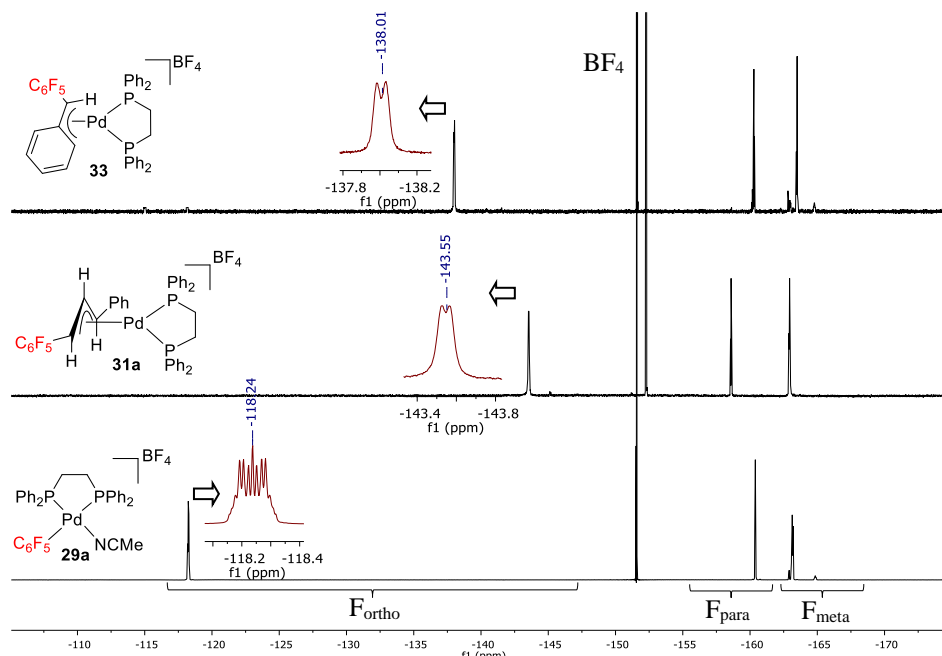


Figure 6.3 ^{19}F NMR (470.17 MHz, CH_3CN , $(\text{CD}_3)_2\text{SO}$ capillary) of the reactions shown in Scheme 6.5, a)).

The analogous solvento acetonitrile complex **44**, but with dppp as a ligand, was generated *in situ* as the *cis*-palladium species (Scheme 6.4). The reaction of complex **44** with an equimolar amount of diazoalkane **30** afforded 46 % of the η^3 -allylic Pd complex **46**. An additional equimolar amount of diazoalkane was added to the same sample, and the reaction proceeded to reach 83 % of **46** and a 17 % of the starting solvento complex which remains unreacted (Scheme 6.5, **b**). Characteristic signals for the migration of the C_6F_5 group to the carbene fragment were observed in the ^{19}F NMR, comparable to the analogous η^3 -allyl complex **31a** (*cf.* Figures 6.5 and 6.3). The F_{ortho} signals show a restricted rotation of the C- C_6F_5 bond at room temperature, presumably caused by the large bite angle of the dppp in comparison to the similar η^3 -allylic complex **31a**. The molecular structure of the η^3 -allyl complex **46**, determined by X-ray diffraction, reveals that both aryl-substituents are in a *syn* arrangement (Figure 6.4).

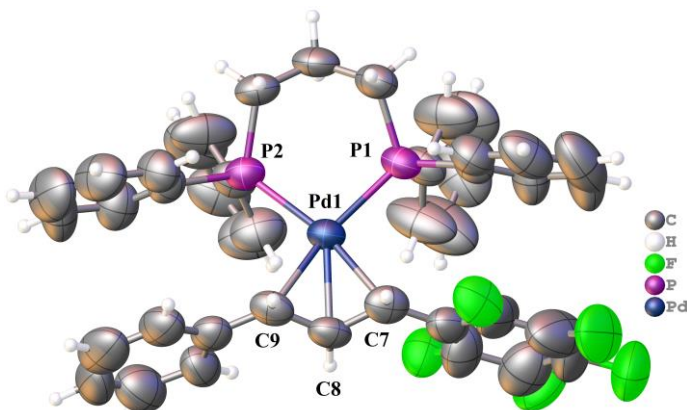


Figure 6.4 X-ray molecular structure of **46** (ORTEP 40% probability ellipsoids). Solvent molecules (CHCl_3) and the BF_4^- anion are omitted for clarity. Selected bond lengths (\AA) and angles ($^\circ$): Pd1-P2, 2.3035(17); Pd1-P1, 2.3057(16); Pd1-C9, 2.229(6); Pd1-C8, 2.196(6), Pd1-C7, 2.226(7); C7-C8, 1.406(10); C8-C9, 1.397(10).

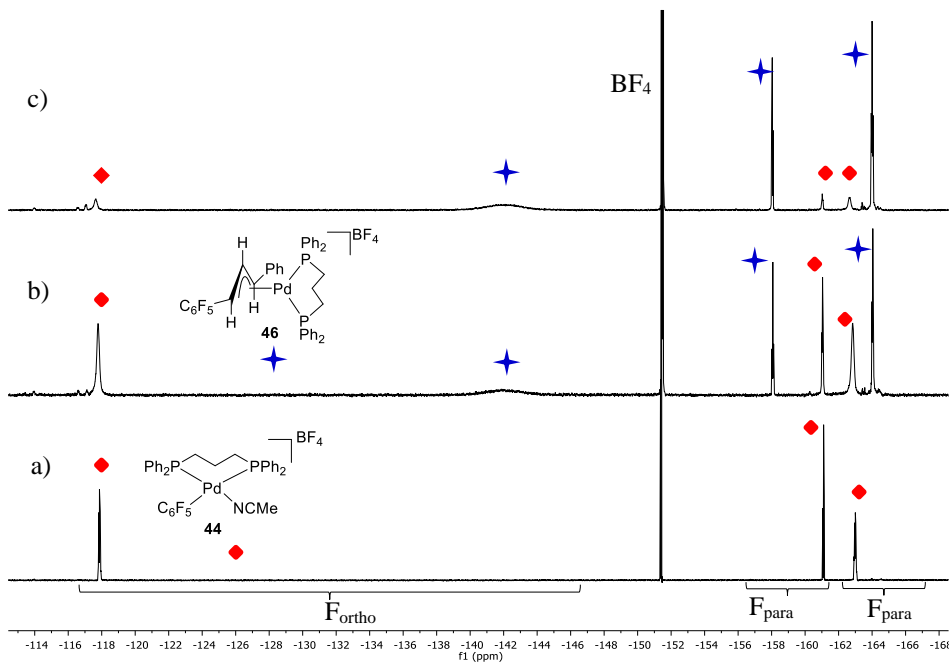


Figure 6.5 ^{19}F NMR (470.17 MHz, CH_3CN , $(\text{CD}_3)_2\text{SO}$ capillary) of reaction shown in Scheme 6.5, **b**) with diazoalkane **30**. **a**) Complex **44**. **b**) Complex **44** upon addition of **30** (Pd:**30** = 1:1 mol ratio) **c**) Sample shown in **b**) upon addition of an additional equimolar amount of **30** (total mol ratio Pd:**30** = 1:2).

In the case of using diazoalkane **32** (Pd:**32** = 1:1.5 mol ratio), a η^3 -benzylic palladium complex was generated (**47**), as a mixture of the *syn* pentafluorophenyl complex and a small amount of a tentatively assigned *anti*- C_6F_5 complex (Scheme 6.5, **b**) and Figure 6.6).

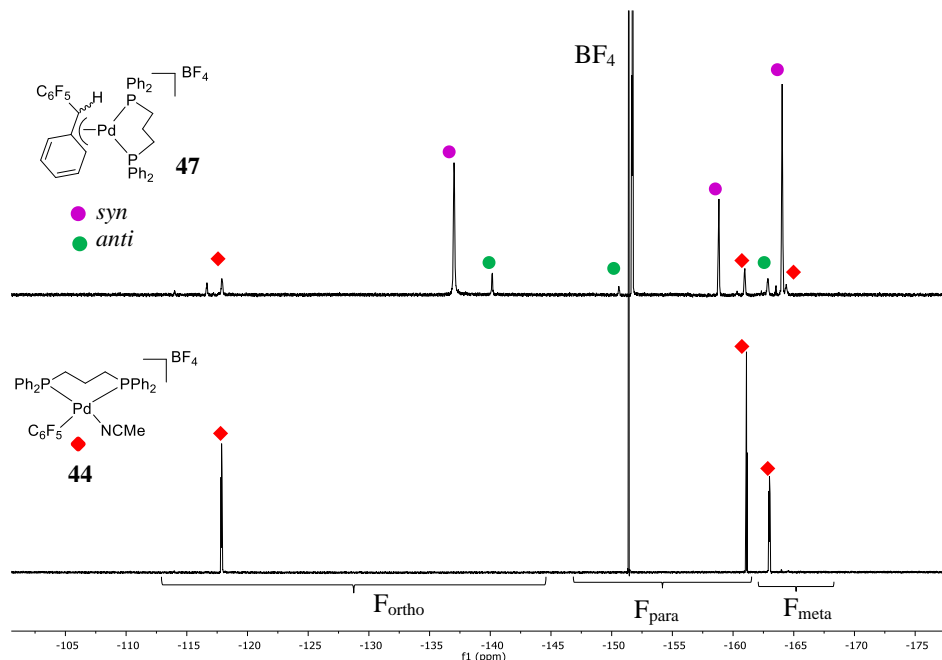
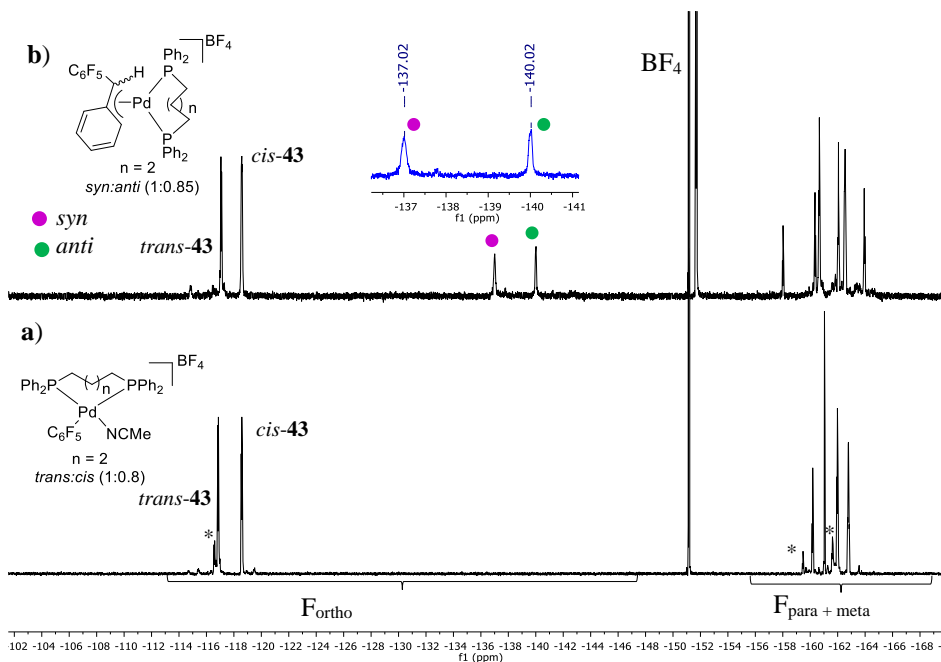
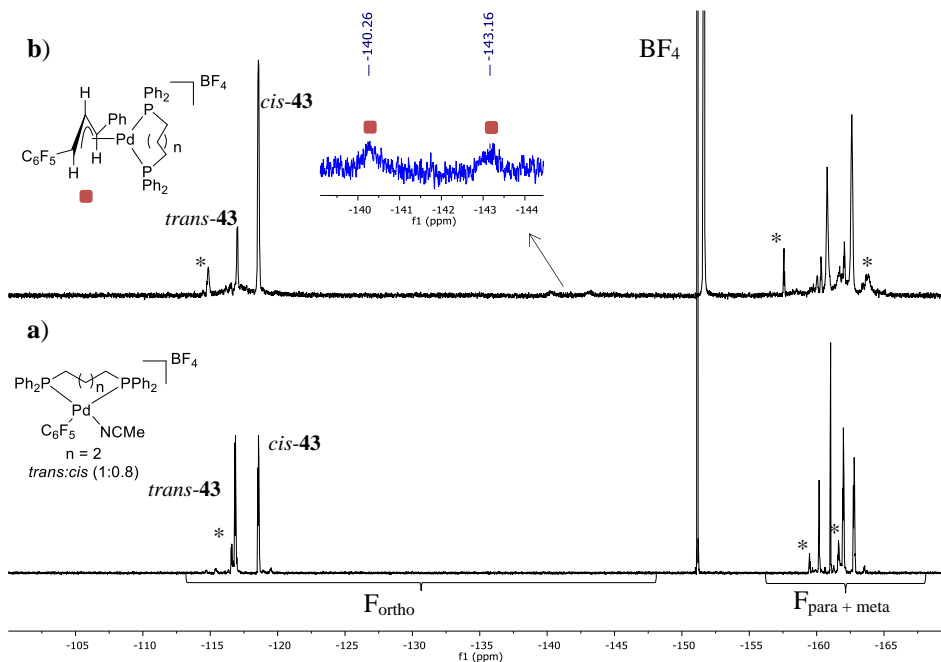


Figure 6.6 ^{19}F NMR (470.17 MHz, CH_3CN , $(\text{CD}_3)_2\text{SO}$ capillary) of reaction shown in Scheme 6.5, **b**) with diazoalkane **32** ($\text{Pd}:\mathbf{32} = 1:1.5$ mol ratio).

As it was mentioned above and shown in Equation 6.2, the freshly prepared complex **43** is a mixture of *trans*:*cis* isomers with a little amount of a non-identified Pd- C_6F_5 species (Figure 6.7, **a**). This equilibrium between isomers introduces a new factor that can distort the observed experimental results since the migratory insertion requires a *cis* arrangement. The reaction with diazoalkane **30** only afforded an 8 % of the η^3 -allyl-palladium complex **48**. The bulky dppb ligand in combination with the aryl groups in the allyl moiety induces a restricted rotation of the C- C_6F_5 bond in solution which leads to broad signals for the $^{19}\text{F}_{\text{ortho}}$ resonances (Figure 6.7, **b**). The remaining starting complex **43** is a mixture of the *trans*:*cis* isomers in a different ratio than that observed minutes before its *in situ* preparation (Figure 6.7, **a**). This means that the equilibrium, presumably slow, was not established at the beginning of the reaction. The analysis of the final reaction mixture indicates that the *cis* isomer is the major one, so the poor formation of the η^3 -allyl-palladium complex **48** is not governed by the availability of *cis*-**43**.

The formation of the η^3 -benzyl-organometallic product **49** when diazoalkane **32** was used is significantly more efficient (30 %). Two new organometallic species appeared which have been tentatively assigned as *anti*-*syn* isomers of **49**, in a 1:1 ratio (Figure 6.8, **b**).



In general, as for most η^3 -allylic compounds, the *syn*-arrangement in the η^3 -benzylic moiety is more favourable than the *anti*-arrangement since it places the

substituent away from the metal and decreases the steric repulsions. However, the bulkiness of the ligands may play a role and this stability order may be reversed. For this reason, DFT calculations were carried out to check the relative stability of the *syn* and *anti*-isomers of the η^3 -benzylic derivatives and compare these results with the experimental observations.

When both *syn* and *anti*-isomers of $[\text{Pd}(\text{dpppe})(\eta^3\text{-Ph-CH-C}_6\text{F}_5)](\text{BF}_4)$ (**33**) were calculated at room temperature, the *syn* isomer is favoured by $1.62 \text{ kcal mol}^{-1}$ (Figure 6.9). This difference explains the observation of the *syn*-isomer as the organometallic product in solution ($\text{syn} \rightleftharpoons \text{anti}$, $K_{\text{equ}} = 6.5 \cdot 10^{-2}$) and this is the isomer present in the solid state as well (X-ray structure, Chapter 5). For complex **47** (L-L = dppp) we propose the *syn*-isomer as the major one by analogy of the ^{19}F NMR data with those for complex **33**: for example, the F_{ortho} NMR resonance appears at about -137 ppm (*syn*) vs. -140 ppm (*anti*). The *syn:anti* ratio for **47** is 9:1 and the DFT calculations show an extremely little difference in energy between both arrangements ($\Delta E = 0.04 \text{ kcal mol}^{-1}$, Figure 6.9). For the η^3 -benzylic complex **49**, the energy difference obtained by DFT is zero. This shows that as the steric demand of the ligand becomes higher, the difference between arrangements decreases to make it negligible, and explains the appearance of both isomers. The calculated energies fit well with the ratio of *syn-49* and *anti-49* observed by ^{19}F NMR ($K_{\text{equ}} = \sim 1$), although deviates a little from the isomer ratio observed for **47**. The most representative structural parameters for these η^3 -benzylic complexes are collected in Table 6.1.

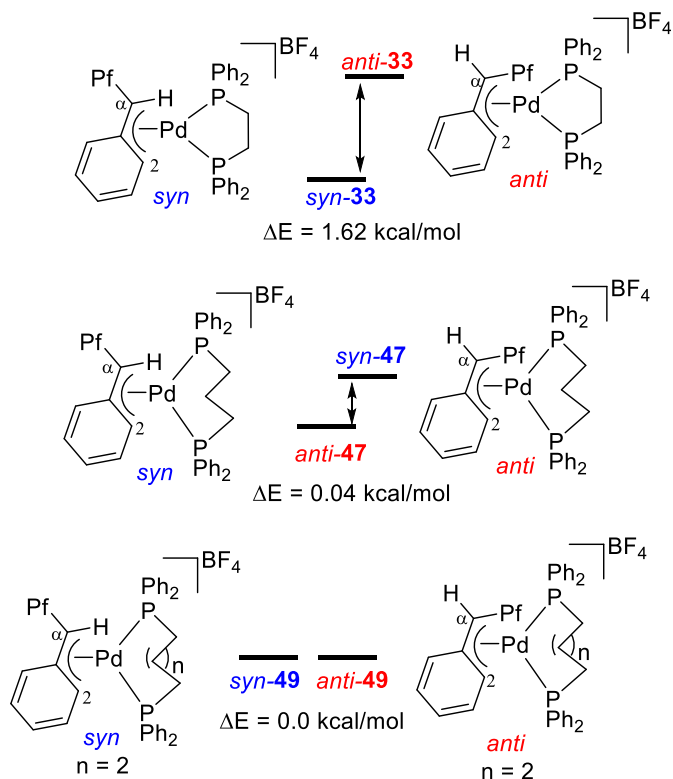


Figure 6.9 Energy difference in kcal mol⁻¹ between the two isomers (*syn* or *anti*) in the complexes **33**, **47** and **49**. Pf = C₆F₅.

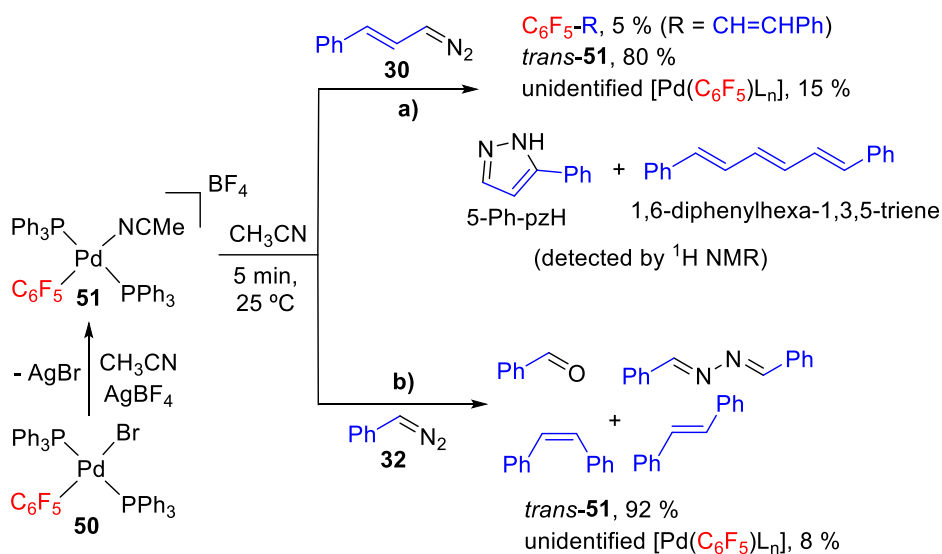
Table 6.1 Geometrical parameters extracted from DFT calculation of the optimized structure. Selected bond lengths (Å) and angles (°).

Geometrical parameters	<i>syn</i> - 33	<i>anti</i> - 33	<i>syn</i> - 47	<i>anti</i> - 47	<i>syn</i> - 49	<i>anti</i> - 49
P-Pd-P	85.4	85.3	96.3	93.2	98.8	98.0
Pd-C ^α	2.144	2.167	2.137	2.156	2.137	2.162
Pd-C ²	2.514	2.311	2.662	2.375	2.662	2.391
K _{eq}	6.5 × 10 ⁻²		1.07		1.0	

6.2.3 Reactions with diazo compounds: triphenylphosphine

PPh_3 was selected as an easily available and commercial monodentate ligand to evaluate the differences in reactivity. As shown in Scheme 6.6, the *trans* diphosphino complex **51** barely reacts with diazoalkane **30**. After the reaction, we could not identify any organometallic product from the migratory insertion of a transient palladium carbene

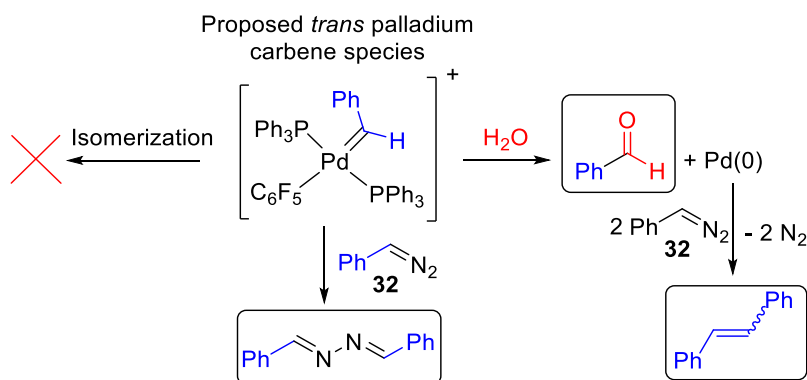
complex into the Pd-C₆F₅ bond and only small amounts of C₆F₅-containing organic products that could be originate by migratory insertion (5 %) were detected by ¹⁹F NMR. Additionally, 5-Ph-pzH, formed by decomposition of the diazoalkane, and 1,6-diphenylhexa-1,3,5-triene, as result of the dimerization of the carbene fragment, were observed by ¹H NMR. Once the diazoalkane replaces the acetonitrile, the intermediate generated is a transient *trans*-[Pd(C₆F₅)(PPh₃)₂(diazoalkane)]⁺ complex where the diazoalkane is located in a *trans* position to the -C₆F₅ group. If this Pd-intermediate undergoes nitrogen extrusion, the resulting Pd-carbene remains in the same *trans*-arrangement and the migratory insertion cannot occur. If the isomerization process to afford a *cis* complex is slower than the decomposition of the diazoalkane and the metal carbene, it could explain the experimental outcome observed.



Scheme 6.6 Reactions of complex **51** with diazoalkanes. Reaction **a**) and **b**) were immediate and no free diazoalkanes were observed after 5 min under these reaction conditions.

Similarly, when diazoalkane **32** interacts with complex **51** no organometallic migratory insertion product could be detected by ¹⁹F NMR, instead, several decomposition products of the diazoalkane **32** such as benzaldehyde, *cis/trans* stilbene and the azine derivative were observed. The formation of the azine derivatives and the benzaldehyde can be explained by the formation of a plausible and elusive Pd-carbene complex that does not evolve by a migratory insertion into the Pd-C₆F₅ bond but *via* nucleophilic attack. The attack of one molecule of the parent diazoalkane **32** on the

Pd-carbene species could form the azine derivative observed.²¹² The attack of water on the Pd-carbene intermediate, gives the corresponding hydrolysis product (benzaldehyde) and Pd(0) species (Scheme 6.7). This Pd(0) species formed in the reaction media could be the responsible for the *cis* and *trans* stilbene which can be generated by a dimerization of two carbene fragment catalyzed by Pd(0) (Scheme 6.7).^{147,148}

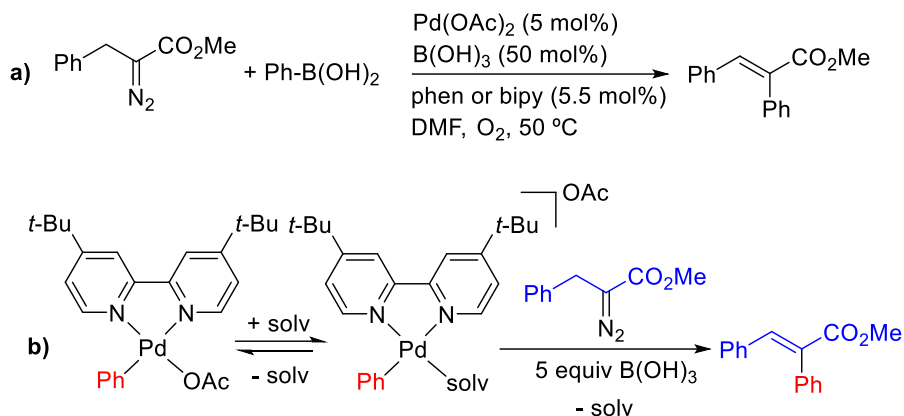


Scheme 6.7 Proposed decomposition routes for the side-products observed in Scheme 6.6, **b**).

6.2.4 Reactions with diazo compounds: bipyridine

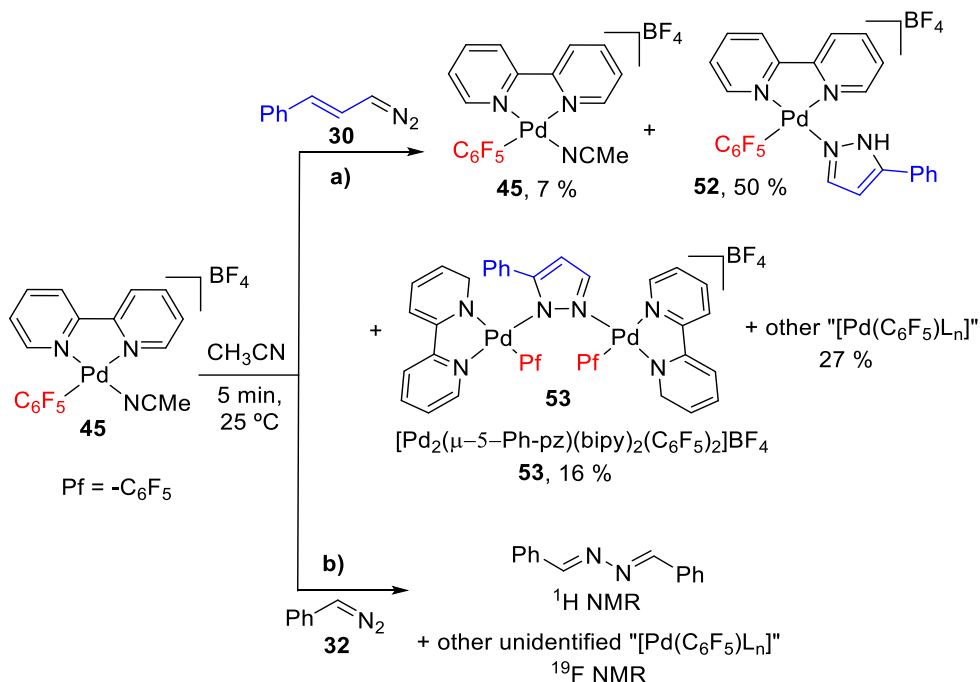
There are very few examples in the literature in which carbene coupling reactions employ *N,N*-chelate ligands. In 2011 Yu *et al.* reported a Pd-catalyzed oxidative reaction of arylboronic acids with diazoesters with a series of nitrogen ligands (Scheme 6.8, **a**). The stoichiometric experiments performed with a well-defined palladium complex bearing bipyridine showed the formation of the diarylacrylate product through a proposed migratory insertion of the metal-carbene generated from diazoesters. To promote the reaction, B(OH)₃ as an additive was essential but its role was not ascertained (Scheme 6.8, **b**).

²¹² The formation of the azine derivative by a bimolecular reaction of the diazo **32** can be also proposed: Griller, D.; Majewski, M.; McGimpsey, W. G.; Nazran, A. S.; Scaiano, J. C. *J. Org. Chem.* **1988**, *53*, 1550–1553.



Scheme 6.8 Pd-catalyzed C-C coupling of diazoester with *N*-donor chelating ligands and B(OH)₃ as an additive.

It is surprising that nitrogen ligands are much less utilized for these reactions and it is worth exploring the reactivity of well-defined bipyridine palladium complex **45** with diazoalkanes (Scheme 6.9) to find out the intrinsic main differences in behavior when compared to the phosphine complexes. Solvento acetonitrile complex **45** immediately reacts with the diazoalkanes **30** and **32** but the reaction does not give rise to the formation of the initially assumed [Pd(η^3 -allyl)(bipy)]⁺ or [Pd(η^3 -benzyl)(bipy)]⁺ complexes by a carbene formation and migratory insertion pathway. The organometallic products observed by ¹⁹F NMR contain the C₆F₅ group bound to palladium and they could only be identified for the reaction with diazoalkane **30**. They consist of different palladium species in which 5-phenyl pyrazole (5-Ph-pzH) has been coordinated: **52** and the dimeric complex [Pd₂(μ -5-Ph-pz)(bipy)₂(C₆F₅)₂]BF₄ (**53**) along with small amount of the starting solvento complex **45** (Scheme 6.9, a)).



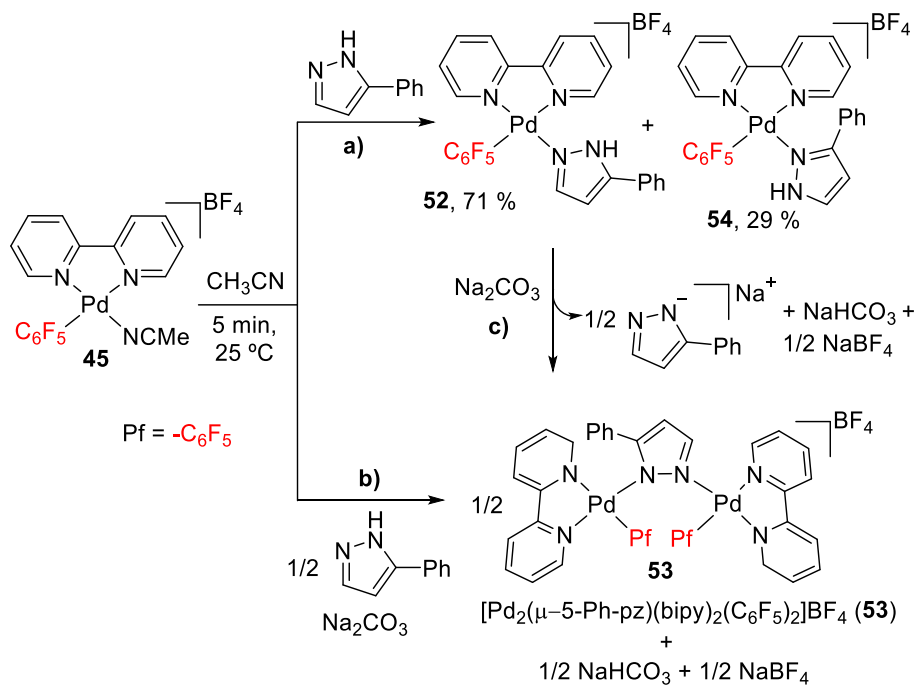
Scheme 6.9 Reactions of complex **45** with diazoalkanes. The percentages of the palladium complexes shown were determined by integration of the signals in the ¹⁹F NMR spectra and given in % F corresponding to the -C₆F₅ groups.

In order to corroborate the species formed in Scheme 6.9, **a**), several control experiments were carried out under different conditions. The reaction of **45** with an equimolar amount of 5-Ph-pzH leads to the formation of a major complex (**52**) and a minor tautomeric complex (**54**) (Scheme 6.10, **a**). The coordination of the 5-Ph-pzH ligand by the more basic iminic nitrogen in these Pd(II)-complexes (**52** and **54**) is proposed based on DFT calculations as well as some analogous reported X-ray molecular structures of [Pd^{II}(5-Ph-pzH)(N,N)X₂] complexes with *N,N*-chelate ligands.²¹³

When a base is added to the preformed mixture of complexes **52** and **54** the formation of the dimer [Pd₂(μ-5-Ph-pz)(bipy)₂(C₆F₅)₂](BF₄) is clearly observed by ¹H and ¹⁹F NMR (Scheme 6.10, **c**). The reaction of complex **45** with 5-Ph-pzH in a Pd:pyrazole = 1:0.5 mol ratio in the presence of a non-coordinating base, also leads to the dimeric derivative **53** (Scheme 6.10, **b**) and Figure 6.10, **d**). Various examples of 2,2'-bipyridine dimeric Pd(II) complexes bearing a pyrazolate-bridge ligands have been

²¹³ a) Uvarova, M. A.; Kushan, E. V.; Nefedov, S. E. *Russ. J. Inorg. Chem.* **2012**, *57*, 676–683.
 b) Zhai, F.; Jordan, R. F. *Organometallics* **2014**, *33*, 7176–7192.

reported where the pyrazolate derivatives is 4-(4-carboxylatephenyl)pyrazolate,²¹⁴ 4-(3,5-dimethyl-pyrazolate-yl)pyridine²¹⁵ and 3,5-dimethylpyrazolate.²¹⁶



Scheme 6.10 Control experiments with complex **45** and 5-Ph-pzH.

²¹⁴ Tong, J.; Lu, H.-L.; Sun, W.-Q.; Yu, S.-Y. *CrystEngComm* **2020**, *22*, 8166–8170.

²¹⁵ Tong, J.; Yu, S.-Y.; Li, H. *Chem. Commun.* **2012**, *48*, 5343–5345.

²¹⁶ Huang, H.-P.; Wu, Q.; Mei, G.-Q. *Acta Crystallogr. Sect. E* **2006**, *62*, m3465–m3466.

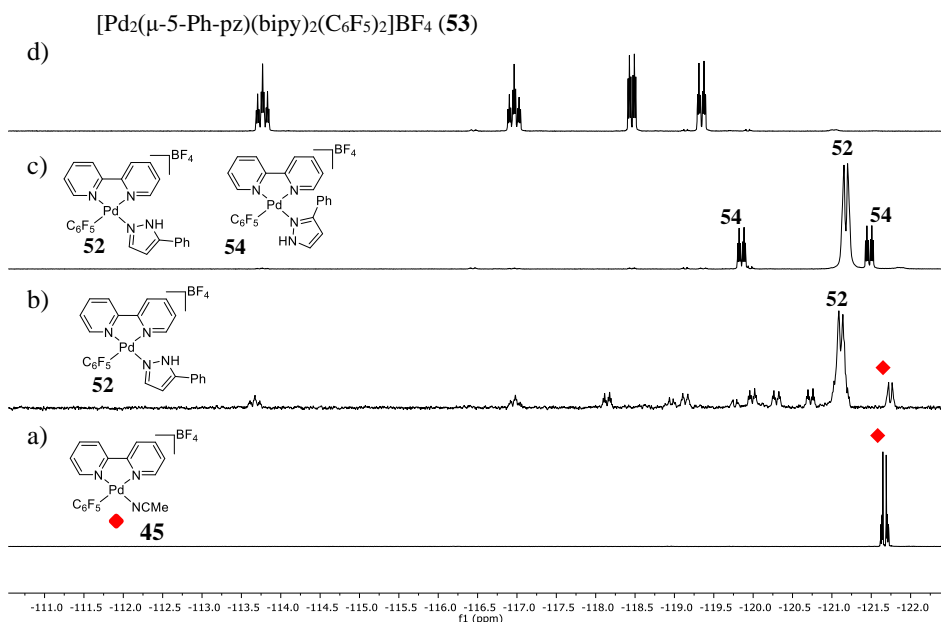
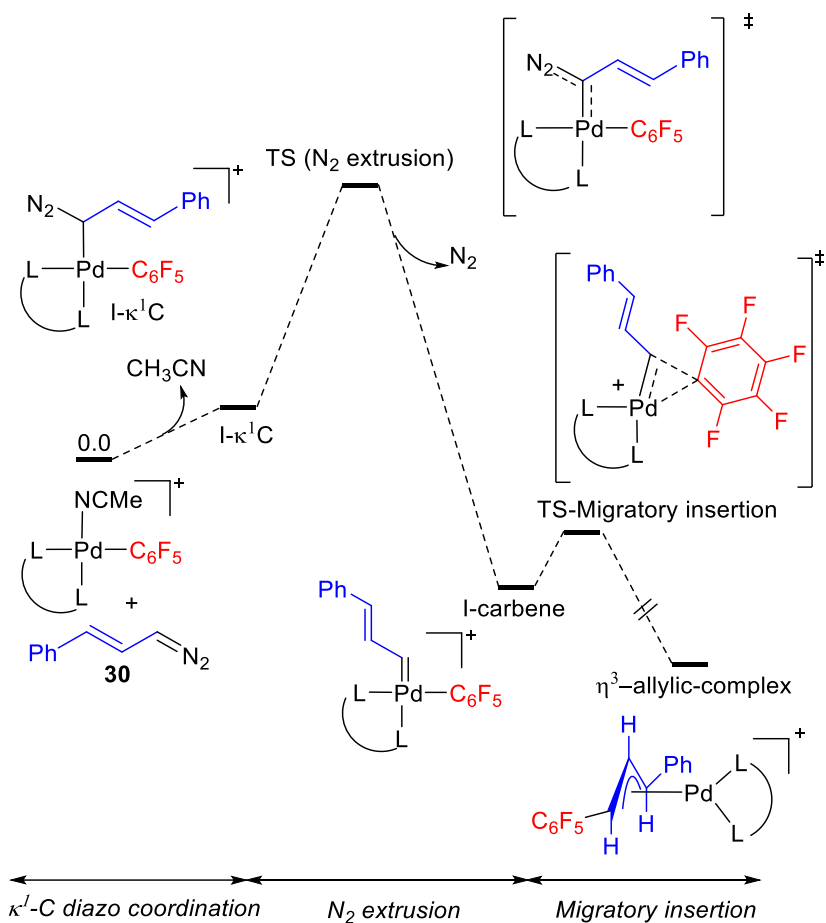
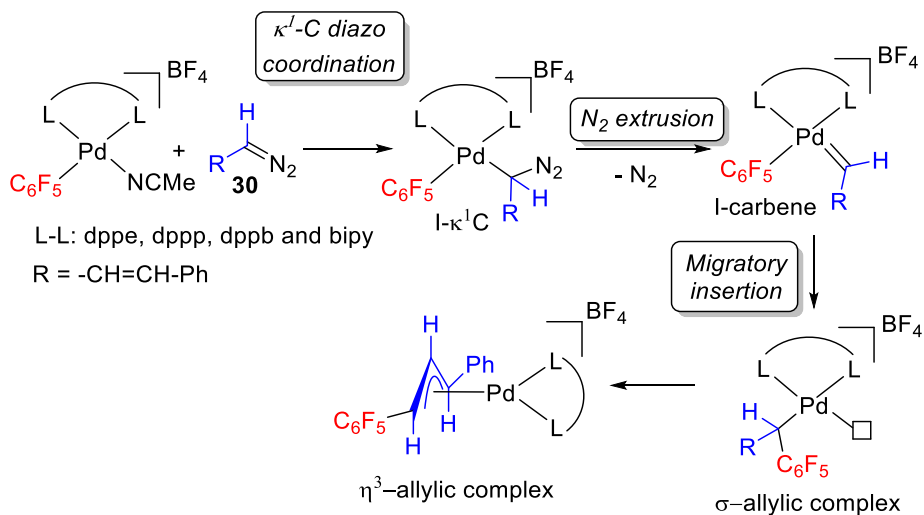


Figure 6.10 ^{19}F NMR, F_{ortho} region (470.17 MHz, δ , CH_3CN , $(\text{CD}_3)_2\text{SO}$ capillary for **a**) and **b**) and CD_3CN for **c**) and **d**) of: **a**) solvento acetonitrile complex **45**; **b**) reaction of complex **45** with an equimolecular amount of diazo **30** (see Scheme 6.9, **a**); **c**) reaction of complex **45** with an equimolecular amount of 5-Ph-pzH after 1 h at room temperature (see Scheme 6.10, **a**); slow rotation of the C_6F_5 group is observed for **54**; **d**) reaction of complex **45** with 5-Ph-pzH (Pd:pyrazole = 1:0.5 mol ratio) in the presence of Na_2CO_3 see Scheme 6.10, **b**).

6.2.5 DFT studies

The nature of the auxiliary ligand and the different number of carbons in the backbone of the diphosphine ligands exert a relevant influence in the outcome of the reaction with diazoalkanes. In a simplified way, the steps involved in the reactions of solvento acetonitrile Pd(II) complexes with diazoalkane **30** are depicted in Scheme 6.11. As it was observed for dppe (*Chapter 5*), only the organometallic products after migratory insertion were detected, so the coordination of the diazoalkane, the formation of the intermediate palladium carbene and the migratory insertion reaction cannot be experimentally studied separately. For this reason, DFT calculations were employed to gain insight into the steps that are responsible for the differences observed. We modelled the energy profiles for the reactions of dppp, dppb and bipy derivatives with diazoalkane **30** and compared them to that of complex **29a** (dppe-system).



Scheme 6.11 Simplified reaction pathway modelled by DFT calculations.

Table 6.2 shows the Gibbs energy barriers for the nitrogen extrusion and migratory insertion key-steps depicted in Scheme 6.11. Both the energy barriers for each step ($\Delta\Delta G^\ddagger$, energy difference between the previous intermediate and the TS) and the Gibbs energy of the TSs taking the reactants as reference are given in the table 6.2. The intermediates proposed in Scheme 6.11 and their corresponding free-energies are given in Table 6.3.

Table 6.2 Free energies in kcal mol⁻¹ for the transition states of nitrogen extrusion and migratory insertion with the different ligands extracted from Figures 6.11, 6.14, 6.24 and 6.25 in the *Experimental part*.

	$\Delta\Delta G^\ddagger$ N ₂ extrusion	$\Delta\Delta G^\ddagger$ mig insert	TS _{N₂ extrusion}	TS _{mig insert}
dppe	11.0	6.1	14.1	-11.6
dppp	10.2	4.5	12.6	-12.2
dppb	8.9	4.6	11.2	-15.5
bipy	3.5	3.3	5.3	-21.3

Table 6.3 Energies in kcal mol⁻¹ for the intermediates proposed in Scheme 6.11.

	I-κ ¹ C	I-carbene	η ³ -allylic palladium complex
dppe	3.1	-17.7	-64.0
dppp	2.4	-17.2	-63.5
dppb	2.3	-20.1	-66.7
bipy	1.8	-24.6	-65.2

The activation barriers for the migratory insertion step ($\Delta\Delta G_{\text{mig insert}}^\ddagger$, Table 6.2) follow the trend: dppe > dppp ≈ dppb > bipy. As the bite angle of the phosphine increases the barrier is lower. This is specially noticeable on going from dppe to dppp and it is the same trend observed for the migratory insertion reaction of CO.^{188b} The barriers for nitrogen extrusion are higher than those for the migratory insertion step and follow the same trend. For 2,2'-bipy, the activation barriers are even lower than those for the diphosphine ligands.

These results do not fit with what was observed experimentally. The efficiency in the formation of the migratory insertion products, *i.e.* dppe > dppp > dppb > bipy; follows the opposite trend to that expected from the barriers in Table 6.2. Therefore, we decided to explore other steps that are also involved in the reaction, *i.e.* the coordination of the diazoalkane to the palladium center.

Two different pathways for the coordination of diazoalkane **30** were computed. i) An associative substitution, where the transition state proposed is a pentacoordinated trigonal-bipyramidal one. ii) A dissociative pathway, where the labile acetonitrile goes

out of the coordination sphere of palladium affording a three-coordinated T-shaped intermediate.

For the dppe derivative **29a**, the complete profile is shown in Figure 6.11. Comparable energetic barriers were obtained in the associative pathway when diazoalkane coordinates to palladium acting as a κ^1 -N donor (**TS-29a-IIN**, 10.5 kcal mol⁻¹) or as a κ^1 -C donor (**TS-29a-IIC**, 11.0 kcal mol⁻¹). On the other hand, a dissociative pathway, where the labile acetonitrile goes out of the coordination sphere affording a three-coordinated T-shaped intermediate **I6** can be proposed. The acetonitrile dissociation has a low energy cost (9.2 kcal mol⁻¹) to give a rather unstable intermediate **I6** (10.9 kcal mol⁻¹). We were unable to locate the transition state for the direct diazo coordination in a κ^1 -C fashion to the three-coordinated intermediate **I6** due to the high stabilization afforded by the coordination of the double bond of the diazo compound (**I7**). DFT-scanning shows that **30** approaches the vacant coordination site in **I6** with a barrierless process (Figure 6.12), affording an intermediate with the olefin coordinated (**I7**).²¹⁷ From this intermediate **I7** the rearrangement to reach a κ^1 -C coordination mode of the diazoalkane is estimated in 11.2 kcal mol⁻¹, which is an accessible energy too.

With these values, the rate-determining step for the reaction of **29a** and the diazoalkane **30** is the nitrogen extrusion (14.1 kcal mol⁻¹), showcasing that all the elementary steps are feasible at low temperature, as it has proven experimentally (Chapter 5).

²¹⁷ A DFT scanning calculates the energies of different structures (partial optimization) as a parameter is varied, in this case the C1-Pd distance (C1 corresponds to the carbon bound to the C1-N₂ functional group of diazoalkane). In this way, plausible intermediates (*minima*) and possible transition states (*maxima*) can be located.

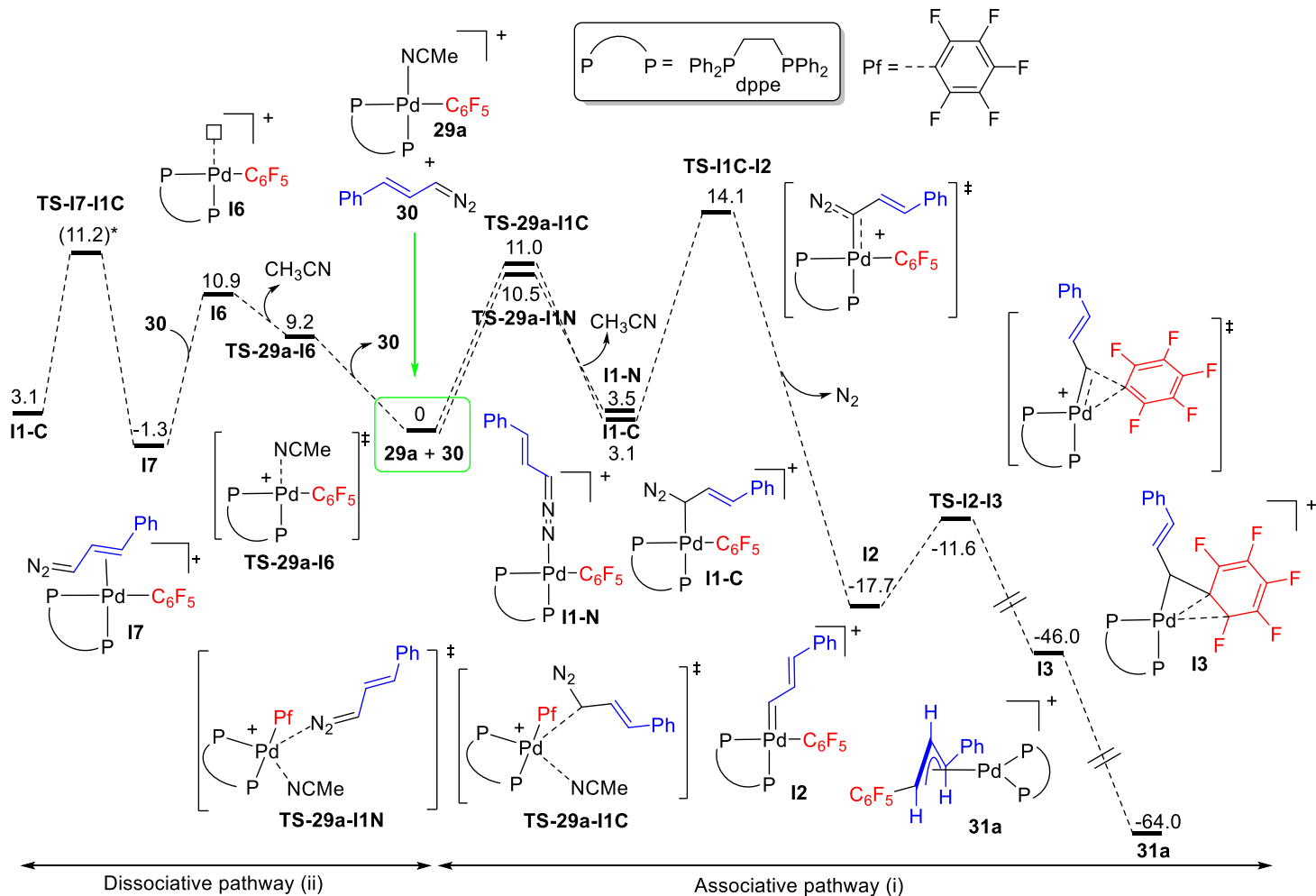


Figure 6.11 Gibbs energy profile for the reaction of complex **29a** with **30** to give the migratory insertion complex **31a**. Energies in kcal mol⁻¹. Energy given with (*) was estimated from the corresponding scanning depicted in Figure 6.12.

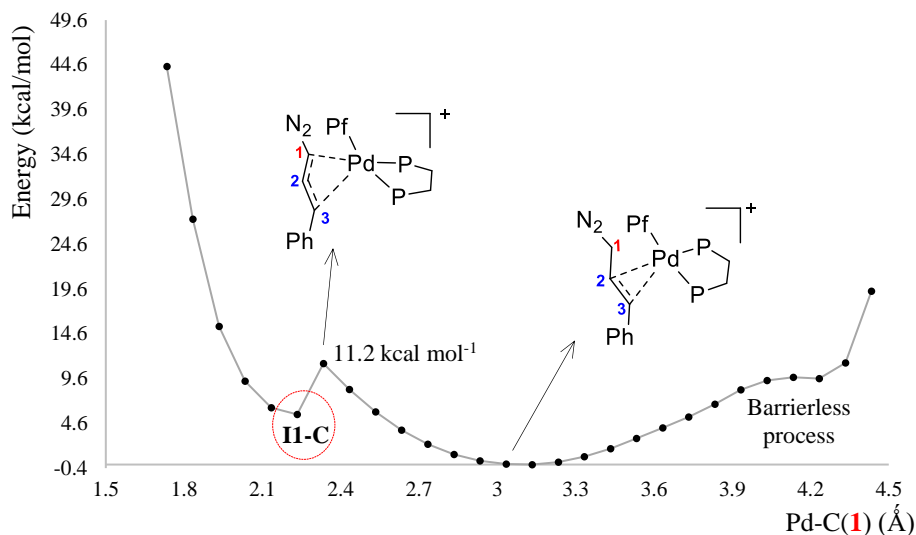


Figure 6.12 Scanning energy profile in the coordination of diazo compound **30** by the κ^1 -C to the three-coordinated intermediate **16**. Pf = C₆F₅.

In the case of the dppp-system, Scheme 6.5, **b**) and Figure 6.5 show that the formation of the migratory insertion product **46** is not complete when the reaction was carried out with a Pd:**30** = 1:1 mol ratio. However, the addition of another portion of diazoalkane **30** on the same sample provide increased conversion of **46**. To test the diazoalkane concentration dependence, three separate reactions with the same initial concentration of the solvento acetonitrile complex **44** ([**44**] = 28.4 mM) were performed with different Pd:**30** mol ratios. Figure 6.13 shows the formation of **46** when diazoalkane **30** was added in a 1, 2 and 3 mol ratio with respect to palladium after 5 min at room temperature.²¹⁸ The values depicted in the plot show a heavy dependence of the reaction rate upon diazoalkane concentration and this allows us to rule out the dissociative pathway in the modelled energy profile for the dppp-system.

²¹⁸ Diazoalkane **30** is synthesized as a CH₂Cl₂ solution with a concentration of 56 mM.

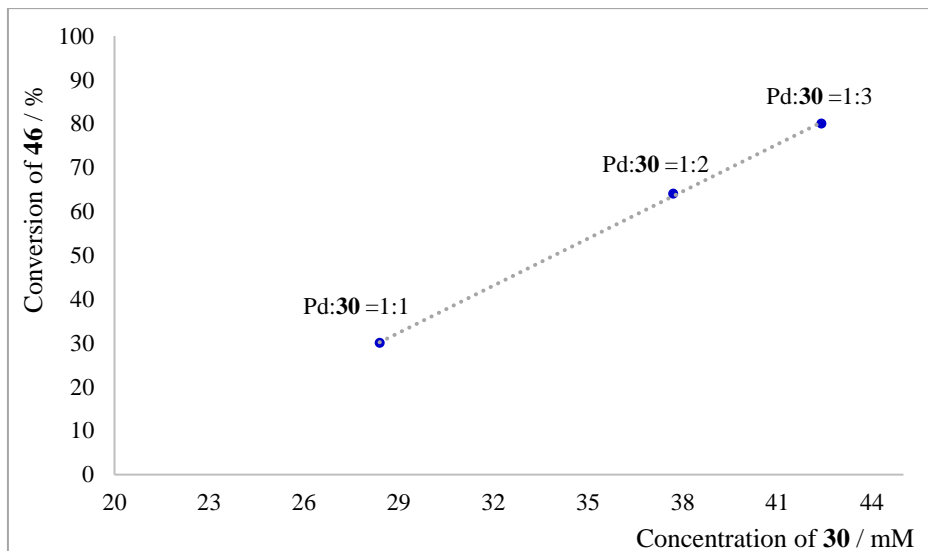


Figure 6.13 Plot of conversion vs. concentration for the reaction of complex **44** with **30**.

The analysis of the energy profile for the reaction of the dppp derivative **44** and diazoalkane **30** shows significant differences in comparison to the energy profile for the dppe analogue (Figure 6.14). The associative pathway to afford diazoalkane intermediates **I8-C** or **I8-N** through a pentacoordinated intermediate leads to TSs quite different in energy, being the one for the coordination in a $\kappa^1\text{-N}$ mode more favorable. This difference can be explained since the sterically less crowded terminal nitrogen can coordinate more easily to the palladium center than the $\kappa^1\text{-C}$. However, the exact TS for the $\kappa^1\text{-C}$ coordination could not be located. An estimation of the energy of this TS *via* a scanning calculation shows an accessible **TS-44-I8C** ($\sim 17.6 \text{ kcal mol}^{-1}$ Figure 6.15). From **I8-C**, the barriers for nitrogen extrusion and the subsequent migratory insertion to afford the η^3 -allylic complex **46** are lower than for the dppe system.

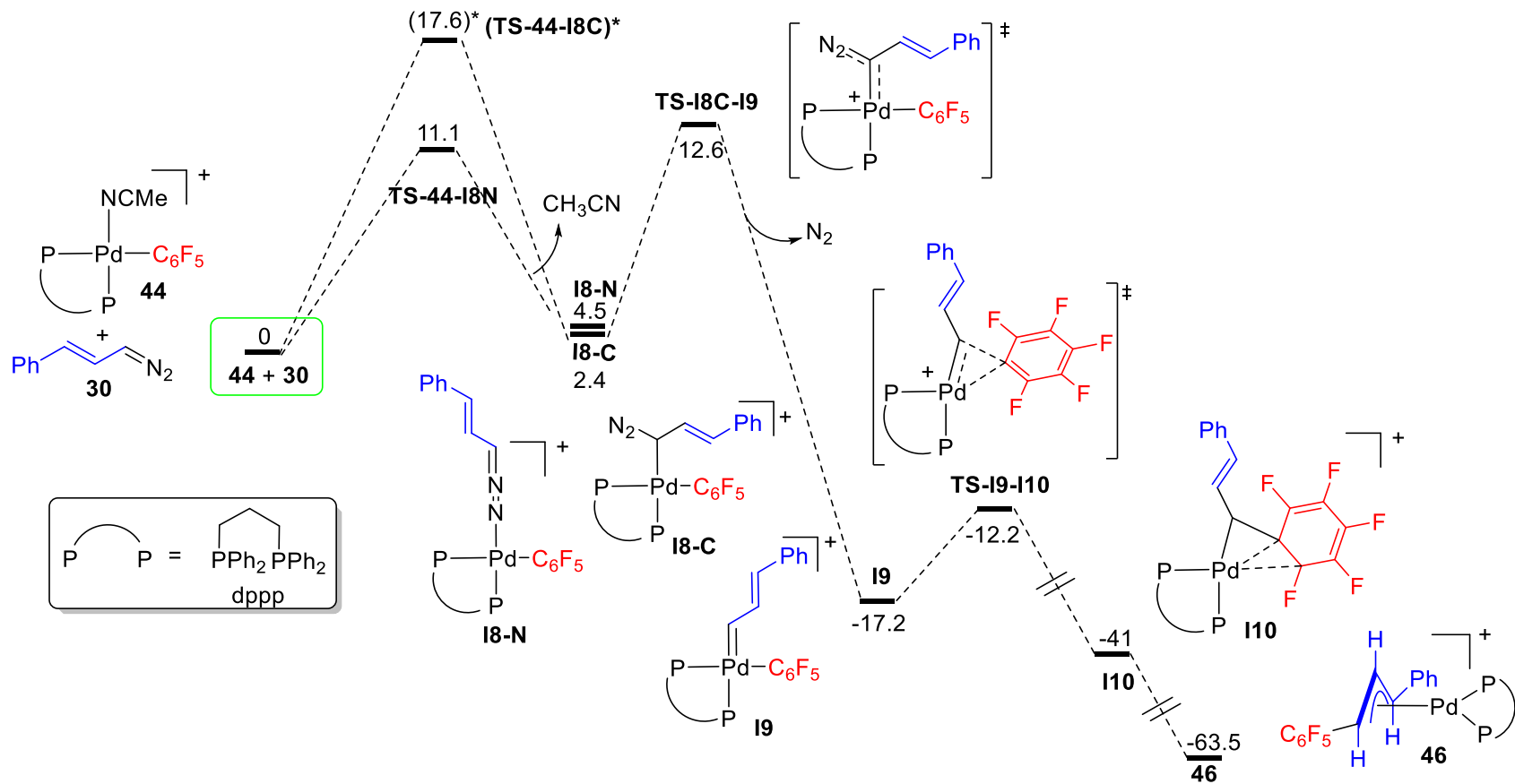


Figure 6.14 Gibbs energy profile for the reaction of complex **44** and the diazo compound **30** to give the migratory insertion complex **46**. Energies in kcal mol⁻¹. Energy given with (*) is estimated from the corresponding scanning depicted in Figure 6.15.

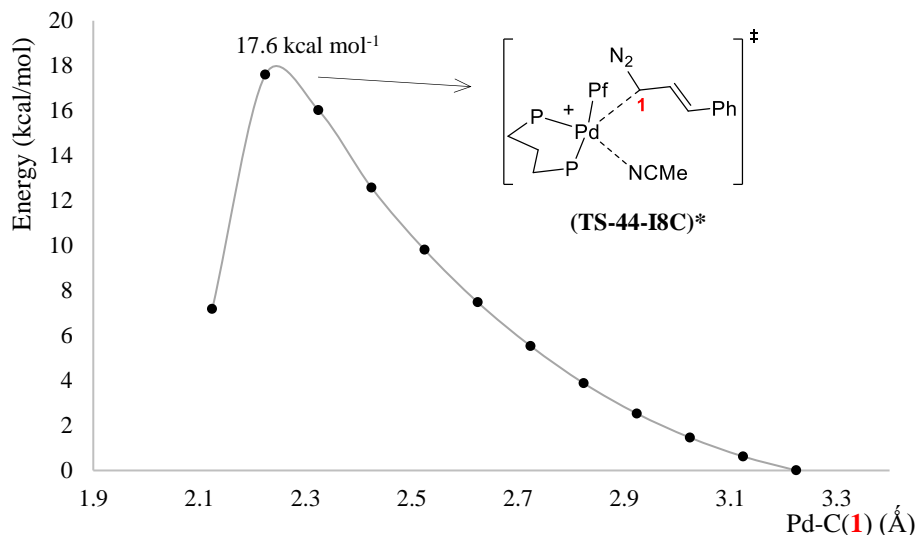


Figure 6.15 Scanning energy profile in the coordination of diazo compound **30** by the κ^1 -C to the solvento complex **44**. Pf = C₆F₅.

The reaction of diazoalkane **30** with the bipy complex **45** was also explored by DFT calculations in an attempt to give a reasonable answer to the different behavior observed experimentally and the formation of the [Pd(5-Ph-pzH)(bipy)(C₆F₅)_x] complexes. As it was discussed above, the energy barriers for nitrogen extrusion and migratory insertion are the lowest found, so these steps are not responsible for not observing the aryl-carbene coupling products (see Table 6.2 and Scheme 6.11).

The two possible pathways in which diazoalkane **30** can replace the labile acetonitrile in the cationic complex **45** were calculated. Figure 6.16 shows the profile for both pathways. Surprisingly, the associative pathway for complex **45** shows the decooordination of a bipyridine *N*-donor ring rather than acetonitrile when diazoalkane **30** approaches in a κ^1 -C fashion, a process with a barrier of 18.8 kcal mol⁻¹ (**TS-45-I11C**). The resulting intermediate **I11C** is not very stable and it undergoes nitrogen extrusion *via* a TS at 17.5 kcal mol⁻¹ to afford the Pd-carbene intermediate **I12**.

The dissociation of the acetonitrile from complex **45** to generate a three-coordinated intermediate **I13** has an energy barrier of 17.3 kcal mol⁻¹. When diazoalkane **30** approaches **I13** the coordination of the double bond is highly favored, the same behaviour observed for the diphosphine complexes. The rearrangement of **I14** to the κ^1 -C diazo compound **I15-C** has a relatively high barrier (TS close to 16.7 kcal mol⁻¹). From **I15-C** the subsequent N₂ extrusion is more facile than that found in the associative pathway. Overall, the dissociative pathway is preferred by 1.5 kcal mol⁻¹

(activation energies 18.8 kcal mol⁻¹ vs. 17.3 kcal mol⁻¹ for the associative and dissociative pathways respectively).

In the course of the reaction, the competitive 1,5-cycloaddition reaction of diazoalkane **30** to give 5-Ph-pzH occurs. The monitoring of the decomposition of free diazoalkane **30** shows a half-life of $t_{1/2} \approx 13$ min (see Figure 5.20, *Chapter 5*). Once it is formed, the coordination of 5-Ph-pzH to the three-coordinated intermediate **I13** is very fast (barrierless, Figures 6.17) while the coordination of diazoalkane **30** in a κ^1 -C mode, a necessary intermediate of the carbene-aryl coupling, always goes through an intermediate [Pd(olefin)]⁺ **I14** and an energy demanding rearrangement (**TS-I14-I15C**, Figure 6.18). The fast 5-Ph-pzH coordination along with the higher thermodynamic stability of complex **52-a** explains the experimental result observed.

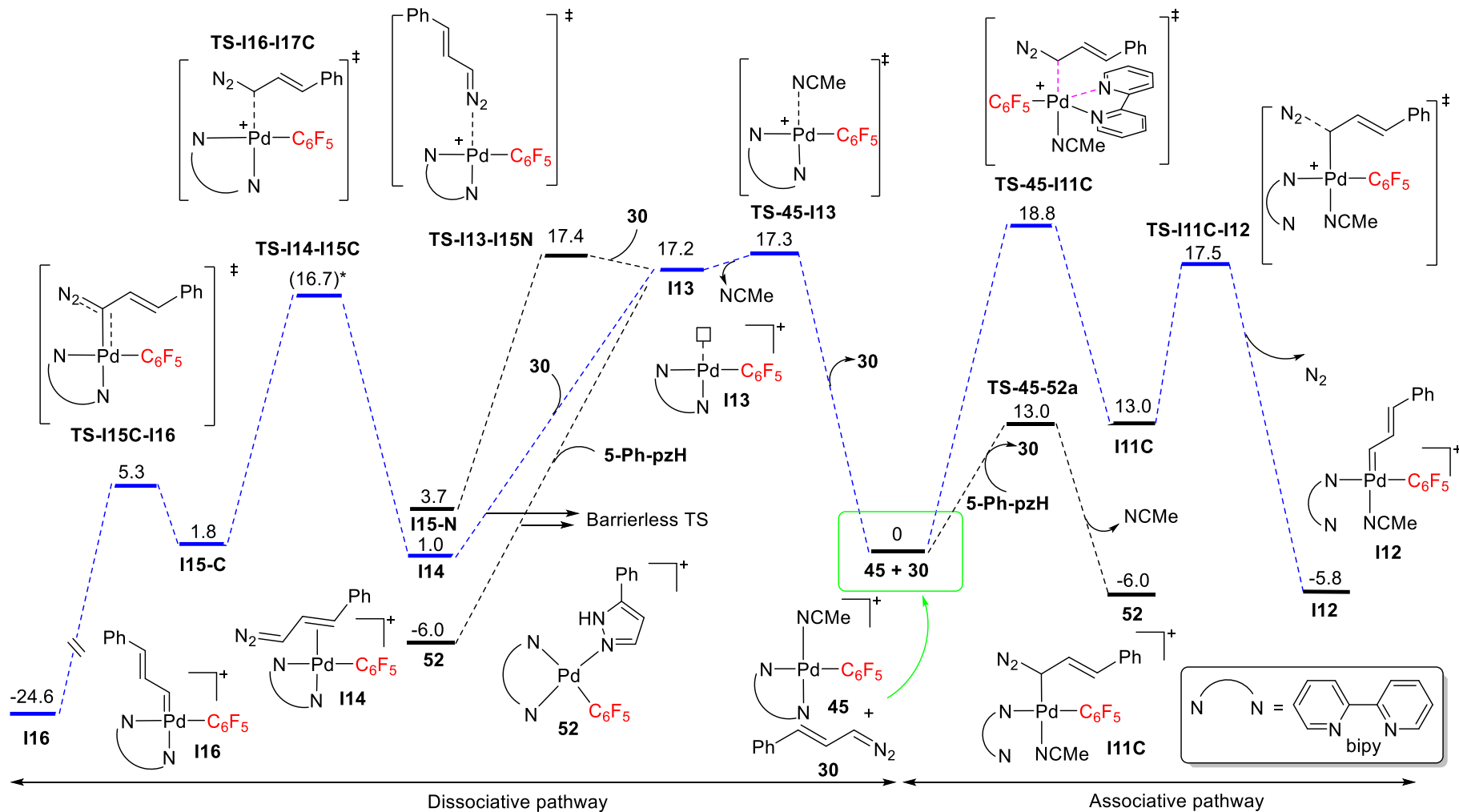


Figure 6.16 Gibbs energy profile for the reaction of complex **45** and the diazo compound **30**. Energies in kcal mol⁻¹. Energy given with (*) was estimated from the corresponding scanning depicted in Figure 6.18.

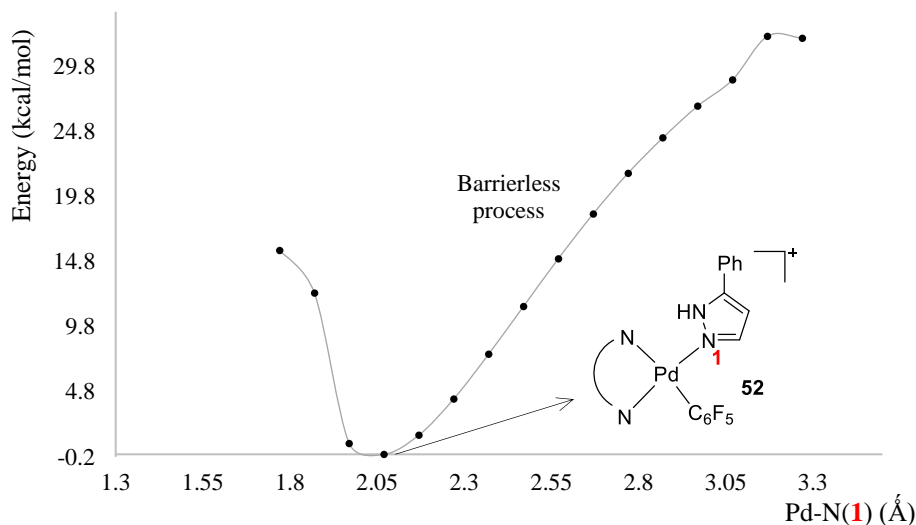


Figure 6.17 Scanning energy profile for the coordination of 5-Ph-pzH to the three-coordinated **I13** intermediate to give complex **52**.

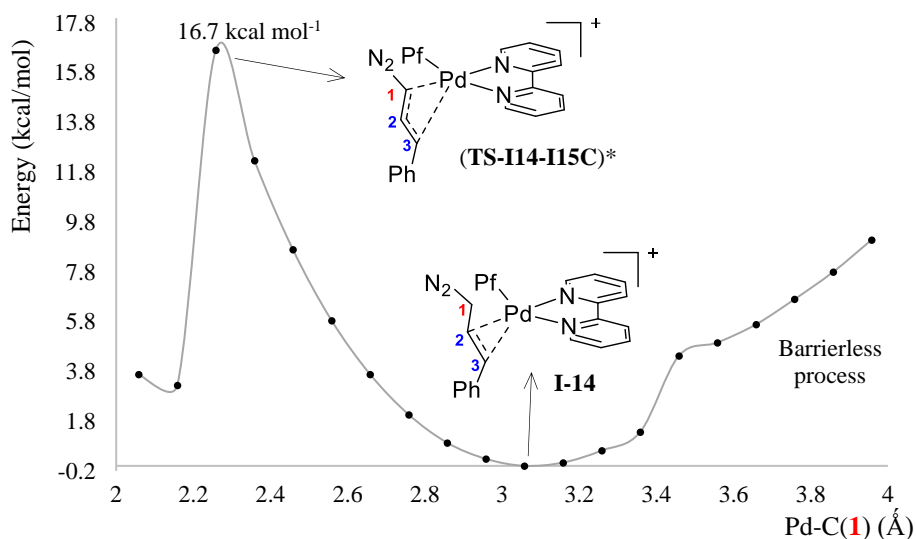
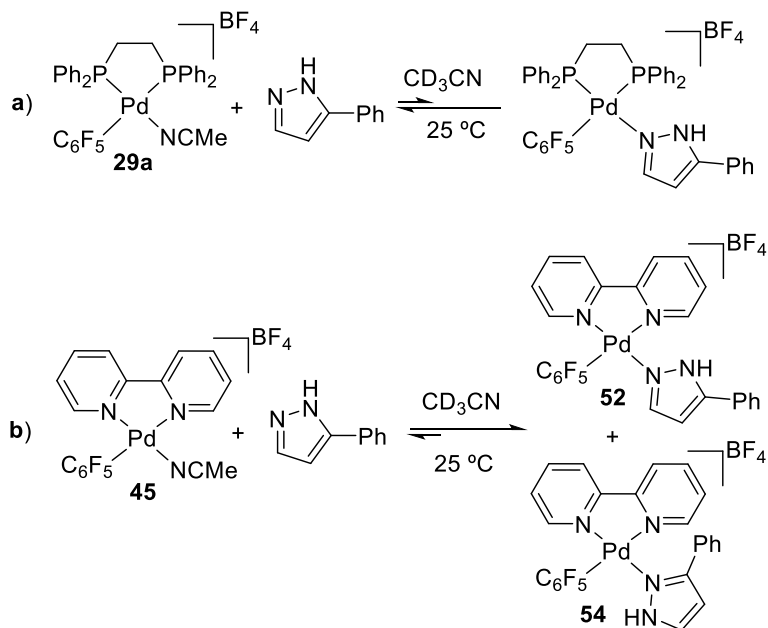


Figure 6.18 Scanning energy profile for the coordination of diazo compound **30** in the κ^1 -C mode to the three-coordinated **I13** intermediate. Pf = C₆F₅.

In the same line, an equimolar amount of 5-Ph-pzH was mixed with the dppe complex **29a**. Only a slight broadening of the signals were observed by ¹⁹F and ¹H NMR which indicate a dynamic equilibrium in solution, shifted to the starting complex **29a**. The bulkier dppe ligand hampers the coordination of 5-Ph-pzH to afford a plausible [Pd(5-Ph-pzH)C₆F₅(dppe)]BF₄ complex. In contrast the reaction of 5-Ph-pzH with the bipy derivative **45** leads to the pyrazole complexes **52** and **54** (Scheme 6.12 and Figures 6.19 and 6.20).



Scheme 6.12 Reaction of solvento complexes **29a** and **45** with an equimolar amount of 5-Ph-pzH.

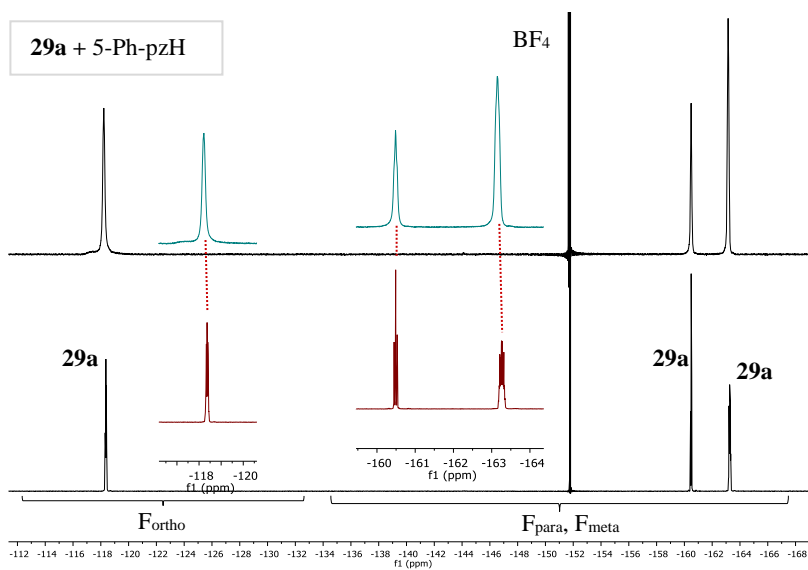


Figure 6.19 ^{19}F NMR (470.17 MHz, CD_3CN) of reaction shown in Scheme 6.12, a).

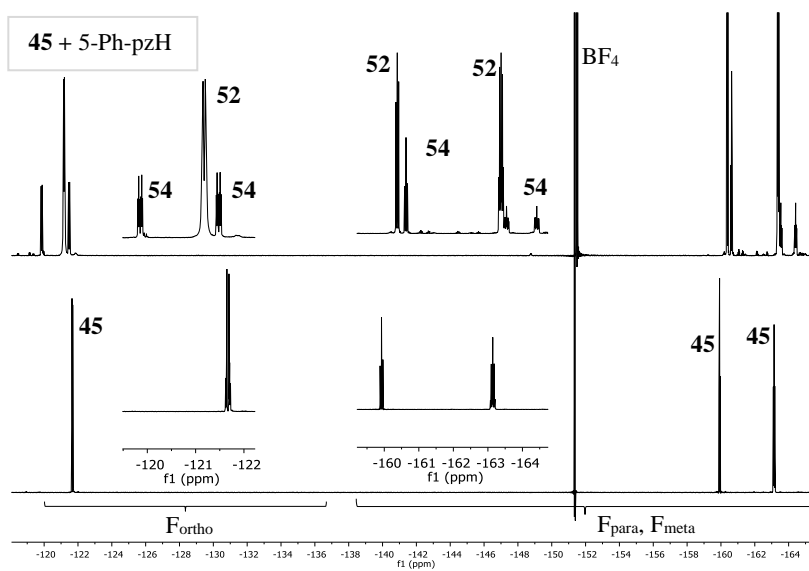


Figure 6.20 ^{19}F NMR (470.17 MHz, CD_3CN) of reaction shown in Scheme 6.12, **b**).

6.3 CONCLUSIONS

The experimental trend for the formation of carbene-aryl coupling products in the reaction of the solvento complexes $[\text{Pd}(\text{C}_6\text{F}_5)(\text{L-L})(\text{NCMe})]\text{BF}_4$ with diazoalkanes for different ancillary diphosphine ligands is: $\text{L-L} = \text{dppe} > \text{dppp} \gg \text{dppb}$. As the electronic features have been maintained with the same substituents on the phosphorus atom, the observed differences in the formation of the migratory insertion organometallic complexes are attributed primarily to the ligand backbone. DFT calculations show that the trend in energy barriers for nitrogen extrusion and migratory insertion do not mirror the experimental outcome, since the bulkier phosphines show lower reaction barriers. The experimental differences can be explained considering the rates of coordination of the diazoalkane to palladium. It has been found that the coordination of the diazoalkane **30** to the palladium complex bearing dppe ligand has a low activation energy, similar for both dissociative and associative pathways, and the nitrogen extrusion in a $\kappa^1\text{-C}$ coordinated diazoalkane is the rate limiting step of the reaction. In contrast, the dppp-system presents a higher activation barrier for the coordination of the diazoalkane, which occurs *via* an associative pathway (about 6.6 kcal mol⁻¹ higher in comparison to the dppe-system). Therefore the coordination of the diazoalkane is controlling the overall reaction rate for large bite angle phosphines.

The reaction of *trans*- $[\text{Pd}(\text{C}_6\text{F}_5)(\text{NCMe})(\text{PPh}_3)_2]\text{BF}_4$ with diazoalkanes does not lead to carbene-aryl coupling. This fact clearly evidences that the *trans* arrangement hampers the migratory insertion process and the required isomerization to a *cis* complex is slower than the decomposition pathways for the diazoalkane and the *trans*-palladium carbene species.

For the solvento acetonitrile complex bearing bipyridine as auxiliary ligand, only palladium complexes containing coordinated 5-Ph-pzH or 5-Ph-pz were detected experimentally. DFT calculations show that the coordination of the diazoalkane is again controlling the reaction rate. The formation of 5-Ph-pzH by decomposition of diazoalkane **30** followed by coordination of the 5-Ph-pzH to the palladium center is favoured *vs.* the $\kappa^1\text{-C}$ diazoalkane coordination needed for the subsequent nitrogen extrusion and migratory insertion steps, which are fast for this ligand.

6.4 EXPERIMENTAL PART

6.4.1 General considerations

^1H , $^{13}\text{C}\{^1\text{H}\}$ ^{31}P and ^{19}F NMR spectra were recorded on an Agilent MR-500 spectrometer equipped with variable-temperature probes at the *Laboratorio de Técnicas Instrumentales* (LTI) of the UVA. Chemical shifts (in δ units, ppm) were referenced to SiMe_4 (^1H and ^{13}C) and CFCl_3 (^{19}F) and H_3PO_4 (85%, ^{31}P). The spectral data were recorded at 298 K unless otherwise noted. The temperature for the NMR probe was calibrated with a methanol standard (low temperature).¹⁹³ Homonuclear (^1H -COSY) and heteronuclear (^1H - ^{13}C HSQC and HMBC) experiments were used to help with the signal assignments. Elemental analyses were carried out in a Carlo Erba 1108 microanalyser (at the Vigo University, Spain). Infrared spectra were recorded (in the range of 4000-200 cm^{-1}) on a Perkin-Elmer FT-IR Spectrum Frontier with an ATR diamond accessory. All stoichiometric reactions were conducted under N_2 atmosphere. Solvents were dried using a solvent purification system SPS PS-MD-5 (ether, hexane, THF and CH_2Cl_2) or distilled from appropriate drying agents under nitrogen prior to use and stored over 3 Å or 4 Å molecular sieves (acetonitrile and acetonitrile- d_3). All commercial reagents and solvents were used as received unless otherwise indicated. $(\text{NBu}_4)_2[\text{Pd}(\mu\text{-Br}_2)\text{Br}_2(\text{C}_6\text{F}_5)_2]$,⁸⁶ $[\text{PdBr}(\text{C}_6\text{F}_5)(\text{bipy})]^{86}$, and $[\text{PdBr}(\text{C}_6\text{F}_5)(\text{PPh}_3)_2]^{86}$ were prepared according to the literature methods.

6.4.2 Synthesis of Palladium complexes

$[\text{PdBr}(\text{C}_6\text{F}_5)(\text{dppp})] \text{ (40)}^{219}$

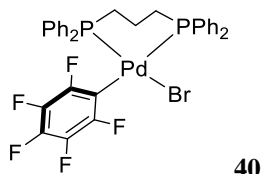
1,3-Bis(diphenylphosphino)propane (dppp) (110.87 mg, 0.268 mmol) was added to a solution of $(\text{NBu}_4)_2[\text{Pd}(\mu\text{-Br}_2)\text{Br}_2(\text{C}_6\text{F}_5)_2]$ (176.5 mg, 0.130 mmol) in acetone (30 mL). The mixture was stirred at room temperature for 1 h. During this time the orange solution became pale-yellow. The solvent was evaporated to dryness and the yellow oil was triturated with cold EtOH until the formation of a pale-yellow solid that was filtered, washed with cold EtOH and air-dried. Yield: 165 mg (83 %).

^1H NMR (499.73 MHz, δ , CDCl_3): 7.78-7.73 (m, 4H, H^{arom}), 7.50-7.42 (m, 6H, H^{arom}), 7.41-7.33 (m, 6H, H^{arom}), 7.17 (td, $J = 5.5$ Hz, 2.4 Hz, 4H, H^{arom}), 2.66 (m, 2H, CH_2), 2.33 (m, 2H, CH_2), 2.03 (m, 2H, CH_2). $^{13}\text{C}\{^1\text{H}\}$ NMR (125.67 MHz, δ , CDCl_3): 138.3 (d, $J_{\text{C-P}} = 11.2$ Hz, C^{arom}), 133.4 (d, $J_{\text{C-P}} = 10.6$ Hz, C^{arom}), 132.7 (d, $J_{\text{C-P}} = 11.0$ Hz, C^{arom}), 131.1 (d, $J_{\text{C-P}} = 2.6$ Hz, C^{para}), 130.8 (d, $J_{\text{C-P}} = 2.5$ Hz, C^{para}), 130.4 (d, $J_{\text{C-P}} = 45.7$ Hz, C^{ipso}), 130.1 (d, $J_{\text{C-P}} = 54.7$ Hz, C^{ipso}), 128.7 (d, $J_{\text{C-P}} = 10.3$ Hz, C^{arom}), 25.8 (dd, $J = 29.2$, 7.3 Hz, CH_2), 25.4 (dd, $J = 25.2$, 7.4 Hz, CH_2), 18.9 (s, CH_2). * ^{19}F NMR (470.17 MHz,

²¹⁹ For synthesis where X = Cl or I see: a) Gaumont, A.-C.; M. Brown, J.; B. Hursthouse, M.; J. Coles, S. *Chem. Commun.* **1999**, 1, 63–64. b) Cullinane, C.; Deacon, G. B.; Drago, P. R.; Erven, A. P.; Junk, P. C.; Luu, J.; Meyer, G.; Schmitz, S.; Ott, I.; Schur, J.; Webster, L. K.; Klein, A. *Dalton Trans.* **2018**, 47, 1918–1932.

δ , CDCl_3): -116.92 (m, 2F, F_{ortho}), -161.77 (t, $J = 20.1$ Hz, 1F, F_{para}), -162.85 (m, 2F, F_{meta}). $^{31}\text{P}\{^1\text{H}\}$ NMR (202.31 MHz, δ , CDCl_3): 13.60 (dt, $J = 42.4$ Hz, 6.4 Hz, 1P), -5.82 (m, 1P). Anal. Calcd. for $\text{C}_{33}\text{H}_{26}\text{BrF}_5\text{P}_2\text{Pd}$: C, 51.46 %; H, 3.42 %. Found: C, 51.60 %; H, 3.26 %.

*The ^{13}C signals for the C_6F_5 group, heavily coupled to ^{19}F , could not be observed.

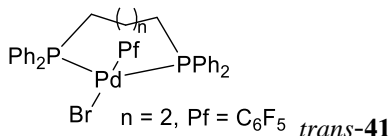


40

trans-[PdBr(C_6F_5)(dppb)] (**41**)

1,4-Bis(diphenylphosphino)butane (dppb) (111.55 mg, 0.256 mmol) was added to a solution of $(\text{NBu}_4)_2[\text{Pd}(\mu\text{-Br}_2)\text{Br}_2(\text{C}_6\text{F}_5)_2]$ (173.0 mg, 0.128 mmol) in acetone (30 mL). The mixture was stirred at room temperature for 1 h. During this time the orange solution became pale-yellow. The solvent was evaporated to dryness and the yellow oil was triturated with cold EtOH until the formation of a pale-yellow solid that was filtered, washed with cold EtOH and air-dried. Yield: 175 mg (88 %).

trans-**41** ^1H NMR (499.72 MHz, δ , CDCl_3): 7.43 (m, 9H, H^{arom}), 7.27 (t, $J = 7.2$ Hz, 4H, H^{arom}), 7.21 (m, 7H, H^{arom}), 2.63 (m, 4H, CH_2), 2.01 (m, 4H, CH_2). $^{13}\text{C}\{^1\text{H}\}$ NMR (125.67 MHz, δ , CDCl_3): 132.9 (br, C^{arom}), 131.4 (d, $J^{\text{C-P}} = 47.1$ Hz, C^{arom}), 130.2 (br, C^{arom}), 128.1 (br, C^{arom}), 27.5 (m, 4C, CH_2). ^{19}F NMR (470.17 MHz, δ , CDCl_3): -116.19 (m, 2F, F_{ortho}), -161.59 (t, $J = 19.7$ Hz, 1F, F_{para}), -162.22 (m, 2F, F_{meta}). $^{31}\text{P}\{^1\text{H}\}$ NMR (202.31 MHz, δ , CDCl_3): 18.92 (s, 2P). Anal. Calcd. for $\text{C}_{34}\text{H}_{26}\text{BrF}_5\text{P}_2\text{Pd}$: C, 52.36 %; H, 3.62 %. Found: C, 52.56 %; H, 3.68 %.



When a solution of complex *trans*-**44** was kept at room temperature for 48 h in CDCl_3 a mixture of the *cis* and *trans* (1:0.8) was formed.

cis-**41**: ^{19}F NMR (470.17 MHz, δ , CDCl_3): -117.15 (m, 2F, F_{ortho}), -161.99 (t, $J = 19.9$ Hz, 1F, F_{para}), -162.83 (m, 2F, F_{meta}). $^{31}\text{P}\{^1\text{H}\}$ NMR (202.31 MHz, δ , CDCl_3): 40.72 (d, $J = 32.5$ Hz, 1P), -1.40 (m, 1P).

[Pd(C_6F_5)(dppb)(NCMe)](BF_4) (**43**)

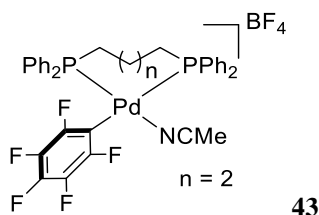
[PdBr(C_6F_5)(dppb)] (52.0 mg, 0.066 mmol) and AgBF_4 (13.0 mg, 0.066 mmol) were mixed in dry MeCN (0.6 mL) and stirred for 15 min at room temperature under nitrogen. The suspension was filtered through Kieselghur to remove the AgBr and the resulting colorless solution was characterized by NMR. The resulting complex is a mixture of *cis/trans* isomers (0.8:1).

cis-**43** + *trans*-**43**: ^1H NMR (499.73 MHz, δ , $\text{CH}_3\text{CN}/(\text{CD}_3)_2\text{SO}$ capillary): 7.92 (m, 1H, H^{arom}), 7.85 (m, 3H, H^{arom}), 7.80 (m, 2H, H^{arom}), 7.77-7.69 (m, 10H, H^{arom}), 7.66 (m, 2H, H^{arom}), 7.57 (td = $J = 7.8, 2.9$ Hz, 2H, H^{arom}).*

cis-**43**: ^{19}F NMR (470.17 MHz, δ , $\text{CH}_3\text{CN}, (\text{CD}_3)_2\text{SO}$ capillary): -118.58 (m 2F, F_{ortho}), -151.11 (BF_4), -161.04 (t, $J = 19.2$ Hz, 1F, F_{para}), -162.78 (m, 2F, F_{meta}). $^{31}\text{P}\{^1\text{H}\}$ NMR (202.31, MHz, δ , $\text{CH}_3\text{CN}, (\text{CD}_3)_2\text{SO}$ capillary): 40.60 (dt, $J = 30.8, 7.2$ Hz, 1P), 7.26 (m, 1P).

trans-**43**: ^{19}F NMR (470.17 MHz, δ , $\text{CH}_3\text{CN}, (\text{CD}_3)_2\text{SO}$ capillary): -116.85 (m 2F, F_{ortho}), -151.11 (BF_4), -160.18 (t, $J = 19.6$ Hz, 1F, F_{para}), -161.98 (m, 2F, F_{meta}). $^{31}\text{P}\{^1\text{H}\}$ NMR (202.31, MHz, δ , $\text{CH}_3\text{CN}, (\text{CD}_3)_2\text{SO}$ capillary): 17.60 (s).

* The CH_2 signals of the dppb ligand are overlapped with the NCCH_3 signal.

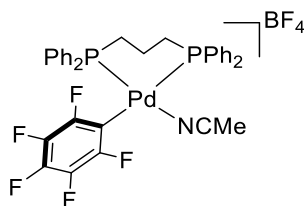


[Pd(C₆F₅)(dppp)(NCMe)](BF₄) (**44**)

[PdBr(C₆F₅)(dppp)] (13.4 mg, 0.017 mmol) and AgBF₄ (3.4 mg, 0.017 mmol) were mixed in dry MeCN (0.6 mL) and stirred for 15 min at room temperature under nitrogen. The suspension was filtered through Kieselghur to remove the AgBr and the resulting colorless solution was characterized by NMR.

^1H NMR (499.73 MHz, δ , $\text{CH}_3\text{CN}/(\text{CD}_3)_2\text{SO}$ capillary): 7.94-7.83 (m, 10H, H^{arom}), 7.71-7.64 (m, 6H, H^{arom}), 7.52 (m, 4H, H^{arom}), 3.18 (m, 2H, CH_2), 2.98 (m, 2H, $\text{C}'\text{H}_2$).* ^{19}F NMR (470.17 MHz, δ , $\text{CH}_3\text{CN}, (\text{CD}_3)_2\text{SO}$ capillary): -117.87 (m 2F, F_{ortho}), -151.42 (BF_4), -161.10 (t, $J = 19.2$ Hz, 1F, F_{para}), -162.99 (m, 2F, F_{meta}). $^{31}\text{P}\{^1\text{H}\}$ NMR (202.31, MHz, δ , $\text{CH}_3\text{CN}, (\text{CD}_3)_2\text{SO}$ capillary): 16.50 (dt, $J = 39.7, 7.2$ Hz, 1P), -4.39 (m, 1P).

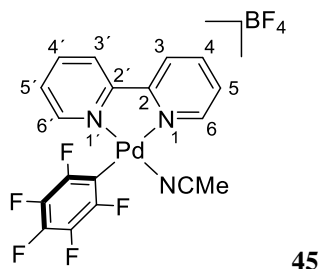
* One CH_2 from dppp is overlapped with the NCCH_3 signal.



[Pd(C₆F₅)(bipy)(NCMe)](BF₄) (45)²²⁰

[PdBr(C₆F₅)(bipy)] (9.16 mg, 0.018 mmol) and AgBF₄ (3.5 mg, 0.018 mmol) were mixed in dry MeCN (0.6 mL) and stirred for 15 min at room temperature under nitrogen. The suspension was filtered through Kieselghur to remove the AgBr and the resulting colorless solution was characterized by NMR.

¹H NMR (499.73 MHz, δ, CH₃CN/(CD₃)₂SO capillary): 8.95 (d, J = 5.4 Hz, 1H, H^{6'}), 8.66-8.59 (m, 3H, H³, H^{3'}, H^{4'}), 8.53 (td, J = 7.8, 1.5 Hz, 1H, H⁴), 8.16 (d, J = 5.7 Hz, 1H, H⁶), 8.08 (m, 1H, H^{5'}), 7.76 (m, 1H, H⁵). ¹⁹F NMR (470.17 MHz, δ, CH₃CN,(CD₃)₂SO capillary): -121.67 (m 2F, F_{ortho}), -151.38 (BF₄), -159.92 (t, J = 19.0 Hz, 1F, F_{para}), -163.14 (m, 2F, F_{meta}).

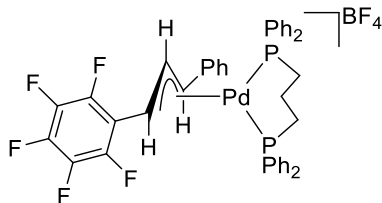
**45****[Pd(dppp)(η³-Ph-CH-CH-CH-C₆F₅)](BF₄) (46)**

[Pd(Br)(C₆F₅)(dppp)] (13.4 mg, 0.017 mmol) and AgBF₄ (3.4 mg, 0.017 mmol) were mixed in dry MeCN (0.6 mL) and stirred for 15 min at room temperature under nitrogen. The suspension was filtered through Kieselghur to remove the AgBr. Addition of a dichloromethane solution of the diazo compound N₂CH-CH=CHPh (2-fold molar amount in two portions, 87 μL, 0.4 M, total of 0.046 mmol) afforded an intense yellow solution, which was stirred at room temperature for 5 min. Then, the solution was characterized by NMR. The crude yield was determined by integration of the ¹⁹F NMR signals in the crude mixture, 83 %.

¹H NMR (499.73 MHz, δ, CH₃CN/(CD₃)₂SO capillary): 7.72-7.36 (m, 25H, H^{arom}), 6.86 (t, J = 12.7 Hz, 1H, H^{allyl1}), 5.36 (t, J = 11.2 Hz, 1H, H^{allyl2}), 4.87 (t, J = 11.2 Hz, 1H, H^{allyl3}).* ¹⁹F NMR (470.17 MHz, δ, CH₃CN, (CD₃)₂SO capillary): -141.99 (br, 2F, F_{ortho}), -151.53 (BF₄), -158.04 (t, J = 20.5 Hz, 1F, F_{para}), -164.00 (m, 2F, F_{meta}). ³¹P{¹H} NMR (202.31, MHz, δ, CH₃CN, (CD₃)₂SO capillary): AB system. ν_A: 8.50 (d, J = 83.2 Hz, 1P), ν_B: 7.06 (d, J = 83.2 Hz, 1P).

* The CH₂ signals of the dppp ligand are overlapped with the NCCH₃ signal.

²²⁰ López-Fernández, R.; Carrera, N.; Albéniz, A. C.; Espinet, P. *Organometallics* **2009**, *28*, 4996–5001.



46

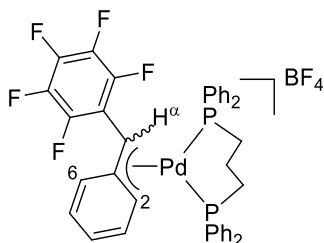
[Pd(dppp)(η^3 -Ph-CH-C₆F₅)](BF₄) (47)

[PdBr(C₆F₅)(dppp)] (17.7 mg, 0.023 mmol) and AgBF₄ (4.5 mg, 0.023 mmol) were mixed in dry MeCN (0.6 mL) and stirred for 15 min at room temperature under nitrogen. The suspension was filtered through Kieselghur to remove the AgBr. The addition of a dichloromethane solution of the diazo compound N₂CHPh (0.0345 mmol, 128 μ L, 0.27 M) afforded an intense yellow solution, which was stirred at room temperature for 5 min. Then, the solution was characterized by NMR. *syn:anti* (89:11), The crude yield was determined by integration of the ¹⁹F NMR signals in the crude mixture, 85 %.

syn-47 ¹H NMR (499.73 MHz, δ , CH₃CN/(CD₃)₂SO capillary): 6.97 (m, 2H, H², H⁶), 4.28 (d, J_{H-P} = 4.28 Hz, 1H, H ^{α}).* ¹⁹F NMR (470.17 MHz, δ , CH₃CN, (CD₃)₂SO capillary): -137.02 (m 2F, F_{ortho}), -151.72 (BF₄), -158.84 (m, 1F, F_{para}), -164.04 (m, 2F, F_{meta}). ³¹P{¹H} NMR (202.31, MHz, δ , CH₃CN, (CD₃)₂SO capillary): 17.29 (dt, J = 81.2, 8.2 Hz, 1P), 4.94 (d, J = 81.2 Hz, 1P).

anti-47 ¹⁹F NMR (470.17 MHz, δ , CH₃CN, (CD₃)₂SO capillary): -140.16 (m 2F, F_{ortho}), -150.59 (m, 1F, F_{para}), -151.72 (BF₄), -162.87 (m, 2F, F_{meta}).

* It has not been possible to characterize the remaining signals.



47

[Pd(dppb)(η^3 -Ph-CH-CH-CH-C₆F₅)](BF₄) (48)

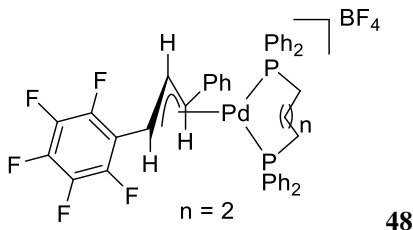
[PdBr(C₆F₅)(dppb)] (25.7 mg, 0.033 mmol) and AgBF₄ (6.4 mg, 0.033 mmol) were mixed in dry MeCN (0.6 mL) and stirred for 15 min at room temperature under nitrogen. The suspension was filtered through Kieselghur to remove the AgBr. Addition of a dichloromethane solution of the diazo compound N₂CH-CH=CHPh (0.033 mmol, 83 μ L, 0.4 M) afforded an intense yellow solution, which was stirred at room temperature for 5 min. Then, the solution was characterized by NMR. The crude yield was determined by integration of the ¹⁹F NMR signals in the crude mixture, 8 %.

¹H NMR (499.73 MHz, δ , CH₃CN/(CD₃)₂SO capillary): 6.59 (t, J = 12.6 Hz, 1H, H^{allyl}), 5.52 (t, J = 11.5 Hz, 1H, H^{allyl}), 4.91 (t, J = 11.5 Hz, 1H, H^{allyl}).* ¹⁹F NMR (470.17 MHz,

δ , CH₃CN, (CD₃)₂SO capillary): -140.31 (br, 1F, F_{ortho}), -143.12 (br, 1F, F_{ortho}), -151.64 (BF₄).[†]

[†] The F_{para} and F_{meta} as well as the ³¹P NMR signals have not been assigned due to the very low concentration of η^3 -allyl-complex in the reaction medium.

* It has not been possible to characterize the remaining signals.



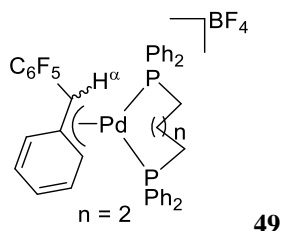
[Pd(dppb)(η^3 -Ph-CH-C₆F₅)](BF₄) (49)

[PdBr(C₆F₅)(dppb)] (52.0 mg, 0.066 mmol) and AgBF₄ (13.0 mg, 0.066 mmol) were mixed in dry MeCN (0.6 mL) and stirred for 15 min at room temperature under nitrogen. The suspension was filtered through Kieselgur to remove the AgBr. Addition of a dichloromethane solution of the diazo compound N₂CHPh (0.1 mmol, 366 μ L, 0.27 M, Pd:**32** = 1.5 mol ratio) afforded an intense yellow solution, which was stirred at room temperature for 5 min. Then, the solution was characterized by NMR. The crude yield was determined by integration of the ¹⁹F NMR signals in the crude mixture, 30 %.

syn-**49** ¹H NMR (499.73 MHz, δ , CH₃CN/(CD₃)₂SO capillary): 6.96 (m, 2H, H², H⁶), 4.17 (d, J = 11.9 Hz, 1H, H ^{α}). * ¹⁹F NMR (470.17 MHz, δ , CH₃CN,(CD₃)₂SO capillary): -137.02 (m 2F, F_{ortho}), -151.66 (BF₄), -158.02 (m, 1F, F_{para}), -163.94 (m, 2F, F_{meta}). ³¹P{¹H} NMR (202.31, MHz, δ , CH₃CN,(CD₃)₂SO capillary): 36.55 (dt, J = 64.0 Hz, 1P), 11.31 (d, J = 64.0 Hz, 1P).

anti-**49** ¹H NMR (499.73 MHz, δ , CH₃CN/(CD₃)₂SO capillary): 6.64 (m, 2H, H², H⁶), 4.72 (m, 1H, H ^{α}). * ¹⁹F NMR (470.17 MHz, δ , CH₃CN,(CD₃)₂SO capillary): -140.02 (m 2F, F_{ortho}), -151.14 (m, 1F, F_{para}), -151.66 (BF₄), -160.67 (m, 2F, F_{meta}). * ³¹P{¹H} NMR (202.31, MHz, δ , CH₃CN,(CD₃)₂SO capillary): 28.35 (d, J = 44.9 Hz, 1P), 14.95 (d, J = 44.9 Hz, 1P).

* Signals for the F_{meta} overlapped with the F_{para} of the *cis*-**43**. It has not been possible to characterize the remaining signals.

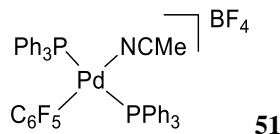


[Pd(C₆F₅)(NCCH₃)(PPh₃)₂](BF₄) (51)

Equimolar amounts of [PdBr(C₆F₅)(PPh₃)₂] (184.3 mg, 0.210 mmol) and AgBF₄ (41 mg, 0.210 mmol) were mixed in dried CH₃CN (10 mL) and stirred for 15 min at room temperature under nitrogen. The suspension was filtered through Kieselgur and the filtrate was evaporated to dryness. The resulting yellow oil was cracked with *n*-hexane until the formation of a pale-yellow solid that was filtered, washed with *n*-hexane and air-dried. Yield: 118 mg, (60 %).

¹H NMR (499.73 MHz, δ, CD₃CN): 7.62 (m, 6H, H_{para} PPh₃) 7.60-7.50 (m, 24H, H_{meta,ortho} PPh₃). ¹³C{¹H} NMR (125.67 MHz, δ, CD₃CN): 144.3 (m, ¹J_{C-F} = 230.5 Hz, C_{ortho}, C₆F₅), 138.2 (m, ¹J_{C-F} = 250 Hz, C_{para}, C₆F₅), 136.3 (m, ¹J_{C-F} = 248 Hz, C_{meta}, C₆F₅), 133.7 (t, J_{C-P} = 6.5 Hz, C_{ortho} PPh₃), 131.9 (C_{para} PPh₃), 129.2 (t, J_{C-P} = 5.3 Hz, C_{meta} PPh₃), 127.5 (t, J_{C-P} = 25.5 Hz, C_{ipso} PPh₃). ¹⁹F NMR (470.17 MHz, δ, CD₃CN): -118.40 (m, 2F, F_{ortho}), -151.70 (BF₄), -161.63 (tt, J = 19.0, 2.4 Hz, 1F, F_{para}), -162.34 (m, 2F, F_{meta}). ³¹P{¹H} NMR (202.29, MHz, δ, CD₃CN): 23.12 (td, J = 6.8, 2.2 Hz). IR (neat, cm⁻¹): C₆F₅: 1501, 1040, 959, 752, 690, CH₃CN: 2319, (BF₄): 1055. Anal. Calcd. for C₄₄H₃₃BF₉NP₂Pd: C, 57.08 %; H, 3.59 %; N, 1.51 %. Found: C, 56.68 %; H, 3.44 %; N, 1.40 %.

*The ¹³C signal for the C_{meta} (C₆F₅ group) is overlapped with other aromatic signals. C_{ipso} has not able to be observed.

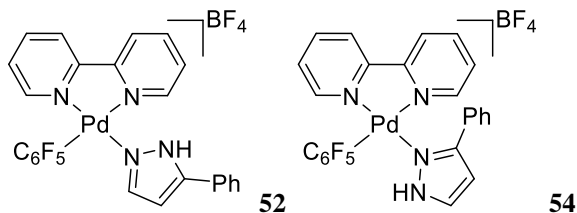
**[Pd(5-Ph-pzH)(C₆F₅)(bipy)](BF₄) (52 and 54)**

[PdBr(C₆F₅)(bipy)] (46.3 mg, 0.09 mmol) and AgBF₄ (17.7 mg, 0.09 mmol) were mixed in dry CD₃CN (0.6 mL) and stirred for 15 min at room temperature under nitrogen. The suspension was filtered through Kieselgur and 5-Ph-pzH (13.0 mg, 0.09 mmol) was added to the resulting colorless solution. The species formed in solution at room temperature were examined by ¹H and ¹⁹F NMR.

52 + 54: ¹H NMR (499.73 MHz, δ, CD₃CN): 12.85 (br, 1H, NH⁵²), 12.55 (br, 0.4H, NH⁵⁴), 8.40 (d, J = 7.9 Hz, 3H), 8.28 (t, J = 7.7 Hz, 3H), 8.09 (d, J = 2.9 Hz, 0.4H, H^{pz-54}), 8.04 (dd, J = 7.4, 3.4 Hz, 0.8H), 7.96 (d, J = 5.6 Hz, 1H), 7.91 (d, J = 2.3 Hz, 1H, H^{pz-52}), 7.90 (m, 0.4H), 7.74 (m, 2H), 7.69 (d, J = 5.3 Hz, 1H), 7.62 (m, 1.6H), 7.56-7.48 (m, 5H), 7.43 (m, 1H), 6.92 (d, J = 2.3, 1H, H^{pz-52}), 6.80 (d, J = 2.9 Hz, 0.4H, H^{pz-54}).

52: ¹⁹F NMR (470.17 MHz, δ, CD₃CN): -121.19 (m 2F, F_{ortho}), -151.53 (BF₄), -160.38 (t, J = 19.3 Hz, 1F, F_{para}), -163.38 (m, 2F, F_{meta}).

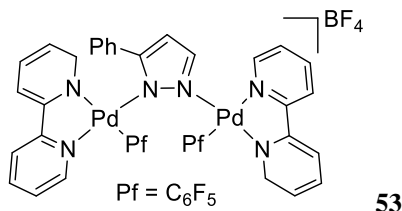
54: ¹⁹F NMR (470.17 MHz, δ, CD₃CN): -119.85 (dt, J = 29.5, 8.2 Hz, 1F, F_{ortho}), -121.48 (dt, J = 29.5, 8.2 Hz, 1F, F_{ortho}), -151.53 (BF₄), -160.63 (t, J = 19.2 Hz, 1F, F_{para}), -163.54 (m, 1F, F_{meta}), -163.41 (m, 1F, F_{meta}).



[Pd₂(μ-5-Ph-pz)(bipy)₂(C₆F₅)₂](BF₄) (53)

[PdBr(C₆F₅)(bipy)] (46.3 mg, 0.09 mmol) and AgBF₄ (17.7 mg, 0.09 mmol) were mixed in dry CD₃CN (0.6 mL) and stirred for 15 min at room temperature under nitrogen. The suspension was filtered through Kieselghur and 5-Ph-pzH (6.5 mg, 0.045 mmol)* and Na₂CO₃ (28.0 mg, 0.27 mmol) were added to the resulting colorless solution. The species formed in solution at room temperature were examined by ¹H and ¹⁹F NMR. * When the reaction was carried out with 0.09 mmol of 5-Ph-pzH (Pd:pyrazole = 1:1 mol ratio), half of the free 5-Ph-pzH was observed in solution, supporting the formation of a dimeric complex (see *Supporting information*).

¹H NMR (499.73 MHz, δ, CD₃CN): 8.60 (d, J = 7.3 Hz, 2H, H^{bipy}), 8.40 (d, J = 8.2 Hz, 1H, H^{bipy}), 8.35 (d, J = 8.0 Hz, 2H, H^{bipy}), 8.30 (d, J = 8.2 Hz, 1H, H^{bipy}), 8.24 (td, J = 7.8, 1.5 Hz, 1H, H^{bipy}), 8.21 (td, J = 7.9, 1.5 Hz, 1H, H^{bipy}), 8.13 (td, J = 7.8, 1.6 Hz, 1H, H^{bipy}), 8.10 (td, J = 7.9, 1.6 Hz, 1H, H^{bipy}), 8.04 (t, J = 2.3 Hz, 1H, H^{pz,C=C}), 7.94 (m, 2H, H^{bipy}), 7.46-7.36 (m, 4H, H^{pz, Ph}), 7.31-7.26 (m, 1H, H^{pz, Ph}), 7.28 (ddd, J = 7.6, 5.5, 1.2 Hz, 1H, H^{bipy}), 7.13 (ddd, J = 7.6, 4.9, 1.2 Hz, 1H, H^{bipy}), 6.99 (t, J = 2.4 Hz, 1H, H^{pz,C=C}), 6.55 (d, J = 5.6 Hz, 1H, H^{bipy}), 6.41 (d, J = 5.5 Hz, 1H, H^{bipy}). ¹⁹F NMR (470.17 MHz, δ, CD₃CN): -113.77 (tt, J = 29.3, 7.9 Hz, 1F, F_{ortho}), -116.96 (tt, J = 29.2, 8.2 Hz, 1F, F_{ortho}), -118.47 (dt, J = 29.6, 8.3 Hz, 1F, F_{ortho}), -119.34 (dt, J = 30.2, 8.3 Hz, 1F, F_{ortho}), -152.53 (BF₄), -161.05 (t, J = 19.4 Hz, 1F, F_{para}), -161.27 (t, J = 19.4 Hz, 1F, F_{para}), -161.44 (m, 1F, F_{meta}), -163.51 (m, 1F, F_{meta}), -164.30 (m, 2F, F_{meta}).



6.4.3 Experiments to evaluate the reactivity of palladium complexes with diazo compounds

PPh₃ experiments:

[PdBr(C₆F₅)(PPh₃)₂] (27.0 mg, 0.030 mmol) and AgBF₄ (6.0 mg, 0.030 mmol) were mixed in dry MeCN (0.6 mL) and stirred for 15 min at room temperature under nitrogen. The suspension was filtered through Kieselghur to remove the AgBr and transferred into

an NMR tube under nitrogen atmosphere. Then the equimolecular amount of diazo compound **30** (136 μL , 0.030 mmol, 0.22 M) or diazo compound **32** (111 μL , 0.030 mmol, 0.27 M) was added and the tube was closed. The reaction was monitored by ^1H , ^{19}F and ^{31}P NMR, at 25 $^\circ\text{C}$.

2,2'-bipyridine experiments:

[PdBr(bipy)(C₆F₅)] (10.2 mg, 0.02 mmol) and AgBF₄ (3.9 mg, 0.02 mmol) were mixed in dry MeCN (0.6 mL) and stirred for 15 min at room temperature under nitrogen. The suspension was filtered through Kieselghur to remove the AgBr and transferred into an NMR tube under nitrogen atmosphere. Then the equimolecular amount of diazo compound (**30**) (91 μL , 0.02 mmol, 0.22 M) or diazo compound (**32**) (74 μL , 0.02 mmol, 0.27 M) was added and the tube was closed. The reaction was monitored by ^1H and ^{19}F NMR, at 25 $^\circ\text{C}$.

Dependence of the formation of η^3 -allylic palladium complex **46** on the concentration of the diazoalkane

[Pd(C₆F₅)(dppp)(NCMe)] (0.028 mmol, [Pd]₀ = 56 mM) and 0.5 mL of dry CH₃CN were added into an NMR tube along with a sealed glass capillary filled with (CD₃)₂SO as NMR lock signal under a nitrogen atmosphere. Addition of a dichloromethane solution of the diazo compound N₂CH-CH=CHPh **30** (Pd:**30** = 1:1, 1:2 and 1:3 mol ratio) afforded an intense yellow solution, which was stirred at room temperature for 5 min. Then, the solution was checked by ^{19}F NMR. The crude yield of **46** was determined by integration of the ^{19}F NMR signals in the mixture: Pd:**30** = 1:1; 30 %. Pd:**30** = 1:2; 64 %. Pd:**30** = 1:3; 80 %. See Figure 6.13.

6.4.4 Data for X-Ray molecular structure determinations

Crystals suitable for X-ray analyses were obtained by: a) slow diffusion of *n*-hexane layered onto a solution of the complex **46** in CHCl₃ at -28 $^\circ\text{C}$; b) slow evaporation of the complex **40** in CHCl₃. In each case, the crystal was attached to the tip of a glass fiber and transferred to an Agilent Supernova diffractometer with an Atlas CCD area detector. Data collection was performed with Mo K α radiation (0.71073 Å) at 298 K. Data integration and empirical absorption correction was carried out using the CrysAlisPro program package. The structures were solved by direct methods and refined by full-matrix least squares against F² with SHELX in OLEX2. The non-hydrogen atoms were refined anisotropically and hydrogen atoms were constrained to ideal geometries and refined with fixed isotropic displacement parameters. Refinement of both structures with the restrictions mentioned above proceeded smoothly to give the residuals shown in Table 6.4.

Two independent molecules were found in the asymmetric unit for **40**.

Complex **46** presents a positional disorder of the -C₆F₅ and -Ph groups in the allyl-fragment. The structure was refined splitting the positions for each atom with different occupancies. As a consequence, the C-C distances in both aromatic rings and

the C-F bond lengths of the -C₆F₅ group are inconsistent with the typical distances of these groups. This positional disorder does not affect the distances and angles of the allylic atoms coordinated to palladium.

Table 6.4 Crystal data and structure refinement parameters for complexes **40** and **46**.

Compound number	40	46
Empirical formula	C ₆₇ H ₅₃ Br ₂ Cl ₃ F ₁₀ P ₄ Pd ₂	C ₄₅ H ₃₇ BCl ₉ F ₉ P ₂ Pd
Formula weight	1650.94	1246.94
Temperature/K	298	298
Crystal system	monoclinic	monoclinic
Space group	P2 ₁ /n	P2 ₁ /n
a/Å	15.0113(2)	13.6190(6)
b/Å	13.1748(3)	14.8420(4)
c/Å	38.0157(8)	26.4643(10)
α/°	90	90
β/°	91.428(2)	96.984(4)
γ/°	90	90
Volume/Å ³	7516.1(3)	5309.6(3)
Z	4	4
ρ _{calc} /cm ³	1.459	1.560
μ/mm ⁻¹	1.794	0.926
F(000)	3272.0	2488.0
Crystal size/mm ³	0.626 × 0.479 × 0.32	0.661 × 0.19 × 0.135
Radiation	Mo Kα (λ = 0.71073)	Mo Kα (λ = 0.71073)
2θ range for data collection/°	6.546 to 59.426	6.826 to 59.332
Index ranges	-20 ≤ h ≤ 15, -17 ≤ k ≤ 14, -52 ≤ l ≤ 52	-12 ≤ h ≤ 18, -20 ≤ k ≤ 19, -36 ≤ l ≤ 36
Reflections collected	41516	29444
Independent reflections	17849 [R _{int} = 0.0274, R _{sigma} = 0.0452]	12962 [R _{int} = 0.0338, R _{sigma} = 0.0564]
Data/restraints/parameters	17849/0/793	12962/0/625
Goodness-of-fit on F ²	1.015	1.064
Final R indexes [I >= 2σ (I)]	R ₁ = 0.0433, wR ₂ = 0.0861	R ₁ = 0.0840, wR ₂ = 0.2388
Final R indexes [all data]	R ₁ = 0.0671, wR ₂ = 0.0954	R ₁ = 0.1404, wR ₂ = 0.2870
Largest diff. peak/hole / e Å ⁻³	0.74/-0.95	1.02/-0.74

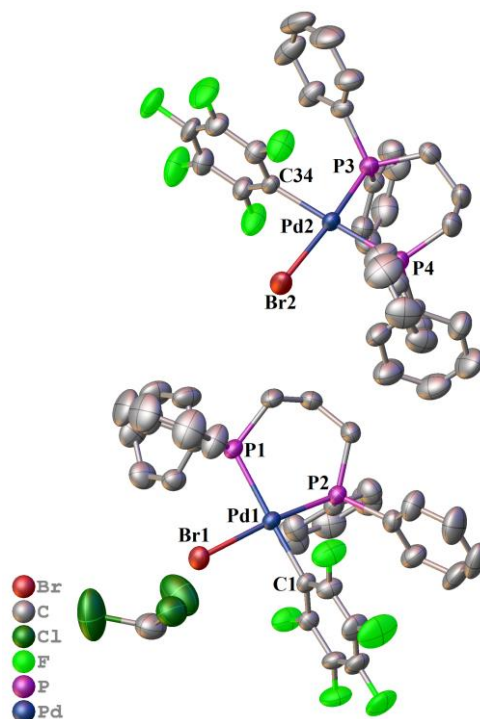


Figure 6.21 X-ray molecular structure of **40** (ORTEP 40% probability ellipsoids). Hydrogen atoms are omitted for clarity. The two independent molecules are shown.

Table 6.5 Selected bond lengths (Å) and angles (°) for complex **40** (for numbering scheme see Figure 6.21).

Pd(1)-Br(1)	2.4756(4)	Pd(2)-Br(2)	2.4752(4)
Pd(1)-P(1)	2.3286(9)	Pd(2)-P(3)	2.2500(8)
Pd(1)-P(2)	2.2483(8)	Pd(2)-P(4)	2.3293(9)
Pd(1)-C(1)	2.062(3)	Pd(2)-C(34)	2.056(3)
P(2)-Pd(1)-P(1)	93.44(3)	P(3)-Pd(2)-P(4)	94.23(3)
C(1)-Pd(1)-Br(1)	88.28(8)	C(34)-Pd(2)-Br(2)	87.36(8)

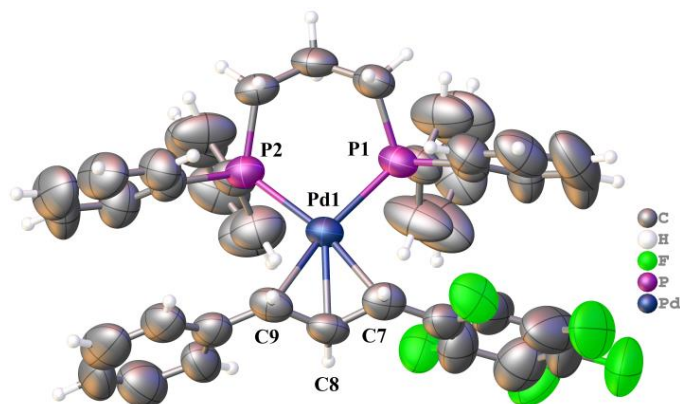


Figure 6.22 X-ray molecular structure of **46** (ORTEP 40% probability ellipsoids). Solvent molecules (CHCl_3) and the BF_4^- anion are omitted for clarity.

Table 6.6 Selected bond lengths (\AA) and angles ($^\circ$) for complex **46** (for numbering scheme see Figure 6.22).

Pd(1)-P(2)	2.3035(17)	P(2)-Pd(1)-P(1)	93.10(6)
Pd(1)-P(1)	2.3057(16)	C(7)-Pd(1)-C(9)	66.9(3)
Pd(1)-C(9)	2.229(6)	C(7)-C(8)-C(9)	122.2(7)
Pd(1)-C(8)	2.196(6)		
Pd(1)-C(7)	2.226(7)		
C(9)-C(8)	1.397(10)		
C(8)-C(7)	1.406(10)		

6.4.5 Computational details

All calculations were performed using the DFT approach with M06 functional, using Gaussian09 as program package. The selected basis set was 6-31+G(d) for C, N, F and H, and LANL2TZ(f) for Pd (Basis set I). Solvation was introduced in all the optimizations, frequency calculations and potential energy refinement through the SMD model, where we applied the experimental solvent, acetonitrile ($\epsilon = 37.5$, at 25°C). All geometry optimizations were carried out in solution with no symmetry restrictions. Free energy corrections were calculated at 298.15 K and 10^5 Pa pressure, including zero-point energy corrections (ZPE), and the energies were converted to 1M standard state in solution (adding/subtracting 1.89 kcal/mol for non-unimolecular processes). Vibrational frequency calculations were performed to establish the stationary points were minima (without imaginary frequencies) or transition states (with one imaginary frequency). Connectivity of the transition state structures were confirmed by relaxing the transition state geometry towards both the reactant and the product. Final potential energies were refined by performing additional single-point energy calculations (also in solution), Pd was still described with LANL2TZ(f) basis set, and the remaining atoms were treated with 6-311++G(d,p) basis set (Basis set II). All reported energies in the manuscript correspond to Gibbs energies in solution, obtained from potential energies (including

solvation) with basis set II plus Gibbs energy corrections with basis set I and are given in kcal mol⁻¹ (see SCF energy and free energy correction values in *Supporting information*).

Additional energy profiles

Due to the high reactivity presented by diazoalkanes **30** and **32**, before studying their interaction with the palladium complexes, we explored whether the free diazoalkanes were able to undergo nitrogen extrusion and generate free carbenes in solution. The energy profiles show that the direct dissociation of N₂ from diazo compounds (**30** and **32**) has a high energetic barrier of 31.0 and 33.0 kcal mol⁻¹ respectively (Figure 6.23). The formation of the free carbenes is endothermic for both the singlet and the triplet carbene. These results indicate that in solution the nitrogen extrusion does not occur spontaneously.

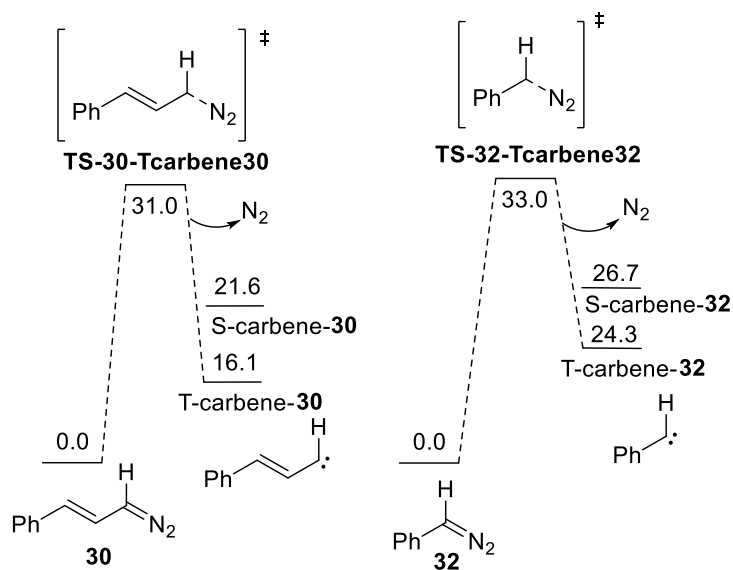


Figure 6.23 Gibbs energy profile for direct nitrogen extrusion from diazo compound (**30** and **32**). T (triplet state), S (singlet state). Energies in kcal mol⁻¹.

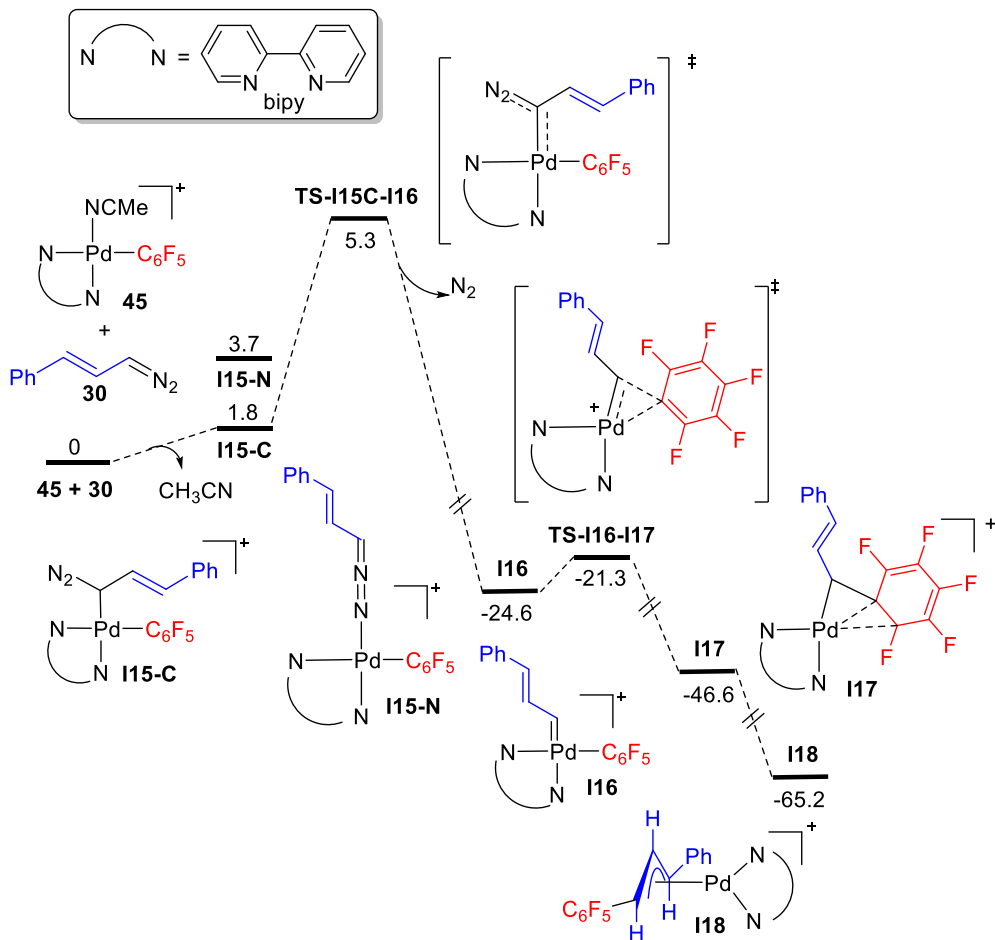


Figure 6.24 Gibbs energy profile for the reaction of complex **45** and the diazo compound **30** according to the model employed with dppe and dppp systems. Energies in kcal mol⁻¹.

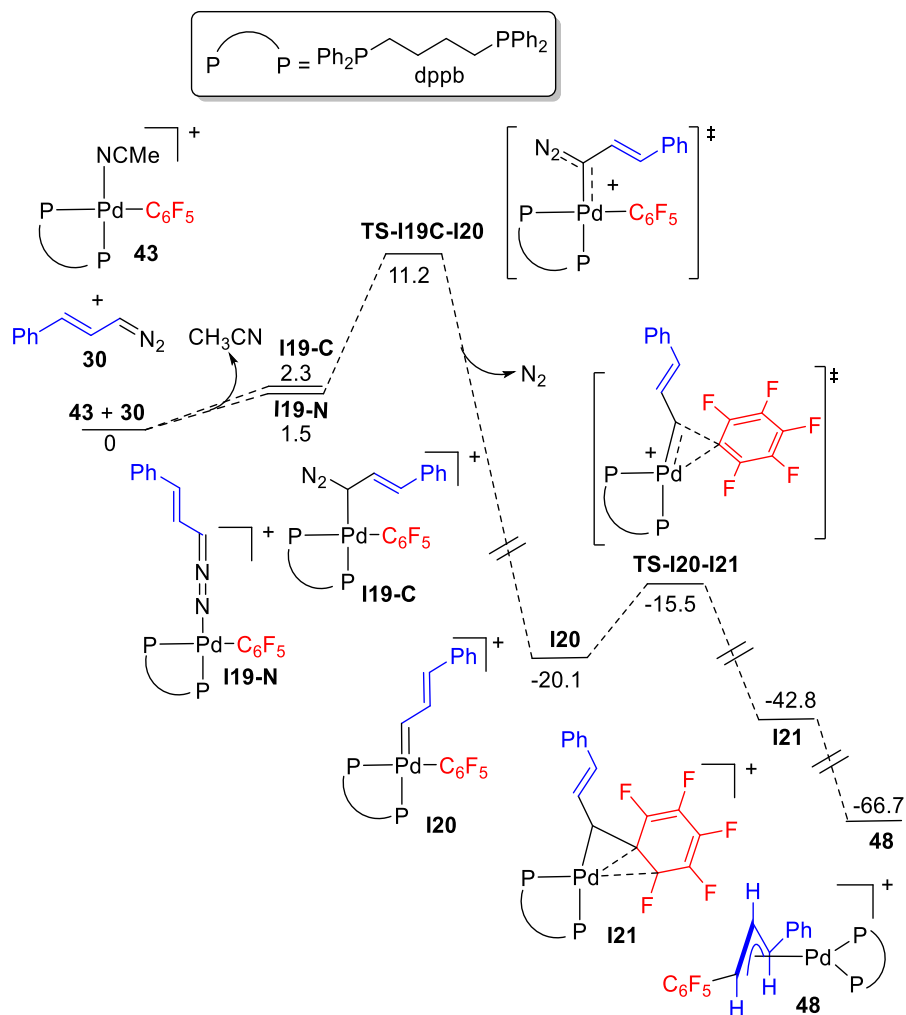


Figure 6.25 Gibbs energy profile for the reaction of complex **43** and the diazo compound **30**. Energies in kcal mol⁻¹.

Chapter 7

7. Reactions of the Simplest Amino Carbene CH(NEt₂): Transmetallation from Cu(I) to Pd(II) and Migratory Insertion

7.1 INTRODUCTION

The transmetallation of the carbene fragment is one of the widely used strategy to access late transition metal carbenes (see *Chapter 4*). Carbene transfer from group 11 metals (coinage metals) has been used in the synthesis of other metal carbenes but these reactions are circumscribed to the transmetallation of *N*-heterocyclic carbenes and other similar stable carbenes.²²¹ In this regard, Ag(I)-NHC carbene complexes represent versatile reagents for the synthesis of numerous late transition metal carbene complexes. The groups of Arduengo,²²² Bertrand²²³ and Lin²²⁴ were the pioneers in the synthesis of well-characterized Ag(I)-NHC complexes that set out the basis for the further development of the carbene transfer applications (Scheme 7.1, **a**).

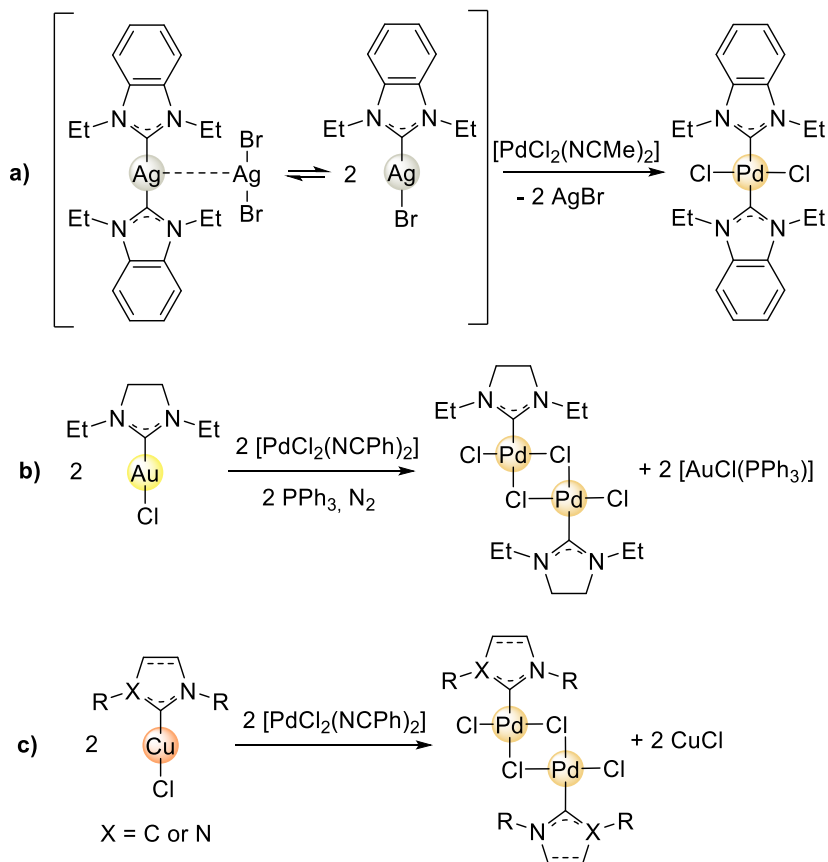
²²¹ a) Lin, J. C. Y.; Huang, R. T. W.; Lee, C. S.; Bhattacharyya, A.; Hwang, W. S.; Lin, I. J. B. *Chem. Rev.* **2009**, *109*, 3561–3598. b) Mikhaylov, V. N.; Balova, I. A. *Russ. J. Gen. Chem.* **2021**, *91*, 2194–2248.

²²² Arduengo, A. J.; Dias, H. V. R.; Calabrese, J. C.; Davidson, F. *Organometallics* **1993**, *12*, 3405–3409.

²²³ Guerret, O.; Solé, S.; Gornitzka, H.; Teichert, M.; Trinquier, G.; Bertrand, G. *J. Am. Chem. Soc.* **1997**, *119*, 6668–6669.

²²⁴ Wang, H. M. J.; Lin, I. J. B. *Organometallics* **1998**, *17*, 972–975.

Apart from these well-known Ag(I)-carbenes, examples of *N*-heterocyclic carbene transfer from other group 11 metals such as gold(I) to Pd(II) are scarce.²²⁵ The group of Chen and Liu reported the NHC carbene transfer from gold(I) promoted by the addition of triphenylphosphine in an oxygen free atmosphere (Scheme 7.1, **b**).²²⁶



Scheme 7.1 Carbene transfer from group 11 to Pd(II) complexes through transmetalation. **a)** see ref: 224. **b)** see ref: 226. **c)** see ref: 227a.

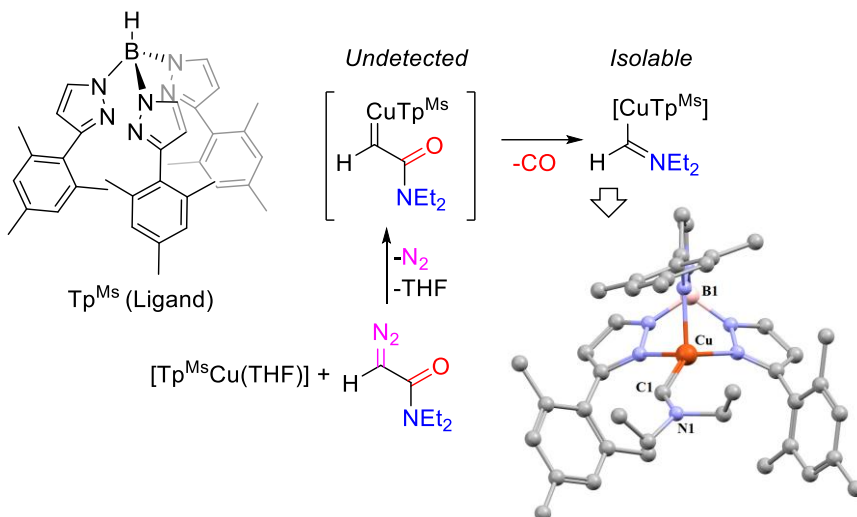
However, the use of silver and gold has some disadvantages: for instance, silver carbenes are air, moisture and light sensitive and both Ag and Au are expensive metals. To move from these drawbacks, the use of Cu(I)-carbenes has emerged as a more convenient route to synthesized late transition metal carbenes. The group of Cazin has been exploring the carbene transmetalation from different Cu(I) carbene precursors

²²⁵ delPozo, J.; Casares, J. A.; Espinet, P. *Chem. Commun.* **2013**, 49, 7246–7248.

²²⁶ Liu, S.-T.; Lee, C.-I.; Fu, C.-F.; Chen, C.-H.; Liu, Y.-H.; Elsevier, C. J.; Peng, S.-M.; Chen, J.-T. *Organometallics* **2009**, 28, 6957–6962.

bearing NHCs, aNHCs, CAACs or MICs to Pd(II) complexes (Scheme 7.1, c)).²²⁷ Aside from the latter stabilized carbenes, there are no examples of the transfer of an unstable carbene group, *i.e.* a fragment with one or no heteroatom-containing substituents (CRX or CRR'; R = H or hydrocarbyl) from copper to a transition metal.

The group of Prof. Pedro Pérez recently reported the isolation of a stable monosubstituted copper carbene complex $[\text{Tp}^{\text{Ms}}\text{Cu}\{\text{CH}(\text{NEt}_2)\}]$ where the ligand Tp^{Ms} provides a high degree of steric protection to the carbene, enough to be isolated. The formation of this monosubstituted copper carbene proceeds from the reaction of the precursor $[\text{Tp}^{\text{Ms}}\text{Cu}(\text{THF})]$ with *N,N*-diethyldiazoacetamide ($\text{N}_2=\text{C}(\text{H})(\text{CONEt}_2)$) followed by a decarbonylation process (Scheme 7.2). In fact, this was the first example of a metal-carbene formed from a diazo compound in which the substituents in the carbenic carbon are different from that in the initial diazo compound.²²⁸



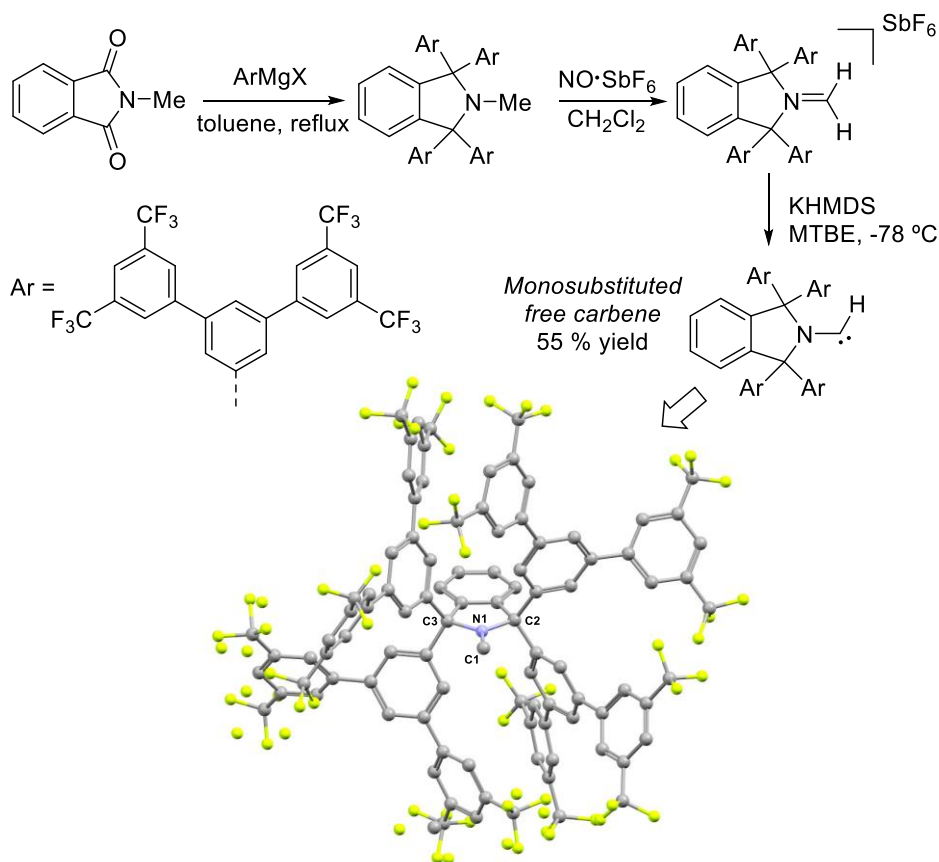
Scheme 7.2 Synthetic route of the monosubstituted Cu(I)-carbene complex and selected bond lengths of the molecular X-ray structure (Å): Cu-C1, 1.874; C1-N1, 1.287.

Monosubstituted $:\text{CHNR}_2$ carbenes are rare either coordinated to metals or as free species. Three years ago, Bertrand *et al.* were able to synthesize the first crystalline monosubstituted free $:\text{CHNR}_2$ carbene by flanking the carbenic carbon with a suitable

²²⁷ a) Furst, M. R. L.; Cazin, C. S. J. *Chem. Commun.* **2010**, 46, 6924–6925. b) Santoro, O.; Lazreg, F.; Cordes, D. B.; Slawin, A. M. Z.; Cazin, C. S. J. *Dalton Trans.* **2016**, 45, 4970–4973. c) Bidal, Y. D.; Santoro, O.; Melaimi, M.; Cordes, D. B.; Slawin, A. M. Z.; Bertrand, G.; Cazin, C. S. J. *Chem. – A Eur. J.* **2016**, 22, 9404–9409. d) Nahra, F.; Gómez-Herrera, A.; Cazin, C. S. J. *Dalton Trans.* **2017**, 46, 628–631.

²²⁸ Álvarez, M.; Besora, M.; Molina, F.; Maseras, F.; Belderrain, T. R.; Pérez, P. J. *J. Am. Chem. Soc.* **2021**, 143, 4837–4843.

pyrrolidine heterocyclic ligand containing bulky substituents on the quaternary carbon adjacent to the nitrogen (Scheme 7.3). Additionally, the study of the electronic, σ -donating and π -accepting, properties of this carbene was carried out by the isolation of a *cis*-[RhCl(CO)₂(CHNR₂)] complex. The donor properties of the monosubstituted carbene can be experimentally measured using the infrared CO stretching frequencies of the corresponding Rh-carbene complex. The authors observe values of 2086 and 2006 cm⁻¹ (average wave number ν = 2046 cm⁻¹). These values in combination with other measures as ³¹P and ⁷⁷Se NMR derived from -P and -Se carbene adducts indicate that this carbene is a weak donor and one of the most electrophilic carbene that can be isolated as a free species.²²⁹



Scheme 7.3 Synthetic route of monosubstituted free :CHNR₂ carbene and selected bond lengths of the molecular X-ray structure (Å): N1-C1, 1.325; N1-C2 = N1-C3, 1.515.

²²⁹ Nakano, R.; Jazzar, R.; Bertrand, G. *Nat. Chem.* **2018**, *10*, 1196–1200.

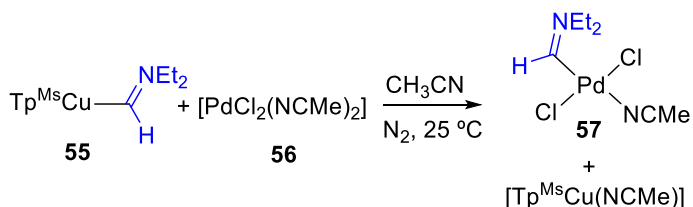
Taking into account the reduced size of the monosubstituted copper-carbene from Prof. Perez's group $\{:\text{CH}(\text{NEt}_2)\}$ in comparison to the monosubstituted carbene from Bertrand *et al.* this fragment could be interesting as a ligand having good σ -donating ability towards the metal but a small size ($\%V_{\text{Bur}}$, buried volume).^{200b,230} The employment of $[\text{Tp}^{\text{Ms}}\text{Cu}\{\text{CH}(\text{NEt}_2)\}]$ as a transmetallating agent could enable the transfer of the unstable $\{:\text{CH}(\text{NEt}_2)\}$ to a wide range of metals, such as 9, 10 or 11 groups. The goal of the work described in this *Chapter* is to explore the transmetallation of the carbene fragment from $[\text{Tp}^{\text{Ms}}\text{Cu}\{\text{CH}(\text{NEt}_2)\}]$ to several Pd(II) complexes and to find out the mechanism behind the carbene transfer. The subsequent reactivity when there is a -R group previously installed on the palladium complex (aryl complexes) has also been studied.

²³⁰ The percent buried volume ($\%V_{\text{Bur}}$) is a molecular descriptor analogous to Tolman's cone angle that measures the percent of the total volume of a sphere occupied by a ligand. Initially, this parameter was developed to be applied to NHC carbene ligands coordinated to metals, but it can be extended to other types of coordinated ligands. Selected examples: a) Poater, A.; Ragone, F.; Giudice, S.; Costabile, C.; Dorta, R.; Nolan, S. P.; Cavallo, L. *Organometallics* **2008**, *27*, 2679–2681. b) Poater, A.; Cosenza, B.; Correa, A.; Giudice, S.; Ragone, F.; Scarano, V.; Cavallo, L. *Eur. J. Inorg. Chem.* **2009**, *2009*, 1759–1766.

7.2 RESULTS AND DISCUSSION

7.2.1 Carbene transmetalation from Cu(I) to Pd(II): Preparation of Pd(II)-aminocarbene complexes

Complexes $[\text{PdCl}_2(\text{NCMe})_2]$ (**56**) and $[\text{Pd}_2(\mu\text{-Cl})_2\text{Cl}_2(\text{PPh}_3)_2]$ (**58**) were chosen as suitable palladium precursors to test the ability of the Cu(I) complex $[\text{Tp}^{\text{Ms}}\text{Cu}\{\text{CH}(\text{NEt}_2)\}]$ (**55**) to transfer the carbene ligand to palladium. Both complexes have easily accessible coordination positions either by substitution of the labile acetonitrile in **56** or bridge cleavage in **58**. The complexes do not bear aryl groups susceptible to undergo a migratory insertion process and, in this way, it could be possible to separate the transmetalation step and trap the carbene complex without further reaction. We first investigated the reaction of $[\text{Tp}^{\text{Ms}}\text{Cu}\{\text{CH}(\text{NEt}_2)\}]$ (**55**) with an equimolar amount of $[\text{PdCl}_2(\text{NCMe})_2]$ (**56**) in CH_3CN at room temperature (Equation 7.1).



Equation 7. 1

Acetonitrile was chosen as solvent because it helps to stabilize the final products by making the decoordination of NCMe more difficult and it also affords a solvento acetonitrile copper byproduct, which precipitates from the reaction mixture.²³¹

Complex **55** has low solubility in CH_3CN but it reacts fast and it disappears in the first registered spectrum (*cf.* **a**) and **b**) in Figure 7.1). After three days at room temperature, the major species in solution was complex **57**, in which the aminocarbene moiety has been transferred to palladium, along with some decomposition products such as diethylformamide (hydrolysis product) and the carbene dimerization product (*cf.* **d**), **e**) and **f**)) in Figure 7.1).

²³¹ Yap, G. P. A.; Jove, F.; Urbano, J.; Alvarez, E.; Trofimenko, S.; Díaz-Requejo, M. M.; Pérez, P. J. *Inorg. Chem.* **2007**, *46*, 780–787.

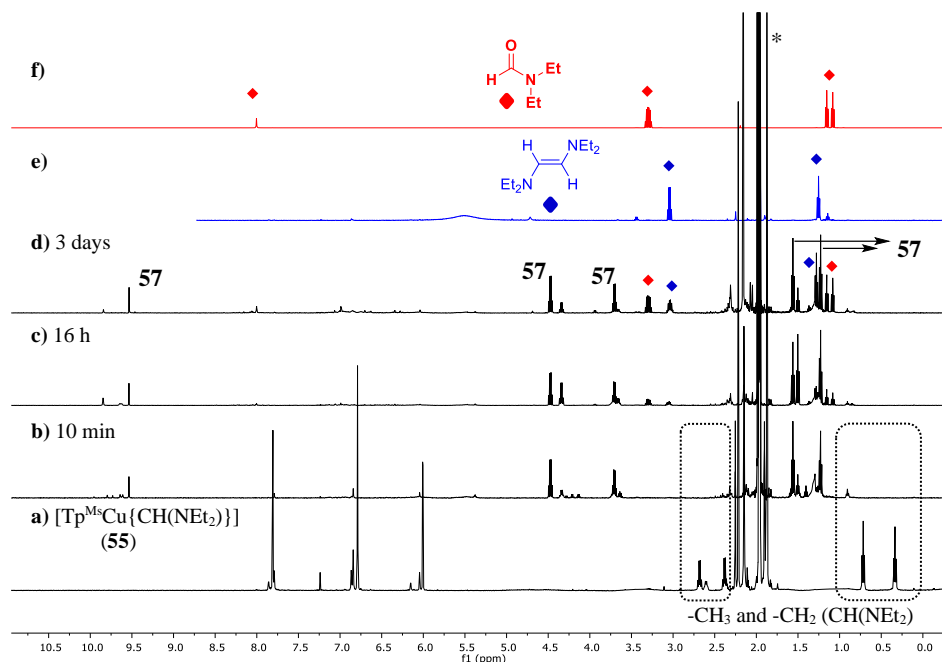


Figure 7.1 ^1H NMR (499.73 MHz, CD_3CN) for: **a)** $[\text{Tp}^{\text{Ms}}\text{Cu}\{\text{CH}(\text{NEt}_2)\}]$ (**55**) in CD_3CN at 298 K. **b), c)** and **d)** The reaction mixture shown in Equation 7.1 after the corresponding time. **e)** and **f)** isolated decomposition products from complex **57** (♦ hydrolysis byproduct (diethylformamide) and (◆ dimerization of the carbene moiety). Signals corresponding to the solvent (solvents and silicone grease).

Complex **57** was prepared in a larger scale and, upon isolation, it loses acetonitrile to give a solid which is a mixture of **57** and two other complexes that were tentatively assigned to dimeric palladium derivatives of formula $[\text{Pd}_2(\mu\text{-Cl})_2\text{Cl}_2\{\text{CH}(\text{NEt}_2)_2\}]$ (Figure 7.2, **a**). A solution of this solid in CDCl_3 reacts with acetonitrile to give **57** as the only species. The identification of complex **57** bearing the carbene fragment $:\text{CH}(\text{NEt}_2)$ was done based on some characteristic spectroscopic values. The ^1H NMR chemical shift for the proton bound to the carbene unit ($\text{Pd}\text{-CH}(\text{NEt}_2)$) is dramatically affected by the metal center, being in the palladium complexes higher than in the copper one (10–9 ppm vs. 8–7 ppm respectively). This proton signal correlates with a ^{13}C signal at 206 ppm in the 2D $^{13}\text{C}\text{-}^1\text{H}$ HSQC NMR experiment (Figure 7.2, **b**). This is within the typical ^{13}C NMR region of $\text{Pd}\text{-C}_{\text{carbene}}$ moieties reported previously. It was not possible to determine the molecular structure of **57** by X-ray diffraction so the *trans* geometry of the complex is proposed based on DFT calculations that indicate that the *trans* arrangement is 2.6 kcal mol $^{-1}$ more stable than the *cis* isomer (see *Experimental part*, Figure 7.20).

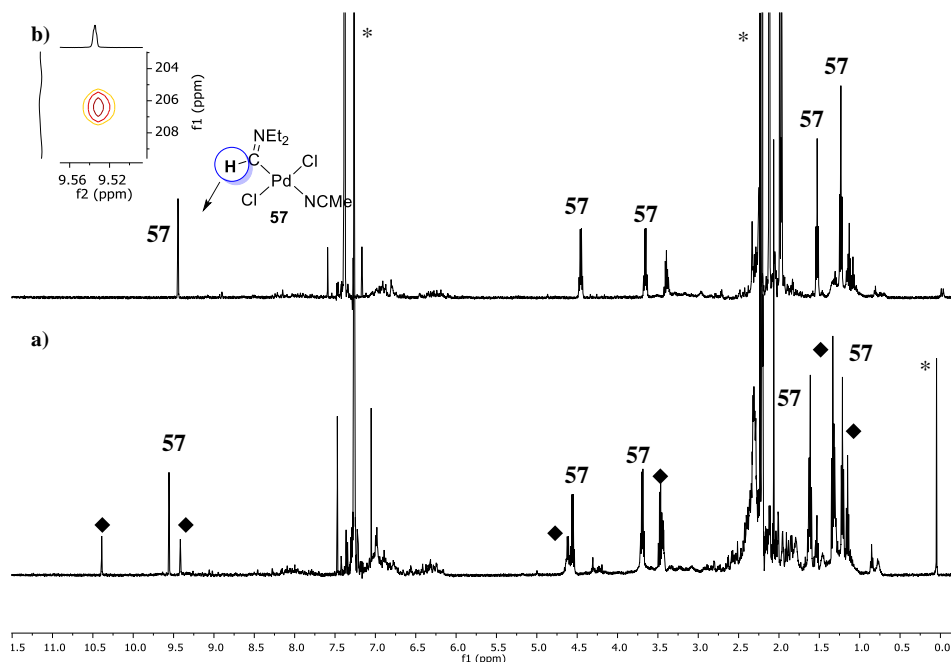
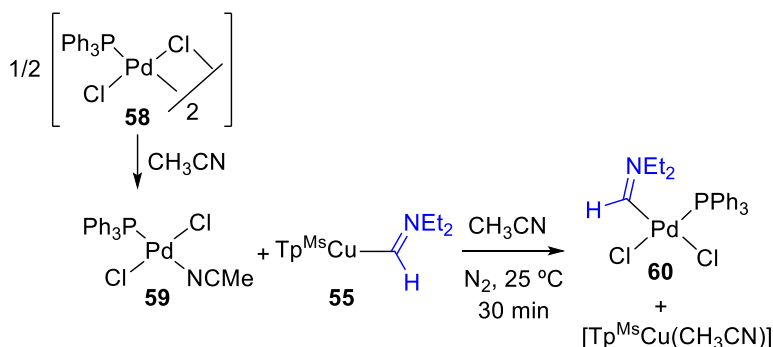


Figure 7.2 ^1H NMR (499.73 MHz, solvent, $-40\text{ }^\circ\text{C}$). **a)** isolated solid in the reaction of **55** and **56** dissolved in CDCl_3 . **b)** isolated solid in CDCl_3 upon addition of 0.1 mL of CD_3CN (inset: cross peak in the ^{13}C - ^1H -HSQC NMR experiment). \blacklozenge tentatively proposed $[\text{Pd}_2(\mu\text{-Cl})_2\text{Cl}_2\{\text{CH}(\text{NEt}_2)_2\}]$ complexes. * Signals corresponding to the solvent (chloroform, acetonitrile and silicone grease).

The reaction of the copper aminocarbene **55** with the dimeric palladium complex **58** was also carried out in acetonitrile. This solvent breaks the chloro-bridges of dimeric complex **58** to afford the mononuclear *trans*- $[\text{PdCl}_2(\text{NCMe})(\text{PPh}_3)]$ (**59**) as it was tested by addition of increasing amounts of acetonitrile to a solution of **58** in chloroform (see *Experimental part*, Figure 7.14). After 30 min at room temperature the transmetalation of the aminocarbene from **55** to **58** occurs leading the formation of complex *cis*- $[\text{Pd}\{\text{CH}(\text{NEt}_2)_2\}\text{Cl}_2(\text{PPh}_3)]$ (**60**) (Scheme 7.4).



Scheme 7.4 Synthesis of complex **60** by transmetalation from complex **55**.

Complex **60** was isolated and fully characterized by NMR spectroscopy, mass spectrometry and X-ray diffraction. The molecular structure of **60** reveals that the chloride groups are in a *cis* arrangement, which could be attributed to the large *trans* influence of PPh_3 and particularly of the carbene unit which favors a mutual *cis* disposition. DFT calculations show that the *cis*-isomer is $5.5 \text{ kcal mol}^{-1}$ thermodynamically more stable than the *trans*-isomer (Figure 7.20, *Experimental part*).

The aminocarbene group lies perpendicular to the palladium coordination plane as has already been reported for other similar palladium aminocarbene complexes.¹⁴⁵ The bond lengths found in the X-ray structure reflect the important donation of the lone electron pair on the nitrogen of the amino group to the vacant *p* orbital of the carbenic carbon atom. Thus, the C1–N1 bond length is consistent with a double bond while the Pd1–C1 bond is consistent with a single one and a negligible back-donation from the metal (Figure 7.3). The ^1H NMR shows a characteristic chemical shift for the aminocarbene proton (Pd–CH(NEt_2)) at 9.32 ppm, similar to that complex **57** (9.46 ppm). Additionally, a doublet of the aminocarbene proton signal is generated due to the coupling with the phosphorus of the triphenylphosphine ligand with a $J_{\text{H-P}} = 8.1 \text{ Hz}$. The 2D ^1H - ^{13}C HSQC NMR experiment shows that the carbenic carbon has a chemical shift of 216 ppm (Figure 7.4).

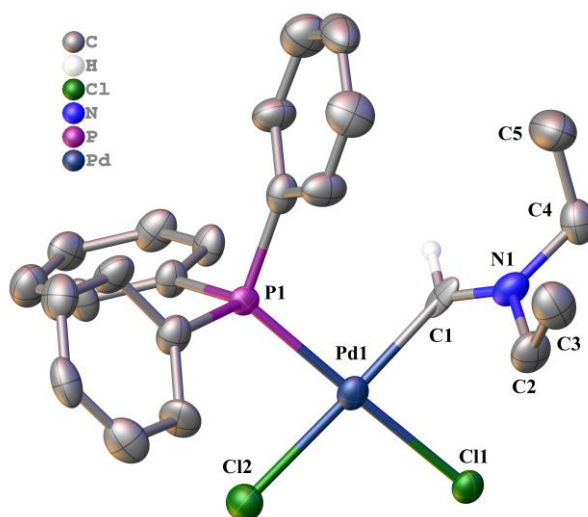


Figure 7.3 Molecular structure of complex *cis*-**60** (ORTEP plot; 40 % probability ellipsoids). Hydrogens have been omitted for clarity except for the hydrogen bound to the carbenic carbon atom. Selected distances (Å) and angles (°): Pd1–Cl1, 2.362(2); Pd1–Cl2, 2.351(3); Pd1–P1, 2.245(2); Pd1–C1, 1.974(11); C1–N1, 1.267(13); P1–Pd1–C1, 91.8(3); Cl1–Pd1–Cl2, 92.25(9).

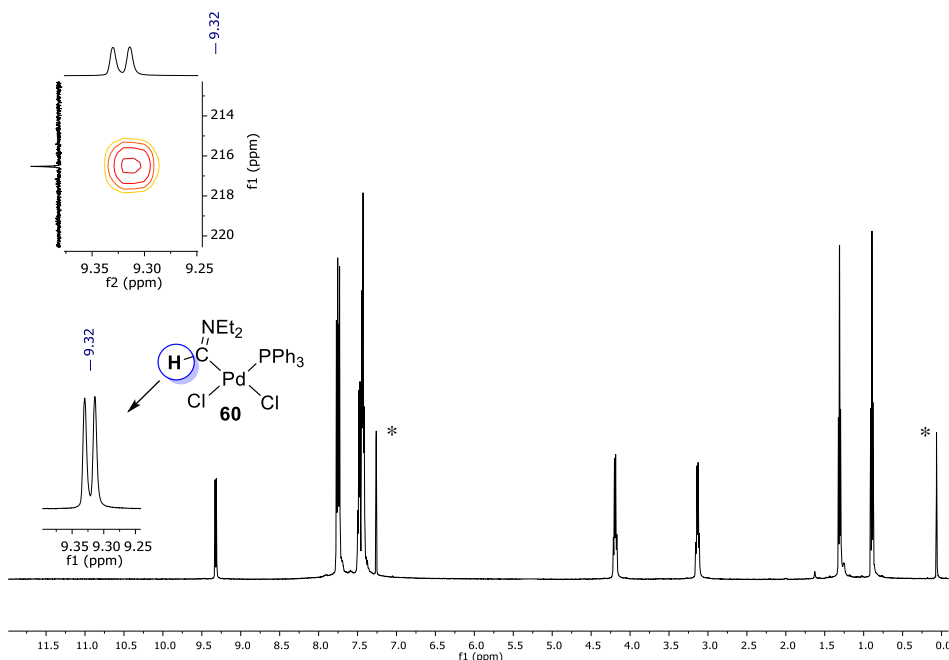


Figure 7.4 ^1H NMR (499.73 MHz, CDCl_3) of isolated complex **60** (inset: cross peak in the ^{13}C - ^1H HSQC NMR experiment) at 298 K. * Signals corresponding to the solvent (chloroform and silicone grease).

The transmetalation of the carbene group from copper to complex **58** was monitored at variable temperature by ^1H NMR. The complexes were mixed at $-40\text{ }^\circ\text{C}$ in a molar ratio **55:58** = 2:1 and the evolution of the low field region corresponding to the Pd-CHNEt₂ resonance is shown in Figure 7.5. It was found that in the $-40\text{ }^\circ\text{C}$ to $-25\text{ }^\circ\text{C}$ temperature interval, the formation of complex *trans*-**60** occurred, and it was the only species observed. *Trans*-**60** shows a similar chemical shift for the proton signal of the aminocarbene to that of *cis*-**60** but with a slightly higher coupling constant to phosphorous (*trans*-**60**, $J_{\text{H-P}} = 11.0\text{ Hz}$ vs. *cis*-**60**, $J_{\text{H-P}} = 8.1\text{ Hz}$). This value fits with the theoretical coupling constants calculated by Gaussian software package on the DFT-optimized *trans*-**60** complex (see *Experimental part*). At $-25\text{ }^\circ\text{C}$, the formation of complexes **57** and *cis*-**60** was observed. In the last interval ($-25\text{ }^\circ\text{C}$ to $-10\text{ }^\circ\text{C}$) both **57** and *trans*-**60** transform into the thermodynamically stable complex *cis*-**60**, which is the final product of the reaction (Figure 7.5).

To check the possible scenario in which the Cu(I) complex can be acting as a trapping agent of PPh₃ during the transmetalation step, and therefore being the cause of the formation of the phosphine-free complex **57**, independent experiments have been carried out. Neither the starting carbene complex $[\text{Tp}^{\text{Ms}}\text{Cu}\{\text{CH}(\text{NEt}_2)\}]$ nor $[\text{Tp}^{\text{Ms}}\text{Cu}(\text{THF})]$ react with PPh₃ (see *Experimental part*, Figure 7.16).

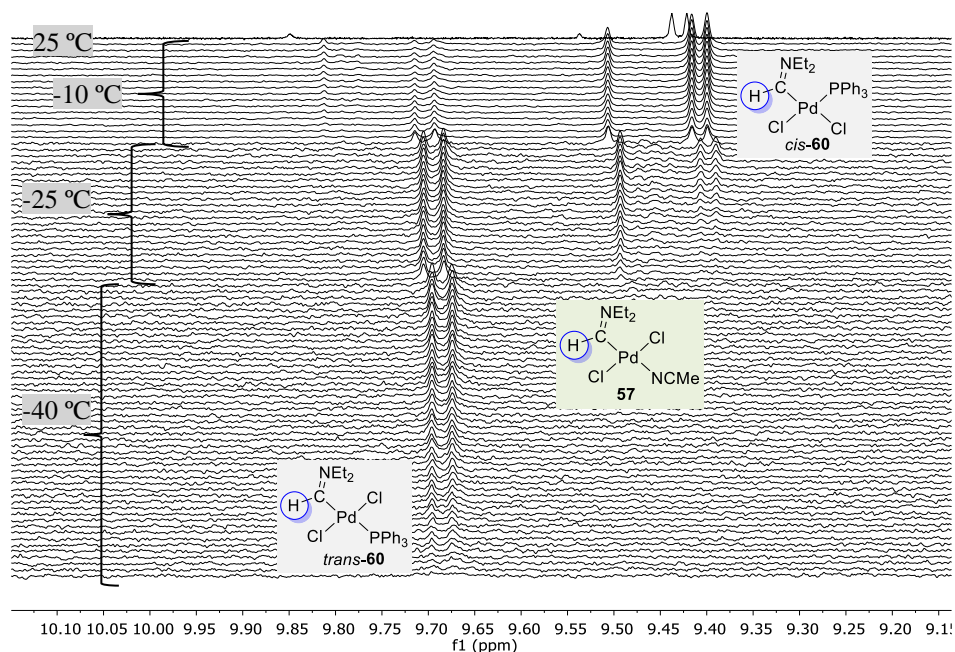


Figure 7.5 ^1H NMR (499.73 MHz, CD_3CN , variable temperature) of reaction shown in Scheme 7.4. Spectra were registered in 3-minute intervals. Only the proton bound to the $\text{C}_{\text{carbenic}}$ region is shown for clarity.

The transmetalation from Cu to Pd when complex **58** was used as palladium precursor was analyzed by DFT calculations carried out by Prof. Agustí Lledós at the *Universitat Autònoma de Barcelona*. The calculations were carried out using the B3LYP-D3/BS2 functional and including solvation through the SMD implicit solvent method for the experimental solvent, acetonitrile. A brief account of the results of those calculations is given here (Figure 7.6 and Scheme 7.5). The interaction of the copper carbene with the monomeric *trans*-[$\text{PdCl}_2(\text{NCMe})(\text{PPh}_3)$] species, formed from complex **58** in acetonitrile, requires the decoordination of one of the pyrazolate rings of the Tp^{Ms} ($\kappa^3\text{Tp}^{\text{Ms}} \rightarrow \kappa^2\text{Tp}^{\text{Ms}}$). This decoordination of one pyrazolate ring allows the approach and subsequent interaction of the *trans*-[$\text{PdCl}_2(\text{NCMe})(\text{PPh}_3)$] complex with the copper center affording **I-1**. The acetonitrile is released at this point from this **I-1** intermediate through a transition state (**TS-1**) with an energy of 17.1 kcal mol $^{-1}$. The resulting Cu-Pd cluster with the aminocarbene acting as a bridge is a high energy intermediate **I-2**. The leaving acetonitrile is now the incoming ligand in the copper center, which requires the decoordination of another pyrazolate ring in the Tp^{Ms} ($\kappa^2\text{Tp}^{\text{Ms}} \rightarrow \kappa^1\text{Tp}^{\text{Ms}}$). This rearrangement involves the highest energy barrier of the reaction (**TS-2**, 18.4 kcal mol $^{-1}$, energetic span). After the acetonitrile coordination, the intermediate **I-3**, which is also high in energy undergoes the complete aminocarbene transfer to the Pd(II) center through

the three-membered bimetallic cluster (**TS-3**). Finally, the aminocarbene is completely transfer to palladium to give *trans*-**60** and [Tp^{Ms}Cu-NCMe]. This DFT energy profile for the transmetallation reaction mirrors the experimental results obtained at low temperature (Figure 7.5) and show that the direct transmetallation from this Cu(I)-aminocarbene to a Pd(II) complex with labile ligands is a rapid process even at low temperature (as indicated by the energy of **TS1** – **TS3** in Figure 7.6). These results indicate that [Tp^{Ms}Cu{CH(NEt₂)}] can be an ideal aminocarbene transfer agent to synthesized Pd(II) complexes.

The computed Gibbs energy profile for the isomerization of *trans*-**60** to *cis*-**60** is depicted in Figure 7.7. The profile summarizes a series of low energy events, being the formation of the thermodynamically more stable *cis*-**60** the driving force of the isomerization process. Complex *trans*-**60** dissociates the triphenylphosphine, favored by the high *trans* effect of the aminocarbene, with a low energy cost (15.4 kcal mol⁻¹) to form a three-coordinated intermediate **I-5**. Intermediate **I-5** is stabilized by the coordination of an acetonitrile molecule to afford **I-6**, which interacts with the incoming triphenylphosphine displacing a chloride ligand (**TS-4**, 17.3 kcal mol⁻¹, energetic span). The resulting chloride approaches to the cationic intermediate **I-8** and displaces the acetonitrile ligand through an energy barrier of 14.9 kcal mol⁻¹ (**TS-5**) to complete the isomerization process.

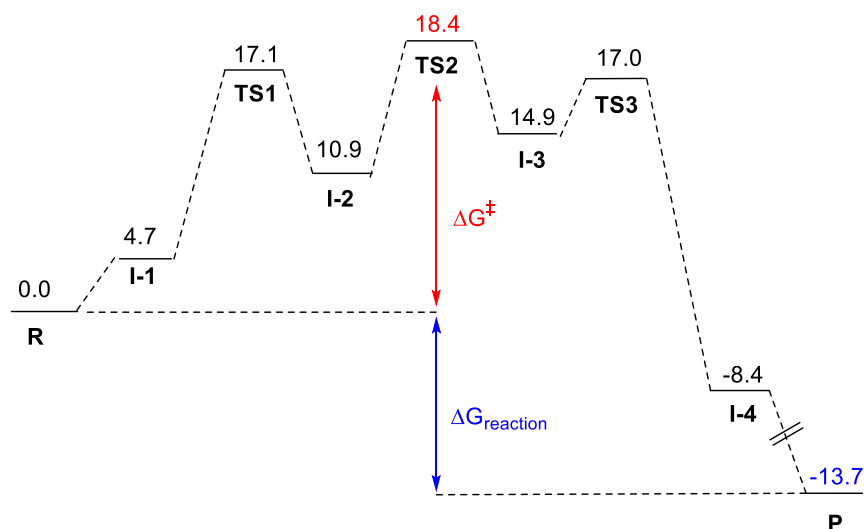
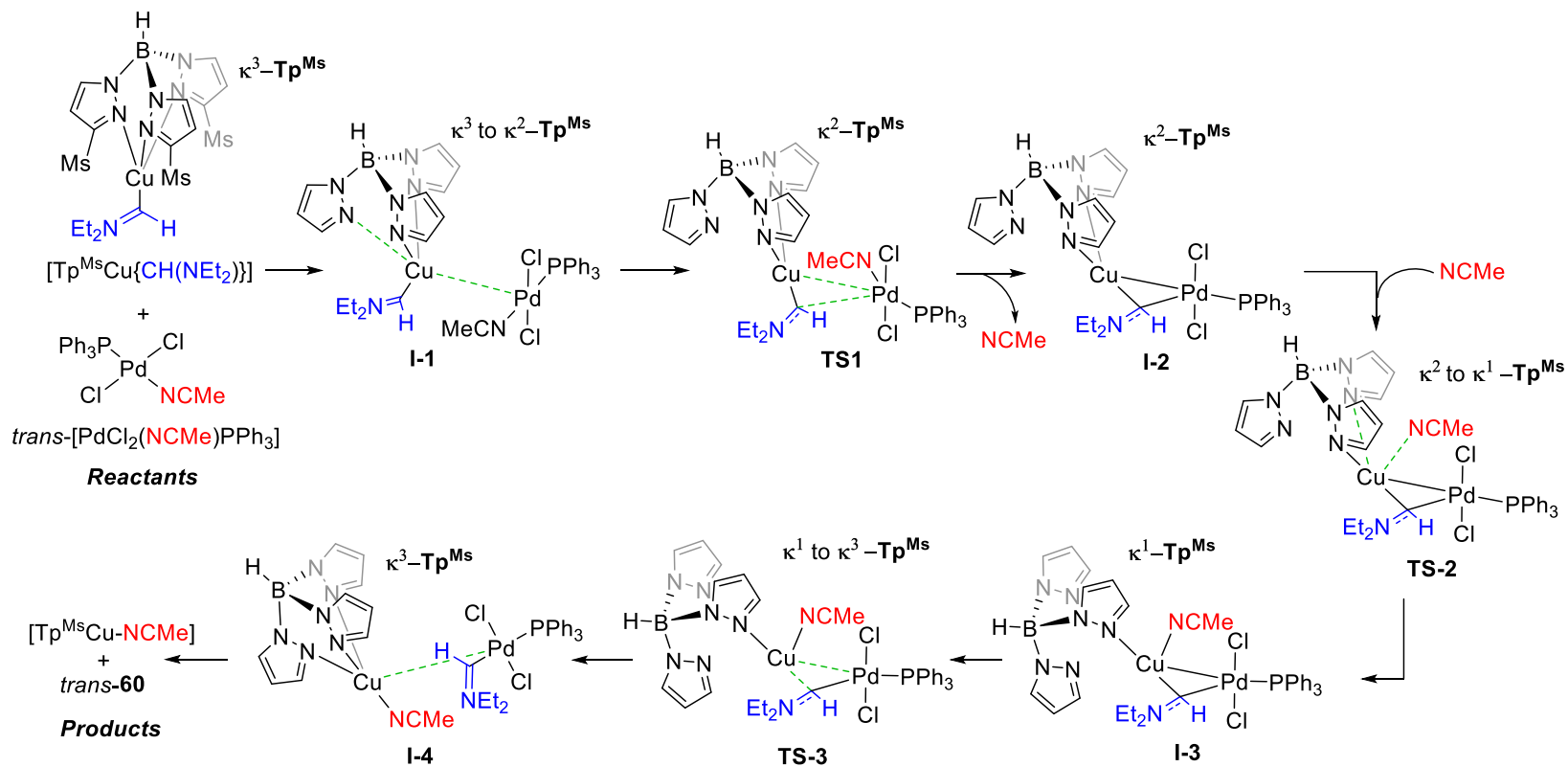


Figure 7.6 Gibbs energy profile for the transmetallation of the aminocarbene from Cu to Pd depicted in Scheme 7.5.



Scheme 7.5 Simplified proposed mechanistic pathway for the aminocarbene transmetalation. Mesityl groups have been omitted for clarity. Gibbs energy profile is depicted in Figure 7.6.

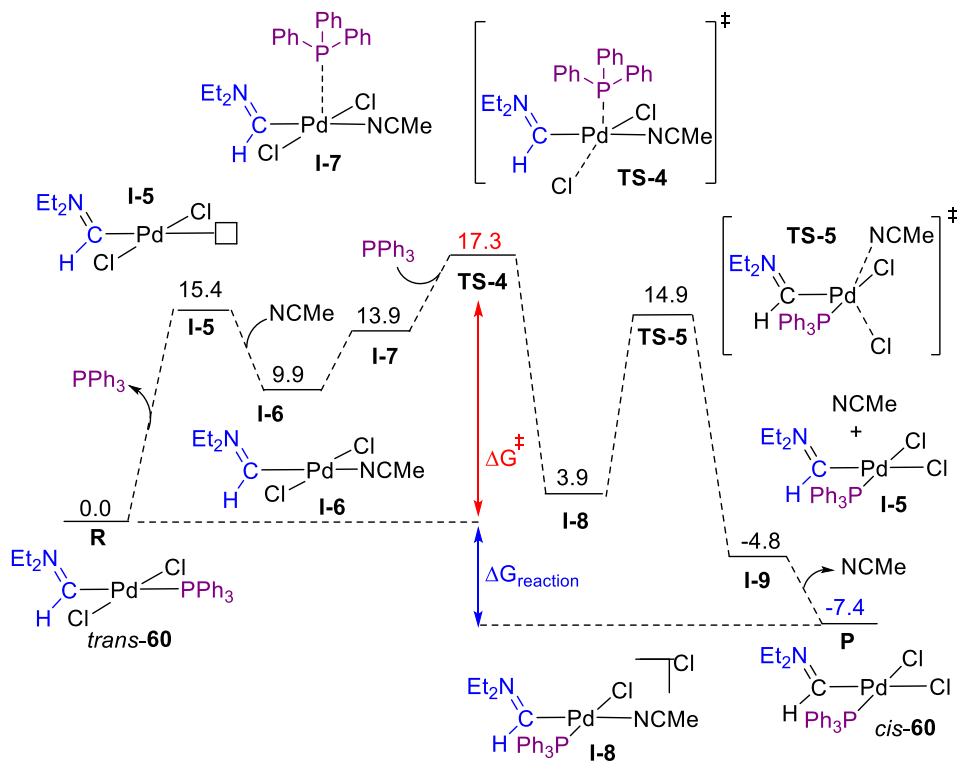
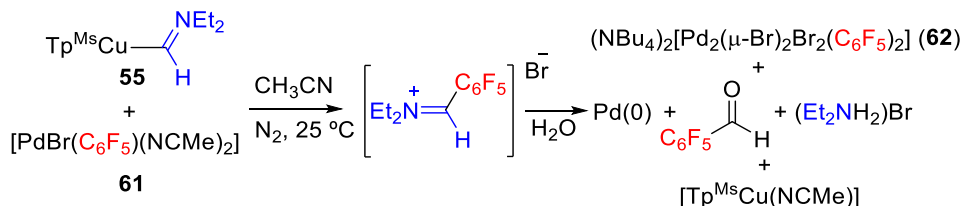


Figure 7.7 Gibbs energy profile for the *trans* to *cis* isomerization of complex **60**.

7.2.2 Study of the transmetalation and migratory insertion reaction in Pd-aryl complexes

As mentioned above, the use of palladium complexes, without -R groups bound to the metal, susceptible to undergo a migratory insertion once the carbene is transferred to the palladium, led us to detect and isolate complexes bearing the aminocarbene unit (complexes **57** and **60**). The following section describes the studies carried out with palladium complexes containing the fluorinated aryl group -C₆F₅ (Pf). In this way, both a transmetalation and a migratory insertion reaction could occur and it will be possible to evaluate if the migratory insertion reaction is favored for this new carbene { :CH(NEt₂)}. As it was mentioned before (*Chapters 5* and *6*) the ¹⁹F NMR signals for the F_{ortho} of the C₆F₅ group show very different chemical shifts for the Pd-C₆F₅ and C-C₆F₅ situations, and therefore the C₆F₅ group is a very convenient tag to study migratory insertion reactions. Scheme 7.6 shows the reaction between copper carbene **55** and the palladium complex **61** in acetonitrile at room temperature. The reaction reveals the formation of two organic products: the iminium salt derived from the carbene-C₆F₅

coupling along with pentafluorobenzaldehyde, the hydrolysis product of the iminium salt (Figure 7.8, ●). Complex $(\text{NBu}_4)_2[\text{Pd}_2(\mu\text{-Br})_2\text{Br}_2(\text{C}_6\text{F}_5)_2]$ (**62**) is formed in the reaction media as a consequence of the coordination of the free bromide to complex **61**. Pentafluorobenzaldehyde (61 mol%) and the dimeric complex $(\text{NBu}_4)_2[\text{Pd}_2(\mu\text{-Br})_2\text{Br}_2(\text{C}_6\text{F}_5)_2]$ (**62**) (39 mol%) were the final products obtained after 4 h in solution.



Scheme 7.6 Transmetalation reaction from **55** to **61** and the products observed.

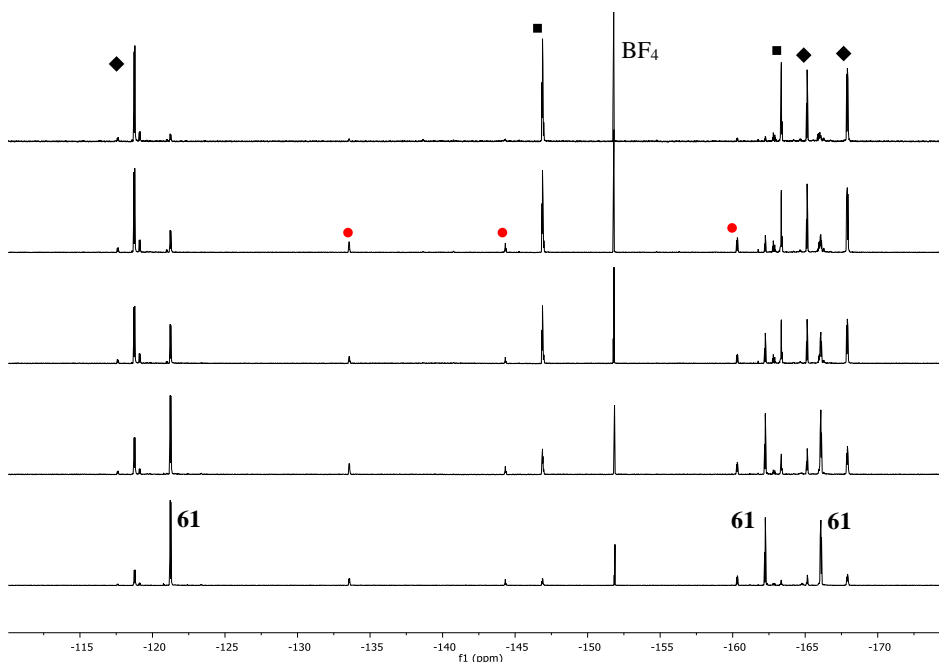
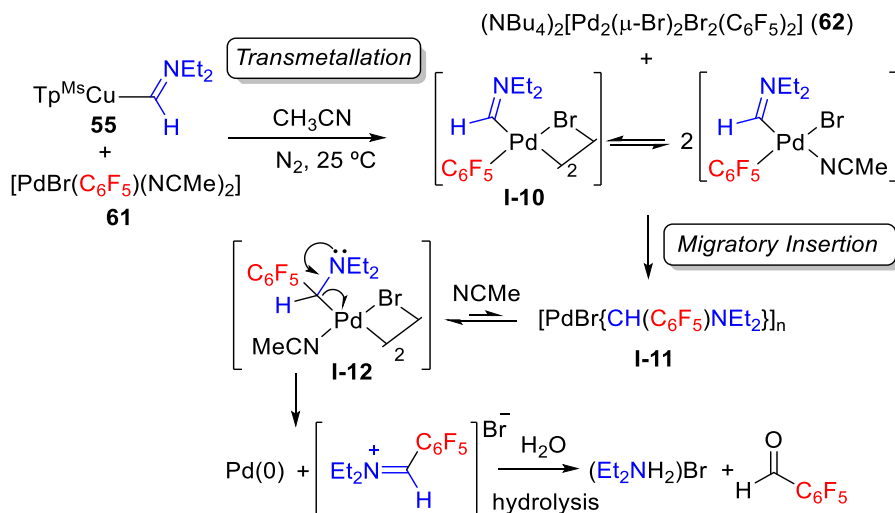


Figure 7.8 ^{19}F NMR (470.17 MHz, CD_3CN) monitoring of reaction shown in Scheme 7.6. ● Iminium salt. ■ Pentafluorobenzaldehyde. ◆ Complex: $(\text{NBu}_4)_2[\text{Pd}_2(\mu\text{-Br})_2\text{Br}_2(\text{C}_6\text{F}_5)_2]$ (**62**). The identity of complex $(\text{NBu}_4)_2[\text{Pd}_2(\mu\text{-Br})_2\text{Br}_2(\text{C}_6\text{F}_5)_2]$ was checked independently by dissolving the isolated complex in CD_3CN at room temperature.

A plausible mechanism for the formation of the products observed in ^{19}F NMR is depicted in Scheme 7.7 where a transient carbene intermediate **I-10**, which could not be detected, undergoes a rapid migratory insertion to afford an intermediate **I-11** with

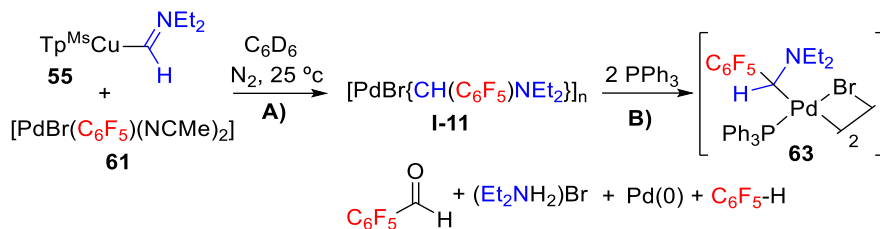
the $-C_6F_5$ group incorporated in the carbene fragment. The formation of the iminium salt can be considered as a reductive elimination from the aminobenzyl-palladium complex (**I-12**). The hydrolysis of the iminium salt produces the corresponding benzaldehyde and ammonium bromide as the final organic products of the reaction.



Scheme 7.7 Mechanistic proposal for the experimental products observed in Scheme 7.6.

When the same reaction was carried out in the much less coordinating benzene solvent, a set of signals consistent with an organometallic complex where the $-C_6F_5$ group is bound to carbon are clearly observed in the ^{19}F NMR spectrum (Figure 7.9, **a**). The decomposition products $C_6F_5\text{H}$ and $C_6F_5\text{CHO}$ are also present (Scheme 7.8, **A** and Figure 7.9, **a**)).

The ^{19}F NMR spectrum of **I-11** shows two sets of $-C_6F_5$ signals with slightly different integrals where all $-F$ atoms of each $-C_6F_5$ group are chemically inequivalent (Figure 7.9, **a**). This indicates a static situation with no free rotation around the $\text{C}-\text{C}_6\text{F}_5$ bond, and two putative isomeric species. We could not determine the exact structure of **I-11** because of the impossibility of isolating it in a pure form. The addition of PPh_3 to **I-11** leads to a single new species (**63**) (Scheme 7.8, **B**) shown by the formation of just two new ^{19}F signals in the region of the F_{para} and F_{meta} . The F_{ortho} signal was not observed due to a fluxional phenomenon and the coalescence at this temperature, $25\text{ }^\circ\text{C}$ (Figure 7.9, **b**)).



Scheme 7.8 Transmetalation reaction from **55** to **61** in non-coordinating solvent.

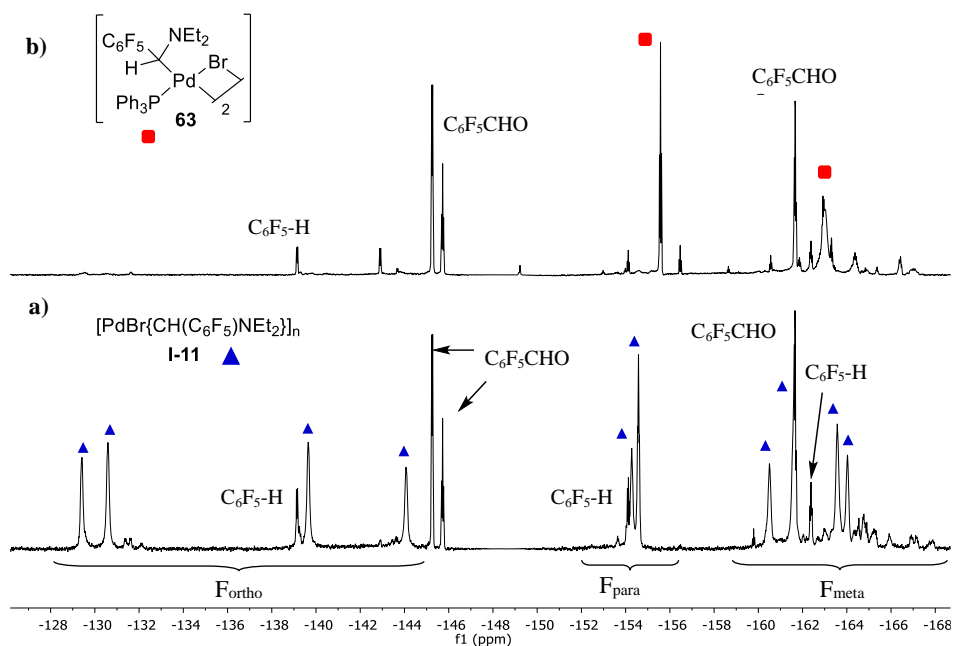
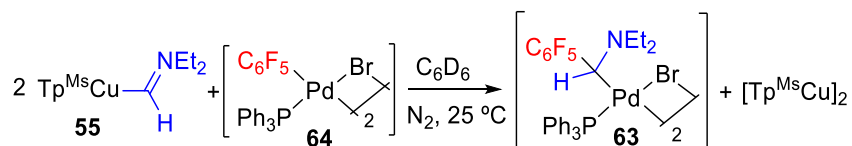


Figure 7.9 ^{19}F NMR (470.17 MHz, C_6D_6) of the reaction shown in Scheme 7.8. **a)** putative proposed intermediate **I-11** (\blacktriangle). **b)** The formation of complex **63** (\blacksquare) when PPh_3 is added to the reaction mixture.

Complex **63** was independently prepared starting from the phosphino dimeric complex **64** (Equation 7.2). The dimeric structure of **63** was confirmed by HRMS and the ^1H and ^{13}C NMR data are consistent with the depicted structure.



Equation 7.2

At low temperatures, the rotation around the C-C₆F₅ bond of **63** is slow, so the two F_{ortho} and F_{meta} are in different chemical environments. As the temperature increases, the peaks begin to broaden until they coalesce into a single broad average peak which is not detected at room temperature for the F_{ortho} but we can see it for the F_{meta} (Figure 7.10). It is noteworthy that only one diastereoisomer is observed for **63** out of the four possible arrangements in the dimer (*cis-trans* and combination of the two configurations for the chiral methine carbon). We could not determine which one is formed.

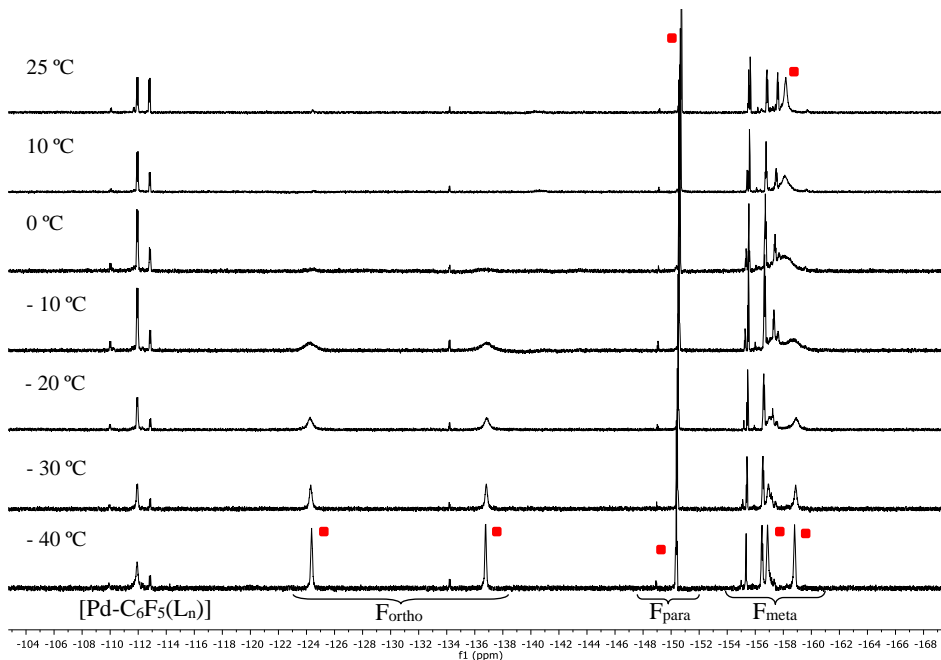


Figure 7.10. ¹⁹F NMR (470.17 MHz, toluene-d₈) of complex **63** (■) at different temperatures. Monitoring of the reaction depicted in Equation 7.2 from -40 °C to room temperature.

The reaction in Equation 7.2 was monitored by ¹⁹F NMR at room temperature. After 4 h, complex **63** was observed as the major species along with a small amount of the starting complex **64** and another unidentified palladium pentafluorophenyl complex (Figure 7.11, **A**). After 8 h in solution at room temperature, the set of signals assigned to **I-11** began to appear (*c.f.* **B**) and **C**) in Figure 7.11) along with [PdBr(C₆F₅)(PPh₃)₂] which led us to propose an equilibrium between the complex **63** and **I-11** which supports the absence of other potential ligands in the coordination sphere of **I-11** (Equation 7.3).

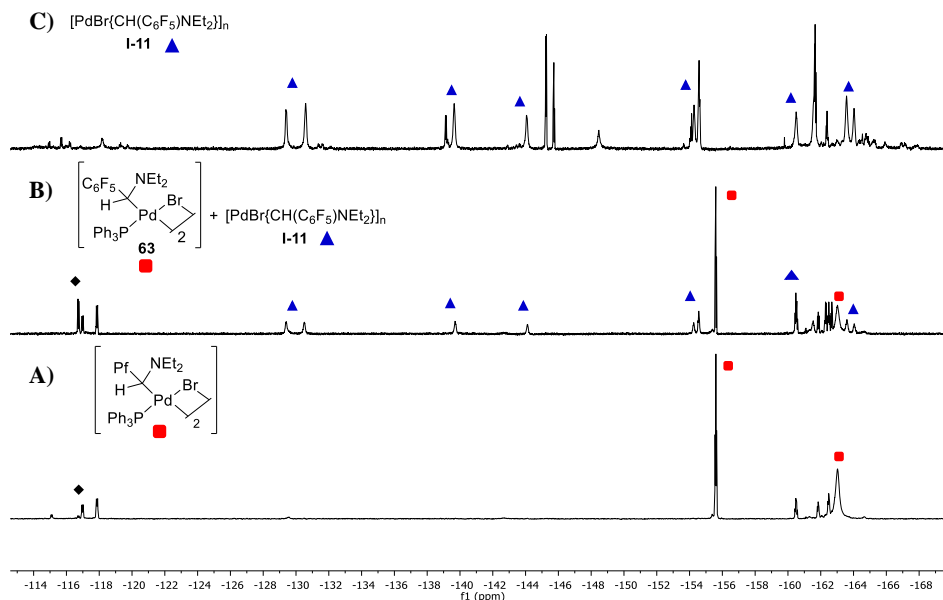
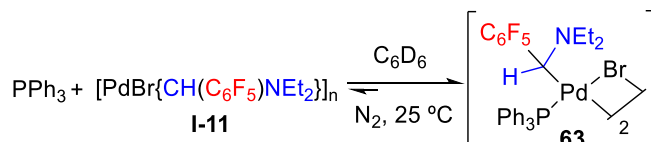


Figure 7.11 ^{19}F NMR (470.17 MHz, C_6D_6) Monitoring of the reaction depicted in Equation 7.2. **A)** Reaction mixture after 4 h at room temperature. **B)** Reaction mixture after 8 h at room temperature. **C)** Comparison with the reaction mixture from reaction of Scheme 7.8. \blacklozenge complex $[\text{PdBr}(\text{C}_6\text{F}_5)(\text{PPh}_3)_2]$.



Equation 7.3

Therefore, from the experiments shown above, the composition of **I-11** is clear but the structure of the complex is not determined. Three possible tentative structures are shown in Figure 7.12 which could react with PPh_3 to give **63** and also have several possible isomeric structures. Bromo-bridged dimeric species with a chelating aminobenzyl group can be considered: Either a η^3 -benzylic complex where the pentafluorophenyl group is involved in the bonding (Figure 7.12, **a**) or a three-membered aminopalladacycle (Figure 7.12, **b**). Another plausible structure would be a tetrameric complex with aminoalkyl and bromo bridges ((Figure 7.12, **c**). To the best of our knowledge, there is no precedent in the literature for η^3 -benzylic Pd-complex where the $-\text{C}_6\text{F}_5$ group is involved in the η^3 -bonding to the Pd. Moreover, several precedents are

described of the proposed intermediate **b**) with a three-membered amino-palladacycle.²³² For the proposed intermediate **c**) the closest precedent found in literature is a Pd(II)-complex bearing thioalkyl and bromo bridges affording a tetranuclear $[\text{Pd}(\mu\text{-Cl})\{\mu\text{-}(\sigma\text{-}\kappa\text{-PhSCHCH}_2\text{C}_6\text{F}_5)\}]_4$ complex.²³³

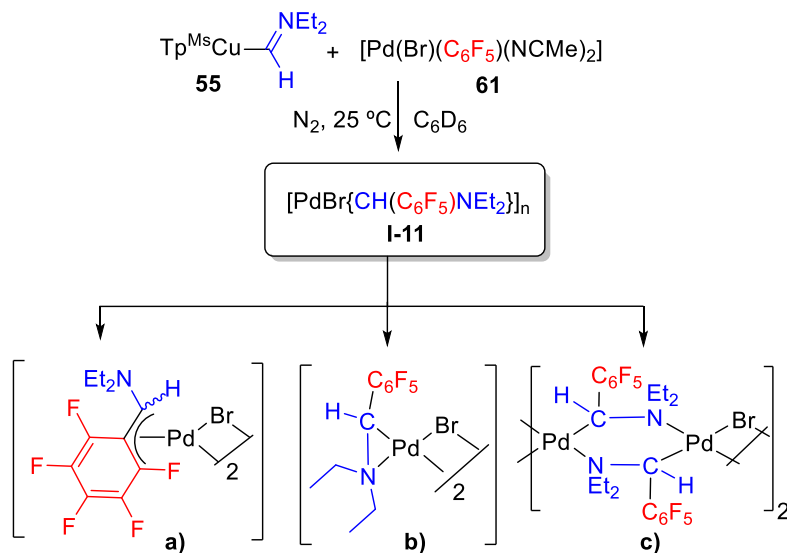


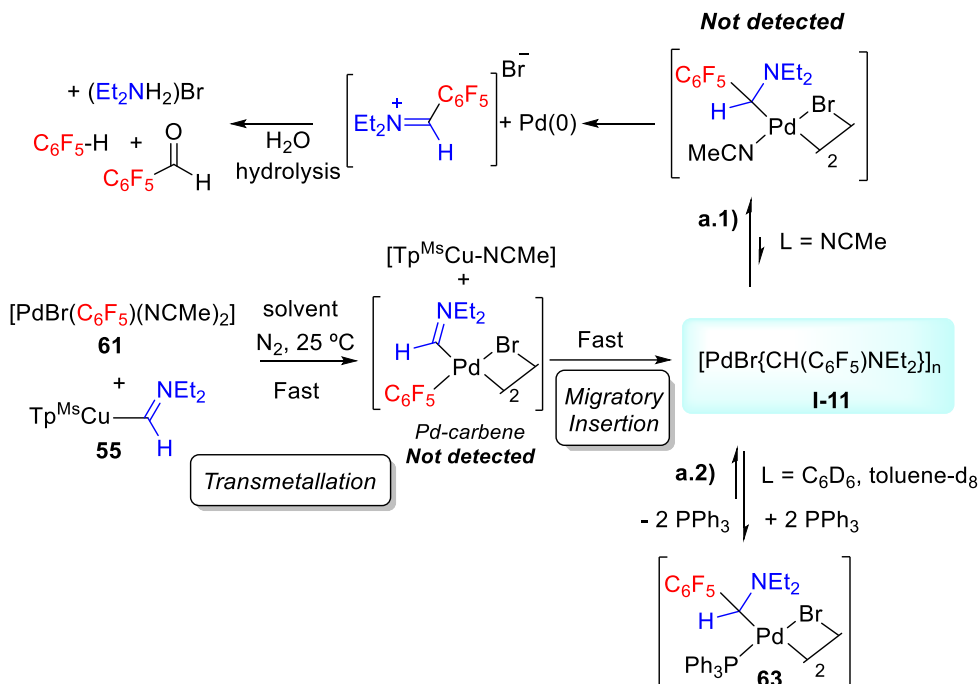
Figure 7.12 Proposed structures for **I-11** ($[\text{PdBr}\{\text{CH}(\text{C}_6\text{F}_5)\text{NEt}_2\}]_n$).

Scheme 7.9 depicts a summary of the data collected for the carbene transmetalation from $[\text{Tp}^{\text{Ms}}\text{Cu}\{\text{CH}(\text{NEt}_2)\}]$ to Pd(II) complex **61**, which bears C_6F_5 as a model aryl group, and the subsequent migratory insertion. It was found that the aminocarbene transmetalation is fast at low temperatures because of the rapid disappearance of the characteristic signals in ^1H NMR of the $\{\text{:CH}(\text{NEt}_2)\}$ fragment bound to Cu(I). No intermediate bearing the Pd– $\text{CH}(\text{NEt}_2)$ and Pd– C_6F_5 bonds could be detected in the monitoring of the reactions because the migratory insertion of the $\text{:CH}(\text{NEt}_2)$ fragment into the Pd– C_6F_5 is also fast and generates intermediate **I-11**. When a coordinating solvent is used (acetonitrile), this intermediate **I-11** undergoes a rapid decomposition towards the iminium salt, which in the presence of water give the hydrolysis product (pentafluorobenzaldehyde) (Scheme 7.9, **a.1**). Nonetheless, when the

²³² a) Owen, G. R.; Vilar, R.; White, A. J. P.; Williams, D. J. *Organometallics* **2003**, *22*, 3025–3027. b) Lu, C. C.; Peters, J. C. *J. Am. Chem. Soc.* **2004**, *126*, 15818–15832. c) Xie, Y.; Hu, J.; Wang, Y.; Xia, C.; Huang, H. *J. Am. Chem. Soc.* **2012**, *134*, 20613–20616.

²³³ Albéniz, A. C.; Espinet, P.; Lin, Y.-S.; Orpen, A. G.; Martín, A. *Organometallics* **1996**, *15*, 5003–5009.

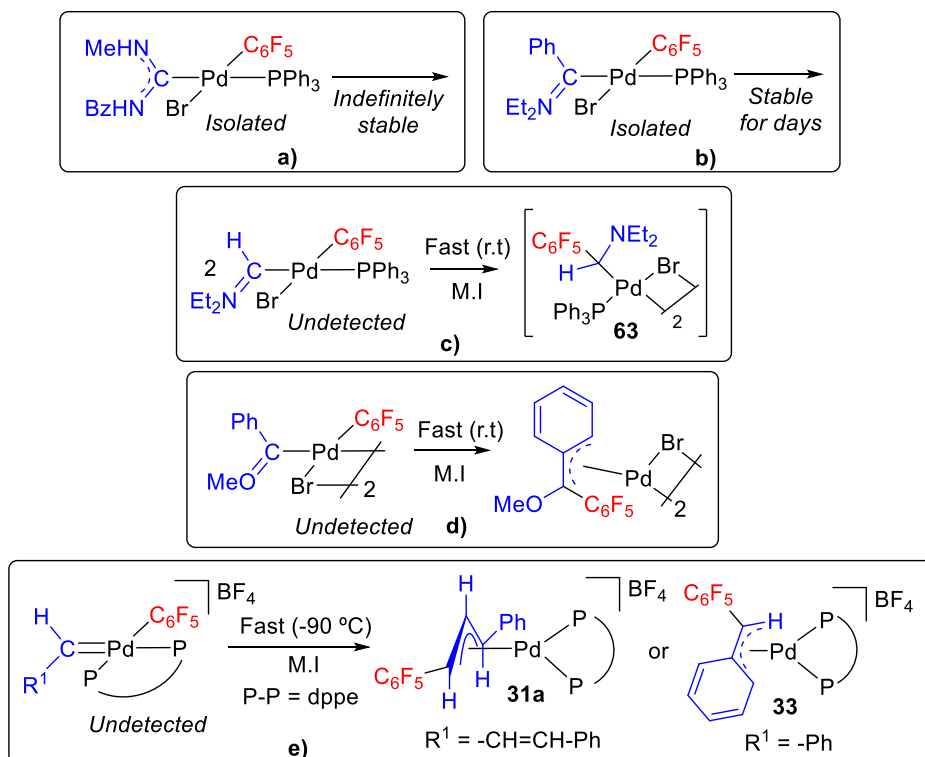
same reaction was carried out in the much less coordinating solvents, such as benzene or toluene, intermediate **I-11** could be detected and it reacts in the presence of triphenylphosphine affording a stable complex **63** which represent the organometallic product obtained just after the migratory insertion step (Scheme 7.9, **a.2**). This situation is comparable to the isolated complexes **31a** and **33** shown in *Chapter 5* when the carbene is originated from a diazoalkane precursor.



Scheme 7.9 Summary of the migratory insertion process depending on the Pd(II) precursor and solvents involved.

The results described in the previous *Chapters 5* and *6* along with the previous studies in our group indicate that the electrophilicity of the carbenic carbon dictates the rates in the migratory insertion into Pd-C₆F₅ bond for Pd(II) complexes (Scheme 7.10). Inasmuch as the migratory insertion can be described as the interaction between the electron density of the Pd-C₆F₅ bond and a vacant orbital of the carbenic carbon, the more electrophilic the carbene is, the faster the migratory insertion occurs. Therefore, we can correlate the migratory insertion rates with the electrophilic nature of the carbene group. For the selected Pd-carbenes show in Scheme 7.10, the reactivity trend towards migratory insertion is the following: C(NHMe)(NHBz) << :C(NEt₂)(R¹) < :C(NEt₂)(H) ~ :C(OMe)(Ph) < :C(R²)(H). This trend is clearly influenced by the number of

heteroatoms bound to the carbenic carbon and also the electronegativity of these heteroatoms which in turn is an indication of the electron deficiency of the carbene carbon (*cf.* **b**) and **d**) in Scheme 7.10) However the reactivity of the $:\text{CH}(\text{NEt}_2)$ fragment observed here is surprising since it is closer to the methoxo carbene than to the analogous monoamino carbene.



Scheme 7.10 Behaviour towards migratory insertion (M.I.) of different Pd(II)-carbenes into Pd-C₆F₅ bond.

Using Density Functional Theory, Prof. Agustí Lledós has calculated some electronic descriptors such as the electrophilicity index (ω) and the nucleophilicity index (N) for a selected number of free carbenes as shown in Table 7.1 and Figure 7.13. Parr, Maynard and other authors defined the “electrophilicity index” (ω) using the electronic chemical potential (μ) and the chemical hardness (η).²³⁴ Both parameters are related to the HOMO and LUMO energies by the following Equations:

²³⁴ a) Pearson, R. G. *Inorg. Chem.* **1988**, *27*, 734–740. b) Maynard, A. T.; Huang, M.; Rice, W. G.; Covell, D. G. *Proc. Natl. Acad. Sci. U.S.A.* **1998**, *95*, 11578. c) Parr, R. G.; Szentpály, L. v.; Liu, S. J. *Am. Chem. Soc.* **1999**, *121*, 1922–1924. c) Chattaraj, P. K.; Roy, D. R. *Chem. Rev.* **2007**, *107*, PR46–PR74.

$$\omega = \frac{\mu^2}{2\eta};$$

$$\mu = (\epsilon_{\text{LUMO}} + \epsilon_{\text{HOMO}})/2 \text{ and } \eta = (\epsilon_{\text{LUMO}} - \epsilon_{\text{HOMO}})$$

The (*N*) nucleophilicity index is related to the energy of the HOMO of the carbene and is correlated with the energy of the HOMO of tetracyanoethylene (TCE) taken as a reference ($N_{\text{TCE}} = 0.0 \text{ eV}$).²³⁵

$$N = (\epsilon_{\text{HOMO}}(\text{carbene}) - \epsilon_{\text{HOMO}}(\text{TCE}))$$

Table 7.1 Values for the ω and *N* for different free carbenes.

Entry	carbenes	ϵ_{HOMO} (eV)	ϵ_{LUMO} (eV)	Global electrophilicity ω (eV)	Global nucleophilicity <i>N</i> (eV)
1	IPr ^a	-5.95	-0.12	0.79(4)	2.56(7)
2	:C(NEt ₂)(Ph)	-4.83	-0.09	0.64(6)	3.68(1)
3	:CH(NEt ₂)	-5.38	-0.02	0.68(5)	3.13(2)
4	:C(OMe)(Ph)	-5.45	-1.70	1.70(1)	3.06(3)

^a IPr = 1,3-bis(2,6-diisopropylphenyl)imidazolin-2-ylidene.

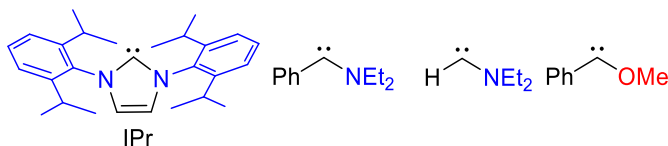


Figure 7.13 Free carbenes depicted in Table 7.1.

From the values of Table 7.1, it is clear the difference between the carbene bearing one alkoxy substituent and those carbenes that bear one or two amino substituents (*cf.* entries 1-3 and entry 4, Table 7.1), in line with the expected trend. The monoamino carbenes :C(R)(NEt₂) (R = Ph or H) have almost identical electrophilicity indexes, which contrasts with the different migratory insertion rates observed experimentally (Scheme 7.10, **b**) and **c**). The ω and *N* descriptors have been calculated for free-carbenes and not for Pd(II)-carbene complexes. Once the carbene is coordinated to the palladium center, the electronic features of the carbene may vary (extent of donation, for example) and this can affect its electrophilicity. However, the discrepancies

²³⁵ a) Domingo, L. R.; Chamorro, E.; Pérez, P. *J. Org. Chem.* **2008**, *73*, 4615–4624. b) Domingo, L. R.; Pérez, P. *Org. Biomol. Chem.* **2011**, *9*, 7168–7175.

observed between the calculated values and the experimental results for the $:\text{CH}(\text{NEt}_2)$ carbene are too high. The abovementioned discussion was focused only on electronic features but the steric hindrance of the carbene substituents has not been considered. This may be an important factor to allow the approach of the carbene and the aryl fragments and facilitate the migratory insertion reaction.

7.3 CONCLUSIONS

The direct aminocarbene transmetallation from $[\text{Tp}^{\text{Ms}}\text{Cu}\{\text{CH}(\text{NEt}_2)\}]$ (**55**) to Pd(II) complexes $[\text{PdCl}_2(\text{NCMe})_2]$ (**56**) and $[\text{Pd}_2(\mu\text{-Cl})_2\text{Cl}_2(\text{PPh}_3)_2]$ (**58**) occurs fast at room temperature and also at $-40\text{ }^\circ\text{C}$. This aminocarbene transmetallation leads to the formation of the Pd(II)-aminocarbene complexes $[\text{Pd}\{\text{CH}(\text{NEt}_2)_2\}\text{Cl}_2(\text{NCMe})]$ (**57**) and *cis*- $[\text{Pd}\{\text{CH}(\text{NEt}_2)_2\}\text{Cl}_2(\text{PPh}_3)]$ (**60**) which can be isolated and characterized. The hydrolysis products observed reveal an electrophilic behaviour of the aminocarbene. DFT calculation which model the transmetallation reaction show accessible activation energy barriers (energetic span of $18.4\text{ kcal mol}^{-1}$) which is consistent with the experimental results. Furthermore, the aminocarbene transfer from Cu(I) to Pd(II) proceeds through a three-membered metallacycle between $[\text{Cu}(\text{I}) - \text{C}_{\text{carbenic}} - \text{Pd}(\text{II})]$ upon decoordination of one pyrazole ring in the $[\text{Tp}^{\text{Ms}}]$ ligand. These reactions show that $[\text{Tp}^{\text{Ms}}\text{Cu}\{\text{CH}(\text{NEt}_2)\}]$ can be used as a source of this unusual monosubstituted carbene fragment to synthesize other metal carbenes.

On the other hand, when the palladium complex bears an aryl group (Pd- C_6F_5 moiety), the Pd-aminocarbene resulting from the transmetallation was not detected. The migratory insertion of the aminocarbene into the Pd- C_6F_5 bond proceeds fast at room temperature, leading the formation of palladium alkyl complexes $[\text{PdBr}\{\text{CH}(\text{C}_6\text{F}_5)\text{NEt}_2\}]_n$ (**I-11**) and $[\text{PdBr}\{\text{CH}(\text{C}_6\text{F}_5)\text{NEt}_2\}(\text{PPh}_3)_2]$ (**63**) in low coordinating solvents. The migratory insertion reaction rate for this carbene is higher than expected from its electronic features, *i.e.* its electrophilicity. The low steric demand of the monosubstituted $\text{CH}(\text{NEt}_2)$ may facilitate the approach to the aryl group and the coupling process.

7.4 EXPERIMENTAL PART

7.4.1 General considerations

^1H , $^{13}\text{C}\{^1\text{H}\}$, ^{19}F and ^{31}P NMR spectra were recorded on an Agilent MR-500 and MR-400 spectrometers equipped with variable-temperature probes at the *Laboratorio de Técnicas Instrumentales* (LTI) of the UVA. Chemical shifts (in δ units, ppm) were referenced to SiMe_4 (^1H and ^{13}C) and CFCl_3 (^{19}F) and H_3PO_4 (85 %, ^{31}P). The temperature for the NMR probe was calibrated with a methanol standard (low temperature).¹⁹³ Homonuclear (^1H and ^{19}F -COSY) and heteronuclear (^1H - ^{13}C HSQC and HMBC) experiments were used to help with the signal assignments. NMR data are given at 298 K unless otherwise noted. Elemental analyses were carried out in a Carlo Erba 1108 microanalyser (at the Vigo University, Spain). All reactions were conducted under a N_2 atmosphere with dry solvents. Solvents were dried using a solvent purification system SPS PS-MD-5 (ether, hexane, THF and CH_2Cl_2) or distilled from appropriate drying agents under nitrogen prior to use and stored over 3 Å or 4 Å molecular sieves (acetonitrile- d_3 , CDCl_3 , C_6D_6 and toluene- d_8). The palladium complexes $[\text{PdCl}_2(\text{NCMe})]$,²³⁶ $[\text{Pd}(\mu\text{-Br})_2(\text{C}_6\text{F}_5)_2(\text{PPh}_3)_2]$ ²³⁷ and $[\text{PdBr}(\text{C}_6\text{F}_5)(\text{PPh}_3)_2]$ ⁸⁶ were prepared as reported before.

7.4.2 Synthesis of Palladium complexes

Preparation of $[\text{PdCl}_2\{\text{CH}(\text{NEt}_2)\text{NCMe}\}]$ (**57**)

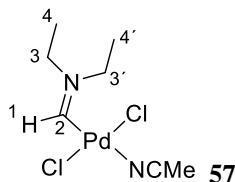
$[\text{Tp}^{\text{Ms}}\text{Cu}\{\text{CH}(\text{NEt}_2)\}]$ (140.7 mg, 0.196 mmol) was added to a solution of $[\text{PdCl}_2(\text{NCMe})]$ (51.0 mg, 0.196 mmol) in CH_3CN anhydrous (5 mL) at 0 °C. The reaction mixture turned to an intense yellow colour and it was stirred under N_2 at room temperature for 16 h. After this time, the mixture was treated with activated carbon, then cannulated into a Schlenk under a nitrogen atmosphere. The intense-yellow solution was concentrated to dryness, obtaining a yellow oil which was characterized by NMR.

When this yellow oil was treated with anhydrous Et_2O and *n*-hexane (15 mL, 1:1 (v/v)) a dark-brown solid was obtained. Yield: 34 mg (66 %). This brown-solid is a mixture of complex **57** along with the tentatively proposed dimeric palladium derivatives of formula $[\text{Pd}_2(\mu\text{-Cl})_2\text{Cl}_2\{\text{CH}(\text{NEt}_2)_2\}]$ that transform into **57** when dissolved in CH_3CN (see Figure 7.2).

^1H NMR (499.73 MHz, δ , CD_3CN): 9.54 (s, 1H, H^1), 4.47 (q, $J = 7.36$ Hz, 2H, H^3), 3.70 (q, $J = 7.26$ Hz, 2H, H^3), 1.56 (t, $J = 7.36$ Hz, 3H, H^4), 1.23 (t, $J = 7.26$ Hz, 3H, H^4). $^{13}\text{C}\{^1\text{H}\}$ NMR (125.67 MHz, δ , CD_3CN): 206.4 (C^2), 55.2 (C^3), 55.1 (C^3), 13.5 (C^4), 12.5 (C^4).

²³⁶ Hartley, F. R.; Murray, S. G.; McAuliffe, C. A. *Inorg. Chem.* **1979**, *18*, 1394–1397.

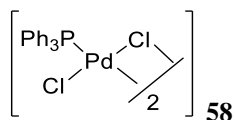
²³⁷ Elia, C.; Elyashiv-Barad, S.; Sen, A.; López-Fernández, R.; Albéniz, A. C.; Espinet, P. *Organometallics* **2002**, *21*, 4249–4256.



Preparation of $[\text{Pd}_2(\mu\text{-Cl})_2\text{Cl}_2(\text{PPh}_3)_2]$ (**58**)

$[\text{PdCl}_2(\text{NCMe})_2]$ (133 mg, 0.513 mmol) was added to a solution of $[\text{Pd}_2\text{Cl}_2(\text{PPh}_3)_2]$ (300 mg, 0.427 mmol) in acetone (100 mL) at room temperature. The reaction mixture turned to an intense yellow colour and it was vigorously stirred at reflux for 16 h. After this time, the solution colour was intense orange. The solvent was evaporated to *ca.* 15 mL and the resulting orange solid was filtered, washed with Et_2O and dried under vacuum. Yield: 311 mg (83 %).

^1H NMR (499.73 MHz, δ , CDCl_3): 7.72 (m, 2H, H^{ortho}), 7.51 (m, 1H, H^{para}), 7.42 (m, 2H, H^{meta}). $^{13}\text{C}\{^1\text{H}\}$ NMR (125.67 MHz, δ , CDCl_3): 135.0 (C^{ipso}), 134.6 (C^{ortho}), 131.7 (C^{para}), 128.4 (C^{meta}). $^{31}\text{P}\{^1\text{H}\}$ NMR (202.31 MHz, δ , CDCl_3): 32.7 (s, 2P). IR (neat, cm^{-1}): (Pd-Cl) 357; (Pd-(μ -Cl)) 259.²³⁸ Anal. Calcd for $\text{C}_{36}\text{H}_{30}\text{Cl}_4\text{P}_2\text{Pd}_2$: C, 49.18 %; H, 3.44. Found: C, 49.23 %; H, 3.48.



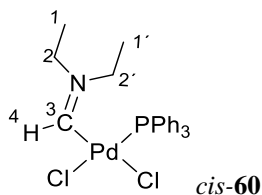
Preparation of *cis*- $[\text{PdCl}_2\{\text{CH}(\text{NEt}_2)\}\text{PPh}_3]$ (*cis*-**60**)

$[\text{Tp}^{\text{Ms}}\text{Cu}\{\text{CH}(\text{NEt}_2)\}]$ (90 mg, 0.125 mmol) was added to a solution of $[\text{Pd}(\mu\text{-Cl})_2\text{Cl}_2(\text{PPh}_3)_2]$ (55.2 mg, 0.062 mmol) in CH_3CN (10 mL) at room temperature. The reaction mixture turned to an intense yellow colour and it was stirred under N_2 at room temperature for 1.5 h. After this time, the suspension was cannulated under a nitrogen atmosphere, removing this way the solid formed in the reaction. The solvent was evaporated to *c.a.* 3 mL and dry-diethyl ether (3 x 10 mL) was added to the suspension. The yellow solid obtained was filtered, washed with dry diethyl ether (2 x 5 mL) and vacuum dried. Finally, complex *cis*-**60** was recrystallized by diffusion of dry *n*-hexane into a solution of the complex in dry dichloromethane at -28°C under a nitrogen atmosphere, giving colourless crystals. Yield: 36 mg (55 %).

^1H NMR (499.73 MHz, δ , CDCl_3): 9.32 (d, $J_{\text{H}^4\text{-P}} = 8.0$ Hz, $^1J_{\text{C}^3\text{-H}^4} = 162$ Hz, 1H, H^4), 7.76 (m, 2H, H^{ortho}), 7.49 (m, 1H, H^{para}), 7.44 (m, 2H, H^{meta}), 4.21 (q, $J = 7.37$ Hz, 2H, H^2), 3.12 (q, $J = 7.26$ Hz, 2H, $\text{H}^{2'}$), 1.33 (t, $J = 7.37$ Hz, 3H, H^1), 0.91 (t, $J = 7.26$ Hz, 3H, $\text{H}^{1'}$). $^{13}\text{C}\{^1\text{H}\}$ NMR (125.67 MHz, δ , CDCl_3): 216.5 (C^3), 134.4 (d, $^2J_{\text{C-P}} = 11.3$ Hz,

²³⁸ a) Lupin, M. S.; Powell, J.; Shaw, B. L. *J. Chem. Soc. A Inorganic, Phys. Theor.* **1966**, 1410–1411 b) Goodfellow, R. J.; Goggin, P. L.; Venanzi, L. M. *J. Chem. Soc. A Inorganic, Phys. Theor.* **1967**, 1897–1900.

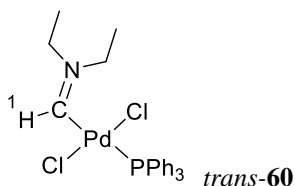
C^{ortho}), 131.3 (d, $^4J_{C-P} = 2.7$ Hz, C^{para}), 130 (d, $^1J_{C-P} = 53.6$ Hz, C^{ipso}), 128.7 (d, $^3J_{C-P} = 11.1$ Hz, C^{meta}), 56.3 (C^2), 54.9 ($C^{2'}$), 12.8 (C^1), 12.4 (C^1). $^{31}\text{P}\{^1\text{H}\}$ NMR (202.31 MHz, δ , CDCl_3): 25.55 (s, 1P). HRMS (ESI-TOF) m/z calcd. for $\text{C}_{23}\text{H}_{26}\text{Cl}_2\text{NNaPPd}$ [$M + \text{Na}$] $^+$ 546.0110. found 546.0113.



Detection of *trans*-[PdCl₂{CH(NEt₂)}PPh₃] at -40 °C. (*trans*-**60**)

[Tp^{Ms}Cu{CH(NEt₂)}] (**55**) (9.3 mg, 0.013 mmol) and 0.6 mL of dry CD₃CN were added into an NMR tube under a nitrogen atmosphere, and placed in cooled bath at -90 °C. Then, [Pd₂(μ -Cl)₂(Cl)₂(PPh₃)₂] (**58**) (5.7 mg, 0.0065 mmol) was added and the tube was closed. The resulting mixture was frozen during the setup of the NMR-experiment. Finally, the sample was shaken vigorously inside the cool bath, wiped externally and introduced in the NMR probe already set at the measurement temperature (-40 °C).

^1H NMR (499.73 MHz, δ , CDCl_3 , 233 K): 9.68 (d, $J = 11.0$ Hz, 1H, H¹), 4.43 (q, $J = 7.3$ Hz, 2H, CH₂), 3.72 (q, $J = 7.3$ Hz, 2H, C¹H₂), 1.56 (t, $J = 7.3$ Hz, 3H, CH₃), 1.25 (t, $J = 7.3$ Hz, 3H, C¹H₃).



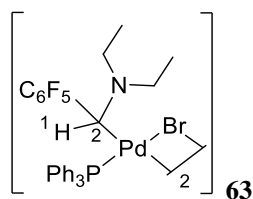
Preparation of [Pd(μ -Br){CH(C₆F₅)(NEt₂)}PPh₃]₂ (**63**)

A solution of [Tp^{Ms}Cu{CH(NEt₂)}] (151.9 mg, 0.212 mmol) in 10 mL of anhydrous toluene was added to [Pd(μ -Br)₂(C₆F₅)₂(PPh₃)₂] (130.5 mg, 0.106 mmol) dissolved in toluene (5 mL) at room temperature. The reaction mixture turned to an intense yellow colour and it was vigorously stirred under N₂ at room temperature for 5 h. After this time, the solution was evaporated to dryness. The off-white solid obtained was redissolved in anhydrous CH₃CN (10 mL) at -30 °C, then the yellow suspension was cannulated to a 50 mL-Schlenk under a nitrogen atmosphere. The resulting solution was evaporated to dryness and 10 mL of dry Et₂O and *n*-hexane (1:1, v/v) were added to redissolve complex **63** and precipitate the Pd byproducts. The yellow suspension was cannulated under a nitrogen atmosphere to a 50 mL-Schlenk and the solvent was evaporated to dryness, obtaining a yellow-solid.

^1H NMR (499.73 MHz, δ , CD_3CN , **298 K**): 7.60 (m, 6H, H^{arom}), 7.42-7.33 (m, 9H, H^{arom}), 4.64 (d, $J_{\text{H-P}} = 4.6$ Hz, 2H, H^1), 3.41 (m, 2H, H^{CH_2}), 3.30 (m, 2H, H^{CH_2}), 2.91 (m, 2H, H^{CH_2}), 2.81 (m, 2H, H^{CH_2}), 1.39 (t, $J = 7.13$ Hz, 6H, H^{CH_3}), 1.30 (t, $J = 7.17$ Hz, 6H, H^{CH_3}). $^{13}\text{C}\{^1\text{H}\}$ NMR (125.67 MHz, δ , CD_3CN , 298 K): 133.7 (d, $J = 13$ Hz, C^{ortho} , PPh_3), 133.3 (d, $J = 42$ Hz, C^{ipso} , PPh_3), 130.0 (d, $J = 2.2$ Hz, C^{para} , PPh_3), 128.2 (d, $J = 10$ Hz, C^{meta} , PPh_3), 55.0 (C^2), 52.2 (CH_2), 46.1 (CH_2), 12.2 (CH_3), 12.5 (CH_3).* ^{19}F NMR (470.17 MHz, δ , CD_3CN , **298 K**): -157.04 (t, $J = 19.8$ Hz, 1F, F_{para}), -164.83 (br, 2F, F_{meta}).† ^{19}F NMR (470.17 MHz, δ , toluene- d_8 , **223 K**): -129.36 (br, 1F, F_{ortho}), -141.81 (br, 1F, F_{ortho}), -155.38 (t, $J = 22$ Hz, 1F, F_{para}), -161.89 (br, 1F, F_{meta}), -163.82 (br, 1F, F_{meta}). $^{31}\text{P}\{^1\text{H}\}$ NMR (202.31 MHz, δ , CD_3CN , **298 K**): 33.76 (t, $J_{\text{P-F}} = 13.2$ Hz). HRMS (ESI-TOF) m/z calcd. for $\text{C}_{58}\text{H}_{52}\text{Br}_2\text{F}_{10}\text{N}_2\text{NaP}_2\text{Pd}_2$ [$\text{M} + \text{Na}$] $^+$ 1420.9790. Found 1420.9774.

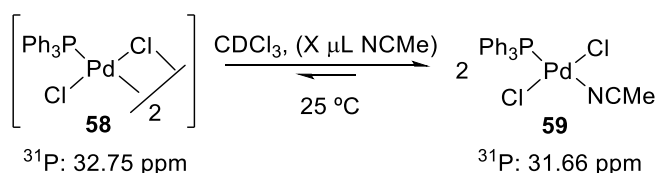
* ^{13}C signals for the C_6F_5 group, heavily coupled to F, could not be located.

† Restricted rotation about the C- C_6F_5 leads to F_{ortho} signals that coalesce at 298 K and are not visible.



7.4.3 Evidence for the chloride bridge cleavage by acetonitrile in complex $[\text{Pd}_2(\mu\text{-Cl})_2(\text{Cl})_2(\text{PPh}_3)_2]$

Palladium complex (**58**) (16.8 mg, 0.019 mmol) was placed into an NMR tube with CDCl_3 (0.6 mL). After that, acetonitrile (1 μL , 0.019 mmol) (mol ratio Pd:NCMe = 1:0.5) was added to the NMR tube. The tube was introduced into the NMR probe and the species formed in solution at room temperature were examined by ^1H and ^{31}P NMR. A second addition of acetonitrile (5 μL , 0.096 mmol) in the same tube sample was performed after 15. Total ratio (Pd:NCMe = 1:3).



Equation 7.4

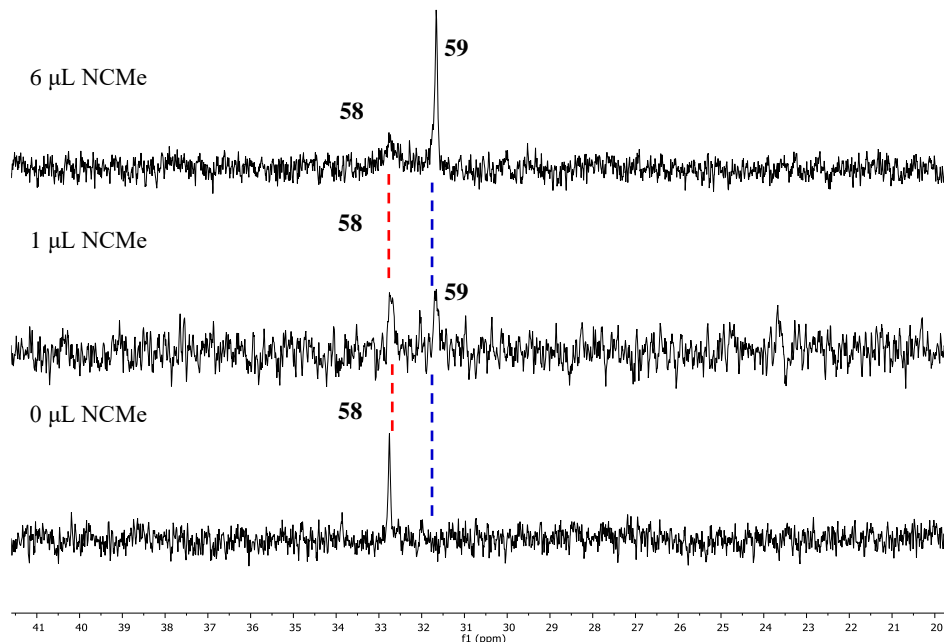
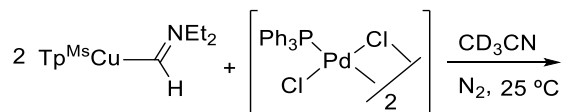


Figure 7.14 $^{31}\text{P}\{^1\text{H}\}$ NMR (202.31 MHz, CDCl_3) of reaction shown in Equation 7.4.

7.4.4 Follow up of the carbene transmetalation from Cu(I) to Pd(II)

Transmetalation to $[\text{Pd}_2(\mu\text{-Cl})_2(\text{Cl})_2(\text{PPh}_3)_2]$ at room temperature

$[\text{Tp}^{\text{Ms}}\text{Cu}\{\text{CH}(\text{NEt}_2)\}]$ (2.0 mg, 0.0028 mmol) and $[\text{Pd}_2(\mu\text{-Cl})_2(\text{Cl})_2(\text{PPh}_3)_2]$ (1.22 mg, 0.0014 mmol) were added into an NMR tube under a nitrogen atmosphere in CD_3CN (0.6 mL). The resulting mixture was frozen during the setup of the NMR experiment ($-50\text{ }^\circ\text{C}$). Finally, the sample was shaken vigorously inside the cool bath, wiped externally and introduced in the NMR probe already set at the measurement temperature ($25\text{ }^\circ\text{C}$). The reaction was monitored by ^1H NMR, at $25\text{ }^\circ\text{C}$ for 25 min (3 min interval) (Equation 7.5, Figure 7.15).



Equation 7.5

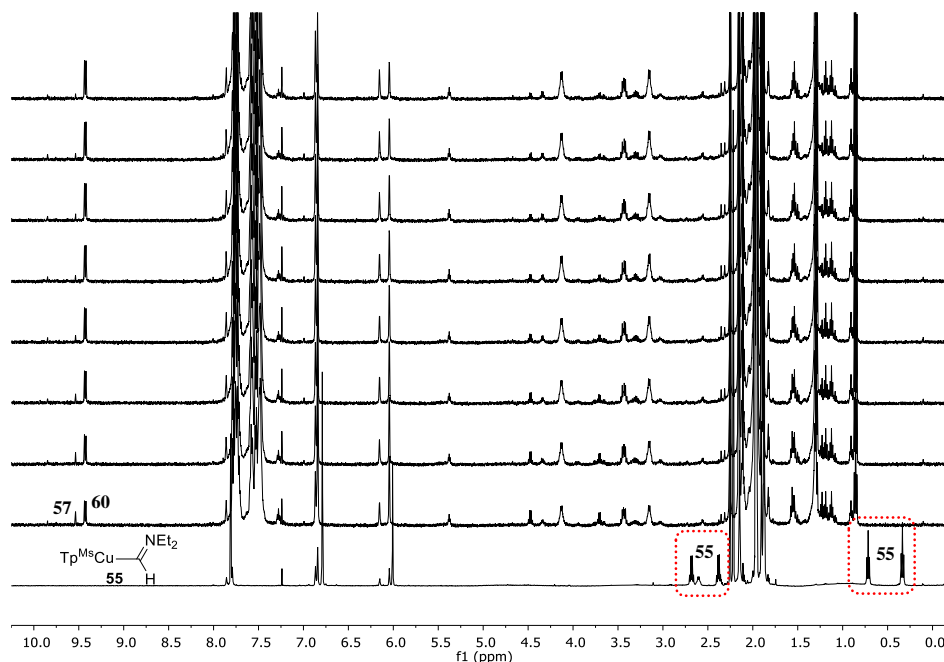
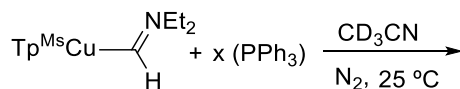


Figure 7.15 ^1H NMR (499.73 MHz, CD_3CN) of reaction shown in Equation 7.5). First spectrum corresponds to the Cu-carbene complex **55** in CD_3CN .

The transmetalation of the carbene from $[\text{Tp}^{\text{Ms}}\text{Cu}\{\text{CH}(\text{NEt}_2)\}]$ to $[\text{Pd}_2(\mu\text{-Cl})_2(\text{Cl})_2(\text{PPh}_3)_2]$ at variable temperature (from $-40\text{ }^\circ\text{C}$ to $25\text{ }^\circ\text{C}$) was carried out in the same way. The spectra are collected in Figure 7.5.

7.4.5 Attempts at detection of a $[\text{Tp}^{\text{Ms}}\text{Cu}(\text{PPh}_3)]$ adduct

$[\text{Tp}^{\text{Ms}}\text{Cu}\{\text{CH}(\text{NEt}_2)\}]$ (9.4 mg, 0.013 mmol) in 0.6 mL of CD_3CN was added into an NMR tube under a nitrogen atmosphere. Then, PPh_3 (0.9 mg, 0.0026 mmol, $\text{Cu}:\text{PPh}_3 = 1:0.2$ mol ratio) was added and the tube was closed. The formation of the species in solution was monitored by ^{31}P NMR at room temperature. After 10 min, PPh_3 (2.5 mg, 0.0096 mmol) was added to the same sample to reach a $\text{Cu}:\text{PPh}_3 = 1:1$ mol ratio (Equation 7.6).



Equation 7.6

When the same reaction was carried out with $[\text{Tp}^{\text{Ms}}\text{Cu}(\text{THF})]^{239}$ instead of complex **55** and PPh_3 ($\text{Pd}:\text{PPh}_3 = 1:1.5$ mol ratio), no $[\text{Tp}^{\text{Ms}}\text{Cu}-\text{PPh}_3]$ adduct was observed in CD_3CN or CD_2Cl_2 solvents at room temperature or $60\text{ }^\circ\text{C}$ in CD_3CN .

²³⁹ Complex $[\text{Tp}^{\text{Ms}}\text{Cu}(\text{THF})]$ is the direct precursor for the synthesis of complex **55** and at the same time bears a labile ligand susceptible to be displaced by the PPh_3 ligand. Schneider, J. L.; Carrier, S. M.; Ruggiero, C. E.; Young, V. G.; Tolman, W. B. *J. Am. Chem. Soc.* **1998**, *120*, 11408–11418.

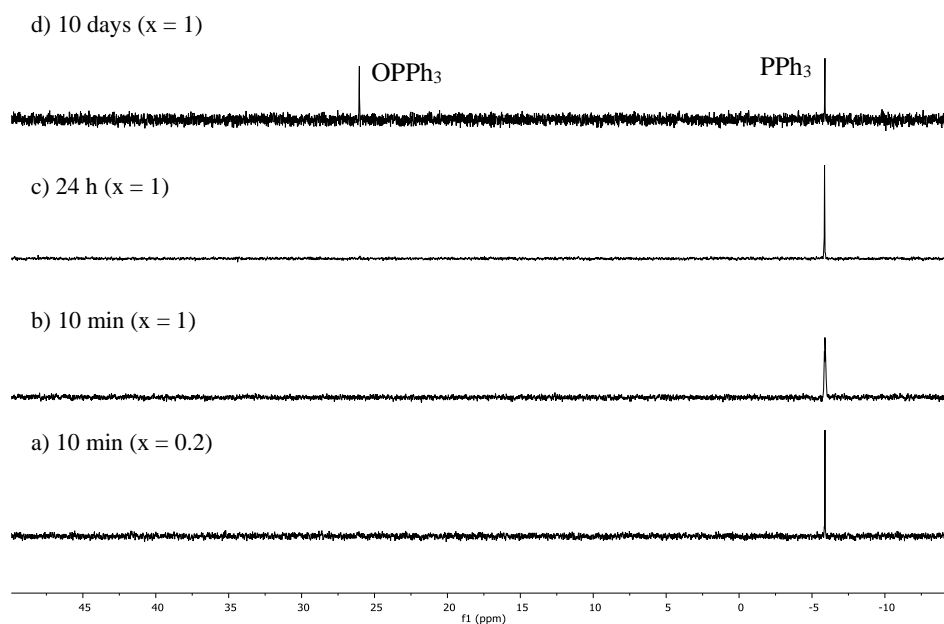


Figure 7.16 ^1H NMR (499.73 MHz, CD_3CN) of reaction shown in Equation 7.6 at 298 K, $\text{Pd}:\text{PPh}_3$ mol ratio (x).

7.4.6 Mass spectra

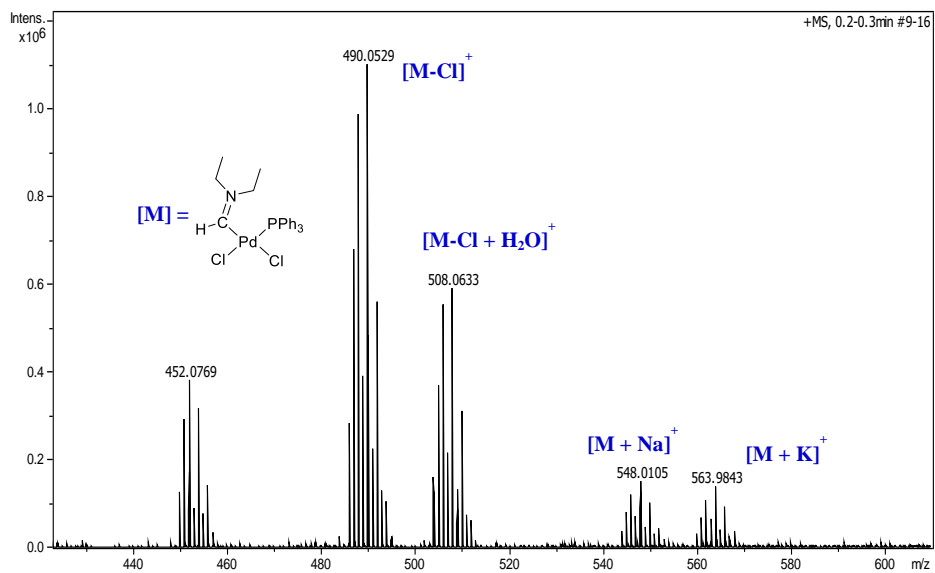


Figure 7.17 HR-MS (ESI-TOF) (positive mode) of complex *cis-60*.

Table 7.2

Meas. m/z (found)	m/z (Calcd)	err [ppm]	mSigma	Ion Formula
488.0536	488.0527	-1.9	38.5	C ₂₃ H ₂₆ CINPPd
506.0640	506.0632	-1.6	25.3	C ₂₃ H ₂₆ CINPPd·H ₂ O
546.0113	546.0110	-0.5	34.0	C ₂₃ H ₂₆ Cl ₂ NNaPPd
561.9852	561.9849	-0.5	10.5	C ₂₃ H ₂₆ Cl ₂ KNPPd

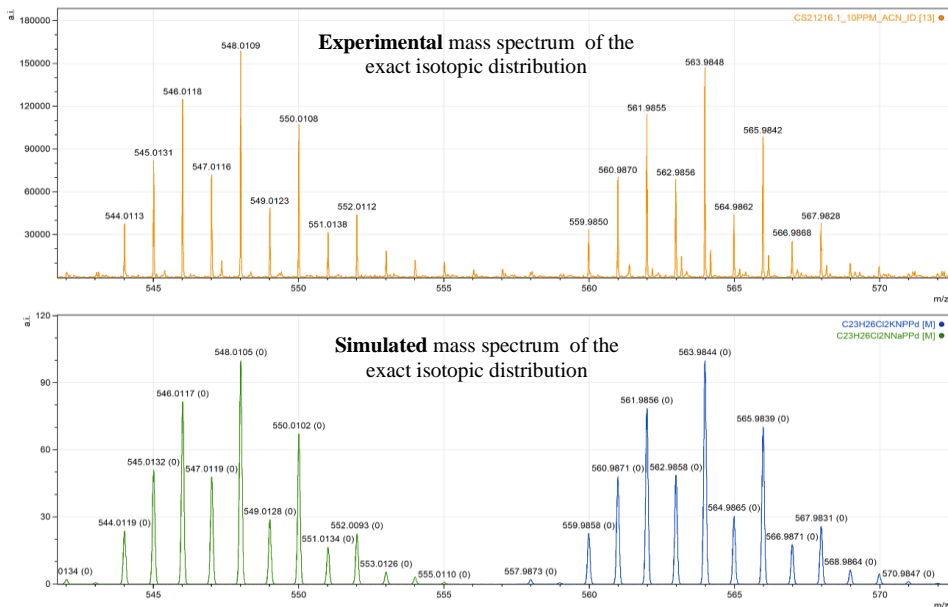


Figure 7.18 HR-MS (ESI-TOF) (positive mode) of complex *cis*-60. Isotope pattern experimental (above) and simulated (bottom). [PdCl₂{CH(NEt₂)}PPh₃·Na]⁺ (left plot) and [PdCl₂{CH(NEt₂)}PPh₃·K]⁺ (right plot).

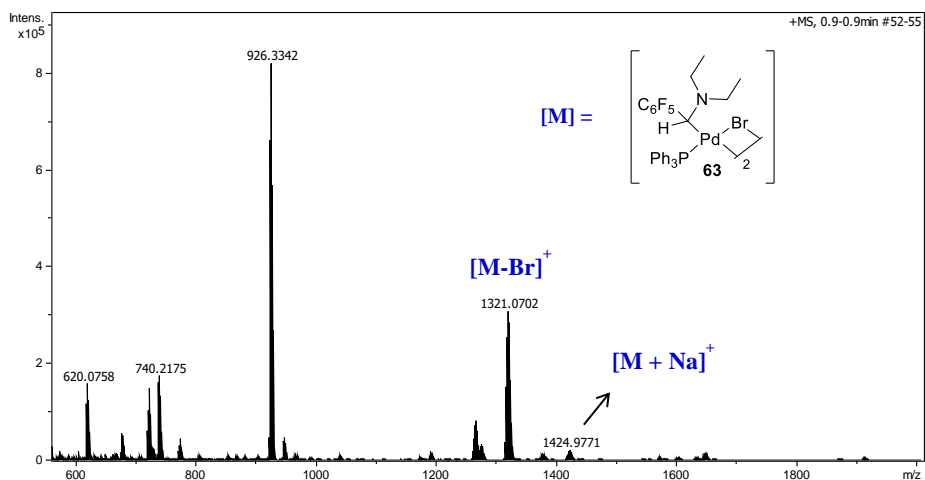


Figure 7.19 HR-MS (ESI-TOF) (positive mode) of complex **63**.

Table 7.3

Meas. m/z (found)	m/z (Calcd)	err [ppm]	mSigma	Ion Formula
1.420,9774	1.420,9790	1.1	19.5	C ₅₈ H ₅₂ Br ₂ F ₁₀ N ₂ P ₂ Pd ₂ Na
1.319,0699	1.319,0714	1.1	23.2	C ₅₈ H ₅₂ BrF ₁₀ N ₂ P ₂ Pd ₂

7.4.7 Computational details

All calculations were initially performed using the DFT approach with the M06 functional using Gaussian 16 as program package. The selected basis set was 6-311++G(d,p) for C, P, N, Cl and H and LANL2TZ(f) for Pd (Basis set I). Solvation was introduced in all the optimizations, frequency calculations and potential energy refinement through the SMD model, where we applied the experimental solvent, acetonitrile ($\epsilon = 35.688$). All geometry optimizations were carried out in solution with no symmetry restrictions. Free energy corrections were calculated at 298.15 K and 10^5 Pa pressure, including zero-point energy corrections (ZPE), and the energies were converted to 1M standard state in solution (adding/subtracting $1.89 \text{ kcal mol}^{-1}$ for non-unimolecular processes). Vibrational frequency calculations were performed to establish the stationary points were minima (without imaginary frequencies) or transition states (with one imaginary frequency). All reported energies in the manuscript correspond to Gibbs energies in solution, obtained from potential energies (including solvation) plus Gibbs energy corrections with basis set I and are given in kcal mol^{-1} (see SCF energy and free energy correction values in *Supporting information*). The constant coupling between the -H proton and the -P atom in the complex *trans-60* was calculated using GIAO (*Gauge-Independent Atomic Orbital*) method, obtaining a simulated value of 11.34 Hz (experimental value 11.0 Hz).

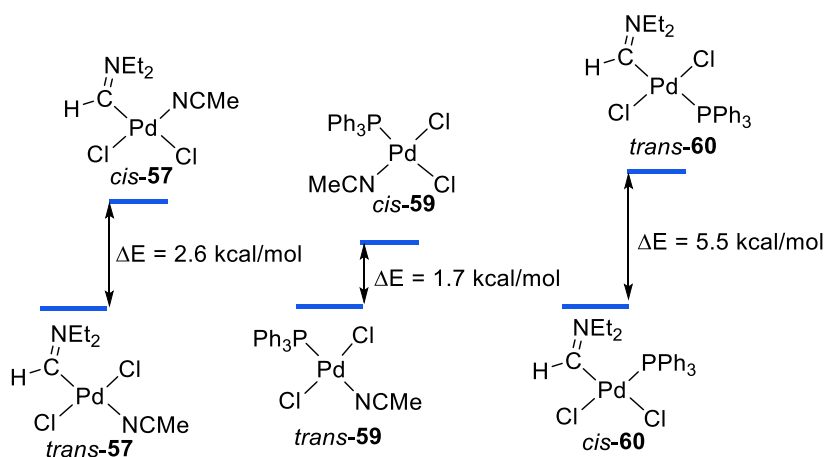


Figure 7.20 Gibbs energies for the *cis:trans* conformations of complexes **57**, **59** and **60**.

*Transformaciones Mediadas por Paladio: C-H
Alquenilación Aeróbica de Arenos Asistida por
Cooperación Metal-Ligando y Reacciones con
Precursores de Carbeno*

Resumen

PREFACIO

Uno de los principales objetivos en Química es conseguir procesos sintéticos mucho más eficientes. Es por ello que, el trabajo contenido en la presente tesis, trata de contribuir a este fin mediante la mejora en la eficiencia de los procesos catalizados por paladio. Con este propósito, mi investigación se ha centrado en desarrollar nuevos catalizadores en combinación con estudios mecanísticos de las etapas que constituyen los ciclos catalíticos. Se han elegido dos tipos de procesos catalíticos de acoplamiento cruzado C-C: El primero de ellos involucra etapas de activación C-H de arenos y el segundo proceso involucra precursores de carbeno y especies carbénicas de paladio. Ambos procesos son interesantes para conseguir complejidad molecular en el menor número de etapas sintéticas. En el primer proceso no se requieren reactivos que hayan sido previamente funcionalizados, empleando de esta manera, las materias primas directamente (hidrocarburos). En el segundo proceso estudiado se puede llevar a cabo la formación de más de un enlace C-C o C-X (X = heteroátomo) en un solo paso de síntesis. El estudio de reacciones catalíticas y estequiométricas junto con estudios cinéticos y computacionales nos ha permitido conseguir información acerca de aspectos mecanísticos de las reacciones y de esta manera aportar un mejor entendimiento de los sistemas catalíticos comentados anteriormente. La discusión de la presente tesis está organizada en dos bloques. Cada bloque se centra en una de las reacciones comentadas y engloba un capítulo introductorio general para establecer el contexto principal y definir los conceptos básicos que se comentarán a lo largo del bloque, así como varios capítulos describiendo el trabajo realizado.

En el primer bloque se desarrolla el trabajo realizado en reacciones de acoplamiento C-C catalizadas por paladio con etapas de activación C-H. Tras la introducción general (*Capítulo 1*), el *Capítulo 2* describe la reacción oxidativa de tipo Heck con oxígeno empleando arenos fluorados y no fluorados catalizada por complejos de paladio. Dichos complejos de paladio contienen ligandos cooperativos de tipo bipyridona que facilitan la ruptura del enlace C-H durante el estado de transición. Las condiciones de reacción, empleando oxígeno como único oxidante y cantidades catalíticas de aditivos, han sido evaluadas para obtener las condiciones óptimas y de esta manera incrementar la sostenibilidad del proceso catalítico global. El *Capítulo 3* explora la especiación en disolución de complejos de paladio con los ligandos cooperativos empleados en el capítulo anterior. Estos estudios han permitido determinar qué

complejos son los más eficientes en reacciones de arilación directa de arenos simples (tolueno).

El segundo Bloque es una contribución a la química de carbenos mediada por paladio, centrándose en los complejos de paladio con carbenos monosustituídos no estabilizados, los cuales han sido muy poco estudiados. Los sustituyentes seleccionados para estos carbenos son grupos alquílicos o fenílicos (:CHR, R = alquilo o fenilo) o el grupo amino (:CH(X), X = NEt₂). Los *Capítulos 5 y 6* describen un estudio completo, mediante métodos experimentales y computacionales, del proceso de inserción migratoria en intermedios muy reactivos de paladio con carbenos no estabilizados (:CHR), generados a partir de diazo compuestos o hidrazonas. Esta etapa, inserción migratoria, es la etapa clave en la formación de enlaces C-C en reacciones catalizadas por paladio con precursores de carbenos como reactivos. Finalmente, el *Capítulo 7* se centra en explorar el comportamiento de complejos de paladio que contienen carbenos con un grupo amino (:CH(X), X = NEt₂) generados a través de una etapa de transmetalación desde el amino-carbeno de cobre(I). Este trabajo ha sido desarrollado en colaboración con el grupo del Prof. Pedro Pérez (CIQSO, Universidad de Huelva) y con el Prof. Agustí Lledós (Universidad Autónoma de Barcelona) quien ha llevado a cabo los cálculos computacionales DFT de este capítulo.

Cinco de los siete capítulos que componen esta tesis están subdivididos en cuatro secciones: Introducción, Resultados y Discusión, Conclusiones y Parte Experimental. Se incluye además un Apéndice con una lista de las abreviaturas utilizadas, y un índice de los compuestos descritos en orden de aparición. Las citas bibliográficas se han presentado como una nota al pie en cada capítulo, y también están recogidas en el Apéndice como un listado para facilitar su búsqueda. Además, se adjunta un documento adicional que contiene todo el material suplementario que no se ha incluido en la tesis. Dado que la tesis se ha escrito en inglés y para cumplir con la normativa sobre Tesis Doctorales de la UVa, se presenta en castellano un breve resumen de los resultados con su propia bibliografía, así como un índice y conclusiones generales.

Capítulo 1: Introducción Parte I

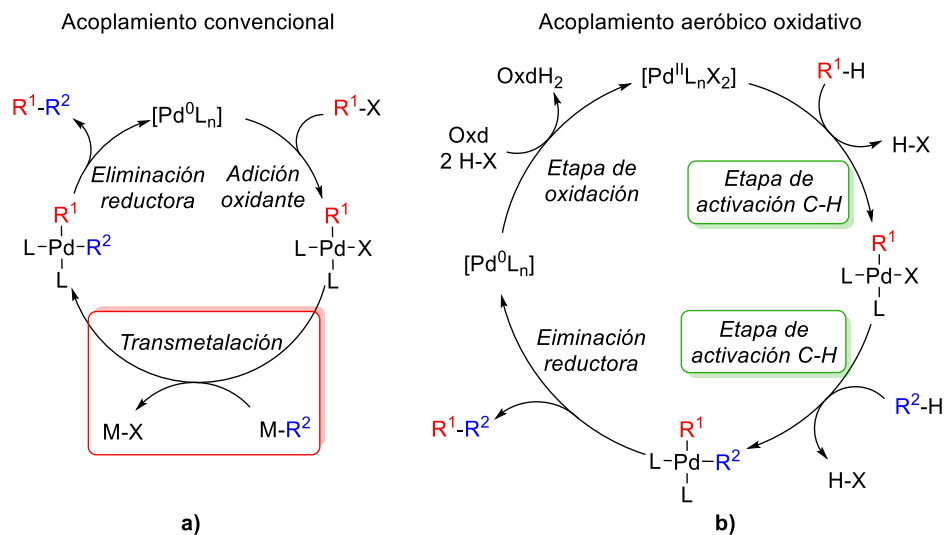
El descubrimiento de las reacciones de acoplamiento C-C catalizadas por metales de transición supuso un avance muy importante en la química sintética aplicada a Química Fina. Las primeras reacciones de acoplamiento C-C estudiadas involucraban un reactivo electrofílico (haluros de arilo) y un reactivo organometálico, que presenta carácter nucleofílico, en presencia de cantidades catalíticas de un metal de transición (generalmente complejos de paladio).^{ccxi} El estudio de estas reacciones permitió proponer un ciclo catalítico general, ampliamente aceptado por la comunidad científica, que consta de tres etapas fundamentales: adición oxidante, transmetalación y eliminación reductora (Esquema I, **a**). Sin embargo, estas reacciones presentan un problema que radica en el empleo de reactivos que requieren etapas previas de funcionalización a la vez que generan subproductos y residuos. Esto incide grave y perjudicialmente en la eficiencia atómica del proceso global junto con posibles problemas de toxicidad asociados a algunos metales empleados.^{ccxii} Como alternativa a este problema, se empezaron a desarrollar reacciones de acoplamiento C-C que no requiriesen reactivos con etapas de funcionalización, usando de esta manera, las materias primas directamente (hidrocarburos). Si se sustituyen los dos reactivos de las reacciones de acoplamiento convencionales por dos hidrocarburos, la reacción necesita habitualmente la presencia de un oxidante. El ciclo catalítico para las reacciones oxidativas de acoplamiento C-C que emplean solo hidrocarburos como reactivos de partida difiere en algunas de las etapas fundamentales con respecto a los acoplamientos C-C convencionales (Esquema I, **b**). Estas nuevas etapas son: activación del enlace C-H del hidrocarburo y la etapa de oxidación del catalizador. Esta última etapa se produce después de la eliminación reductora, generando una especie intermedia del catalizador en un estado de oxidación dos unidades menor. Para que el ciclo catalítico se reinicie, es necesario añadir un oxidante externo (Esquema I, **b**).

De entre todos los oxidantes estudiados y utilizados para las reacciones de acoplamiento oxidante C-C, cabe destacar que el oxígeno es uno de los más limpios

^{ccxi} a) Heck, R. F. *J. Am. Chem. Soc.* **1968**, *90*, 5518–5526. b) Mizoroki, T.; Mori, K.; Ozaki, A. *Bull. Chem. Soc. Jpn.* **1971**, *44*, 581–581. c) Kumada, M. *Pure Appl. Chem.* **1980**, *52*, 669–679. d) Negishi, E-I. *Acc. Chem. Res.* **1982**, *15*, 340–348. e) Stille, J. K. *Angew. Chem. Int. Ed.* **1986**, *25*, 508–524. f) Sonogashira, K.; Tohda, Y.; Hagihara, N. *Tetrahedron Lett.* **1975**, 4467–4470. g) Louie, J.; Hartwig, J. F. *Tetrahedron Lett.* **1995**, *36*, 3609–3612. h) Guram, A. S.; Rennels, R. A.; Buchwald, S. L. *Angew. Chem., Int. Ed.* **1995**, *34*, 1348–1350.

^{ccxii} a) Anastas, P. T.; Mary, M. *Acc. Chem. Res.* **2002**, *35*, 686–694. b) Dalton, T.; Faber, T.; Glorius, F. *ACS Cent. Sci.* **2021**, *7*, 2, 245–261.

desde el punto de vista medioambiental ya que genera únicamente peróxido de hidrógeno o agua como subproducto.^{ccxlii}



Esquema I

La etapa de activación C-H del hidrocarburo a menudo presenta ciertos problemas; entre ellos, cabe destacar la elevada energía de disociación y la poca polaridad que presenta el enlace C-H. Estas características lo convierten en poco reactivo en comparación con los enlaces C-X (X = halógeno) o M-C.^{ccxliii} También existen problemas en la regioselectividad del producto de acoplamiento final ya que a menudo los hidrocarburos, como cualquier molécula orgánica, presentan múltiples enlaces C-H susceptibles de ser funcionalizados en las condiciones de reacción.

Una de las estrategias que se han desarrollado en las últimas décadas para abordar el problema relacionado con el alto coste energético que implica la ruptura del enlace C-H es el desarrollo de ligandos que faciliten esta ruptura, disminuyendo la energía del correspondiente estado de transición. A estos ligandos se los ha denominado “ligandos cooperativos”,^{ccxliv} siendo los ligandos de tipo aminoácido^{ccxlv} y derivados de piridona los que más se han estudiado hasta el momento. En la mayoría de los ligandos

^{ccxlii} Ejemplos seleccionados de reacciones oxidativas acoplamiento C-C catalizadas por metales de transición con oxígeno. a) Campbell, A. N.; Stahl, S. S. *Acc. Chem. Res.* **2012**, *45*, 851–863. b) Piera, J.; Bäckvall, J.-E. *Angew. Chem. Int. Ed.* **2008**, *47*, 3506–3523. c) Stahl, S. S. *Angew. Chem. Int. Ed.* **2004**, *43*, 3400–3420. d) Shi, Z.; Zhang, C.; Tanga, C.; Jiao, N. *Chem. Soc. Rev.*, **2012**, *41*, 3381–3430.

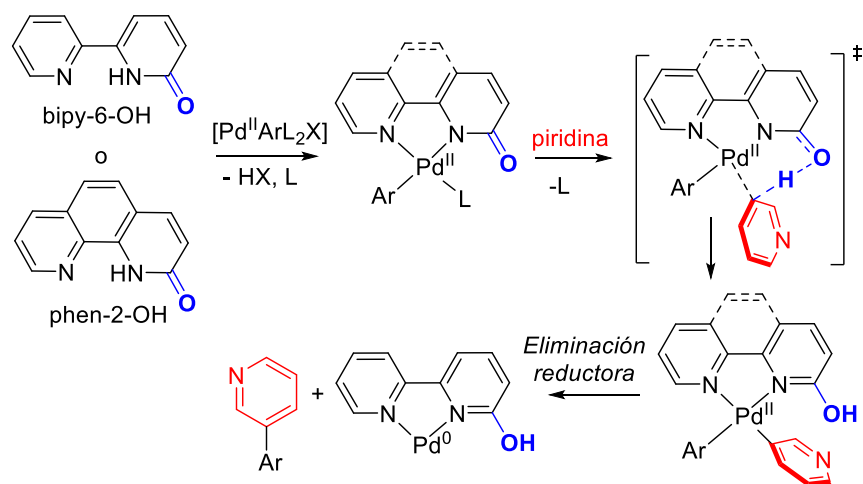
^{ccxliii} Luo, Y. R. *Comprehensive Handbook of Chemical Bond Energies*, CRC Press, **2007**.

^{ccxliv} Khusnutdinova, J. R.; Milstein, D. *Angew. Chem. Int. Ed.* **2015**, *54*, 12236–12273.

^{ccxlv} Shi, B.-F.; Mangel, N.; Zhang, Y.-H.; Yu, J.-Q. *Angew. Chem. Int. Ed.* **2008**, *47*, 4882–4886.

cooperativos estudiados se ha visto que operan a través de un mecanismo de tipo concertado, involucrando una parte del ligando, la cual actúa como base, y al mismo tiempo el centro metálico. A este mecanismo, el más energéticamente favorable para arenos simples, se lo ha denominado “metalación-deprotonación concertada” (MDC o CMD en sus siglas en inglés).^{cexlvi} Siguiendo esta línea, se han desarrollado en nuestro grupo de investigación, dos ligandos quelatos *N,N*-dadores derivados de la piridona: [2,2'-bipiridin]-6(1*H*)-ona y 1,10-fenantrolin-2-(1*H*)-ona (bipy-6-OH and phen-2-OH respectivamente) los cuales han demostrado ser eficientes en reacciones de arilación directa de arenos simples (Esquema II).^{cexlvii}

La parte I de esta memoria tiene como objetivo aplicar este tipo de ligandos a reacciones de acoplamiento oxidativo de arenos con oxígeno como oxidante y estudiar su mecanismo de actuación para conseguir reacciones más sostenibles. Asimismo, se pretende conocer las especies que forman estos ligandos con paladio en las mezclas precatalíticas habitualmente empleadas.



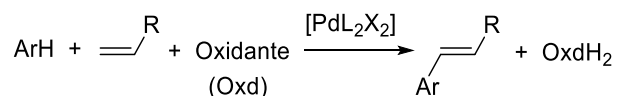
Esquema II

^{cexlvi} a) Campeau, L.-C.; Parisien, M.; Leblanc, M.; Fagnou, K. *J. Am. Chem. Soc.* **2004**, *126*, 9186–9187. b) García-Cuadrado, D.; Braga, A. A. C.; Maseras, F.; Echavarren, A. M. *J. Am. Chem. Soc.* **2006**, *128*, 1066–1067. c) Lafrance, M.; Rowley, C. N.; Woo, T. K.; Fagnou, K. *J. Am. Chem. Soc.* **2006**, *128*, 8754–8756. d) García-Cuadrado, D.; de Mendoza, P.; Braga, A. A. C.; Maseras, F.; Echavarren, A. M. *J. Am. Chem. Soc.* **2007**, *129*, 6880–6886. e) Stuart, D. R.; Fagnou, K. *Science*. **2007**, *316*, 1172–1175. f) Gorelsky, S. I.; Lapointe, D.; Fagnou, K. *J. Am. Chem. Soc.* **2008**, *130*, 10848–10849.

^{cexlvii} a) Salamanca, V.; Toledo, A.; Albéniz, A. C. *J. Am. Chem. Soc.* **2018**, *140*, 17851–17856. b) Salamanca, V.; Albéniz, A. C. *Org. Chem. Front.* **2021**, *8*, 1941–1951.

Capítulo 2: Reacción de Heck oxidativa de fluorobencenos y otros arenos: ¿En qué casos necesita ayuda la activación C-H?

La reacción de Fujiwara-Moritani^{cexlviii} o también llamada Heck oxidativa para la funcionalización de arenos tiene un enorme interés en química sintética (Ecuación I). El mecanismo aceptado establece dos etapas clave: una etapa de activación C-H del areno y una etapa de coordinación-inserción migratoria de la olefina en el enlace Pd-C generado en la etapa anterior.^{cexlix}



Ecuación I

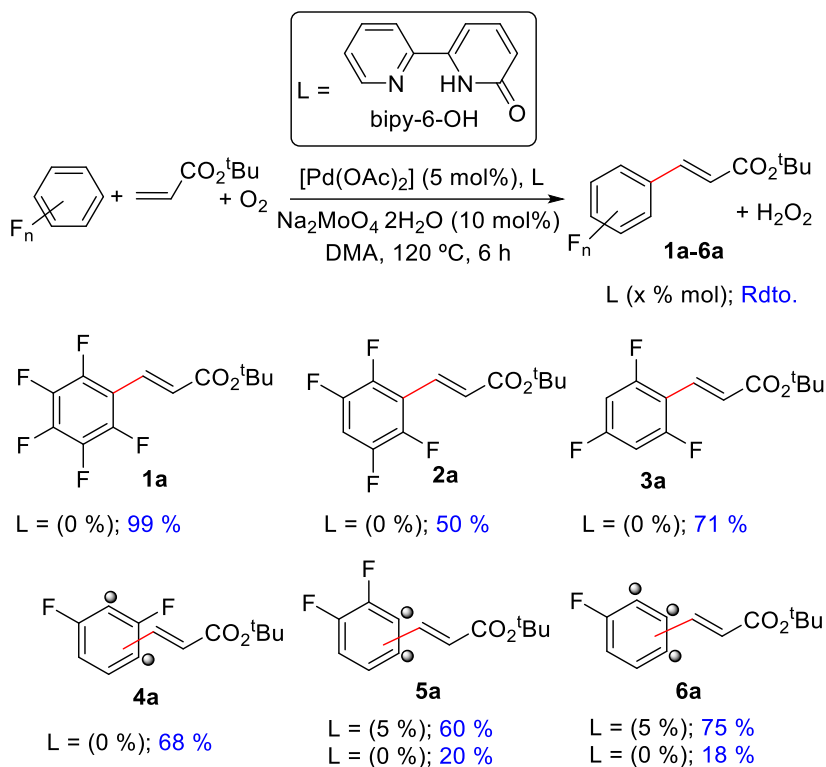
Usando pentafluorobenceno (C₆F₅H) como areno modelo y acrilato de *tert*-butilo como alqueno se han explorado las condiciones óptimas para llevar a cabo la reacción catalizada por complejos de paladio. Empleando oxígeno como único oxidante en la reacción y cantidades subestequiométricas de Na₂MoO₄·2H₂O como aditivo a 120 °C se han conseguido excelentes resultados en la formación del producto de acoplamiento **1a** (Esquema III). Se han realizado estudios independientes para conocer cuál podría ser el papel del molibdato sódico empleado como aditivo, resultando que un papel similar al de una base débil es el que mejor se ajusta a los resultados obtenidos.^{cecl} Una vez optimizadas las condiciones de la reacción modelo, se procedió a estudiar otros arenos fluorados (Esquema III). Se observa que la facilidad con la que se produce la etapa de activación C-H del areno depende del número de átomos de flúor que contiene la molécula. Para arenos fluorados con más de dos átomos de flúor, el precatalizador [Pd(OAc)₂] produce buenas conversiones del producto de acoplamiento sin necesidad de ligandos adicionales (compuestos **1a-4a**, Esquema III). Esto puede explicarse debido a la mayor acidez del -H que va a ser activado durante la etapa de ruptura del enlace C-H en las moléculas con mayor contenido en átomos de flúor. Sin embargo, al llevar a cabo

^{cexlviii} Moritani, I.; Fujiwara, Y. *Tetrahedron Lett.* **1967**, *8*, 1119–1122.

^{cexlix} a) Le Bras, J.; Muzart, J. *Chem. Rev.* **2011**, *111*, 1170–1214. b) Yeung, C. D.; Dong, V. M. *Chem. Rev.* **2011**, *111*, 1215–1292. c) Odell, L. R.; Sävmarker, J.; Lindh, J.; Nilsson, P.; Larhed, M. *Addition Reactions with Formation of Carbon-Carbon Bonds: (V) The Oxidative Heck Reaction*, Elsevier Ltd., **2014**. d) Kancherla, S.; Jørgensen, K. M.; Fernández-Ibáñez, M. A. *Synthesis*, **2019**, *51*, 643–663. e) Gunnoe, T. B.; Schinski, W. L.; Jia, X.; Zhu, W. *ACS Catal.* **2020**, *10*, 14080–14092. f) Ali, W.; Prakash, G.; Maiti, D. *Chem. Sci.* **2021**, *12*, 2735–2759. g) Zhu, W.; Gunnoe, T. B. *J. Am. Chem. Soc.* **2021**, *143*, 6746–6766.

^{cecl} a) Cruywagen, J. J.; Rohwer, E. F. C. H. *Inorg. Chem.* **1975**, *14*, 3136–3137. b) Liu, X.; Cheng, J.; Sprik, M.; Lu, X. *J. Phys. Chem. Lett.* **2013**, *4*, 2926–2930

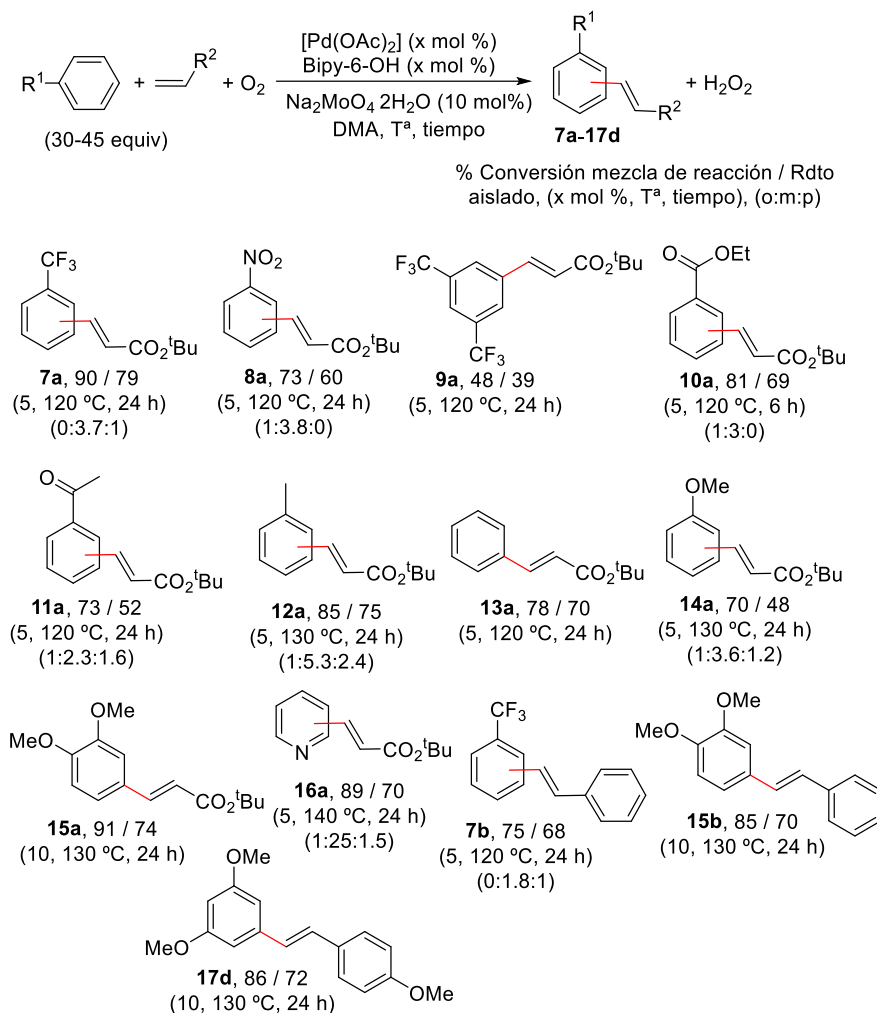
la reacción con 1,2-difluorobenceno o fluorobenceno se observa que la reacción fracasa incluso cuando se emplean grandes concentraciones de estos arenos. Para estos arenos se observó que el empleo de un ligando cooperativo (bipy-6-OH) en combinación con [Pd(OAc)₂] como precatalizador es necesario para obtener buenas conversiones del producto de olefinación del areno fluorado (compuestos **5a** y **6a**, Esquema III).



Esquema III

La reacción se puede extender a otros arenos simples no fluorados. Las condiciones de reacción óptimas para cada uno de ellos, así como las conversiones y rendimientos aislados se muestran en el Esquema IV. Todos los arenos utilizados en el Esquema IV requieren la presencia de un ligando cooperativo (bipy-6-OH o phen-2-OH) para llevar a cabo la formación del acoplamiento C-C entre el areno y la olefina de manera eficiente.

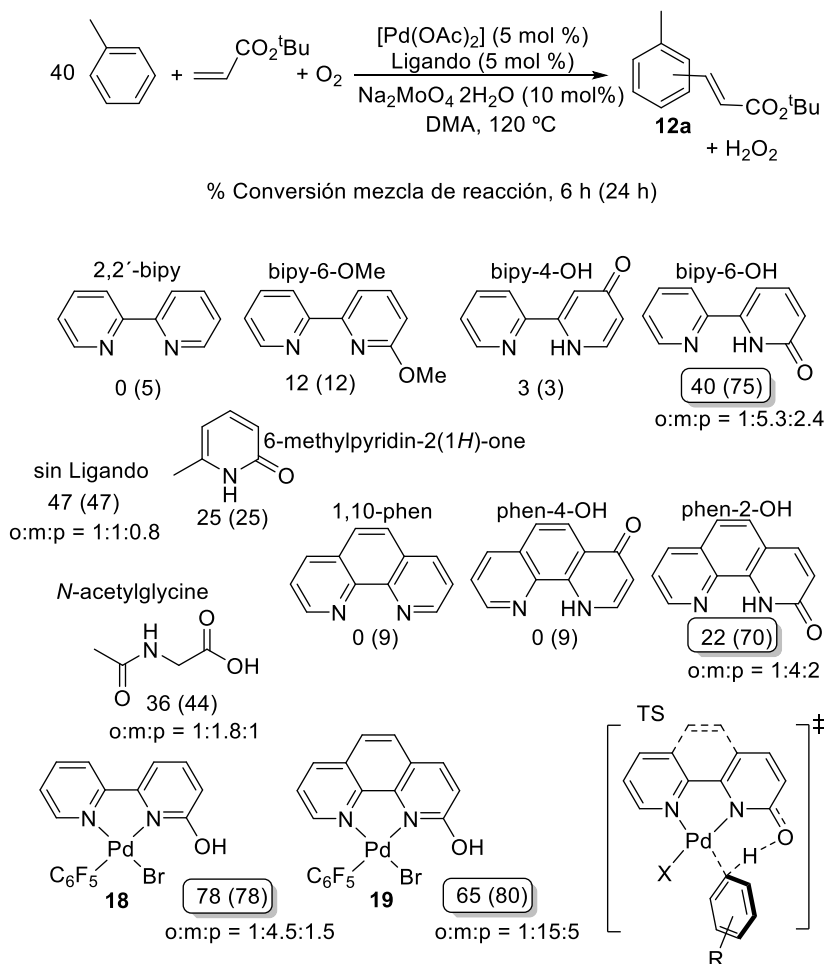
Resumen



Esquema IV

Se llevaron a cabo diferentes reacciones catalíticas empleando tolueno como areno modelo en la reacción de Heck oxidativa para conocer mejor el papel que desempeña el ligando cooperativo durante la catálisis. Se observó que la reacción catalítica generaba mejores resultados (conversión y rendimiento) cuando se emplea una mezcla del ligando cooperativo (bipy-6-OH o phen-2-OH) + [Pd(OAc)₂] o bien cuando se añadía un complejo aislado de paladio con el ligando cooperativo previamente coordinado (**18** o **19**, Esquema V). La misma reacción no es eficaz con otros ligandos no cooperativos como son 2,2'-bipy, bipy-6-OMe, bipy-4-OH o ligandos cooperativos como piridonas monodentadas o aminoácidos. En ausencia de ligando externo, se observa que la reacción procede hasta un 47 % de conversión del producto **12a** lo cual indica que la etapa de activación C-H posiblemente la esté llevando a cabo el acetato.

Para conocer quién es el responsable en dicha etapa de activación C-H cuando se emplea el ligando cooperativo bipy-6-OH se realizaron cálculos computacionales DFT del estado de transición de dicha etapa. Los cálculos indican que la activación mediada por el ligando bipy-6-OH a través de un estado de transición como el representado en el Esquema V (X = OAc) es 11.7 kcal/mol más baja que cuando se lleva a cabo a través del acetato, indicando que el ligando bipy-6-OH está actuando como un ligando cooperativo en la reacción estudiada.



Esquema V

Se ha observado que, en el caso de arenos polifluorados la presencia del ligando cooperativo bipy-6-OH no sólo no es necesaria, sino que es perjudicial (Tabla I). Se han realizado experimentos mecanísticos con complejos modelo que indican que la presencia del ligando dificulta la etapa de coordinación-inserción de la olefina en el enlace

Resumen

Pd-C(arilo). De este modo, el ligando sólo favorece la reacción en el caso de que la activación C-H sea difícil y limitante en la reacción, lo que ocurre para la mayoría de los arenos excepto para los polifluorados.

Tabla I. Efecto del ligando cooperativo bipy-6-OH en la reacción de tipo Heck oxidativa.^a

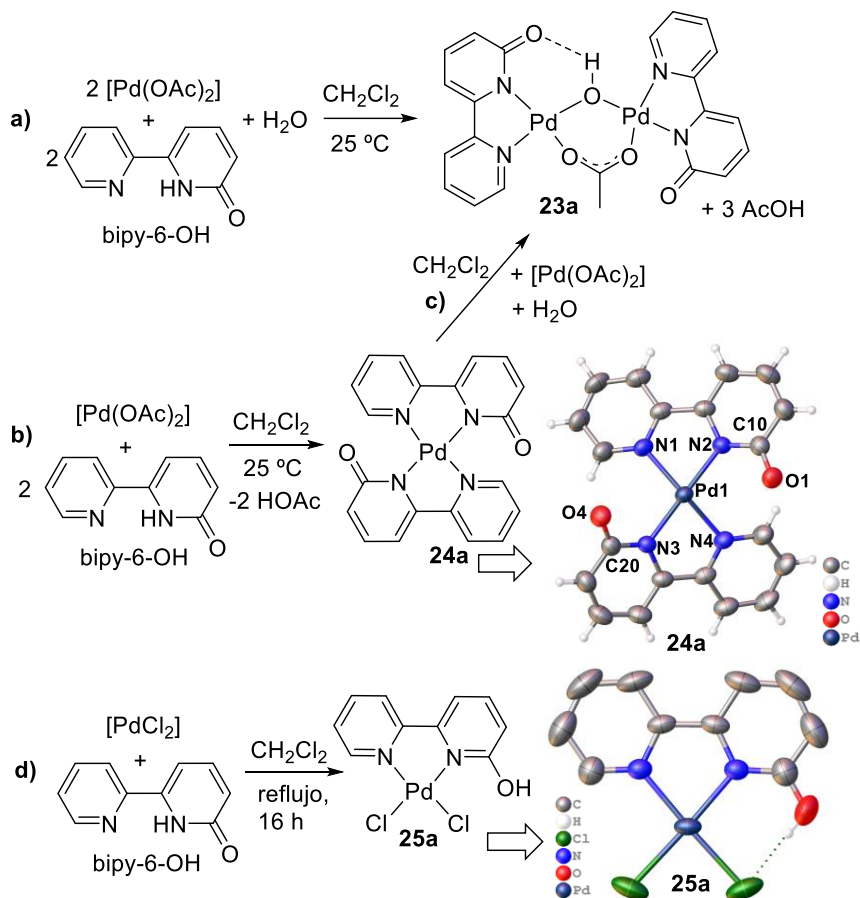
Entrada	Ligando	Areno	Producto	Rdto bruto, %	
				6 h ^b	24h ^b
1 ^c	bipy-6-OH	C ₆ F ₅ H	1a	0	0
2 ^c	–	C ₆ F ₅ H	1a	86	90
3	bipy-6-OH	PhF	6a	75	87
4	–	PhF	6a	18	18
5	bipy-6-OH	PhMe	12a	40	75
6	–	PhMe	12a	47	47

^a Condiciones de reacción: [Pd(OAc)₂] (0.017 mmol, 5 mol %), Na₂MoO₄·2H₂O (0.034 mmol, 10 mol %), acrilato de *tert*-butilo (0.341 mmol), Areno:DMA = 1:1 v/v (volumen total, 3 mL), O₂ (1 atm), 120 °C.^b Los rendimientos fueron determinados mediante ¹H RMN empleando dodecano como patrón interno. ^c Areno:alqueno = 2.5:1 relación molar.

Capítulo 3: Arrojando luz sobre las especies presentes en la mezcla precatalítica de $[Pd(OAc)_2]$ y ligandos cooperativos de tipo bipyridona para activaciones C-H de arenos

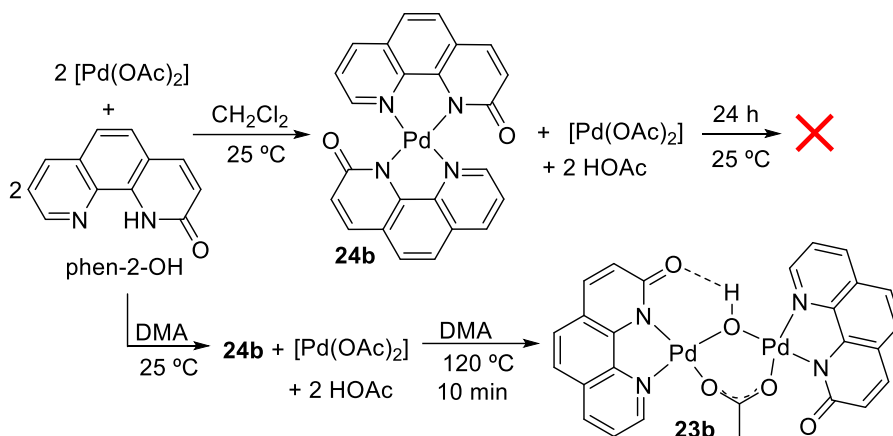
El uso de una mezcla de ligando cooperativo en combinación con un derivado comercial o fácilmente accesible de paladio es habitual en las reacciones catalíticas de acoplamiento C-C con etapas de activación C-H. Sin embargo, apenas existen estudios que hayan ahondado en las diferentes especies que se forman al mezclar el ligando y el precatalizador de paladio y esto es importante para conocer cómo se forman las especies catalíticamente activas. Esta información puede ayudar a evitar tiempos de inducción largos o elegir condiciones que eviten la descomposición del precatalizador. En este capítulo se presentan los resultados obtenidos en el estudio de la mezcla de los ligandos cooperativos [2,2'-bipiridin]-6(1*H*)-ona y 1,10-fenantrolin-2(1*H*)-ona con dos de los precatalizadores de Pd(II) más utilizados: $[Pd(OAc)_2]$ y $PdCl_2$.

Cuando se hace reaccionar el ligando bipy-6-OH con $[Pd(OAc)_2]$ en relación 1:1 se observa la formación de un complejo dímero de Pd(II) (**23a**), con grupos acetato e hidroxilo como puentes (Esquema VI, **a**). Por el contrario, cuando la relación ligando:Pd es 2:1, la evolución de la reacción genera un complejo monómero de Pd(II) (**24a**) donde los dos ligandos bipy-6-OH se encuentran deprotonados y quelatando al centro metálico (el ligando bipy-6-O deprotonado actúa como ligando monoaniónico L,X, Esquema VI, **b**). En disolución a temperatura ambiente el complejo **24a** experimenta una rápida reorganización en presencia de un equivalente de $[Pd(OAc)_2]$ para generar el complejo **23a** (Esquema VI, **c**). Esta reorganización es más rápida en presencia de pequeñas cantidades de agua y en disolventes polares y coordinantes como DMSO y en menor medida DMA. Cuando se hace reaccionar con $PdCl_2$ el ligando bipy-6-OH se coordina al centro metálico sin deprotonarse generando **25a** (se mantiene como ligando neutro L,L, Esquema VI, **d**).



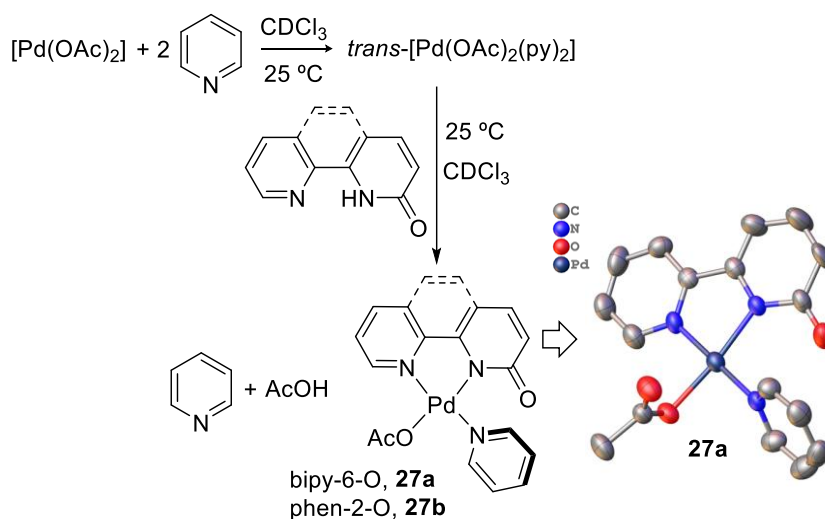
Esquema VI

Cuando se estudia la reactividad del ligando phen-2-OH en presencia de $[\text{Pd}(\text{OAc})_2]$ en relación 1:1, solo se observa la formación del dímero de paladio (**23b**) en un disolvente polar como DMSO a temperatura ambiente o DMA a alta temperatura, 120 °C (Esquema VII). Estos resultados indican que, pese a que la bipy-6-OH y la phen-2-OH son ligandos muy similares, su comportamiento en disolución con $[\text{Pd}(\text{OAc})_2]$ difiere, siendo los complejos resultantes con phen-2-OH mucho menos solubles y reactivos.



Esquema VII

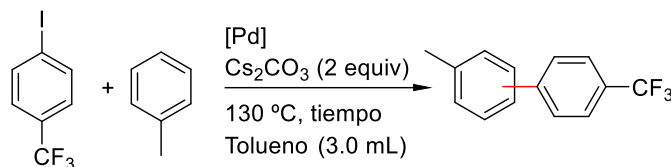
Debido a que muchas reacciones catalíticas que involucran etapas de activación C-H emplean una combinación de dos ligandos, habitualmente uno de ellos de tipo cooperativo y el otro de tipo piridina,^{ccli} se decidió estudiar la reactividad de los ligandos bipy-6-OH y phen-2-OH en presencia de $[\text{Pd}(\text{OAc})_2]$ y piridina. Con ambos ligandos se observa la formación de complejos monómeros (**27a-b**) donde el ligando bipyridona se encuentra deprotonado junto con un ligando piridina y acetato que completan la esfera de coordinación del centro metálico (Esquema VIII).



Esquema VIII

ccli a) Zhang, S.; Shi, L.; Ding, Y. *J. Am. Chem. Soc.* **2011**, *133*, 20218–20229. b) Chen, H.; Mondal, A.; Wedi, P.; van Gemmeren, M. *ACS Catal.* **2019**, *9*, 1979–1984.

Una vez realizado el estudio de la especiación de nuestros ligandos bipy-6-OH y phen-2-OH con $[\text{Pd}(\text{OAc})_2]$ se decidió explorar las diferencias de actividad como precatalizadores en una reacción de arilación directa de tolueno (Ecuación II).^{ccxlvii}



Ecuación II

Los resultados obtenidos de las reacciones catalíticas se muestran en la Tabla II, donde se puede observar que la reacción no genera el producto de acoplamiento cruzado cuando solo se emplea $[\text{Pd}(\text{OAc})_2]$, sin embargo, en presencia de la mezcla $[\text{Pd}(\text{OAc})_2]$ + ligando cooperativo se observa la formación del producto, pero en bajas conversiones tras 6 h de reacción (entradas 2 y 3, Tabla II). Cuando se realiza la misma catálisis con los complejos aislados dímeros **23a-b** se produce un incremento en la conversión hacia el producto de interés, especialmente notable para el complejo **23a** (entrada 4, Tabla II). Los complejos monómeros **24a-b** que presentan una relación Pd:Ligando de 1:2 muestran resultados peores para las mismas condiciones de reacción (entradas 6 y 7, Tabla II). Finalmente se estudió la actividad catalítica para los complejos **25a-b** en los cuales el ligando presenta una coordinación de tipo L,L (ligando protonado). De los dos complejos, solo **25a** es capaz de generar una buena conversión a las 6 h (65 %) (entrada 8, Tabla II).

Tabla II. Arilación directa de tolueno con $p\text{-CF}_3\text{C}_6\text{H}_4\text{I}$ empleando diferentes catalizadores.^a

Entrada	[Pd] (5 mol %)	Rdto bruto de reacción, %, (6 h) ^b
1	$[\text{Pd}(\text{OAc})_2]$	- (6 h)
2	$[\text{Pd}(\text{OAc})_2]$ + bipy-6-OH	20 (6h)
3	$[\text{Pd}(\text{OAc})_2]$ + phen-2-OH	6 (6h)
4	23a	82 (6h)
5	23b	15 (6h)
6	24a	18 (6h)
7	24b	3 (6h)
8	25a	65 (6h)
9	25b	4 (6h)

^a Condiciones de reacción: $p\text{-CF}_3\text{C}_6\text{H}_4\text{I}$ (51 μL , 0.34 mmol), tolueno (3 mL), [Pd] (5 mol %), Cs_2CO_3 (222 mg, 0.68 mmol); 130 °C. ^b Conversiones determinadas del crudo de reacción mediante ^{19}F RMN. El producto de reducción del haluro de arilo ($p\text{-CF}_3\text{C}_6\text{H}_4\text{-H}$) así como el producto de acoplamiento son los subproductos de la reacción observados.

Por tanto, el uso como precatalizadores de complejos que contengan el ligando ya coordinado a paladio en relación Pd:ligando = 1:1 llevan a reacciones más rápidas, previsiblemente porque el tiempo necesario para genera las especies activas es menor. Hay que destacar que las diferencias observadas se producen en tolueno como reactivo y disolvente. Cuando se emplea una mezcla de tolueno y DMA (tolueno:DMA = 1:1 v/v) estas diferencias no son tan importantes debido a la mayor facilidad de coordinación del ligando y reorganización de los complejos observada en disolventes más polares.

La reacción del complejo **23a** en tolueno a alta temperatura (130 °C) lleva a la formación de dimetilbifenilo y Pd(0) mediante doble activación C-H de dos moléculas de tolueno y eliminación reductora. Este es por tanto un mecanismo probable de generación de especies de Pd(0) activas, necesarias en las reacciones de arilación directa ensayadas, desde los complejos precatalizadores de Pd(II) (Figura I).

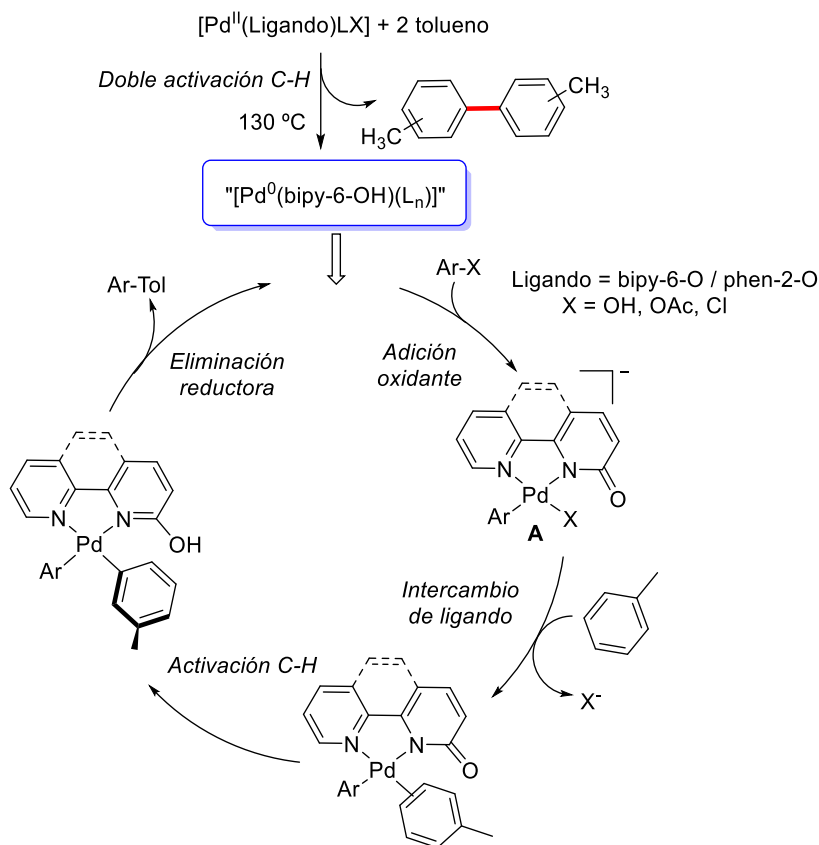


Figura I

Capítulo 4: Introducción Parte II.

Los carbenos más estables son aquellos en los que la presencia de sustituyentes dadores de densidad electrónica compensa la deficiencia del carbono carbénico y los hacen menos reactivos. Por esta razón, se ha desarrollado una amplia química alrededor de los carbenos *N*-heterocíclicos (NHC) y análogos (CAAC, MIC, etc).^{cclii} Estos carbenos presentan dos grupos amino que se encuentran adyacentes al carbono carbénico, formando en muchas ocasiones una estructura cíclica. Coordinados a un metal de transición, y en particular a paladio, actúan como ligandos auxiliares en numerosos procesos catalíticos (Figura II).^{ccliii}

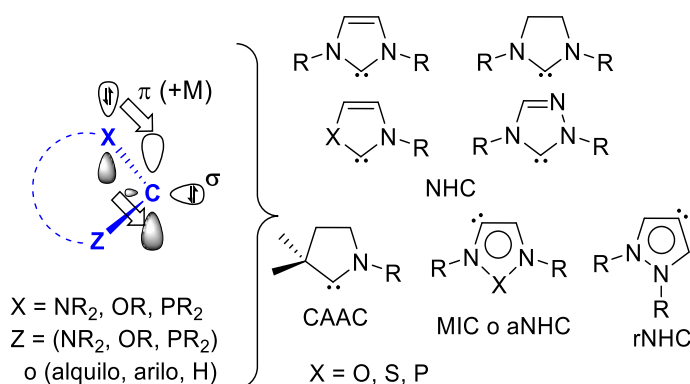


Figura II

En nuestro grupo se han aislado y se ha estudiado la reactividad de carbenos de paladio mucho menos estables que los NHCs, ya que solo presentan un solo grupo electro-dador contiguo al carbono carbénico. De estos estudios, junto con lo que ya se habían publicado previamente, se puede hacer una estimación de la reactividad del carbono carbénico en estos complejos de paladio. La tendencia observada es la siguiente: $[:\text{C}(\text{NR}^1\text{R}^1)_2] \ll : \text{CR}^2(\text{NR}^1\text{R}^1) < : \text{CR}^2(\text{OR}^1) < : \text{CR}^2(\text{R}^1) \sim : \text{CH}(\text{R}^1)$ (R^1 = grupo alquilo o arilo).^{ccliv} La síntesis de los complejos de paladio con carbenos que solo contienen un grupo electro-dador puede llevarse a cabo por cuatro rutas sintéticas principalmente; i) transmetalación desde complejos metálicos del grupo 6;^{ccliv} ii) mediante protonación de

^{cclii} a) Arduengo, A. J.; Harlow, R. L.; Kline, M. *J. Am. Chem. Soc.* **1991**, *113*, 361–363.

b) Arduengo, A. J.; Bertrand, G. *Chem. Rev.* **2009**, *109*, 3209–3210.

^{ccliii} Bourissou, D.; Guerret, O.; Gabbai, F. P.; Bertrand, G. *Chem. Rev.* **2000**, *100*, 39–91.

^{ccliv} a) Albéniz, A. C.; Espinet, P.; Manrique, R.; Pérez-Mateo, A. *Angew. Chem. Int. Ed.* **2002**, *41*, 2363–2366. b) Albéniz, A. C. *Eur. J. Inorg. Chem.* **2018**, *33*, 3693–3705.

un grupo alcoxovinílico coordinado a un complejo de Pd(II);^{cclv} iii) mediante el ataque nucleofílico a un ligando isocianuro previamente coordinado a Pd(II);^{cclvi} iv) mediante una etapa de adición oxidante de un complejo de Pd(0) a un derivado de 2-cloroimidazolio.^{cclvii}

La situación más reactiva y de mayor inestabilidad para un carbeno metálico de Pd(II) se produce cuando los dos sustituyentes adyacentes al carbono carbénico son restos hidrocarbonados (alquilos o arilos). En esta situación, el carbeno metálico resultante es una especie altamente reactiva y a menudo difícil de detectar incluso a baja temperatura. Sin embargo, este tipo de carbenos metálicos desempeñan un papel muy importante como intermedios en la síntesis de compuestos de mayor complejidad molecular, donde el carbeno pasa a formar parte del producto final. Para sintetizar estos carbenos metálicos se han desarrollado diferentes metodologías, entre las que cabe destacar, el uso de diazo compuestos como precursores carbénicos,^{cclviii} fuentes de carbenos reactivos que no proceden de diazo compuestos (ciclopropeno, triazoles, alenos entre otros)^{cclix} y mediante transmetalación desde carbenos metálicos del grupo 6.

Los diazo compuestos se encuentran entre los precursores carbénicos más estudiados, sin embargo, cómo interaccionan con el paladio solo se ha podido averiguar para unos pocos complejos de paladio(0).^{cclx} El análisis de la estructura molecular mediante difracción de rayos X, muestra que los dos nitrógenos del diazo compuesto se coordinan al Pd(0) en un modo de coordinación de tipo *side-on* (Esquema IX, a)). Este modo de coordinación es el más estable para complejos de Pd(0) pero para generar el intermedio carbeno metálico, es necesaria una etapa de extrusión de nitrógeno molecular, la cual solo se puede llevar a cabo cuando el diazo compuesto se coordina al centro metálico través del carbono contiguo al grupo funcional “diazo” (Esquema IX, b)).

^{cclv} a) Wada, M.; Koyama, Y. *J. Organomet. Chem.* **1980**, *201*, 477–491. b) Wada, M.; Koyama, Y.; Sameshima, K. *J. Organomet. Chem.* **1981**, *209*, 115–121.

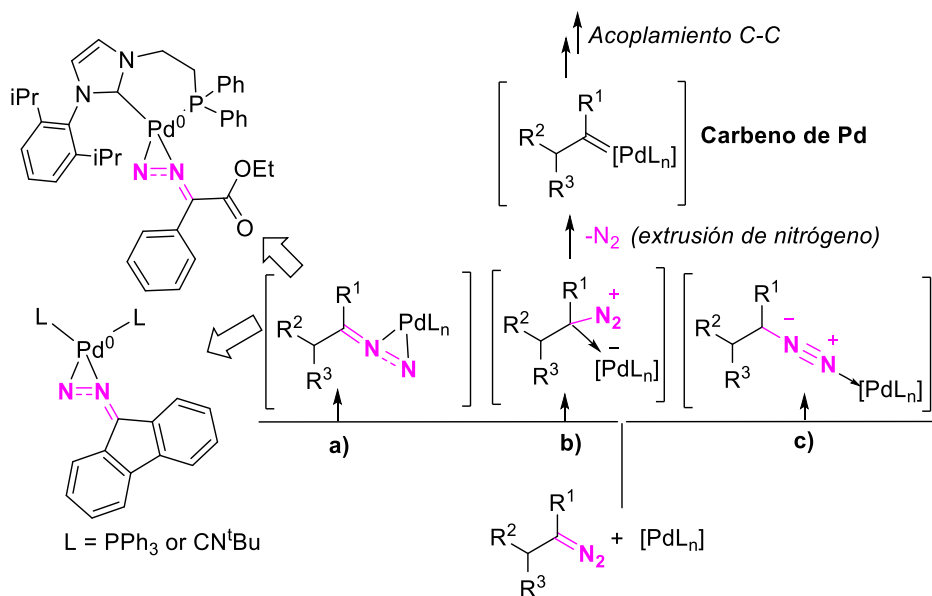
^{cclvi} Crociani, B.; Nicolini, M.; Boschi, T. *J. Organomet. Chem.* **1971**, *33*, C81–C83.

^{cclvii} Kremzow, D.; Seidel G.; Lehmann, C. W.; Fürstner, A. *Chem. Eur. J.* **2005**, *11*, 1833–1853.

^{cclviii} a) Regitz, M.; Maas, G. *Diazo Compounds Properties and Synthesis*, Academic Press, Orlando, **1986**. b) Gerhard Maas, G. *Angew. Chem. Int. Ed.* **2009**, *48*, 8186–8195. c) Akter, M.; Rupa, K.; Anbarasan, P. *Chem. Rev.* **2022**, *122*, 13108–13205.

^{cclix} a) Jia, M.; Ma, S. *Angew. Chem. Int. Ed.* **2016**, *55*, 9134–9166. b) Wang, K.; Wang, J. *Synlett*, **2019**, *30*, 542–551. c) Mayakrishnan, S.; Tamizmani, M.; Maheswari, N. U. *Chem. Commun.* **2020**, *56*, 15462–15465. d) Zhu, D.; Chen, L.; Fan, H.; Yao, Q.; Zhu, S. *Chem. Soc. Rev.* **2020**, *49*, 908–950.

^{cclx} a) Rull, S. G.; Álvarez, E.; Fructos, M. R.; Belderrain, T. R.; Pérez, P. J. *Chem. Eur. J.* **2017**, *23*, 7667–7671. b) Otsuka, S.; Nakamura, A.; Koyama, T.; Tatsuno, Y. *Justus Liebigs Ann. Chem.* **1975**, 626–635.



La aplicación sintética más importante de los complejos de paladio con carbenos reactivos es la formación de enlaces C-C a través de una etapa de inserción migratoria del grupo carbeno en el enlace Pd-R (R = alquilo, arilo). Van Vranken y colaboradores fueron los pioneros en desarrollar reacciones catalíticas empleando esta estrategia sintética donde los carbenos metálicos se generaban desde diazo compuestos como precursores (Esquema X).^{cclxi} Los diazo compuestos son una excelente fuente de carbenos metálicos, sin embargo, debido a los problemas de seguridad y de estabilidad que presentan algunos de ellos, las *N*-tosilhidrazonas se han convertido en una alternativa mucho más segura para generar *in situ* el diazo compuesto, evitando así los riesgos asociados a la síntesis y manipulación de éstos.^{cclxii,cclxiii} En concreto las *N*-tosilhidrazonas se descomponen fácilmente en presencia de base y calor mediante la reacciones de Bamford-Stevens (Esquema X).^{cclxiv} Esta estrategia fue empleada por primera vez por el grupo de Barluenga y Valdés en reacciones catalíticas para la formación de enlaces

^{cclxi} a) Greenman, K. L.; Carter, D. S.; Van Vranken, D. L. *Tetrahedron* **2001**, *57*, 5219–5225.

b) Greenman, K. L.; Van Vranken, D. L. *Tetrahedron* **2005**, *61*, 6438–6441.

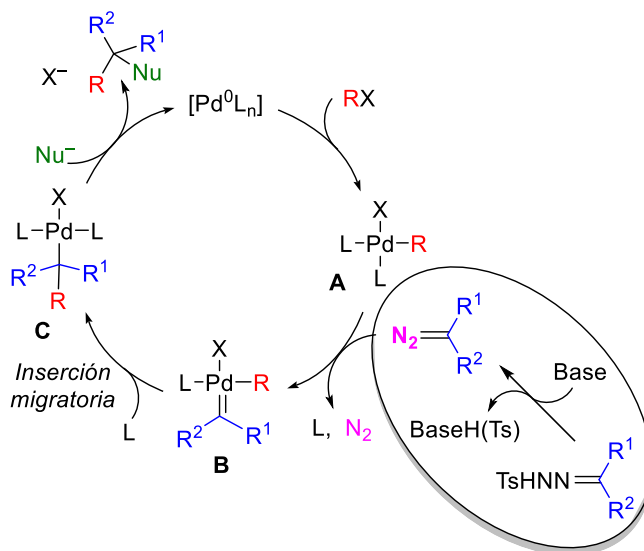
^{cclxii} a) Fulton, J. R.; Aggarwal, V. K.; de Vicente, J. *Eur. J. Org. Chem.* **2005**, 1479–1492.

b) Green, S. P.; Wheelhouse, K. M.; Payne, A. D.; Hallett, J. P.; Miller, P. W.; Bull, J. A. *Org. Process. Res. Dev.* **2020**, *24*, 67–84.

^{cclxiii} Xia, Y.; Qiu, D.; Wang, J. *Chem. Rev.* **2017**, *117*, 13810–13889.

^{cclxiv} Bamford, W. R.; Stevens, T. S. *J. Chem. Soc.* **1952**, 4735–4740.

C-C.^{cclxv} El Esquema X representa de una manera simplificada, el ciclo catalítico general propuesto para este tipo de reacciones.



Esquema X

La etapa de inserción migratoria (**B** a **C**) en complejos bien definidos de paladio sólo se ha podido demostrar con carbenos donde uno de los sustituyentes es un grupo amino o alcoxo.^{ccliv,cclxvi} Sin embargo la mayoría de las reacciones de acoplamiento C-C con precursores de carbeno catalizadas por paladio usan derivados $:CR^2(R^1)$ con $R^1, R^2 =$ alquilo, arilo, H. Por ello el objetivo del trabajo descrito en la Parte II de esta memoria es estudiar la reactividad de complejos de paladio bien definidos con este tipo de fragmentos generados desde diazo compuestos o hidrazonas. Asimismo, se estudiará la reactividad de complejos de otros fragmentos carbénicos poco estabilizados.

^{cclxv} a) Barluenga, J.; Moriel, P.; Valdés, C.; Aznar, F. *Angew. Chem. Int. Ed.* **2007**, *46*, 5587–5590.

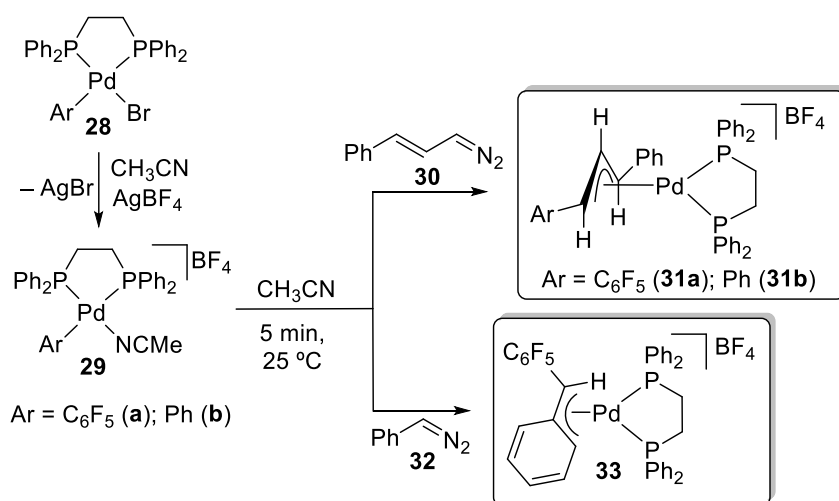
b) Barluenga, J.; Valdés, C. *Angew. Chem. Int. Ed.* **2011**, *50*, 7486–7500.

^{cclxvi} a) Albéniz, A. C.; Espinet, P.; Manrique, R.; Pérez-Mateo, A. *Chem. Eur. J.* **2005**, *11*, 1565–1573. b) Albéniz, A. C.; Espinet, P.; Pérez-Mateo, A.; Nova, A.; Ujaque, G. *Organometallics*, **2006**, *25*, 1293–1297. c) Pérez-Mateo, A.; Espinet, P.; Albéniz, A. C. *J. Organomet. Chem.* **2010**, *695*, 441–445.

Capítulo 5: Diazo-compuestos, hidrazonas y sus reacciones con complejos arílicos de paladio

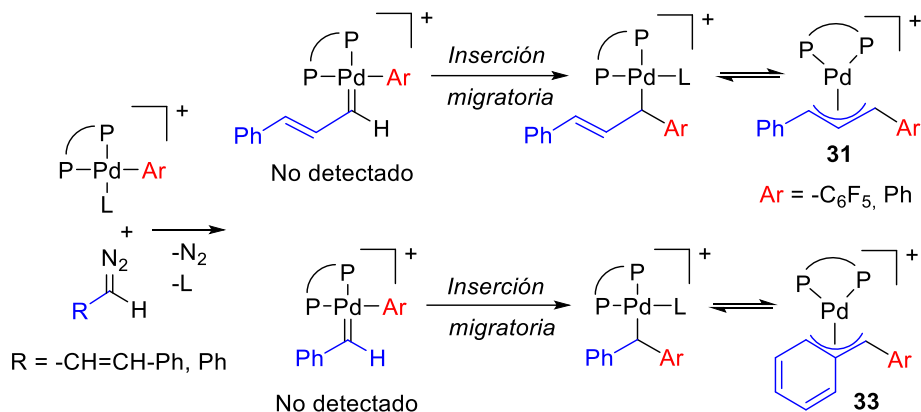
En este Capítulo se describe la reactividad de diazoalcanos e hidrazonas con complejos de paladio bien definidos.

Se han sintetizado diferentes complejos de paladio modelo: [PdArBr(dppe)] (**28**) y [PdAr(dppe)(NCMe)](BF₄) (**29**) y se ha llevado a cabo su reacción con los diazo compuestos **30** y **32**. La reacción es inmediata a temperatura ambiente y genera los correspondientes complejos organometálicos **31** y **33** como se muestra en el Esquema XI.



Esquema XI

Estos complejos organometálicos, son el resultado de una secuencia de etapas, como son la formación del carbeno de paladio (tras extrusión de nitrógeno) e inserción migratoria del grupo carbeno en el enlace Pd-arilo (Esquema XII). Los complejos **31** y **33** se estabilizan debido a presencia de un doble enlace o un arilo contiguo al carbono carbénico, lo cual permite que sean lo suficientemente estables para poder aislarlos y caracterizarlos, mediante la formación de un alilo o bencilo de paladio.

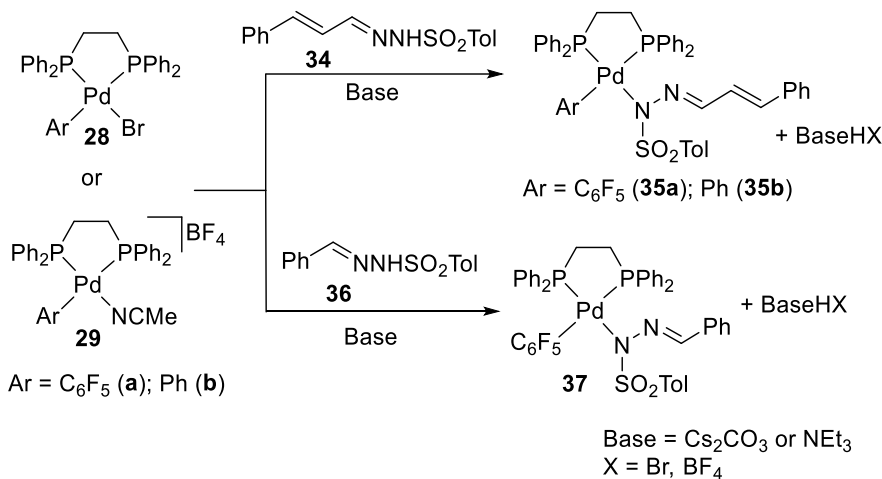


Esquema XII

Cuando las mismas reacciones mostradas en el Esquema XIII se llevan a cabo a $-90\text{ }^\circ\text{C}$ monitorizándolas por ^1H , ^{19}F y ^{31}P RMN no se pudo observar ni detectar ningún intermedio donde el diazo estuviera coordinado al paladio ni la formación de ningún carbeno de paladio.

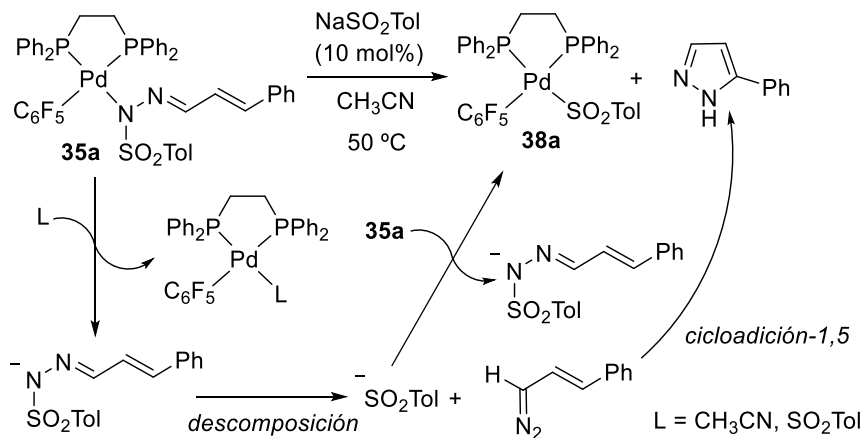
El perfil energético de las etapas de coordinación del diazo compuesto, extrusión de nitrógeno e inserción migratoria de las reacciones mostradas en el Esquema XIII se han modelizado empleando DFT debido a la imposibilidad de observar ningún intermedio a baja temperatura. La etapa de extrusión de nitrógeno para complejos **31** y **33** es la etapa limitante de la velocidad de la reacción. Los intermedios calculados con el diazo compuesto coordinado presentan una energía mayor que los correspondientes reactivos de partida, impidiendo de esta manera, su detección por RMN. Una vez superada la barrera energética de la extrusión de nitrógeno para la formación del intermedio carbeno de paladio, la barrera energética de la inserción migratoria es muy pequeña (6.1 y 6.2 kcal/mol para la formación de los complejos **31a** y **33** respectivamente).

Debido a que las *N*-tosilhidrazonas representan grandes ventajas como sustitutos de los diazo compuestos en muchas reacciones catalíticas, se ha estudiado la reactividad del complejo modelo **29** con las *N*-tosilhidrazonas **34** y **36** (Esquema XIV). La deprotonación de la *N*-tosilhidrazona asistida por una base no coordinante (Cs_2CO_3) resulta en la formación del *N*-tosilhidrazonato correspondiente, el cual es un excelente ligando para complejos de Pd(II), generando los correspondientes complejos con el *N*-tosilhidrazonato coordinado **35** y **37** (Esquema XIV).



Esquema XIII

Ambos complejos se descomponen a 50 °C con formación del derivado **38**, donde el grupo tosilo se ha coordinado al paladio por el átomo de azufre. Se observa también la formación del 5-fenil-pirazol derivado, formado por ciclación-1,5 del diazo compuesto generado por descomposición del hidrazonato (Esquema XIV).^{cclxvii}

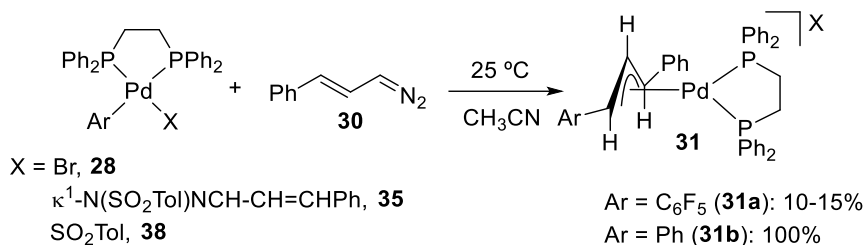


Esquema XIV

El seguimiento cinético de la reacción y experimentos cruzados entre dos complejos de paladio con *N*-tosilhidrazonatos coordinados y diferentes ligandos quelatos difosfinas han demostrado que el *N*-tosilhidrazonato se descoordina y se descompone fuera de la esfera de coordinación del paladio.

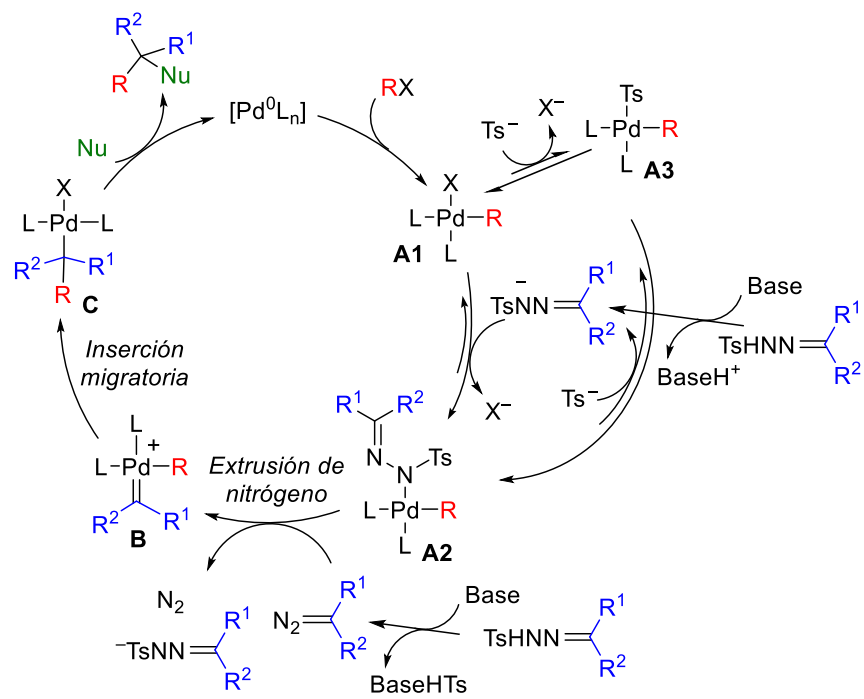
^{cclxvii} Brewbaker, J. L.; Hart, H. *J. Am. Chem. Soc.* **1969**, *91*, 711–715.

Se han llevado a cabo experimentos de sustitución de ligandos que indican que la coordinación del *N*-tosilhidrazonato a paladio es más favorable que la coordinación de bromuro o tosilato. De este modo en una reacción catalítica donde se empleen hidrazonas como precursores de carbeno, se pueden formar diferentes especies, pero los complejos hidrazonato son previsiblemente las especies predominantes (*resting state*). La sustitución del hidrazonato por un diazo compuesto es posible como se muestra en los experimentos independientes realizados de la Ecuación III.



Ecuación III

En conjunto, estos experimentos permiten completar el ciclo catalítico propuesto para las reacciones de acoplamiento C-C con precursores carbenos como reactivos tal y como muestra el Esquema XV.



Esquema XV

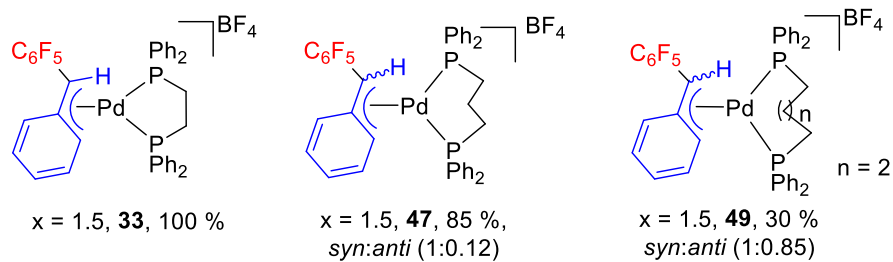
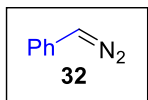
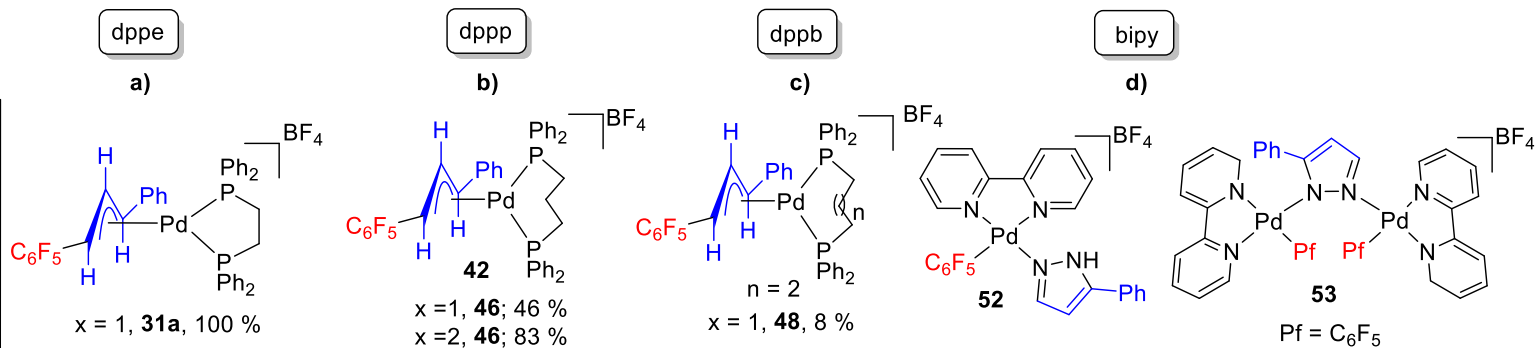
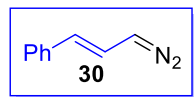
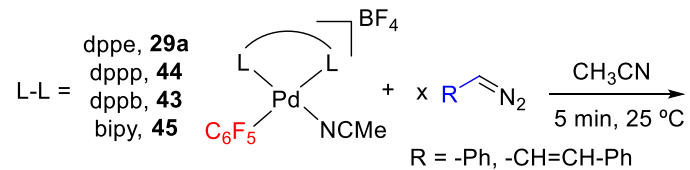
Capítulo 6: Entendiendo la influencia de los ligandos en la reacción multietapa de diazo compuestos con complejos de paladio con acoplamiento carbeno-arilo.

En la literatura se encuentran ejemplos en los que la elección de diferentes ligandos auxiliares en reacciones catalíticas de acoplamiento C-C que involucran carbenos reactivos (generados a partir de diazo compuestos o hidrazonas) puede llevar a la formación de diferentes productos partiendo de los mismos reactivos de partida.^{cclxviii} Tomando como base las reacciones modelo estudiadas en el *Capítulo 5*, se ha extendido su investigación a complejos similares donde el ligando quelato fosfina (dppe) se ha sustituido por otros ligandos (dppp, dppb, PPh₃ o bipy).

El Esquema XVI recoge los datos obtenidos por ¹H, ¹⁹F y ³¹P RMN para la reacción de los complejos de paladio modelo (**29**, **43**, **44** y **45**) con los dos diazo compuestos (**30** y **32**). Se observa una clara disminución en la cantidad del producto de inserción migratoria cuando que sustituimos el ligando auxiliar dppe por otros más voluminosos (dppp o dppb). Estos resultados experimentales indican que el ligando auxiliar está teniendo un papel importante durante la reacción.

Cuando se estudia la reactividad con biperidina como ligando auxiliar no se observa ningún producto derivado de inserción migratoria. Los únicos complejos de paladio observados tras la reacción corresponden a la coordinación del pirazol-derivado, generado por cicloadición intramolecular del diazo compuesto (Esquema XVI, **d**)).

^{cclxviii} a) Ren, X.; Zhu, L.; Yu, Y.; Wang, Z.-X.; Huang, X. *Org. Lett.* **2020**, *22*, 3251–3257. b) Chen, Z.-S.; Duan, X.-H.; Wu, L.-Y.; Ali, S.; Ji, K.-G.; Zhou, P.-X.; Liu, X.-Y.; Liang, Y.-M. *Chem. – A Eur. J.* **2011**, *17*, 6918–6921. c) Ping, W.-W.; Jin, L.; Wu, Y.; Xue, X.-Y.; Zhao, X. *Tetrahedron* **2014**, *70*, 9373–9380.



Esquema XVI

El complejo *trans*-[PdBr(C₆F₅)(PPh₃)₂] no genera ningún producto organometálico de inserción migratoria cuando reacciona con los diazo compuestos **30** y **32**. La disposición *trans* del complejo de partida, impide que el posible carbeno de paladio (formado tras la etapa de extrusión de nitrógeno) pueda interactuar con el enlace Pd-arilo llevando a cabo la etapa de inserción migratoria. La reorganización en disolución hacia el isómero *cis* es más lenta que la descomposición por otras vías del carbeno de paladio, explicando así la presencia de benzaldehído (producto de hidrólisis) o derivados de azina.

A la vista de los resultados experimentales recogidos en el Esquema XVI, se decidió modelar las reacciones mediante cálculos computacionales DFT para averiguar qué etapas eran claves para explicar la velocidad de formación de los complejos organometálicos. La Tabla III muestra los valores obtenidos para la barrera de extrusión de nitrógeno y de inserción migratoria para los diferentes ligandos auxiliares estudiados. Todos ellos presentan energías de activación muy bajas donde la tendencia es justo la contraria a la observada experimentalmente. Por tanto, se decidió explorar otras etapas que también están involucradas en la reacción y que no se habían contemplado hasta el momento, como es la coordinación del diazo compuesto al centro metálico.

Tabla III.

L-L	$\Delta\Delta G^\ddagger$ extrusión de N ₂	$\Delta\Delta G^\ddagger$ inserción migratoria	TS extrusión de N ₂	TS _{inserción migratoria}
dppe	11.0	6.1	14.1	-11.6
dppp	10.2	4.5	12.6	-12.2
dppb	8.9	4.6	11.2	-15.5
bipy	3.5	3.3	5.3	-21.3

Se analizó el mecanismo de sustitución asociativo entre el diazo compuesto **30** y los complejos de partida **29** y **44** (Figura III). Experimentos cinéticos realizados para la reacción del complejo **44** (dppp) con diferentes concentraciones del ligando entrante (diazoalcano) indican que este es el mecanismo que opera. La energía de activación para el estado de transición en el sistema dppe es de 11.0 kcal mol⁻¹, mientras que el mismo mecanismo para el sistema dppp presenta una barrera de activación estimada de 17.6 kcal mol⁻¹. Esta diferencia energética permite explicar la diferente facilidad de formación de los complejos organometálicos de inserción migratoria **31** vs. **46**.

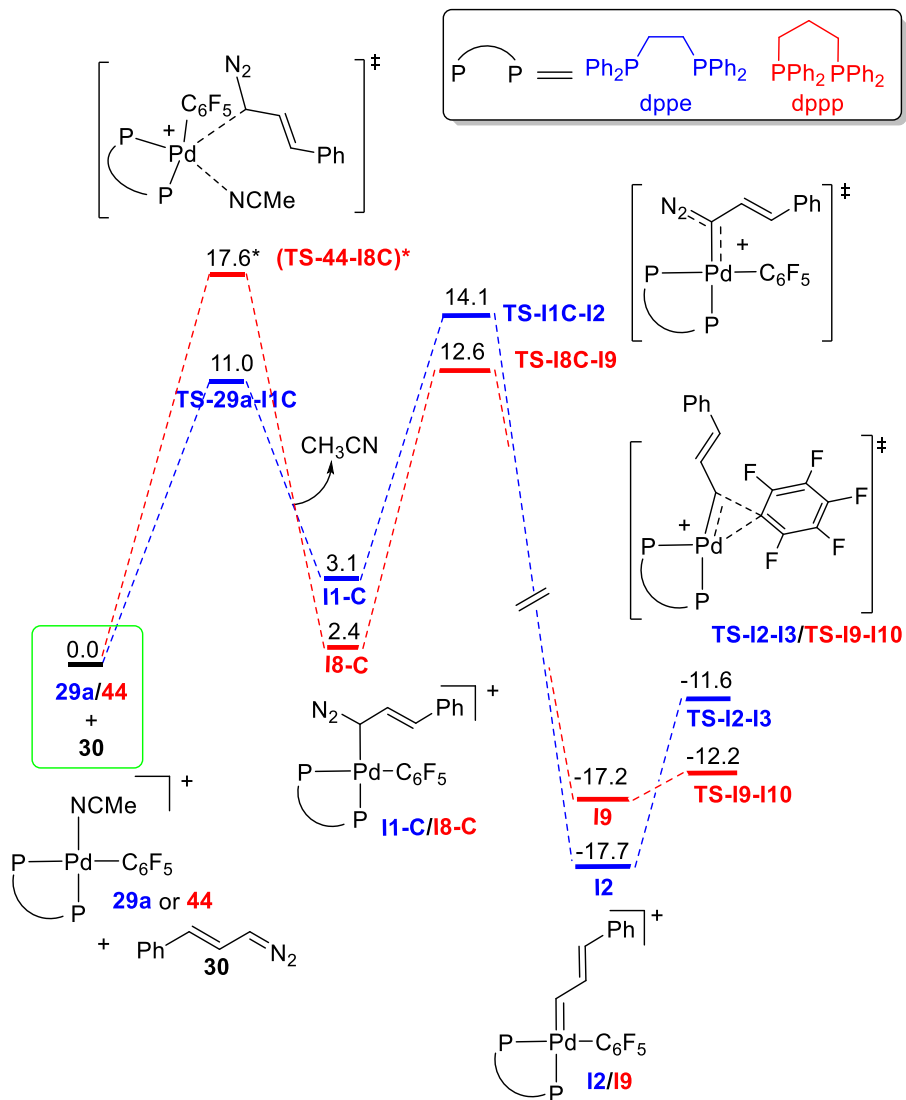


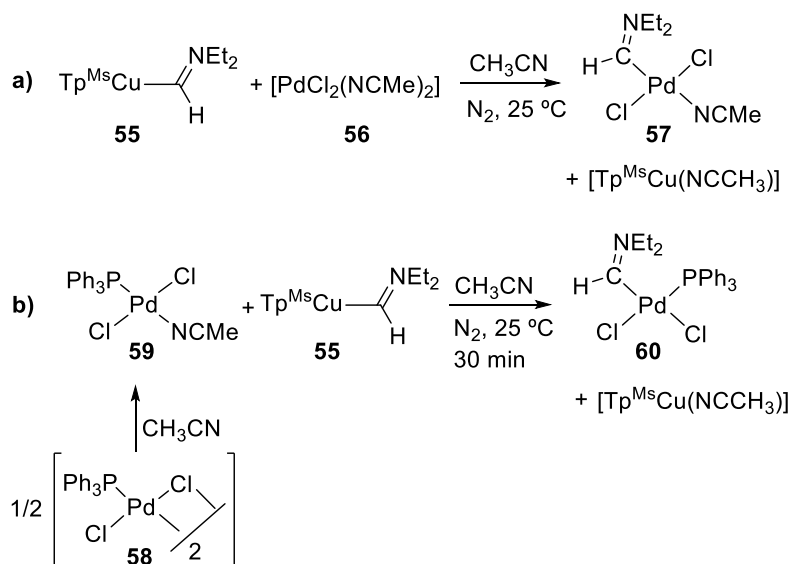
Figura III

Capítulo 7: Reacciones del aminocarbeno más simple $CH(NEt_2)$: Transmetalación desde Cu(I) a Pd(II) e inserción migratoria.

A lo largo de este capítulo se aborda el estudio de reacciones donde se produce una transferencia de carbeno entre un complejo de cobre(I) ($[Tp^{Ms}Cu\{CH(NEt_2)\}]$) y complejos de paladio(II).^{ccclix} Este trabajo se ha llevado a cabo en colaboración con el grupo de investigación del Prof. Pedro Pérez de la Universidad de Huelva (CIQSO) y con el Prof. Agustí Lledós de la Universidad Autónoma de Barcelona.

El complejo $[Tp^{Ms}Cu\{CH(NEt_2)\}]$ representa el primer ejemplo de un aminocarbeno monosustituido que se ha podido aislar y caracterizar completamente. Al no encontrar ningún precedente en la literatura que sea similar, se decidió estudiar su transferencia a complejos de Pd(II) y sobre éstos últimos, realizar un estudio de su reactividad.

Empleando los complejos de paladio **56** y **58** se ha conseguido aislar los complejos **57** y **60** donde el aminocarbeno se encuentra coordinado (Esquema XVII). Ambos complejos han sido caracterizados por RMN, espectrometría de masas (complejo **60**) y difracción de rayos X (complejo **60**).



Esquema XVII

^{ccclix} Álvarez, M.; Besora, M.; Molina, F.; Maseras, F.; Belderrain, T. R.; Pérez, P. J. *J. Am. Chem. Soc.* **2021**, *143*, 4837–4843.

Resumen

La reacción b) del Esquema XVII se ha monitorizado por ^1H RMN a baja temperatura ($-40\text{ }^\circ\text{C}$). El proceso comienza con la transmetalación del aminocarbeno desde el complejo de cobre **55** al complejo **59** (generado *in situ* en el medio de reacción cuando se emplea acetonitrilo como disolvente). El primer complejo que se observa es el intermedio *trans*- $[\text{PdCl}_2(\text{PPh}_3)(\text{carbeno})]$ (*trans*-**60**) estable solo a baja temperatura ($-40\text{ }^\circ\text{C}$). A medida que se incrementa la temperatura se observa la aparición de dos complejos; **57** (previa disociación de una PPh_3) y el complejo *cis*- $[\text{PdCl}_2(\text{PPh}_3)(\text{carbeno})]$ (*cis*-**60**). Este último (*cis*-**60**) es la especie estable termodinámicamente y la única especie que se observa a temperatura ambiente (Figura IV).

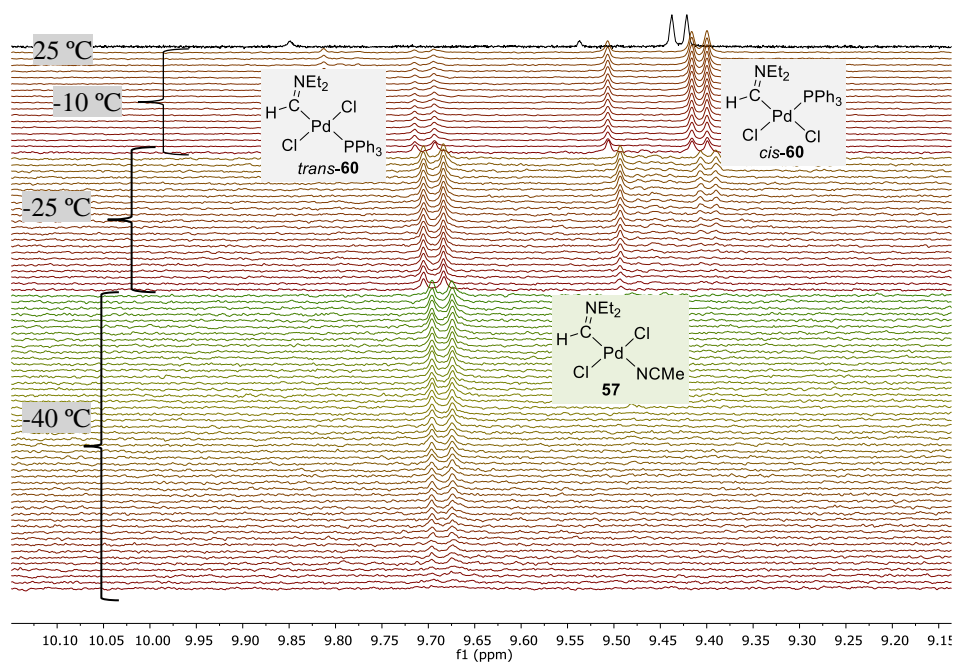


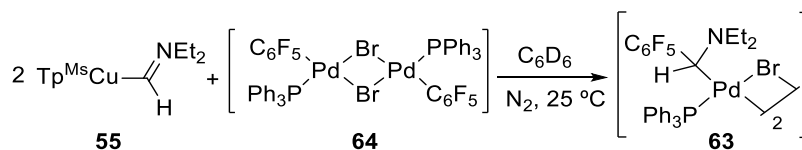
Figura IV

Con los datos experimentales obtenidos a partir de la reacción mostrada en el Esquema XVII, b) y la Figura IV, el Prof. Agustí Lledós ha modelizado por cálculos computacionales DFT las diferentes etapas que se producen para llevar a cabo la transmetalación del aminocarbeno desde el complejo de Cu(I) **55** al complejo de Pd(II) **59**. La etapa más alta en energía para todo el proceso presenta un valor de $18.4\text{ kcal mol}^{-1}$, esta barrera de activación es fácil de superar a bajas temperaturas como se ha demostrado en el seguimiento de la reacción. El estudio computacional de la etapa de isomerización *trans*-*cis* del complejo **60** muestra que el proceso transcurre con disociación de la fosfina

y formación del carbeno con acetonitrilo coordinado **57** durante el proceso, como se observa experimentalmente.

Tras analizar la etapa de transmetalación en complejos de paladio que no contienen grupos arilo, se procedió a estudiar la reactividad de complejos de paladio que contuviesen un arilo coordinado de forma que, tras la etapa de transmetalación, el aminocarbeno pudiera insertarse en el enlace Pd-C(arilo).

El complejo dímero de paladio(II) **64** demostró ser idóneo para llevar a cabo este tipo de reacción, ya que permite aislar el complejo resultante de las etapas de transmetalación y de inserción migratoria del aminocarbeno en el enlace Pd-C₆F₅ (**63**). El complejo resultante es un dímero de paladio(II) (**63**) que se encuentra estabilizado por la imposibilidad de llevar a cabo procesos de descomposición de tipo β-eliminación de hidrógeno (Ecuación IV). No se detecta el carbeno de paladio intermedio, lo que indica que para este fragmento la inserción migratoria es un proceso rápido.



Ecuación IV

Conclusiones Generales

Capítulo 2. Se ha desarrollado la reacción de tipo Heck oxidativa para arenos simples con oxígeno como único oxidante y sin presencia de mediadores de oxidación, empleando la mínima cantidad de aditivos, solo molibdato sódico en cantidades catalíticas. Esto permite unas condiciones de reacción sin necesidad de usar bases fuertes o ácidos. La presencia de los ligandos cooperativos [2, 2'-bipiridin]-6(1*H*)-ona (bipy-6-OH) y 1,10-fenantrolin-2(1*H*)-ona (phen-2-OH) facilita la reacción para arenos mono- y disustituídos con diferentes propiedades electrónicas, asistiendo en la etapa de ruptura del enlace C-H. Sin embargo, la presencia del ligando cooperativo es perjudicial en la reacción de polifluoroarenos $C_6F_nH_{6-n}$ ($n \geq 3$) y 1,3- $C_6F_2H_4$ donde la fácil activación C-H no requiere de una cooperación adicional por parte del ligando. Es más, se genera un efecto desfavorable en la etapa de coordinación-inserción de la olefina. Por eso en el caso de polifluoroarenos no es recomendable el uso de un ligando cooperativo pero la etapa de activación C-H de cualquier otro areno en estas condiciones de reacción sí requiere la presencia del ligando cooperativo para llevar a cabo la reacción con buenos rendimientos.

Capítulo 3. Todos los complejos de paladio aislados de la reacción entre bipy-6-OH o phen-2-OH con $[Pd(OAc)_2]$ exhiben un modo de coordinación de tipo L,X (monoaniónico). Independientemente de la relación Pd:ligando empleada (1:1 o 1:2) la formación del complejo monómero neutro $[Pd(L-X)_2]$ (L-X = bipy-6-O, phen-2-O, **24**) ocurre en primer lugar. Este complejo **24** es el único producto que se observa para una relación Pd:ligando = 1:2. Si la relación es 1:1, se produce una reorganización del complejo **24** con el $[Pd(OAc)_2]$ que no ha reaccionado para formar el complejo dímero $[Pd_2(bipy-6-O)_2(\mu-OAc)(\mu-OH)]$ (**23a**) que se han aislado y caracterizado. La formación del complejo **23a** es rápida en disolventes coordinantes como el DMSO. Además, se ha observado que la formación del complejo **23a** tiene una fuerte dependencia con la cantidad de agua que haya presente en el disolvente. El ligando phen-2-OH tiende a formar complejos mucho menos solubles, lo cual lleva a un comportamiento menos activo al requerir mayores temperaturas para llevar a cabo el proceso de reorganización para generar **23b**.

En contraste con el acetato de paladio, la reacción de $PdCl_2$, como precursor, genera complejos neutros (**25**, coordinación de tipo L,L).

La actividad como precatalizadores de los complejos aislados ha sido evaluada en la reacción de arilación directa de tolueno en comparación con la mezcla

[Pd(OAc)₂]/bipy-6-OH o phen-2-OH. Cuando la reacción catalítica se lleva a cabo en un medio polar, por ejemplo, una mezcla de tolueno/DMA, apenas hay diferencias en el rendimiento final sin importar el precatalizador empleado, muy probablemente debido a la rápida coordinación y posterior reorganización del ligando en el centro metálico que lleva a las especies activas. Sin embargo, cuando la reacción se lleva a cabo en un medio no-polar (tolueno), los complejos **23a** y **25a** aceleran la reacción incrementando el rendimiento final en las primeras 6 h en comparación con la mezcla [Pd(OAc)₂]/bipy-6-OH. Esto demuestra que la precoordinación del ligando deprotonado al centro metálico en relación Pd:ligando = 1:1 facilita la formación de especies activas. Los precatalizadores de Pd(II) sintetizados pueden transformarse en especies de Pd(0) activas en la reacción de arilación directa mediante una doble activación C-H del areno (tolueno) y posterior eliminación reductora.

Capítulo 5. Empleando complejos arílicos de paladio se ha podido conseguir información acerca de la interacción con diazo compuestos y *N*-tosilhidrazonas. No se ha podido detectar complejos carbeno de paladio debido al alto carácter electrofílico que presentan y que conlleva a una rápida inserción migratoria, generando los correspondientes alilos y bencilos de paladio que sí se han podido aislar y caracterizar completamente. Estos complejos demuestran de manera inequívoca que la inserción migratoria ocurre para carbenos de paladio generados a partir de diazo compuestos.

Por otra parte, los tosilhidrazonatos han demostrado ser excelentes ligandos en complejos de paladio bajo condiciones de catálisis (altas concentraciones de hidrazona y de base en el medio). Cuando los complejos con tosilhidrazonato coordinado se descomponen, generan tosilato libre que compite como ligando, formando complejos de paladio con el tosilo coordinado. Se ha demostrado mediante experimentos cruzados que la descomposición del tosilhidrazonato no se produce dentro de la esfera de coordinación del paladio, sino que requiere de una descoordinación previa. Con todos los resultados obtenidos en el aislamiento y estudio de complejos de paladio con tosilhidrazonatos coordinados, así como reacciones competitivas de sustitución de ligandos, es posible proponer a los complejos hidrazonato como posibles “*resting states*” del ciclo catalítico de acoplamiento C-C con precursores de carbenos como reactivos. A partir de ahí la sustitución del hidrazonato por el diazoalcano es posible seguida de una rápida formación del carbeno e inserción migratoria.

Capítulo 6. Se ha estudiado la reacción con diazoalcanos de una serie de complejos de Pd(II) con el arilo C₆F₅ y ligandos auxiliares de tipo difosfina con diferentes

ángulos de mordedura $[\text{Pd}(\text{C}_6\text{F}_5)(\text{NCMe})(\text{L-L})]\text{BF}_4$ El orden de reactividad obtenido experimentalmente para la formación de los productos de inserción migratoria es el siguiente: $\text{L-L} = \text{dppe} > \text{dppp} \gg \text{dppb}$. Los cálculos computacionales realizados para los diferentes perfiles de las disfosfinas muestran que a medida que aumenta el ángulo de mordedura de la difosfina, las energías de las etapas de extrusión de nitrógeno desde el diazo compuesto y de inserción migratoria disminuyen. Por lo tanto, las diferencias de reactividad no se deben a estas etapas sino a la velocidad de coordinación del diazo compuesto al paladio, como se ha corroborado experimental y computacionalmente.

La reacción de los complejos análogos *trans*- $[\text{Pd}(\text{C}_6\text{F}_5)(\text{NCMe})(\text{PPh}_3)_2]\text{BF}_4$ y $[\text{Pd}(\text{C}_6\text{F}_5)(\text{NCMe})(\text{bipy})]\text{BF}_4$ no llevan productos de acoplamiento carbeno-arilo. En el primer caso porque no se produce la isomerización del complejo que permita la disposición *cis*-carbeno arilo necesaria para la inserción migratoria. En el segundo caso porque la coordinación de 5-fenil-pirazol, producto de la descomposición del diazoalcano empleado, es más favorable que la coordinación $\kappa^1\text{-C}$ del diazoalcano.

Capítulo 7. La transmetalación del fragmento carbeno desde el complejo $[\text{Tp}^{\text{Ms}}\text{Cu}\{\text{CH}(\text{NEt}_2)\}]$ (**55**) a los complejos $[\text{PdCl}_2(\text{NCMe})\text{L}]$ ($\text{L} = \text{NCMe}$, **56**; PPh_3 , **59**) ocurre muy rápido tanto a temperatura ambiente como a baja temperatura para **59** (-40°C). Se han podido aislar y caracterizar los correspondientes complejos de Pd(II) con el aminocarbeno coordinado $[\text{Pd}\{\text{CH}(\text{NEt}_2)\text{Cl}_2(\text{NCMe})\}]$ (**57**) y *cis*- $[\text{Pd}\{\text{CH}(\text{NEt}_2)\text{Cl}_2(\text{PPh}_3)\}]$ (**60**). Se ha observado que estos complejos con el grupo aminocarbeno presentan un comportamiento electrofílico, como muestra la formación de subproductos de hidrólisis durante las reacciones y seguimientos. Los estudios sobre la etapa de transmetalación desde el aminocarbeno de Cu(I) al complejo **59** llevados a cabo por el Prof. Agustí Lledós revelan un perfil energético con barreras de activación bajas, siendo el *energetic span* de la reacción de 18.4 kcal/mol. La transferencia del grupo carbeno desde el Cu(I) hasta el Pd(II) se produce a través de un puente aminocarbeno a los dos centros metálicos.

Cuando se estudia la reacción de $[\text{Tp}^{\text{Ms}}\text{Cu}\{\text{CH}(\text{NEt}_2)\}]$ (**55**) con complejos de paladio con grupos arilo ($-\text{C}_6\text{F}_5$) no se ha podido detectar ningún intermedio con el carbeno coordinado al paladio, sino la formación del complejo de paladio dímero **63**, resultado de la inserción migratoria del carbeno en el enlace Pd- C_6F_5 , el cual ha podido ser aislado y caracterizado. Esto implica que la etapa de inserción migratoria es muy rápida para el aminocarbeno $\text{CH}(\text{NEt}_2)$ que en este comportamiento se asemeja a carbenos más electrofílicos que lo que su estructura electrónica permite predecir.

Appendix

List of abbreviations and acronyms**General Abbreviations**

5-Ph-pz	5-phenyl-pyrazolate
5-Ph-pz-H	5-phenyl-1 <i>H</i> -pyrazole
2,6-F-F-Bz-Leu-OH	2,6-difluorobenzoyl-protected leucine
acac	Acetylacetonate
AcOH	Acetic acid
Anal.	Elemental Analysis
Ar	Aryl group
bipy	2,2'-bipyridine
bipy-6-OH	[2,2'-bipyridin]-6(1 <i>H</i>)-one
bipy-6-O	[2,2'-bipyridin]-6-one
CAAC	Cyclic Alkyl Amino Carbene
C ^{carbenic}	Carbon atom of the carbene unit
CMD	Concerted Metalation-Deprotonation
Cpd.	Compound
D	Diffusion coefficient
DDQ	2,3-Dichloro-5,6-dicyano-1,4-benzoquinone
DFT	Density Functional Theory
DGs	Directing Groups
DMA	<i>N,N</i> -dimethylacetamide
DMSO	Dimethyl sulfoxide
dppb	1,4-Bis(diphenylphosphino)butane
dppe	1,2-Bis(diphenylphosphino)ethane
dppm	1,1-Bis(diphenylphosphino)methane
dppp	1,3-Bis(diphenylphosphino)propane
dippp	1,4-Bis(diphenylphosphino)butane
dpbz	1,2-Bis(diphenylphosphino)ethane
dmpe	1,3-Bis(diphenylphosphino)propane
dppee	1,2-Bis-(diphenylphosphino)benzene
EDG	Electron-Donating Groups
equiv	Equivalent
ETMs	Electron-Transfer Mediators
ESI-TOF	Electrospray Ionisation- Time-Of-Flight
EWG	Electron-Withdrawing Groups
GC	Gas Chromatography
GIAO	Gauge-Independent Atomic Orbital
IR	Infrared
Isol.	Isolated
KIE	Kinetic Isotope Effect
KHMDS	Potassium bis(trimethylsilyl)amide
L	Monodentate neutral ligand
MS	Mass Spectrometry
MTBE	<i>Tert</i> -butyl methyl ether
M.I.	Migratory insertion
MPAA	Monoprotected amino acid
NAC	Nitrogen Acyclic Carbene
NHC	Nitrogen Heterocyclic Carbene
OAc	Acetate
Ox	Oxidized / Oxidant

Abbreviations

Pf	Pentafluorophenyl (-C ₆ F ₅) group
PfH	Pentafluorobenzene
phen	1,10-Phenanthroline
phen-2-OH	[1,10-Phenanthroline]-2(1 <i>H</i>)-one
phen-2-O	[1,10-Phenanthroline]-2-one
Py	Pyridine
PivOH	2,2-Dimethylpropanoic acid (pivalic acid)
Ref.	Reference
Rf	3,5-dichloro-2,4,6-trifluorophenyl
SMD	Solvation Model based on Density
Solv	Solvent in general
TFA	Trifluoroacetic acid
THF	Tetrahydrofuran
TP ^{Ms}	Hydrotris(3-mesitylpyrazolyl)borate
Ts	Tosylate
TS	Transition State
TsNIK	<i>N</i> -Iodo <i>p</i> -toluenesulfonamide
TEMPO	(2,2,6,6-Tetramethylpiperidin-1-yl)oxyl
VTNA	Variable Time Normalization Analysis
X	Halogen in general
Z-Phe-OH	L-Phenylalanine

Abbreviations used in NMR spectroscopy

NMR	Nuclear Magnetic Resonance
s	singlet
d	doublet
t	triplet
m	multiplet
br	broad
J	Coupling constant
ppm	Parts per million
COSY	(<i>C</i> orrelation <i>S</i> pectroscop <i>Y</i>)
HSQC	(<i>H</i> eteronuclear <i>S</i> ingle <i>Q</i> uantum <i>C</i> oherence <i>S</i> pectroscop <i>Y</i>)
HMBC	(<i>H</i> eteronuclear <i>M</i> ultiple <i>B</i> ond <i>C</i> orrelation)
ROESY	(<i>R</i> otating <i>f</i> rame <i>O</i> verhauser <i>E</i> ffect <i>S</i> pectroscop <i>Y</i>)

Abbreviations used in X-Ray diffraction

CCD	Charge Coupled Device
ORTEP	Oak Ridge Thermal Ellipsoid Plot

References

1. A presentation of the topic can be found in: a) de Meijere, A.; Negishi, E-i. *Handbook of Organopalladium Chemistry for Organic Synthesis, Vol 1 and 2*, Wiley-Interscience, New York, **2002**. b) Miyaura, N.; *Cross-Coupling Reactions: A practical Guide; Topics in Current Chemistry*, Series 219; **2002**, Springer, Berlin. c) De Meijere, A; Dietrich, F.; *Metal-Catalyzed Cross-Coupling Reactions*, 2nd ed. **2004**, Wiley-VCH: Weinheim. d) de Meijere, A.; Bräse, S.; Oestreich, M. *Metal-Catalyzed Cross-Coupling Reactions and More, Vol 1, 2 and 3.*; Wiley-VCH: Weinheim, **2013**.
2. a) Heck, R. F. *J. Am. Chem. Soc.* **1968**, *90*, 5518–5526. b) Mizoroki, T.; Mori, K.; Ozaki, A. *Bull. Chem. Soc. Jpn.* **1971**, *44*, 581–581. c) Heck, R. F. *Org. React.* **1982**, *27*, 345–390.
3. a) Louie, J.; Hartwig, J. F. *Tetrahedron Lett.* **1995**, *36*, 3609–3612. b) Guram, A. S.; Rennels, R. A.; Buchwald, S. L. *Angew. Chem., Int. Ed.* **1995**, *34*, 1348–1350. For recent reviews see: a) Ruiz-Castillo, P.; Buchwald, S. L. *Chem. Rev.* **2016**, *116*, 12564–12649. b) Heravi, M. M.; Kheilkordi, Z.; Zadsirjan, V.; Heydari, M.; Malmir, M. *J. Organomet. Chem.* **2018**, *861*, 17–104. c) Dorel, R.; Grugel, C. P.; Haydl, A. M. *Angew. Chem. Int. Ed.* **2019**, *58*, 17118–17129.
4. Zhao, B.; Rogge, T.; Ackermann, L.; Shi, Z. *Chem. Soc. Rev.* **2021**, *50*, 8903–8953.
5. a) Li, J.; Yang, S.; Wu, W.; Jiang, H. *Org. Chem. Front.* **2020**, *7*, 1395–1417. b) Beletskaya, I. P.; Ananikov, V. P. *Chem. Rev.* **2022**, *122*, 16110–16293.
6. Kumada, M. *Pure Appl. Chem.* **1980**, *52*, 669–679.
7. Negishi, E-I. *Acc. Chem. Res.* **1982**, *15*, 340–348.
8. a) Stille, J. K. *Angew. Chem. Int. Ed.* **1986**, *25*, 508–524. b) Stille, J. K. *Angew. Chem.* **1986**, *98*, 504–519. c) Espinet, P.; Echavarren, A. M. *Angew. Chem. Int. Ed.* **2004**, *43*, 4704–4734.
9. a) Miyaura, N.; Yanagi, T.; Suzuki, A. *Synth. Commun.* **1981**, *11*, 513–519. b) Miyaura, N.; Suzuki, A. *Chem. Rev.* **1995**, *95*, 2457–2483.
10. a) Hiyama, T.; Shirakawa, E. *Top. Curr. Chem.* **2002**, *219*, 61–85. b) Hiyama, T.; *J. Organomet. Chem.* **2002**, *653*, 58–61.
11. a) Sonogashira, K.; Tohda, Y.; Hagihara, N. *Tetrahedron Lett.* **1975**, 4467–4470. b) Sonogashira, K. in *Comprehensive Organic Synthesis* (Eds.: B. M. Trost, I. Fleming), Pergamon Press, Oxford, **1991**, vol. 3, pp. 521–549.
12. a) Anastas, P. T.; Mary, M. *Acc. Chem. Res.* **2002**, *35*, 686–694. b) Dalton, T.; Faber, T.; Glorius, F. *ACS Cent. Sci.* **2021**, *7*, 2, 245–261.
13. a) He, J.; Wasa, M.; Chan, K. S. L.; Shao, Q.; Yu, J-Q. *Chem. Rev.* **2017**, *117*, 8754–8786. b) Newton, C. G.; Wang, S.-G.; Oliveira, C. C.; Cramer, N. *Chem. Rev.* **2017**, *117*, 8908–8976. c) Crabtree, R. H.; Lei, A. *Chem. Rev.* **2017**, *117*, 8481–8482. d) Zhang, L.; Ritter, T. *J. Am. Chem. Soc.* **2022**, *144*, 2399–2414.
14. Altus, K. M.; Love, J. A. *Commun. Chem.* **2021**, *4*, 173.
15. In the context of fundamental organometallic chemistry oxidative coupling has a different meaning: it is a reaction where two coordinated ligands form a new bond to each other while changing from 2 L ligands to an X₂ ligand and therefore producing the oxidation of the metal center.
16. Li, H.; Liu, J.; Sun, C.-L.; Li, B.-J.; Shi, Z.-J. *Org. Lett.* **2011**, *13*, 276–279.

17. a) Li, C.-J. *Acc. Chem. Res.* **2009**, *42*, 335–344. b) Scheuermann, C. J. *Chem. Asian J.* **2010**, *5*, 436–451. c) Krylov, I. B.; Vil', V. A.; Terent'ev, A. O. *Beilstein J. Org. Chem.* **2015**, *11*, 92–146. d) Yang, Y.; Lan, J.; You, J.-Q. *Chem. Rev.* **2017**, *117*, 8787–8863. e) Huang, C.-Y.; Kang, H.; Li, J.; Li, C.-J. *J. Org. Chem.* **2019**, *84*, 12705–12721.
18. Moritanl, I.; Fujiwara, Y. *Tetrahedron Lett.* **1967**, *8*, 1119–1122.
19. Zhang, X.; Fan, S.; He, C.-Y.; Wan, X.; Min, Q.-Q.; Yang, J.; Jiang, Z.-X. *J. Am. Chem. Soc.* **2010**, *132*, 4506–4507.
20. a) Tang, S.; Zeng, L.; Lei, A. *J. Am. Chem. Soc.* **2018**, *140*, 13128–13135. b) Zhang, D.; Hui, X.; Wu, C.; Zhu, Y. *ChemCatChem* **2021**, *13*, 3370–3380. c) Liu, Q.; Wu, L.-Z. Cross-Coupling Hydrogen Evolution to Avoid the Use of External Oxidants BT - Springer Handbook of Inorganic Photochemistry; Bahnemann, D., Patrocínio, A. O. T., Eds.; Springer International Publishing: Cham, **2022**; pp 1457–1480.
21. For reviews on transition-metal catalyzed oxidative reactions with oxygen see: a) Stahl, S. S. *Angew. Chem. Int. Ed.* **2004**, *43*, 3400–3420. b) Piera, J.; Bäckvall, J.-E. *Angew. Chem. Int. Ed.* **2008**, *47*, 3506–3523. c) Campbell, A. N.; Stahl, S. S. *Acc. Chem. Res.* **2012**, *45*, 6, 851–863. d) Shi, Z.; Zhang, C.; Tanga, C.; Jiao, N. *Chem. Soc. Rev.*, **2012**, *41*, 3381–3430.
22. a) Liu, J.; Guðmundsson, A.; Bäckvall, J.-E. *Angew. Chem. Int. Ed.* **2021**, *60*, 15686–15704.
23. a) Steinhoff, B. A.; Stahl, S. S. *J. Am. Chem. Soc.* **2006**, *128*, 4348–4355. b) Quaranta, M.; Murkovic, M.; Klimant, I. *Analyst* **2013**, *138*, 6243–6245. c) Sato, T.; Hamada, Y.; Sumikawa, M.; Araki, S.; Yamamoto, H. *Ind. Eng. Chem. Res.* **2014**, *53*, 19331–19337.
24. a) Muzart, J. *Chem. Asian J.* **2006**, *1*, 508–515. b) Wang, D.; Weinstein, A. B.; White, P. B.; Stahl, S. S. *Chem. Rev.* **2018**, *118*, 5, 2636–2679.
25. a) Stahl, S. S.; Thorman, J. L.; Nelson, R. C.; Kozee, M. A. *J. Am. Chem. Soc.* **2001**, *123*, 7188–7189. b) Steinhoff, B. A.; Fix, S. R.; Stahl, S. S. *J. Am. Chem. Soc.* **2002**, *124*, 766–767. c) Steinhoff, B. A.; Guzei, I. A.; Stahl, S. S. *J. Am. Chem. Soc.* **2004**, *126*, 11268–11278. d) Rogers, M. M.; Wendlandt, J. E.; Guzei, I. A.; Stahl, S. S. *Org. Lett.* **2006**, *8*, 2257–2260. e) Cai, X.; Majumdar, S.; Fortman, G. C.; Cazin, C. S. J.; Slawin, A. M. Z.; Lhermitte, C.; Prabhakar, R.; Germain, M. E.; Palluccio, T.; Nolan, S. P.; Rybak-Akimova, E. V.; Temprado, M.; Captain, B.; Hoff, C. D. *J. Am. Chem. Soc.* **2011**, *133*, 1290–1293. f) Scheuermann, M. L.; Boyce, D. W.; Grice, K. A.; Kaminsky, W.; Stoll, S.; Tolman, W. B.; Swang, O.; Goldberg, K. I. *Angew. Chem. Int. Ed.* **2014**, *53*, 6492–6495.
26. a) Popp, B. V.; Stahl, S. S. *J. Am. Chem. Soc.* **2007**, *129*, 4410–4422. b) Konnick, M. M.; Stahl, S. S. *J. Am. Chem. Soc.* **2008**, *130*, 5753–5762. c) Popp, B. V.; Stahl, S. S. *Chem. Eur. J.* **2009**, *15*, 2915–2922.
27. a) Keith, J. M.; Goddard III, W. A. *J. Am. Chem. Soc.* **2009**, *131*, 1416–1425. b) Konnick, M. M.; Decharin, N.; Popp, B. V.; Stahl, S. S. *Chem. Sci.* **2011**, *2*, 326–330.
28. a) Ingram, A. J.; Solis-Ibarra, D.; Zare, R. N.; Waymouth, R. M. *Angew. Chem. Int. Ed.* **2014**, *53*, 5648–5652. b) Ingram, A. J.; Walker, K. L.; Zare, R. N.; Waymouth, R. M. *J. Am. Chem. Soc.* **2015**, *137*, 13632–13646.
29. Luo, Y. R. *Comprehensive Handbook of Chemical Bond Energies*, CRC Press, **2007**.

30. For a comprehensive revision see: a) Chen, Z.; Wang, B.; Zhang, J.; Yu, W.; Liu, Z.; Zhang, Y. *Org. Chem. Front.* **2015**, *2*, 1107–1295. b) Ghosh, K.; Rit, R. K.; Shankar, M.; Mukherjee, K.; Sahoo, A. K. *Chem. Rec.* **2020**, *20*, 1017–1042.
31. Kuhl, N.; Hopkinson, M. N.; Wencel-Delord, J.; Glorius, F. *Angew. Chem. Int. Ed.* **2012**, *51*, 10236–10254.
32. Balcells, D.; Clot, E.; Eisenstein, O. *Chem. Rev.* **2010**, *110*, 749–823.
33. a) Fujiwara, Y.; Moritani, I.; Danno, S.; Asano, R.; Teranishi, S. *J. Am. Chem. Soc.* **1969**, *91*, 7166–7169. b) Ryabov, A. D.; Sakodinskaya, I. K.; Yatsimirsky, A. K. *J. Chem. Soc., Dalton Trans.* **1985**, 2629–1638. c) Yokoyama, Y.; Matsumoto, T.; Murakami, Y. *J. Org. Chem.* **1995**, *60*, 1486–1487. d) Jia, C.; Piao, D.; Oyamada, J.; Lu, W.; Kitamura, T.; Fujiwara, Y. *Science* **2000**, *287*, 1992–1995. e) Lane, B. S.; Brown, M. A.; Sames, D. *J. Am. Chem. Soc.* **2005**, *127*, 8050–8057. f) Lebrasseur, N.; Larrosa, I. *J. Am. Chem. Soc.* **2008**, *130*, 2926–2927
34. Canty, A. J.; van Koten, G. *Acc. Chem. Res.* **1995**, *28*, 406–413.
35. a) Watson, P. L. *J. Am. Chem. Soc.* **1983**, *105*, 6491–6493. b) Thompson, M. E.; Baxter, S. M.; Bulls, A. R.; Burger, B. J.; Nolan, M. C.; Santarsiero, B. D.; Schaefer, W. P.; Bercaw, J. E. *J. Am. Chem. Soc.* **1987**, *109*, 203–219. c) Lin, Z. *Coord. Chem. Rev.* **2007**, *251*, 2280–2291.
36. Winstein, S.; Traylor, T. G. *J. Am. Chem. Soc.* **1955**, *77*, 3747–3752.
37. a) Kurzeev, S. A.; Kazankov, G. M.; Ryabov, A. D. *Inorganica Chim. Acta* **2002**, *340*, 192–196.
38. Davies, D. L.; Donald, S. M. A.; Macgregor, S. A. *J. Am. Chem. Soc.* **2005**, *127*, 13754–13755.
39. a) Ackermann, L. *Chem. Rev.* **2011**, *111*, 1315–1345. b) Davies, D. L.; Macgregor, S. A.; McMullin, C. L. *Chem. Rev.* **2017**, *117*, 8649–8709.
40. a) García-Cuadrado, D.; Braga, A. A. C.; Maseras, F.; Echavarren, A. M. *J. Am. Chem. Soc.* **2006**, *128*, 1066–1067. b) García-Cuadrado, D.; de Mendoza, P.; Braga, A. A. C.; Maseras, F.; Echavarren, A. M. *J. Am. Chem. Soc.* **2007**, *129*, 6880–6886.
41. a) Campeau, L.-C.; Parisien, M.; Leblanc, M.; Fagnou, K. *J. Am. Chem. Soc.* **2004**, *126*, 9186–9187. b) Lafrance, M.; Rowley, C. N.; Woo, T. K.; Fagnou, K. *J. Am. Chem. Soc.* **2006**, *128*, 8754–8756. c) Stuart, D. R.; Fagnou, K. *Science* **2007**, *316*, 1172–1175. d) Gorelsky, S. I.; Lapointe, D.; Fagnou, K. *J. Am. Chem. Soc.* **2008**, *130*, 10848–10849.
42. a) Pascual, S.; de Mendoza, P.; Braga, A. A. C.; Maseras, F.; Echavarren, A. M. *Tetrahedron* **2008**, *64*, 6021–6029. b) Sun, H.-Y.; Gorelsky, S. I.; Stuart, D. R.; Campeau, L.-C.; Fagnou, K. *J. Org. Chem.* **2010**, *75*, 8180–8189.
43. a) Wang, L.; Carrow, B. P. *ACS Catal.* **2019**, *9*, 6821–6836. b) Carrow, B. P.; Sampson, J.; Wang, L. *Isr. J. Chem.* **2020**, *60*, 230–258. c) Evans, R.; Sampson, J.; Wang, L.; Lückemeier, L.; Carrow, B. P. *Chem. Commun.* **2021**, *57*, 9076–9079.
44. Khusnutdinova, J. R.; Milstein, D. *Angew. Chem. Int. Ed.* **2015**, *54*, 12236–12273.
45. Shi, B.-F.; Maugel, N.; Zhang, Y.-H.; Yu, J.-Q. *Angew. Chem. Int. Ed.* **2008**, *47*, 4882–4886.
46. a) Liu, L.-Y.; Qiao, J. X.; Yeung, K.-S.; Ewing, W. R.; Yu, J.-Q. *Angew. Chem. Int. Ed.* **2020**, *59*, 13831–13835. b) Park, H. S.; Fan, Z.; Zhu, R.-Y.; Yu, J.-Q. *Angew. Chem. Int. Ed.* **2020**, *59*, 12853–12859. c) Sinha, S. K.; Panja, S.; Grover, J.; Hazra,

- P. S.; Pandit, S.; Bairagi, Y.; Zhang, X.; Maiti, D. *J. Am. Chem. Soc.* **2022**, *144*, 12032–12042.
47. a) Yang, Y.-F.; Hong, X.; Yu, J.-Q.; Houk, K. N. *Acc. Chem. Res.* **2017**, *50*, 2853–2860. b) Shao, Q.; Wu, K.; Zhuang, Z.; Qian, S.; Yu, J.-Q. *Acc. Chem. Res.* **2020**, *53*, 833–851.
48. Cheng, G.-J.; Yang, Y.-F.; Liu, P.; Chen, P.; Sun, T.-Y.; Li, G.; Zhang, X.; Houk, K. N.; Yu, J.-Q.; Wu, Y.-D. *J. Am. Chem. Soc.* **2014**, *136*, 894–897.
49. a) Naksomboon, K.; Valderas, C.; Gómez-Martínez, M.; Álvarez-Casao, Y.; Fernández-Ibáñez, M. Á. *ACS Catal.* **2017**, *7*, 6342–6346. b) Álvarez-Casao, Y.; Fernández-Ibáñez, M. Á. *European J. Org. Chem.* **2019**, *2019*, 1842–1845. c) Sukowski, V.; Jia, W.-L.; van Diest, R.; van Borselen, M.; Fernández-Ibáñez, M. Á. *European J. Org. Chem.* **2021**, *2021*, 4132–4135.
50. Wang, P.; Verma, P.; Xia, G.; Shi, J.; Qiao, J. X.; Tao, S.; Cheng, P. T. W.; Poss, M. A.; Farmer, M. E.; Yeung, K. S.; Yu, J.-Q. *Nature*, **2017**, *551*, 489–493.
51. Wang, Y.-J.; Yuan, C.-H.; Chu, D.-Z.; Jiao, L. *Chem. Sci.* **2020**, *11*, 11042–11054.
52. a) Salamanca, V.; Toledo, A.; Albéniz, A. C. *J. Am. Chem. Soc.* **2018**, *140*, 17851–17856. b) Salamanca, V.; Albéniz, A. C. *Org. Chem. Front.* **2021**, *8*, 1941–1951.
53. a) Kawahara, R.; Fujita, K.; Yamaguchi, R. *J. Am. Chem. Soc.* **2012**, *134*, 3643–3646. b) Wang, W.-H.; Muckerman, J. T.; Fujita, E.; Himeda, Y. *ACS Catal.* **2013**, *3*, 856–860. c) Zheng, G.; Sakaki, S.; Fujita, K.; Sano, H.; Yamaguchi, R. *ACS Catal.* **2014**, *4*, 1010–1020. d) Fujita, K.; Tanaka, Y.; Kobayashi, M.; Yamaguchi, R. *J. Am. Chem. Soc.* **2014**, *136*, 4829–4832. e) Wang, R.; Ma, J.; Li, F. *J. Org. Chem.* **2015**, *80*, 10769–10776. f) Xu, Z.; Yan, P.; Li, H.; Liu, K.; Liu, X.; Jia, S.; Zhang, Z. C. *ACS Catal.* **2016**, *6*, 3784–3788. g) Suna, Y.; Himeda, Y.; Fujita, E.; Muckerman, J. T.; Ertem, M. Z. *ChemSusChem* **2017**, *10*, 4535–4543. h) Siek, S.; Burks, D. B.; Gerlach, D. L.; Liang, G.; Tesh, J. M.; Thompson, C. R.; Qu, F.; Shankwitz, J. E.; Vasquez, R. M.; Chambers, N.; Szulczewski, G. J.; Grotjahn, D. B.; Webster, C. E.; Papish, E. T. *Organometallics* **2017**, *36*, 1091–1106.
54. a) Nieto, L.; Livings, M. S.; Sacci, J. B., III; Reuther, L. E.; Zeller, M.; Papish, E. T. *Organometallics* **2011**, *30*, 6339–6342. b) Moore, C. M.; Szymczak, N. K. *Chem. Commun.* **2013**, *49*, 400–402. c) Roy, B. C.; Chakrabarti, K.; Shee, S.; Paul, S.; Kundu, S. *Chem. Eur. J.* **2016**, *22*, 18147–18155. d) Yu, F.; Shen, C.; Zheng, T.; Chu, W.-K.; Xiang, J.; Luo, Y.; Ko, C.-C.; Guo, Z.-Q.; Lau, T.-C. *Eur. J. Inorg. Chem.* **2016**, *2016*, 3641–3648. e) Shen, C.; Yu, F.; Chu, W.-K.; Xiang, J.; Tan, P.; Luo, Y.; Feng, H.; Guo, Z.-Q.; Leung, C.-F.; Lau, T.-C. *RSC Adv.* **2016**, *6*, 87389–87399.
55. Zhang, C.; Hu, B.; Chen, D.; Xia, H. *Organometallics* **2019**, *38*, 3218–3226.
56. a) Tomás-Mendivil, E.; Díez, J.; Cadierno, V. *Catal. Sci. Technol.* **2011**, *1*, 1605–1615. b) Hu, L.-L.; Shen, C.; Chu, W.-K.; Xiang, J.; Yu, F.; Xiang, G.; Nie, Y.; Kwok, C.-L.; Leung, C.-F.; Ko, C.-C. *Polyhedron* **2017**, *127*, 203–211.
57. a) Ying, C.-H.; Yan, S.-B.; Duan, W.-L. *Org. Lett.* **2014**, *16*, 500–503. b) Ying, C.-H.; Duan, W.-L. *Org. Chem. Front.* **2014**, *1*, 546–550. c) Zhen Li, Z.; Duan, W.-L. *Angew. Chem. Int. Ed.* **2018**, *57*, 16041–16045.
58. a) Wang, Z.; Hu, L.; Chekshin, N.; Zhuang, Z.; Qian, S.; Qiao, J. X.; Yu, J.-Q. *Science*. **2021**, *374*, 1281–1285. b) Zhen, L.; Zhen, W.; Nikita, C.; Qian, S.; Qiao, J. X.; Cheng, P. T.; Yeung, K.-S.; Ewing, W. R.; Yu, J.-Q. *Science*. **2021**, *372*, 1452–

1457. c) Chan, H. S. S.; Yang, J.-M.; Yu, J.-Q. *Science*. **2022**, *376*, 1481–1487.
d) Hu, L.; Meng, G.; Yu, J.-Q. *J. Am. Chem. Soc.* **2022**, *144*, 20550–20553.
59. a) Le Bras, J.; Muzart, J. *Chem. Rev.* **2011**, *111*, 1170–1214. b) Yeung, C. D.; Dong, V. M. *Chem. Rev.* **2011**, *111*, 1215–1292. c) Odell, L. R.; Sävmarker, J.; Lindh, J.; Nilsson, P.; Larhed, M. *Addition Reactions with Formation of Carbon-Carbon Bonds: (V) The Oxidative Heck Reaction*, Elsevier Ltd., **2014**. d) Kancherla, S.; Jørgensen, K. M.; Fernández-Ibáñez, M. A. *Synthesis*, **2019**, *51*, 643–663.
e) Gunnoe, T. B.; Schinski, W. L.; Jia, X.; Zhu, W. *ACS Catal.* **2020**, *10*, 14080–14092. f) Ali, W.; Prakash, G.; Maiti, D. *Chem. Sci.* **2021**, *12*, 2735–2759. g) Zhu, W.; Gunnoe, T. B. *J. Am. Chem. Soc.* **2021**, *143*, 6746–6766.
60. Mondal, A.; van Gemmeren, M. *Angew. Chem. Int. Ed.* **2022**, e202210825.
61. Babu, B. P.; Meng, X.; Bäckvall, J. E. *Chem. Eur. J.* **2013**, *19*, 4140–4145.
62. Zhang, Y.-H.; Shi, B.-F.; Yu, J.-Q. *J. Am. Chem. Soc.* **2009**, *131*, 5072–5074.
63. a) Engle, K. M.; Wang, D. H.; Yu, J.-Q. *J. Am. Chem. Soc.* **2010**, *132*, 14137–14151.
b) Baxter, R. D.; Sale, D.; Engle, K. M.; Yu, J.-Q.; Blackmond, D. G. *J. Am. Chem. Soc.* **2012**, *134*, 4600–4606.
64. a) He, C. Y.; Qing, F. L.; Zhang, X. *Tetrahedron Lett.* **2014**, *55*, 2962–2964.
b) Huang, Q.; Zhang, X.; Qiu, L.; Wu, J.; Xiao, H.; Zhang, X.; Lin, S. *Adv. Synth. Catal.* **2015**, *357*, 3753–3757.
65. a) Beck, E. M.; Grimster, N. P.; Hatley, R.; Gaunt, M. J. *J. Am. Chem. Soc.* **2006**, *128*, 2528–2529. b) Ye, M.; Gao, G. L.; Yu, J.-Q. *J. Am. Chem. Soc.* **2011**, *133*, 6964–6967. c) Chen, W. L.; Gao, Y. R.; Mao, S.; Zhang, Y. L.; Wang, Y. F.; Wang, Y. Q. *Org. Lett.* **2012**, *14*, 5920–5923. d) Vasseur, A.; Harakat, D.; Muzart, J.; Le Bras, J. *Adv. Synth. Catal.* **2013**, *355*, 59–67. e) Zhang, X.; Su, L.; Qiu, L.; Fan, Z.; Zhang, X.; Lin, S.; Huang, Q. *Org. Biomol. Chem.* **2017**, *15*, 3499–3506. f) Gorsline, B. J.; Wang, L.; Ren, P.; Carrow, B. P. *J. Am. Chem. Soc.* **2017**, *139*, 9605–9614.
66. a) Yokota, T.; Tani, M.; Sakaguchi, S.; Ishii, Y. *J. Am. Chem. Soc.* **2003**, *125*, 1476–1477. b) Dams, M.; De Vos, D. E.; Celen, S.; Jacobs, P. A. *Angew. Chem. Int. Ed.* **2003**, *42*, 3512–3515. c) Cong, X.; Hang, H.; Wu, C.; Zeng, X. *Organometallics* **2013**, *32*, 6565–6575. d) Harada, S.; Yano, H.; Obora, Y. *ChemCatChem* **2013**, *5*, 121–125. e) Gigant, N.; Bäckvall, J. E. *Org. Lett.* **2014**, *16*, 1664–1667. f) Kim, H. T.; Kang, E.; Kim, M.; Joo, J. M. *Org. Lett.* **2021**, *23*, 3657–3662.
67. a) Chen, H.; Wedi, P.; Meyer, T.; Tavakoli, G.; van Gemmeren, M. *Angew. Chem. Int. Ed.* **2018**, *57*, 2497–2501. b) Yin, B.; Fu, M.; Wang, L.; Liu, J.; Zhu, Q. *Chem. Commun.* **2020**, *56*, 3293–3296. c) Wedi, P.; Farizyan, M.; Bergander, K.; Mück-Lichtenfeld, C.; van Gemmeren, M. *Angew. Chem. Int. Ed.* **2021**, *60*, 15641–15649.
68. a) Wang, D.-H.; Engle, K. M.; Shi, B.-F.; Yu, J.-Q. *Science*, **2010**, *327*, 315–319.
b) Xiao, K. J.; Chu, L.; Yu, J.-Q. *Angew. Chem. Int. Ed.* **2016**, *55*, 2856–2860.
69. a) Chen, X. Y.; Wu, Y.; Zhou, J.; Wang, P.; Yu, J.-Q. *Org. Lett.* **2019**, *21*, 1426–1429. b) Fan, Z.; Bay, K. L.; Chen, X.; Zhuang, Z.; Park, H. S.; Yeung, K.; Houk, K. N.; Yu, J.-Q. *Angew. Chem. Int. Ed.* **2020**, *59*, 4770–4777.
70. a) Toledo, I. Funes-Ardoiz, F. Maseras, A. C. Albéniz, *ACS Catal.* **2018**, *8*, 7495–7506.
71. a) Cruywagen, J. J.; Rohwer, E. F. C. H. *Inorg. Chem.* **1975**, *14*, 3136–3137. b) Liu, X.; Cheng, J.; Sprik, M.; Lu, X. *J. Phys. Chem. Lett.* **2013**, *4*, 2926–2930.

72. a) Adam, W. A.; Kazakov, D. V.; Kazakov, V. P. *Chem. Rev.* **2005**, *105*, 3371–3387. b) Montagnon, T.; Tofi, M.; Vassilikogiannakis, G. *Acc. Chem. Res.* **2008**, *41*, 1001–1011. c) Ghogare, A. A.; Greer, A. *Chem. Rev.* **2016**, *116*, 9994–10034.
73. a) Aubry, J. M.; Bouttemy, S. *J. Am. Chem. Soc.* **1997**, *119*, 5286–5294. b) Li, W.; Li, L.; Xiao, H.; Qi, R.; Huang, Y.; Xie, Z.; Ling, X.; Zhang, H. *RSC Adv.* **2013**, *3*, 13417–13421.
74. Boehme, K.; Brauer, H. D. *Inorg. Chem.* **1992**, *31*, 3468–3471.
75. a) Rubio-Presa, R.; Fernández-Rodríguez, M. A.; Pedrosa, M. R.; Arnáiz, F. J.; Sanz, R. *Adv. Synth. Catal.* **2017**, *359*, 1752–1757. b) García, N.; García-García, P.; Fernández-Rodríguez, M. A.; García, D.; Pedrosa, M. R.; Arnáiz, F. J.; Sanz, R. *Green Chem.* **2013**, *15*, 999–1005.
76. Bokare, A. D.; Choi, W. *Environ. Sci. Technol.* **2015**, *49*, 14392–14400.
77. a) Tarabanko, V. E.; Kozhevnikov, I. V.; Matveev, K. I. *React. Kinet. Catal. Lett.* **1978**, *8*, 77–79. b) Weinstock, A.; Schreiber, R. E.; Neumann, R. *Chem. Rev.* **2018**, *118*, 2680–2717.
78. a) Yokota, T.; akakura, A.; Tani, M.; Sakaguchi, S.; Ishii, Y. *Tetrahedron Lett.* **2002**, *43*, 8887–8891. b) Yamada, T.; Sakaguchi, S.; Ishii, Y. *J. Org. Chem.* **2005**, *70*, 5471–5474. c) Mizuta, Y.; Obora, Y.; Shimizu, Y.; Ishii, Y. *ChemCatChem* **2012**, *4*, 187–191.
79. Yokota, T.; Fujibayashi, S.; Nishiyama, Y.; Sakaguchi, S.; Ishii, Y. *J. Mol. Catal. A Chem.* **1996**, *169*, 113–122.
80. See for example: Albéniz, A. C.; Espinet, P.; López-Fernández, R.; *Organometallics*, **2003**, *22*, 4206–4212.
81. Salamanca, V.; Albéniz, A. C. *Eur. J. Org. Chem.* **2020**, 3206–3212.
82. Eisenstein, O.; Milani, J.; Perutz, R. N. *Chem. Rev.* **2017**, *117*, 8710–8753.
83. These two elementary steps are inseparable when analyzing the reaction experimentally in Heck processes and therefore are referred to as one.
84. a) Albéniz, A. C.; Espinet, P.; Martín-Ruiz, B.; Milstein, D. *J. Am. Chem. Soc.* **2001**, *123*, 11504–11505. b) Albéniz, A. C.; Espinet, P.; Martín-Ruiz, B.; Milstein, D. *Organometallics* **2005**, *24*, 3679–3684.
85. Albéniz, A. C.; Espinet, P. *Organometallics* **1990**, *9*, 1079–1085.
86. Usón, R.; Forniés, J.; Nalda, J. A.; Lozano, M. J.; Espinet, P.; Albéniz, A. C. *Inorg. Chim. Acta* **1989**, *156*, 251–256.
87. Tomon, T.; Koizumi, T. A.; Tanaka, K. *Eur. J. Inorg. Chem.* **2005**, *2005*, 285–293.
88. Krapcho, A. P.; Sparapani, S. *J. Heterocycl. Chem.* **2008**, *45*, 1167–1170.
89. Ferretti, F.; Ragaini, F.; Lariccia, R.; Gallo, E.; Cenini, S. *Organometallics* **2010**, *29*, 1465–1471.
90. a) Wenkert, D.; Woodward, R. B. *J. Org. Chem.* **1983**, *48*, 283–289. b) Hong, Y. R.; Gorman, C. B. *J. Org. Chem.* **2003**, *68*, 9019–9025.
91. Wu, C-Z.; He, C-Y.; Huang, Y.; Zhang, X. *Org. Lett.* **2013**, *15*, 5266–5269.
92. Davies, S. G.; Fletcher, A. M.; Lv, L.; Roberts, P. M.; Thomson, J. E. *Tetrahedron: Asymmetry*, **2012**, *23*, 910–925.
93. Liu, J.; Zhao, Y.; Zhou, Y.; Li, L.; Zhang, T. Y.; Zhang, H. *Org. Biomol. Chem.* **2003**, *1*, 3227–3231.
94. Zhu, M-K.; Zhao, J-F.; Loh, T-P. *Org. Lett.* **2011**, *13*, 6308–6311.

95. Youn, S. W.; Kim, B. S.; Jagdale, B. A. R. *J. Am. Chem. Soc.* **2012**, *134*, 11308–11311.
96. Lakshminarayana, B.; Mahendar, L.; Ghosal, P.; Sreedhar, B.; Satyanarayana, G.; Subrahmanyam, C. *New J. Chem.* **2018**, *42*, 1646–1654.
97. Enquist, P. A.; Lindh, J.; Nilsson, P.; Larhed, M. *Green Chem.* **2006**, *8*, 338–343.
98. Patureau, F. W.; Besset, T.; Glorius, F. *Angew. Chem. Int. Ed.* **2011**, *50*, 1064–1067.
99. Jadhav, S. N.; Rode, C. V. *Green Chem.* **2017**, *19*, 5958–5970.
100. Davies, S. G.; Mulvaney, A. W.; Russell, A. J.; Smith, A. D. *Tetrahedron: Asymmetry*, **2007**, *18*, 1554–1566.
101. Li, J-H.; Wang, D-P.; Xie, Y-X.; *Synthesis*, **2005**, *13*, 2193–2197.
102. Sore, H. F.; Boehner, C. M.; MacDonald, S. J. F.; Norton, D.; Fox, D. J.; Spring, D. R. *Org. Biomol. Chem.* **2009**, *7*, 1068–1072.
103. Liu, J.; Liu, H.; Wang, L. *Appl. Organomet. Chem.* **2010**, *24*, 386–391.
104. Borate, H. B.; Dumbre, D. K.; Wakharkar, R. D.; Choudhary, V. R. *J. Chem. Res.* **2008**, 495–499.
105. Belhateche, D.; Symons, J. M. *Journal AWWA*, **1991**, *83*, 70–73.
106. Aubry, J. M. *J. Am. Chem. Soc.* **1985**, *107*, 5844–5849.
107. a) Burés, J. *Angew. Chem. Int. Ed.* **2016**, *55*, 16084–16087. b) Burés, J. *Angew. Chem. Int. Ed.* **2016**, *55*, 2028–2031.
108. Zhao, Y.; Truhlar, D. G. *J. Chem. Phys.* **2006**, *125*, 194101–194118.
109. Zhao, Y.; Truhlar, D. G. *Theor. Chem. Acc.* **2006**, *120*, 215–241.
110. Gaussian 09, Revision D.01, Frisch, M. J.; Trucks, G. W.; Schlegel, H. B.; Scuseria, G. E.; Robb, M. A.; Cheeseman, J. R.; Scalmani, G.; Barone, V.; Mennucci, B.; Petersson, G. A.; Nakatsuji, H.; Caricato, M.; Li, X.; Hratchian, H. P.; Izmaylov, A. F.; Bloino, J.; Zheng, G.; Sonnenberg, J. L.; Hada, M.; Ehara, M.; Toyota, K.; Fukuda, R.; Hasegawa, J.; Ishida, M.; Nakajima, T.; Honda, Y.; Kitao, O.; Nakai, H.; Vreven, T.; Montgomery, J. A., Jr.; Peralta, J. E.; Ogliaro, F.; Bearpark, M.; Heyd, J. J.; Brothers, E.; Kudin, K. N.; Staroverov, V. N.; Kobayashi, R.; Normand, J.; Raghavachari, K.; Rendell, A.; Burant, J. C.; Iyengar, S. S.; Tomasi, J.; Cossi, M.; Rega, N.; Millam, J. M.; Klene, M.; Knox, J. E.; Cross, J. B.; Bakken, V.; Adamo, C.; Jaramillo, J.; Gomperts, R.; Stratmann, R. E.; Yazyev, O.; Austin, A. J.; Cammi, R.; Pomelli, C.; Ochterski, J. W.; Martin, R. L.; Morokuma, K.; Zakrzewski, V. G.; Voth, G. A.; Salvador, P.; Dannenberg, J. J.; Dapprich, S.; Daniels, A. D.; Farkas, Ö.; Foresman, J. B.; Ortiz, J. V.; Cioslowski, J.; Fox, D. J. Gaussian, Inc., Wallingford CT, **2009**.
111. Francl, M. M.; Petro, W. J.; Hehre, W. J.; Binkley, J. S.; Gordon, M. S.; DeFrees, D. J.; Pople, J. A. *J. Chem. Phys.* **1982**, *77*, 3654–3665.
112. Clark, T.; Chandrasekhar, J.; Schleyer, P. V. R. *J. Comput. Chem.* **1983**, *4*, 294–301.
113. Ehlers, A. W.; Böhme, M.; Dapprich, S.; Gobbi, A.; Höllwarth, A.; Jonas, V.; Köhler, K. F.; Stegmann, R.; Veldkamp, A.; Frenking, G. *Chem. Phys. Lett.* **1993**, *208*, 111–114.
114. Roy, L. E.; Hay, P. J.; Martin, R. L. *J. Chem. Theory Comput.* **2008**, *4*, 1029–1031.
115. CrysAlisPro Software system, version 1.171.33.51, 2009, Oxford Diffraction Ltd, Oxford, UK.
116. Sheldrick, G. M. *Acta Crystallogr. Sect. C* **2015**, *71*, 3–8.

117. Dolomanov, O. V.; Bourhis, L. J.; Gildea, R. J.; Howard, J. A. K.; Puschmann, H. *J. Appl. Crystallogr.* **2009**, *42*, 339–341.
118. Villalba, F.; Albéniz, A. C. *Adv. Synth. Catal.* **2021**, *363*, 4795–4804.
119. Plata, R. E.; Hill, D. E.; Haines, B. E.; Musaev, D. G.; Chu, L.; Hickey, D. P.; Sigman, M. S.; Yu, J. Q.; Blackmond, D. G. *J. Am. Chem. Soc.* **2017**, *139*, 9238–9245.
120. Mandal, N.; Datta, A. *J. Org. Chem.* **2020**, *85*, 13228–13238.
121. Selected examples of Pd-catalyzed C-H activation reaction with a ratio of ligand:Pd > 1 or 2: a) Engle, K. M.; Wang, D.-H.; Yu, J.-Q. *Angew. Chem. Int. Ed.* **2010**, *49*, 6169–6173. b) Ye, M.; Gao, G. L.; Edmunds, A. J. F.; Worthington, P. A.; Morris, J. A.; Yu, J. Q. *J. Am. Chem. Soc.* **2011**, *133*, 19090–19093. c) Provencher, P. A.; Hoskin, J. F.; Wong, J. J.; Chen, X.; Yu, J.-Q.; Houk, K. N.; Sorensen, E. J. *J. Am. Chem. Soc.* **2021**, *143*, 20035–20041.
122. Pinilla, C.; Salamanca, V.; Lledós, A.; Albéniz, A. C. *ACS Catal.* **2022**, *12*, 14527–14532.
123. Milani, B.; Alessio, E.; Mestroni, G.; Sommazzi, A.; Garbassi, F.; Zangrando, E.; Bresciani-Pahor, N.; Randaccio, L. *J. Chem. Soc. Dalton Trans.* **1994**, 1903–1911.
124. Milani, B.; Anzilutti, A.; Vicentini, L.; Sessanta o Santi, A.; Zangrando, E.; Geremia, S.; Mestroni, G. *Organometallics* **1997**, *16*, 5064–5075.
125. a) Farizyan, M.; Mondal, A.; Mal, S.; Deufel, F.; van Gemmeren, M. *J. Am. Chem. Soc.* **2021**, *143*, 16370–16376. b) Santiago, C.; Chen, H.; Mondal, A.; van Gemmeren, M. *Synlett*, **2022**, *33*, 357–360.
126. a) Zhang, S.; Shi, L.; Ding, Y. *J. Am. Chem. Soc.* **2011**, *133*, 20218–20229. b) Chen, H.; Mondal, A.; Wedi, P.; van Gemmeren, M. *ACS Catal.* **2019**, *9*, 1979–1984.
127. It is not possible to determine if the deprotonation of the bipyridone ligand occurs inside or outside the palladium coordination sphere.
128. Ritter, S. K. A User's Guide for Palladium Acetate. *C&EN Glob. Enterp.* **2016**, *94*, 20–21.
129. Shaughnessy, K. H. *Isr. J. Chem.* **2020**, *60*, 180–194.
130. Geary, W. J. *Coord. Chem. Rev.* **1971**, *7*, 81–122.
131. Lian, Z.-Y.; Yuan, J.; Yan, M.-Q.; Liu, Y.; Luo, X.; Wu, Q.-G.; Liu, S.-H.; Chen, J.; Zhu, X.-L.; Yu, G.-A. *Org. Biomol. Chem.* **2016**, *14*, 10090–10094.
132. Shi, S.; Meng, G.; Szostak, M. *Angew. Chem. Int. Ed.* **2016**, *55*, 6959–6963.
133. a) Bourissou, D.; Guerret, O.; Gabbai, F. P.; Bertrand, G. *Chem. Rev.* **2000**, *100*, 39–91. b) Crabtree, R. H. *The Organometallic Chemistry of the Transition Metals*. 6th ed.; Wiley-VCH: Weinheim, **2014**.
134. Igau, A.; Grutzmacher, H.; Baccaredo, A.; Bertrand, G. *J. Am. Chem. Soc.* **1988**, *110*, 6463–6466.
135. a) Arduengo, A. J.; Harlow, R. L.; Kline, M. *J. Am. Chem. Soc.* **1991**, *113*, 361–363. b) Arduengo, A. J.; Bertrand, G. *Chem. Rev.* **2009**, *109*, 3209–3210.
136. a) Nolan, S. P. *N-Heterocyclic Carbenes: Effective Tools for Organometallic Synthesis*; Wiley-VCH: Weinheim, **2014**. b) Huynh, H. V. *The Organometallic Chemistry of N-Heterocyclic Carbenes*. Wiley-VCH: Weinheim, **2017**. c) Biju, A. T. *N-Heterocyclic Carbenes in Organocatalysis*. Wiley-VCH: Weinheim, **2019**. d) Jazzar, R.; Soleilhavoup, M.; Bertrand, G. *Chem. Rev.* **2020**, *120*, 4141–4168.

- e) Kim, H.; Lee, E. *Bull. Korean Chem. Soc.* **2022**, <https://doi.org/10.1002/bkcs.12620>.
- 137.** A mesoionic compound can be defined as: dipolar five- (possibly six-) membered heterocyclic compounds in which both the negative and the positive charge are delocalized, for which a totally covalent structure cannot be written, and which cannot be represented satisfactorily by any one polar structure. The formal positive charge is associated with the ring atoms, and the formal negative charge is associated with ring atoms or an exocyclic nitrogen or chalcogen atom. PAC, 1995, 67, 1307. (*Glossary of class names of organic compounds and reactivity intermediates based on structure (IUPAC Recommendations 1995)*) on page 1349. <https://doi.org/10.1351/goldbook.M03842>.
- 138.** For reviews of MICs see: a) Vivancos, A.; Segarra, C.; Albrecht, M. *Chem. Rev.* **2018**, *118*, 9493–9586. b) Sierra, M. A.; de la Torre, M. C. *ACS Omega*, **2019**, *4*, 12983–12994.
- 139.** For isolation of crystalline “abnormal” N-heterocyclic carbene see: a) Aldeco-Perez, E.; Rosenthal, A. J.; Donnadiou, B.; Parameswaran, P.; Frenking, G.; Bertrand, G. *Science*. **2009**, *326*, 556–559. b) Guisado-Barrios, G.; Bouffard, J.; Donnadiou, B.; Bertrand, G. *Angew. Chem. Int. Ed.* **2010**, *49*, 4759–4762.
- 140.** Fischer, E. O.; Maasböl, A. *Angew. Chem. Int. Ed.* **1964**, *3*, 580–581.
- 141.** Schrock, R. R. *J. Am. Chem. Soc.* **1974**, *96*, 6796–6797.
- 142.** Selected reviews: a) Nelson, D. J.; Nolan, S. P. *Chem. Soc. Rev.* **2013**, *42*, 6723–6753. b) Hopkinson, M. N.; Richter, C.; Schedler, M.; Glorius, F. *Nature* **2014**, *510*, 485–496. c) Zhao, Q.; Meng, G.; Nolan, S. P.; Szostak, M. *Chem. Rev.* **2020**, *120*, 1981–2048.
- 143.** Albéniz, A. C. *Eur. J. Inorg. Chem.* **2018**, *33*, 3693–3705.
- 144.** Fischer, E. O.; Beck, H.-J. *Angew. Chem. Int. Ed.* **1970**, *9*, 72–73.
- 145.** a) Albéniz, A. C.; Espinet, P.; Manrique, R.; Pérez-Mateo, A. *Angew. Chem. Int. Ed.* **2002**, *41*, 2363–2366. b) Albéniz, A. C.; Espinet, P.; Manrique, R.; Pérez-Mateo, A. *Chem. Eur. J.* **2005**, *11*, 1565–1573. c) Albéniz, A. C.; Espinet, P.; Pérez-Mateo, A.; Nova, A.; Ujaque, G. *Organometallics*, **2006**, *25*, 1293–1297. d) Pérez-Mateo, A.; Espinet, P.; Albéniz, A. C. *J. Organomet. Chem.* **2010**, *695*, 441–445.
- 146.** Meana, I.; Albéniz, A. C.; Espinet, P. *Organometallics*, **2008**, *27*, 4193–4198.
- 147.** Meana, I.; Toledo, A.; Albéniz, A. C.; Espinet, P. *Chem. Eur. J.* **2012**, *18*, 7658–7661.
- 148.** Gómez-Gallego, M.; Mancheño, M. J.; Sierra, M. A. *Acc. Chem. Res.* **2005**, *38*, 44–53.
- 149.** a) Sierra, M. A.; Mancheño, M. J.; Sáez, E.; del Amo, J. C. *J. Am. Chem. Soc.* **1998**, *120*, 6812–6813. b) Sierra, M. A.; del Amo, J. C.; Mancheño, M. J.; Gómez-Gallego, M. *J. Am. Chem. Soc.* **2001**, *123*, 851–861. c) Lage, M. L.; Curiel, D.; Fernández, I.; Mancheño, M. J.; Gómez-Gallego, M.; Molina, P.; Sierra, M. A. *Organometallics* **2011**, *30*, 1794–1803.
- 150.** Fernández, I.; Mancheño, M. J.; Vicente, R.; López, L. A.; Sierra, M. A. *Chem. – A Eur. J.* **2008**, *14*, 11222–11230. López-Alberca, M. P.; Fernández, I.; Mancheño, M. J.; Gómez-Gallego, M.; Casarrubios, L.; Sierra, M. A. *European J. Org. Chem.* **2011**, *2011*, 3293–3300.

151. Wang, K.; Lu, Y.; Hu, F.; Yang, J.; Zhang, Y.; Wang, Z.-X.; Wang, J. *Organometallics* **2018**, *37*, 1–10.
152. a) Liu, S.-T.; Hsieh, T.-Y.; Lee, G.-H.; Peng, S.-M. *Organometallics* **1998**, *17*, 993–995. b) Ku, R.-Z.; Huang, J.-C.; Cho, J.-Y.; Kiang, F.-M.; Reddy, K. R.; Chen, Y.-C.; Lee, K.-J.; Lee, J.-H.; Lee, G.-H.; Peng, S.-M.; Liu, S.-T. *Organometallics* **1999**, *18*, 2145–2154. c) Kessler, F.; Szesni, N.; Maaß, C.; Hohberger, C.; Weibert, B.; Fischer, H. *J. Organomet. Chem.* **2007**, *692*, 3005–3018.
153. a) Wada, M.; Koyama, Y. *J. Organomet. Chem.* **1980**, *201*, 477–491. b) Wada, M.; Koyama, Y.; Sameshima, K. *J. Organomet. Chem.* **1981**, *209*, 115–121.
154. Crociani, B.; Nicolini, M.; Boschi, T. *J. Organomet. Chem.* **1971**, *33*, C81–C83.
155. Kremzow, D.; Seidel G.; Lehmann, C. W; Fürstner, A. *Chem. Eur. J.* **2005**, *11*, 1833–1853.
156. a) Regitz, M.; Maas, G. *Diazo Compounds-Properties and Synthesis*, Academic Press, Orlando, **1986**. b) Gerhard Maas, G. *Angew. Chem. Int. Ed.* **2009**, *48*, 8186–8195. c) Akter, M.; Rupa, K.; Anbarasan, P. *Chem. Rev.* **2022**, *122*, 13108–13205.
157. a) Jia, M.; Ma, S. *Angew. Chem. Int. Ed.* **2016**, *55*, 9134–9166. b) Wang, K.; Wang, J. *Synlett*, **2019**, *30*, 542–551. c) Mayakrishnan, S.; Tamizmani, M.; Maheswari, N. U. *Chem. Commun.* **2020**, *56*, 15462–15465. d) Zhu, D.; Chen, L.; Fan, H.; Yao, Q.; Zhu, S. *Chem. Soc. Rev.* **2020**, *49*, 908–950.
158. a) Zhang, L.; DeMuynck, B. M.; Paneque, A. N.; Rutherford, J. E.; Nagib, D. A. *Science*. **2022**, *377*, 649–654. b) West, M. S.; Rousseaux, S. A. L. *Science*. **2022**, *377*, 580–581.
159. Proctor, L. D.; Warr, A. J. *Org. Process. Res. Dev.* **2002**, *6*, 884–892.
160. a) Poh, J.-S.; Tran, D. N.; Battilocchio, C.; Hawkins, J. M.; Ley, S. V. *Angew. Chem. Int. Ed.* **2015**, *54*, 7920–7923. b) Hock, K. J.; Koenigs, R. M. *Chem. Eur. J.* **2018**, *24*, 10571–10583. c) Sullivan, R. J.; Freure, G. P. R.; Newman, S. G. *ACS Catal.* **2019**, *9*, 5623–5630. d) Empel, C.; Koenigs, R. M. *J. Flow Chem.* **2020**, *10*, 157–160.
161. a) Dingwall, P.; Greb, A.; Crespin, L. N. S.; Labes, R.; Musio, B.; Poh, J.-S.; Pasau, P.; Blakemore, D. C.; Ley, S. V. *Chem. Commun.*, **2018**, *54*, 11685. b) Ciszewski, Ł. W.; Rybicka-Jasińska, K.; Gryko, D. *Org. Biomol. Chem.*, **2019**, *17*, 432–448. c) Jana, S.; Li, F.; Empel, C.; Verspeek, D.; Aseeva, P.; Koenigs, R. M. *Chem. Eur. J.* **2020**, *26*, 2586–2591.
162. Sutton, D. *Chem. Rev.* **1993**, *93*, 995–1022.
163. Pereira, A.; Champouret, Y.; Martín, C.; Álvarez, E.; Etienne, M.; Belderraín, T. R.; Pérez, P. J. *Chem. Eur. J.* **2015**, *21*, 9769–9775.
164. Deydier, E.; Menu, M.-J.; Dartiguenave, M.; Dartiguenave, Y.; Simard, M.; Beauchamp, A. L.; Brewer, J. C.; Gray, H. B. *Organometallics*. **1996**, *15*, 1166–1175.
165. Schramm, K. D.; Ibers, J. A. *Inorg. Chem.* **1980**, *19*, 2441–2448.
166. a) Otsuka, S.; Nakamura, A.; Koyama, T.; Tatsuno, Y. *Justus Liebigs Ann. Chem.* **1975**, *1975*, 626–635. b) Rull, S. G.; Álvarez, E.; Fructos, M. R.; Belderraín, T. R.; Pérez, P. J. *Chem. Eur. J.* **2017**, *23*, 7667–7671.
167. a) Murahashi, S.-I.; Kitani, Y.; Hosokawa, T.; Miki, K.; Kasai, N. *J. Chem. Soc., Chem. Commun.*, **1979**, 450–451. b) Murahashi, S.-I.; Kitani, Y.; Uno, T.; Hosokawa, T.; Miki, K.; Yonezawa, T.; Kasai, N. *Organometallics*, **1986**, *5*, 356–365.

168. a) M. Bröring, C. D. Brandt, S. Stellwag. *Chem. Commun.* **2003**, 2344–2345.
b) Taubmann, C.; Ofele, K.; Herdtweck, E.; Herrmann, W. A. *Organometallics*, **2009**, *28*, 4254–4257. c) Barrett, B. J.; Iluc, V. M. *Organometallics*, **2017**, *36*, 730–741.
169. a) Greenman, K. L.; Carter, D. S.; Van Vranken, D. L. *Tetrahedron* **2001**, *57*, 5219–5225. b) Greenman, K. L.; Van Vranken, D. L. *Tetrahedron* **2005**, *61*, 6438–6441.
170. Selected reviews: a) Liu, Z.; Wang, J. *J. Org. Chem.* **2013**, *78*, 10024–10030.
b) Barroso, R.; Cabal, M. P.; Valdés, C. *Synth.* **2017**, *49*, 4434–4447 c) Xia, Y.; Qiu, D.; Wang, J. *Chem. Rev.* **2017**, *117*, 13810–13889. d) Chen, G.; Yu, Y.; Huang, X. *Synlett* **2018**, *29*, 2087–2092. e) Wang, X.; Wang, X.; Wang, J. *Tetrahedron* **2019**, *75*, 949–964. f) Xiang, Y.; Wang, C.; Ding, Q.; Peng, Y. *Adv. Synth. Catal.* **2019**, *361*, 919–944. g) Jha, N.; Khot, N. P.; Kapur, M. *Chem. Rec.* **2021**, *21*, 4088–4122.
171. a) Liu, Y.; Zhang, Z.; Zhang, S.; Zhang, Y.; Wang, J.; Zhang, Z. *Chem. – An Asian J.* **2018**, *13*, 3658–3663. b) Zhou, Q.; Gao, Y.; Xiao, Y.; Yu, L.; Fu, Z.; Li, Z.; Wang, J. *Polym. Chem.* **2019**, *10*, 569–573. c) Pérez-Gómez, M.; Azizollahi, H.; Franzoni, I.; Larin, E. M.; Lautens, M.; García-López, J.-A. *Organometallics* **2019**, *38*, 973–980. d) Yu, Y.; Ma, L.; Xia, J.; Xin, L.; Zhu, L.; Huang, X. *Angew. Chem. Int. Ed.* **2020**, *59*, 18261–18266. e) Yu, Y.; Chakraborty, P.; Song, J.; Zhu, L.; Li, C.; Huang, X. *Nat. Commun.* **2020**, *11*, 461. f) Huo, J.; Zhong, K.; Xue, Y.; Lyu, M.; Ping, Y.; Liu, Z.; Lan, Y.; Wang, J. *J. Am. Chem. Soc.* **2021**, *143*, 12968–12973. g) Cheng, M.; Huang, X.-Y.; Yang, F.; Zhao, D.-M.; Ji, K.; Chen, Z.-S. *Org. Lett.* **2022**, *24*, 1237–1242. h) X.-Q.; Wang, Y.-S.; Wang, J. *Chem. Commun.* **2022**, *58*, 4032–4035.
172. Xiao, Q.; Zhang, Y.; Wang, J. *Acc. Chem. Res.* **2013**, *46*, 236–247.
173. a) Wang, H.; Deng, Y. H.; Shao, Z. *Synth.* **2018**, *50*, 2281–2306 b) Xia, Y.; Wang, J. *J. Am. Chem. Soc.* **2020**, *142*, 10592–10605. c) Radolko, J.; Ehlers, P.; Langer, P. *Adv. Synth. Catal.* **2021**, *363*, 3616–3654.
174. Wade Wolfe, M. M.; Shanahan, J. P.; Kampf, J. W.; Szymczak, N. K. *J. Am. Chem. Soc.* **2020**, *142*, 18698–18705.
175. Danopoulos, A. A.; Tsoureas, N.; Green, J. C.; Hursthouse, M. B. *Chem. Commun.* **2003**, *6*, 756–757.
176. Solé, D.; Vallverdú, L.; Solans, X.; Font-Bardia, M.; Bonjoch, J. *Organometallics* **2004**, *23*, 1438–1447.
177. a) Yu, W.-Y.; Tsoi, Y.-T.; Zhou, Z.; Chan, A. S. C. *Org. Lett.* **2009**, *11*, 469–472.
b) Tsoi, Y.-T.; Zhou, Z.; Chan, A. S. C.; Yu, W.-Y. *Org. Lett.* **2010**, *12*, 4506–4509.
178. a) Shao, Z.; Zhang, H. *Chem. Soc. Rev.* **2012**, *41*, 560–572.
179. *N*-tosylhydrazones are the most commonly *N*-sulfonylhydrazones used, but other hydrazone derivatives such as *N*-2-(trifluoromethyl)benzenesulfonylhydrazone (*i.e.* *N*-trifosylhydrazone) have been reported since 2014 by Xihe Bi's group as an efficient diazo surrogate that decomposes at very low temperatures (–40 °C). These mild reaction conditions allow them to carry out a range of challenging transformations that require functional group tolerance and/or chemo- and stereoselectivity. Liu, Z.; Sivaguru, P.; Zaroni, G.; Bi, X. *Acc. Chem. Res.* **2022**, *55*, 1763–1781.

180. a) Fulton, J. R.; Aggarwal, V. K.; de Vicente, J. *Eur. J. Org. Chem.* **2005**, 1479–1492. b) Green, S. P.; Wheelhouse, K. M.; Payne, A. D.; Hallett, J. P.; Miller, P. W.; Bull, J. A. *Org. Process. Res. Dev.* **2020**, *24*, 67–84.
181. Bamford, W. R.; Stevens, T. S. *J. Chem. Soc.* **1952**, 4735–4740.
182. a) Barluenga, J.; Moriel, P.; Valdés, C.; Aznar, F. *Angew. Chem. Int. Ed.* **2007**, *46*, 5587–5590. b) Barluenga, J.; Valdés, C. *Angew. Chem. Int. Ed.* **2011**, *50*, 7486–7500.
183. a) Ping, Y.; Wang, R.; Wang, Q.; Chang, T.; Huo, J.; Lei, M.; Wang, J. *J. Am. Chem. Soc.* **2021**, *143*, 9769–9780. b) Yang, B.; Cao, K.; Zhao, G.; Yang, J.; Zhang, J. *J. Am. Chem. Soc.* **2022**, *144*, 15468–15474.
184. a) Gutman, E. S.; Arredondo, V.; Van Vranken, D. L. *Org. Lett.* **2014**, *16*, 5498–5501. b) Wu, Q.; Muto, K.; Yamaguchi, J. *Org. Lett.* **2022**, *24*, 4129–4134.
185. a) Zhou, P.-X.; Luo, J.-Y.; Zhao, L.-B.; Ye, Y.-Y.; Liang, Y.-M. *Chem. Commun.* **2013**, *49*, 3254–3256. b) Zhou, P.-X.; Ye, Y.-Y.; Zhao, L.-B.; Hou, J.-Y.; Kang, X.; Chen, D.-Q.; Tang, Q.; Zhang, J.-Y.; Huang, Q.-X.; Zheng, L.; Ma, J.-W.; Xu, P.-F.; Liang, Y.-M. *Chem. – A Eur. J.* **2014**, *20*, 16093–16096. c) Li, J.; Qin, G.; Liu, Y.; Huang, H. *Org. Chem. Front.* **2016**, *3*, 259–267.
186. a) Becker, Y.; Stille, J. K. *J. Am. Chem. Soc.* **1978**, *100*, 845–850. b) Craswell, L. E.; Spencer, J. L. *J. Chem. Soc. Dalton Trans.* **1992**, 3445–3452. c) Gatti, G.; López, J. A.; Mealli, C.; Musco, A. *J. Organomet. Chem.* **1994**, *483*, 77–89. d) Rix, F. C.; Brookhart, M.; White, P. S. *J. Am. Chem. Soc.* **1996**, *118*, 2436–2448. e) Martín-Ruiz, B.; Pérez-Ortega, I.; Albéniz, A. C. *Organometallics* **2018**, *37*, 1074–1085.
187. a) Hosokawa, T.; Maitlis, P. M. *J. Am. Chem. Soc.* **1972**, *94*, 3238–3240. b) Johns, A. M.; Utsunomiya, M.; Incarvito, C. D.; Hartwig, J. F. *J. Am. Chem. Soc.* **2006**, *128*, 1828–1839.
188. a) Shultz, C. S.; Ledford, J.; DeSimone, J. M.; Brookhart, M. *J. Am. Chem. Soc.* **2000**, *122*, 6351–6356. b) Ledford, J.; Shultz, C. S.; Gates, D. P.; White, P. S.; DeSimone, J. M.; Brookhart, M. *Organometallics* **2001**, *20*, 5266–5276.
189. a) Ye, F.; Qu, S.; Zhou, L.; Peng, C.; Wang, C.; Cheng, J.; Hossain, M. L.; Liu, Y.; Zhang, Y.; Wang, Z.-X.; Wang, J. *J. Am. Chem. Soc.* **2015**, *137*, 4435–4444. b) Yu, Y.; Lu, Q.; Chen, G.; Li, C.; Huang, X. *Angew. Chem. Int. Ed.* **2018**, *57*, 319–323. c) Yue, X.; Shan, C.; Qi, X.; Luo, X.; Zhu, L.; Zhang, T.; Li, Y.; Li, Y.; Bai, R.; Lan, Y. *Dalton Trans.* **2018**, *47*, 1819–1826. d) Qi, X.; Lan, Y. *Acc. Chem. Res.* **2021**, *54*, 2905–2915.
190. Hartwig, J. F. *Angew. Chem. Int. Ed.* **1998**, *37*, 2090–2093.
191. Brewbaker, J. L.; Hart, H. *J. Am. Chem. Soc.* **1969**, *91*, 711–715.
192. a) Pelzer, G.; Herwig, J.; Keim, W.; Goddard, R. *Russ. Chem. Bull.* **1998**, *47*, 904–912. b) Shavnya, A.; Hesp, K. D.; Mascitti, V.; Smith, A. C. *Angew. Chem. Int. Ed.* **2015**, *54*, 13571–13575.
193. Ammann, C.; Meier, P.; Merbach, A. E. *J. Magn. Reson.* **1982**, *321*, 319–321.
194. a) Aggarwal, V. K.; Alonso, E.; Bae, I.; Hynd, G.; Lydon, K. M.; Palmer, M. J.; Patel, M.; Porcelloni, M.; Richardson, J.; Stenson, R. A.; Studley, J. R.; Vasse, J.-L.; Winn, C. L. *J. Am. Chem. Soc.* **2003**, *125*, 10926–10940. b) Li, P.; Zhao, J.; Wu, C.; Larock, R. C.; Shi, F. *Org. Lett.* **2011**, *13*, 3340–3343.

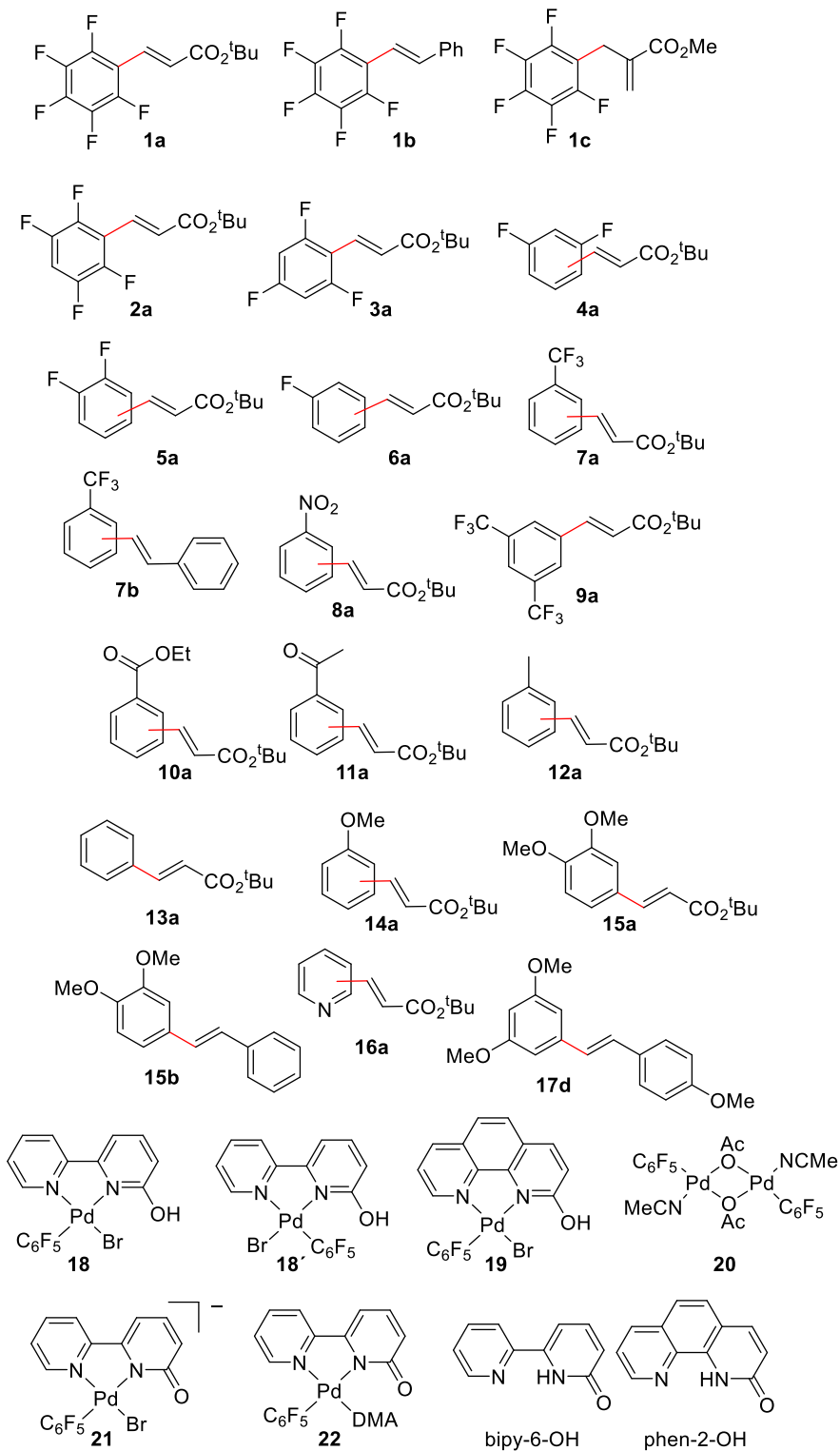
195. a) Morrison, H.; Danishefsky, S.; Yates, P. *J. Org. Chem.* **1961**, *26*, 2617–2618. b) Doyle, M. P.; Yan, M. *J. Org. Chem.* **2002**, *67*, 602–604. c) Friscourt, F.; Fahrni, C. J.; Boons, G.-J. *Chem. – A Eur. J.* **2015**, *21*, 13996–14001.
196. Wen, J.; Fu, Y.; Zhang, R.-Y.; Zhang, J.; Chen, S.-Y.; Yu, X.-Q. *Tetrahedron* **2011**, *67*, 9618–9621.
197. Russavskaya, N. V.; Grabel'nykh, V. A.; Levanova, E. P.; Sukhomazova, E. N.; Deryagina, E. N. *Russ. J. Org. Chem.* **2002**, *38*, 1498–1500.
198. Chen, Z.-S.; Duan, X.-H.; Wu, L.-Y.; Ali, S.; Ji, K.-G.; Zhou, P.-X.; Liu, X.-Y.; Liang, Y.-M. *Chem. – A Eur. J.* **2011**, *17*, 6918–6921.
199. Ping, W.-W.; Jin, L.; Wu, Y.; Xue, X.-Y.; Zhao, X. *Tetrahedron* **2014**, *70*, 9373–9380.
200. a) Gillespie, J. A.; Dodds, D. L.; Kamer, P. C. J. *Dalton Trans.* **2010**, *39*, 2751–2764. b) Durand, D. J.; Fey, N. *Chem. Rev.* **2019**, *119*, 6561–6594.
201. Casey, C. P.; Whiteker, G. T. *Isr. J. Chem.* **1990**, *30*, 299–304.
202. Koide, Y.; Bott, S. G.; Barron, A. R. *Organometallics* **1996**, *15*, 2213–2226.
203. a) Kamer, P. C.J.; van Leeuwen, P. W. N. M.; Reek, J. N. H. *Acc. Chem. Res.* **2001**, *34*, 895–904. b) Grushin, V. V.; Marshall, W. J. *J. Am. Chem. Soc.* **2006**, *128*, 12644–12645. c) Ferguson, D. M.; Bour, J. R.; Canty, A. J.; Kampf, J. W.; Sanford, M. S. *Organometallics*, **2019**, *38*, 519–526.
204. a) Brown, J. M.; Guiry, P. J. *Inorg. Chim. Acta.* **1994**, *220*, 249–259. b) Hamann, B. C.; Hartwig, J. F. *J. Am. Chem. Soc.* **1998**, *120*, 3694–3703. c) Freixa, Z.; van Leeuwen, P. W. N. M. *Dalton Trans.* **2003**, 1890–1901.
205. a) Luinstra, G. A.; Brinkmann, P. H. P. *Organometallics* **1998**, *17*, 5160–5165. b) Reddy, K. R.; Surekha, K.; Lee, G.-H.; Peng, S.-M.; Chen, J.-T.; Liu, S.-T. *Organometallics* **2001**, *20*, 1292–1299.
206. Grushin, V. V.; Marshall, W. J. *J. Am. Chem. Soc.* **2006**, *128*, 4632–4641.
207. Herrmann, W. A.; Broßmer, C.; Priermeier, T.; Öfele, K. *J. Organomet. Chem.* **1994**, *481*, 97–108.
208. Takemoto, S.; Grushin, V. V. *J. Am. Chem. Soc.* **2013**, *135*, 16837–16840.
209. The percentage given for the mixture of the monomeric and dimeric “[PdBr(C₆F₅)dppm]” was obtained from the crude reaction mixture by ¹⁹F and ³¹P NMR integration.
210. a) Puddephatt, R. J. *Chem. Soc. Rev.* **1983**, *12*, 99–127. b) Usón, R.; Forniés, J.; Espinet, P.; Navarro, R.; Fortuño, C. *J. Chem. Soc. Dalton Trans.* **1987**, *8*, 2077–2081.
211. Chlorinated solvents (CDCl₃ or CD₂Cl₂) and coordinating solvent such as acetonitrile have been tested in these reactions. All the following reactions with different ligands have been carried out in acetonitrile as a solvent to prevent side-reactions like reorganizations of the -C₆F₅ groups, observed for complex **29a** in CD₂Cl₂.
212. The formation of the azine derivative by a bimolecular reaction of the diazo **32** can be also proposed: Griller, D.; Majewski, M.; McGimpsey, W. G.; Nazran, A. S.; Scaiano, J. C. *J. Org. Chem.* **1988**, *53*, 1550–1553.
213. a) Uvarova, M. A.; Kushan, E. V.; Nefedov, S. E. *Russ. J. Inorg. Chem.* **2012**, *57*, 676–683. b) Zhai, F.; Jordan, R. F. *Organometallics* **2014**, *33*, 7176–7192.
214. Tong, J.; Lu, H.-L.; Sun, W.-Q.; Yu, S.-Y. *CrystEngComm* **2020**, *22*, 8166–8170.

215. Tong, J.; Yu, S.-Y.; Li, H. *Chem. Commun.* **2012**, *48*, 5343–5345.
216. Huang, H.-P.; Wu, Q.; Mei, G.-Q. *Acta Crystallogr. Sect. E* **2006**, *62*, m3465–m3466.
217. A DFT scanning calculates the energies of different structures (partial optimization) as a parameter is varied, in this case the C1-Pd distance. In this way, plausible intermediates (*minima*) and possible transition states (*maxima*) can be located.
218. Diazoalkane **30** is synthesized as a CH₂Cl₂ solution with a concentration of 56 mM.
219. For synthesis where X = Cl or I see: a) Gaumont, A.-C.; M. Brown, J.; B. Hursthouse, M.; J. Coles, S. *Chem. Commun.* **1999**, *1*, 63–64. b) Cullinane, C.; Deacon, G. B.; Drago, P. R.; Erven, A. P.; Junk, P. C.; Luu, J.; Meyer, G.; Schmitz, S.; Ott, I.; Schur, J.; Webster, L. K.; Klein, A. *Dalton Trans.* **2018**, *47*, 1918–1932.
220. López-Fernández, R.; Carrera, N.; Albéniz, A. C.; Espinet, P. *Organometallics* **2009**, *28*, 4996–5001.
221. a) Lin, J. C. Y.; Huang, R. T. W.; Lee, C. S.; Bhattacharyya, A.; Hwang, W. S.; Lin, I. J. B. *Chem. Rev.* **2009**, *109*, 3561–3598. b) Mikhaylov, V. N.; Balova, I. A. *Russ. J. Gen. Chem.* **2021**, *91*, 2194–2248.
222. Arduengo, A. J.; Dias, H. V. R.; Calabrese, J. C.; Davidson, F. *Organometallics* **1993**, *12*, 3405–3409.
223. Guerret, O.; Solé, S.; Gornitzka, H.; Teichert, M.; Trinquier, G.; Bertrand, G. *J. Am. Chem. Soc.* **1997**, *119*, 6668–6669.
224. Wang, H. M. J.; Lin, I. J. B. *Organometallics* **1998**, *17*, 972–975.
225. delPozo, J.; Casares, J. A.; Espinet, P. *Chem. Commun.* **2013**, *49*, 7246–7248.
226. Liu, S.-T.; Lee, C.-I.; Fu, C.-F.; Chen, C.-H.; Liu, Y.-H.; Elsevier, C. J.; Peng, S.-M.; Chen, J.-T. *Organometallics* **2009**, *28*, 6957–6962.
227. a) Furst, M. R. L.; Cazin, C. S. J. *Chem. Commun.* **2010**, *46*, 6924–6925. b) Santoro, O.; Lazreg, F.; Cordes, D. B.; Slawin, A. M. Z.; Cazin, C. S. J. *Dalton Trans.* **2016**, *45*, 4970–4973. c) Bidal, Y. D.; Santoro, O.; Melaimi, M.; Cordes, D. B.; Slawin, A. M. Z.; Bertrand, G.; Cazin, C. S. J. *Chem. – A Eur. J.* **2016**, *22*, 9404–9409. d) Nahra, F.; Gómez-Herrera, A.; Cazin, C. S. J. *Dalton Trans.* **2017**, *46*, 628–631.
228. Álvarez, M.; Besora, M.; Molina, F.; Maseras, F.; Belderrain, T. R.; Pérez, P. J. *J. Am. Chem. Soc.* **2021**, *143*, 4837–4843.
229. Nakano, R.; Jazzar, R.; Bertrand, G. *Nat. Chem.* **2018**, *10*, 1196–1200.
230. The percent buried volume (%V_{Bur}) is a molecular descriptor analogous to Tolman's cone angle that measures the percent of the total volume of a sphere occupied by a ligand. Initially, this parameter was developed to be applied to NHC carbene ligands coordinated to metals, but it can be extended to other types of coordinated ligands. Selected examples: a) Poater, A.; Ragone, F.; Giudice, S.; Costabile, C.; Dorta, R.; Nolan, S. P.; Cavallo, L. *Organometallics* **2008**, *27*, 2679–2681. b) Poater, A.; Cosenza, B.; Correa, A.; Giudice, S.; Ragone, F.; Scarano, V.; Cavallo, L. *Eur. J. Inorg. Chem.* **2009**, *2009*, 1759–1766.
231. Yap, G. P. A.; Jove, F.; Urbano, J.; Alvarez, E.; Trofimenko, S.; Díaz-Requejo, M. M.; Pérez, P. J. *Inorg. Chem.* **2007**, *46*, 780–787.
232. a) Owen, G. R.; Vilar, R.; White, A. J. P.; Williams, D. J. *Organometallics* **2003**, *22*, 3025–3027. b) Lu, C. C.; Peters, J. C. *J. Am. Chem. Soc.* **2004**, *126*, 15818–

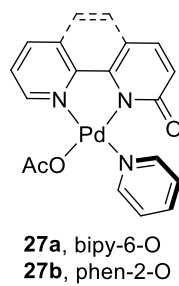
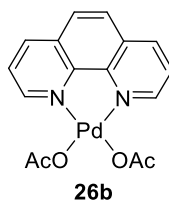
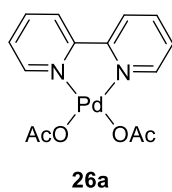
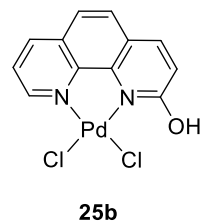
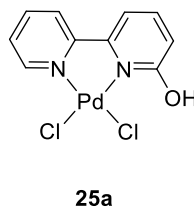
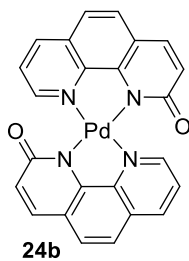
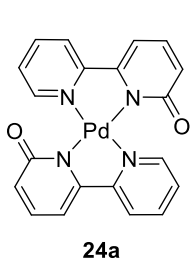
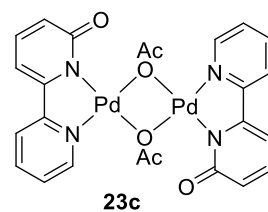
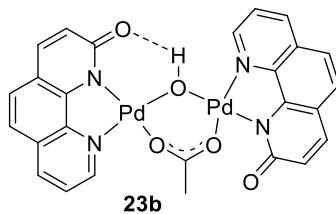
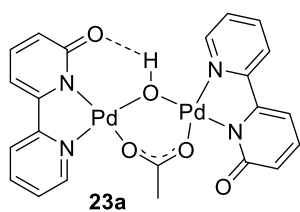
15832. c) Xie, Y.; Hu, J.; Wang, Y.; Xia, C.; Huang, H. *J. Am. Chem. Soc.* **2012**, *134*, 20613–20616.
- 233.** Albéniz, A. C.; Espinet, P.; Lin, Y.-S.; Orpen, A. G.; Martín, A. *Organometallics* **1996**, *15*, 5003–5009.
- 234.** a) Pearson, R. G. *Inorg. Chem.* **1988**, *27*, 734–740. b) Maynard, A. T.; Huang, M.; Rice, W. G.; Covell, D. G. *Proc. Natl. Acad. Sci. U.S.A.* **1998**, *95*, 11578. c) Parr, R. G.; Szentpály, L. v.; Liu, S. *J. Am. Chem. Soc.* **1999**, *121*, 1922–1924. c) Chattaraj, P. K.; Roy, D. R. *Chem. Rev.* **2007**, *107*, PR46–PR74.
- 235.** a) Domingo, L. R.; Chamorro, E.; Pérez, P. *J. Org. Chem.* **2008**, *73*, 4615–4624. b) Domingo, L. R.; Pérez, P. *Org. Biomol. Chem.* **2011**, *9*, 7168–7175.
- 236.** Hartley, F. R.; Murray, S. G.; McAuliffe, C. A. *Inorg. Chem.* **1979**, *18*, 1394–1397.
- 237.** Elia, C.; Elyashiv-Barad, S.; Sen, A.; López-Fernández, R.; Albéniz, A. C.; Espinet, P. *Organometallics* **2002**, *21*, 4249–4256.
- 238.** a) Lupin, M. S.; Powell, J.; Shaw, B. L. *J. Chem. Soc. A Inorganic, Phys. Theor.* **1966**, 1410–1411 b) Goodfellow, R. J.; Goggin, P. L.; Venanzi, L. M. *J. Chem. Soc. A Inorganic, Phys. Theor.* **1967**, 1897–1900.
- 239.** Complex [Tp^{Ms}Cu(THF)] is the direct precursor for the synthesis of complex **55** and at the same time bears a labile ligand susceptible to be displaced by the PPh₃ ligand. Schneider, J. L.; Carrier, S. M.; Ruggiero, C. E.; Young, V. G.; Tolman, W. B. *J. Am. Chem. Soc.* **1998**, *120*, 11408–11418.

Compound index

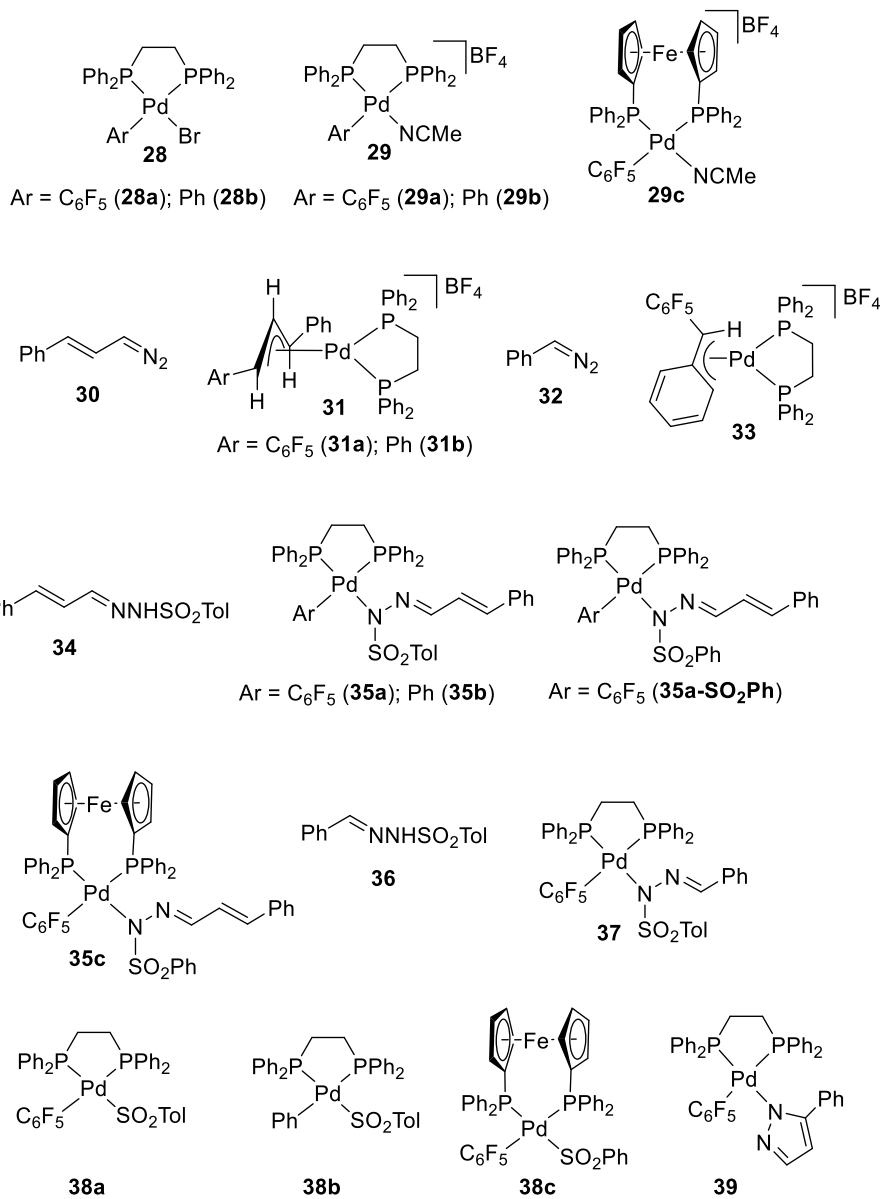
Chapter 2



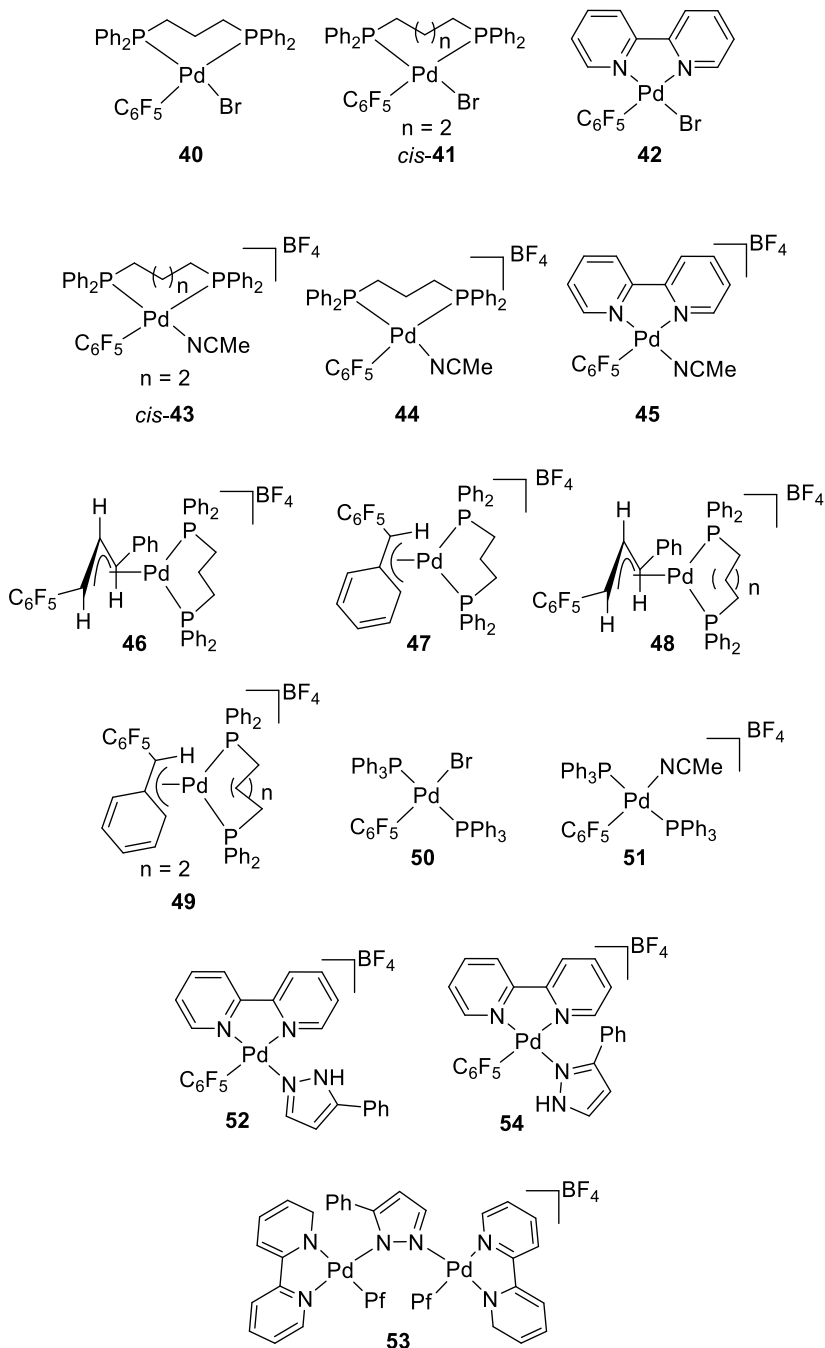
Chapter 3



Chapter 5



Chapter 6



Chapter 7

